Development of Novel Fluorogenic Antioxidants for Imaging Reactive Oxygen Species in Live Cells

Katerina Krumova

Degree of Doctor of Philosophy

Department of Chemistry
McGill University
Montreal, Quebec, Canada
H3A 2K6

August, 2012

A Thesis submitted to McGill University in partial fulfillment of the requirements for the degree of Doctor of Philosophy

Dedication

This thesis is dedicated to my parents Ana and Georgi, and my sister Lubomira.

Abstract

This thesis describes our advances in the preparation of lipophilic fluorogenic probes for the specific imaging of reactive oxygen species (ROS) in the lipid membrane of live cells. The work revolves around a simple design involving the preparation of a two segment receptor-reporter type free radical scavenger-fluorophore probe (an off-on fluorogenic antioxidant indicator). The receptor segment in the probe mimics the structure and activity of the naturally occurring antioxidant α-tocopherol. A covalently tethered lipophilic fluorophore serves the purpose of reporting, via emission enhancement, structural changes at the receptor end following its reaction with free radicals.

In this thesis we initially explore the off/on molecular switch mechanism operating in the first generation fluorogenic probe we prepared, a Bodipy-Trolox adduct that we named B-TOH. Through mechanistic studies including oxygen uptake, laser flash photolysis, electrochemistry, and DFT calculations we were able to establish that photoinduced electron transfer (PeT) occurs from the receptor to the reporter segment.

Molecular imaging of lipid peroxyl radicals in model lipid membranes and in live cells are next reported and we lay out the potential and drawbacks for utilizing B-TOH towards monitoring lipid peroxyl radicals in the lipid membrane of live cells. The information gained in these two chapters allowed us to determine the reporter (fluorophore) electrochemical and spectroscopic requirements that need to be met in order to modulate the sensitivity of B-TOH.

We subsequently describe the preparation, spectroscopic, and electrochemical characterization of a family of 16 new Bodipy dyes with tuneable redox potentials and versatile functional groups. Electron withdrawing or donating groups (Et, H, Cl or CN) at positions C2 and C6 enabled tuning the redox potentials within a *ca.* 0.7 eV window without significantly affecting either the HOMO-LUMO gap or the absorption and emission spectra. Hydroxymethyl or formyl groups at the *meso* (C8) position in turn provided functionality for covalent tethering to receptors and biomolecules of interest. The dyes can thus be coupled to both electrophiles and nucleophiles.

We subsequently generate two new fluorogenic probes (second generation) where we exploit the new Bodipy chromophores synthesized. We further optimize the linker moiety between receptor and reporter segment in order to control the chemical reactivity of the probes. The development of a high-throughput fluorescence assay for monitoring kinetics of peroxyl radical reactions in liposomes is described where the evolution of the fluorescence intensity over time provides a rapid facile method to conduct competitive kinetic studies in the presence of α-tocopherol and analogues

We additionally explore the selective targeting of cell organelles, specifically mitochondria (third generation probes). A chapter is devoted to describe the synthesis and mechanistic studies of mitochondria-targeting probes.

We conclude this thesis with a chapter dedicated to Conclusions and New directions. The new probes here described will allow a non-invasive spatial and temporal monitoring of the oxidative state in live cell on an organelle level. We may foresee that imaging studies with specific sensors will ultimately enable us to better understand vital links between the chemistry and the biology of ROS.

Résumé

Cette thèse discute de la préparation et du développement de sondes fluorescentes pour l'imagerie spécifique des espèces réactives de l'oxygène (ERO) dans les membranes de cellules vivantes. Le travail est centré sur une conception simple impliquant la préparation d'une sonde piégeuse de radicaux libres en deux segments récepteur-reporteur (un indicateur antioxydant fluorescent arrêt-marche). Le segment récepteur de la sonde mimique la structure et l'activité de l'antioxydant naturel α-tocophérol. Un fluorophore lipophile lié par un lien covalent rapporte, à l'aide d'une augmentation de la fluorescence, les changements structurels du côtè récepteur suite à sa réaction avec des radicaux libres.

Cette thèse explore initialement le mécanisme de fonctionnement de l'interrupteur arrêt / marche moléculaire dans la sonde de première génération que nous avons préparée, un produit d'addition Bodipy-Trolox que nous avons nommé B-TOH. Par l'entremise d'études mécanistiques incluant l'absorption d'oxygène, la photolyse éclair au laser, électrochimie et calculs sur la théorie de la fonctionnelle de la densité, nous étions capable de déterminer que le transfert d'électron photoinduit se produit du segment récepteur au segment reporteur.

L'imagerie moléculaire de radicaux peroxydes lipidiques dans les membranes lipides modèles et dans les cellules vivantes sont ensuite rapportées et nous mentionnons les inconvénients potentiels reliés à l'utilisation de B-TOH à l'évaluation de radicaux peroxydes lipidiques dans la membrane lipide de cellules vivantes. L'information acquise durant ces deux chapitres nous a permis de déterminer les exigences électrochimiques et spectroscopiques du reporteur (fluorophore) qui doivent être remplies afin de moduler la sensibilité de B-TOH.

Par la suite, nous décrivons la préparation ainsi que la caractérisation spectroscopique et électrochimique de 16 nouvelles molécules Bodipy avec des potentiels d'oxydoréduction variables et groupes fonctionnels polyvalents. Des groupes donneur ou accepteur d'électrons (Et, H, Cl ou CN) aux positions C2 et C6 permettent de changer le potentiel d'oxydoréduction dans une fenêtre de ca. 0.7 eV sans changer significativement ni l'écart HOMO-LUMO ni les spectres

d'absorption ou d'émission. Des groupes hydroxymethyl ou formyl à la position méso (C8) quant à eux fournissent la fonctionnalité requise pour la formation de liens covalents avec des récepteurs et molécules biologiques d'intérêts. Ces molécules fluorescentes peuvent donc être couplées non seulement aux électrophiles mais, également aux nucléophiles.

Nous générons ensuite deux nouvelles sondes fluorescentes (deuxième génération) en exploitant les nouveaux chromophores Bodipy synthétisés. Nous optimisons davantage le groupe caractéristique lieur entre les segments récepteurs et reporteur afin de contrôler la réactivité chimique des sondes. Le développement d'une analyse à haut débit qui suit la cinétique de la réaction des radicaux peroxydes dans des liposomes est décrite où l'évolution de l'intensité de la fluorescence avec le temps nous fournie une méthode rapide et facile pour mener des études cinétiques compétitives dans la présence de α-tocophérol et ses analogues.

Nous explorons additionnellement le ciblage sélectif d'organelle cellulaire, spécifiquement des mitochondries (sonde de troisième génération). Un chapitre est dévoué à la description de la synthèse et aux études mécanistiques de sondes cibleuses de mitochondrie.

Nous concluons cette thèse par un chapitre dédié aux conclusions et aux nouvelles directions. Les nouvelles sondes décrites ici permettront l'évaluation spatiotemporelle et non-invasive de l'état d'oxydation de cellules vivantes au niveau des organelles. Nous pouvons prévoir que des études d'imageries avec des sondes spécifiques vont éventuellement nous permettre de mieux comprendre des liens vitaux entre la chimie et la biologie des ERO.

Acknowledgements

First, I would like to thank my supervisor Professor Gonzalo Cosa for his constant guidance and support throughout my PhD. He has always been able to motivate and encourage me when I needed it the most. He has been a great mentor and I will be forever grateful for his confidence in my capabilities as a scientist and for getting the best out of me.

I would like to also thank all the past and current Cosa lab members for their help and support. Paul Oleynik, Pierre Karam, An Ngo, Wayne Mah, Robert Godin, Lana Green, Hsiao-Wei Liu, Richard Lincoln, Amani Hariri, Ryan Marko, Christina Calver, Viktorija Glembockyte, Mathieu Frenette, you all made my PhD a fun and unforgettable experience. I need to especially thank a few people in our lab: Paul for being an incredible friend and helping me deal with my problems both personal and work related in my first year in Canada; Pierre for always having my back and managing to make me laugh; Robert for being so patient and for listening to my constant complaining and at the same time providing great ideas and insightful comments for my research; Lana for being a great person to work with and putting up with my weird working habits. I am also grateful to all the students I supervised, Sayuri Friedland, Mien Chien Yu, Mark Maclean, Genevieve Redstone, Richard Lincoln, for helping me become a better teacher.

I am also grateful to all the administrative staff without whose help I would not have been able to graduate. Special thanks go to Chantal Marotte who has been so helpful with everything and always managing to keep us all on track. I also want to thank all the people at McGill whose help allowed me to carry out my research: Fred Morin for keeping up the NMR facilities, Nadim Saade for his assistance with MS, Dr. Claire Brown from the McGill Imaging Facility.

I especially want to thank all my friends for always being there for me helping me every step of the way. I will mention a few: Rodrigo Mendosa Sancez for many helpful discussions about organic synthesis; Rami Hourani for always being able to cheer me up; Chris McLaughlin and Adrienne Langille for surviving living with me and patiently listening to my endless talking. I need to especially thank Matthew Hassler for making my stay in Canada more interesting than I

expected. Despite his constant teasing and generally annoying behaviour he has always been a great friend and his help and support has always been really appreciated.

Last but not least, I would like to thank the most important people in my life my family, my sister Lubomira, my mother Ana, and my father Georgi for their unconditional love and support. I cannot put in words my gratitude for all they have sacrificed throughout my whole life so I can follow my dreams. You have always been my inspiration.

Contributions of Authors

All papers presented in chapters 2 to 6 were co-authored with Prof. Gonzalo Cosa (Department of Chemistry, McGill University), who acted as a research advisor. He also conducted the DFT calculations included in chapters 2 and 4.

- Katerina Krumova, Paul Oleynik, Pierre Karam and Gonzalo Cosa, Phenol-based Lipophilic Fluorescent Antioxidant Indicators: a Rational Approach. *J. Org. Chem.* **2009**, 74, 3641–3651

Katerina Krumova contributed to project design, performed spectroscopic characterization of B-TOH and B-BHB, laser flash photolysis experiments, oxygen uptake studies, and kinetic studies in homogeneous solution. Contributions also include data analysis, interpretation of the acquired data, and manuscript writing and editing.

Paul Oleynik conducted preliminary kinetic studies on the peroxyl radical scavenging activity of B-TOH and B-BHB in homogeneous media.

Pierre Karam acquired cyclic voltammograms for PM605 and PMOH.

- Armen Khatchadourian, Katerina Krumova, Sebastien Boridy, An Thien Ngo, Dusica Maysinger, Gonzalo Cosa, Molecular Imaging of Lipid-Peroxyl Radicals in Living Cells with a Bodipy-α-Tocopherol Adduct. *Biochemistry* **2009**, 48, 5658–5668

Armen Khatchadourian contributed to project design, performed confocal fluorescence imaging of live cell (rat pheochromocytoma, PC12 cells) stressed with CdTe nanoparticles using B-TOH, conducted kinetic studies of lipid peroxidation in PC 12 cells and co-localization studies of B-TOH with Nile Red. Contributions also include data analysis, interpretation of the acquired data, and manuscript writing and editing.

Katerina Krumova contributed to project design, development and performance of experimental procedures for measuring partition coefficients of B-TOH and PMOH, fluorescence lifetimes of B-TOH and PMOH in liposomes, kinetic studies

of radical scavenging activity of B-TOH in heterogeneous media, and pH dependence studies of the reactivity of B-TOH. Contributions also include data analysis, interpretation of the acquired data, and manuscript writing and editing.

Sebastien Boridy conducted confocal fluorescence imaging of lipid peroxidation in live cells (primary culture of mouse hippocampus) stressed with methyl viologen using B-TOH and Lysotracker Red DND-99.

An Thien Ngo contributed to liposome extrusion and manuscript editing.

Prof. Dusica Maysinger contributed to project design, data analysis, interpretation of the acquired data, manuscript writing and editing.

- Katerina Krumova and Gonzalo Cosa, Bodipy Dyes with Tunable Redox Potentials and Functional Groups for Further Tethering: Preparation, Electrochemical and Spectroscopic Characterization. *J. Am. Chem. Soc.,* **2010**, 132, 17560–17569

Katerina Krumova contributed to project design, synthesis, electrochemical and spectroscopic characterization of the Bodipy dyes reported in the manuscript, and manuscript writing and editing.

- Katerina Krumova, Sayuri Friedland and Gonzalo Cosa, How Lipid Unsaturation, Peroxyl Radical Partitioning and Chromanol Lipophilic Tail Affect the Antioxidant Activity of α-Tocopherol: Direct Visualization via High Throughput Fluorescence Studies Conducted with Fluorogenic α-Tocopherol Analogues *J. Am. Chem. Soc*. **2012** DOI: 10.1021/ja301680m

Katerina Krumova contributed to project design, synthesis of second generation of fluorogenic antioxidants (H_2B-TOH and H_2B-PMHC), and development of high-throughput fluorescence method for monitoring kinetics of peroxyl radical reactions in liposomes. Contributions also include performing the experimental procedures reported in the manuscript, data analysis, interpretation of the acquired data, and manuscript writing and editing.

Sayuri Friedland assisted in performing competitive kinetic studies in liposome suspensions using H_2B-TOH as a signal carrier.

- Katerina Krumova, Lana Greene and Gonzalo Cosa, Imaging Peroxyl Radicals within the Mitochondrial Lipid Membrane of Live Cells. *Manuscript in preparation*

Katerina Krumova contributed to project design, synthesis of third generation of fluorogenic antioxidants (mitochondria-targeting probes) and their spectroscopic characterization, development and performance of experimental procedures for kinetic studies of the radical scavenging activity of the mitochondria-targeting fluorogenic probes in homogeneous and heterogeneous media, co-localization studies of mitochondria-targeting probes with MitoTracker Deep Red in live cells, and imaging of the emission enhancement of the probes in live cells under oxidative stress using confocal fluorescence microscopy. Contributions also include data analysis, interpretation of the acquired data, and manuscript writing and editing.

Lana Greene performed cell culturing, cell treatment, and assisted with confocal fluorescence live cell imaging.

Table of Contents

List of Figures

List of Schemes

List of Tables

List of Abbreviations

ABAP	2,2'-Azobis-(2-methylpropionamide) dihydrochloride
Abs	Absorbance
ACN	Acetonitrile
AIBN	2,2'-Azobis-(2-isobutyronitrile)
AMBN	2,2'-Azobis-(2-methylbutyronitrile)
AOH	Phenolic Antioxidant
ATP	Adenosine Triphosphate
B-BHB	3,5-Di-tert-butyl-4-hydroxybenzoic acid-Bodipy adduct
BDE	Bond Dissociation Enthalpy
BHT	Butylated Hydroxytoluene
Bodipy	Boron-dipyrromethene (4,4-difluoro-4-bora-3a,4a-diaza-s-indacene)
B-TOH	8-((±) 6-Hydroxy-2,5,7,8-tetramethylchromane-2-carbonyloxy)-methyl-2,6-diethyl-1,3,5,7-tetramethyl pyrromethene fluoroborate (Bodipy-Trolox adduct)
CdTe np	Cadmium Telluride nanoparticle
DCFH	Dichlorodihydrofluorescein
DCM	Dichloromethane
DFT	Density Functional Theory
DIPEA	Diisopropylethilamine
DLPC	1,2-Dilinoleoyl-*sn*-glycero-3-phosphocholine
DMAP	4-Dimethylaminopyridine
DMEM	Dulbecco's Modified Eagle Medium
DMF	Dimethylformamide
DMPC	1,2-Dimyristoyl-*sn*-glycero-3-phosphocholine
DMSO	Dimethylsulfoxide
DNA	Deoxyribonucleic acid
DOPC	1,2-Dioleoyl-*sn*-glycero-3-phosphocholine
DPPC	1,2-Dipalmitoyl-*sn*-glycero-3-phosphocholine
EA	Electron Affinity
EDC	1-Ethyl-3-(3-dimethylaminopropyl) carbodiimide
EDG	Electron-Donating Group
EggPC	L-α-phosphocholine

Em	Emission
EPR	Electron Paramagnetic Resonance
ESI	Electron Spray Ionization
EWG	Electron-Withdrawing Group
FBS	Fetal Bovine Serum
FRET	Förster Resonance Energy Transfer
HAT	Hydrogen Atom Transfer
H_2B-PMHC	8-((6-hydroxy-2,5,7,8-tetramethylchroman-2-yl)-methyl)-1,3,5,7-tetramethyl Pyrromethene Fluoroborate (H_2-Bodipy-PMHC adduct)
HBSS	Hank's Balanced Salt Solution
H_2B-TOH	8-((±)-6-Hydroxy-2,5,7,8-tetramethylchromane-2-carbonyloxy)-methyl-1,3,5,7-tetramethyl pyrromethene fluoroborate (H_2-Bodipy-Trolox adduct)
HNE	4-Hydroxy-2-nonenal
HOMO	Highest Occupied Molecular Orbital
HPLC	High Performance Liquid Chromatography
HPODE	Hydroperoxyoctadecadienoates
HRMS	High Resolution Mass Spectrometry
IC	Internal Conversion
ICT	Intramolecular Charge Transfer
IMM	Inner Mitochondrial Membrane
IMS	Intermembrane Space
IP	Ionization Potential
IR	Infrared
ISC	Intersystem Crossing
LAMP1	Lysosomal-Associated Membrane Protein-1
LDL	Low-Density Lipoproteins
LFP	Laser Flash Photolysis
LH	Lipids
LUMO	Lowest Occupied Molecular Orbital
MeO-AMVN	2,2'-Azobis(4-methoxy-2.4-dimethyl valeronitrile)
MeOH	Methanol
MPA	Mercaptopropionic acid
MV^{2+}	N,N'-dimethyl-4,4'-bipyridinium dichloride (Methyl Viologen)

NAC	N-acetylcysteine
NADPH	Nicotinamide Adenine Dinucleotide Phosphate
NCS	N-chlorosuccinimide
NMR	Nuclear Magnetic Resonance
OMM	Outer Mitochondrial Membrane
ONE	4-oxo-2-nonenal
PBS	Phosphate Buffer Saline
PC12 cells	Pheochromocytoma cells
PCET	Proton Coupled Electron Transfer
PeT	Photoinduced electron Transfer
PMHC	2,2,5,7,8-Pentamethyl-6-hydroxychroman
PM605	8-Acetoxymethyl-2,6-diethyl -1,3,5,7-tetramethyl pyrromethene fluoroborate
PMOH	8-Hydroxymethyl-2,6-diethyl -1,3,5,7-tetramethyl pyrromethene fluoroborate
PS	Phosphatidyl Serine
PUFA	Polyunsaturated Fatty Acids
POPC	1-Palmitoyl-2-oleoyl-*sn*-glycero-3-phosphocholine
RNS	Reactive Nitrogen Species
ROS	Reactive Oxygen Species
SCE	Standard Calomel Electrode
SH-SY5Y	Neuroblastoma cells
SOD	Superoxide Dismutases
SOMO	Semi-Occupied Molecular Orbital
SPLET	Sequential Proton Loss Electron Transfer
TEA	Triethylamine
THF	Tetrahydrofuran
TMP	Tocopherol-Mediated Peroxidation
TOH	α-Tocopherol
TPP	Triphenylphosphine or triphenylphosphonium cation
VR	Vibrational relaxation

1. Introduction

Reactive oxygen species (ROS) are formed following electron transfer to molecular oxygen and are related to the toxicity of oxygen at the cellular and organismal level. They are often responsible for mediating modifications of biomolecules that are central to life such as DNA, proteins, and lipids.[1] The overproduction of ROS is associated with oxidative stress and is implicated in various diseases, aging, and death.[2] However, new evidences are emerging for the more complex and beneficial role ROS play in physiological processes associated with cell signaling.[3]

This introduction highlights the production and chemistry of the major types of ROS and how they affect biological systems. The focus will be on the role ROS play in changing the lipid cell milieu and more specifically in the oxidative process known as lipid peroxidation. The biology, chemistry, and kinetic considerations of lipid peroxidation and its inhibition by phenolic antioxidants will be discussed in detail. Crucial for elucidating the biological consequences of the chemistry of ROS and lipid peroxidation in particular, is the development of chemical tools that can give real-time information about cell changes triggered by ROS. An overview of recent advances in the development of molecular probes for imaging of ROS and their specific targeting of organelles (e.g. mitochondria) will be given.

1.1 Reactive Oxygen Species

Reactive oxygen species (ROS) is a collective term describing the chemical species that are formed upon incomplete reduction of oxygen. The major ROS in living systems are singlet oxygen ($^1O_2$), superoxide radical anion ($O_2^{\bullet -}$), hydrogen peroxide (H_2O_2), hydroxyl radicals ($OH^{\bullet}$), lipid peroxides ($LOO^{\bullet}$), and hypochlorous acid (HOCl). They are produced in a wide range of chemical and physiological processes (Figure 1.1). Sources of ROS are UV radiation, the metabolism of drugs, and various redox reactions. Most of the redox processes responsible for the production of ROS occur in the mitochondrial respiratory

chains in cell membranes, or in the endoplasmic reticulum through oxidative protein folding.

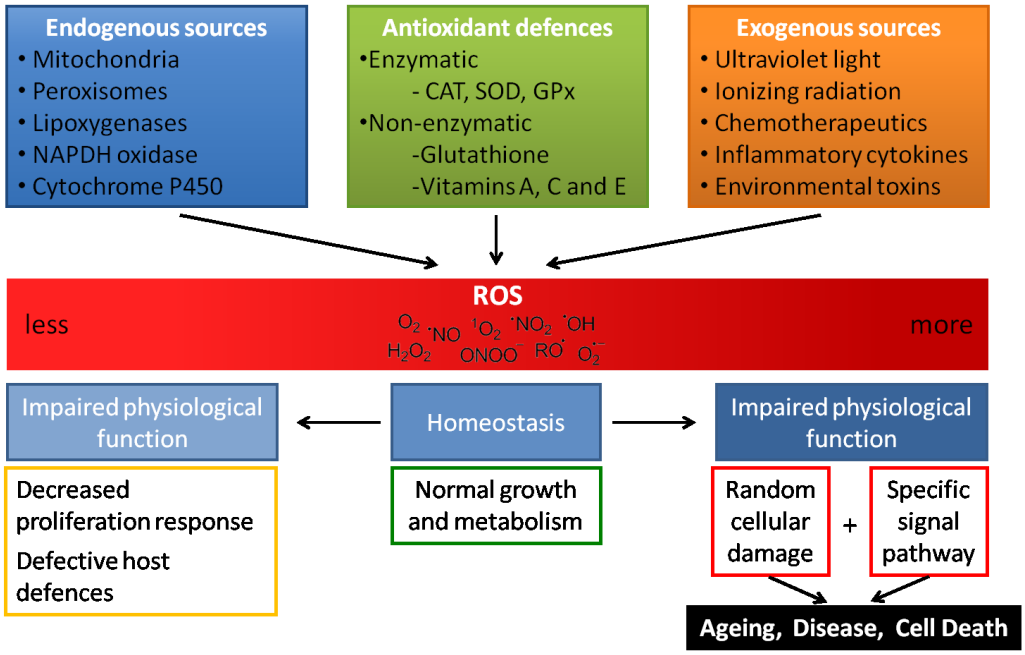

Figure 1.1 Sources of ROS, antioxidant defences, and subsequent biological effects depending on the level of ROS production.[4]

While the controlled release of ROS is crucial to maintain normal homeostasis,[3] their overproduction is associated with numerous disorders.[4] Oxidative stress caused by the imbalance between excessive formation of ROS and limited antioxidant defences is connected to many diseases including age-related disorders, cancer, cardiovascular, inflammatory, and neurodegenerative diseases such as Parkinson's and Alzheimer's diseases.[2,5-8]

Due to their redox properties ROS are often responsible for modifications of biomolecules such as lipids, DNA bases, and aminoacids, which trigger cellular damage. Polyunsaturated fatty acids in membranes are particularly susceptible to oxidative modifications and lipid peroxidation is a sensitive marker of oxidative stress.[8] Oxidative damage to lipids leads to changes in the membrane fluidity and is one of the most prevalent mechanisms of cellular injury.[9,10] Additionally, the breakdown products of lipid peroxidation, including α,β-unsaturated aldehydes, can attack aminoacids and nucleobases resulting in site-specific chemical

modifications of proteins and DNA. This can lead to damage and fragmentation of the peptide backbone or to mutations and other lethal genetic effects.[11]

Numerous physiological functions are controlled by redox-responsive signaling pathways. Mounting evidence suggest that ROS can operate as intracellular signaling molecules.[3,6,9,12-14] The redox regulation typically involves controlled production of reactive oxygen and nitrogen species. They can in turn react with specific functional groups of target proteins (e.g. [Fe-S] clusters, cysteins, etc.) that lead to covalent protein modifications.[15] ROS as second messengers are important for the expression of several transcription factors and other signal transduction molecules such as heat shock-inducing factor and nuclear factor. They also participate in the regulation of cell adhesion, redox-mediated amplification of immune response and programmed cell death.[7]

1.1.1. Precursor-Product Relationship of Various ROS

In order to understand the chemical and the associated biological impact of ROS, we need to know their origin, type, and reactivity.

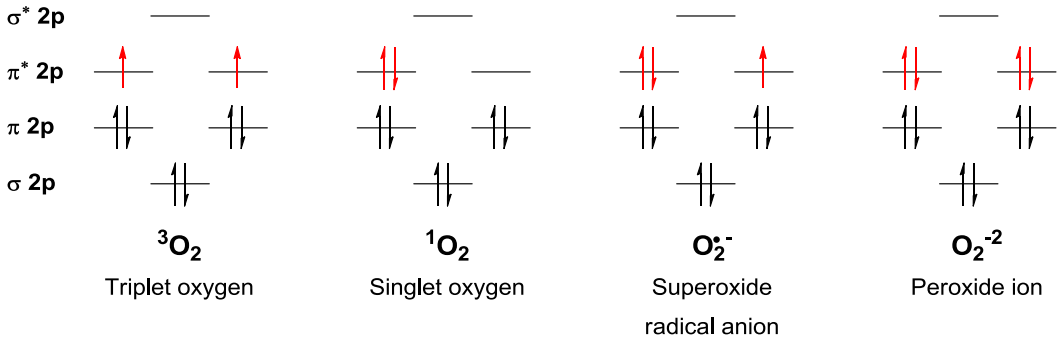

Figure 1.2. Molecular orbital diagrams for ground state molecular oxygen ($^3O_2$), singlet oxygen ($^1O_2$), and ROS (superoxide radical anion $O_2^{\bullet-}$ and peroxide ion O_2^{-2}, deprotonated form of hydrogen peroxide H_2O_2).[1]

Ground state triplet molecular oxygen ($^3O_2$) is a paramagnetic diradical with its two valent electrons occupying separate orbitals with parallel spins (Figure 1.2). In order for molecular oxygen to participate in redox reactions with other atoms or molecules it has to accept a pair of electrons with the same spin so they can fit into the vacant spaces in the π^* orbitals. Most non-radical organic

molecules are diamagnetic, with pairs of electrons with opposite spins. Thus oxygen is unable to efficiently oxidize biomolecules. The spin restriction results in oxygen preferably accepting one electron at a time during redox reactions.

Ground state $^3O_2$ can be converted to more reactive oxygen containing forms. Energy transfer to $^3O_2$ leads to the formation of the more reactive molecular oxygen form singlet oxygen ($^1O_2$). Singlet oxygen has paired electrons with opposite spins and is not a radical (Figure 1.2). The spin restriction is removed therefore $^1O_2$ has an increased oxidizing ability compared to $^3O_2$.

$^3O_2$ can react fast with other radicals by single electron transfer. The unpaired electrons of triplet oxygen can readily react with the unpaired electrons of transition metals such as Fe found in [Fe-S] clusters in mitochondrial respiratory chains. The one electron reduction of oxygen results in the formation of superoxide radical anion ($O_2^{\bullet-}$). The main site of generation of superoxide radical anion ($O_2^{\bullet-}$) is the inner mitochondrial membrane. It is formed through reduction of molecular oxygen by semiquinone or by NADH dehydrogenase in the respiratory chains[11] and through various enzymatic oxidation reactions catalyzed by cytochromes P450.[4,16] Despite its high reduction potential of +0.94 V (Scheme 1.1) $O_2^{\bullet-}$ can oxidize very few biological compounds. It has limited reactivity with electron-rich centers because of its anionic charge. Once formed superoxide can react at diffusion controlled rates with nitric oxide ($NO^{\bullet}$) to form peroxynitrile ($ONOO^-$) which is a potent oxidant.

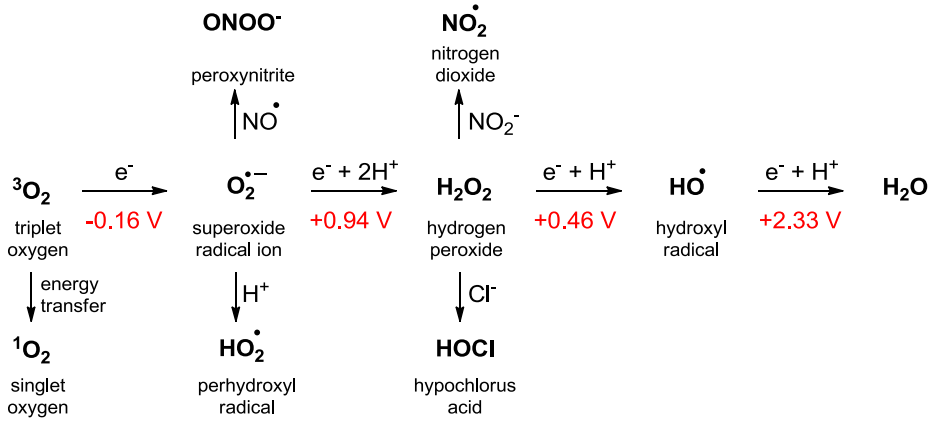

Scheme 1.1. Formation of ROS through energy and electron transfer reactions. Reduction potentials for the major ROS are shown.[7,11]

One-electron reduction of $O_2^{\bullet-}$ leads to the formation of other ROS (Scheme 1.1) such as hydrogen peroxide (H_2O_2) and subsequently hydroxyl radicals ($OH^{\bullet}$). $O_2^{\bullet-}$ can dismutate enzymatically (by superoxide dismutases, SODs) and non-enzymatically to oxygen and hydrogen peroxide (H_2O_2).[7] Hydrogen peroxide is uncharged (Figure 1.2) and readily diffuses through biological membranes. In neutrophils (immune cells) it is produced in milimolar quantities and stored in specific organelles called phagosomes for the purpose of microbial killing.[13] It is involved in cellular redox signaling pathways such as programmed cell death and apoptosis through its direct reaction with specific thiol proteins.[17]

H_2O_2 can be reduced by transition metals (Fe^{2+} or Cu^{2+}) through Fenton chemistry to hydroxyl radical ($HO^{\bullet}$). $HO^{\bullet}$ is the most reactive oxygen radical. It reacts with biomolecules with diffusion controlled rates. Hydroxyl radicals can also initiate chain reactions such as lipid peroxidation.

All these ROS are stronger oxidants than molecular oxygen as indicated by their redox potentials (Figure 1.2) thus accounting for their higher reactivity towards biomolecules.

1.2. Lipid Peroxidation

1.2.1. Biology of Lipid Peroxidation

Lipids are essential components of cell membranes. They participate in maintaining the cell structure and integrity and control the proper functioning of the cell. The lipid bilayer of biological membranes is composed of a complex mixture of various types of lipids. This complex composition reflects the different functions membranes have in specific parts of the cell. For example the fluidity of the membrane depends on the percentage of polyunsaturated lipids in its composition. Chemical changes of the unsaturated lipids can lead to *cis-trans* isomerisation thus changing their packing characteristics.[10,18] This has dramatic effects on the structure and therefore functions of these membranes. Lipids are primary target of ROS. The oxidative reactions of lipids are combined under the term lipid peroxidation, also known as autoxidation. Polyunsaturated fatty acids (PUFA) and esters are particularly prone to undergo autoxidation due to the

presence of activated C-H bonds. Details on the specific structural and chemical requirements for lipid peroxidation to occur and the subsequent products formed in this process will be discussed in following sections.

The biological role of lipid peroxidation and its products have received a lot of attention in past decades. This oxidation process leads to changes in the integrity, fluidity and permeability of biomembranes. Many of the decomposition products of oxidized PUFA are highly reactive and modify biologically essential molecules such as proteins and DNA bases. α,β-Unsaturated aldehydes are commonly produced in lipid peroxidation. Due to their electrophilic nature they readily participate in Michael type nucleophilic addition reactions with nucleobases and amino acids (Scheme1.2.).

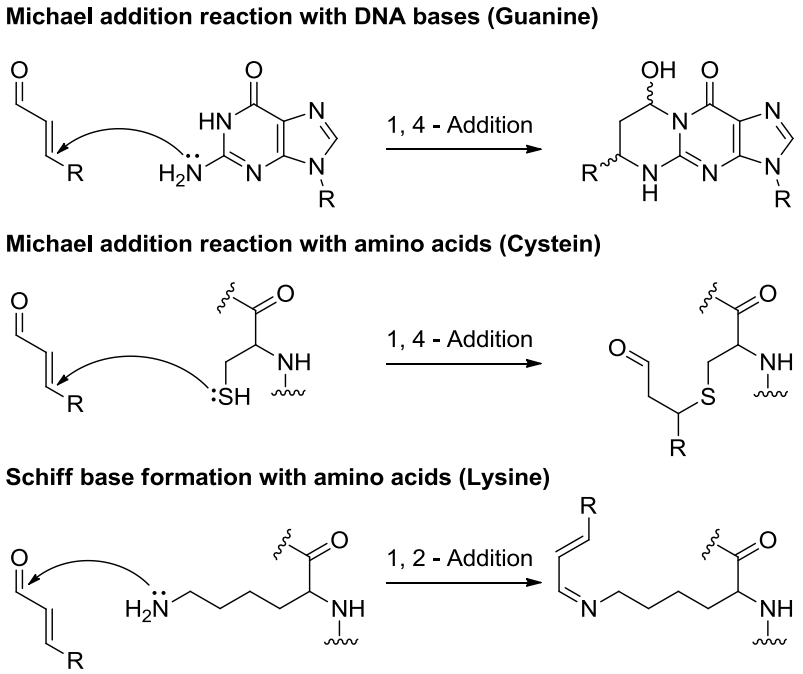

Scheme 1.2. Chemical modifications of DNA bases and protein amino acids nucleophilic addition reactions to α,β-unsaturated aldehydes.[19]

Additionally, electrophilic aldehydes produced during lipid peroxidation induce rapid depletion of glutathione, leading to intracellular change in redox equilibrium.[20] Thus, lipid peroxidation and its products are implicated in numerous disorders and diseases such as cardiovascular and liver diseases,[21] cancer,[22] neurodegenerative disorders such as Alzheimer's and Parkinson's disease,[8,23] and aging.[4,24] At the same time, the involvement of oxidatively

modified lipids has become more evident in different signalling pathways such as regulation of gene expression,[25] activation of receptors and nuclear transcription factors,[26] and adaptive responses.[27] Studies of these signalling mechanisms represent the expanding field of oxidative lipidomics that is bridging the lipid biochemistry and biophysics with free radical chemistry and cell biology.[14]

1.2.2 Kinetic Analysis and Products of Lipid Peroxidation

The biomedical aspects of the oxidation of lipids have led to the extensive studies of the mechanisms, dynamics, and products of lipid peroxidation. Significant contributions to this field have been made by Ingold starting from the 1960's to present time. His research is spanning from studies on reactions of free radicals and their intermediates with oils and lipids, to development of quantitative kinetic analysis of autoxidation and its inhibition by antioxidants (e.g. vitamin C, vitamin E, and their analogues) in homogeneous solutions[28-30] and heterogeneous environments such as aqueous micelles and phospholipids bilayers.[31-38] Additional mechanistic understanding of the effects of antioxidants has been provided by Barclay.[34,39-45] Porter and coworkers have been able to analyze lipid peroxidation products and elucidate the mechanisms behind their formation.[46,47]

The primary reactions involved in lipid peroxidation are hydrogen-atom abstraction by peroxyl or alkoxyl radicals, oxygen addition to carbon-centered radicals, and peroxyl-peroxyl termination. The free radical chain mechanism for autoxidation of lipids in biological systems is generally represented by the reaction sequence shown in Scheme 1.3. The mechanism and kinetic rate laws describing the oxidation process were first developed for reactions in homogeneous solutions and further extended to heterogeneous systems closely mimicking the lipid bilayer in cell membranes.

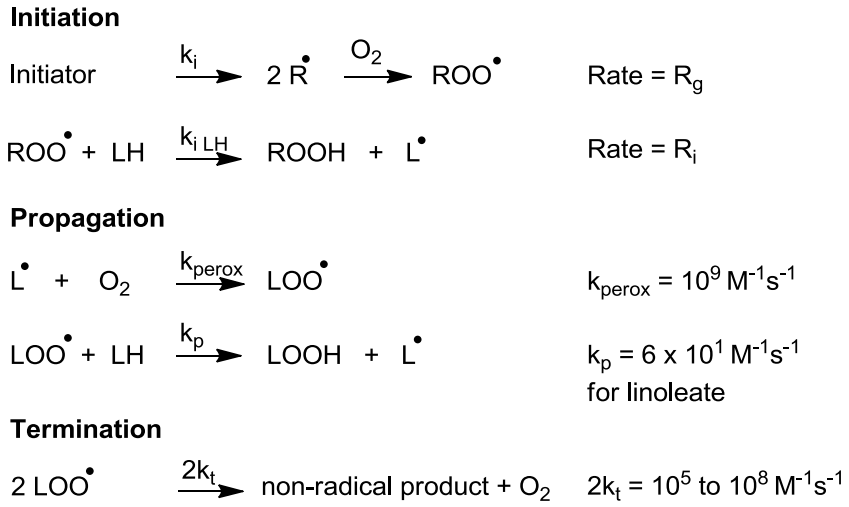

Scheme 1.3. Mechanism of lipid peroxidation in the presence of radical initiator. ROO• represents a general peroxyl radical regardless of the source and LH is polyunsaturated fatty acid in lipids. Rate constants are obtained from studies in homogeneous solution (k_{perox}[48], k_p[49], k_t[47]).

1.2.2.1. Initiation

In the initiation step, the key event is the formation of a lipid carbon-centered radical L• from a molecular precursor. In a biological system, cellular membrane lipid oxidation can be induced by exogenous physical (heat and light) and chemical reagents, or endogenous enzymatic and non-enzymatic systems. In vitro oxidation of unsaturated fatty acid-containing lipids can be initiated by a variety of methods, including the use of transition metals such as copper and iron, enzymes, hydroxyl radicals, or reactive nitrogen species (RNS).[47]

In mechanistic studies, it is important to have free radical generation at a known and well-defined rate. Under experimental conditions, lipid peroxidation is normally initiated at a constant rate, R_i, by thermal decomposition of azo-compounds, RN=NR. Azo-compounds decompose by first order kinetics. This process results in the formation of two carbon-centered radicals R•, which rapidly trap molecular oxygen to form peroxyl radicals ROO• (see Scheme 1.4.).

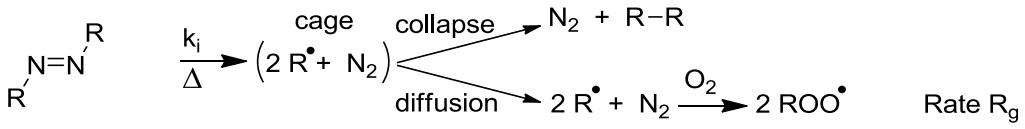

Scheme 1.4. Generation of peroxyl radicals through thermal initiation of azo-compounds.[34,50,51]

Peroxyl radicals are generated at a rate R_g that can be controlled by using an initiator with a known rate constant of initiation, k_i, and a known initiator efficiency, *e*. The correction *e* is needed since only those radicals which escape the solvent cage in which they are formed can react with oxygen to next initiate reaction on the substrate.[52-54] The initiation (or decomposition) rate constant, k_i, for an azo initiator at a given temperature varies depending on the structure. It can be calculated for a certain temperature using the Arrhenius equation:

$$k_i = Ae^{-E_a/RT} \qquad (1)$$

where E_a is the activation energy of the reaction and A is the pre-exponential factor. The structures, E_a, A, as well as k_i values determined at 37 °C for some of the most commonly used hydrophylic and lipophilic radical azo-initiators are given in Figure 1.3.

Lipophilic Radical Initiators

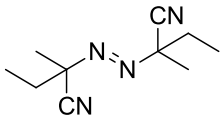

2,2'-Azobis(2-methylbutyronitrile)
(AMBN)
E_a=1.25 x 10^5 J/mol; A = 3.08 x 10^{14}
k_i = 0.27 x 10^{-6} s^{-1}; $t_{1/2}$ = 722 hs at 37 °C

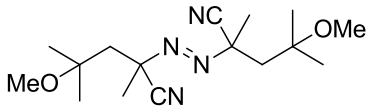

2,2'-Azobis(4-methoxy-2.4-dimethyl valeronitrile)
(MeO-AMVN)
E_a=1.15 x 10^5 J/mol; A = 1.29 x 10^{15}
k_i = 54 x 10^{-6} s^{-1}; $t_{1/2}$ = 3.5 hs at 37 °C

Hydrophilic Radical Initiators

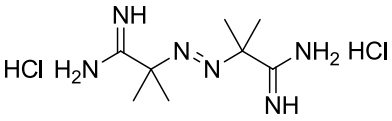

2,2'-Azobis(2-methylpropionamidine)
dihydrochloride **(ABAP)**
E_a=1.24x10^5 J/mol; A = 9.39 x 10^{14}
k_i = 1.2 x 10^{-6} s^{-1}; $t_{1/2}$ = 161 hs at 37 °C

Figure 1.3. Structures, activation energy (E_a), decomposition rate constants (k_i), and half-life times for selected azo-initiators.[47,55]

Under steady state conditions, the rate of generation (R_g) and the rate of chain initiation (R_i) are equal to the rate of termination and is expressed by equation (2)

$$R_i = R_g = 2k_i e[RN = NR] = 2k_t[ROO^{\bullet}]^2 \quad (2)$$

Peroxyl radicals ROO$^{\bullet}$ initiate the chain reaction of lipid peroxidation by abstracting a hydrogen atom from the polyunsaturated fatty acids forming a lipid carbon-centered radical L$^{\bullet}$ that further propagates the reaction (Scheme 1.5).

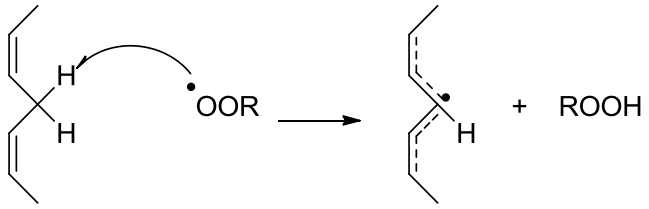

Scheme 1.5. H-abstraction by a peroxyl radical from PUFA forming a resonance stabilized lipid carbon-centered radical.

Since the H-abstraction involves homolytic cleavage of a C-H bond (Scheme 1.5.) the reaction will depend on the strength of this bond and the stability of the so formed carbon-centered radical. The strength of the bond is defined as bond dissociation enthalpy (BDE). The **C-H** BDE of LH must be lower than that of the newly formed RO**O-H** which is about 88 kcal/mol for R being an alkyl group.[56] Polyunsaturated fatty acids and esters are particularly prone to undergo autoxidation due to the presence of activated C-H bonds and the subsequent formation of stabilized bis-allilyc radicals. Linoleate and arachidonate are examples of such fatty acid esters (Figure 1.4.).

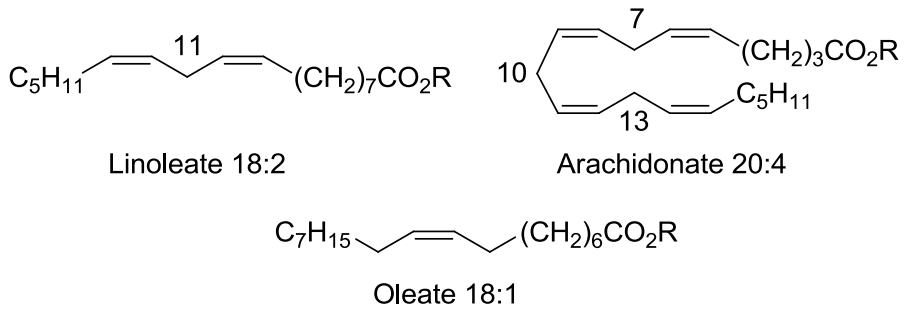

Figure 1.4. Structures of monounsaturated (oleate) and polyunsaturated (linoleate and arachidonate) fatty esters.

The C-H bonds at the bis-allylic positions, C-11 in linoleate, and C-7, C-10, C-13 in arachidonate, are the weakest C-H bonds in these molecules. Their homolytic bond dissociation enthalpies (BDE) are about 78-80 kcal/mol.[56] The hydrogen

atoms at these positions are preferentially abstracted by peroxyl radicals. Oleate, a monounsaturated fatty acid, is much less prone to undergo oxidation because the allylic C-H bonds at C-8 and C-11 are about 10 kcal/mol higher in energy than the corresponding bis-allylic substructures in linoleate.[47] Saturated lipids have even higher BDE's of around 100 kcal/mol and do not participate in lipid peroxidation.[56]

1.2.2.2. Propagation

Propagation of the chain reaction of oxidation of lipids consists of two steps. The first one is addition of molecular oxygen to the lipid carbon-centered radical $L^{\bullet}$ to generate a lipid peroxyl radical $LOO^{\bullet}$. The peroxyl radicals $LOO^{\bullet}$ next propagate the chain reaction by abstracting a hydrogen atom from activated C-H bonds in bis-allylic position in the polyunsaturated fatty acids (PUFA) of lipid membranes. Since the reaction of $L^{\bullet}$ with oxygen to form $LOO^{\bullet}$ is close to diffusion controlled, with a reaction rate constant larger than 1 x 10^8 $M^{-1}s^{-1}$, the rate determining step will be the H-atom abstraction (Scheme 1.3.).[47,54] Under steady state conditions the values for $[LOO^{\bullet}]$ and $[L^{\bullet}]$ can be determined solving the following differential equations

$$\frac{d[LOO^{\bullet}]}{dt} = 0 = R_i + k_{perox}[L^{\bullet}][O_2] - k_p[LOO^{\bullet}][LH] - 2k_t[LOO^{\bullet}]^2 \qquad (3)$$

$$\frac{d[L^{\bullet}]}{dt} = 0 = k_p[LOO^{\bullet}][LH] - k_{perox}[L^{\bullet}][O_2] \qquad (4)$$

Algebraic rearrangement of equation (4), followed by its substitution into (3), gives equation (5)

$$\frac{d[LOO^{\bullet}]}{dt} = 0 = R_i - 2k_t[LOO^{\bullet}]^2 \qquad (5)$$

After integration of equation (5), the values for $[LOO^{\bullet}]$ at steady state can be obtained

$$[LOO^{\bullet}] = \left(\frac{R_i}{2k_t}\right)^{1/2} \qquad (6)$$

The consumption of oxygen during oxidation of lipids will follow the rate law shown in equation (7)

$$-\frac{d[O_2]}{dt} = k_p[LOO^{\bullet}][LH] \quad (7)$$

Substituting for the reactive intermediate, [LOO$^{\bullet}$], from equation (6), the general expression for oxygen uptake is

$$-\frac{d[O_2]}{dt} = \frac{k_p}{(2k_t)^{1/2}}[LH]R_i^{1/2} \quad (8)$$

From this relationship the susceptibility of a substrate to undergo oxidation, known as oxidizability, can be quantified by rearranging the equation into

$$Oxidizability = \frac{k_p}{(2k_t)^{1/2}} = \frac{-d[O_2]/dt}{[LH]\times R_i^{1/2}} \quad (9)$$

For a successful chain reaction to occur the rate of propagation reactions must be much greater than the rate of termination reactions such that many cycles of the propagation sequence are completed for each radical initiation and termination reaction. The efficiency of the chain reaction is measured by the number of oxygen molecules consumed per radical initiated, which is the chain length ν and is expressed by equation (10)

$$\nu = \left(\frac{d[O_2]}{dt} \Big/ R_i\right) = \frac{k_p}{(2k_tR_i)^{1/2}}[LH] \quad (10)$$

1.2.2.3. Products of Lipid Peroxidation

The products deriving from the free radical mediated lipid peroxidation have been studied extensively, most notably by Porter and his colleagues.[46,47] All of the peroxidation products are highly reactive and exhibit their own set of damaging effects discussed in the Section 1.2.1.

The addition of oxygen to lipid carbon-centered radicals is a reversible process. This determines the products observed in the chain oxidation and can be well illustrated by the product distribution in the linoleate oxidation (Scheme 1.6.).

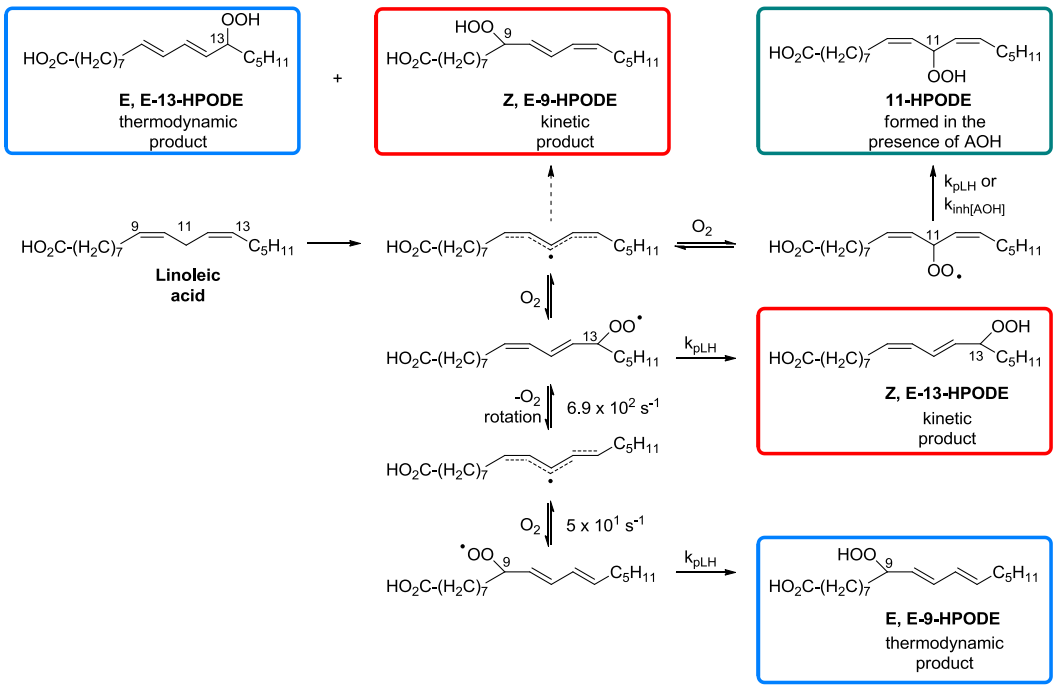

Scheme 1.6. Mechanism of linoleate oxidation. Hydroperoxy-octadecadienoates (HPODE's) are formed following addition of oxygen to pentadienyl radical intermediates (C-9, C-11, C-13 positions).[47]

In linoleate the carbon-centered radical is delocalized between five carbons with electron spin distributed on the two terminal and one central carbon of the diene. Oxygen addition could occur at any of these three positions (C-9, C-11, and C-13) resulting in the formation of three peroxyl radical products (hydroperoxyoctadecadienoates or HPODE's) under kinetic control. Two of the products are *cis, trans*-conjugated dienes with oxygen substitution at C-9 and C-13 (Z,E-9-HPODE and Z,E-13-HPODE) and one non-conjugated diene with oxygen substitution at C-11 (11-HPODE).[47] Further *cis-trans* isomerisation to form the more thermodynamically stable *trans*-radical, followed by addition of oxygen, will lead to the formation of two more products (E,E-9-HPODE and E,E-13-HPODE). These are the thermodynamically more stable products.[47] Some HPODE's can cyclise to form epoxides or alternatively the molecules can undergo a second peroxidation at a different site of unsaturation. These doubly oxidized lipids can decompose to form α,β-unsaturated 2-nonenals (4-hydroxy- and 4-oxo-2-nonenals, Scheme 1.7.).

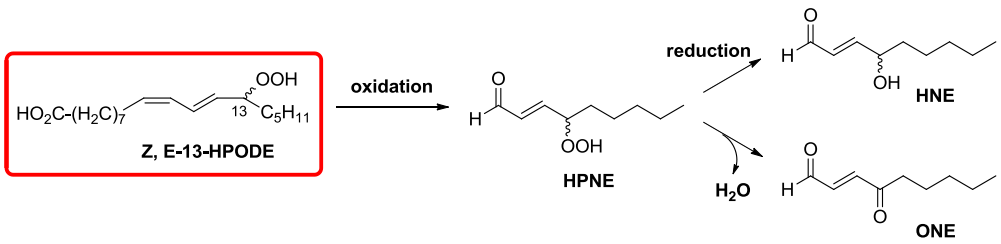

Scheme 1.7. Decomposition of hydroperoxides (HPODE) to α,β-unsaturated aldehydes (4-hydroxy-2-nonenal **HNE** and 4-oxo-2-nonenal **ONE**)[19]

1.2.2.4. Inhibition by Phenols

The protection against oxidative degradation of organic materials, including lipids in living organisms, is provided by specific compounds called antioxidants. They can be divided into two classes, referred to as preventative and chain-breaking antioxidants. The first class reduces the rate of chain initiation, whereas the second interferes with one or more of the propagation steps. Most phenols are chain-breaking antioxidants.[38] Some of the commonly used antioxidants are presented in Figure 1.5.

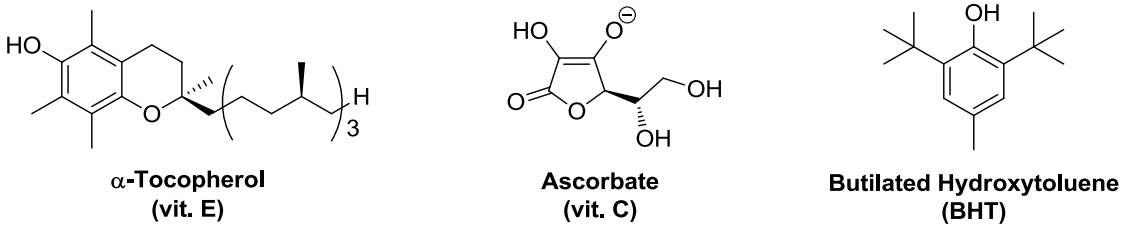

Figure 1.5. Structures of some well-known chain breaking antioxidants.

The main reactions for phenol inhibited oxidation are outlined bellow (Scheme 1.8.)

The chain-carrying peroxyl radicals are scavenged by H-atom abstraction from a phenolic hydroxyl group (Inhibition steps in Scheme 1.8). The resulting phenoxyl radical rapidly recombines with another peroxyl radical to form non-radical adducts, thus breaking the chain oxidation.

Initiation

Initiator $\xrightarrow{}$ $R^{\bullet}$ $\xrightarrow{O_2}$ $ROO^{\bullet}$ Rate = R_g

$ROO^{\bullet}$ + LH $\xrightarrow{k_{i\,LH}}$ ROOH + $L^{\bullet}$ Rate = R_i

Propagation

$L^{\bullet}$ + O_2 $\xrightarrow{k_{perox}}$ $LOO^{\bullet}$ k_{perox}~ 1-10x10^8 $M^{-1}s^{-1}$

$LOO^{\bullet}$ + LH $\xrightarrow{k_p}$ LOOH + $L^{\bullet}$ k_p~ 1x10^1 $M^{-1}s^{-1}$

Inhibition

$LOO^{\bullet}$ + AOH $\xrightarrow{k_{inh}}$ LOOH + $AO^{\bullet}$ k_{inh}~ 3x10^6 $M^{-1}s^{-1}$

$LOO^{\bullet}$ + $AO^{\bullet}$ $\xrightarrow{k_{coup}}$ non-radical products k_{coup}~ 1- 8x10^8 $M^{-1}s^{-1}$

Scheme 1.8. Mechanism of inhibited lipid peroxidation by phenolic antioxidant (AOH). $ROO^{\bullet}$ represents a general peroxyl radical regardless of the source and LH is polyunsaturated fatty acid in lipids. Rate constants are obtained from studies in homogeneous solution using α-tocopherol as an inhibitor (k_{perox}[48], k_p[49], k_{inh}[38], k_{coup}[57]).

In the presence of an efficient antioxidant most peroxyl radicals are scavenged so that a new steady-state approximation applies, where the rate of chain initiation now equals the rate of inhibition by phenols and can be expressed by equation (11)

$$R_i = 2k_i e[RN=NR] = nk_{inh}[AOH][ROO^{\bullet}] \quad (11)$$

Due to the change in the termination of the chain reaction which now is inhibited, the production of $LOO^{\bullet}$ and $L^{\bullet}$ will now be expressed by equations (12) and (13)

$$\frac{d[LOO^{\bullet}]}{dt} = 0 = R_i + k_{perox}[L^{\bullet}][O_2] - k_p[LOO^{\bullet}][LH] - nk_{inh}[LOO^{\bullet}][AOH] \quad (12)$$

$$\frac{d[L^{\bullet}]}{dt} = 0 = k_p[LOO^{\bullet}][LH] - k_{perox}[L^{\bullet}][O_2] \quad (13)$$

After applying the same algebraic rearrangement as for equation (5), the rate of $LOO^{\bullet}$ production can be expressed by equation (14)

$$\frac{d[LOO^{\bullet}]}{dt} = 0 = R_i - nk_{inh}[LOO^{\bullet}][AOH] \quad (14)$$

Subsequent integration leads to equation (15) expressing $[LOO^{\bullet}]$

$$[LOO^{\bullet}] = \left(\frac{R_i}{nk_{inh}[AOH]}\right) \quad (15)$$

Additionally the rate of inhibition by phenols can be expressed by equation (16)

$$-\frac{d[AOH]}{dt} = k_{inh}[LOO^{\bullet}][AOH] \quad (16)$$

Further substitution for [LOO$^{\bullet}$] from equation (15) transforms the equation into equation (17)

$$-\frac{d[AOH]}{dt} = \frac{R_i}{n} \quad (17)$$

This shows that the rate law for consumption of AOH is zero order in antioxidant concentration. Substituting for [LOO$^{\bullet}$] in the equation (7) for the rate-limiting reaction of peroxyl radicals gives the basic expression for antioxidant inhibited oxygen uptake

$$-\frac{d[O_2]}{dt} = \frac{k_p}{k_{inh}}[LH]\frac{R_i}{n[AOH]} \quad (18)$$

The factor *n* is the stoichiometric factor which represents the number of peroxyl radicals trapped by the antioxidant. For a compound to effectively protect against lipid peroxidation in living organisms a molecule of antioxidant (AOH) should be able to protect a much larger amount of lipids [LH]>>[AOH]. Therefore, an efficient radical scavenger should have an inhibition rate constant (k_{inh}) that is several orders of magnitude greater than the propagation rate constant (k_p), or $k_{inh} >> k_p$. The inhibition rate constants for some well-known phenolic antioxidants are in the order of 1 x 10^5 $M^{-1}s^{-1}$ (e.g. α-tocopherol k_{inh} = 32 x 10^5 $M^{-1}s^{-1}$, BHT k_{inh} = 0.14 x 10^5 $M^{-1}s^{-1}$, dihydroduroquinone k_{inh} = 3.9 x 10^5 $M^{-1}s^{-1}$; all k_{inh} are measured in styrene at 30 °C)[33,38], whereas the k_p for the oxidation of linoleate is k_p = 6 x 10^1 $M^{-1}s^{-1}$.[47]

1.2.2.5. Structural Effects on Efficiencies of Antioxidants

The key factors that determine the phenolic antioxidant activity preventing lipid peroxidation are:[58,59]

1) No direct reaction of the phenol with molecular oxygen.

2) Low O-H bond dissociation enthalpy (BDE), which facilitates the H-abstraction reaction between antioxidant and radical.

3) High ionization potential (IP), which decreases the electron-transfer rate between antioxidant and oxygen, and thus, reduces the pro-oxidative potency of the antioxidant.

3) Formation of a stable radical of the antioxidant after the H-abstraction reaction, which decreases the toxicity of the antioxidant.

4) No reaction of the phenoxyl radical ($AO^{\bullet}$) formed with either molecular oxygen or lipids (LH).

5) Solubility that determines mobility of the antioxidant between membranes and lipoproteins.

Substituent effects

The antioxidant properties of phenols result from their ability to inhibit the chain reaction of peroxyl radicals with a substrate, by providing a competing reaction involving hydrogen atom transfer from the phenol hydroxyl group to form lipid hydroperoxides. The rate constant of this reaction depends on the strength of the O-H bond, or the O-H bond dissociation enthalpy (BDE), of phenolic derivatives, so it is important to understand how the strength of the O-H bond is affected by the nature and position of substituents.

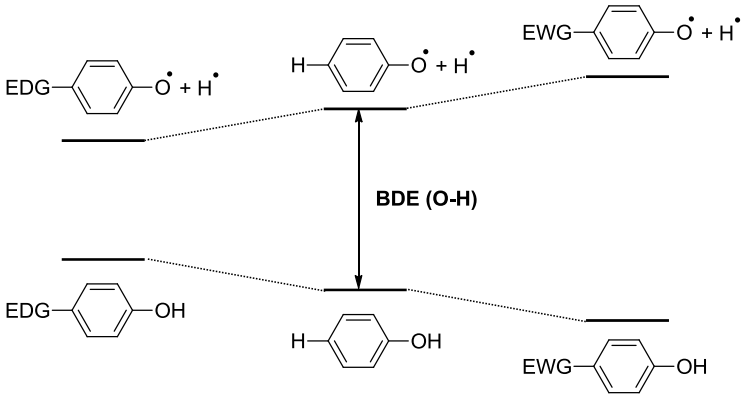

Figure 1.6. Effect of *para*-substituents (EDG and EWG) in phenols on O-H bond dissociation enthalpies (BDE).[60]

The BDE is given by the difference between the energy of the phenoxyl radical (plus the hydrogen atom) and that of the starting phenol (Figure 1.6.). With electron withdrawing substituents (EWG) containing heteroatoms such as CN, NO_2, COR, etc., the *para* interaction is stabilizing in the phenol and

destabilizing in the phenoxyl radical, thus producing an increase of the O-H bond strength. Electron donating groups (EDG) in *para* position, lower the phenolic O-H BDE by destabilizing the phenol (ground-state effect) and/or stabilizing the phenoxyl radical (radical effect). An example of the effect of para-subtituents is the change in BDE for derivatives of 4-X-2,6-di-*tert*-butylphenol shown in Figure 1.7.

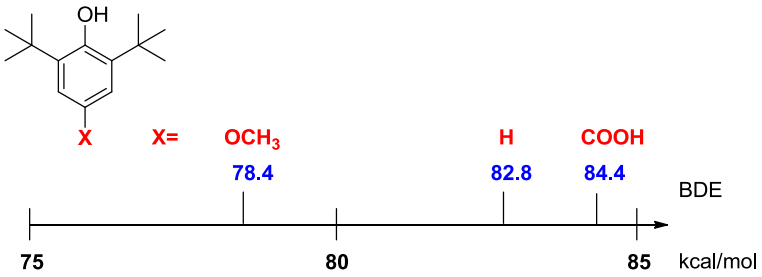

Figure 1.7. Effect of *para*-subtitution in phenols on BDE. BDE values are given for derivatives of 4-X-2,6-di-*tert*-butylphenol.[60]

Alkyl groups stabilize the phenoxyl radical by inductive effect and hyperconjugation. A heteroatom (e.g. in alkoxyl groups) at the *para* position provides additional resonance stabilization of the phenoxyl radical by conjugative electron delocalization.[38]

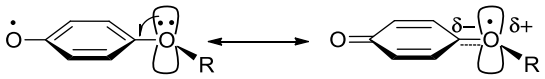

The *ortho* groups increase steric hindrance to reduce side reactions such as pro-oxidation:

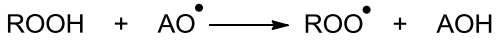

Stereoelectronic Effects

Stereoelectronic effects of *para*-substituents in phenols are important in controlling their antioxidant activity. These effects are concerned with the orientation of the p-type lone pair on the *para*-heteroatom to the phenoxyl radical with respect to the aromatic plane. The extent of overlap between the p-type orbital on X and the semi-occupied molecular orbital (SOMO) in the radical affects the reactivity of *para*-X-substituted phenols.

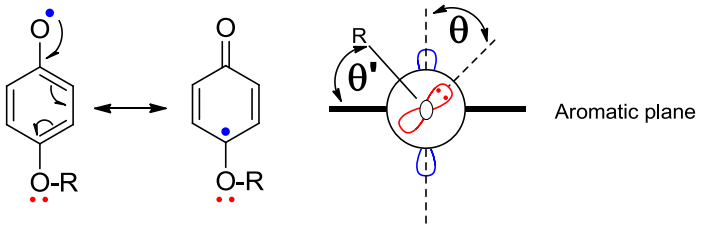

Figure 1.8. Schematic representation of the dihedral angle between the *para*-alkoxyl group and the phenoxyl radical.[33,38]

The extent of the overlap depends on the dihedral angle θ between the p-type orbital on the oxygen atom and a perpendicular to the aromatic plane. This angle should be equal to the dihedral angle θ′, between the O-R bond and the aromatic plane. Stabilization of the phenoxyl radical will be maximized when θ=0° and will be at minimum when the two orbitals are orthogonal, i.e. θ=90°. The rate constant for H-abstraction from the phenol by a peroxyl radical (k_{inh}) increases as θ decreases (Figure 1.8).[33,38]

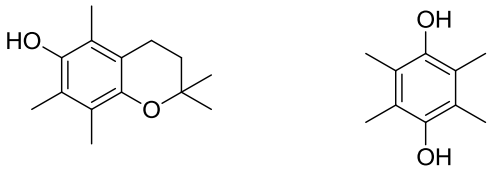

PMHC
θ = 17°
BDE = 78.9 kcal/mol
k_{inh}= 38 x 10^5 $M^{-1}s^{-1}$

HydroQuinone
θ = 89°
BDE = 82.3 kcal/mol
k_{inh}= 3.9 x 10^5 $M^{-1}s^{-1}$

Figure 1.9. Examples of the relationship between dihedral angle, BDE, and k_{inh} for phenolic antioxidants.[33,38]

1.3. Vitamin E

Vitamin E compounds, classified as chromanols, are phenolic antioxidants that are effective inhibitors of lipid peroxidation in biological systems. They are synthesized by plants, while animals and humans acquire tocopherols through their diet. Vitamin E includes two main classes of compounds: tocopherols and tocotrienols. They differ in the degree of unsaturation of the long hydrocarbon chain (phytyl tail) which is necessary for the proper orientation of the molecule in membranes. Each class has four homologues (α, β, γ, and δ forms) differing by the number and site of methyl groups on the chromanol ring (Figure 1.10). The

relative antioxidant activity is determined by the chromanol ring, where the order is α > β > γ > δ. α-Tocopherol (α-TOH) is the most active naturally occurring lipid soluble antioxidant, due to its chemical reactivity towards reactive oxygen and nitrogen species at physiological concentration.[38] α-TOH has a beneficial effect on chronic diseases with oxidative stress components such as cardiovascular and neurodegenerative diseases (Alzheimer's disease),[61,62] artherosclerosis, and cancer, and most recently promoting plasma membrane repair.[63] α-TOH has also attracted attention due to its nonantioxidant functions, in particular its emerging role as a cellular signaling molecule, including modulation of the activity of protein kinase C and phosphatidylinositol 3-kinase,[64] as well as regulation of a number of genes.

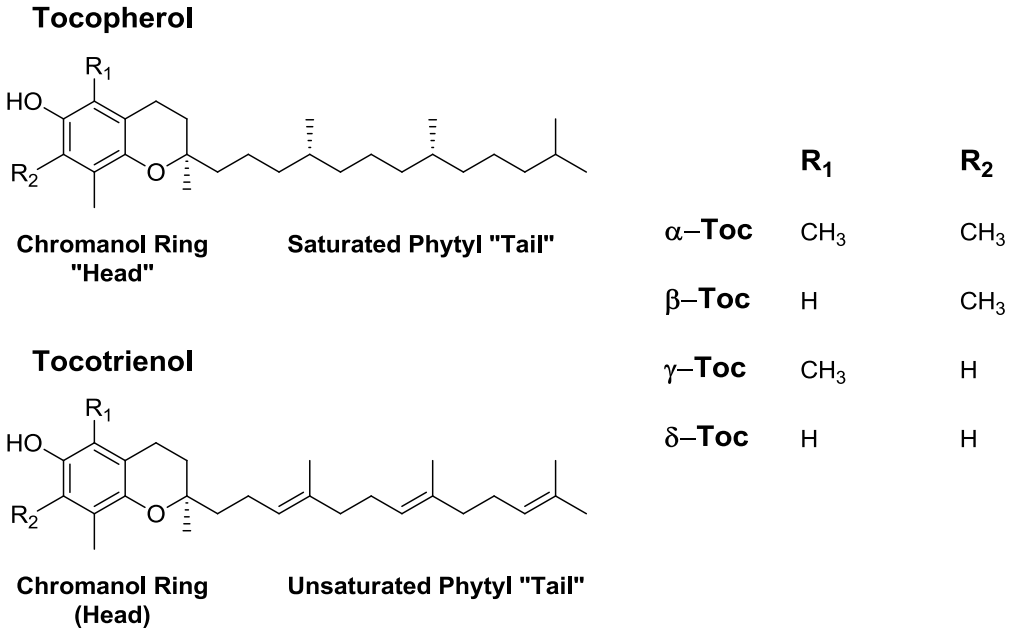

Figure 1.10. Structures of Tocopherol and Tocotrienol conpounds.

1.3.1. Inhibition of Lipid peroxidation in Homogeneous Solutions

The mechanism of inhibition of oxidation by α-TOH and its analogues in homogeneous solutions was proposed by Ingold and coworkers.[28,31,38,65,66] α-TOH is a phenolic chain-breaking antioxidant that prevents the propagation of free radical reactions by scavenging two peroxyl radicals at a time.

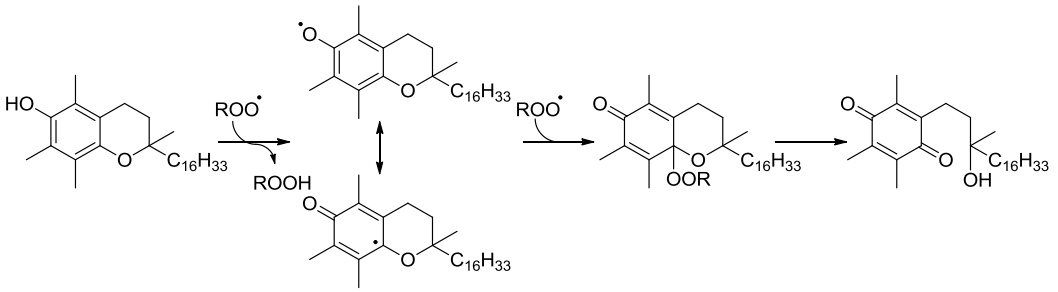

Scheme 1.9. Reaction of α-TOH with peroxyl radicals.

The rapid hydrogen transfer to peroxyl radicals in organic solvents is controlled by structural and stereoelectronic effects discussed above. In biological systems the inherent chemical reactivity of α-TOH is modulated by the heterogeneity of the environment. Factors such as localization, concentration, and mobility in the microenvironment contribute to the relative rate of radical scavenging.

1.3.2. Vitamin E in Heterogeneous Systems (Lipid Membranes)

The antioxidant activity of α-TOH *in vivo* depends both on its localization and on its intrinsic chemical reactivity.[49] The main factors determining the radical scavenging activity of α-TOH in the lipid bilayer are 1) the position and orientation of the chromanol head group relative to the phospholipids, 2) the dynamics of the antioxidant mobility in membranes, and 3) the partitioning of α-TOH in regions enriched with a specific type of lipids (lipid domains).

1.3.2.1. Localization

Studies done by Barclay and Ingold in bilayers and micelles show the ability of α-TOH to access both peroxidizing unsaturated lipids within membranes, as well as aqueous reductants like ascorbic acid.[38,41] This comes to show that α-TOH does not sit in a static position in lipid membranes, but can move within the bilayer. A series of three models were proposed by Fukuzawa for the positioning of the antioxidant in lipid membranes which could account for its hydrophilic and lipophilic reactivity (Figure 1.11.).[67] In model A the phenol hydroxyl group is positioned at the water/lipid interface, accessible for reaction with ascorbic acid.

In model B, the chromanol may be hydrogen bonded to either phosphate oxygen or acyl-ester oxygen atoms thus sinking slightly in the bilayer. Model C has the chromanol deeply submerged into the bilayer, closer to the unsaturated sites that would generate peroxyl radicals during PUFA oxidation. The three models were investigated by different techniques including fluorescence quenching of membrane resident probes by α-TOH,[68] ^{13}C-NMR,[69] and small-angle X-ray diffraction of brominated δ-TOH.[70] These studies concluded that the average position of α-TOH would be given by an equilibrium between models B and C. Recent work by Katsaras and co-workers on neutron diffraction of deuterium–labeled tocopherol places the hydroxyl group of the chromanol ring at the same depth as the phospholipid glycerol backbone ester. They also concluded that tocopherol stands in an upright position with the phytyl chain extending to the center of the bilayer.[71,72]

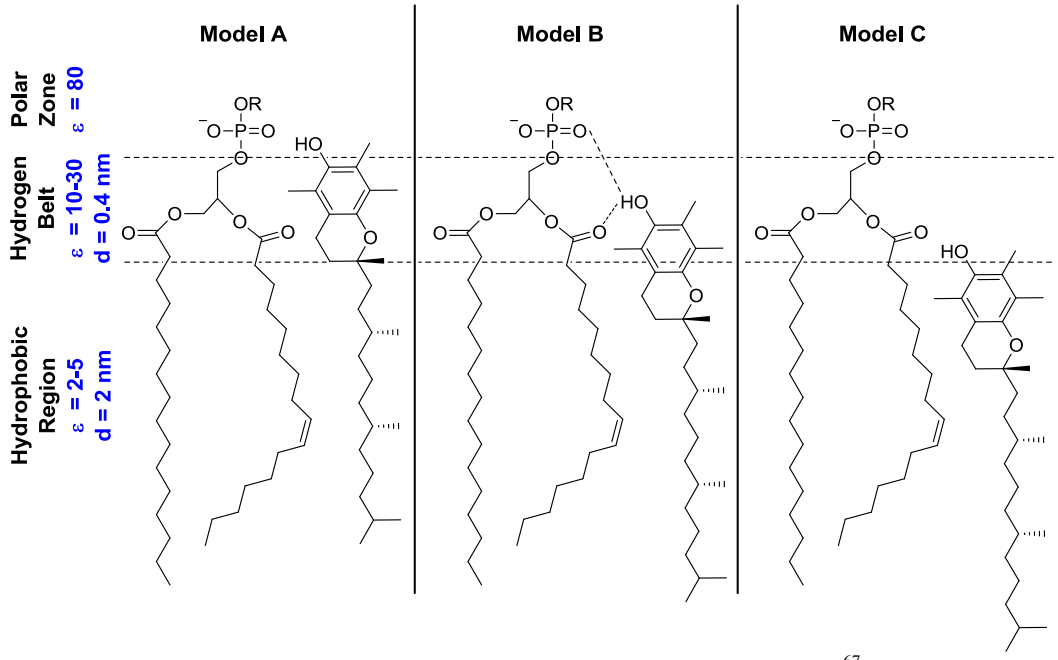

Figure 1.11. Proposed modes of localization of α-TOH in lipid membranes.[67] Palmitoyl oleoyl phosphatidylcholine (POPC) is a representative membrane phospholipid.

1.3.2.2. Mobility

The mobility of α-TOH within the lipid bilayer is a factor that affects its antioxidant activity. The phytyl side chain of α-TOH determines its dominant partitioning in the membrane over water but it also reduces its mobility and

radical scavenging efficiency. The apparent antioxidant activity of α-TOH (k_{inh}/k_p) has been found to be 100 times smaller in membranes compared to homogeneous solutions.[49] A significant effect of the side chain has been observed for intermembrane mobility by Niki and Noguchi. Comparison between the antioxidant activity of α-TOH and an analogue with one carbon side chain 2,2,5,7,8-pentamethyl-6-hydroxychroman (PMHC) in homogeneous and heterogeneous media demonstrates this effect. While no difference in activity is observed in solution, in liposomal membranes PMHC shows much more pronounced radical scavenging ability.[49]

1.3.2.3. Association of α-TOH with Specific Lipids

Association of α-TOH with unsaturated fatty lipids has been observed in model membranes. Urano and co-workers have shown that the chromanol methyl groups fit well into the Z-double bonds of PUFA. Their flexible side chains also provide suitable environment for α-TOH's phytyl chain. Spontaneous intermembrane transfer of α-TOH is favoured when the donor membrane is PUFA rich. This shows that unsaturated lipids serve to concentrate α-TOH but not to hold it indefinitely.[73-75]

1.3.3. Tocopherol Mediated Peroxidation (TMP)

Tocopherol-mediated peroxidation (TMP), where α-TOH acts as both a *pro*-oxidant and an antioxidant, has been suggested as a new mechanism describing the molecular action of the vitamin in oxidizing low-density lipoproteins (LDL). LDLs are small ca. 20 nm particles containing a [LH]/[α-TOH] ratio of ca. 150 to 300 and would not be expected to peroxidize in a chain reaction if there are TOH molecules present. However, lipid peroxidation occurs and is attributed to the reaction of tocopherol radicals ($TO^{\bullet}$) with LH[76]

$$TO^{\bullet} + LH \longrightarrow TOH + L^{\bullet}$$

This reaction is very slow (k_{TMP}=0.1 $M^{-1}s^{-1}$) but it occurs because the lipophilic tocopherol radical ($TO^{\bullet}$) is isolated within the LDL particle in which it is formed

and is only destroyed when that LDL particle encounters and reacts with a second ROO$^{\bullet}$ from the aqueous phase.[77]

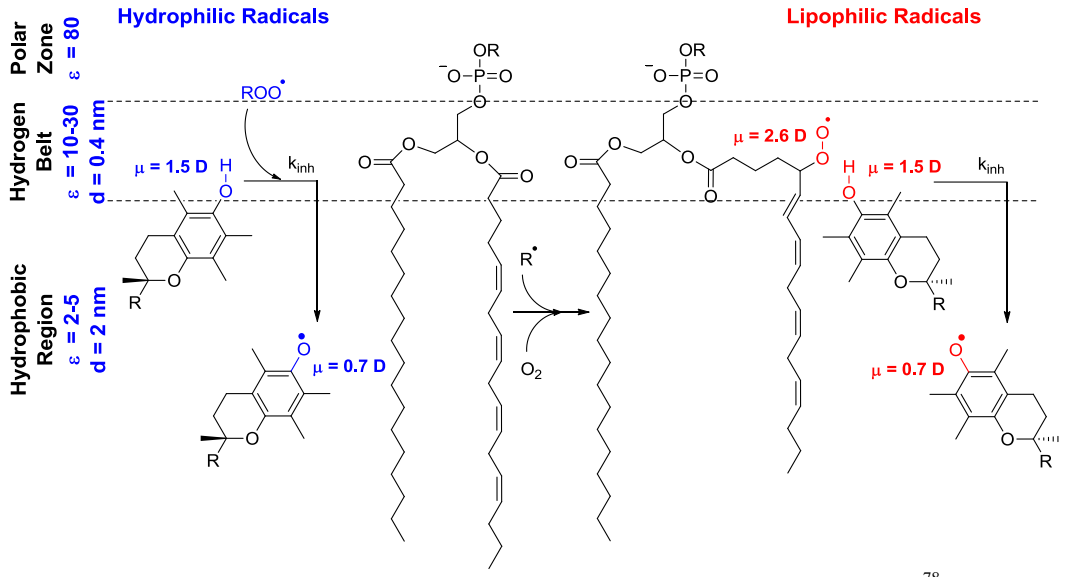

Figure 1.12. Proposed mechanism for tocopherol mediated lipid peroxidation (TMP).[78]

A model developed by Stocker explains the TMP in LDL taking into account some physical properties of the reactants involved.[78]

1) The reactive hydroxyl group of the chromanol ring sits in the so called "hydrogen belt" which is at the water-lipid interface (Figure 1.12). This conclusion is based on the static dielectric constant of this region (ε=10-30) and the polarity of the TO-H bond (μ=1.5 D). 2) Following hydrogen abstraction by a peroxyl radial ROO$^{\bullet}$ the newly formed TO$^{\bullet}$ has different polarity (μ=0.7 D). 3) Given its lower polarity TO$^{\bullet}$ sinks deeper in the LDL particle where it can undergo reaction with LH and form L$^{\bullet}$ and subsequently LOO$^{\bullet}$. 4) The lipid peroxyl radical LOO$^{\bullet}$ is very polar (μ=2.6 D) and tends to "float" on the surface of the LDL where it can react with another TOH molecule. The compartmentalization of TO$^{\bullet}$ in the small volume of the LDL particle results in increase of its effective concentration, thus increasing the rate of reaction with LH. This model explains why particles without a lipid core will not undergo TMP whereas particles with a lipid core will undergo TMP.[35]

1.4. Experimental Methods for Studying Lipid Peroxidation

Various techniques are available to measure the antioxidant effectiveness in relation to lipid peroxidation. We may cite monitoring the suppression of oxygen uptake during oxidation of a substrate, or product studies over time facilitated by HPLC. More detailed information of the absolute rate constants of hydrogen abstraction from phenolic antioxidants by free radicals can be obtained by laser flash photolysis studies (LFP). Studies with these techniques have yielded valuable information on the mechanistic aspect of lipid peroxidation and provide means to monitor real-time the production and/ or consumption of free radicals.

Product studies and oxygen uptake however require large amounts of sample. Additionally, the sample cannot be recovered. These limitations prevent the use of these techniques in live cell studies. What is required in biologically relevant studies is a non-invasive technique that may readily report on the oxidative status of the cell. Fluorescence imaging overcomes some of these limitations. It is a useful technique for studying chemical and biological processes *in vivo*. Fluorescence-based techniques enable highly sensitive, non-invasive, and safe detection of ROS.

1.4.1. Fluorescence Techniques

Over the past decade a variety of fluorescence-based assays involving the use of fluorogenic probes have been developed. Fluorescent probes are compounds which upon reaction with an analyte experience a change in fluorescence intensity. Such probes are widely used to monitor various different chemical species in live cell studies. The assays rely on built in molecular switches that turn either on or off the emission of a fluorescent dye. The molecular switches may in turn rely on a number of photophysical and photochemical phenomena including:[79]

1) Photoinduced electron Transfer (PeT)
2) Förster Resonance Energy Transfer (FRET)
3) Intramolecular Charge Transfer (ICT)
4) Spirocyclization Mechanism

Rational approach for the design of fluorescent probes is of critical importance, since it can determine their sensitivity and specificity towards a target of interest. In the following sections we will center our discussion to the development of fluorescent probes to detect ROS in a highly sensitive and specific manner.

1.5. Fluorescence

1.5.1. Photoexcited State, Jablonski Diagram, and Fluorescence

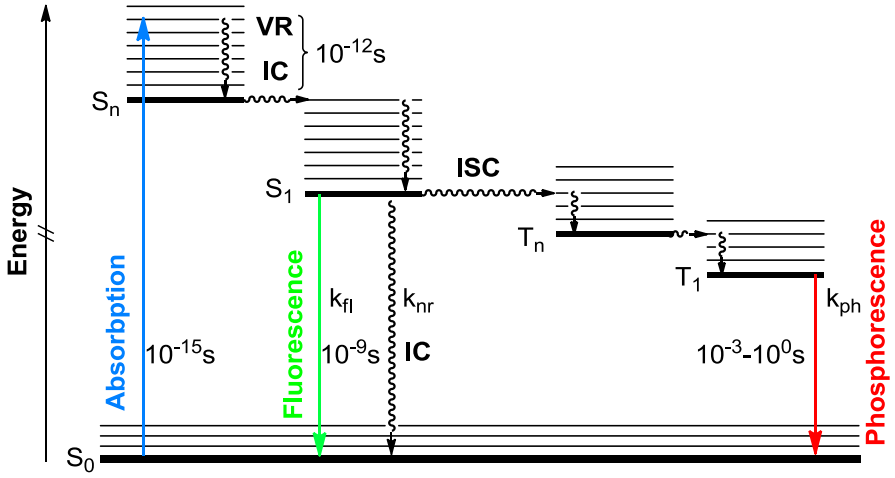

Figure 1.13. Jablonski diagram,[80] where VR is vibrational relaxation, IC is internal conversion, and ISC is intersystem crossing.

The first process that occurs is the absorption of energy (light), which excites an electron from the singlet ground state (S_0) to one of the vibrational levels of a higher singlet electronic state (S_n). Absorbance is a very fast transition in the order of 10^{-15} s. Once an electron is excited there are multiple ways for the energy to be dissipated. The first is through vibrational relaxation (between vibrational levels of the same electronic state), followed by internal conversion (between electronic states S_n to S_1 or S_1 to S_0). These non-radiative processes are very fast, with characteristic lifetimes ranging from 10^{-14} to 10^{-11} s. Another way energy in S_1 is dissipated is by emission of a photon and return to the ground state (S_0). This process is called fluorescence. Fluorescence may extend from femtoseconds to nanoseconds. Molecules that can undergo fluorescence are called fluorophores. An alternative pathway a molecule may take is intersystem crossing. This is a transition between an excited singlet state (S_1) to an excited

triplet state (T_n). In many fluorophores triplet vibrational energy levels overlap with the lowest energy level in S_1, thus favouring intersystem crossing. In this process the electron changes spin multiplicity by undergoing reversal in spin so that the former pair of electrons is now parallel. From a quantum theory prospective, this is a forbidden transition. Emission of a photon from the first triplet state (T_1) to the singlet ground state (S_0) is possible, albeit formally forbidden. This process is called phosphorescence. Phosphorescence is much slower than fluorescence with characteristic lifetimes ranging from 10^{-3} to 10^{0} s.

1.5.2. Fluorescence Quenching

Fluorescence quenching refers to any process that decreases the fluorescence intensity of a fluorophore. There are two main quenching mechanisms, dynamic and static quenching. Dynamic quenching requires the diffusion and encounter of the fluorophore in the excited state with a quencher. Static quenching on the other hand requires ground-state complex formation or chemical tethering of quencher and fluorophore so no diffusion is required.

1.5.3. Fluorescence Quantum Yield and Fluorescence Lifetime

The most important parameters related to fluorescence are the fluorescence spectrum, fluorescence quantum yield, fluorescence lifetime, and fluorescence polarization.

The emission spectrum is given by the energy gap between S_1 and S_0.

The quantum yield (Φ) is the ratio of the number of emitted to the number of absorbed photons. It can also be represented in terms of rates of transitions (equation 19)

$$\Phi = \frac{k_r}{k_r + \sum k_{nr}} \tag{19}$$

$$\sum k_{nr} = k_{IC} + k_{ISC} \tag{20}$$

where k_r is the rate constant of radiative decay and Σk_{nr} is the sum of the rate constants of all non-radiative deactivation pathways. The quantum yield will be close to unity the smaller the rate of the non-radiative decay or the larger k_r is.

The lifetime of an excited state is the average time a molecule spends in the excited state before it disappears via emission of a photon (fluorescence), IC, ISC, or any other physical or chemical process, including chemical reactions in the excited state:

Radiative decay pathway

$$M^{1*} \xrightarrow{k_r} M + h\upsilon$$

Non-radiative decay pathways

$$M^{1*} \xrightarrow{k_{IC}} M + \Delta$$

$$M^{1*} \xrightarrow{k_{ISC}} M^{3*}$$

$$M^{1*} + Q \xrightarrow{k_q[Q]} M - Q \text{ or } M + Q^{1*} etc.$$

where Q is a quencher molecule.

The decay rate constant of the singlet excited state (k_{dec}) is expressed by equation (21)

$$k_{dec} = k_r + \sum k_{nr} + k_q[Q] \tag{21}$$

The rate equation for [M^*] can be written as

$$\frac{\delta[M^*]}{\delta t} = -k_{dec}[M^*], \tag{22}$$

or after integration with respect to initial conditions

$$[M^*] = [M^*]_0 e^{-k_{dec} \times t} \tag{23}$$

The population of excited molecules generated immediately after excitation, t=0, starts decreasing exponentially with time as both radiative and non-radiative transitions to the ground state take place. The intensity decays exponentially with time

$$I_t = I_0 e^{-t \times k_{dec}}, \tag{24}$$

where I_0 and I_t are the initial fluorescence intensity and intensity at time t=t, respectively. The decay lifetime or average lifetime in the excited state can be defined as

$$\tau = \frac{1}{k_{dec}} = \frac{1}{k_r + \sum k_{nr} + k_q[Q]} \tag{25}$$

The ratios of the fluorescence intensities in the absence (I_0) and in the presence of a quencher (I) can be expressed as a ratio of the decay rates

$$\frac{I_0}{I} = \frac{k_r + \sum k_{nr} + k_q[Q]}{k_r + \sum k_{nr}} = 1 + \frac{k_q}{k_r + \sum k_{nr}}[Q] \quad (26)$$

or as the Stern-Volmer equation

$$\frac{I_0}{I} = 1 + k_q \tau_o [Q] = 1 + K_{sv}[Q] \quad (27)$$

where τ_o is the fluorescent lifetime in the absence of quencher and K_{sv} is the Stern-Volmer quenching constant. K_{sv} and k_q can be obtained experimentally as the slope from a plot of I_0 / I versus [Q].

There are numerous applications of fluorescence quenching both in chemistry and biology. Quenching measurements can reveal changes in the accessibility of a fluorophore to a quencher due to micro-environmental changes such as protein binding, localization of a molecule in membranes, or effects of conformational changes.

1.5.4. Photoinduced Electron Transfer

One of the mechanisms of fluorescence quenching is photoinduced electron transfer (PeT). This is a process in which an electron is transferred from an electron donor (D) to an electron acceptor (A). This results in the formation of a charge separated state which consists of the corresponding radical cation and anion. Prior to the electron transfer one of the species is excited with light. The excited species can be either the donor or the acceptor (Figure 1.14). Whether the excited species serves as a donor or acceptor will be determined by the electronic characteristics and energies of the HOMO and LUMO of both molecules participating in the electron transfer.

The process may occur only if it is energetically favoured ($\Delta G_{eT}<0$). In case A (Figure 1.14) the excited molecule is the acceptor because the half filled HOMO of A^* lies lower in energy than the HOMO of the donor (ground state molecule). In case B (Figure 1.14) electron transfer occurs between the half filled LUMO of the excited molecule (D^*) which donates an electron to the lower lying

LUMO of the ground state molecule (A). In both case A and B the process is downhill energetically therefore it is considered plausible.[81]

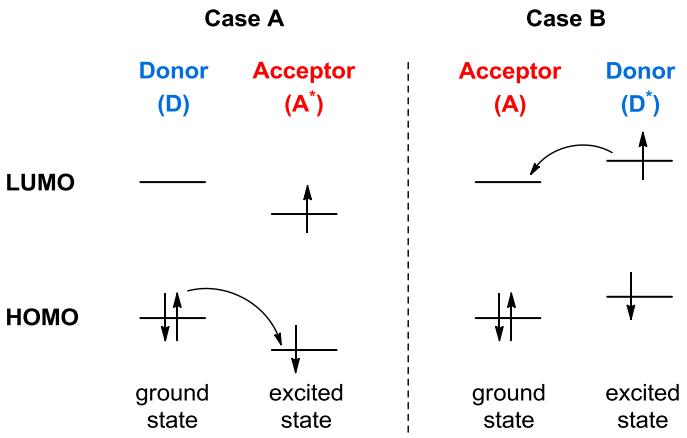

Figure 1.14. Photoindiced electron transfer (PeT)

The direction of the electron transfer is determined by the redox potentials of the ground and excited states intervening. PeT can be explained in terms of energy change due to electron transfer using basic principles of electrochemistry. Excited states of diamagnetic molecules with closed shell ground states are always better oxidizing and reducing agents than their corresponding ground states.[81] This can be visualized in Figure 1.15.

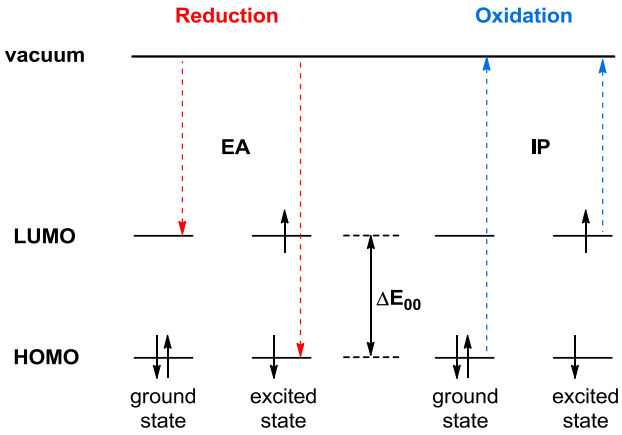

Figure 1.15. Reduction and oxidation processes and the corresponding electron affinities (EA) and ionization potentials (IP) of ground state and excited state molecules.[81]

The energy released from the acceptor upon electron binding (electron affinity, EA) is larger for the excited state, whereas the energy required to remove an electron completely from the donor (ionization potential, IP) is lower for the

excited state. In gas phase, the free energy change for excited state electron transfer for the following process

$$D + A^* \longrightarrow D^{+\bullet} + A^{-\bullet}$$

will be given by equation (28)

$$\Delta G^o_{eT} = (IP)_D - (EA)_A - \Delta E_{00} \qquad (28)$$

ΔE_{00} is the excitation energy, which provides the energy to drive charge separation.

In solution, the solvation of the charged species produced by electron transfer significantly changes the values of ΔG_{eT} compared to gas phase. A correction term is necessary to account for this change. Thus, the energy change for PeT is given by the Rehm-Weller equation:

$$\Delta G^o_{eT} = \left[\left(E^o_{D^{+\bullet}/D} - E^o_{A/A^{-\bullet}}\right) - \Delta E_{00} + \varpi\right] \qquad (29)$$

The value $E°_{D+^{\bullet}/D}$ is the potential required for reducing $D^{+\bullet}$ to D and $E°_{A/A-^{\bullet}}$ is the potential required for reducing A to $A^{-\bullet}$. ΔE_{00} is the energy of the S_0 to S_1 transition of the fluorophore, which can be either D or A. The term ϖ is the Coulombic correction term which takes into consideration the Coulombic energy gain from bringing two particles of opposite charge together. It is given by

$$\varpi = -N_A \frac{e^2}{4\pi\varepsilon_0 \varepsilon r} \qquad (30)$$

or

$$\varpi = -\frac{331.5}{\varepsilon \times r} kcal/mol \qquad \text{when r is in Å} \qquad (31)$$

N_A is the Avogadro's constant (6.02×10^{23} mol^{-1}), e is the charge of the electron (1.60×10^{-19} C), ε_0 is the permittivity of vacuum (8.85×10^{-12} $C^2N^{-1}m^{-1}$), ε is the dielectric constant of the solvent, and *r* is the distance between the two charges. For an electron transfer process the two charges have to be separated. From equations (29) and (30) we can appreciate that the final contribution of the Coulombic term to ΔG_{eT} will decrease as the separation between the charged species increases and as the dielectric constant of the solvent increases. Thus, it will have very small contribution to the overall energy change of PeT for polar

solvents. For example for complete separation of one electron charge in acetonitrile with ε = 37.5 the Coulombic term is ϖ = - 0.064 eV for r = 6 Å.[82] In contrast the term may become sufficiently large in non-polar solvents to favour ionic association, rather than dissociation.[80] The value of ΔG_{eT} (free energy for electron transfer) can be calculated from the electrochemical oxidation potential of the donor, the reduction potential of the acceptor, and excited state energy data according to equation (32)[81]

$$\Delta G_{eT} = E^{ox}_{1/2}(D) - E^{red}_{1/2}(A) - E_{exc}(A) + \Delta E_{Coulombic} \qquad (32)$$

The rate constant for quenching via electron transfer k_{eT} can be experimentally determined using the Stern-Volmer analysis or calculated using activation free energy for electron transfer $\Delta G^{\ddagger}_{eT}$.

According to Marcus theory electron transfer is accompanied by solvent reorganization. This positive energy (λ) corresponds to the total internal and external reorganization energy required for an electron transfer to occur.[81] Thus the activation energy ($\Delta G^{\ddagger}_{eT}$) of electron transfer is expressed in terms of both the free energy of the reaction (ΔG^{0}_{eT}) and the reorganization energy (λ)

$$\Delta G^{\neq}_{eT} = \frac{\left(\Delta G^{0}_{eT} + \lambda\right)^2}{4\lambda} \qquad (33)$$

The rate constant for electron transfer is then expressed by equation (34)

$$k_{eT} = \nu_N \kappa \exp\left(\frac{\Delta G^{\neq}_{eT}}{RT}\right) \qquad (34)$$

where the term ν_N is an electronic factor and κ is the transition coefficient. Equation (34) provides the theoretical link between the experimental rate constant k_{eT}, the activation energy $\Delta G^{\ddagger}_{eT}$, the reaction exothermicity ΔG^{0}_{eT}, and the reorganization energy λ.

1.6. Fluorescent Probes

Fluorescent probes based on small organic molecules are promising tools for revealing the biological role of biomolecules. Their use allows for gathering information on localization and quantity of the molecules of interest. Fluorescent

probes in conjunction with fluorescence microscopy can provide high level of sensitivity and specificity combined with temporal and spatial information in live cell studies.

The development of fluorescent probes was pioneered in the 80's by the group of Tsien with experimental studies on Ca^{2+}-dependent signal transduction in cells using fluorescent indicators.[83,84] Since then the field has expanded and now many fluorescent probes are available for sensing variety of ions such as Cu^{+}, K^{+}, F^{-},[85-87] toxic species such as Cd^{2+}, Hg^{2+},[88-90] or highly reactive chemicals such as ROS and RNS.[91-97]

In order to achieve successful imaging the probes should be properly designed to activate only in the presence of the biomolecule of interest. This activation can cause increase or decrease in the fluorescence of the probe, thus separating them into two main classes namely off/on (fluorogenic probes) and on/off switches. Disadvantage of the on/off type of probes is that many events can cause decrease in fluorescence such as photobleaching of the fluorophore, changes in the microenvironment that can affect quantum yield and fluorescence lifetime, intermolecular quenching with molecules other then the molecule of interest, etc. A false positive is thus highly plausible when working with on/off probes. Fluorogenic probes based on off/on switches eliminate these problems, as not many processes can lead to an increase in the fluorescence. As discussed earlier there are several mechanisms that could be applied for the development of off/on fluorogenic probes.

Fluorescent signalling via the PeT strategy is widely used in the design of off/on probes. Typically these probes consist of two segments, a receptor and a covalently linked reporter (fluorophore). The receptor moiety is designed to specifically interact with the analyte thus determining the specificity of the probe. The fluorophore is the site of both excitation and emission, shaping its role as a reporter of changes in the molecule and affecting the sensitivity of the probe.[98] Electron transfer to deactivate the photoinduced excited state can successfully compete with the radiative relaxation of the excited electron to the ground state (fluorescence). This renders the molecule non-fluorescent (k_{eT}, which is part of

the Σk_{nr}, outcompetes k_r in equation 19). Upon chemical reaction of the receptor the PeT is deactivated and fluorescence is restored. Since PeT is dependent on the oxidation potential of the donor and the reduction potential of the acceptor, almost any receptor of a given analyte can be converted into a fluorogenic probe by labeling it with a fluorophore with a suitable redox potential. The choice of fluorophore is not purely based on the electrochemistry but also on factors such as high extinction coefficient and quantum yield, emission in the visible range to avoid autofluorescence from aromatic aminoacids in cells, large Stoke's shift, and sufficient photostability.

1.6.1. Fluorogenic Probes for Detection of ROS

In the last decade remarkable progress has been made in the development of fluorogenic probes capable of detecting ROS. These probes have been widely used to monitor oxidative stress and evaluate antioxidant activities. One of the commonly used fluorescence sensors for detecting ROS and more specifically hydrogen peroxide in live cells is dichlorodihydrofluorescein (DCFH). In its reduced form it is non-emissive and upon oxidation by H_2O_2 it becomes highly fluorescent (Scheme.1.10).[99]

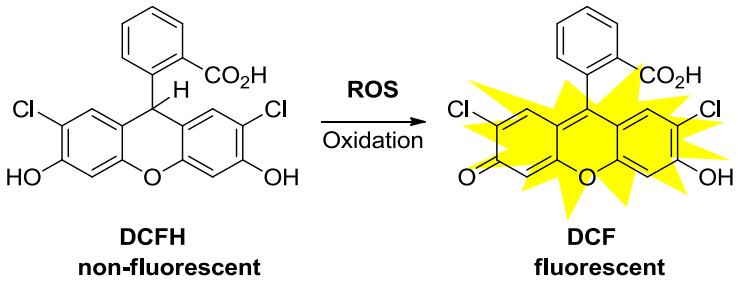

Scheme.1.10. Traditional pre-fluorescent probe 2',7'-dichlorodihydro-fluorescein (DCFH) for detection of ROS generation. Upon oxidation it converts into the highly fluorescent 2',7'-dichlorofluorescein (DCF).[99]

The DFCH probe and all the subsequent derivatives developed from it have serious drawbacks. They are not strictly specific towards ROS due to their non-specific reactions with oxidants. Their ability to undergo autoxidation upon light irradiation also produces large background fluorescence in the absence of ROS. Although these probes are not applicable to selective ROS detection they are still

suitable for detection of oxidative activity in cells.[100] However, there is a high demand for novel probes with high selectivity for individual ROS. This arises from the need to elucidate the ROS unique physiological activity in relation not only to oxidative stress but also to cell signalling. Main contributions to the development of ROS specific fluorogenic probes come from the groups of Chang and Nagano, amongst others (Figure 1.16.).

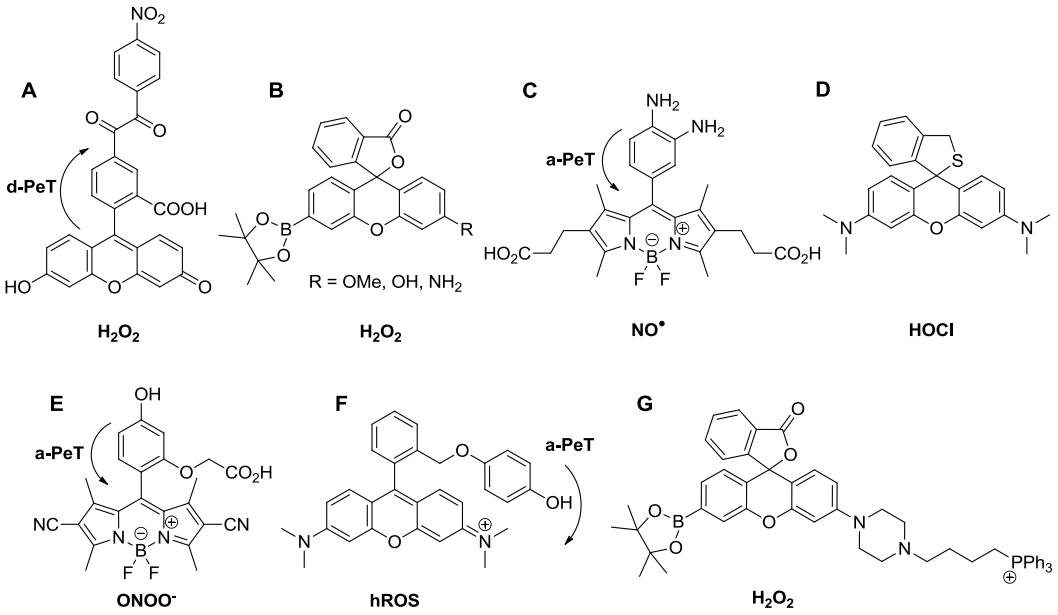

Figure 1.16. Fluorogenic probes for sensing ROS: **A)** hydrogen peroxide (H_2O_2);[101] **B)** hydrogen peroxide (H_2O_2);[92] **C)** nitric oxide (NO•);[93] **D)** hypochloric acid (HOCl);[95] **E)** peroxynitrite ($ONOO^-$);[97] **F)** mitochondria targeting probe for highly reactive ROS (e.g.OH•);[102] **G)** mitochondria targeting probe for hydrogen peroxide (H_2O_2);[103]

Chang and coworkers prepared a family of fluorogenic probes with varying emission colours for selective imaging of H_2O_2 signaling in living cells.[92] The probes are based on boronate caged fluorescein or rhodamine fluorophores (Figure 1.16 B). Deprotection of the boronate by H_2O_2 leads to an increase in fluorescence. The emission enhancements reported are from 10 to 40 fold for the different fluorophores used. Although the boronate-caged probes can detect low concentrations of endogenous H_2O_2 (5 μM) their reaction rates are relatively slow. They are also reported to show some fluorescence response to nitric oxide in addition to H_2O_2.[104]

An improved design of H_2O_2-specific fluorogenic probe was reported by Nagano utilizing the PeT strategy (Figure 1.16 A).[101] The probe relies on the

specific reactivity between benzil and H_2O_2 to form benzoic anhydride which upon hydrolysis gives benzoic acid. The fluorescence is quenched through donor-excited photoinduced electron transfer process (d-PeT). Upon reaction with H_2O_2 the probe is converted to carboxyfluorescein which is highly fluorescent. This fluorogenic probe has a similar detection limit and rate of reaction with H_2O_2 as the boronate-caged probes. However it shows a much better emission enhancement as high as 150 fold. Additionally, it exhibits a unique selectivity for H_2O_2 among ROS such as nitric oxide, superoxide, hydroxyl radicals, hypochlorite, and singlet oxygen.

1.6.2. Fluorogenic Probes for Specific Organelle Targeting

The complex biology of ROS is dictated by the chemical properties of each type of oxygen metabolite, their production sites, and further trafficking of the ROS themselves and the products of their reactions at cellular level.[5] This provides a motivation for developing tools to study the chemistry and biology of ROS in specific organelles in the cell. Fluorescence imaging with fluorogenic probes that can target specific organelles emerges as a valuable method for site-specific imaging of the different types of ROS exploring their complex contributions to physiological processes in living organisms.

For a molecule to target an organelle it must first cross the cellular membrane, which possesses a complex structure that prohibits access to intracellular compartments. Additionally, all organelles are separated from the cytosol by lipid membranes that might differ in lipid composition but have no distinguishing features that can afford directing molecules in a specific manner. The unique nature of mitochondria distinguishes it from all the other organelles, making it an attractive target for the development of organelle specific fluorogenic probes. The presence of ion channel pumps and oxidation pathways in the inner mitochondrial membrane leads to a strong negative potential of -180 mV maintained through the membrane. One way to selectively target mitochondria is thus to take advantage of this electrochemical potential.

A few strategies have emerged as viable approaches to target mitochondria. These involve the use of proteins, short cationic peptide sequences, as well as lipophilic cationic compounds.[105,106] Commercially available mitochondria-targeting lipophilic cations are the MitoTracker series of fluorophores (Figure 1.17). They are analogues of rhodamine and cyanine dyes with a cationic functionality and otherwise nonpolar frameworks. Additionally, triphenylphosphonium (TTP) salts are commonly used mitochondrial targeting agents that traverse the mitochondrial membrane by using the negative potential gradient as an electrostatic driving force.[106,107] TTP accumulates several hundred-fold within the mitochondria relative to the cytosol.[105,108]

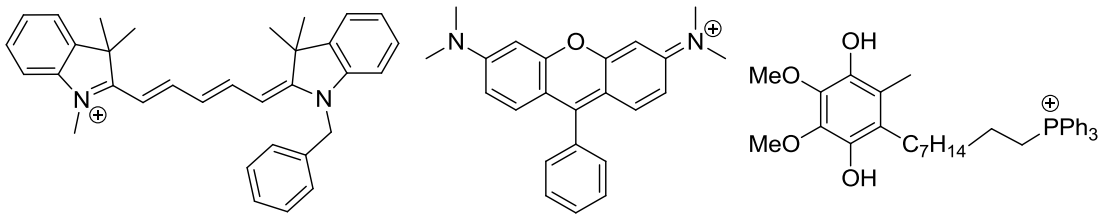

Figure.1.17 Structures of mitochondria-targeting molecules: MitoTracker® dyes (commercially available) and Mito Q.[107]

Lipophilic cationic compounds have been applied for the development of fluorogenic probes for imaging ROS directly in their generation site, the mitochondria. The most noticeable examples come from the groups of Nagano and Chang. Nagano and coworkers developed a fluorogenic probe for detection of highly reactive ROS like $OH^{\bullet}$, $ONOO^{-}$, and OCl^{-} in mitochondria. It relies on PeT between a quinol moiety and a rhodamine dye (Figure 1.16. F). Upon reaction with hROS the quinol is oxidized to quinone and cleaved from the molecule thus restoring the fluorescence. The rhodamine dye assures the accumulation of the probe in mitochondria by virtue of its positive charge.

The group of Chang applied the H_2O_2-sensitive fluorogenic probes they had previously developed based on boronate deprotection to monitor ROS in the cell mitochondria by tagging the probe with TTP through an alkyl linker (Figure 1.16 G).

1.6.3. Fluorescent Probes for Detection of Lipid Peroxidation and Antioxidant Activity

As discussed earlier the main site of ROS production are the electron transport chains located in the mitochondrial membrane. Lipids are a major target for ROS leading to amplification of the ROS through formation of peroxyl radicals in an autoxidation chain reaction. Additionally, the release of reactive aldehydes as products of lipid peroxidation can affect many cellular functions.

To date a significant body of work has been dedicated to the development and application of fluorogenic probes enabling monitoring of ROS and the correlation of their concentration and sites of production to important physiological processes. Most of the fluorogenic probes for sensing ROS however are water soluble preventing their use in the hydrophobic media of lipid membranes. Further, the available lipophilic fluorescent probes are not based on quenched emission being restored upon chemical reaction with lipid peroxyl radical (off/on) but rater on the emission quenching (on/off).

The first fluorescent probe used in lipid peroxidation assays and in the evaluation of antioxidants was developed by Hudson and co-workers in the 70's.[109] They used the naturally occurring polyunsaturated fatty acid *cis*-parinaric acid. The oxidation of the probe is accompanied by decreased fluorescence and absorption due to break in the conjugation of the double bonds, thus serving as an on/off fluorescent probe for lipid peroxidation. There are several problems associated with the use of parinaric acid as a fluorescent probe. It absorbs in the UV region thus limiting its use in cell studies. It is extremely air sensitive, photolabile, and undergoes photodimerization resulting in loss of fluorescence.[110] The probes developed from thereon rely on the same oxidation mechanism, but have increased photostability and emit in the visible range. The lipid peroxidation sensors commercially available Bodipy® 665/676,[111] as well as its analogue C11-Bodipy 581/591,[112] have a similar design to that of *cis*-parinaric acid. Both probes are distinguished by their highly conjugated structure and red shifted emission. Upon oxidation by alkoxyl and peroxyl radicals the conjugation is broken and the emission is shifted to lowed wavelengths. Such probes are called

ratiometric since they depend on the ratio of emission at two different wavelengths.

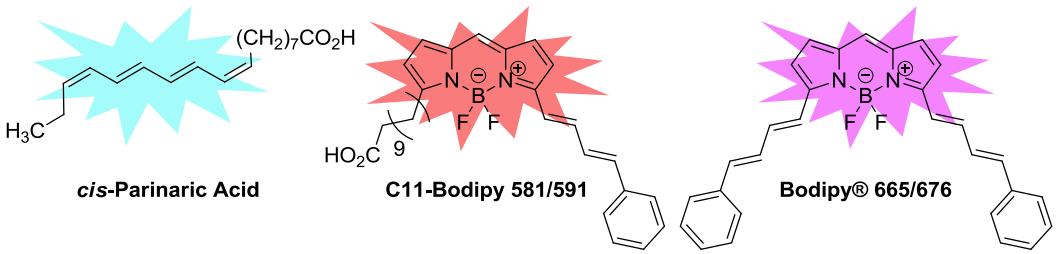

Figure 1.18. Fluorescent probes mimicking the structure of polyunsaturated fatty acids for lipid peroxidation studies.[109,111,112]

The above mentioned probes may be utilized in developing fluorimetric assays for measuring peroxyl radical scavenging activities of lipophilic antioxidants (e.g. α-tocopherol). However they are all on/off probes and suffer from the general limitations of this class of compounds.

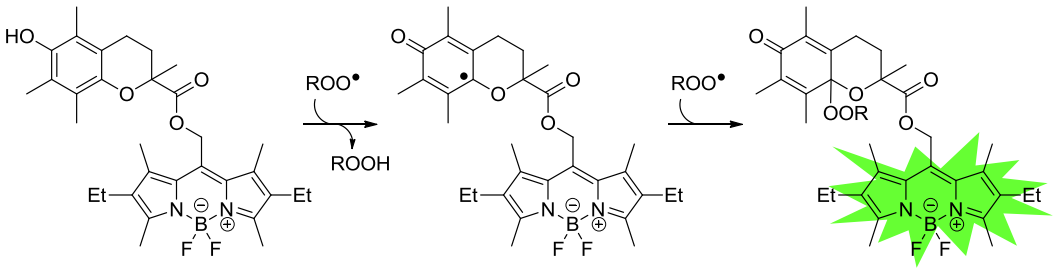

Scheme 1.11. Reaction of BTOH with peroxyl radicals.

Recently in our lab a novel lipophilic fluorogenic ROS sensor, B-TOH, was developed.[113] The probe is designed as a fluorogenic antioxidant mimicking the structure and activity of α-tocopherol. B-TOH is a two segment receptor-reporter type probe that relies on an intramolecular PeT off/on switching mechanism (Scheme 1.11). The receptor in the probe consists of a chromanol moiety with an activity similar to α-tocopherol. This segment contributes to the free radical scavenging activity of the probe and determines the selectivity towards lipid peroxyl radicals. The reporter segment serves the purpose of detecting, via emission enhancement, structural changes at the receptor end which result from the reaction with radicals. The lipophilic Bodipy fluorophore used as a reporter ensures partitioning in the lipid membrane and determines the sensitivity (off/on

ratio) of the probe. Upon ROS oxidation of the chromanol ring the PeT is deactivated and fluorescence is restored. Up to 10-fold emission enhancement is observed following reaction with peroxyl and alkoxyl radicals in homogeneous solutions.

1.7. Research Goals

The free radical mediated oxidation of biological molecules and the formation of toxic by-products have been the subject of extensive studies in relation to oxidative damage leading to numerous disorders. The recent discovery of the involvement of free radicals in signaling pathways has sparked a renovated interest in the chemistry and biology of ROS. However, the methods available to study these processes in cells and in vivo are generally destructive and with limited sensitivity. Advances in fluorescence microscopy now allow for the development of non-invasive tools that provide high sensitivity combined with spatial and temporal resolution for imaging live cell systems under oxidative stress.

Previously in our lab a fluorogenic sensor, B-TOH, was prepared which is capable of reporting via emission enhancement on the depletion of peroxyl radical scavengers and the onset of the lipid chain autoxidation in homogeneous solutions. Expanding on this work, the initial goals of my work were two pronged: i) Investigate the molecular mechanism operating in B-TOH off-on switching. This, we anticipated, would allow us to delineate the criteria to be considered in optimizing phenol-based lipophilic fluorogenic antioxidant sensors. ii) To explore the potential of the fluorogenic antioxidant as an imaging tool in living cells.

Building on these two initial premises, this thesis provides insights on improving the sensitivity and reactivity of the first generation fluorogenic lipophilic ROS sensor B-TOH, and on further optimizing the probes to confer organelle targeting. The following 5 chapters discuss our efforts towards achieving these goals.

The molecular level of understanding gained in Chapter 2 on the mechanism accounting for B-TOH intramolecular emission quenching and subsequent emission enhancement upon reaction with free radicals provides us with a base for the development of fluorogenic sensors.

In Chapter 3 we demonstrate the scope and limitations for the potential application of B-TOH as a novel sensor suitable for peroxyl radical detection in cells both under physiological and pathological conditions.

Based on these results, we show in Chapter 4 that in order to change the sensitivity of the probes we need to tune the electrochemical properties of the reporter molecule (Bodipy fluorophore) for an exergonic PeT from the receptor moiety (chromanol ring) to occur. The redox potentials of the Bodipy fluorophores are largely affected by the electron donating or withdrawing properties of the substituents at positions C2 and C6 of the Bodipy core (Et, H, Cl, or CN). Creating such library of Bodipy fluorophores provides us with a platform for labeling a broad spectrum of molecules for studies of biological systems.

Further, in Chapter 5 we determine that utilizing different linkers between the receptor and reporter moieties allows for modulating the free radical scavenging activity of the fluorogenic probes. We additionally explore the newly developed fluorogenic ROS sensors with improved reactivity and sensitivity as tools for investigating the effects of lipid membrane composition on the ROS scavenging activity of antioxidants.

Chemical modifications to the fluorogenic antioxidants discussed in Chapter 6 also enable targeting of specific organelles (e.g. mitochondria), thus advancing the development of new methods for visualizing localized production of ROS in living cells. Ultimately such a tool will enable us in the future to better understand the vital links between the chemistry and the biology of ROS.

1.8. References

1. Halliwell, B. & Gutteridge, J.M.C. Free Radicals in Biology and Medicine. *4th ed; Oxford University Press: Oxford* **2007**.
2. Finkel, T., Serrano, M. & Blasco, M.A. The common biology of cancer and ageing. *Nature* 448, 767-774, **2007**.
3. D'Autreaux, B. & Toledano, M.B. ROS as signalling molecules: mechanisms that generate specificity in ROS homeostasis. *Nat Rev Mol Cell Biol* 8, 813-824, **2007**.
4. Finkel, T. & Holbrook, N.J. Oxidants, oxidative stress and the biology of ageing. *Nature* 408, 239-247, **2000**.
5. Dickinson, B.C. & Chang, C.J. Chemistry and biology of reactive oxygen species in signaling or stress responses. *Nat Chem Biol* 7, 504-511, **2011**.
6. Dröge, W. Free Radicals in the Physiological Control of Cell Function. *Physiological Reviews* 82, 47-95, **2002**.
7. Winterbourn, C.C. Reconciling the chemistry and biology of reactive oxygen species. *Nat Chem Biol* 4, 278-286, **2008**.
8. Barnham, K.J., Masters, C.L. & Bush, A.I. Neurodegenerative diseases and oxidative stress. *Nat Rev Drug Discov* 3, 205-214, **2004**.
9. Lesser, M.P. Oxidative stress in marine environments: Biochemistry and physiological ecology. in *Annual Review of Physiology*, Vol. 68 253-278 (Annual Reviews, Palo Alto, 2006).
10. Chatgilialoglu, C. & Ferreri, C. Trans Lipids: The Free Radical Path. *Accounts of Chemical Research* 38, 441-448, **2005**.
11. Imlay, J.A. Pathways of Oxidative Damage. *Annual Review of Microbiology* 57, 395-418, **2003**.
12. Apel, K. & Hirt, H. Reactive oxygen species: Metabolism, oxidative stress, and signal transduction. *Annual Review of Plant Biology* 55, 373-399, **2004**.
13. Rhee, S.G. H2O2, a Necessary Evil for Cell Signaling. *Science* 312, 1882-1883, **2006**.
14. Kagan, V.E. & Quinn, P.J. Toward oxidative lipidomics of cell signaling. *Antioxidants & redox signaling* 6, 199-202, **2004**.
15. Nathan, C. Specificity of a third kind: reactive oxygen and nitrogen intermediates in cell signaling. *The Journal of Clinical Investigation* 111, 769-778, **2003**.
16. Pryor, W.A. Oxy-Radicals and Related Species: Their Formation, Lifetimes, and Reactions. *Annual Review of Physiology* 48, 657-667, **1986**.
17. Stone, J.R. & Yang, S. Hydrogen Peroxide: A Signaling Messenger. *Antioxidants & Redox Signaling* 8, 243-270, **2006**.
18. Chatgilialoglu, C., Ferreri, C., Ballestri, M., Mulazzani, Q.G. & Landi, L. cis−trans Isomerization of Monounsaturated Fatty Acid Residues in Phospholipids by Thiyl Radicals. *Journal of the American Chemical Society* 122, 4593-4601, **2000**.
19. West, J.D. & Marnett, L.J. Endogenous Reactive Intermediates as Modulators of Cell Signaling and Cell Death. *Chemical Research in Toxicology* 19, 173-194, **2006**.
20. Uchida, K., Shiraishi, M., Naito, Y., Torii, Y., Nakamura, Y. & Osawa, T. Activation of Stress Signaling Pathways by the End Product of Lipid Peroxidation. *Journal of Biological Chemistry* 274, 2234-2242, **1999**.
21. Poli, G., Biasi, F. & Leonarduzzi, G. 4-Hydroxynonenal–protein adducts: A reliable biomarker of lipid oxidation in liver diseases. *Molecular Aspects of Medicine* 29, 67-71, **2008**.
22. Wu, R.P., Hayashi, T., Cottam, H.B., Jin, G., Yao, S., Wu, C.C.N., Rosenbach, M.D., Corr, M., Schwab, R.B. & Carson, D.A. Nrf2 responses and the therapeutic selectivity of electrophilic compounds in chronic lymphocytic leukemia. *Proceedings of the National Academy of Sciences* 107, 7479-7484, **2010**.
23. Simonian, N.A. & Coyle, J.T. Oxidative Stress in Neurodegenerative Diseases. *Annual Review of Pharmacology and Toxicology* 36, 83-106, **1996**.
24. Koji, U. 4-Hydroxy-2-nonenal: a product and mediator of oxidative stress. *Progress in Lipid Research* 42, 318-343, **2003**.

25. Etsuo, N. Lipid peroxidation: Physiological levels and dual biological effects. *Free Radical Biology and Medicine* 47, 469-484, **2009**.
26. Poli, G., Schaur, R.J., Siems, W.G. & Leonarduzzi, G. 4-Hydroxynonenal: A membrane lipid oxidation product of medicinal interest. *Medicinal Research Reviews* 28, 569-631, **2008**.
27. Noguchi, N. Role of Oxidative Stress in Adaptive Responses in Special Reference to Atherogenesis. *Journal of Clinical Biochemistry and Nutrition* 43, 131-138, **2008**.
28. Ingold, K.U. Inhibition of the Autoxidation of Organic Substances in the Liquid Phase. *Chemical Reviews* 61, 563-589, **1961**.
29. Ingold, K.U. *Spec. Publ.-Chem. Soc.*, 285-293, **1971**.
30. Ingold, K.U. Rate constants for radical reactions in solution. *J.K. Kochi (Ed.), Free Radicals (3rd edn.), Wiley-Interscience, New York* Vol. 1., 37–112, **1973**.
31. Burton, G.W. & Ingold, K.U. Autoxidation of biological molecules. 1. Antioxidant activity of vitamin E and related chain-breaking phenolic antioxidants in vitro. *Journal of the American Chemical Society* 103, 6472-6477, **1981**.
32. Barclay, L.R.C. & Ingold, K.U. Autoxidation of biological molecules. 2. Autoxidation of a model membrane. Comparison of the autoxidation of egg lecithin phosphatidylcholine in water and in chlorobenzene. *Journal of the American Chemical Society* 103, 6478-6485, **1981**.
33. Burton, G.W., Doba, T., Gabe, E., Hughes, L., Lee, F.L., Prasad, L. & Ingold, K.U. Autoxidation of biological molecules. 4. Maximizing the antioxidant activity of phenols. *Journal of the American Chemical Society* 107, 7053-7065, **1985**.
34. Barclay, L.R.C., Locke, S.J., MacNeil, J.M., VanKessel, J., Burton, G.W. & Ingold, K.U. Autoxidation of micelles and model membranes. Quantitative kinetic measurements can be made by using either water-soluble or lipid-soluble initiators with water-soluble or lipid-soluble chain-breaking antioxidants. *Journal of the American Chemical Society* 106, 2479-2481, **1984**.
35. Alessi, M., Paul, T., Scaiano, J.C. & Ingold, K.U. The Contrasting Kinetics of Peroxidation of Vitamin E-Containing Phospholipid Unilamellar Vesicles and Human Low-Density Lipoprotein1. *Journal of the American Chemical Society* 124, 6957-6965, **2002**.
36. Litwinienko, G. & Ingold, K.U. Solvent Effects on the Rates and Mechanisms of Reaction of Phenols with Free Radicals. *Accounts of Chemical Research* 40, 222-230, **2007**.
37. Bowry, V.W. & Ingold, K.U. The Unexpected Role of Vitamin E (α-Tocopherol) in the Peroxidation of Human Low-Density Lipoprotein1. *Accounts of Chemical Research* 32, 27-34, **1998**.
38. Burton, G.W. & Ingold, K.U. Vitamin E: application of the principles of physical organic chemistry to the exploration of its structure and function. *Accounts of Chemical Research* 19, 194-201, **1986**.
39. Barclay, L.R.C. 1992 Syntex Award Lecture Model biomembranes: quantitative studies of peroxidation, antioxidant action, partitioning, and oxidative stress. *Canadian Journal of Chemistry* 71, 1-16, **1993**.
40. Barclay, L.R.C., Baskin, K.A., Dakin, K.A., Locke, S.J. & Vinqvist, M.R. The antioxidant activities of phenolic antioxidants in free radical peroxidation of phospholipid membranes. *Canadian Journal of Chemistry* 68, 2258-2269, **1990**.
41. Barclay, L.R.C., Locke, S.J. & MacNeil, J.M. Autoxidation in micelles. Synergism of vitamin C with lipid-soluble vitamin E and water-soluble Trolox. *Canadian Journal of Chemistry* 63, 366-374, **1985**.
42. Barclay, L.R.C., Baskin, K.A., Kong, D. & Locke, S.J. Autoxidation of model membranes. The kinetics and mechanism of autoxidation of mixed phospholipid bilayers. *Canadian Journal of Chemistry* 65, 2541-2550, **1987**.
43. Barclay, L.R.C., Vinqvist, M.R., Mukai, K., Itoh, S. & Morimoto, H. Chain-breaking phenolic antioxidants: steric and electronic effects in polyalkylchromanols, tocopherol analogs, hydroquinones, and superior antioxidants of the polyalkylbenzochromanol and naphthofuran class. *The Journal of Organic Chemistry* 58, 7416-7420, **1993**.

44. Barclay, L.R.C., Edwards, C.E. & Vinqvist, M.R. Media Effects on Antioxidant Activities of Phenols and Catechols. *Journal of the American Chemical Society* 121, 6226-6231, **1999**.
45. Barclay, L.R.C. & Vinqvist, M.R. Membrane peroxidation: Inhibiting effects of water-soluble antioxidants on phospholipids of different charge types. *Free Radical Biology and Medicine* 16, 779-788, **1994**.
46. Porter, N.A., Weber, B.A., Weenen, H. & Khan, J.A. Autoxidation of polyunsaturated lipids. Factors controlling the stereochemistry of product hydroperoxides. *Journal of the American Chemical Society* 102, 5597-5601, **1980**.
47. Yin, H., Xu, L. & Porter, N.A. Free Radical Lipid Peroxidation: Mechanisms and Analysis. *Chemical Reviews* 111, 5944-5972, **2011**.
48. Hasegawa, K. & Patterson, L.K. PULSE RADIOLYSIS STUDIES IN MODEL LIPID SYSTEMS: FORMATION AND BEHAVIOR OF PEROXY RADICALS IN FATTY ACIDS. *Photochemistry and Photobiology* 28, 817-823, **1978**.
49. Niki, E. & Noguchi, N. Dynamics of Antioxidant Action of Vitamin E. *Accounts of Chemical Research* 37, 45-51, **2003**.
50. Bedard, L., Young, M.J., Hall, D., Paul, T. & Ingold, K.U. Quantitative Studies on the Peroxidation of Human Low-Density Lipoprotein Initiated by Superoxide and by Charged and Neutral Alkylperoxyl Radicals1. *Journal of the American Chemical Society* 123, 12439-12448, **2001**.
51. Noguchi, N., Yamashita, H., Gotoh, N., Yamamoto, Y., Numano, R. & Niki, E. 2,2′-Azobis (4-Methoxy-2,4-Dimethylvaleronitrile), a New Lipid-Soluble Azo Initiator: Application to Oxidations of Lipids and Low-Density Lipoprotein in Solution and in Aqueous Dispersions. *Free Radical Biology and Medicine* 24, 259-268, **1998**.
52. Culbertson, S.M. & Porter, N.A. Unsymmetrical Azo Initiators Increase Efficiency of Radical Generation in Aqueous Dispersions, Liposomal Membranes, and Lipoproteins. *Journal of the American Chemical Society* 122, 4032-4038, **2000**.
53. Maillard, B., Ingold, K.U. & Scaiano, J.C. Rate constants for the reactions of free radicals with oxygen in solution. *Journal of the American Chemical Society* 105, 5095-5099, **1983**.
54. Barclay, L.R.C. & Vinqvist, M.R. Phenols as Antioxidants. in *The Chemistry of Phenols* 839-908 (John Wiley & Sons, Ltd, 2003).
55. http://www.wako-chem.co.jp/specialty/waterazo/index.htm.
56. Blanksby, S.J. & Ellison, G.B. Bond Dissociation Energies of Organic Molecules. *Accounts of Chemical Research* 36, 255-263, **2003**.
57. Jonsson, M., Lind, J., Reitberger, T., Eriksen, T.E. & Merenyi, G. Free radical combination reactions involving phenoxyl radicals. *The Journal of Physical Chemistry* 97, 8229-8233, **1993**.
58. Zhang, H.-Y., Sun, Y.-M. & Wang, X.-L. Substituent Effects on O□H Bond Dissociation Enthalpies and Ionization Potentials of Catechols: A DFT Study and Its Implications in the Rational Design of Phenolic Antioxidants and Elucidation of Structure–Activity Relationships for Flavonoid Antioxidants. *Chemistry – A European Journal* 9, 502-508, **2003**.
59. Mulder, P., Korth, H.-G. & Ingold, K.U. Why Quantum-Thermochemical Calculations Must Be Used with Caution to Indicate 'a Promising Lead Antioxidant'. *Helvetica Chimica Acta* 88, 370-374, **2005**.
60. Brigati, G., Lucarini, M., Mugnaini, V. & Pedulli, G.F. Determination of the Substituent Effect on the O−H Bond Dissociation Enthalpies of Phenolic Antioxidants by the EPR Radical Equilibration Technique. *The Journal of Organic Chemistry* 67, 4828-4832, **2002**.
61. Singh, U., Devaraj, S. & Jialal, I. VITAMIN E, OXIDATIVE STRESS, AND INFLAMMATION. *Annual Review of Nutrition* 25, 151-174, **2005**.
62. Sano, M., Ernesto, C., Thomas, R.G., Klauber, M.R., Schafer, K., Grundman, M., Woodbury, P., Growdon, J., Cotman, C.W., Pfeiffer, E., Schneider, L.S. & Thal, L.J. A Controlled Trial of Selegiline, Alpha-Tocopherol, or Both as Treatment for Alzheimer's Disease. *New England Journal of Medicine* 336, 1216-1222, **1997**.

63. Howard, A.C., McNeil, A.K. & McNeil, P.L. Promotion of plasma membrane repair by vitamin E. *Nat Commun* 2, 597, **2011**.
64. Boscoboinik, D., Szewczyk, A., Hensey, C. & Azzi, A. Inhibition of cell proliferation by alpha-tocopherol. Role of protein kinase C. *Journal of Biological Chemistry* 266, 6188-6194, **1991**.
65. Bowry, V.W. & Ingold, K.U. Extraordinary Kinetic Behavior of the a-Tocopheroxyl (Vitamin E) Radical. *Journal of Organic Chemistry* 60, 5456-67, **1995**.
66. Valgimigli, L., Ingold, K.U. & Lusztyk, J. Antioxidant Activities of Vitamin E Analogues in Water and a Kamlet−Taft β-Value for Water1. *Journal of the American Chemical Society* 118, 3545-3549, **1996**.
67. Fukuzawa, K. Dynamics of Lipid Peroxidation and Antioxidion of α-Tocopherol in Membranes. *Journal of Nutritional Science and Vitaminology* 54, 273-285, **2008**.
68. Kagan, V.E. & Quinn, P.J. The interaction of α-tocopherol and homologues with shorter hydrocarbon chains with phospholipid bilayer dispersions. *European Journal of Biochemistry* 171, 661-667, **1988**.
69. Perly, B., Smith, I.C.P., Hughes, L., Burton, G.W. & Ingold, K.U. Estimation of the location of natural α-tocopherol in lipid bilayers by 13C-NMR spectroscopy. *Biochimica et Biophysica Acta (BBA) - Biomembranes* 819, 131-135, **1985**.
70. Katsaras, J., Stinson, R.H., Davis, J.H. & Kendall, E.J. Location of two antioxidants in oriented model membranes. Small-angle x-ray diffraction study. *Biophysical journal* 59, 645-653, **1991**.
71. Atkinson, J., Harroun, T., Wassall, S.R., Stillwell, W. & Katsaras, J. The location and behavior of α-tocopherol in membranes. *Molecular Nutrition & Food Research* 54, 641-651, **2010**.
72. Kučerka, N., Marquardt, D., Harroun, T.A., Nieh, M.-P., Wassall, S.R. & Katsaras, J. The Functional Significance of Lipid Diversity: Orientation of Cholesterol in Bilayers Is Determined by Lipid Species. *Journal of the American Chemical Society* 131, 16358-16359, **2009**.
73. Atkinson, J., Epand, R.F. & Epand, R.M. Tocopherols and tocotrienols in membranes: A critical review. *Free Radical Biology and Medicine* 44, 739-764, **2008**.
74. Urano, S., Shichita, N. & Matsuo, M. Interaction of vitamin E and its model compounds with unsaturated fatty acids in homogeneous solution. *Journal of Nutritional Science and Vitaminology* 34, 189-94, **1988**.
75. Urano, S., Iida, M., Otani, I. & Matsuo, M. Membrane stabilization of vitamin E; interactions of α-tocopherol with phospholipids in bilayer liposomes. *Biochemical and Biophysical Research Communications* 146, 1413-1418, **1987**.
76. Bowry, V.W., Ingold, K.U. & Stocker, R. Vitamin E in human low-density lipoprotein. When and how this antioxidant becomes a pro-oxidant. . *Biochem. J.* , 341-344, **1992**.
77. Ingold, K.U., Bowry, V.W., Stocker, R. & Walling, C. Autoxidation of lipids and antioxidation by alpha-tocopherol and ubiquinol in homogeneous solution and in aqueous dispersions of lipids: unrecognized consequences of lipid particle size as exemplified by oxidation of human low density lipoprotein. *Proceedings of the National Academy of Sciences* 90, 45-49, **1993**.
78. Waldeck, A.R. & Stocker, R. Radical-Initiated Lipid Peroxidation in Low Density Lipoproteins: Insights Obtained from Kinetic Modeling. *Chemical Research in Toxicology* 9, 954-964, **1996**.
79. Nagano, T. Development of fluorescent probes for bioimaging applications. *Proceedings of the Japan Academy, Series B* 86, 837-847, **2010**.
80. Lakowicz, J.R. in *Principles of Fluorescence Spectroscopy* (ed. Lakowicz, J.R.) 1-26 (Springer US, 2006).
81. Turro, N.J., Ramamurthy, V. & Scaiano, J.C. *Principles of Molecular Photochemistry: An Introduction*, 495 (University Science Books, Sausalito, CA, 2009).
82. Tachiya, M. Energetics of electron transfer reactions in polar solvents. *Chemical Physics Letters* 230, 491-494, **1994**.

83. Grynkiewicz, G., Poenie, M. & Tsien, R.Y. A new generation of Ca2+ indicators with greatly improved fluorescence properties. *Journal of Biological Chemistry* 260, 3440-3450, **1985**.
84. Minta, A., Kao, J.P. & Tsien, R.Y. Fluorescent indicators for cytosolic calcium based on rhodamine and fluorescein chromophores. *Journal of Biological Chemistry* 264, 8171-8178, **1989**.
85. Baruah, M., Qin, W., Vallée, R.A.L., Beljonne, D., Rohand, T., Dehaen, W. & Boens, N. A Highly Potassium-Selective Ratiometric Fluorescent Indicator Based on BODIPY Azacrown Ether Excitable with Visible Light. *Organic Letters* 7, 4377-4380, **2005**.
86. Bozdemir, O.A., Sozmen, F., Buyukcakir, O., Guliyev, R., Cakmak, Y. & Akkaya, E.U. Reaction-Based Sensing of Fluoride Ions Using Built-In Triggers for Intramolecular Charge Transfer and Photoinduced Electron Transfer. *Organic Letters* 12, 1400-1403, **2010**.
87. Zeng, L., Miller, E.W., Pralle, A., Isacoff, E.Y. & Chang, C.J. A Selective Turn-On Fluorescent Sensor for Imaging Copper in Living Cells. *Journal of the American Chemical Society* 128, 10-11, **2005**.
88. Peng, X., Du, J., Fan, J., Wang, J., Wu, Y., Zhao, J., Sun, S. & Xu, T. A Selective Fluorescent Sensor for Imaging Cd2+ in Living Cells. *Journal of the American Chemical Society* 129, 1500-1501, **2007**.
89. Wang, J. & Qian, X. A Series of Polyamide Receptor Based PET Fluorescent Sensor Molecules: Positively Cooperative Hg2+ Ion Binding with High Sensitivity. *Organic Letters* 8, 3721-3724, **2006**.
90. Yuan, M., Li, Y., Li, J., Li, C., Liu, X., Lv, J., Xu, J., Liu, H., Wang, S. & Zhu, D. A Colorimetric and Fluorometric Dual-Modal Assay for Mercury Ion by a Molecule. *Organic Letters* 9, 2313-2316, **2007**.
91. Albers, A.E., Okreglak, V.S. & Chang, C.J. A FRET-Based Approach to Ratiometric Fluorescence Detection of Hydrogen Peroxide. *Journal of the American Chemical Society* 128, 9640-9641, **2006**.
92. Dickinson, B.C., Huynh, C. & Chang, C.J. A Palette of Fluorescent Probes with Varying Emission Colors for Imaging Hydrogen Peroxide Signaling in Living Cells. *Journal of the American Chemical Society* 132, 5906-5915, **2010**.
93. Gabe, Y., Urano, Y., Kikuchi, K., Kojima, H. & Nagano, T. Highly Sensitive Fluorescence Probes for Nitric Oxide Based on Boron Dipyrromethene ChromophoreRational Design of Potentially Useful Bioimaging Fluorescence Probe. *Journal of the American Chemical Society* 126, 3357-3367, **2004**.
94. Gomes, A., Fernandes, E. & Lima, J.L.F.C. Fluorescence probes used for detection of reactive oxygen species. *Journal of Biochemical and Biophysical Methods* 65, 45-80, **2005**.
95. Kenmoku, S., Urano, Y., Kojima, H. & Nagano, T. Development of a Highly Specific Rhodamine-Based Fluorescence Probe for Hypochlorous Acid and Its Application to Real-Time Imaging of Phagocytosis. *Journal of the American Chemical Society* 129, 7313-7318, **2007**.
96. Srikun, D., Albers, A.E., Nam, C.I., Iavarone, A.T. & Chang, C.J. Organelle-Targetable Fluorescent Probes for Imaging Hydrogen Peroxide in Living Cells via SNAP-Tag Protein Labeling. *Journal of the American Chemical Society* 132, 4455-4465, **2010**.
97. Ueno, T., Urano, Y., Kojima, H. & Nagano, T. Mechanism-Based Molecular Design of Highly Selective Fluorescence Probes for Nitrative Stress. *Journal of the American Chemical Society* 128, 10640-10641, **2006**.
98. de Silva, A.P., Gunaratne, H.Q.N., Gunnlaugsson, T., Huxley, A.J.M., McCoy, C.P., Rademacher, J.T. & Rice, T.E. Signaling Recognition Events with Fluorescent Sensors and Switches. *Chemical Reviews* 97, 1515-1566, **1997**.
99. Keston, A.S. & Brandt, R. The fluorometric analysis of ultramicro quantities of hydrogen peroxide. *Analytical Biochemistry* 11, 1-5, **1965**.
100. Soh, N. Recent advances in fluorescent probes for the detection of reactive oxygen species. *Analytical and Bioanalytical Chemistry* 386, 532-543, **2006**.

101. Abo, M., Urano, Y., Hanaoka, K., Terai, T., Komatsu, T. & Nagano, T. Development of a Highly Sensitive Fluorescence Probe for Hydrogen Peroxide. *Journal of the American Chemical Society* 133, 10629-10637, **2011**.
102. Koide, Y., Urano, Y., Kenmoku, S., Kojima, H. & Nagano, T. Design and Synthesis of Fluorescent Probes for Selective Detection of Highly Reactive Oxygen Species in Mitochondria of Living Cells. *Journal of the American Chemical Society* 129, 10324-10325, **2007**.
103. Dickinson, B.C. & Chang, C.J. A Targetable Fluorescent Probe for Imaging Hydrogen Peroxide in the Mitochondria of Living Cells. *Journal of the American Chemical Society* 130, 9638-9639, **2008**.
104. Lippert, A.R., Van de Bittner, G.C. & Chang, C.J. Boronate Oxidation as a Bioorthogonal Reaction Approach for Studying the Chemistry of Hydrogen Peroxide in Living Systems. *Accounts of Chemical Research* 44, 793-804, **2011**.
105. Yousif, L.F., Stewart, K.M. & Kelley, S.O. Targeting Mitochondria with Organelle-Specific Compounds: Strategies and Applications. *ChemBioChem* 10, 1939-1950, **2009**.
106. Hoye, A.T.D., Jennifer E.; Wipf, Peter; Fink, Mitchell P.; Kagan, Valerian E. Targeting Mitochondria. *Accounts of Chemical Research* 41, 87-97, **2008**.
107. Murphy, M.P. Development of lipophilic cations as therapies for disorders due to mitochondrial dysfunction. *Expert Opinion on Biological Therapy* 1, 753-764, **2001**.
108. Murphy, M.P. & Smith, R.A.J. Targeting Antioxidants to Mitochondria by Conjugation to Lipophilic Cations. *Annual Review of Pharmacology and Toxicology* 47, 629-656, **2007**.
109. Sklar, L.A., Hudson, B.S. & Simoni, R.D. Conjugated polyene fatty acids as membrane probes: preliminary characterization. *Proceedings of the National Academy of Sciences* 72, 1649-1653, **1975**.
110. Naguib, Y.M.A. A Fluorometric Method for Measurement of Peroxyl Radical Scavenging Activities of Lipophilic Antioxidants. *Analytical Biochemistry* 265, 290-298, **1998**.
111. http://www.invitrogen.com/1/1/5907-bodipy-665-676-lipid-peroxidation-sensor.html.
112. Drummen, G.P.C., van Liebergen, L.C.M., Op den Kamp, J.A.F. & Post, J.A. C11-BODIPY581/591, an oxidation-sensitive fluorescent lipid peroxidation probe: (micro)spectroscopic characterization and validation of methodology. *Free Radical Biology and Medicine* 33, 473-490, **2002**.
113. Oleynik, P., Ishihara, Y. & Cosa, G. Design and Synthesis of a BODIPY-a-Tocopherol Adduct for Use as an Off/On Fluorescent Antioxidant Indicator. *Journal of the American Chemical Society* 129, 1842-1843, **2007**.

Phenol-based Lipophilic Fluorescent Antioxidant Indicators: a Rational Approach

Katerina Krumova, Paul Oleynik, Pierre Karam and Gonzalo Cosa, *J. Org. Chem.* **2009**, 74, 3641–3651

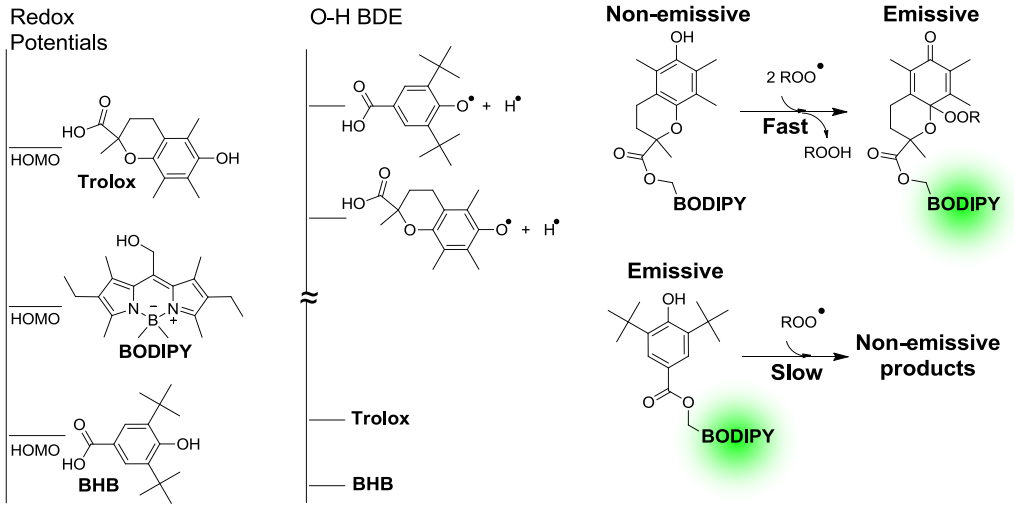

Preface

The fluorogenic probe B-TOH was recently developed in our lab for detecting ROS in the lipid membranes of live cells. B-TOH is a two segment probe with an α-tocopherol analogue as a receptor and a lipophilic Bodipy fluorophore as a reporter segment. Upon scavenging peroxyl or alkoxyl radicals in homogeneous solution B-TOH yields a highly fluorescent product. In this chapter we explore the off/on molecular switch mechanism operating in B-TOH. Our current objective is to gain a molecular level understanding regarding the off/on switch mechanism. We further seek to establish the scope and limitations of B-TOH as a fluorogenic antioxidant indicator, *i.e.*, an antioxidant which becomes emissive following free radical scavenging by the receptor moiety of the probe. In general, we aim at delineating the criteria for preparing new phenol-fluorophore based probes relying on the off/on switch first reported in B-TOH. In order to accomplish these goals we have performed reactivity, electrochemical and photophysical studies on B-TOH and on a newly synthesized control compound, the two segment receptor-reporter substrate 3,5-di-tert-butyl-4-hydroxybenzoic acid-Bodipy adduct (B-BHB). We have also performed theoretical calculations on HOMO energy levels for the receptors and reporters used. Our results highlight the potential of B-TOH as a fluorogenic antioxidant indicator and help illustrate the considerations to be taken into account in preparing a receptor-reporter type fluorogenic antioxidant indicator.

2.1 Introduction

Chemical functionalization of organic dyes has yielded a plethora of fluorescent chemosensors enabling real time detection of analytes with high spatial and temporal resolution and exquisite chemical specificity.[1,2] Advances over the last eight years include the synthesis of receptor-reporter fluorescent probes which are sensitive to reactive oxygen species (ROS).[3-6] These newly developed probes rely on an intramolecular photoinduced electron transfer (PeT) off/on switch mechanism operating between the receptor and reporter segments.[7]

We are working on the preparation of phenol-fluorophore lipophilic antioxidant indicators for detecting peroxyl radicals in the lipid membrane of live cells. Lipid peroxidation studies both in solution but especially within live-cell membranes will dramatically benefit from using a real time off/on fluorescent indicator of the antioxidant status, i.e. a probe capable of reporting via emission enhancement the depletion of peroxyl radical scavengers and the onset of the lipid chain autoxidation. This type of probes will ultimately allow a non-invasive spatial and temporal monitoring of the oxidative state in live-cell studies. We may foresee that imaging studies with specific sensors will ultimately enable us to better understand vital links between the chemistry and the biology of ROS.

Having recognized that α-tocopherol (an amphiphilic chromanol antioxidant and most abundant form of vitamin E, see Scheme 2.1) is the most active lipid soluble antioxidant present in mammalian tissues,[8] we have recently prepared the two segment receptor-reporter type fluorescent antioxidant indicator B-TOH (Figure 2.1).[9] B-TOH is an α-tocopherol analogue provided with a lipophilic Bodipy reporter segment. Upon scavenging peroxyl or alkoxyl radicals in homogeneous solution B-TOH yields a highly fluorescent product.[9]

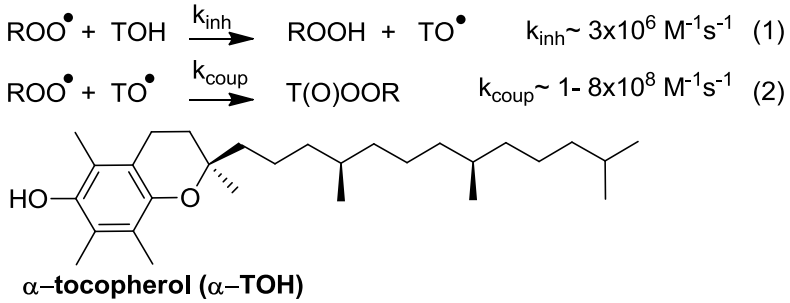

Scheme 2.1: Peroxyl radical (ROO•) scavenging by α-tocopherol (TOH)[8,10] and α-tocopheroxyl radical (TO•).[11-13]

The choice of a chromanol receptor moiety with a similar structure to that of α-tocopherol was based on our interest in preparing a probe whose reaction mechanism would be on par with that of α-tocopherol (see Scheme 2.1). The goal was thus to prepare a very potent peroxyl radical scavenger. α-Tocopherol and analogues such as trolox (a water soluble compound where the α-tocopherol phytyl tail has been replaced by a carboxylic acid moiety) and 2,2,5,7,8-pentamethyl-6-hydroxychroman (PMHC, an α-tocopherol analogue lacking the phytyl tail) have been shown to undergo the series of elementary reactions shown in Equations 1 and 2 (Scheme 2.1) under free radical chain autoxidation conditions.[8] Presumably, the same elementary reactions should also apply to B-TOH under similar reaction conditions. Additionally we synthesized a control compound, the two segment receptor-reporter substrate 3,5-di-tert-butyl-4-hydroxybenzoic acid-Bodipy adduct (B-BHB) (see Figure 2.1).

In the following sections we compare the reactivity of α-tocopherol, B-TOH and B-BHB in the presence of peroxyl radicals and discuss the differences in terms of the phenol O-H bond dissociation energy (BDE). We have thus determined the antioxidant activity of B-TOH and B-BHB by measuring the inhibition rate constant (during the induction periods) of styrene autoxidation in homogeneous solution. We have also estimated the stochiometric factor for peroxyl radical scavenging by B-TOH and B-BHB. We have additionally conducted competitive kinetic studies (B-TOH/α-tocopherol and B-BHB/α-tocopherol). Finally, we have measured absolute rate constants for H-atom abstraction from B-TOH by cumyloxyl radicals via laser flash photolysis (LFP).

These studies reveal similar reactivity patterns for B-TOH and α-tocopherol whereas B-BHB is observed to lack any antioxidant properties.

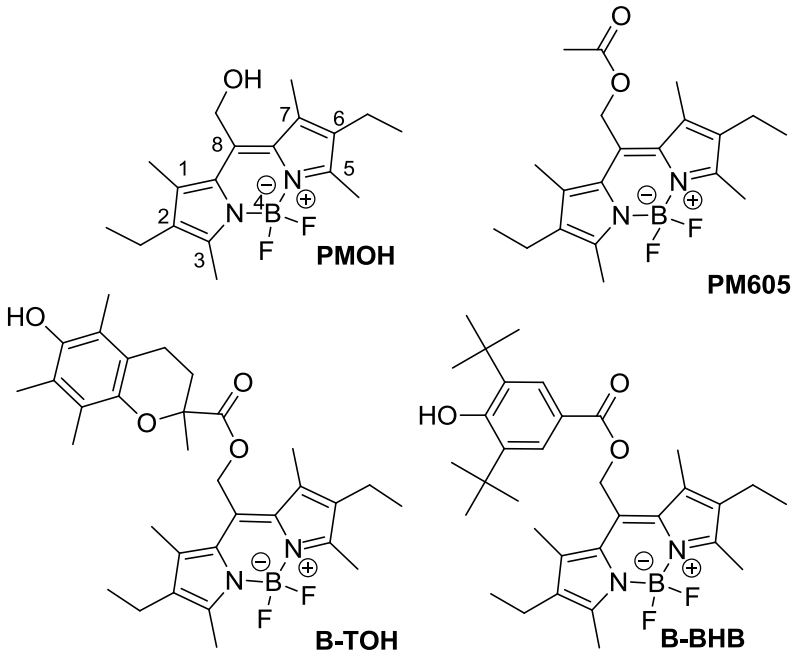

Figure 2.1: Fluorophores studied.

Our results also include redox potential measurements which together with theoretical calculations performed at the B3LYP/6-31G(d) level on the HOMO energy levels support a photoinduced electron transfer off/on switch mechanism. Fluorescence lifetimes and fluorescence quantum yields measured in a range of solvent polarities, from hexane to acetonitrile, for both B-TOH and B-BHB and their Bodipy precursors PM605 or PMOH are consistent with an intramolecular non-radiative decay pathway operative in B-TOH. This pathway is not operative in B-BHB where photoinduced electron transfer is deemed highly endergonic based on electrochemical studies.

The electrochemical, photophysical and reactivity experiments described underscore the potential of B-TOH as a lipophilic fluorogenic antioxidant indicator. Altogether, the information provided illustrates the steps to be taken in selecting the components necessary to prepare lipophilic phenol-fluorophore based antioxidant indicators. The criteria are based on the redox potentials of both receptor and reporter segments, the O-H BDE on the receptor phenol moiety

and the photophysical and solubility characteristics of the reporter end. This work provides substantial amount of information useful in the rational design of phenol-fluorophore based off/on fluorogenic antioxidant indicators for detection of peroxyl radicals.

2.2 Results and Discussion

Two major conditions must be fulfilled by phenol-based fluorogenic antioxidant indicators, *i.e.*, nonemissive antioxidants which become highly emissive upon peroxyl radical scavenging. They must have I) a high antioxidant activity and II) an intramolecular off/on switch which activates following peroxyl radical scavenging. In preparing a lipophilic phenol-fluorophore antioxidant indicator it is therefore of primordial importance to evaluate the chemical reactivity of the phenol moiety towards peroxyl radicals and to consider the mechanism by which the resultant phenoxyl radical further decays.

2.2.1 Reactivity

The antioxidant activity of phenols relies on their ability to quench peroxyl radicals via H-atom transfer from the phenol hydroxyl group to yield a phenoxyl radical and a hydroperoxide. The major considerations in determining antioxidant activity involve the rate of hydrogen atom transfer from phenols to peroxyl radicals and the subsequent reaction of the phenoxyl radicals formed.[8,10,11,14-18] The rates of formal abstraction of the phenol H-atom by free radicals have been shown to be influenced by the phenol's ring substituents, as well as by the nature of the free radical and the solvent. The reactions of phenols with free radicals may occur by at least three different mechanisms which have been recently reviewed.[19]

Motivated by our interest in determining the antioxidant activity for B-TOH (and the control compound B-BHB), we measured the inhibition rate constant (or rate constant for H-atom transfer, k_{inh}, Equation 1) of styrene autoxidation initiated by 2,2'-Azobisisobutyronitrile (AIBN) in a toluene solution at 30 ^{o}C under air atmosphere (Equations 3 to 6 in Scheme 2.2). We also determined the

stoichiometric coefficient (n) for peroxyl radical scavenging by B-TOH. As a standard we evaluated PMHC under identical experimental conditions (see Figures 2.2A and 2.2B).

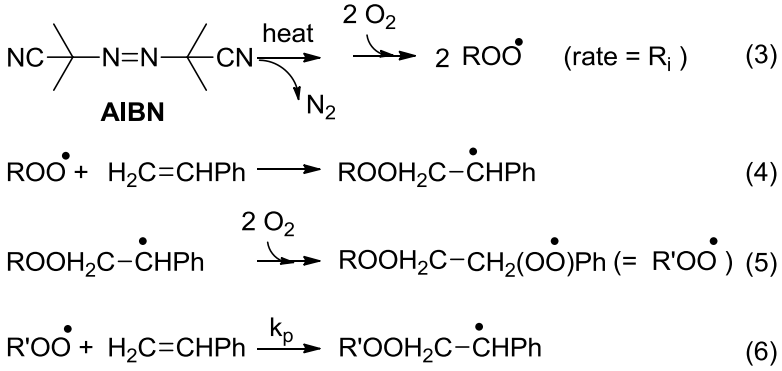

Scheme 2.2: Homolytic cleavage of AIBN and styrene autoxidation under O_2 atmosphere.[20-23]

The quantitative kinetic method we employed to determine k_{inh} has been amply discussed and applied by Barclay and Ingold.[8,14,24-26] Under our experimental conditions the autoxidation of styrene in toluene is initiated following thermolysis of AIBN[20,21,23] to give two carbon-centered radicals which readily trap molecular oxygen (with a reaction rate constant larger than 1 x 10^8 $M^{-1}s^{-1}$)[22] to yield two peroxyl radicals. The subsequent propagation reactions taking place are illustrated in Scheme 2.2.

The differential rate equation describing the oxygen consumption during the induction period is given by Equation 7, where k_{inh}, R_i and k_p are defined by equations 1, 3 and 6, respectively and where τ is the inhibition period of styrene autoxidation (τ is determined from the intercept of the straight lines tangential to the oxygen consumption curve during inhibition and once inhibition is over; see Figure 2.2A).

$$\frac{-d[O_2]}{dt} = k_p\left(\frac{R_i}{2k_{inh}[antioxidant]}\right)[H_2C=CHPh] \qquad (7)$$

Upon integration of Equation 7 we obtain equation 8 which we further use in the data analysis. From the slope of $\triangle[O_2]_t$ vs -ln (1-t/τ) we obtain the ratio $k_p[H_2C=CHPh]/k_{inh}$, and given the experimental value of $[H_2C=CHPh]$ and known values of k_p, the k_{inh} value may be readily determined.

$$\Delta[O_2]_t = k_p \frac{-\ln\left(1-\frac{t}{\tau}\right)}{k_{inh}}[H_2C=CHPh] \quad (8)$$

Finally, the stoichiometric coefficient *n* is determined form the τ value upon rearranging Equation 9.

$$\tau = \frac{n[antioxidant]}{R_i} \quad (9)$$

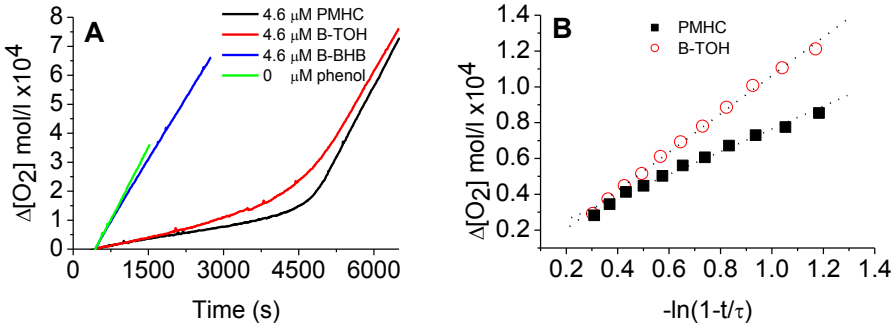

Figure 2.2: A) Profiles of oxygen-uptake during styrene (2.61 M) autoxidation initiated by 19 mM AIBN in toluene at 30°C under air. The rate of initiation, calculated based on Arrhenius parameters for AIBN homolysis is R_i= 1.98 x 10^{-9} Ms^{-1}. **Green**: Uninhibited rate of oxidation; R_i= 2.31 x 10^{-9} Ms^{-1}; **Blue**: Inhibition with 4.6 μM B-BHB; τ = 0 s, R_i= 1.98 x 10^{-9} Ms^{-1}, n = 0; **Black**: Inhibition with 4.6 μM PMHC; τ = 4670 s, R_i= 1.97 x 10^{-9} Ms^{-1}, n = 2; **Red**: Inhibition with 4.6 μM B-TOH; τ = 4500 s, R_i= 1.98 x 10^{-9} Ms^{-1}, n = 1.92. B) Plot of oxygen uptake versus –ln(1-t/τ) during the inhibition period in the AIBN initiated peroxidation of styrene in the presence of ■) PMHC and ○) B-TOH. Also shown is the linear fit to the experimental points. In the case of PMHC the value we obtained for k_{inh} is 1.6 x 10^6 $M^{-1}s^{-1}$. The B-TOH k_{inh} value is 1.6 fold smaller than that for PMHC, k_{inh} = 1.0 x 10^6 $M^{-1}s^{-1}$ for B-TOH.

Figure 2.2 illustrates the O_2 consumption for styrene autoxidation in the presence of B-TOH, B-BHB and PMHC, where the latter is known to have a stoichiometric factor *n* = 2 for peroxyl radical scavenging[8] and as such serves as a standard in our experiments. From the analysis of the data on Figures 2.2A and 2.2B we obtained a stoichiometric coefficient of 1.92 for B-TOH in comparison to PMHC. The small difference may arise in uncertainties in determining B-TOH concentration, which were based on a molar absorptivity at 549 nm of 70,000$M^{-1}cm^{-1}$ for the antioxidant indicator. From Equation 8 and the ratio of the slopes in Figure 2.2B we determined the ratio of k_{inh}(PMHC)/k_{inh}(B-TOH) to be equal to 1.6, *i.e.*, PMHC inhibition rate constant is only 1.6 fold larger than that of B-TOH.

In order to determine an absolute value for k_{inh} we first need a value for the styrene autoxidation rate constant k_p in toluene. k_p is relatively insensitive to the solvent, indeed, k_p for styrene in chlorobenzene and benzene are extremely similar (k_p = 19 and 21 $M^{-1}s^{-1}$, respectively, at 13 ^oC).[27] Assuming k_p in toluene ~ k_p in chlorobenzene = 41 $M^{-1}s^{-1}$ at 30 ^oC,[27] and from the experimental data in Figure 2.2B, and the styrene concentration used in our experiments ([styrene] = 2.61 M) we obtain k_{inh} = 1.58 x 10^6 $M^{-1}s^{-1}$ for PMHC and k_{inh} = 1.0 x 10^6 $M^{-1}s^{-1}$ for B-TOH.

Whereas B-TOH showed a similar antioxidant activity to that of PMHC, B-BHB, did not exhibit any antioxidant activity. These results are not surprising. The rate constant for H-atom transfer (k_{inh}) depends largely on the phenol O-H bond dissociation energy (BDE).[28] Unique stereoelectronic effects give α-tocopherol a distinctively low BDE[10] for the O-H bond (77.8 kcal/mol, determined via EPR).[18,29] The reported k_{inh} value for α-tocopherol in chlorobenzene is 3.2 x 10^6 $M^{-1}s^{-1}$.[8] Similar k_{inh} values have been reported for PMHC (k_{inh} = 3.8 x 10^6 $M^{-1}s^{-1}$)[8] and for trolox (k_{inh} = 1.1 x 10^6 $M^{-1}s^{-1}$)[8] in the same solvent. The smallest value recorded for trolox is consistent with the electron withdrawing effect of the carboxylic moiety which strengthens the phenol O-H bond.[8] A similar explanation would account for the slightly lower reactivity we have measured for B-TOH compared to PMHC under identical experimental conditions. In summary, the value of k_{inh} we have measured for B-TOH, in the range of those listed above, is in line with a chemical structure which preserves intact the α-tocopherol chromanol ring leading to a low O-H BDE.

The BDE for the phenolic O-H bond in 3,5-di-tert-butyl-4-hydroxybenzoic acid is reported to be 83.0 kcal/mol (determined via EPR).[29,30] Such a high BDE value should in turn result in a *ca.* 3 to 4 orders of magnitude drop in k_{inh}, at room temperature for 3,5-di-tert-butyl-4-hydroxybenzoic acid or B-BHB in comparison to that of α-tocopherol. As such, B-BHB is expected to have negligible antioxidant activity in the autoxidation of styrene, as experimentally observed.

We further estimated via laser flash photolysis (LFP) the absolute rate constant for H-atom abstraction (k_H) for B-TOH, PMHC and B-BHB by

cumyloxyl radicals generated upon 355 nm laser excitation of dicumyl peroxide (Scheme 2.3). Irradiation of 1 M dicumyl peroxide in air saturated benzene solutions with a short (*ca*. 6 ns) laser pulse leads to the formation of cumyloxyl radicals within the duration of the laser pulse (where O_2 quenched any Bodipy in its excited triplet state). The cumyloxyl radicals next react either by β-scission to give acetophenone and methyl radical (Equation 11) or by H-atom abstraction from the phenol to form cumyl alcohol (Equation 12).[31,32] The decay rate of the cumyloxyl radical, k_{exp}, was indirectly monitored following the growth rate, at 420 nm, of the phenoxyl radical derived from PMHC or B-TOH. Phenoxyl radicals have absorption bands in the range of 370 to 505 nm,[33,34] B-TOH phenoxyl radical has an absorption maximum at *ca.* 420 nm, similar to the absorption maximum reported for α-tocopherol phenoxyl radical in benzene.[35] As expected from the high BDE for B-BHB and 3,5-di-tert-butyl-4-hydroxybenzoic acid, we were unable to observe the formation of the phenoxyl radical derived from these two phenols in the presence of cumyloxyl radical (*vide infra*).

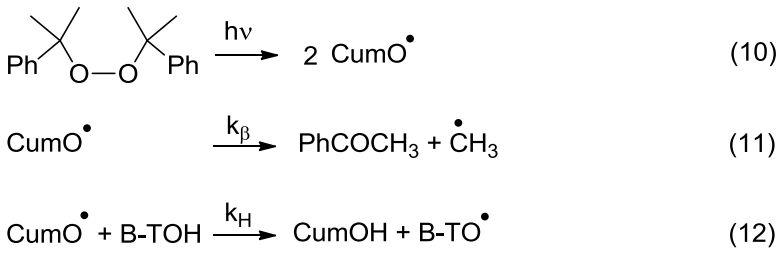

Scheme 2.3: Cumyloxyl radical formation and reaction upon β-scission and H-atom transfer.

The rate constant for H-atom abstraction, k_H, by cumyloxyl radical was determined from the experimental growth rate of phenoxyl radicals under pseudo first order conditions at increasing concentrations of the phenol substrate, according to Equation 13.[36,37]

$$k_{\exp} = k_{\beta} + k_H \times [phenol] \qquad (13)$$

By plotting k_{exp} values vs. increasing phenol concentration (Figure 2.3), we obtained a k_H value of 33 x 10^8 ± 1 x 10^8 $M^{-1}s^{-1}$ and a k_β value of 6 x 10^5 ± 1 x 10^5 s^{-1} for PMHC. Similar k_H values have been measured for α-tocopherol upon reaction with *tert*-butoxyl radicals photogenerated in a 1:1 *tert*-butyl

peroxide:benzene solution.[35] The high molar absorptivity of B-TOH at 420 nm constrained the experiments to low B-TOH concentration to ensure the probe beam could be detected in our LFP setup; thus, only two data points were measured for B-TOH at concentrations of 0.1 mM and 0.2 mM. Within the experimental error, B-TOH is observed to be as reactive as PMHC towards cumyloxyl radicals.

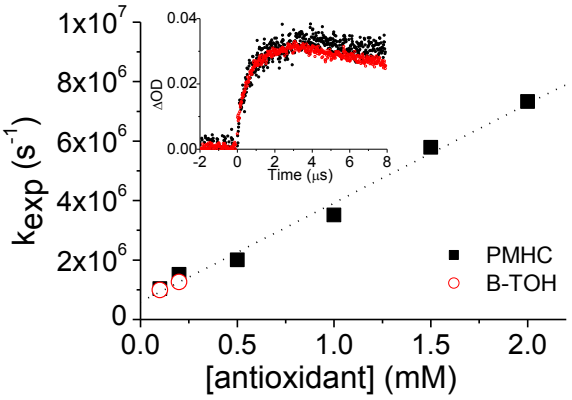

Figure 2.3: Observed growth rate constant (k_{exp}) for the formation of the phenoxyl radical upon 355 nm excitation of cumyl peroxide. Also shown is the linear fit to k_{exp} values vs. [PMHC]. The growth rates were recorded at 420 nm in the presence of increasing [PMHC] or [B-TOH] in air saturated benzene. The inset shows the time profiles for (○) the absorption of the B-TOH phenoxyl radical obtained upon excitation of cumyl peroxide in the presence of 0.2 mM B-TOH and (■) the absorption of the PMHC phenoxyl radical obtained upon excitation of cumyl peroxide in the presence of 0.2 mM PMHC. The larger dispersion in the data points observed with B-TOH is due to the low intensity of the probe beam which is significantly attenuated by absorption from B-TOH even at the low B-TOH concentrations employed.

In line with the k_{inh} values determined above for the H-atom abstraction by peroxyl radicals, PMHC was observed to be as reactive as B-TOH towards H-atom abstraction by alkoxyl radicals. In the case of 3,5-di-tert-butyl-4-hydroxybenzoic and B-BHB, no phenoxyl radical formation was observed even at concentrations of 3,5-di-tert-butyl-4-hydroxybenzoic = 7.64 mM. The k_H value for 3,5-di-tert-butyl-4-hydroxybenzoic (and B-BHB) is therefore at least one order of magnitude smaller than that for B-TOH.

In order to establish the scope and limitations of the prefluorescent antioxidant indicators it is important to determine their sensing potential for peroxyl radicals. The emissive properties of B-TOH and B-BHB were thus

investigated in the presence of peroxyl radicals generated via thermolysis of 67 mM AIBN in air saturated toluene at 37 ^{o}C (Figures 2.4A to 2.4D).

Figure 2.4A displays the changes in fluorescence intensity observed upon thermolysis of AIBN under increasing [B-TOH] in toluene solutions under air. Curves are normalized to the intensity value at time t = 0. Concomitant with the scavenging of peroxyl radicals by the receptor segment a linear increase in fluorescence intensity (and a linear decrease in [B-TOH]) is observed over time. The linear increase in intensity is consistent with the rate law which is expected to be zero order in antioxidant concentration. Given the measured stoichiometric factor of ~2 for peroxyl radical scavenging by B-TOH (*vide supra*) one may show that the rate law for B-TOH consumption follows Equation 14.

$$\frac{-d[B-TOH]}{dt} = \frac{R_i}{2} \qquad (14)$$

Upon free radical reaction with the receptor segment, prolonged exposure of B-TOH to peroxyl radicals leads to a slow decrease in fluorescence (and parallel decrease in absorption) intensity with time (see curves obtained with low initial B-TOH concentration in Figure 2.4A). This result is consistent with the onset of radical-mediated Bodipy degradation following the end of the induction period, i.e., upon consumption of the antioxidant receptor segment.[9] The situation is similar at high B-TOH concentration, where however the drop in Bodipy absorption concomitant with its degradation reduces inner filter effects. Thus, rather than a drop in intensity, the degradation of Bodipy leads to a moderate increase in intensity over time when the initial concentration of B-TOH is larger than 15 μM.

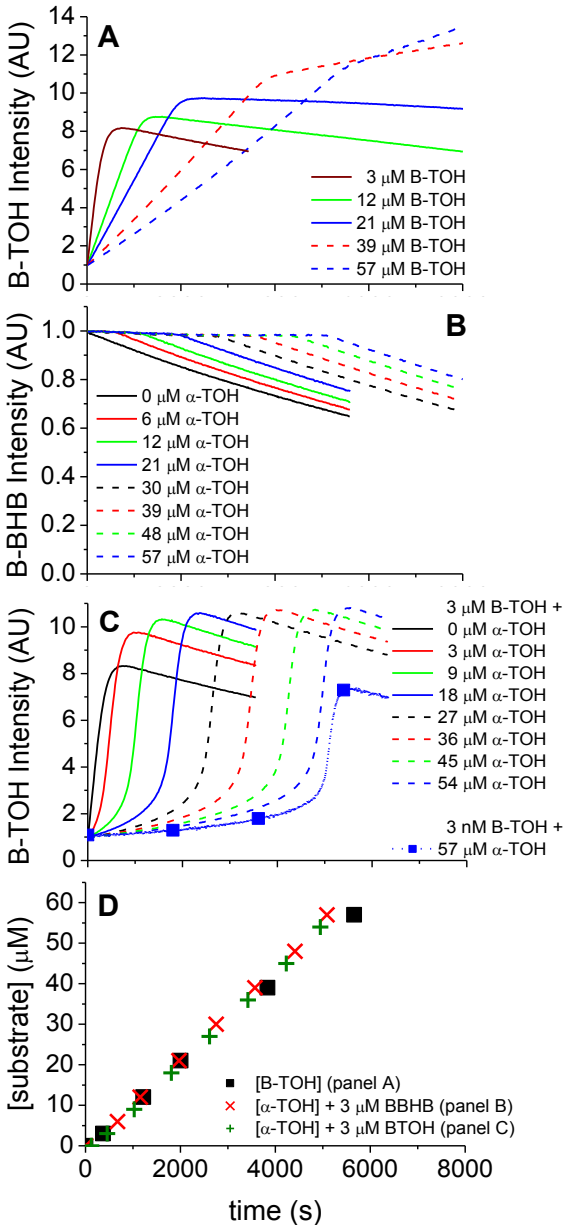

Figure 2.4: Emission intensity profiles in toluene solutions incubated at 37°C with 67 mM AIBN for A) increasing [B-TOH]. B) [B-BHB] = 3 μM with increasing [α-tocopherol]. C) [B-TOH] = 3 μM with increasing [α-tocopherol] (note that (■) consisted of 3 nM B-TOH). All samples were air equilibrated, the fluorescence intensity was recorded at 567 nm upon exciting at 520 nm, data points were taken every 2.5 s, excitation and emission slits were set at 2.5 nm except for the experiment with [B-TOH] = 3 nM, where slits were set at 5 nm. D) Increasing substrate concentration (either [B-TOH] for panel A or [α-tocopherol] for panels B and C) vs. induction period as calculated from the data in panels (■) A, (×) B and (+) C.

Figure 2.4A underscores the tremendous potential of B-TOH to follow *in situ* induction periods by simply monitoring the emission over time. We may thus

determine the inhibition period τ directly from the intercept of the straight lines tangential to the linear increase in intensity and the subsequent linear change in intensity arising from Bodipy degradation. Figure 2.4D illustrates the linear increase in τ with increasing [B-TOH], where the slope is directly proportional to the stoichiometric coefficient. One may also show that the rate of production of peroxyl radicals upon AIBN thermolysis, R_i, may be directly estimated from the values of τ.[9]

Figure 2.4B displays changes in fluorescence intensity observed upon thermolysis of AIBN under [B-BHB] = 3 μM and upon increasing concentrations of α-tocopherol in toluene solutions under air. Curves are normalized to the intensity value at time t = 0. Consistent with our expectations based on BDE values, the receptor segment in B-BHB does not serve a protecting antioxidant role and B-BHB undergoes peroxyl radical mediated degradation of the Bodipy reporter segment at much the same rate as observed for PMOH (data not shown) or for B-TOH once the receptor segment is scavenged (see the trace obtained with [B-TOH] = 3 μM). Indeed, one may conclude from the B-BHB results described above that the reaction of the peroxyl radicals with 3,5-di-tert-butyl-4-hydroxybenzoic acid is slower than the reaction of peroxyl radicals with the Bodipy chromophores PMOH or PM605. Addition of increasing amounts of α-tocopherol illustrate the inhibition effect in the Bodipy degradation exerted in this case by an external (rather than covalently linked as in B-TOH) antioxidant. The inhibition periods τ measured for increasing [α-tocopherol] are plotted in Figure 2.4D together with those recorded for B-TOH. We note that the slopes of [substrate] vs. τ are the same, within experimental error, for B-TOH and α-tocopherol. This result is consistent with both the prefluorescent antioxidant and α-tocopherol having the same stoichiometric coefficient for peroxyl radical scavenging.

Important to note is that the fluorescence quantum yield (ϕ_f) for B-BHB is close to 1 (*vide infra)*, and as such the probe would not manifest a fluorescence enhancement even if the receptor segment was reactive towards peroxyl radicals.

Figure 2.4C in turn displays changes in fluorescence intensity observed upon thermolysis of AIBN under constant [B-TOH] = 3 μM and with increasing concentrations of α-tocopherol in toluene solutions under air. Rather than a linear increase in intensity over time, as observed in Figure 2.4A, we observe that the increase in intensity follows a sigmoid behavior. The result is consistent with B-TOH having a slightly smaller k_{inh} in comparison with α-tocopherol, and therefore the fluorescence intensity enhancement and B-TOH consumption only occurs once significant portions of α-tocopherol have reacted. Once again we have determined the inhibition period τ which in this case was given by the time at the inflection point of the sigmoid curve (and which was extracted from the first derivative of the fluorescence intensity vs. time trajectory). The inhibition period determined is consistent with that obtained with increasing [B-TOH] and with that for B-BHB with increasing [α-tocopherol]. Close inspection of the [substrate] vs. τ experimental points obtained either with increasing [α-tocopherol] and either constant [B-BHB] or constant [B-TOH], reveal that in order to achieve the same τ value, the necessary [α-tocopherol] is *ca.* 3 μM smaller in experiments run with B-TOH vs. those run with B-BHB, consistent with B-TOH exerting an antioxidant effect of its own.

Two additional pieces of information may be extracted from the analysis of Figure 2.4C. Careful inspection of the intensity vs. time trajectories in this figure reveal that the enhancement is significantly smaller for pure B-TOH (a *ca.* 8 fold fluorescence enhancement is observed) compared to B-TOH solutions to which α-tocopherol was previously added (a *ca.* 11 fold fluorescence enhancement is observed). Whereas the intensity vs. time trajectories shown are normalized to the intensity value at time t = 0, in reality all trajectories reach the same final value of fluorescence, and rather start at slightly larger fluorescence values when [α-tocopherol] is low. The marked difference in emission enhancement reveals that partial oxidation of the probe occurs upon contact with the solvent, and that oxidation is prevented by sacrificial amounts of α-tocopherol when it is first added to the solutions.

The second relevant result is that the fluorescent antioxidant indicator B-TOH readily reports the onset of oxidation and the end of the inhibition period even when in the presence of large excesses of α-tocopherol, i.e., with a ratio of α-tocopherol/B-TOH ~ 20,000/1 (see the curve obtained with [α-tocopherol] = 57 μM and [B-TOH] = 3 nM). The low limit for [B-TOH] is set by the fluorimeter background, which would make measurements at lower [B-TOH] unreliable. These results underscore the scope and potential of B-TOH as a prefluorescent antioxidant indicator. We may realize that only trace amounts of B-TOH are necessary to follow e.g. peroxidation of lipid membranes in live cells containing physiological amounts of α-tocopherol. One may alternatively conceive kinetic experiments to test peroxidation in solution studies, where an *in situ* simple fluorescence method relaying on B-TOH (or new generation probes prepared under the same considerations) may be employed.

Whereas the reaction of B-TOH with an alkoxyl radical readily forms a phenoxyl radical with identical spectroscopic properties to that of α-tocopherol phenoxyl radical[35] (data not shown), and whereas a similar radical is conceivably formed following H-atom abstraction from B-TOH by peroxyl radicals, the fate of the phenoxyl radical is more difficult to establish. In general, the reaction of a phenoxyl radical formed upon scavenging an initial peroxyl radical can take any of four different pathways. They may I) undergo rapid reaction with the oxygen centered radicals, II) undergo dimerization with a second phenoxyl radical, III) initiate a new chain reaction upon H-abstraction and IV) undergo regeneration.[28] Whereas pathways III and IV are highly improbable under high free radical concentration conditions, pathways I and II are certainly viable ones. We may further rule out pathway II by considering that this pathway is sterically demanding and should play a minor role, if any, in the sterically crowded receptor-reporter molecules described.[28,38]

For pathway I, numerous products are expected for different phenols, involving the addition of peroxyl radicals to the phenoxyl radical and the subsequent rearrangement. In the specific case of the chromanoxyl radical of α-tocopherol a chromanone moiety which may further rearrange to a

chromaquinone is the major expected product.[12,13,39] We have previously detected the formation of an addition product upon B-TOH scavenging of peroxyl radicals.[9] These results were based on the UV absorption and mass spectra of the reaction product. The nature of the addition product (i.e., tocopherone or tocopheroquinone analogue) however remains elusive.

In closing the reactivity section, we may speculate as to the nature of the mechanism of reaction of B-TOH with peroxyl and alkoxyl free radicals. Three mechanisms have been recently reviewed, which involve hydrogen atom transfer (HAT), proton coupled electron transfer (PCET) and sequential proton loss electron transfer (SPLET).[19] In analogy with α-tocopherol, we expect B-TOH to follow a hydrogen atom transfer (HAT) mechanism under the experimental conditions discussed (low polarity solvents). Importantly, SPLET might become the most probable mechanism in aqueous solutions, where water makes electron transfer far more common than in organic solvents.[19] B-TOH should certainly lend itself as a convenient substrate to perform mechanistic studies in order to evaluate the importance of SPLET in aqueous solution.

2.2.2 Electrochemistry

Having discussed the reactivity of B-TOH and B-BHB and the importance of the O-H BDE in choosing a phenol receptor segment, we discuss next the electrochemical and photophysical properties of the probes and their precursor reporter segments. These experiments are intended to provide a molecular level understanding of the off/on switch mechanism observed in B-TOH.

We have previously hypothesized that an intramolecular photoinduced electron transfer (PeT) from the receptor segment to the photoexcited reporter segment renders B-TOH non-emissive. Free radical mediated oxidation of the chromanol receptor segment to a chromanone or chromoquinone increases its redox potential, thus deactivating the PeT quenching mechanism and leading to a fluorescence enhancement (Scheme 2.4).[9] We have speculated that the chromanol to chromanone/chromaquinone transformation leads to a significant increase in the redox potential of the substrate at the receptor end in B-TOH, i.e.; $E^{o}_{D^{+\bullet}/D}$ will

increase upon α-tocopherone formation yielding an emissive molecule. We have conducted experimental work and DFT calculations to test this hypothesis.

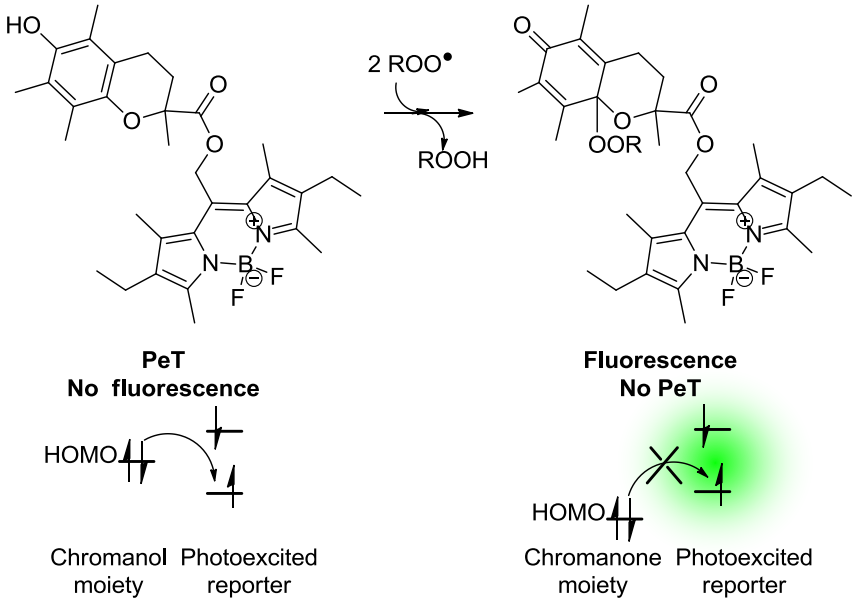

Scheme 2.4: Proposed off/on sensing mechanism for B-TOH relying on PeT from the chromanol moiety and lack of PeT from the chromanone moiety generated following peroxyl radical scavenging by the chromanol moiety.

In order to test the PeT hypothesis we calculated the standard Gibbs free energy for the process according to Equation 15:[40,41]

$$\Delta G^{o}_{eT} = \left[e\left(E^{o}_{D^{+\bullet}/D} - E^{o}_{A/A^{-\bullet}}\right) + \varpi\right] - \Delta E_{00} \qquad (15)$$

where e is the elementary charge, ω is the electrostatic work term that accounts for the effect of Coulombic interaction of the radical ions formed upon reduction/oxidation, ΔE_{00} is the vibrational zero electronic energy of the excited fluorophore, $E^{o}_{A/A^{-\bullet}}$ is the one-electron redox potential for the electron acceptor (Bodipy), and $E^{o}_{D^{+\bullet}/D}$ is the one-electron redox potential for the electron donor (phenol).

The Born correction term ω is usually taken as a simple Coulombic correction given by Equation 16, where q is the electron charge, ε is the solvent dielectric constant and R is the distance that separate reactants at charge transfer. Values in the range of -0.10 eV are typically used for ω in the case of acetonitrile (ε=37.5). This value corresponds to a separation distance R of *ca.* 0.38 nm.[42]

$$\varpi_{(R)} = \frac{-q^2}{4\pi\varepsilon_o \varepsilon R} \qquad (16)$$

The vibrational zero electronic energy of the excited PM605, ΔE_{00}, was calculated from the intersection point of the normalized absorption and emission spectra for PM605 in acetonitrile, we found a ΔE_{00} value of 2.22 eV (see also Table 2.2).

There are only few electrochemical studies on Bodipy dyes and none of these recent studies have explored the electrochemical properties of PMOH or PM605. We therefore conducted cyclic voltammetry experiments for both dyes in order to establish their redox potentials.

Figure 2.5A shows the cyclic voltammogram for PM605 acquired in Ar-saturated 0.1 M Tetrabutylammonium hexafluorophosphate vs. a Fc/Fc^+ internal standard. In this solvent, PM605 showed irreversible reduction and reversible oxidation waves when scanning at 200 mV/s. One reversible oxidation wave was observed for PM605 with a redox potential of +0.70 V. The negative scan showed two-electron reduction leading to two peaks with E_{pc} values of -1.45 V and -1.63 V. Electrochemical reversibility in the reduction was not observed at scan rates up to 10 V/s.

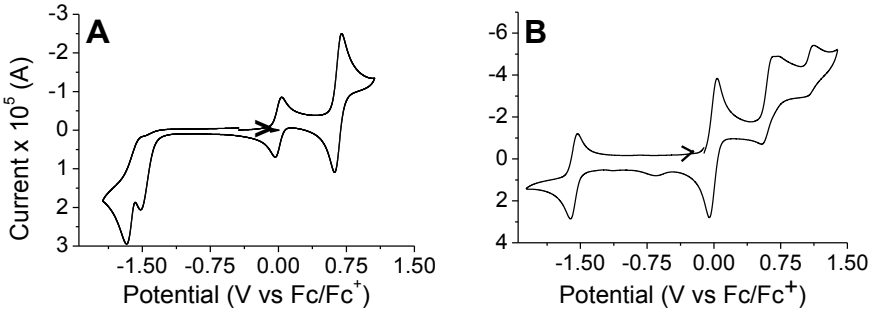

Figure 2.5: Cyclic voltammograms of A) PM605 and B) PMOH in degassed, Ar-saturated acetonitrile (0.1 M Tetrabutylammonium hexafluorophosphate) versus Fc/Fc^+. Scan rate = 200 mV s^{-1}. The scan direction is indicated by an arrow. The wave at a potential = 0 V corresponds to Fc/Fc^+.

Figure 2.5B shows the cyclic voltammogram for PMOH obtained under identical conditions as for PM605. Contrary to the results for PM605, PMOH showed reversible reduction and irreversible oxidation waves at 200 mV/s. The

positive scan showed a two step oxidation. Electrochemical reversibility in the oxidation was observed at scan rates > 1 V/s, wherefrom a redox potential of +0.61 V was determined. One reversible reduction wave was observed for PMOH with a redox potential of -1.56 V. Table 2.1 summarizes the electrochemical data. The observed peak separation for the reversible waves at 0.70 for PM605 and 0.61 and -1.57 for PMOH was ~ 60 mV demonstrating near Nernstian behavior. Also for the reversible reduction of PMOH and the reversible oxidation of PM605 at 200 mV/s, the peak current ratio (i_{pa}/i_{pc} or i_{pc}/i_{pa}) were approximately unity indicating that the radical ions were fairly stable and no additional chemical reactions took place.

	V vs. Fc/Fc^+						
	$E^o_{B/B^{-}\bullet}$	$E^o_{B^{+}\bullet/B}$	E_{pa1}	E_{pa2}	E_{pc1}	E_{pc2}	E_g (eV)
PMOH (1 V/s)	-1.57	0.61					2.18
PMOH (200 mV/s)	-1.56		1.10	0.74			NA
PM605 (200 mV/s)		0.70			-1.45	-1.63	NA

Table 2.1: Electrochemical data for PMOH and PM605.

The redox potentials measured are consistent with those reported for the series of commercial Bodipy derivatives having a methyl substituent in position 8 and ethyl (PM567), n-butyl (PM580) and isobutyl (PM597) substituents in positions 2 and 6 (note that PMOH has an hydroxyl group in position 8 and ethyl substituents in positions 2 and 6, see Figure 2.1). For PM567, PM580 and PM597 the reported $E^o_{B/B^{-}\bullet}$ values range between 0.53 V to 0.60 V, those for $E^o_{B^{+}\bullet/B}$ range between -1.66 V to -1.71 V (values originally reported vs. SCE, converted to values vs. Fc/Fc^+).[43]

The one-electron redox potential for PMOH ($E^o_{B/B^{-}\bullet}$) was found to be -1.56 V (vs. Fc/Fc^+). The $E^o_{B/B^{-}\bullet}$ value for PM605 could not be directly determined ever since it undergoes an irreversible reaction. This value may however be estimated from the spectroscopic HOMO-LUMO gap (E_g) and the electrochemical oxidation potential value of +0.70 V obtained for PM605. In effect, there is a good

agreement between both electrochemical (E_g = 2.18 eV) and spectroscopic (E_g = 2.28 eV, see Table 2.2) HOMO-LUMO gaps for PMOH in acetonitrile. Assuming both electrochemical and spectroscopic E_g values are similar for PM605, we may then estimate $E^o_{B/B^{-}\bullet}$ from E_g - $E^o_{B^{+}\bullet/B}$ (see Tables 2.1 and 2.2 for PM605 $E^o_{B^{+}\bullet/B}$ and E_g values in acetonitrile, respectively). A value of $E^o_{B/B^{-}\bullet}$ = -1.53 V was found for PM605.

Under most experimental conditions the oxidation of phenols occurs concomitant with deprotonation of the radical cation formed, and as such irreversible oxidation waves are generally obtained.[44-46] Given the difficulty in obtaining reliable one-electron oxidation potential for phenols ($E^o_{D^{+}\bullet/D}$) we used the literature value of 0.6 V vs. Fc/Fc^{+} recently reported by Webster *et al.* for the oxidation potential of trolox ethyl ester.[44-46]

Consistent with our original hypothesis[9] PeT from trolox ester (the electron donor D) to Bodipy (the electron acceptor A) was found to be exergonic. We thus found that ΔG^o_{eT} is *ca.* -0.15 eV for the PM605/trolox ethyl ester system in acetonitrile.

Upon rearranging Equation 15 we may further estimate the maximum value the receptor segment redox potential ($E^o_{D^{+}\bullet/D}$) may have which will satisfy that electron transfer to the photoexcited reporter segment occurs spontaneously. For PMOH based sensors, the $E^o_{D^{+}\bullet/D}$ for the receptor segment has to be smaller than *ca.* 0.76 V in acetonitrile, *i.e.*, $E^o_{D^{+}\bullet/D} < E^o_{A/A^{-}\bullet} + \Delta E_{00} - \varpi$ = 0.76 V.

For 3,5-di-tert-butyl-4-hydroxybenzoic acid, the one-electron redox potential is not observed within the acetonitrile solvent window. As such, we may estimate that $E^o_{D^{+}\bullet/D}$ > 1.25 eV (vs Fc/Fc^{+}) for 3,5-di-tert-butyl-4-hydroxybenzoic acid, way above the 0.76 V threshold. We may thus infer that for the system consisting of PM605 and 3,5-di-tert-butyl-4-hydroxybenzoic acid, intermolecular PeT will be endergonic. Consistent with this assumption, no Bodipy quenching is observed in the presence of 3,5-di-tert-butyl-4-hydroxybenzoic acid (*vide infra*).

Complementary to our experimental work, we conducted DFT calculations. The calculations on the HOMO energy levels relative to vacuum were performed at the B3LYP/6-31G(d) level.[47,48] Figure 2.6 displays the HOMO values calculated for the reporter precursor PM605, the receptor precursors trolox and 3,5-di-tert-butyl-4-hydroxybenzoic acid adduct (BHB in the plot) and the oxidized receptors trolox chromanone and duroquinone (duroquinone was chosen as a suitable model for trolox chromaquinone). Trolox is observed to have the HOMO at higher energy values than the HOMO of the reporter segment (PM605), whereas oxidized trolox (either in a chromanone or chromaquinone form) or 3,5-di-tert-butyl-4-hydroxybenzoic acid all have their HOMO lying at significantly lower energy values with respect to PM605. As such electron transfer to the photoexcited receptor can only be exergonic in the case of trolox, whereas it will be endergonic for the oxidized receptor and 3,5-di-tert-butyl-4-hydroxybenzoic acid.

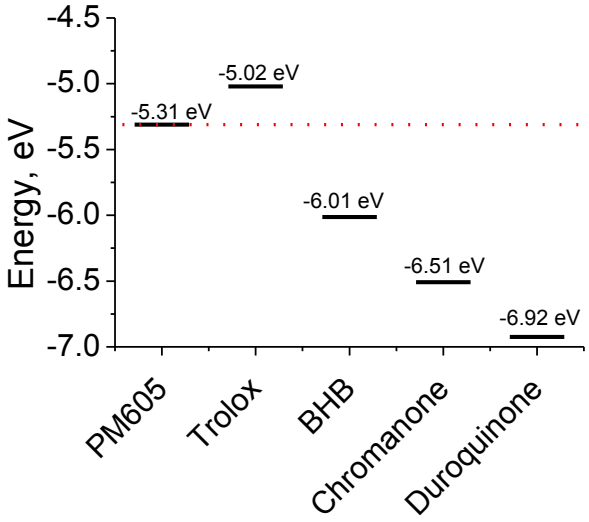

Figure 2.6: HOMO energy levels (in eV) calculated at the B3LYP/6-31G(d) level implemented through Gaussian 03.

2.2.3 Steady-state and Time-resolved Fluorescence

Experiments performed with PM605 and increasing concentrations of trolox or 3,5-di-tert-butyl-4-hydroxybenzoic acid are consistent with the expectations based on Equation 15. Thus, no intermolecular quenching of PMOH is observed when 3,5-di-tert-butyl-4-hydroxybenzoic acid is used as a quencher (see Figure

2.6). Trolox on the other hand efficiently quenches the PMOH emission, from the analysis of the I_0/I ratio vs. trolox concentration a Stern-Volmer fluorescence quenching constant K_{SV} = 19.3 M^{-1} was determined in acetonitrile (Figure 2.3). From the knowledge of K_{SV} together with the knowledge of PMOH fluorescence lifetime in acetonitrile (τ_{dec} = 7.2 ns), it is possible to estimate the fluorescence quenching constant for PMOH by trolox; $k_q = 2.6 \times 10^9$ $M^{-1}s^{-1}$.[9] This quenching rate constant is one order of magnitude smaller than the diffusion controlled rate constant $k_d = 2 \times 10^{10}$ s^{-1} in acetonitrile. The low value of k_q possibly reflects the low driving force for PeT (*i.e.* $\Delta G^0_{eT} \sim -0.15$ eV).

The emission quantum yield (ϕ_f) of the B-BHB adduct is similar to that of its precursor PM605, whereas the emission quantum yield for B-TOH is more than 10 fold smaller than that of PM605 (Table 2.2). These results are consistent with the intermolecular quenching studies and the thermodynamic calculations described above.

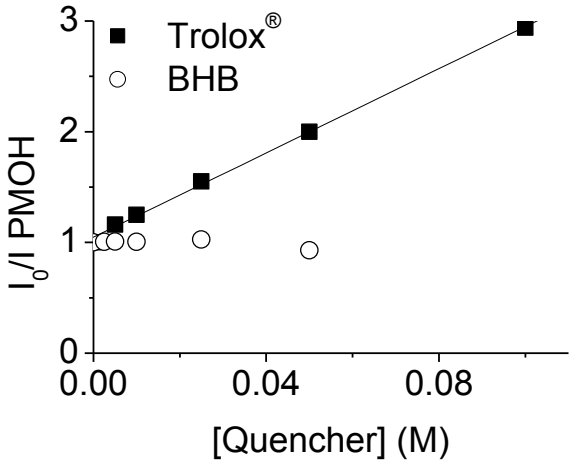

Figure 2.7: Stern-Volmer plot for the fluorescence quenching of PMOH in the presence of (■) increasing trolox and (○) increasing 3,5-di-tert-butyl-4-hydroxybenzoic acid (BHB) in aerated acetonitrile solution.

Time resolved data acquired for B-TOH, B-BHB, PM605 and PMOH in solutions of hexane, acetonitrile or toluene further illustrate that the drop in B-TOH ϕ_f arises from a dynamic intramolecular quenching. Thus, whereas the fluorescence decay lifetimes (τ_{dec}) of PMOH, PM605 and B-BHB are similar and

show little solvent dependence, with τ_{dec} values close to 7 ns in all solvents (see Table 2.2), a significant reduction is observed in the case of B-TOH, where τ_{dec} = 0.44 ns, 0.74 and 0.92 ns in hexane, acetonitrile and toluene, respectively (Figure 2.7 and Table 2.2).[49] From the analysis of the fluorescence decay rate constant and the emission quantum yields it is further possible to estimate the non-radiative decay (τ_{nr}) for the dyes according to Equation 17.

$$\tau_{nr} = \frac{\tau_{dec}}{1-\phi_f} \qquad (17)$$

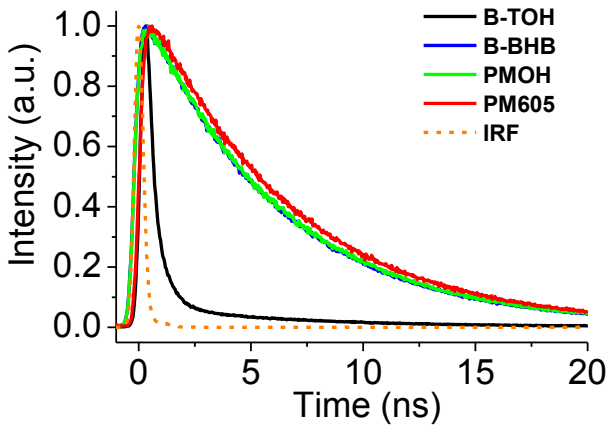

Figure 2.8: Normalized fluorescence decay profiles for B-TOH, B-BHB, PMOH and PM605 in toluene. Fluorophore concentration was *ca.* 3 to 6 μM in all cases.

In the case of B-TOH a dramatic decrease in τ_{nr} (or increase of $k_{nr} = 1/\tau_{nr}$, the non radiative decay rate constant) can be observed from the analysis of Table 2.2. This is consistent with the introduction of an intramolecular quenching mechanism which is not present in either the precursor dyes (PM605 and PMOH), or in B-BHB, all characterized by their large τ_{nr} values. From the ratio of the first-order rate constant k_{nr} for B-TOH intramolecular quenching and the second-order rate constant for intermolecular quenching k_q (obtained from the quenching of PMOH by trolox) we may further estimate, upon applying Equation 18, that the effective trolox molarity [$trolox_{effective}$] is *ca.* 0.5 to 1 M for B-TOH in the various solvents studied.

$$\left[trolox_{effective}\right] = \frac{k_{nr}}{k_q} \qquad (18)$$

In summary, B-BHB, PMOH and PM605 exhibit similar spectroscopic properties, whereas B-TOH is characterized by significantly smaller values of ϕ_f and τ_{dec}. It follows from the previous electrochemical and spectroscopic studies and DFT calculations that the B-TOH off-state arises due to an intramolecular PeT from the receptor end to the reporter end.

Compound	Solvent	Abs. λ_{max} (nm)	Em λ_{max} (nm)	Φ_f	τ_{dec} (ns)	τ_{rad} (ns)	τ_{nr} (ns)	E_g (eV)
PMOH	Hexanes	543	557	0.832	6.57±0.02	7.9	39.0	2.26
	Acetonitrile	536	552	0.838	6.90±0.02	8.2	42.5	2.28
	Toluene	545	560	0.995	6.02±0.02	6.1	1187.0	2.25
PM605	Hexanes	546	561	0.755	6.31±0.02	8.4	25.8	2.25
	Acetonitrile	542	561	0.722	6.76±0.02	9.4	24.3	2.26
	Toluene	549	566	0.894	6.43±0.02	7.2	60.8	2.23
B-TOH	Hexanes	549	555	0.063	0.44±0.02	6.9	0.47	2.24
	Acetonitrile	544	565	0.039	0.74±0.02	18.9	0.77	2.26
	Toluene	549	567	0.137	0.92±0.02	6.7	1.1	2.22
B-BHB	Hexanes	545	564	0.764	6.75±0.02	8.8	28.6	2.25
	Acetonitrile	540	560	0.450	6.79±0.02	15.1	12.4	2.26
	Toluene	549	567	0.882	5.94±0.02	6.7	50.2	2.23

Table 2.2: Spectroscopic properties for PMOH, PM605, B-TOH and B-BHB.

The results discussed above illustrate what are the redox and photophysical criteria that need to be considered in choosing a receptor-reporter system. Based on the redox potentials characterizing the receptor and reporter ends, and upon considering the first excited singlet state energy of the reporter, we can estimate

which receptor/reporter combinations are feasible to undergo PeT when the receptor is in its reduced form. The search for fluorophores readily excitable in the visible region of the spectrum, thus avoiding autofluorescence from biological tissue, is yet another criterion to consider in choosing the reporter end for probes to be used in biological studies.

Whereas the emphasis on our work has been on the role of the phenol receptor segment, it is worthwhile noting that by replacing the reporter Bodipy segment one may further control the extent to which PeT is exergonic. Bodipy fluorophores where the ethyl groups (electron releasing substituents) at positions 2 and 6 are replaced by H atoms or cyano substituents lead to larger $E^{o}_{A/A^{-}\cdot}$ values. Using BDIPY fluorophores with electron withdrawing substituents should result in fluorescent antioxidant indicators with improved sensitivity (*i.e.* larger on/off intensity ratio).

2.3. Conclusions

A comparison between the prefluorescent antioxidant indicator B-TOH and the control molecule B-BHB has allowed us to gain a molecular level understanding of the mechanism accounting for B-TOH intramolecular emission quenching and subsequent emission enhancement upon reaction with free radicals. Photoinduced electron transfer is the plausible mechanism accounting for the Bodipy intramolecular fluorescence quenching observed in B-TOH. Reactivity studies have underscored the antioxidant activity of B-TOH and the importance of BDE in preparing a phenol based prefluorescent antioxidant indicator. The studies reported here allow us to delineate a series of criteria to be considered in selecting the receptor and reporter components to prepare phenol-based lipophilic fluorescent antioxidant sensors.

The choice has to be primarily based on the redox properties of the phenol and fluorophore segments as well as the first excited singlet state energy of the latter in order that PeT from the phenol to the fluorophore is exergonic. Intermolecular quenching via PeT should ideally be diffusion controlled, this will ensure that upon tethering the reporter and receptor segment a significant decrease

in the emission quantum yield of the former will be observed given the high effective quencher concentrations achieved following covalent binding. Our interest in preparing lipophilic fluorescent antioxidants to monitor the oxidative stress in lipid bilayers reduces the choice of fluorophores mostly to those derived from Bodipy. Cyanine dyes among others, frequently bearing a formal charge, are not suitable candidates for lipophilic fluorescent antioxidant indicators. However they would certainly be suitable candidates to be considered in preparing water soluble antioxidant indicators.

The chemical reactivity of the phenol moiety plays a significant role in the choice of the receptor end. Whereas phenols containing a low BDE hydroxyl group readily scavenge peroxyl radicals, phenols with a high BDE hydroxyl group are poor antioxidants. Interestingly, the BDE in phenols decreases upon substituting H-atoms with electron donating groups in the aromatic ring and it increases upon substituting H-atoms with electron withdrawing groups.[30] The former substitution pattern further favors PeT from the phenol to the fluorophore moiety, whereas the later disfavor this PeT mechanism as can be observed with B-TOH and B-BHB.

The peroxyl radical mediated degradation observed for PMOH or B-BHB, albeit slow, further underscores the necessity of choosing a fluorophore whose chemical structure minimizes the possibility of side reactions with free radicals.

2.4. Experimental Section

Materials. 8-Acetoxymethyl-2,6-diethyl -1,3,5,7-tetramethyl pyrromethene fluoroborate (PM605) was purchased from Exciton, Inc. (±) 6-Hydroxy-2,5,7,8-tetramethylchromane-2-carboxylic acid (trolox), 3,5-di-tert-butyl-4-hydroxybenzoic acid, N-(3-dimethylaminopropyl)-N'-ethylcarbodiimide (EDC), Dimethylamino pyridine (DMAP), 2,2,5,7,8-pentamethyl-6-hydroxychroman (PMHC), dicumylperoxide, 2,2´-Azobis-(2-methylpropionitrile) (AIBN) and α-tocopherol were used as received; styrene was distilled prior to use. Solvents were used without further purification unless otherwise specified in the text.

Absorption. Absorption spectra were recorded employing 1cm x 1cm quartz cuvettes.

Oxygen uptake studies. Autoxidation studies were carried out at 30 °C under air (760 Torr) in a dual-channel oxygen uptake apparatus equipped with a sensitive pressure transducer described previously.[50]

Known volumes of substrate (styrene) and solvent (toluene) were placed in both reaction chambers of the system (sample cell and reference cell) and left to equilibrate with a water bath at 30°C. The volume of toluene employed was 1.3 mL in the sample cell and 1.4 mL in the reference cell. The final styrene concentration in the reaction chambers was 2.61 M. The initiator solution (0.1 mL of a 0.373 M AIBN solution in toluene) was injected in the sample cell to yield a final AIBN concentration of 19 mM. A steady rate of oxidation was next established. Known amounts of the inhibitors in toluene (30μL of 0.312 mM PMHC, 0.312 mM B-TOH and 0.321 mM B-BHB) were then injected into the sample cell to determine their antioxidant activity. The same amount of antioxidants was added to the reference cell so as to prevent oxygen uptake due to self initiation. The oxygen uptake was measured until the rate returned to the uninhibited rate.

Laser flash photolysis studies. Experiments were carried out in a commercially available Luzchem 212 LFP setup provided with a Tektronix TDS 2000 digitizer for signal capture. A Nd:Yag laser (Continuum model Surelite I-10) was used for excitation at a wavelength of 355 nm. The laser was attenuated yielding 9 mJ laser pulses with a pulse width of ~ 6 ns. Cuvettes, 1 cm in path length, were utilized in all experiments. The solutions consisted of 1 M dicumylperoxide in benzene to ensure absorption of 0.3 at the excitation wavelength. We chose 355 nm as the excitation wavelength to minimize direct excitation of B-TOH (molar absorptivity ε_{355nm} = 3.4 x 10^3 for B-TOH). Air saturated solutions were utilized to rapidly quench any triplet Bodipy which may form under our experimental conditions. Experiments were conducted at room temperature. The growth of the phenoxyl radical was monitored at 420 nm following laser excitation of the dicumylperoxide solutions containing increasing

concentrations of PMHC or B-TOH. In order to minimize sample degradation, fresh samples were irradiated with a total of 10 laser shots to acquire the △OD temporal evolution and the k_{exp} for the various antioxidant concentrations, the solutions were further agitated in-between shots (prolonged irradiation of the solutions containing B-TOH and dicumylperoxide (12 or more laser shots) lead to an observable emission enhancement arising from B-TOH oxidation upon reaction with cumyloxyl radicals).

Steady state fluorescence studies. A Cary Eclipse Spectrophotometer with temperature controller was utilized to measure the emission intensity profiles of 3 μM B-TOH and 3 μM B-BHB solutions in toluene. Fluorescence was recorded at 567 nm upon exciting at 520 nm using 2.5 nm excitation and emission slits. 2.2 mL of toluene solutions containing B-TOH or B-BHB with or without α-tocopherol were incubated for 10 min at 37°C before 804 μL of AIBN 250 mM in toluene were added to each cuvette for final AIBN concentration of 67 mM. The emission intensity was followed at 2.5 s intervals for 8000 s.

The emission quantum yield for PM605 in ethanol (ϕ_s = 0.74) was used as the standard to calculate the emission quantum yield for the various dyes in the different solvents (ϕ_u). Optically matched solutions of PM605 in ethanol and of a dye of interest were excited at the same wavelength, and the emission recorded and integrated over all the wavelength range. The emission quantum yield was calculated according to Equation 19, where A stands for the absorption, I for the integrated intensity and n for the refractive index for the unknown (u) or the standard sample (s).

$$\phi_u = \phi_s \times \frac{A_s \times I_u \times n_u^2}{A_u \times I_s \times n_s^2} \qquad (19)$$

Electrochemical studies. Voltammetric experiments were conducted with a computer controlled BASi EC Epsilon potentiostat with a BASi C3 cell stand. The working electrode was a 2 mm Pt electrode with a Pt wire auxiliary electrode and a 0.01 M $Ag/AgNO_3$ solution reference electrode. A 0.1 M solution of tetrabutylammonium hexafluorophosphate in dry acetonitrile was used as the electrolyte solvent, in to which the species of interest were dissolved for analysis.

The solution was purged with argon with simultaneous stirring and left under a blanket of argon. All values are reported vs. ferrocene, with the oxidation of ferrocene explicitly measured and corrected to zero for each experiment.

Fluorescence lifetime studies. The fluorescence lifetime measurements were carried out using a Picoquant Fluotime 200 Time Correlated Single Photon Counting setup employing an LDH 470 picosecond diode laser (Picoquant) with excitation wavelength at 470 nm as the excitation source. The laser was controlled by a PDL 800 B picosecond laser driver from Picoquant. The excitation rate was 10 MHz and the detection frequency was less than 100 kHz. Photons were collected at the magic angle.

Computational methods. All structures were computed using the density functional theory at the B3LYP/6-31G(d) level implemented through Gaussian 03.[47] Several starting geometries were utilized to get geometry optimization in order to ensure that the optimized structure corresponds to a global minimum.

Synthesis. **8-Hydroxymethyl-2,6-diethyl -1,3,5,7-tetramethyl pyrromethene fluoroborate (PMOH)** and **8-((±) 6-Hydroxy-2,5,7,8-tetramethylchromane-2-carbonyloxy)methyl-2,6-diethyl -1,3,5,7-tetramethyl pyrromethene fluoroborate (B-TOH)** were prepared as described in the literature.[9,51]

3,5-di-tert-butyl-4-hydroxybenzyloxymethyl-2,6-diethyl -1,3,5,7-tetramethyl pyrromethene fluoroborate (B-BHB): To 5 mL of anhydrous CH_2Cl_2 under Argon atmosphere and constant stirring were added PMOH (15.5 mg, 0.0464 mmol, 1 eq), 3,5-di-tert-butyl-4-hydroxybenzoic acid (11.6 mg, 0.0463 mmol, 1 eq), EDC (8.9 mg, 0.046 mmol, 1 eq) and DMAP (5.1 mg, 0.042 mmol, 0.9 eq). The resulting solution was refluxed under Argon in the dark for 1 hour. The reaction mixture was then cooled to room temperature and quenched with 10 mL of saturated aqueous solution of NH_4Cl. The phases were separated and the aqueous phase was extracted three times with CH_2Cl_2 . The combined organic fractions were dried with anhydrous $MgSO_4$, followed by concentration under reduced pressure. The residue was loaded onto a silica gel flash column and eluted with 1/1 CH_2Cl_2/hexanes mixture. The clean fractions were

condensed, redissolved in ethyl acetate and washed 10 times with 10% K_2CO_3 (aq) to afford the coupling product as a dark purple solid in 45% yield. ^{1}H-NMR (400 MHz, $CDCl_3$) δ ppm 8.05 (s, 4H), 5.79 (s, 1H), 5.55 (s, 2H), 2.54 (s, 6H), 2.41 (q, J = 7.6 Hz, 4H), 2.33 (s, 6H), 1.50 (s, 18H), 1.35 (s, 18H), 1.06 (t, J = 7.6 Hz, 6H). ^{13}C (75 MHz, $CDCl_3$) δ ppm 166.9, 158.8, 154.9, 137.0, 136.2, 133.7, 132.8, 132.4, 127.5, 120.3, 58.8, 34.7, 30.5, 17.5, 15.1, 13.1, 13.0. LRMS (EI, 70 eV) *m*/*z* (%) 566.4 (M^+ 100), 303.2 (30), 235.1 (54); HRMS (EI) for $C_{33}H_{45}N_2O_3BF_2$ (M^+) calculated: 566.34913, found: 566.35017. IR (neat) ν cm^{-1} 3586(m), 2963(m), 2934(m), 2876(m), 1713(m), 1556(s), 979(s). Absorption λ_{max} = 549 nm in toluene; Emission λ_{max} = 567 nm in toluene.

2.5. References

1. Lavis, L.D. & Raines, R.T. Bright Ideas for Chemical Biology. *ACS Chemical Biology* 3, 142-155, **2008**.
2. Tsien, R.Y. & Waggoner, A. Fluorophores for Confocal Microscopy Photophysics and Photochemistry. in *Handbook of Biological Confocal Microscopy* (ed. Pawley, J.B.) 338-348 (Springer, 2006).
3. Gabe, Y., Urano, Y., Kikuchi, K., Kojima, H. & Nagano, T. Highly Sensitive Fluorescence Probes for Nitric Oxide Based on Boron Dipyrromethene ChromophoreRational Design of Potentially Useful Bioimaging Fluorescence Probe. *Journal of the American Chemical Society* 126, 3357-3367, **2004**.
4. Tanaka, K.M., Tetsuo; Umezawa, Naoki; Urano, Yasuteru; Kikuchi, Kazuya; Higuchi, Tsunehiko; Nagano, Tetsuo. Rational Design of Fluorescein-Based Fluorescence Probes. Mechanism-Based Design of a Maximum Fluorescence Probe for Singlet Oxygen. *Journal of the American Chemical Society* 123, 2530-2536, **2001**.
5. Ueno, T., Urano, Y., Kojima, H. & Nagano, T. Mechanism-Based Molecular Design of Highly Selective Fluorescence Probes for Nitrative Stress. *Journal of the American Chemical Society* 128, 10640-10641, **2006**.
6. Ueno, T.U., Yasuteru; Setsukinai, Kenichi; Takakusa, Hideo; Kojima, Hirotatsu; Kikuchi, Kazuya; Ohkubo, Kei; Fukuzumi, Shunichi; Nagano, Tetsuo. Rational principles for modulating fluorescence properties of fluorescein. *Journal of the American Chemical Society* 126, 14079-14085, **2004**.
7. de Silva, A.P., Gunaratne, H.Q.N., Gunnlaugsson, T., Huxley, A.J.M., McCoy, C.P., Rademacher, J.T. & Rice, T.E. Signaling Recognition Events with Fluorescent Sensors and Switches. *Chemical Reviews* 97, 1515-1566, **1997**.
8. Burton, G.W., Doba, T., Gabe, E., Hughes, L., Lee, F.L., Prasad, L. & Ingold, K.U. Autoxidation of biological molecules. 4. Maximizing the antioxidant activity of phenols. *Journal of the American Chemical Society* 107, 7053-7065, **1985**.
9. Oleynik, P., Ishihara, Y. & Cosa, G. Design and Synthesis of a BODIPY-a-Tocopherol Adduct for Use as an Off/On Fluorescent Antioxidant Indicator. *Journal of the American Chemical Society* 129, 1842-1843, **2007**.
10. Burton, G.W. & Ingold, K.U. Vitamin E: application of the principles of physical organic chemistry to the exploration of its structure and function. *Accounts of Chemical Research* 19, 194-201, **1986**.
11. Jonsson, M., Lind, J., Reitberger, T., Eriksen, T.E. & Merenyi, G. Free radical combination reactions involving phenoxyl radicals. *The Journal of Physical Chemistry* 97, 8229-8233, **1993**.
12. Liebler, D.C., Baker, P.F. & Kaysen, K.L. Oxidation of vitamin E: evidence for competing autoxidation and peroxyl radical trapping reactions of the tocopheroxyl radical. *Journal of the American Chemical Society* 112, 6995-7000, **1990**.
13. Liebler, D.C., Matsumoto, S., Iitaka, Y. & Matsuo, M. Reactions of vitamin E and its model compound 2,2,5,7,8-pentamethylchroman-6-ol with ozone. *Chemical Research in Toxicology* 6, 69-74, **1993**.
14. Barclay, L.R.C. 1992 Syntex Award Lecture Model biomembranes: quantitative studies of peroxidation, antioxidant action, partitioning, and oxidative stress. *Canadian Journal of Chemistry* 71, 1-16, **1993**.
15. Barclay, L.R.C., Edwards, C.E. & Vinqvist, M.R. Media Effects on Antioxidant Activities of Phenols and Catechols. *Journal of the American Chemical Society* 121, 6226-6231, **1999**.
16. Bowry, V.W. & Ingold, K.U. The Unexpected Role of Vitamin E (α-Tocopherol) in the Peroxidation of Human Low-Density Lipoprotein1. *Accounts of Chemical Research* 32, 27-34, **1998**.
17. Niki, E. & Noguchi, N. Dynamics of Antioxidant Action of Vitamin E. *Accounts of Chemical Research* 37, 45-51, **2003**.
18. Lucarini, M., Pedulli, G.F. & Cipollone, M. Bond Dissociation Enthalpy of a-Tocopherol and Other Phenolic Antioxidants. *Journal of Organic Chemistry* 59, 5063-70, **1994**.

19. Litwinienko, G. & Ingold, K.U. Solvent Effects on the Rates and Mechanisms of Reaction of Phenols with Free Radicals. *Accounts of Chemical Research* 40, 222-230, **2007**.
20. Boozer, C.E., Hammond, G.S., Hamilton, C.E. & Sen, J.N. Air oxidation of hydrocarbons. II. The stoichiometry and fate of inhibitors in benzene and chlorobenzene. *Journal of the American Chemical Society* 77, 3233-3237, **1955**.
21. Burton, G.W. & Ingold, K.U. Autoxidation of biological molecules. 1. Antioxidant activity of vitamin E and related chain-breaking phenolic antioxidants in vitro. *Journal of the American Chemical Society* 103, 6472-6477, **1981**.
22. Maillard, B., Ingold, K.U. & Scaiano, J.C. Rate constants for the reactions of free radicals with oxygen in solution. *Journal of the American Chemical Society* 105, 5095-5099, **1983**.
23. Niki, E., Saito, T., Kawakami, A. & Kamiya, Y. Inhibition of oxidation of methyl linoleate in solution by vitamin E and vitamin C. *Journal of Biological Chemistry* 259, 4177-4182, **1984**.
24. Barclay, L.R.C., Baskin, K.A., Dakin, K.A., Locke, S.J. & Vinqvist, M.R. The antioxidant activities of phenolic antioxidants in free radical peroxidation of phospholipid membranes. *Canadian Journal of Chemistry* 68, 2258-2269, **1990**.
25. Barclay, L.R.C. & Ingold, K.U. Autoxidation of biological molecules. 2. Autoxidation of a model membrane. Comparison of the autoxidation of egg lecithin phosphatidylcholine in water and in chlorobenzene. *Journal of the American Chemical Society* 103, 6478-6485, **1981**.
26. Barclay, L.R.C., Locke, S.J. & MacNeil, J.M. Autoxidation in micelles. Synergism of vitamin C with lipid-soluble vitamin E and water-soluble Trolox. *Canadian Journal of Chemistry* 63, 366-374, **1985**.
27. Howard, J.A. & Ingold, K.U. Absolute rate constants for hydrocarbon autoxidation. I. Styrene. *Canadian Journal of Chemistry* 43, 2729-36, **1965**.
28. Barclay, L.R.C. & Vinqvist, M.R. Phenols as Antioxidants. in *The Chemistry of Phenols* 839-908 (John Wiley & Sons, Ltd, 2003).
29. Mulder, P., Korth, H.-G., Pratt, D.A., DiLabio, G.A., Valgimigli, L., Pedulli, G.F. & Ingold, K.U. Critical Re-evaluation of the O−H Bond Dissociation Enthalpy in Phenol. *The Journal of Physical Chemistry A* 109, 2647-2655, **2005**.
30. Brigati, G., Lucarini, M., Mugnaini, V. & Pedulli, G.F. Determination of the Substituent Effect on the O−H Bond Dissociation Enthalpies of Phenolic Antioxidants by the EPR Radical Equilibration Technique. *The Journal of Organic Chemistry* 67, 4828-4832, **2002**.
31. Avila, D.V., Ingold, K.U., Di Nardo, A.A., Zerbetto, F., Zgierski, M.Z. & Lusztyk, J. Electronic Absorption Spectra of Some Alkoxyl Radicals. An Experimental and Theoretical Study. *Journal of the American Chemical Society* 117, 2711-2718, **1995**.
32. Avila, D.V., Lusztyk, J. & Ingold, K.U. Color benzyloxyl and cumyloxyl orange and 4-methoxycumyloxyl blue. Unexpected discovery that arylcarbinyloxyl radicals have strong absorptions in the visible. *Journal of the American Chemical Society* 114, 6576-6577, **1992**.
33. Das, P.K., Encinas, M.V., Steenken, S. & Scaiano, J.C. Reaction of *tert*-Butoxy Radicals with Phenols. Comparison with the Reactions of Carbonyl Triplets. *J. Am. Chem. Soc.* 103, 4162-4166, **1981**.
34. Land, E.J. & Porter, G. Primary photochemical processes in aromatic molecules. VII. Spectra and kinetics of some phenoxyl derivatives. *Transactions of the Faraday Society* 59, 2016-26, **1963**.
35. Evans, C., Scaiano, J.C. & Ingold, K.U. Absolute kinetics of hydrogen abstraction from alpha-tocopherol by several reactive species including an alkyl radical. *Journal of the American Chemical Society* 114, 4589-4593, **1992**.
36. Cosa, G. Photodegradation and photosensitization in pharmaceutical products: assessing drug phototoxicity. *Pure and Applied Chemistry* 76, 263-275, **2004**.
37. Cosa, G. & Scaiano, J.C. Laser techniques in the study of drug photochemistry. *Photochemistry and Photobiology* 80, 159-174, **2004**.

38. Bowry, V.W. & Ingold, K.U. Extraordinary Kinetic Behavior of the a-Tocopheroxyl (Vitamin E) Radical. *Journal of Organic Chemistry* 60, 5456-67, **1995**.
39. Kamal-Eldin, A. & Appelqvist, L.-Å. The chemistry and antioxidant properties of tocopherols and tocotrienols. *Lipids* 31, 671-701, **1996**.
40. Rehm, D. & Weller, A. KINETICS OF FLUORESCENCE QUENCHING BY ELECTRON AND H-ATOM TRANSFER. *Israel Journal of Chemistry* 8, 259-&, **1970**.
41. Turro, N.J., Ramamurthy, V. & Scaiano, J.C. *Principles of Molecular Photochemistry: An Introduction*, 495 (University Science Books, Sausalito, CA, 2009).
42. Tachiya, M. Energetics of electron transfer reactions in polar solvents. *Chemical Physics Letters* 230, 491-4, **1994**.
43. Lai, R.Y. & Bard, A.J. Electrogenerated Chemiluminescence 71. Photophysical, Electrochemical, and Electrogenerated Chemiluminescent Properties of Selected Dipyrromethene-BF2 Dyes. *Journal of Physical Chemistry B* 107, 5036-5042, **2003**.
44. Moore, G.F., Hambourger, M., Gervaldo, M., Poluektov, O.G., Rajh, T., Gust, D., Moore, T.A. & Moore, A.L. A Bioinspired Construct That Mimics the Proton Coupled Electron Transfer between $P680^{+}$ and the TyrZ-His190 Pair of Photosystem II. *Journal of the American Chemical Society* 130, 10466-10467, **2008**.
45. Webster, R.D. New Insights into the Oxidative Electrochemistry of Vitamin E. *Accounts of Chemical Research* 40, 251-257, **2007**.
46. Williams, L.L. & Webster, R.D. Electrochemically Controlled Chemically Reversible Transformation of α-Tocopherol (Vitamin E) into Its Phenoxonium Cation. *Journal of the American Chemical Society* 126, 12441-12450, **2004**.
47. Frisch, M.J.T., G. W.; Schlegel, H. B.; Scuseria, G. E.; Robb, M. A.; Cheeseman, J. R.; Montgomery, Jr., J. A.; Vreven, T.; Kudin, K. N.; Burant, J. C.; Millam, J. M.; Iyengar, S. S.; Tomasi, J.; Barone, V.; Mennucci, B.; Cossi, M.; Scalmani, G.; Rega, N.; Petersson, G. A.; Nakatsuji, H.; Hada, M.; Ehara, M.; Toyota, K.; Fukuda, R.; Hasegawa, J.; Ishida, M.; Nakajima, T.; Honda, Y.; Kitao, O.; Nakai, H.; Klene, M.; Li, X.; Knox, J. E.; Hratchian, H. P.; Cross, J. B.; Bakken, V.; Adamo, C.; Jaramillo, J.; Gomperts, R.; Stratmann, R. E.; Yazyev, O.; Austin, A. J.; Cammi, R.; Pomelli, C.; Ochterski, J. W.; Ayala, P. Y.; Morokuma, K.; Voth, G. A.; Salvador, P.; Dannenberg, J. J.; Zakrzewski, V. G.; Dapprich, S.; Daniels, A. D.; Strain, M. C.; Farkas, O.; Malick, D. K.; Rabuck, A. D.; Raghavachari, K.; Foresman, J. B.; Ortiz, J. V.; Cui, Q.; Baboul, A. G.; Clifford, S.; Cioslowski, J.; Stefanov, B. B.; Liu, G.; Liashenko, A.; Piskorz, P.; Komaromi, I.; Martin, R. L.; Fox, D. J.; Keith, T.; Al-Laham, M. A.; Peng, C. Y.; Nanayakkara, A.; Challacombe, M.; Gill, P. M. W.; Johnson, B.; Chen, W.; Wong, M. W.; Gonzalez, C.; and Pople, J. A.; . *Gaussian 03, Revision C.02, Gaussian, Inc., Wallingford CT,* **2004**.
48. Koch, W.H., M. C. A Chemist's Guide to Density Functional Theory. *Second edition ed.; Wiley-VCH: Weinheim, Germany* **2000**.
49. We note that the decay arises mostly from a short lived species, but a secondary long lived species is also observed. We have repeated this experiment a considerable number of times with different B-TOH batches, and in all cases we obtain the same result, we attribute the long lived intermediate to the partial oxidation of the probe taking place upon preparing the solution (see also the text related to Figure 4C).
50. Wayner, D.D.M. & Burton, G.W. in *Handbook of Free Radicals and Antioxidants in Biomedicine*, Vol. 3 223-232 (CRC Press, Boca Raton, Fl, 1989).
51. Amat-Guerri, F., Liras, M., Carrascoso, M.L. & Sastre, R. Methacrylate-tethered analogs of the laser dye PM567-synthesis, copolymerization with methyl methacrylate and photostability of the copolymers. *Photochemistry and Photobiology* 77, 577-584, **2003**.

Molecular Imaging of Lipid-Peroxyl Radicals in Living Cells with a Bodipy-α-Tocopherol Adduct

Armen Khatchadourian, Katerina Krumova, Sebastien Boridy, An Thien Ngo, Dusica Maysinger, Gonzalo Cosa; *Biochemistry* 2009, 48, 5658–5668

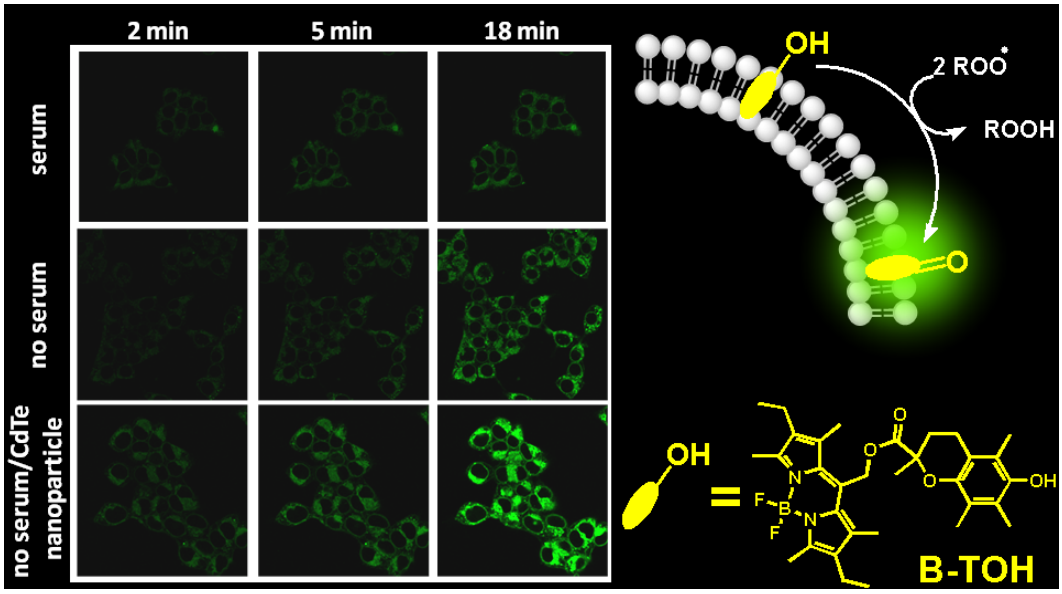

Preface

In Chapter 2 we showed that B-TOH is nearly as reactive as α-tocopherol towards H-atom abstraction by peroxyl radicals. B-TOH marked sensitivity arises from an intramolecular photoinduced electron transfer (PeT) "off-on" switch. Upon peroxyl radical scavenging, oxidation of the receptor segment deactivates PeT leading to a 10-fold fluorescence enhancement observed in homogeneous solutions. Critical to establishing the potential of B-TOH as a lipophilic ROS sensor *in vivo* is to test its chemical sensitivity and molecular specificity in model lipid membranes and further to extend the studies to imaging ROS in the lipid membrane of live cells.

In this chapter we show that in model lipid membranes a 5-fold fluorescence enhancement is observed upon reaction of liposome-embedded B-TOH with peroxyl radicals. The enhancement is independent of the solution pH and membrane composition. In studies with live cells performed under states of growth factor withdrawal and externally induced oxidative stress a significant increase in B-TOH emission was also observed. As exogenous sources of free radicals methyl viologen and uncoated non-emissive CdTe nanoparticles were utilized. The recorded fluorescence intensity of B-TOH was proportional to the concentration of the dye and to the level of cellular oxidative stress. By employing B-TOH in conjunction with fluorescent dyes such as Lysotracker and Nile Red we demonstrate the formation of peroxyl radicals under oxidative stress conditions in subcellular locations (lysosomes) in rat pheochromocytoma (PC12 cells) and in primary mouse hippocampal neural cells.

3.1. Introduction

Reactive oxygen species (ROS) such as peroxyl radicals, hydrogen peroxide or superoxide radical anion have long been implicated in oxidative damage inflicted on fatty acids, DNA and proteins as well as other cellular components.[1] Mounting evidence suggests that ROS act as messengers in cellular signaling, a new paradigm in the rich and diverse chemistry of ROS which has attracted increased attention in the last decade.[1-8]

A significant body of work, both in model membrane systems and in live cells, has examined the role lipid peroxyl radicals play in damaging the cell lipid milieu. Autoxidation of polyunsaturated fatty acid residues is initiated by a free radical such as the hydroxyl radical, which upon reaction with fatty acids generate lipid carbon centered radicals (Equation 1, Scheme 3.1).[9-13] Lipid carbon centered radicals in turn readily trap molecular oxygen under physiological conditions to form lipid peroxyl radicals,[14,15] effective chain carriers in the lipid chain auto-oxidation (Equations 2 and 3, Scheme 3.1). In the oxidation processes fatty acyl chains mostly in their *cis* configuration are either converted to the *trans* configuration,[13,16-18] or form corresponding hydroperoxides and alcohols[13,19] or may fragment into electrophilic αβ-unsaturated aldehydes,[19,20] among others. Peroxidation and destruction of the *cis* double bonds may in turn lead to a reduction in the membrane fluidity[21] and appearance of liquid order domains.[22] Autoxidation of polyunsaturated fatty acid residues ultimately generates a variety of secondary cytotoxic products which account for pathological effects *e.g.*, neurodegenerative diseases,[23] atherosclerosis,[24] and cell apoptosis.[25]

In recent years, it has become apparent that chemical reactions between peroxyl radicals and lipids may in addition play a critical role in cellular signaling.[7,8,26] Oxidative signaling pathways arise from the formation of electrophilic αβ-unsaturated aldehydes which may undergo reaction with nucleotides (indirect signaling).[8] Additional oxidative signaling pathways have been reported which involve cardiolipin peroxidation and release of proapoptotic factors from mitochondria,[27] as well as phosphatidyl serine (PS) oxidation in the

plasma membrane leading to externalization and recognition of PS on the cell surface by phagocytes.[25]

Critical to elucidating the underlying chemical mechanism behind cellular pathologies and cellular signaling process is the development of novel probes with the partition, chemical sensitivity, and molecular specificity enabling the spatial and temporal imaging of peroxyl radicals in the lipid membranes of live cells. We have recently made significant progress in this direction by preparing a lipid soluble probe capable of reporting the presence of peroxyl radicals in homogeneous solution. The two-segment receptor-reporter type free radical scavenger-fluorophore probe B-TOH (a Bodipy-α-tocopherol adduct, Scheme 3.1) satisfies the necessary specificity, sensitivity, and spectroscopic requirements.[28,29]

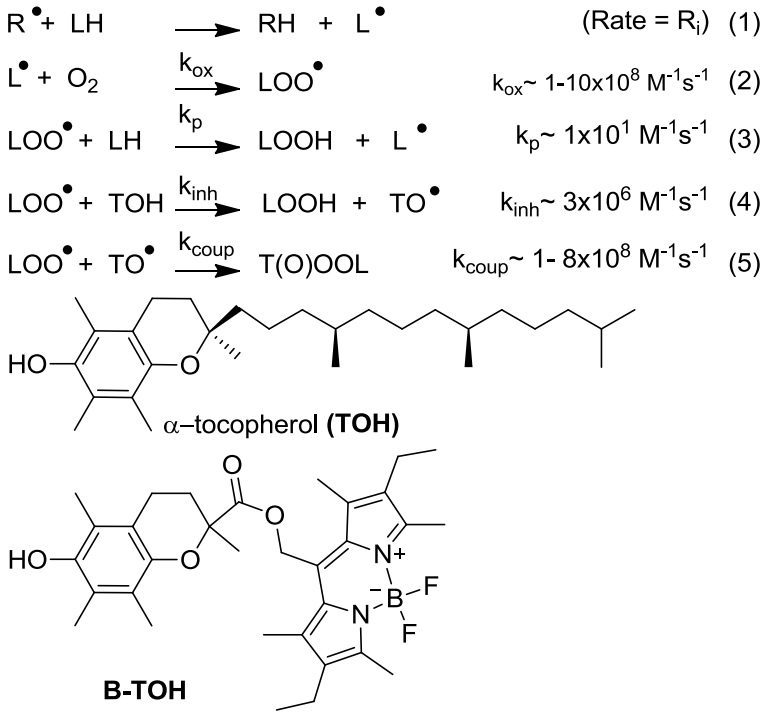

Scheme 3.1: Lipid (L) oxidation in the presence of a free radical initiator (R•) and α-tocopherol (TOH); eq 2,[14] 3,[15] 4,[30] 5.[31] Also shown are the structures of α-tocopherol (TOH) and B-TOH. Note that equations 4 and 5 are also applicable to B-TOH.[28]

The molecular specificity of B-TOH arises from the potent lipid peroxyl radical-scavenging activity conferred by the chromanol ring in the receptor segment. This chromanol ring architecture mirrors that found in α-tocopherol, the

most active naturally-occurring lipid soluble antioxidant[32] (see Equations 4 and 5 in Scheme 3.1 for rate constant values for radical scavenging by α-tocopherol). We have shown that B-TOH is nearly as reactive as α-tocopherol in the reaction involving H-atom transfer to a peroxyl radical (Equation 4 in Scheme 1). The rate constant for H-atom transfer measured for B-TOH in toluene (k_{inh} = 1.0 x 10^6 $M^{-1}s^{-1}$) is only 0.63-fold that of 2,2,5,7,8-pentamethyl-6-hydroxychroman (k_{inh} = 1.6 x 10^6 $M^{-1}s^{-1}$), an α-tocopherol analogue lacking the phytyl tail.[28]

B-TOH sensitivity is given by an intramolecular photoinduced electron transfer (PeT) "off-on" switch activated following reaction with peroxyl radicals.[28,33] Fast intramolecular PeT from the receptor segment (chromanol ring) to the reporter segment (Bodipy dye) renders the probe non-emissive. Upon peroxyl radical scavenging, oxidation of the receptor segment deactivates PeT leading to a 10-fold fluorescence enhancement.

Here we report results on the detection of peroxyl radicals in model lipid membranes and real-time imaging of peroxyl radicals in the lipid membranes of live cells, studies which were conducted with B-TOH.

To explore the role of membrane composition and pH on the activity and sensitivity of B-TOH, we initially characterized the fluorescent properties of B-TOH in liposomes (water filled unilamellar lipid bilayers). This was a necessary preliminary step to our studies within the complex environment of the cell milieu. We next performed experiments with live cells. Our ultimate objective was to assess the suitability of B-TOH for detecting peroxyl radicals in the lipid membrane of living cells in two different models: rat pheochromocytoma (PC12 cells) and mouse primary hippocampal cells. Our aim was also to reveal the subcellular localization where B-TOH undergoes fluorescence enhancement in states of growth factor withdrawal and increased oxidative stress. We explored the consequences that exposure to either N,N'-dimethyl-4,4'-bipyridinium dichloride (also known as methyl viologen or paraquat) or CdTe nanoparticles has on cells deprived of serum, a state known to induce mild to moderately intense oxidative stress. The choice of these reagents as source of oxidative stress is ultimately guided by the well understood effect of methyl viologen on biological

systems[34-39] and by our own interest and ongoing work in assessing and quantifying markers of the toxicity that CdTe nanoparticles exert in biological tissues.[40-43] By employing specific, established dyes for the labeling of multiple cell components, we demonstrate peroxyl radical formation at multiple sites in these cells. Our results underscore the potential of B-TOH as a sensitive and specific probe enabling the molecular imaging of peroxyl radicals in the lipid membrane of live cells.

3.2. Results

3.2.1. Partition Coefficient

We first measured the partition coefficient ($P_{O:W}$) of the probe between *n*-octanol and water in order to estimate the affinity of B-TOH for the lipid membrane. A value of $P_{O:W} = 1.9 \times 10^4 \pm 1 \times 10^3$ was obtained for B-TOH. The value we measured for the B-TOH precursor PMOH was $P_{O:W} = 9 \times 10^3 \pm 1 \times 10^3$. Reported *n*-octanol:water partition coefficients for α-tocopherol range from 3.9×10^{10} to 1.6×10^{12}.[44,45] We may thus conclude that B-TOH has a high affinity for the lipid membrane, albeit smaller than that of α-tocopherol.

3.2.2. Liposome Studies

We next evaluated the reactivity and emissive properties of B-TOH when embedded in the lipid membrane of liposomes at different pH conditions and in the presence or absence of peroxyl radicals. Control experiments were performed with PMOH. Two different lipid compositions were utilized in preparing the liposomes: 1,2-dimyristoyl-*sn*-glycero-3-phosphocholine (DMPC, saturated fatty acid chains, 14 carbon atoms in length) and egg phosphatidylcholine (EggPC, consisting of a mixture of various phospholipids containing polyunsaturated, unsaturated and saturated fatty acids with chain lengths of 16 or more carbon atoms, with a saturated to unsaturated mole ratio of 0.82).

In the first set of experiments, we monitored the emission of liposome-embedded B-TOH in the presence of peroxyl radicals generated at a constant rate

upon thermolysis of 2,2'-azobis(2-methylpropionamide) dihydrochloride (ABAP) under air (Scheme 3.2).[10,46]

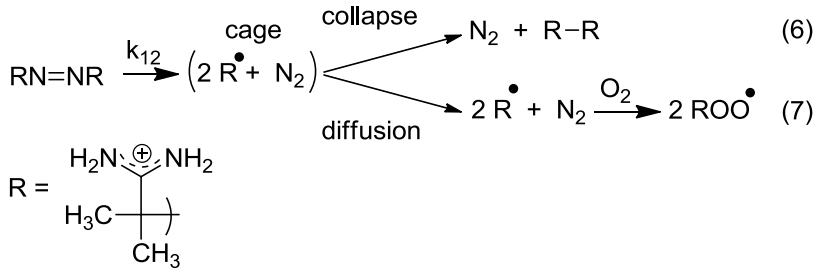

Scheme 3.2: Production of peroxyl radicals (ROO$^{\bullet}$) following thermolysis of ABAP. ABAP initially decomposes in a first order reaction to yield two geminate carbon centered radicals which may either recombine (Equation 6) or diffuse away (Equation 7). In air equilibrated solutions radicals that escape cage recombination will readily trap molecular oxygen[47] to yield two water soluble peroxyl radicals.

Liposomes 100 nm in diameter containing on average 13 B-TOH molecules each (lipid:fluorophore mole ratio = 7,700:1) were prepared in a pH 7.0 phosphate buffer solution and incubated at 37 ^{o}C in the presence of 9 mM ABAP. A linear increase in emission intensity was observed over time for B-TOH when embedded both in DMPC and EggPC liposomes. The intensity increase was faster in DMPC liposome solutions than in EggPC liposome solutions, yet in both cases it leveled off once a *ca.* 5-fold enhancement had occurred (Figure 3.1). Upon prolonged exposure to peroxyl radicals, the emission intensity slowly decreased in EggPC liposome solutions, a *ca.* 9-fold faster drop in intensity was initially observed in DMPC. In the case of control experiments with PMOH, the fluorescence intensity dropped from the start of the experiment, and it qualitatively followed the same rate as that observed for B-TOH samples once they had reached their maximum emission enhancement. In the absence of ABAP we observed no changes in emission intensity over a period of 2 hours either for B-TOH or P-MOH (see below).

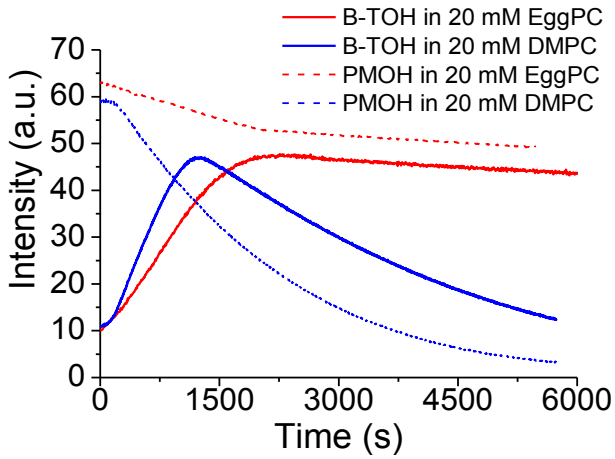

Figure 3.1: Emission intensity time profiles for B-TOH and PMOH embedded in DMPC and EggPC liposome suspensions incubated at 37°C with ABAP, λ_{exc} = 514 nm, λ_{em} = 565 nm.. Samples were air equilibrated, solutions 2.6 μM in B-TOH, 9 mM in ABAP and 20 mM in DMPC or 20 mM in EggPC were prepared in a pH 7.0 phosphate buffer. Data points were taken every 5 seconds.

We also tested what effect, if any, the solution pH has on membrane-embedded B-TOH reactivity. DMPC liposomes *ca.* 100 nm in diameter containing *ca.* 13 B-TOH or PMOH molecules each (lipid:fluorophore mole ratio = 7,700:1) were prepared in various buffers with pH values ranging between 2.2 and 10.3. ABAP was added to one set of solutions at each pH for each dye. A second set was left as a control. In the absence of peroxyl radicals (Figure 3.2) we observed that the emission intensity for both dyes remained constant with time at all pH values under these conditions. In the presence of peroxyl radicals, generated at a constant rate upon thermolysis of ABAP at 37 °C in air saturated solutions (see Scheme 3.2), we observed a 4-fold increase in the emission of B-TOH (Figure 3.2). In conclusion, neither the reactivity of B-TOH nor its emission properties changed with pH.

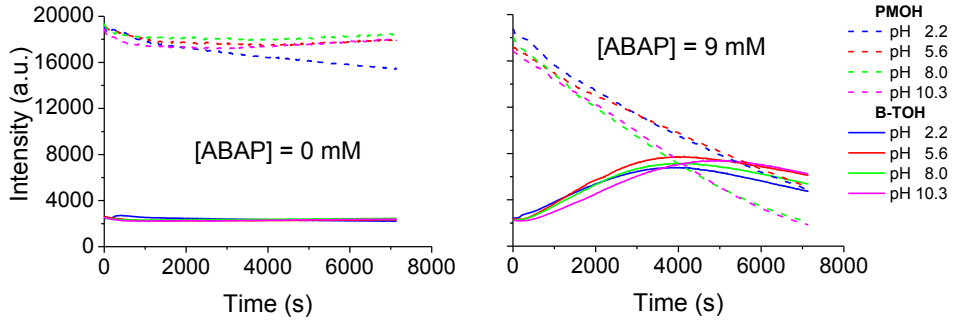

Figure 3.2: Emission intensity time profiles for B-TOH and PMOH embedded in DMPC liposome suspensions incubated at 37°C without (left) and with (right) ABAP. Samples were air equilibrated. Solutions of 2.59 μM dye, 10 mM DMPC and 9 mM ABAP were prepared in pH values of 2.2, 5.6, 8.0 and 10.3. Data points were taken every 19 seconds. The liposome dispersion prepared at pH 2.2 was significantly less turbid than the others, and its emission was ca. 1.45 larger than that measured at all other pH values, thus the traces obtained at this pH were divided by the 1.45 factor in this figure.

In addition to the steady state emission experiments described above, we measured the fluorescence lifetime for B-TOH when embedded within lipid membranes, in an attempt to establish the reason for the lower sensitivity observed in liposome membranes (on:off ratio of 5) as compared to homogeneous solutions in toluene or hexanes (on:off ratio $\geq$ 10). Liposomes 100 nm in diameter containing on average 260 B-TOH or PMOH molecules each (lipid:fluorophore mole ratio = 385:1) were prepared in a pH 7.0 phosphate buffer. Under these loading conditions, no fluorescence self-quenching is expected to take place within the bilayer. Figure 3.3 shows the fluorescence decay for B-TOH and PMOH when embedded in EggPC and DMPC liposomes.

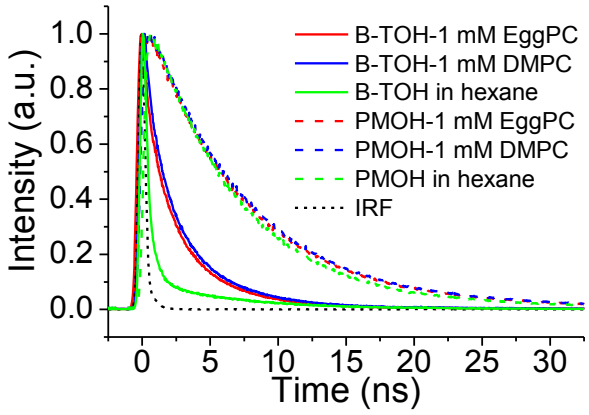

Figure 3.3: Fluorescence decay profiles for 2.6 μM B-TOH and PMOH in 1 mM DMPC or 1 mM EggPC liposomes; λ_{exc} = 470 nm, λ_{em} = 565 nm. Also shown are the decays of PMOH and B-TOH in hexane.

Table 3.1 summarizes the relevant emission decay lifetimes (τ_{decay}). Whereas PMOH has a single exponential decay in both lipid systems, B-TOH reveals multiexponential decays which can be fitted with a biexponential function as shown in Equation 8, where $k_{decay(i)}$ is the decay rate constant and a_i is the preexponential factor or weight. The average emission decay lifetime for B-TOH is *ca.* 4-fold smaller than the fluorescence decay lifetime for PMOH.

$$I = a_1 \times \exp^{-(k_{decay(1)} \times t)} + a_2 \times \exp^{-(k_{decay(2)} \times t)} \qquad (8)$$

	lipid	τ_{decay1} (ns)	a_1	τ_{decay2} (ns)	a_2	$\langle\tau_{decay}\rangle$ (ns)
PMOH	DMPC	7.27	1	N.A.	N.A.	7.27
	EggPC	7.19	1	N.A.	N.A.	7.19
	Hexanes	[a]6.57	1	N.A.	N.A.	6.57
B-TOH	DMPC	1.18	0.52	3.88	0.48	1.8
	EggPC	1.12	0.51	3.63	0.49	1.7
	Hexanes	[a]0.44	1	N.A.	N.A.	0.44

Table 3.1: Fluorescence decay lifetime values for B-TOH and PMOH when embedded in lipid membranes. $\tau_{decay(i)} = 1/k_{decay(i)}$; see equation 8 for a_i and $k_{decay(i)}$ definitions. [a]From reference [28].

3.2.3. Live Cell Studies

Our next goal was to apply B-TOH for detection and imaging of peroxyl radicals in the lipid membrane in live cells. We chose as sources of reactive oxygen species methyl viologen, a well established pro-oxidant agent, and unprotected CdTe nanoparticles known to leak Cd^{2+} into the solution, thus indirectly promoting the formation of ROS.[48]

Treatment of PC12 cells with CdTe nanoparticles or methyl viologen in the absence of trophic factors leads to severe oxidative stress and cell death.[43] We first established the concentration of B-TOH required for the detection of peroxyl radicals in living (unfixed) PC12 cells under optimal and stressed (*i.e.* serum-starved) conditions using a wide field fluorescent microscope. A series of B-TOH concentrations were tested (Figure 3.4A). In PC12 cells deprived of growth factors there was a marked increase in the B-TOH fluorescence intensity when CdTe nanoparticles, known to enhance oxidative stress in serum-deprived conditions, were added.[43]

A concentration dependent increase in fluorescence intensity was observed when treating cells with 4–24 μM B-TOH for 10 minutes. The presence of peroxyl radicals in cells exposed to CdTe nanoparticles was easily detectable by employing any B-TOH concentration between 4 and 24 μM (Figure 3.4A). The green fluorescent signal was diffuse within the cells at higher concentrations. This diffuseness could be partly caused by the leakiness of cellular membranes damaged by the CdTe nanoparticles, as demonstrated in previous studies employing propidium iodide as a label.[43]

We carried out all subsequent experiments with either 1 μM or 5 μM concentrations, since the signal saturated above 8 μM B-TOH (see Figure 3.4A). These experiments were conducted using a confocal microscope to gain a detailed spatial resolution in terms of probe localization in membranes and organelles (Figure 3.4B). Confocal micrographs from these studies show that PC12 cells stressed with CdTe nanoparticles (10 μg/ml, 4h) become highly emissive at the cell membrane and at the membranes of multiple organelles (Figure 3.4B).

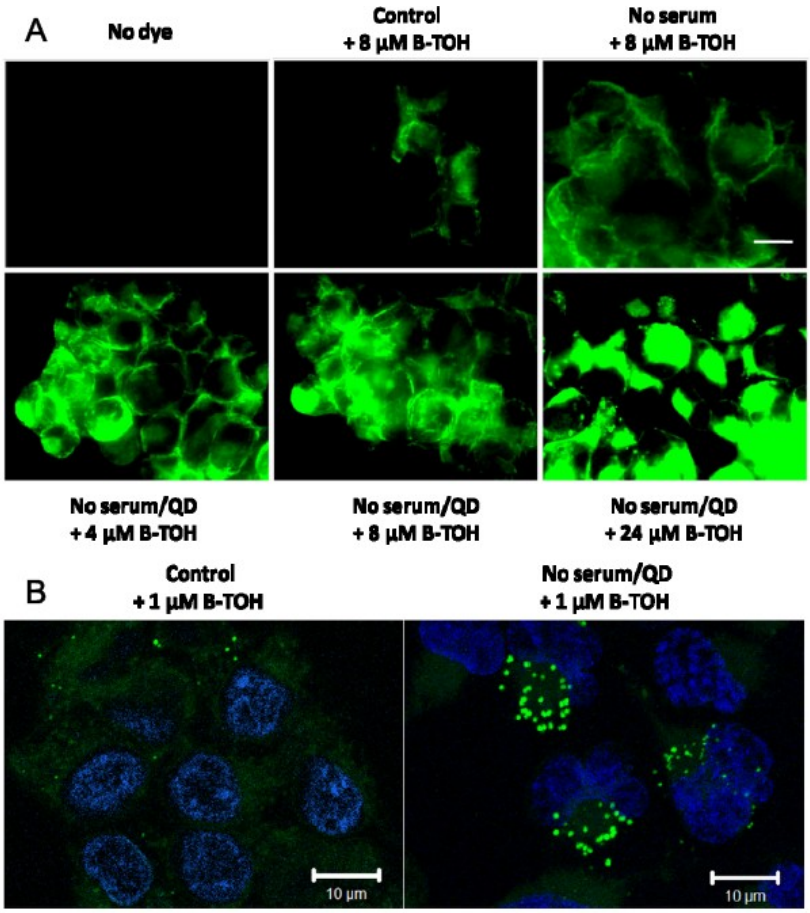

Figure 3.4: Detection of lipid peroxidation with B-TOH under different conditions in PC12 cells. A) Live adherent PC12 cells were stained with increasing concentrations of B-TOH in the absence of treatment, 20 h serum withdrawal or 4h CdTe nanoparticle (CdTe np)/serum free (10 µg/ml). Cell images were taken within 10 minutes of B-TOH staining. Bar = 20 µm. B) Confocal micrographs showing B-TOH staining in untreated (left) and CdTe nanoparticle treated (right) (10 µg/ml, 4h) live PC12 cells. Nuclei (blue) were stained with Hoechst 33342 (10 µM) for 30 min. Bars 10 µM.

To examine the dynamics and quantify the relative amount of lipid peroxyl radicals in live PC12 cells, we performed time lapse experiments with a confocal microscope. PC12 cells were deprived of serum overnight, and one fraction of the cells was additionally treated with CdTe nanoparticles (5 µg/ml) for 4h. Subsequently each set of cells was incubated with B-TOH (5µM) for up to 18 min. Excitation of B-TOH at 488 nm was performed to image the cells. For those cells that were incubated overnight without trophic factors (serum deprived), we observed that the fluorescence of B-TOH increased in a time-dependent manner (Figures 3.5A and 3.6). Additionally, treating serum deprived cells with CdTe nanoparticles caused an even larger amplification in the

fluorescence of B-TOH (Figures 3.5B and 3.6). Following 18 min incubation, we observed a 19-fold increase (relative to autofluorescence) in the B-TOH emission signal for the CdTe nanoparticle treated cells, compared to 15-fold in the serum free (no CdTe nanoparticle) condition (Figure 3.5). The induction of lipid peroxidation by CdTe nanoparticles was partially inhibited by the addition of a commonly used antioxidant molecule N-acetylcysteine (NAC).[40,43] Treatment with NAC for 2h prior to CdTe nanoparticle addition attenuated the magnitude of the B-TOH fluorescence enhancement observed with the CdTe nanoparticles (Figure 3.5B *vs.* 3.5C, also see Figure 3.6). At 18 min, the increase in the B-TOH signal in NAC-treated samples was 15-fold (relative to autofluorescence), compared to 19-fold in CdTe nanoparticle treated cells. Finally, at 18 min the increase in the magnitude of the B-TOH signal for control cells incubated with serum was 5-fold. A similar result was obtained for cells incubated with serum but treated with CdTe nanoparticle. Arguably, the small increase in intensity is due to low levels of lipid peroxidation in cells cultured in serum-containing media. The increase may also be in part due to slow uptake of B-TOH via endocytic process, what has been shown to take place over several minutes for labeled α-tocopherol in hepatocytes.[49]

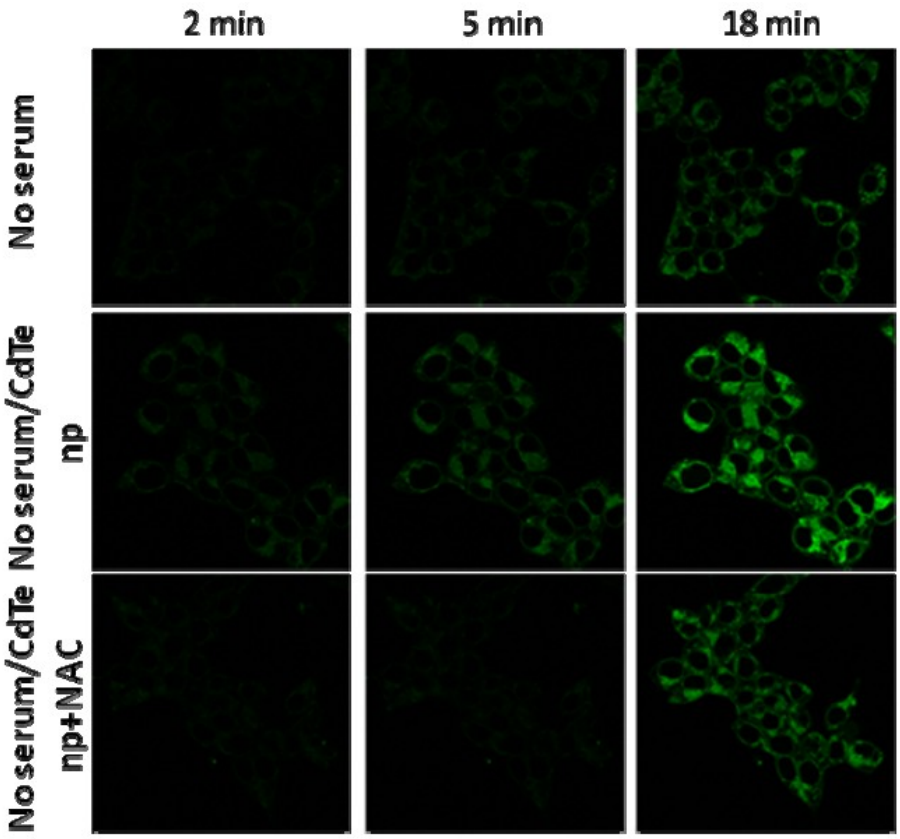

Figure 3.5: B-TOH as a sensor for dynamic changes in peroxyl radical formation in PC12 cells. The top three panels illustrate the time dependent increase of B-TOH fluorescence for A) serum-deprived PC12 cells, B) serum-deprived and CdTe nanoparticle (CdTe np) treated PC12 cells, and C) serum-deprived, CdTe nanoparticle treated and N-acetylcysteine (NAC) treated PC12 cells. The bar is 20 μM in all cases. PC12 cells were deprived of serum overnight and treated with CdTe np (5 μg/ml) for 4h. NAC (2 mM) was added to the cell culture medium 2h prior to the addition of CdTe np. Cells were then incubated with B-TOH (5 μM) for the indicated periods of time.

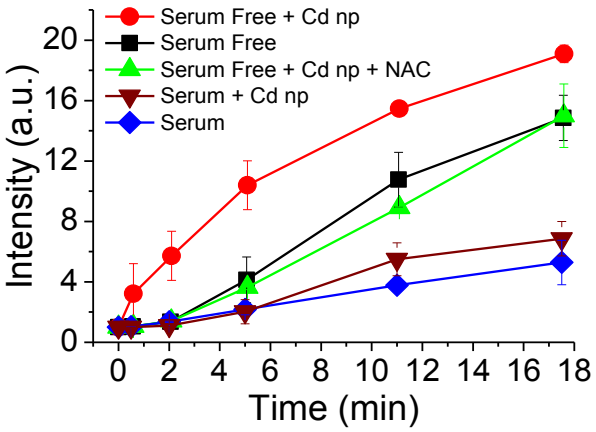

Figure 3.6: B-TOH fluorescence intensity *vs.* time plot recorded for PC12 cells that were ●) deprived of serum and treated with CdTe np, ■) deprived of serum, ▲) deprived of serum, treated with CdTe np and treated with NAC, ▼) incubated with serum and treated with CdTe np, and ◆) incubated with serum. The fluorescence intensity was normalized by the number of cells present

in each field of view, the increase in B-TOH emission intensity is normalized to the autofluorescence of the cells (emission at t =0). Y-Axis values represent means of at least two independent experiments. PC12 cells were deprived of serum overnight and treated with CdTe nanoparticles (5 µg/ml) for 4h. NAC (2 mM) was added to the cell culture medium 2h prior to the addition of CdTe nanoparticles. Cells were then incubated with B-TOH (5 µM) for the indicated periods of time.

Altogether, these experiments report on the relative concentration of lipid peroxyl radicals in live cells under various treatments/conditions and underscore that changes in the extent of lipid peroxidation can be measured with B-TOH.

We additionally examined the presence of peroxyl radicals in the membranes of different subcellular structures of growth factor-deprived PC12 cells. Imaging was done with a confocal microscope upon staining with B-TOH (1 µM for 10 min) and with Nile Red (1.57 µM for 10 min), a commonly used dye for labeling neutral lipids and phospholipids in living and fixed cells [50] (Figure 3.7).

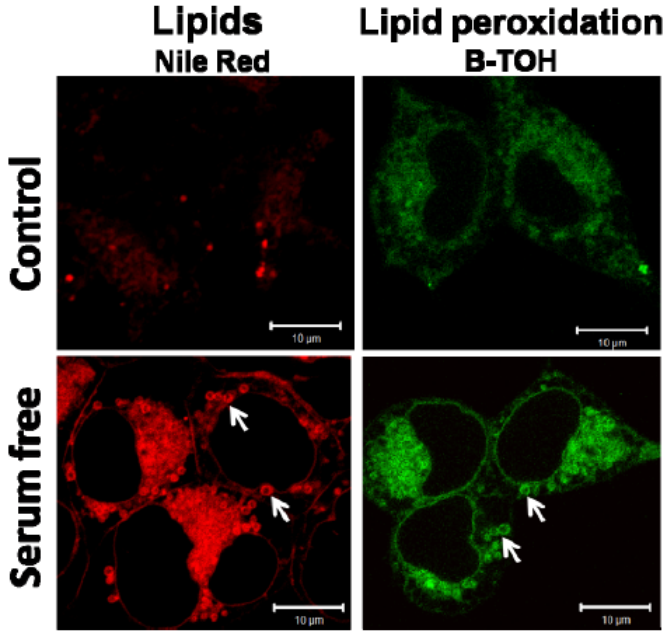

Figure 3.7: Detection of peroxyl radicals by B-TOH and of cytoplasmic compartments by staining with Nile Red. Living PC12 cells in serum-containing and serum-free medium (24h) were stained with Nile Red (1.57 µM for 10 min) for lipids and with B-TOH (1 µM for 10min) for peroxyl radicals. Arrows indicate ring-like structures reminiscent of autophagic vacuoles. The bars are 10 µm.

Under growth factor deprivation conditions, B-TOH localized in ring-like structures in PC12 cells where Nile Red also localized. The observed ring-like

structures are reminiscent of a specific vesicular structure, the autophagosomes, which typically develop in cells under oxidative stress and starvation.[51,52]

We then examined peroxyl radical formation on another subcellular compartment, the lysosome. Lysotracker Red DND-99 is an acidotropic dye used to stain lysosomes. The colocalization of oxidized B-TOH (1μM for 10 min) and of Lysotracker Red DND-99 (500 nM for 3 min), ultimately reveals the presence of peroxyl radicals in lysosomes (Figure 3.8). B-TOH and Lysotracker labeling in mouse hippocampal cultures stressed with methyl viologen (10μM for 24h, see Figure 3.8), conveys a similar message: B-TOH reports on the presence of lipid peroxyl radicals in lysosomes of live cells under oxidative stress and growth factor deprivation.

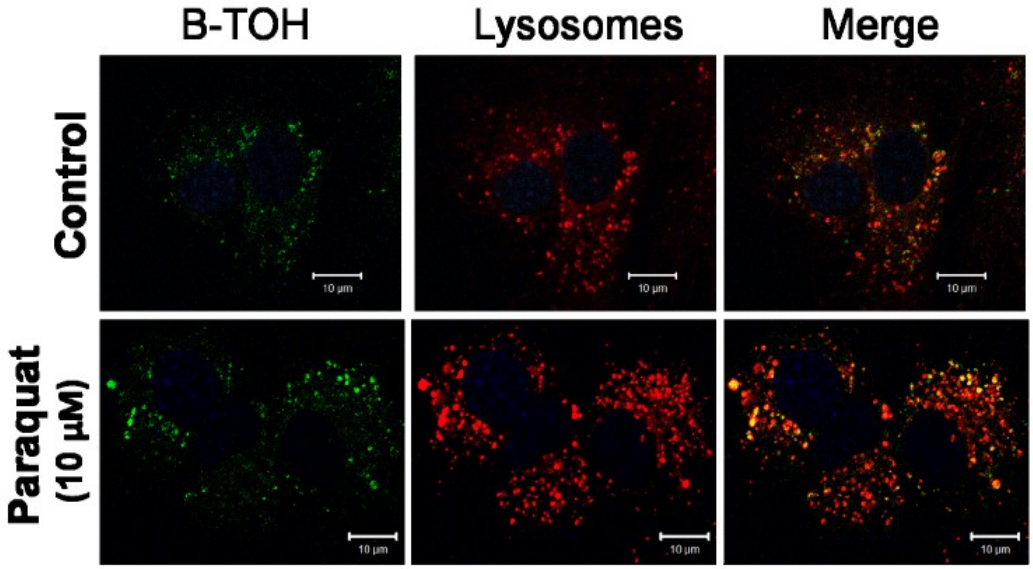

Figure 3.8: Lipid peroxidation and acidic cytoplasmic compartments in primary culture of mouse hippocampus. Lipid peroxidation was induced by treating hippocampal neural cultures with methyl viologen (10 μM) for 24h. Lipid peroxidation is colored green and was detected by B-TOH (1μM for 10 min), and lysosomes (red) were detected using lysotracker DND-99 (500 nM for 3 min). Hoechst (10 μM for 30min) staining reveals nuclei (blue). The bars are 10 μm.

3.3. Discussion

3.3.1. Liposome Studies

The observed fluorescence enhancement of B-TOH upon reaction with peroxyl radicals when embedded in either liposomes or cellular lipid organelles is consistent with B-TOH molecular mechanism of action. The scavenging of two lipid peroxyl radicals by B-TOH, concomitant with the oxidation of the

chromanol head in the receptor segment, deactivates the PeT quenching mechanism (off-state), leading to emission enhancement (on-state).[28,29] We observed no pH dependence on the B-TOH fluorescence enhancement when embedded within liposomes; we can thus rule out any contribution arising from the hydrolysis of the ester linkage between the receptor and reporter end. The fluorescent enhancement is due solely to the reaction of B-TOH with peroxyl radicals.

Under the experimental conditions employed, the emission enhancement is *ca.* 5-fold in the presence of peroxyl radicals produced upon ABAP thermolysis under air. This value is lower than that anticipated from homogeneous solution studies, where enhancements of *ca.* 10-fold have been measured. We thus conducted fluorescence lifetime studies on B-TOH and PMOH to elucidate the photophysical behavior of the probe within the lipid media.

PMOH decay is monoexponential and its characteristic decay rate constant is similar to that determined in homogeneous solutions (see Table 3.1).[28] This is not surprising since the photophysical properties of Bodipy fluorophores do not show a significant solvent effect.[53] B-TOH undergoes multiexponential fluorescence decay when intercalated within the lipid membrane, where the decay rate can be fit by a minimum of two exponential terms. Further, the average fluorescence lifetime is significantly larger than that for B-TOH in homogeneous solution (1.7 and 0.44 ns, respectively).

One may show (see Equation 9) that given the average fluorescence lifetime (τ_{decay}) for B-TOH is *ca.* 4-fold smaller than the emission decay lifetime for PMOH in the lipid membrane, and considering that the Bodipy radiative lifetime (τ_r) is not be affected by the solvent,[53] the intensity enhancement for B-TOH upon oxidation by peroxyl radicals should not surpass a value of 4 or 4.5, consistent with our experimental observations.

$$\phi_f = \frac{\tau_{decay}}{\tau_r} \qquad (9)$$

The multiexponential behavior in B-TOH decay is consistent with the probe experiencing a range of environments within the lipid bilayer. Motion restriction

of the receptor-reporter segments provides a plausible explanation for B-TOH's larger τ_{decay} during its "off" state in lipid membrane vs. in homogeneous solution, where one may foresee that the receptor and reporter segments are required to mutually approach in order for intramolecular electron transfer to occur. Interestingly, in EggPC membranes the B-TOH fluorescence lifetime is somewhat shorter than in DMPC membranes. This most probably reflects a more fluid environment for the probe in the former case.[54]

Having discussed the photophysics for B-TOH and PMOH when membrane-intercalated, we next address its reactivity in model lipid membranes. The linear growth in intensity (and consumption of B-TOH) over time is consistent with a rate law which is zero order with respect to the receptor (antioxidant) segment in B-TOH. By analogy to our previous studies in homogeneous solution, we assign the initial rise in intensity to the two-radical oxidation of the chromanol head in B-TOH into a chromanone or chromoquinone.[23]

Significant information on the probe reactivity may be obtained from our studies under controlled generation of peroxyl radicals.[10,46,55] According to Equation 10, at any given time "t" the total yield of peroxyl radicals can be estimated based on the rate of thermolysis of ABAP at 37°C (k_{12}), on the fraction of geminate radicals that escape recombination (e) and on the initial concentration of ABAP (see Scheme 3.2, Equations 1 and 2).

$$\left[ROO^{\bullet}\right]_t = 2ek_{12}\left[ABAP\right]\times t \qquad (10)$$

The time for complete consumption of the probe (or induction period τ) can be then estimated and compared to the experimental values (see Equation 11). Our estimates yield a τ value of 517 s under the experimental conditions (2.6 μM B-TOH and 9 mM ABAP, 37°C). A main assumption in the above estimate is that all peroxyl radicals formed are scavenged by B-TOH, *i.e.* $2[\text{B-TOH}]_0 = [ROO^{\bullet}]_t$, where we utilized a stoichiometric factor of 2 for B-TOH scavenging of peroxyl radicals (see also Equations 4 and 5 in Scheme 3.1).[28] We further used the value for the escape fraction e = 0.43 obtained for ABAP in the presence of multilamellar liposomes prepared from dilinoleoylphosphatidylcholine (DLPC)[10]

and the rate constant of thermolysis value k_{12} = 1.3 x 10^{-6} s^{-1} at 37°C in buffer solution.[46]

$$\tau = \frac{2[B-TOH]}{2ek_{12}[ABAP]} \quad (11)$$

Experimentally, the time for B-TOH consumption can be obtained from the analysis of the time profile for the emission intensity growth and subsequent decay.[56] We obtained the following values: τ = 1.0 x 10^3 s in DMPC and τ = 1.6 x 10^3 s in EggPC. These values are significantly larger than the theoretical estimate of 517 s.

We may conclude based on the above observations that the probe is moderately sensitive to the membrane system under study, where we observe differences in the rate of B-TOH consumption by water-soluble peroxyl radicals. A plausible explanation for the larger than expected τ measured in EggPC and DMPC is the low availability of B-TOH to the water-soluble peroxyl radicals.[57] A low B-TOH availability will in turn lead to a larger fraction of the water soluble radicals undergoing bimolecular self-reaction to yield non-radical products.[55] In DMPC liposomes the larger rate of intensity growth recorded upon free-radical scavenging by B-TOH receptor segment correlates with the faster rate of intensity drop once the receptor segment in B-TOH is consumed. Arguably, the intercalation within DMPC and EggPC is different for the lipophilic fluorophore (either PMOH or B-TOH). Based on the above results the fluorophore lies more exposed to water soluble peroxyl radicals in DMPC than in EggPC, *i.e.* B-TOH and PMOH penetrate more readily in EggPC than in DMPC membranes. B-TOH is membrane-embedded both in EggPC and DMPC, which can be concluded both from the large octanol:water partition coefficient and from the observed emission for both probes in the lipid media (B-TOH and PMOH are non-emissive in aqueous dispersions, where they most probably form non-emissive aggregates).

A considerable body of work has gone into gaining a molecular-level understanding of the interaction of α-tocopherol with lipids in the lipid membranes. Major aspects of this topic have been recently reviewed.[58-61] Three models have been proposed to describe where tocopherols reside within

membranes,[62] where differences in the models arise on pinpointing the depth of α-tocopherol location within the membrane. Discrepancies are the result both of the different experimental methods employed as well as the type of lipids used in the studies. A prevailing picture is the one where the chromanol is recessed into the membrane, possibly involved in hydrogen bonding with either phosphate oxygen or acyl-ester oxygen atoms in the lipid.[58] It has been recently observed that whereas in palmitolyl-oleoylphosphatidylcholine (POPC) tocopherol is found high in the membrane, in dioleoylphosphatidylcholine (DOPC) it sits much deeper. It has been proposed along those lines that α-tocopherol penetration depth may increase with a greater degree of unsaturation.[58] In related work, Maggio *et al*. described the penetration of α-tocopherol and derivatives into monolayers at the air water interface.[63] They found that α-tocopherol and derivatives penetrate more readily into monolayers prepared from phospholipids with unsaturated fatty acid substituents than in monolayers prepared from their saturated counterparts. The presence of unsaturated phospholipids in mixed saturated-unsaturated lipid mixtures was also shown to facilitate the penetration of α-tocopherol and its derivatives.[63] When discussing the lipophilic tail in B-TOH, we may further point out that Bodipy preferentially partitions in membranes rich in unsaturated fatty acids as compared to membranes rich in saturated ones. This phenomena has been exploited for imaging lipid domains within lipid bilayers.[64]

Our results on the reactivity of B-TOH and its position within the membrane are in line with the results recently reviewed, *i.e.*, we observe a larger penetration depth by B-TOH in EggPC than in DMPC.[58] We note, however, that there exist significant differences in the lipophilic tail in B-TOH vs. that in α-tocopherol. Nonetheless, our data emphasizes how important the surrounding lipid structure may be in determining the peroxyl radical scavenging ability of α-tocopherol and other members of the vitamin E family, a key concept in assessing vitamin E antioxidant activity.[58]

3.3.2. Live Cell Studies

In studies at the cellular level, B-TOH was able to report both methyl viologen and CdTe nanoparticle-induced lipid peroxidation in a concentration dependent manner in PC12 cells. Methyl viologen catalyzes the reduction of molecular oxygen to water yielding various ROS intermediates along the way (Scheme 3.3).[34,35] In the presence of an electron donor methyl viologen undergoes reduction to a radical cation within the cell milieu. The radical cation may be subsequently oxidized back to methyl viologen upon reaction with molecular oxygen, yielding superoxide radical anion. A series of subsequent electron transfer and proton uptake reactions may lead to the formation of various intermediate ROS species such as hydrogen peroxide and hydroxyl radical (Scheme 3.3). Particularly, methyl viologen readily accepts electrons from hydrogen/alkylperoxides (Equation 15 in Scheme 3.7) to produce hydroxyl/alkoxyl radicals, which may in turn act as free radical initiators.

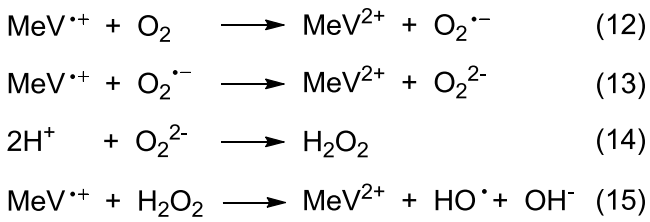

Scheme 3.3: Methyl viologen (MeV^{2+})-catalyzed reduction of oxygen into water with the formation of various ROS intermediates such as superoxide radical anion (12) hydrogen peroxide (14 and 15) and hydroxyl radical (15).[34] In the case of metal-catalyzed reduction of oxygen into water the reaction sequence is similar to that described for MeV^{2+} but replacing $Metal^{(n-1)+}$ and $Metal^{n+}$ for $MeV^{\bullet+}$ and MeV^{2+}, respectively.[34]

Previous studies indicate that CdTe nanoparticles induce ROS formation and produce lipid peroxidation in several cell types, namely in PC12 (pheochromocytoma) and SH-SY5Y (neuroblastoma) cells.[40,42] Cadmium nanoparticles, like the ones used in our experiments, release Cd^{2+} ions from their core when they are degraded. Whereas Cd^{2+} is unable to directly produce ROS, it acts by displacing iron and copper from various proteins;[39] the resulting free iron and copper ions in turn take place in a metal-catalyzed reduction of oxygen into water with the formation of various ROS intermediates along the way.[36-38] Cd^{2+} ions produce ROS by interfering with antioxidant enzymes and by causing

mitochondrial membrane dysfunction.[65,66] ROS generated by free Cd^{2+} could be responsible for initiating or reinforcing the propagation of lipid peroxidation in cells.[65]

Labeling with Nile Red clearly shows vesicular structures with double membranes in cells exposed to nutrient deprivation. Some of these double-membrane structures are stained with B-TOH, suggesting that lipid peroxidation may occur on lipidic membrane vacuoles. The localization of fluorescent B-TOH within lysosomes would be consistent with the high content of α-tocopherol that has been reported to exist within these organelles. Indeed, in rat liver subcellular membranes the α-tocopherol:phospholipid mole ratio was found to be 1:65 in lysosomes and Golgi membranes, which is an order of magnitude larger than in mithochondria, microsomes, or nuclear fraction.[59,67] Experiments with labeled α-tocopherol have also shown that it is incorporated via an endocytic process in hepatocytes, where shortly following uptake it is found within the lysosomes.[49] Whereas lysosome staining by B-TOH (visible following oxidation of B-TOH by peroxyl radicals) is indeed a reasonable assumption, this needs to be proved by detecting colocalization of B-TOH with lysosomal resident proteins, such as lysosomal-associated membrane protein-1 (LAMP1).[68]

Pretreatment with the antioxidant NAC significantly reduced the B-TOH signal in CdTe nanoparticle-treated PC12 cells, suggesting a protective role of NAC against CdTe nanoparticle-induced lipid peroxidation. The protective effects of NAC against CdTe nanoparticle-induced cytotoxicity have been demonstrated in several cell lines by several groups.[40,42] More specifically, pretreatment of cells with NAC prevented significant enhancement in lipid peroxidation following CdTe nanoparticle treatment,[40] and it reduced the levels of lipid peroxidation markers (*e.g.* 4-hydroxy-2-nonenal (HNE)) in skin fibroblasts from Alzheimer's disease (AD) patients.[69]

3.4. Conclusions

Our studies in liposomes and live cells underscore the potential of B-TOH for molecular imaging of lipid peroxyl radicals in the membrane of live cells. Numerous studies have shown that reactive oxygen species accumulate during aging and that they contribute to neurodegenerative disorders. In this study, B-TOH has been successfully used to track the formation of lipid peroxides in primary hippocampal neural cultures from mice following an oxidative insult, as illustrated in Figure 3.8. This example clearly demonstrates the potential application of B-TOH as a novel sensor suitable for peroxyl radical detection in model cells and eventually in tissues both under physiological and pathological conditions.

Our results show the following. (i) There is a 5-fold increase in emission upon reaction of lipid-intercalated B-TOH with peroxyl radicals. (ii) B-TOH is very reactive and readily traps a large fraction of peroxyl radicals when embedded within lipid membranes. (iii) B-TOH can be used as a fluorescent biomarker to examine the relative concentration of lipid peroxyl radicals in live cells under various treatments and conditions. (iv) It is possible to detect lipid peroxyl radicals in different subcellular structures, including lipid-rich vesicles and lysosomes when cells are deprived of nutrient and trophic factors.

The critical importance of monitoring lipid peroxyl radicals cannot be overemphasized. Whereas the chemistry of lipid peroxyl radicals is becoming well understood, it is unclear how this translates into cellular mechanisms. Imaging studies with specific sensors will help provide a molecular-level understanding of the role lipid peroxyl radicals play in the cellular mechanisms of pathologies and signaling. We strongly believe that our results are a step forward in this direction

3.5. Experimental Section

Preparation and characterization of B-TOH. B-TOH was prepared as described in the literature.[29]

Preparation and characterization of CdTe nanoparticles. The CdTe nanoparticles used (commonly known as quantum dots or QD) are spherical nanoparticles (2.8 nm diameter) consisting of a core rich in metals (cadmium and telluride) and coated with mercaptopropionic acid (MPA), which increases their hydrophilicity and contributes to a negatively charged surface. These nanoparticles were prepared as previously described.[43] Cells were exposed to CdTe nanoparticles at a concentration of 5 (or 10) μg/ml, which is equivalent to a 23 (or 46) nM concentration. These particles ($\lambda_{max(em)}$ = 520 nm) are not visible under our cell imaging experimental conditions (low concentration of nanoparticles and 520 nm long pass filter, see below).

B-TOH partition coefficient. The partition coefficient of B-TOH between *n*-octanol and water was measured following previously described methods.[70] A 1 mM B-TOH solution in 1:1 *n*-octanol/water was stirred for 2 h at 37 ^{o}C. The absorbance of aliquots of the aqueous and organic layer was measured at the maximum of B-TOH absorption, and blanks were prepared with a water-equilibrated *n*-octanol solution and *n*-octanol-equilibrated water solution, respectively. The absorption was used to calculate the B-TOH concentration in water ($[B\text{-}TOH]_W$) and in *n*-octanol ($[B\text{-}TOH]_O$). The *n*-octanol:water partition coefficient $P_{O:W}$ is defined according to Equation 16:

$$P_{O:W} = \frac{[B-TOH]_O}{[B-TOH]_W} \tag{16}$$

Liposome preparation. Aqueous solutions 20 mM in lipids were prepared as follows. First, 135 mg of dimirystoylphosphatidylcholine powder (DMPC, from Avanti Polar Lipids, Alabaster, Al) or 152 mg of egg phosphatidylcholine (EggPC, from Avanti Polar Lipids, Alabaster, Al) were weighed in two dry vials and dissolved with chloroform. The solvent was evaporated while rotating the sample vial to create a thin film on the vial wall. The films were left under vacuum to remove excess solvent. After 1 hour, the aliquots of DMPC and

EggPC were hydrated with 10 mL of pH 7.0, 10 mM phosphate buffer saline solution 150 mM in NaCl yielding a 20 mM DMPC and 20 mM EggPC suspensions, respectively. The lipid suspensions were subjected to 5 freeze-thaw-sonicate-vortex cycles, where each cycle involved storing the vials with the solutions in dry ice for 4 min followed by a 4 min thawing at 37 ^{o}C and a 4 min sonication at 37 ^{o}C. After the fifth cycle the lipid suspensions were extruded 15 times using an Avanti mini-extruder provided with one 100 nm polycarbonate membrane. Liposomes roughly 100 nm in diameter and each containing *ca.* 100,000 DMPC or EggPC lipids were thus obtained.[71]

We next embedded B-TOH or PMOH (the precursor to the reporter segment in B-TOH) in the liposome membranes. Each sample of DMPC and EggPC was divided into 2 equal 1.5 ml aliquots. A total of 50 μl of a DMSO solution 80.6 μM in B-TOH was injected in half of the 1.5 ml aliquots of EggPC and DMPC. The other half of the aliquots was injected with 50 μl of a DMSO solution 80.6 μM in PMOH. The DMSO solutions of B-TOH and PMOH were prepared in order to yield an absorbance of 0.18 upon diluting 50 μl of a DMSO solution in 1.5 ml of methanol. The same absorbance is expected upon their injection in the liposome dispersion. We obtained a final solution 20 mM in lipids, *ca.* 200 nM in liposomes and 2.6 μM in dye (either B-TOH or PMOH). Liposomes were prepared each containing on average 13 fluorophores with a DMPC:fluorophore mole ratio of 7,700:1. Under these loading conditions, no fluorescence self-quenching is expected to occur within the bilayer.

To conduct time resolved studies in a time correlated single photon counting setup, the 20 mM liposome solutions were first diluted 20-fold with phosphate buffer (pH 7.0) and then B-TOH or PMOH were added to yield a final solution 1 mM in lipids, *ca.* 10 nM in liposomes and 2.6 μM in dye (either B-TOH or PMOH). Solutions were 1 mM in lipids to minimize scattering in the time correlated single photon counting setup. Liposomes each containing on average 260 fluorophores, with a DMPC:fluorophore mole ratio of 380:1, were thus obtained.

Liposome preparation for pH experiments. DMPC liposomes were prepared in a similar manner as that described above, where lipid films were hydrated with 150 mM NaCl, phosphate buffer saline solutions with pH values of 2.2, 5.6, 8.0 or 10.3 yielding a 10 mM DMPC suspension

Each lipid suspension was subjected to 20 freeze-thaw-sonicate-vortex cycles (no extrusion), where each cycle involved storing the vial with the solution in dry ice for 4 min followed by a 4 min thawing at 37 ^{o}C and a 4 min sonication at 37 ^{o}C. Throughout the 20 cycles the solutions became translucent, indicating a reduction in particle size. As a result of sonication with no extrusion the liposomes obtained are roughly 100 nm in diameter with a large size distribution.[71]

We next embedded B-TOH or PMOH in the membrane of the liposomes prepared. Each sample at a given pH was divided into 5 aliquots of 0.35 ml each. Two aliquots were injected with 15 µl each of a DMSO solution 63.2 µM in B-TOH, two were injected with 15 µl each of a DMSO solution 63.2 µM in PMOH, and a fifth aliquot was left as a blank for the spectroscopy studies. The DMSO solutions of B-TOH and PMOH were prepared in order to yield an absorbance of 0.18 upon diluting 15 µl of a DMSO solution in 0.35 ml of methanol. The same absorbance is expected upon their injection in the liposome dispersion. We thus obtained a final solution 20 mM in lipids, 200 nM in liposomes and 2.6 µM in dye (either B-TOH or PMOH). Liposomes were prepared each containing on average 13 fluorophores, with a DMPC/fluorophore mole ratio of 7,700/1. Under these low loading conditions, no fluorescence self-quenching is expected to take place within the bilayer.

Spectroscopy. A Cary Eclipse Spectrophotometer with temperature controller and water circulation was utilized to measure the liposome suspension fluorescence emission at 565 nm upon exciting at 514 nm using 2.5 nm excitation and emission slits. 1.5 ml of each sample were placed into triangular cuvettes and incubated at 37°C. To each sample was added 45 µl of a 0.3 M aqueous solution of 2,2′-Azobis-(2-methyl-propionamidine) dihydrochloride (ABAP) (Sigma-Aldrich, Oakville, Ontario, Canada) after equilibrating at 37 ^{o}C, to yield a final

concentration of ABAP of 9 x 10^{-3} M. Fluorescence emission was monitored for 2 h periods at 5 s time intervals to assess the effect of the peroxyl radicals on the B-TOH emission enhancement.

The fluorescence lifetime measurements were carried out using a Picoquant Fluotime 200 Time Correlated Single Photon Counting setup employing an LDH 470 picosecond diode laser (Picoquant) with excitation wavelength at 470 nm. The laser was controlled by a PDL 800 B picosecond laser driver from Picoquant. The excitation rate was 10 MHz and the detection frequency was less than 100 kHz. Photons were collected at the magic angle.

A Gemini XS fluorescence well-plate reader was utilized to measure the emission from the liposome suspensions; the emission was collected at 565 nm upon exciting at 514 nm. A total of 300 µl of each sample were placed into 20 separate wells and incubated at 37°C. After equilibrating at 37 ^{o}C, 15 µl of a 0.18 M aqueous solution of 2,2´-Azobis-(2-methylpropionamidine) dihydrochloride (ABAP) were added to one sample at each pH, to yield a final ABAP concentration of 9 x 10^{-3} M. Fluorescence emission was monitored for 2 h periods at 19 s time intervals to explore the effects of pH and peroxyl radicals on the B-TOH emission enhancement.

Cell cultures. Rat pheochromocytoma cells (PC12), (ATCC, USA) were cultured in RPMI 1640 media containing 10% FBS (Gibco, Burlington, ON, Canada). Cells were maintained at 37˚C (5% CO_2) in a humidified atmosphere. All media contained 1% penicillin-streptomycin and were free of phenol-red. Cells were seeded in 24-well plates (Sarstedt, Montreal, QC, Canada) at a density of 4 x 10^4 cells/cm^2, and a density of 10^4 cells/cm^2 was used in 8-well chambers (Lab-Tek, Nalge Nunc International, Rochester, NY, USA).

Primary hippocampal cell cultures. The study was performed with the approval of an institutional ethics committee and all experiments were conducted according to standard stipulated guidelines of animal care. Primary hippocampal neurons and glia from 5-day-old mouse pups (129T2/SV EmsJ, kindly provided by Dr. R.Sairam, IRCM, Montreal) were isolated and trypsinized, and the cells were dissociated by repetitive trituration through a Pasteur glass pipette, counted

and seeded (5 x 10^4 cells/well) onto collagen-coated glass coverslips, and grown in a 24-well cell culture plate (Corning) at 37 °C and 5% CO_2 initially in Dulbecco's Modified Eagle's Medium without phenol red (Invitrogen), 1mM L-Glutamine (Sigma), sodium pyruvate, and PSN (Invitrogen). On the second day in vitro, cells were cultured in Neurobasal A medium without phenol red (Invitrogen) supplemented with 2% (v/v) B-27 supplement (Invitrogen), PSN (Invitrogen), and 1mM L-Glutamine (Sigma) until the eighth day in vitro. On average, four hippocampi per one 24 well plate were required.

Cell Treatment. Cells were washed and maintained in serum-free media with CdTe nanoparticles (10 μg/mL) for 4 hr or 10 μM methyl viologen (Sigma-Aldrich, Oakville, Ontario, Canada) for 24 hr. Primary hippocampal cultures were treated with methyl viologen (10 μM) for 24 hours.

Live cell imaging. To assess the optimal B-TOH concentration range (λ_{max} absorption = 544 nm; λ_{max} emission = 565 nm in acetonitrile)[28] an initial screening was done using a wide field fluorescent microsope (Olympus BX-51, Center Valley, Pennsylvania, USA) at 40x magnification. All other images were acquired with a Zeiss LSM 510 NLO laser scanning confocal inverted microscope at 63X magnification using the Plan Apochromat 63x/1.4 Oil objective. Cells were grown on poly-D-Lysine HBr (Sigma, P7886) coated 8-well chambers (Lab-Tek, Nalge Nunc International, Rochester, NY, USA) or in 24 well plates with inserted glass coverlips (Fisher 12-545-80) coated with collagen (Sigma, C7661). CdTe nanoparticles or methyl viologen were added to designated wells and the cells were incubated at 37°C for 4 or 24 h, respectively. The B-TOH fluorescence enhancement was monitored over time upon exciting with the 488 nm laser line of an Ar^+ laser using an HFT 488 beam splitter and a LP520 emission filter. Detection of lysosomes with Lysotracker DND-99 (500 nM, Molecular Probes) was achieved upon exciting with the 543 nm laser line of a HeNe laser using an HFT 543 beam splitter and an LP560 emission filter. Lipid staining was performed by incubating cells with Nile Red (1.57 μM) for 10-15 min. Before imaging, cells were washed with PBS or with serum-free medium. Hoechst 33342 (10 μM, 30 min, Molecular Probes; λ_{ex} 350 nm, λ_{em} 461 nm) was used for

nuclear staining. No background fluorescence of cells was detected under the settings used. The images (512 x 512 or 1024 x 1024) were recorded upon laser scanning and registering the emission on a photo Multiplier tube. Triplicate samples were analyzed in all the imaging experiments. The region scanned was 146.2 x 146.2 μm^2. Figures were created using Adobe Photoshop.

Fluorescent enhancement analysis for time lapse experiments. Confocal pictures of PC12 cells stained with B-TOH were analyzed using Image J software (version 1.38). Quantification of the florescent signal was achieved by calculating the area (%) occupied by B-TOH using an identical threshold of detection for all images. The area (%) of B-TOH fluorescence was normalized to the green autofluorescent signal of PC12 cells, which were the same as the ones being analyzed for fluorescent enhancement.

Statistical analysis. Data were analyzed using SYSTAT 10 (SPSS, Chicago, IL, USA). Statistical significance was determined by Student's t-tests with Bonferroni correction. Differences were considered significant where $p<0.05$.

3.6. References

1. Halliwell, B. & Gutteridge, J.M.C. *Free Radicals in Biology and Medicine*, 851 (Oxford University Press, Oxford, 2007).
2. Winterbourn, C.C. Reconciling the chemistry and biology of reactive oxygen species. *Nature Chemical Biology* 4, 278-286, **2008**.
3. Droge, W. Free Radicals in the Physiological Control of Cell Function. *Physiol. Rev.* 82, 47-95, **2002**.
4. Apel, K. & Hirt, H. REACTIVE OXYGEN SPECIES: Metabolism, Oxidative Stress, and Signal Transduction. *Annual Review of Plant Biology* 55, 373-399, **2004**.
5. Rhee, S.G. CELL SIGNALING: H2O2, a Necessary Evil for Cell Signaling. *Science* 312, 1882-1883, **2006**.
6. Lesser, M.P. OXIDATIVE STRESS IN MARINE ENVIRONMENTS: Biochemistry and Physiological Ecology. *Annual Review of Physiology* 68, 253-278, **2006**.
7. Kagan, V.E. & Quinn, P.J. Toward Oxidative Lipidomics of Cell Signaling. *Antioxidants & Redox Signaling* 6, 199-202, **2004**.
8. West, J.D. & Marnett, L.J. Endogenous Reactive Intermediates as Modulators of Cell Signaling and Cell Death. *Chemical Research in Toxicology* 19, 173-194, **2006**.
9. Barclay, L.R.C. & Ingold, K.U. Autoxidation of biological molecules. 2. Autoxidation of a model membrane. Comparison of the autoxidation of egg lecithin phosphatidylcholine in water and in chlorobenzene. *Journal of the American Chemical Society* 103, 6478-6485, **1981**.
10. Barclay, L.R.C., Locke, S.J., MacNeil, J.M., VanKessel, J., Burton, G.W. & Ingold, K.U. Autoxidation of micelles and model membranes. Quantitative kinetic measurements can be made by using either water-soluble or lipid-soluble initiators with water-soluble or lipid-soluble chain-breaking antioxidants. *Journal of the American Chemical Society* 106, 2479-2481, **1984**.
11. Cosgrove, J., Church, D. & Pryor, W. The kinetics of the autoxidation of polyunsaturated fatty acids. *Lipids* 22, 299-304, **1987**.
12. Yamamoto, Y., Haga, S., Niki, E. & Kamiya, Y. Oxidation of lipids. V. Oxidation of methyl linoleate in aqueous dispersion. *Bulletin of the Chemical Society of Japan* 57, 1260-4, **1984**.
13. Porter, N.A. Mechanisms for the autoxidation of polyunsaturated lipids. *Accounts of Chemical Research* 19, 262-8, **1986**.
14. Hasegawa, K. & Patterson, L.K. PULSE RADIOLYSIS STUDIES IN MODEL LIPID SYSTEMS: FORMATION AND BEHAVIOR OF PEROXY RADICALS IN FATTY ACIDS. *Photochemistry and Photobiology* 28, 817-823, **1978**.
15. Niki, E. & Noguchi, N. Dynamics of Antioxidant Action of Vitamin E. *Accounts of Chemical Research* 37, 45-51, **2004**.
16. Barclay, L.R.C. Model biomembranes: quantitative studies of peroxidation, antioxidant action, partitioning, and oxidative stress. *Canadian Journal of Chemistry* 71, 1-16, **1993**.
17. Chatgilialoglu, C. & Ferreri, C. Trans Lipids: The Free Radical Path. *Accounts of Chemical Research* 38, 441-448, **2005**.
18. Chatgilialoglu, C., Ferreri, C., Ballestri, M., Mulazzani, Q.G. & Landi, L. Cis-trans Isomerization of Monounsaturated Fatty Acid Residues in Phospholipids by Thiyl Radicals. *Journal of the American Chemical Society* 122, 4593-4601, **2000**.
19. Sun, M. & Salomon, R.G. Oxidative Fragmentation of Hydroxy Octadecadienoates Generates Biologically Active γ-Hydroxyalkenals. *Journal of the American Chemical Society* 126, 5699-5708, **2004**.
20. Esterbauer, H., Schaur, R.J. & Zollner, H. Chemistry and biochemistry of 4-hydroxynonenal, malonaldehyde and related aldehydes. *Free Radical Biology and Medicine* 11, 81-128, **1991**.
21. Borst, J.W., Visser, N.V., Kouptsova, O. & Visser, A.J.W.G. Oxidation of unsaturated phospholipids in membrane bilayer mixtures is accompanied by membrane fluidity changes. *Biochimica et Biophysica Acta* 1487, 61-73, **2000**.

22. Yuan, J., Hira, S.M., Strouse, G.F. & Hirst, L.S. Lipid Bilayer Discs and Banded Tubules: Photoinduced Lipid Sorting in Ternary Mixtures. *Journal of the American Chemical Society* 130, 2067-2072, **2008**.
23. Barnham, K.J., Masters, C.L. & Bush, A.I. Neurodegenerative diseases and oxidative stress. *Nature Reviews Drug Discovery* 3, 205-214, **2004**.
24. Bowry, V.W. & Ingold, K.U. The Unexpected Role of Vitamin E (α-Tocopherol) in the Peroxidation of Human Low-density Lipoprotein. *Acc. Chem. Res.* 32, 27-34, **1999**.
25. Kagan, V.E., Fabisiak, J.P., Shvedova, A.A., Tyurina, Y.Y., Tyurin, V.A., Schor, N.F. & Kawai, K. Oxidative signaling pathway for externalization of plasma membrane phosphatidylserine during apoptosis. *FEBS Letters* 477, 1-7, **2000**.
26. Berliner, J.A. & Zimman, A. Future of Toxicology-Lipidomics, an Important Emerging Area for Toxicologists: Focus on Lipid Oxidation Products. *Chem. Res. Toxicol.* 20, 849-853, **2007**.
27. Kagan, V.E., Tyurin, V.A., Jiang, J., Tyurina, Y.Y., Ritov, V.B., Amoscato, A.A., Osipov, A.N., Belikova, N.A., Kapralov, A.A., Kini, V., Vlasova, I.I., Zhao, Q., Zou, M., Di, P., Svistunenko, D.A., Kurnikov, I.V. & Borisenko, G.G. Cytochrome c acts as a cardiolipin oxygenase required for release of proapoptotic factors. *Nature Chemical Biology* 1, 223-232, **2005**.
28. Krumova, K., Oleynik, P., Karam, P. & Cosa, G. Phenol-Based Lipophilic Fluorescent Antioxidant Indicators: A Rational Approach. *The Journal of Organic Chemistry* 74, 3641-3651, **2009**.
29. Oleynik, P., Ishihara, Y. & Cosa, G. Design and Synthesis of a BODIPY-a-Tocopherol Adduct for Use as an Off/On Fluorescent Antioxidant Indicator. *Journal of the American Chemical Society* 129, 1842-1843, **2007**.
30. Burton, G.W. & Ingold, K.U. Vitamin E: application of the principles of physical organic chemistry to the exploration of its structure and function. *Accounts of Chemical Research* 19, 194-201, **1986**.
31. Jonsson, M., Lind, J., Reitberger, T., Eriksen, T.E. & Merenyi, G. Free radical combination reactions involving phenoxyl radicals. *Journal of Physical Chemistry* 97, 8229-33, **1993**.
32. Burton, G.W., Doba, T., Gabe, E., Hughes, L., Lee, F.L., Prasad, L. & Ingold, K.U. Autoxidation of biological molecules. 4. Maximizing the antioxidant activity of phenols. *Journal of the American Chemical Society* 107, 7053-7065, **1985**.
33. de Silva, A.P., Gunaratne, H.Q.N., Gunnlaugsson, T., Huxley, A.J.M., McCoy, C.P., Rademacher, J.T. & Rice, T.E. Signaling Recognition Events with Fluorescent Sensors and Switches. *Chemical Reviews* 97, 1515-1566, **1997**.
34. Cadenas, E. Biochemistry of Oxygen Toxicity. *Annual Review of Biochemistry* 58, 79-110, **1989**.
35. Farrington, J.A., Ebert, M., Land, E.J. & Fletcher, K. Bipyridylium quaternary salts and related compounds. V. Pulse radiolysis studies of the reaction of paraquat radical with oxygen. Implications for the mode of action of bipyridyl herbicides. *Biochimica et Biophysica Acta* 314, 372-381, **1973**.
36. Lai, C.-S. & Piette, L.H. Spin-trapping studies of hydroxyl radical production involved in lipid peroxidation. *Archives of Biochemistry and Biophysics* 190, 27-38, **1978**.
37. Halliwell, B. & Gutteridge, J.M.C. Biologically relevant metal ion-dependent hydroxyl radical generation An update. *FEBS Letters* 307, 108-112, **1992**.
38. Casalino, E., Sblano, C. & Landriscina, C. Enzyme Activity Alteration by Cadmium Administration to Rats: The Possibility of Iron Involvement in Lipid Peroxidation. *Archives of Biochemistry and Biophysics* 346, 171-179, **1997**.
39. Price, D.J. & Joshi, J.G. Ferritin. Binding of beryllium and other divalent metal ions. *Journal of Biological Chemistry* 258, 10873-10880, **1983**.
40. Choi, A.O., Cho, S.J., Desbarats, J., Lovric, J. & Maysinger, D. Quantum dot-induced cell death involves Fas upregulation and lipid peroxidation in human neuroblastoma cells. *J Nanobiotechnology* 5, 1, **2007**.

41. Funnell, W.R. & Maysinger, D. Three-dimensional reconstruction of cell nuclei, internalized quantum dots and sites of lipid peroxidation. *J Nanobiotechnology* 4, 10, **2006**.
42. Lovric, J., Bazzi, H.S., Cuie, Y., Fortin, G.R., Winnik, F.M. & Maysinger, D. Differences in subcellular distribution and toxicity of green and red emitting CdTe quantum dots. *J Mol Med* 83, 377-85, **2005**.
43. Lovric, J., Cho, S.J., Winnik, F.M. & Maysinger, D. Unmodified cadmium telluride quantum dots induce reactive oxygen species formation leading to multiple organelle damage and cell death. *Chem Biol* 12, 1227-34, **2005**.
44. Tafazoli, S., Wright, J.S. & O'Brien, P.J. Prooxidant and Antioxidant Activity of Vitamin E Analogues and Troglitazone. *Chemical Research in Toxicology* 18, 1567-1574, **2005**.
45. Cooper, D.A., Webb, D.R. & Peters, J.C. Evaluation of the Potential for Olestra To Affect the Availability of Dietary Phytochemicals. *Journal of Nutrition* 127, 1699S-, **1997**.
46. Bedard, L., Young, M.J., Hall, D., Paul, T. & Ingold, K.U. Quantitative Studies on the Peroxidation of Human Low-Density Lipoprotein Initiated by Superoxide and by Charged and Neutral Alkylperoxyl Radicals. *Journal of the American Chemical Society* 123, 12439-12448, **2001**.
47. Maillard, B., Ingold, K.U. & Scaiano, J.C. Rate constants for the reactions of free radicals with oxygen in solution. *Journal of the American Chemical Society* 105, 5095-5099, **1983**.
48. Valko, M., Rhodes, C.J., Moncol, J., Izakovic, M. & Mazur, M. Free radicals, metals and antioxidants in oxidative stress-induced cancer. *Chemico-Biological Interactions* 160, 1-40, **2006**.
49. Qian, J., Morley, S., Wilson, K., Nava, P., Atkinson, J. & Manor, D. Intracellular trafficking of vitamin E in hepatocytes: the role of tocopherol transfer protein. *J. Lipid Res.* 46, 2072-2082, **2005**.
50. Greenspan, P., Mayer, E.P. & Fowler, S.D. Nile red: a selective fluorescent stain for intracellular lipid droplets. *J Cell Biol* 100, 965-73, **1985**.
51. Terman, A., Gustafsson, B. & Brunk, U.T. Autophagy, organelles and ageing. *J Pathol* 211, 134-43, **2007**.
52. Kroemer, G. & Jaattela, M. Lysosomes and autophagy in cell death control. *Nat Rev Cancer* 5, 886-97, **2005**.
53. Arbeloa, F.L., Banuelos, J., Martinez, V., Arbeloa, T. & Arbeloa, I.P. Structural, photophysical and lasing properties of pyrromethene dyes. *International Reviews in Physical Chemistry* 24, 339-374, **2005**.
54. Ueno, T., Urano, Y., Kojima, H. & Nagano, T. Mechanism-Based Molecular Design of Highly Selective Fluorescence Probes for Nitrative Stress. *Journal of the American Chemical Society* 128, 10640-10641, **2006**.
55. Alessi, M., Paul, T., Scaiano, J.C. & Ingold, K.U. The Contrasting Kinetics of Peroxidation of Vitamin E-Containing Phospholipid Unilamellar Vesicles and Human Low-Density Lipoprotein. *Journal of the American Chemical Society* 124, 6957-6965, **2002**.
56. Zeng, L., Miller, E.W., Pralle, A., Isacoff, E.Y. & Chang, C.J. A Selective Turn-On Fluorescent Sensor for Imaging Copper in Living Cells. *Journal of the American Chemical Society* 128, 10-11, **2005**.
57. Srikun, D., Albers, A.E., Nam, C.I., Iavarone, A.T. & Chang, C.J. Organelle-Targetable Fluorescent Probes for Imaging Hydrogen Peroxide in Living Cells via SNAP-Tag Protein Labeling. *Journal of the American Chemical Society* 132, 4455-4465, **2010**.
58. Atkinson, J., Epand, R.F. & Epand, R.M. Tocopherols and tocotrienols in membranes: A critical review. *Free Radical Biology and Medicine* 44, 739-764, **2008**.
59. Wang, X. & Quinn, P.J. Vitamin E and its function in membranes. *Progress in Lipid Research* 38, 309-336, **1999**.
60. Wang, X. & Quinn, P.J. The location and function of vitamin E in membranes (Review). *Molecular Membrane Biology* 17, 143 - 156, **2000**.

61. Quinn, P.J. Molecular associations of vitamin E. in *Vitamin E: Vitamins and Hormones Advances in Research and Applications*, Vol. 76 67-+ (Elsevier, Amsterdam, 2007).
62. Fukuzawa, K., Ikebata, W., Shibata, A., Kumadaki, I., Sakanaka, T. & Urano, S. Location and dynamics of [alpha]-tocopherol in model phospholipid membranes with different charges. *Chemistry and Physics of Lipids* 63, 69-75, **1992**.
63. Maggio, B., Diplock, A.T. & Lucy, J.A. Interactions of tocopherols and ubiquinones with monolayers of phospholipids. *Biochemical Journal* 161, 111-121, **1977**.
64. Korlach, J., Schwille, P., Webb, W.W. & Feigenson, G.W. Characterization of lipid bilayer phases by confocal microscopy and fluorescence correlation spectroscopy. *Proceedings of the National Academy of Sciences of the United States of America* 96, 8461-8466, **1999**.
65. Lopez, E., Arce, C., Oset-Gasque, M.J., Canadas, S. & Gonzalez, M.P. Cadmium induces reactive oxygen species generation and lipid peroxidation in cortical neurons in culture. *Free Radic Biol Med* 40, 940-51, **2006**.
66. Cho, S.J., Maysinger, D., Jain, M., Roder, B., Hackbarth, S. & Winnik, F.M. Long-term exposure to CdTe quantum dots causes functional impairments in live cells. *Langmuir* 23, 1974-80, **2007**.
67. Buttriss, J.L. & Diplock, A.T. The ga-tocopherol and phospholipid fatty acid content of rat liver subcellular membranes in vitamin E and selenium deficiency. *Biochimica et Biophysica Acta (BBA) - Lipids and Lipid Metabolism* 963, 61-69, **1988**.
68. Czibener, C., Sherer, N.M., Becker, S.M., Pypaert, M., Hui, E., Chapman, E.R., Mothes, W. & Andrews, N.W. Ca^{2+} and synaptotagmin VII-dependent delivery of lysosomal membrane to nascent phagosomes. *Journal of Cell Biology* 174, 997-1007, **2006**.
69. Moreira, P.I., Harris, P.L., Zhu, X., Santos, M.S., Oliveira, C.R., Smith, M.A. & Perry, G. Lipoic acid and N-acetyl cysteine decrease mitochondrial-related oxidative stress in Alzheimer disease patient fibroblasts. *J Alzheimers Dis* 12, 195-206, **2007**.
70. Liao, K.l. & Yin, M.c. Individual and Combined Antioxidant Effects of Seven Phenolic Agents in Human Erythrocyte Membrane Ghosts and Phosphatidylcholine Liposome Systems: Importance of the Partition Coefficient. *Journal of Agricultural and Food Chemistry* 48, 2266-2270, **2000**.
71. Torchilin, V.P. & Weissig, V. (eds.). *Liposomes*, (Oxford University Press Inc. , NY, 2003).

Bodipy Dyes with Tunable Redox Potentials and Functional Groups for Further Tethering: Preparation, Electrochemical and Spectroscopic Characterization

Katerina Krumova and Gonzalo Cosa, *J. Am. Chem. Soc.,* **2010**, 132, 17560–17569

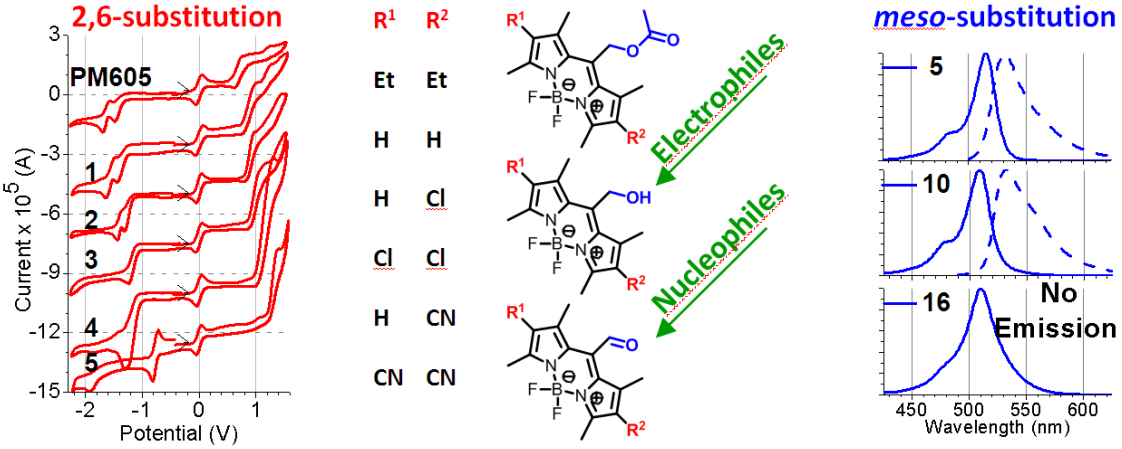

Preface

In chapters 2 and 3 we determined the scope and limitations of B-TOH. Studies in homogeneous and heterogeneous media show that the reactivity of B-TOH is on par with that of α-tocopherol. However, when B-TOH is embedded in lipid membranes we observed a marked decrease in sensitivity leading to only 5-fold emission enhancement upon scavenging peroxyl radicals. We established that the fluorogenic antioxidant operates on a PeT "off-on" switch mechanism and that the process is moderately exergonic. We can foresee that using a fluorophore with higher reduction potential (less negative) will make the PeT process more exergonic. Facilitating PeT will in turn lead to improvements on the on/off ratio of the fluorogenic probe, where we anticipate that more exergonic electron transfer will lead to a faster rate constant for electron transfer from the receptor to the reporter segment. In chapter 4 we report on the preparation, spectroscopic and electrochemical characterization of a family of 16 new Bodipy dyes with tunable redox potentials and versatile functional groups. Electron withdrawing or donating groups (Et, H, Cl or CN) at positions C2 and C6 of the Bodipy core enable tuning the redox potentials within a *ca.* 0.7 eV window without significantly affecting either the HOMO-LUMO gap or the absorption and emission spectra. Hydroxymethyl or formyl groups at the *meso* (C8) position in turn provided functionality for covalent tethering to receptors and biomolecules of interest.

4.1. Introduction

Following the first report in 1968, boron dipyrromethene or Bodipy dyes[1] have been increasingly adopted for various different fluorescence imaging applications.[2,3] To a great extent Bodipy dyes owe popularity to their relative ease of preparation[4-6] and optimal spectroscopic properties (high emission quantum yields, high extinction coefficients, and narrow absorption and emission bands).[7-10] Bodipy dyes have been utilized, among others, as fluorescent positional tags in the form of lipid membrane markers in model membranes[3,11] or live cells;[12-14] as donor or acceptor fluorophores in FRET schemes to probe conformational rearrangements in biomolecules;[15,16] and as sensors/analyte indicators of ions[17-22] or reactive oxygen and nitrogen species.[12,13,23-31]

In the case of sensors/analyte indicators, most Bodipy-based probes described rely on the action of an intramolecular off-on switch based on a photoinduced electron transfer (PeT) mechanism (receptor-reporter probes).[32-34] Tuning the redox potentials of the Bodipy dyes, in order that PeT processes are thermodynamically feasible is thus of primary importance in designing and developing novel sensors. It is important to emphasize that introducing new functional groups for highly versatile tethering is critical in designing new Bodipy dyes in order to enable their tagging to receptors and to other molecules of interest.

Here we describe the preparation, electrochemical and spectroscopic characterization of a series of new Bodipy dyes (see Figure 4.1). These dyes contain electron donating or withdrawing groups including Et, H, Cl and CN at positions C2 and C6 of the backbone enabling tuning of the redox potential within a 0.7 eV window. The *meso* position is functionalized with hydroxymethyl or formyl group for further tethering. The rationale for this design is **i**) to provide a suitable functional group to tether molecules of interest, where our criteria is to minimize the distance between the Bodipy dye (reporter) and a covalently linked receptor in order to facilitate photoinduced electron transfer processes[35] in receptor-reporter systems; and **ii**) to dispense with the use of a *meso*-aryl moiety as a handle where to tether molecules of interest. Whereas a *meso*-aryl moiety is

currently the preferred method to introduce a handle on Bodipy dyes, it enhances the non-radiative excited state deactivation via internal conversion processes arising from rotation along the bond connecting the aryl moiety and the boron dipyrromethene backbone.[36-38] The aryl moiety may further insulate the dye (reporter) from a receptor segment in receptor-reporter probes, since typically the Bodipy plane and that of the *meso* aromatic moiety lie at 90° with respect to each other (propeller like) and are thus conjugatively uncoupled.[31,39]

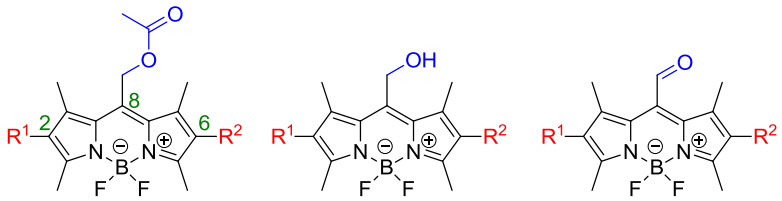

	R^1	R^2
PM605	Et	Et
1	H	H
2	H	Cl
3	Cl	Cl
4	H	CN
5	CN	CN

	R^1	R^2
PMOH	Et	Et
6	H	H
7	H	Cl
8	Cl	Cl
9	H	CN
10	CN	CN

	R^1	R^2
11	Et	Et
12	H	H
13	H	Cl
14	Cl	Cl
15	H	CN
16	CN	CN

Figure 4.1: Structure of the Bodipy dyes prepared and characterized in this work (**1-16**). Also shown are the structures of the commercially available dye PM605 and its derivative PMOH. Positions 2, 6 and 8 (*meso*) are shown in green.[5]

4.2. Results and Discussion

In the following section we first describe the preparation of the new Bodipy dyes and subsequently we discuss their photophysical properties and electrochemical potentials.

4.2.1. Preparation of Bodipy Dyes

Bodipy dyes are usually synthesized by the condensation reaction between a carbonyl (either acyl chlorides or aromatic aldehydes) and a pyrrole followed by *in situ* complexation with BF_3•OEt_2 in the presence of a base.[5] We identified the condensation between substituted pyrroles and acetoxyacetyl chloride[40] (See Schemes 4.1 and 4.2) as the preferred method to prepare the Bodipy dyes described here. Precursor pyrroles bearing either electron withdrawing or donating groups at C3 position were utilized, this translated to C2 and C6

substitution in the resulting Bodipy dyes. Whereas this substitution had only a minor effect on the HOMO-LUMO gap of these dyes (ranging between 2.26 and 2.42 eV), it had a dramatic effect on their redox potentials which spanned over 0.7 eV (see below). The condensation also allowed us to introduce the acetoxy group at the *meso* position which could be then converted first to a *meso*-hydroxymethyl Bodipy (**6-10**) upon ester hydrolysis, and, via subsequent oxidation, to a *meso*-formyl Bodipy (**11-16**). New dyes were thus obtained with diverse electrochemical properties and versatile tethering potential.

Compound **1** was synthesized in two steps in 75% overall yield by condensation of acetoxyacetyl chloride and 2 equivalents of 2,4-dimethyl pyrrole under reflux in dichloromethane followed by treatment of the reaction mixture with 4 equivalents of BF_3•OEt_2 and diisopropylethilamine at room temperature.

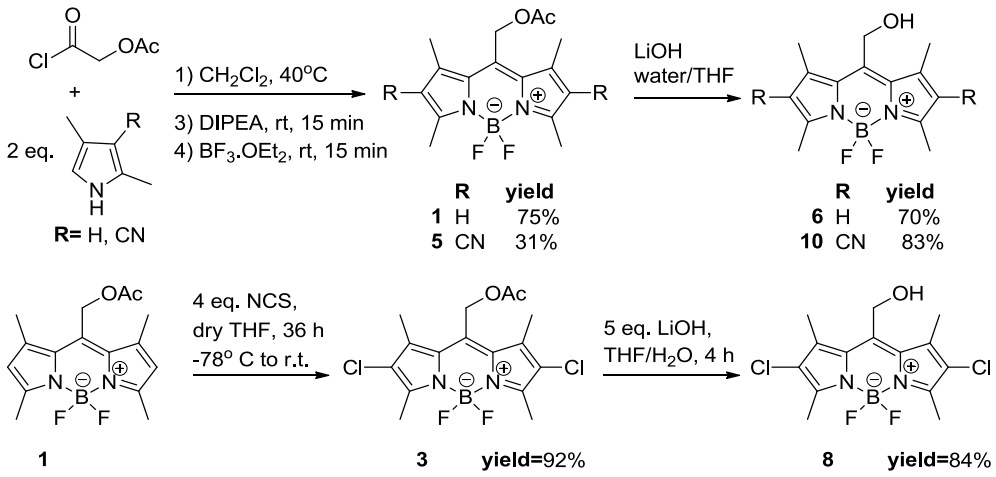

Scheme 4.1: Synthesis of symmetric Bodipy dyes**.**

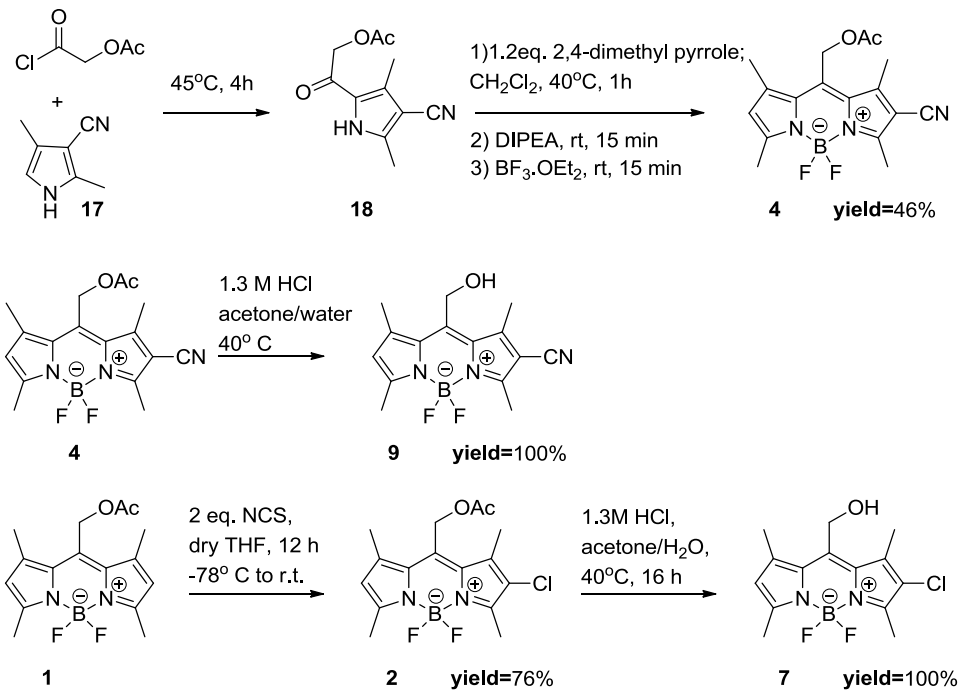

Scheme 4.2: Synthesis of asymmetric Bodipy dyes.

Chlorination of compound **1** using N-chlorosuccinimide[41] afforded either compounds **2** (Scheme 4.2) or **3** (Scheme 4.1) depending on the reaction conditions. Compound **2** was obtained in 76% yield after 12 hours of reaction. Leaving the reaction for 36 h gave compound **3** in 92% yield, where additional reaction time was necessary due to the deactivation of the aromatic system upon introduction of the first chlorine atom. Compound **5** was prepared in 30% overall yield via condensation of 3-cyano-2,4-dimethyl pyrrole (**17**, prepared following a modified literature procedure[33,42]) with acetoxyacetyl chloride followed by addition of diisopropylethilamine and 4 equivalents of BF_3•OEt_2 (Scheme 4.1). Extended heating was required during the condensation due to the lower nucleophilicity of **17**.

Asymmetric Bodipy dyes are usually prepared by condensation of 2-formyl-pyrroles with a second pyrrole bearing a free α-position.[5] This procedure however does not allow for the introduction of a handle at the *meso* position.

We envisioned that using 2-ketopyrrole (**18**) as a precursor would provide us with a necessary handle. In order to prepare this compound, we exploited the

low reactivity of **17** in its condensation with acetoxyacetylchloride which allowed us to stop the reaction at the formation of **18** (see Scheme 4.2). The latter was next coupled with the more reactive 2,4-dimethyl pyrrole. After 1 h of reflux the reaction was cooled to room temperature; upon 10-fold dilution[43] and addition of an excess of DIPEA and BF_3•OEt_2 we obtained compound **4** in 46% yield (see Scheme 4.2).

The *meso*-acetoxymethyl Bodipy derivatives **1** to **5** were easily hydrolyzed to the corresponding *meso*-hydroxymethyl Bodipy **6** to **10** under basic or acidic conditions. Specifically for the symmetric compounds **1, 3** and **5** hydrolysis was performed in basic media. [40]

It is interesting to note that when performing the basic hydrolysis of compounds **3** and **5** discoloration and loss of fluorescence occurred upon addition of the aqueous solution of LiOH to the solution of the dyes in THF, yet discoloration was not observed in the hydrolysis of compound **1**. Notably the discoloration we observed in **3** and **5** was reversed when acidifying the solution following addition of 3M HCl. The solution turned orange pink and compounds **8** and **10** were isolated in 80 and 83 % yields respectively. It is worth mentioning that discoloration has also been observed for other nitrile substituted Bodipy dyes.[44,45] In all cases these changes occurred under significantly milder conditions than those we employed in the hydrolysis of **3** and **5**.[44-46] Discoloration was not reversible, but it was pH sensitive.[44,45]

Basic hydrolysis of compounds **2** and **4** was initially attempted under identical conditions to those employed for the hydrolysis of **1**, **3** and **5** yet it did not lead to the formation of the desired *meso*-hydroxymethyl Bodipy dyes but rather resulted in the decomposition of the dye and the generation of secondary fluorescent products. The hydrolysis of compounds **2** and **4** was ultimately accomplished under acidic conditions (1.3 M HCl in acetone, 40 ^{o}C)[40] affording the alcohol in quantitative yield after 3 h or 16 h of reaction, respectively. No change in either absorption or emission occurred under these hydrolysis conditions. These conditions however led to decomposition of the symmetric Bodipy dyes PM605 and **1**, **3** and **5**.

	R^1	R^2	yield
11	Et	Et	74%
12	H	Cl	80%
13	Cl	Cl	80%
14	H	H	86%
15	H	CN	91%
16	CN	CN	97%

Scheme 4.3: Conversion of *meso*-hydroxymethyl to *meso*-formyl Bodipy.

Oxidation of PMOH and compounds **6** to **10** to the corresponding *meso*-formyl Bodipy (compounds **11** to **16**) was done using standard Dess-Martin oxidation conditions (see Scheme 4.3).[47] The reaction yields increased with the increase in the number of electron withdrawing groups introduced in the Bodipy core (reactions **11**, **12** and **13** were quenched before completion due to the formation of side products). The resultant compounds **11**, **12**, **13**, **14**, **15** and **16** were obtained in 74%, 80%, 80%, 86%, 91% and 97% yields, respectively.

4.2.2. Electrochemistry of Bodipy Dyes

In order to monitor how electron withdrawing and donating groups at positions C2 and C6 modify the redox potential of the Bodipy dyes we next conducted electrochemical studies on compounds **1** to **16** and compared these with similar studies we previously performed on PM605 and PMOH.[23]

The redox potentials of the Bodipy dyes were measured via cyclic voltammetry. Throughout, acetonitrile solutions and a scan rate of 0.2 V/s and up to 10 V/s were used. All measurements were performed in Ar saturated solutions 0.1 M in tetrabutylammonium hexafluorophosphate and 0.4 mM in the internal standard ferrocene (Fc/Fc^+). Solutions were *ca.* 0.72 mM for each of the Bodipy dyes studied, as determined from their extinction coefficients.

The cyclic voltammograms for compounds **1** to **16**, PM605 and PMOH are shown in Figure 4.2. Table 4.1 summarizes the electrochemical data. Similar trends were noticed within each group i.e., for acetoxymethyl, hydroxymethyl and

formyl derivatives. Introduction of H and/or electron-withdrawing groups (*e.g.* Cl or CN) at position C2 and C6 lead to an increase in both the reduction and oxidation potentials with respect to Et substituted Bodipy chromophores.

The acetoxymethyl derivatives appeared to be more versatile in their electrochemistry than either the hydroxymethyl or formyl substituted Bodipy dyes. Compounds **1** to **4** showed irreversible reduction and oxidation waves when scanning at 0.2 V/s. Scanning in the negative direction gave two reduction peaks for **1**, **2** and **4** with E_{pc} values of -1.44 and -1.64 V for **1** and -1.30 and -1.44 V for **2**. For compound **4** the two peaks overlapped into one two-electron peak as can be judged by comparing the integral of the peak with that of the ferrocene standard. Electrochemical reversibility was not observed for these three acetoxymethyl derivatives at scan rates up to 10 V/s. This is in agreement with the electrochemical studies reported for PM605.[23] Compound **3** showed one irreversible reduction peak at scan rate 0.2 V/s, which became reversible only at 10 V/s scan rate. Compound **5** had a different electrochemistry compared to the other acetoxymethyl derivatives. As expected, it showed a much higher reduction potential due to the electron withdrawing cyano groups at positions C2 and C6. It was the only compound in its group that had reversible reduction at a 0.2 V/s scanning rate ($E^0_{B/B-.}$ = -0.77 V). A different behavior was observed for the oxidation of all acetoxymethyl derivatives compared to PM605. While the oxidation peak for PM605 was reversible at 0.2 V/s scan rate, all other acetoxymethyl derivatives gave an irreversible oxidation peak at the same scan rate. Their oxidation became reversible only at scan rates of 10 V/s and the oxidation potential increased in the order from **1** to **5**.

A one-electron oxidation and reduction waves were observed for alcohols PMOH and **6** to **10**. A reversible reduction was recorded for PMOH and compounds **6** to **9**, whereas **10** did not show reversibility even at scan rates of 10 V/s. Unlike **PMOH**, **6**, and **7**, which showed reversible oxidation at 200 mV/s and **8** which showed reversible oxidation at 1 V/s, compounds **9** and **10** did not display reversible oxidation at scan rates up to 10 V/s.

The cyclic voltammograms of *meso*-formyl Bodipy dyes had two one-electron reduction waves (reversible at scan rates of 0.2 V/s) and a one-electron oxidation wave. We assigned the first reduction wave (at higher potential) to the one-electron reduction of the carbonyl group and the second wave (at lower potential) to the one-electron reduction of the Bodipy core. The oxidation wave was reversible at scan rates of 0.2 V/s only for **11** and **12**. Reversibility was observed for **13** and **14** at scan rates of 1 V/s, whereas compounds **15** and **16** remained irreversible even at 10 V/s scan rates. The reduction and oxidation potentials followed the same trend as the acetoxymethyl and hydroxymethyl derivatives and increased with the introduction of electron withdrawing groups.

The observed peak separation for the reversible waves was *ca.* 100 mV which is larger than expected for nernstian behavior, where one-electron waves are expected to have a peak separation of 59 mV. The peak separation for the ferrocence internal standard, which is known to have a nernstian behavior, was also 100 mV under our experimental conditions (similar results have been previously observed and were attributed to ohmic drop (1 kohm) that is often observed within aprotic solvents).[48] Also for the reversible reductions and the reversible oxidations, the peak current ratio (i_{pa}/i_{pc} or i_{pc}/i_{pa}) were approximately unity indicating that the radical ions were fairly stable and no additional chemical reactions took place.[49]

	$E_2^{0}{}_{B/B^{-\cdot}}$	$E_1^{0}{}_{B/B^{-\cdot}}$	E_{pc1}	E_{pc2}	$E^{0}{}_{B^{+\cdot}/B}$	E_{pa1}	[a]E_g (eV)	[b]E_g (eV)	[c]E_{00} (eV)	[c]HOMO (eV)
[d]**PM605**	-		-1.48	-1.69	0.70		2.18[e]	2.26	2.79	-5.31
1	-		-1.44	-1.64		0.88	2.32[e]	2.38	2.86	-5.55
2	-		-1.30	-1.44		0.97	2.27[e]	2.32	2.82	-5.71
3	-		-1.24			1.07	2.31[e]	2.25	2.77	-5.86
4	-		-1.24	-1.31		1.31	2.55[e]	2.42	2.87	-6.05
5	-	-0.77		-1.91		1.39	2.16[e]	2.38	2.84	-6.49
[d]**PMOH**	-	-1.58			0.63		2.21[f]	2.28	-	-
6	-	-1.48			0.77		2.25[f]	2.41	-	-
7	-	-1.36			0.82		2.18[f]	2.34	-	-
8	-	-1.23				0.97	2.14[g]	2.28	-	-
9	-	-1.24				1.15	2.39[e]	2.45	-	-
10	-		-0.9			1.39	2.29[e]	2.41	-	-
11	-1.12	-1.58			0.73		1.85[f]	N.A.[h]	-	-
12	-1.05	-1.60			0.86		1.91[f]	N.A.[h]	-	-
13	-0.97	-1.50				1.07	1.97[g]	N.A.[h]	-	-
14	-0.89	-1.44				1.05	1.94[g]	N.A.[h]	-	-
15	-0.82	-1.38				1.23	2.05[e]	N.A.[h]	-	-
16	-0.52	-1.12				1.42	1.94[e]	N.A.[h]	-	-

Table 4.1: Electrochemical data acquired at 200 mV/s and HOMO-LUMO gaps determined from spectroscopy and DFT calculations.
E_{pc} –cathodic peak potential; E_{pa} –anodic peak potential; $E^{0}{}_{B/B^{-\cdot}}$ –reversible reduction potential; $E^{0}{}_{B^{+\cdot}/B}$ –reversible oxidation potential; E_g - HOMO-LUMO gap. [a]Obtained from CV measurements; [b]obtained from the intercept of the normalized absorption and emission spectra; [c]obtained from DFT calculations, HOMO values are with respect to vacuum. [d]Data from reference [23]. [e]Calculated from ($E_{pa} - E_{pc}$) at 0.2 V/s scan rate. [f]Calculated from ($E^{0}{}_{B^{+\cdot}/B}$ - $E_1{}^{0}{}_{B/B^{-\cdot}}$) at 0.2 V/s scan rate. [g]Calculated from ($E^{0}{}_{B^{+\cdot}/B}$ - $E_1{}^{0}{}_{B/B^{-\cdot}}$) at 1 V/s scan rate. [h]Non available due to the lack of emission from *meso*-formyl Bodipys.

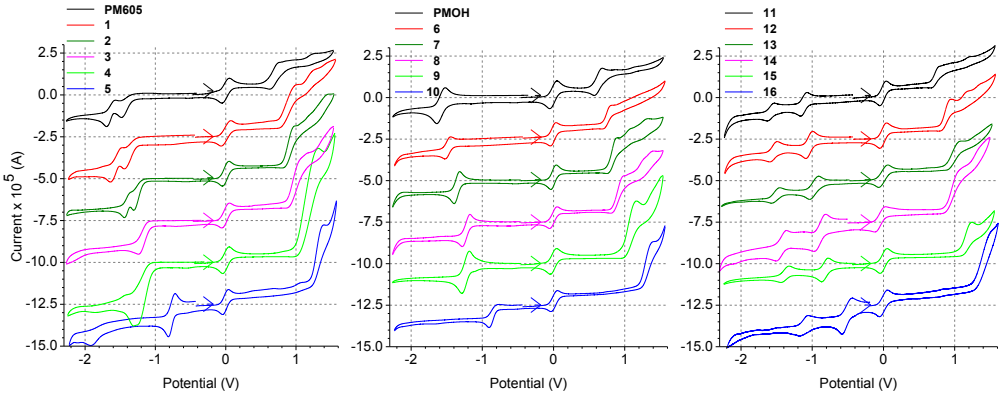

Figure 4.2: Cyclic voltammograms for 0.72 μM solutions of compounds **1**–**16**, PM605 and PMOH. Note that the plots are offset by 25 μA with respect to each other in the ordinate axis to facilitate comparison. Voltammograms were acquired in degassed, Ar-saturated acetonitrile (0.1 M tetrabutylammonium hexafluorophosphate) versus 0.40 mM Fc/Fc^{+}. Scan rate = 200 mV s^{-1}. The scan direction is indicated by an arrow. The wave at a potential = 0 V corresponds to Fc/Fc^{+}. All voltammograms were normalized to the ferrocene anodic peak.

We additionally conducted DFT calculations at the B3LYP/6-31G(d) level[50,51] to estimate the HOMO and LUMO energy levels for compounds **1** to **5**. Table 4.1 lists the calculated HOMO and LUMO values relative to vacuum as well as the energy band gap for compounds **1**-**5** and **PM605**.[23] There is a good correlation between electrochemical studies and DFT calculations on the decrease in HOMO and LUMO values with substitution (Et, H, Cl and CN), there is also a linear dependence on the energy band gaps obtained from spectroscopic studies and those determined from DFT, however the calculated energy band gap values amply surpass those obtained experimentally (Table 4.1 and 4.2). *Ab initio* methods have been shown to overestimate the energy gap but they successfully predict the effect of substitution on spectroscopy based on the electronic densities of HOMO and LUMO orbitals (see below).[8]

4.2.3. Spectroscopy of Bodipy Dyes

Listed in Table 4.2 are the main photophysical properties of compounds **1** to **16** determined in acetonitrile. Figure 4.3 displays the absorption and emission spectra for these compounds.

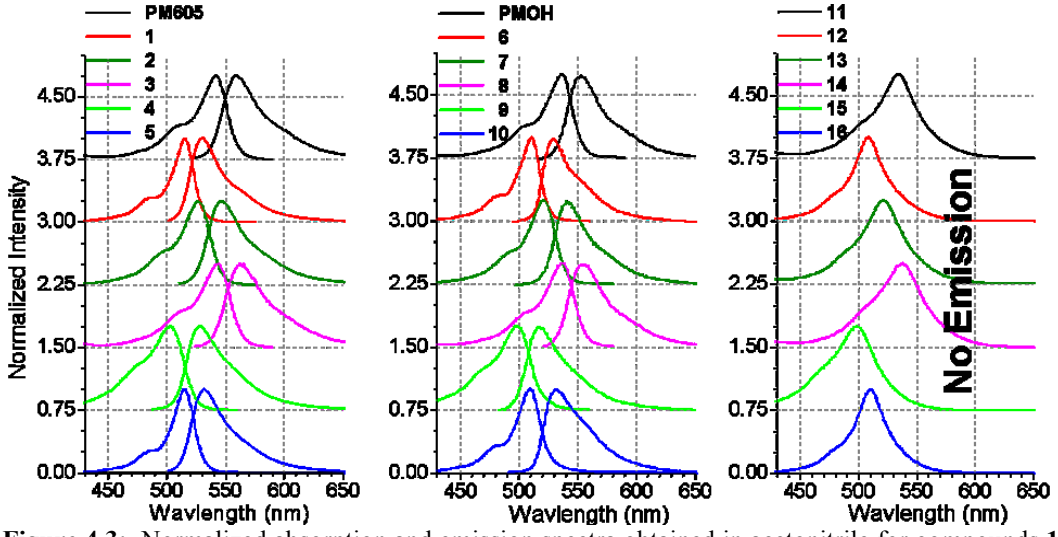

Figure 4.3: Normalized absorption and emission spectra obtained in acetonitrile for compounds **1** - **16**, PM605 and PMOH. Note that the plots are offset with respect to each other in the ordinate axis to facilitate comparison.

The lowest energy absorption band (S_0 to S_1 0-0 transition) is centered in the green region of the visible spectrum (in the range of 489 nm to 566 nm) for

compounds **1**-**10.** It shows a higher energy vibronic shoulder at *ca.* 1,100 cm^{-1} from the main peak (in the range of 470 nm to 510 nm). For a given family of compounds the absorption and emission bands shift to lower energies when positions C2 and C6 bear electron donating groups (see Table 4.2 and Figure 4.3). A drop of *ca.* 0.1 eV in the HOMO-LUMO energy gap (Eg) is also observed (see Table 4.1). Our results are consistent with expectations from previous DFT calculations[8,46] on the electronic density of the HOMO and LUMO for the commercially available Bodipy dyes PM567 and PM650 (dyes bearing H or CN groups, respectively, at positions C2 and C6 and a methyl substituent at position C8). These calculations show a significant depletion in the electronic density at positions C2 and C6 in the excited state in comparison to the ground state, it is therefore expected that electron withdrawing groups such as the nitriles found in compounds **4** and **5** as well as **9** and **10** will increase the HOMO-LUMO energy gap by stabilizing the HOMO relative to the LUMO. On the contrary, electron donating groups such as ethyl groups in PM605, and PMOH will stabilize the LUMO relative to the HOMO level thus decreasing the energy gap. Interestingly, in case of substitution with Cl at C 2 and C6 (see compounds **3** and **8**) the resonance (donating) effects dominate over the inductive effect. Thus the energy gap and absorption and emission λ_{max} for these compounds are comparable to those observed with the Bodipy dyes PM605, and PMOH. Asymmetric dyes **2** and **7** (Cl, H) or **4** and **9** (CN, H) all show significantly higher HOMO-LUMO energy gaps than their symmetric counterparts **3** and **8** (Cl, Cl) or **5** and **10** (CN, CN).

The lower absorption, emission and band gap energies measured for the acetoxymethyl substituted Bodipy dyes compared to their hydroxymethyl substituted counterparts may be rationalized by the electron withdrawing nature of the acyl group (compare PM605 and compounds **1** to **5** vs. PMOH and compounds **6** to **10**, respectively). Since *ab initio* calculations have shown an increase in electron density in the *meso* position for the LUMO vs. the HOMO level, the acyl groups will preferentially stabilize the former over the latter.[8,46]

The fluorescence lifetimes for *meso*-acetoxymethyl (PM605, and **1-3**) or *meso*-hydroxymethyl (PMOH, and **6-8**) Bodipy dyes range between 6.5 and 7.5 ns with the exception of the nitrile bearing Bodipy dyes **4**, **5**, **9** and **10**. The fluorescence lifetimes for the latter compounds are somewhat shorter; we recorded values in the range of 4.65-5.24 ns in all solvents. Given the high emission quantum yields for **4**, **5**, **9** and **10** (see Table 4.2), the shorter lifetimes indicate a faster radiative decay taking place in 2- or 2,6- CN substituted Bodipy chromophores. We were not able to measure fluorescence lifetimes for compounds **11-16** since they are non emissive (see below).

	Abs λ_{max} (nm)	Em λ_{max} (nm)	Φ_f	τ_{dec} (ns)	$\varepsilon \times 10^3$ ($M^{-1}cm^{-1}$)
[a]**PM605**	542	561	0.72	6.76	70
1	515	530	0.87	6.66	81
2	526	546	0.88	6.31	66
3	543	560	0.68	6.46	58
4	503	526	0.86	4.68	46
5	515	531	0.76	5.24	96
[a]**PMOH**	536	552	0.84	6.90	70
6	510	523	0.98	6.65	100
7	521	535	0.82	6.31	70
8	537	554	0.79	6.46	53
9	498	517	0.87	4.65	51
10	509	525	1.00	5.05	94
11	535	N.A.	N.A.	N.A.	16
12	509	N.A.	N.A.	N.A.	18
13	520	N.A.	N.A.	N.A.	43
14	538	N.A.	N.A.	N.A.	16
15	499	N.A.	N.A.	N.A.	57
16	510	N.A.	N.A.	N.A.	42

Table 4.2: Photophysical properties of dyes **1** to **16** in various solvents at room temperature. Also shown for comparison are the photophysical properties of the commercially available dye PM605 and its alcohol derivative PMOH. [a]Data from reference [23].

The absorption spectra of *meso*-formyl Bodipy dyes **11** to **16** are unique since they display an additional (lower-energy) transition buried within the major absorption peak, extending beyond 600 nm for some of these compounds, and

which is likely arising from an n-π* transition. These absorption spectra are much broader than the ones recorded for compounds **1 to 10** (Figure 4.3). *meso*-Formyl Bodipy dyes also have a smaller HOMO-LUMO energy gap when compared to their hydroxymethyl and acetoxymethyl counterparts as observed from the electrochemical studies (Table 4.1), this is consistent with a lower energy n-π* transition. No reliable HOMO-LUMO energy gap estimation can be done for **11-16** based on spectroscopic measurements due to their lack of emission (see below).

The most striking difference between compounds **1** to **10**, PMOH and PM605, vs. compounds **11** to **16** is the difference in emission quantum yield (Φ_f) and molar extinction coefficient (ε), reflecting the forbidden nature of the lowest energy electronic excitation and emission transition for the *meso*-formyl Bodipy dyes. Compounds **1** to **10**, together with PM605 and PMOH, have high molar extinction coefficients (70000 to 90000 $M^{-1}cm^{-1}$) and relatively high fluorescence quantum yield values ranging from 0.7 to 1 in acetonitrile. Substituents at positions C2 and C6 do not dramatically affect either the Φ_f or the molar extinction coefficient. In marked contrast, *meso*-formyl Bodipy dyes show up to 4-fold reduction in the molar extinction coefficient (16000 to 60000 $M^{-1}cm^{-1}$). Most importantly, these compounds are non-emissive. No emission was recorded upon exciting these compounds at their absorption maximum.

The non-emissive formyl dyes provide unique opportunities as fluorogenic probes of nucleophilic attack by *e.g.* alcohols and amine groups. Studies conducted in our group reveal that emission is rapidly restored following hemiacetal formation upon addition of **13** to methanol at room temperature (compound **19**, Scheme 4.4 and Figure 4.4). Compound **11**, being much less reactive towards nucleophiles, did not react with methanol under the same conditions and no emission enhancement was observed. Compound **13** readily underwent reaction with n-butyl amine to form non-emissive intermediate imine **21** which upon reduction gave a highly emissive **23** with Φ_f values of 0.9 in toluene. A catalyst and high temperatures (90^oC in toluene) were however required to form the corresponding imine **20** following reaction of **11** and n-butyl

amine. Reduction of **20** in methanol yielded **22** with Φ_f values of 0.13 in acetonitrile. M*eso*-formyl Bodipy dyes with electron withdrawing groups at positions C2 and C6 are highly reactive given their enhanced electrophilicty.

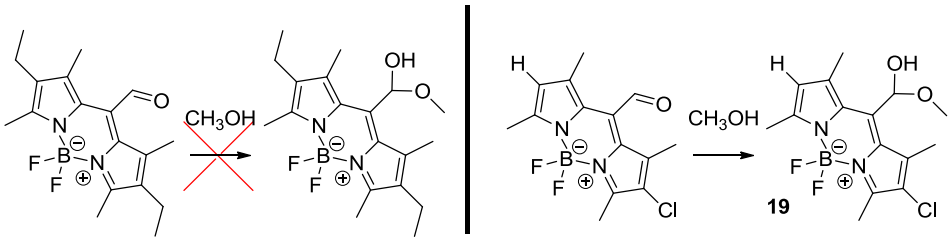

Scheme 4.4: Hemiacetal formation in methanol**.**

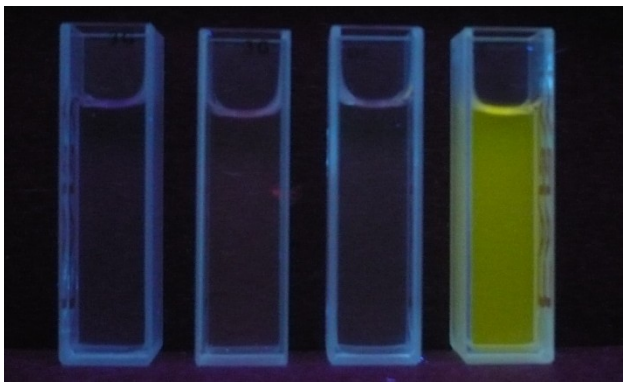

Figure 4.4: From left to right, solutions of compounds **11** in acetonitrile and methanol and solutions of compound **13** in acetonitrile and methanol, all at room temperature, portrayed upon UV excitation. Rapid emission enhancement was observed upon preparing the solution in methanol due to nucleophilic addition of methanol to compound **13**.

4.3. Conclusion

New Bodipy dyes were obtained with versatile tethering potential and diverse electrochemical properties. Hydroxymethyl or formyl groups at the *meso* position provided a handle for covalent tethering to receptors and biomolecules of interest, which dispenses with the more commonly used *meso*-aryl moiety as a means to tag molecules and thus avoid the undesired internal conversion dissipation mechanisms attributed to such a moiety. The new dyes may be coupled to both electrophiles and nucleophiles. Substitution at positions C2 and C6 with electron withdrawing or donating groups (Et, H, Cl or CN) enabled tuning the redox potentials within a *ca.* 0.7 eV, importantly, no substantial changes were observed in either the absorption or emission spectra, or the HOMO-LUMO bandgap. *Meso*-acetoxymethyl and *meso*-hydroxymethyl Bodipy dyes showed, in general, irreversible and reversible electrochemical reductions,

respectively. In the case of *meso*-formyl compounds a reversible two-electron reduction was recorded. A one-electron electrochemical oxidation was recorded for all compounds reported. *Meso*-acetoxymethyl and *meso*-hydroxymethyl are characterized by their high emission quantum yields (in the range of 0.7 to 1) and extinction coefficients (in the range of 50,000 to 100,000). Fluorescence lifetimes in the range of 4.5 to 7.0 ns are further recorded for these compounds. In contrast *meso*-formyl compounds show an up to 4-fold reduction in the molar extinction coefficient and are non-emissive, consistent with a forbidden n-π^* transition from the ground state to lowest singlet excited state. The non-emissive *meso*-formyl Bodipy dyes thus provide unique opportunities as fluorogenic probes of nucleophilic attack by *e.g.* alcohols, thiols and amine groups and as fluorescent labeling agents where uncoupled fluorophores will not contribute to the fluorescence background. Overall, the new Bodipy dyes reported here are promising candidates for the preparation of fluorescent sensors relying in photoinduced electron transfer and may find use in a number of fluorescent-labeling protocols.

4.4. Experimental Section

Materials. 8-Acetoxymethyl-2,6-diethyl-1,3,5,7-tetramethyl-pyrromethene fluoroborate (PM605) was purchased from Exciton, Inc. All other chemicals were supplied by Sigma-Aldrich, Co and used without further purification.

Instrumentation. Absorption and emission spectra were recorded on a Cary 5000 UV-VIS-NIR and Cary Eclipse Fluorescence Spectrophotomeres, using 1 cm x 1 cm quartz quvettes. 1H NMR and 13C NMR spectra were recorded on a Varian VNMRS 500 instrument at 500MHz and 125 MHz respectively. ESI mass spectra were measured on a Thermo Scientific Exactive Orbitrap. Voltammetric experiments were conducted with a computer-controlled CHI760C potentiostat with a BASi C3 cell stand.

Fluorescence Quantum Yield. PM605 in ethanol (Φ_{st}=0.74) was used as a standard to calculate the emission quantum yields of the compounds (Φ_x). The absorption spectra of solutions of PM605 in ethanol and the dye of interest in

acetonitrile at five different concentrations were matched at 375 nm. Emission spectra were recorded for all solutions using excitation and emission slits of 2.5 nm upon excitation at 375 nm. Relative quantum efficiencies with respect to the standard were obtained from the slope of the product of absorption for the standard A_{st}, integrated emission I_x and solvent refractive index n_x for the unknown Φ_x vs. the product of absorption for the unknown A_x, integrated emission I_{st} and solvent refractive index n_{st} for the standard (see Equation 1 below).

$$A_{st} I_x n_x^2 = \frac{\phi_x}{\phi_{st}} A_x I_{st} n_{st}^2 \qquad (1)$$

Electrochemical Studies. Electrochemical experiments were performed using a three electrode system. The working electrode was 2 mm Pt with a Pt mesh as auxilary electrode and a 0.01 M aqueous Ag/AgCl solution as a reference electrode. A 0.1 M solution of tetrabutylammonium hexafluorophosphate in dry acetonitrile was used as the electrolyte solvent in which the compounds were dissolved to a final 0.72 mM concentration. Solutions also contained ferrocene with a concentration of 0.40 mM as an internal standard. The solutions were purged with argon and all measurements were conducted under inert atmosphere. Formal redox potentials were calculated from the midpoint of the cathodic and anodic peak potentials observed in the cyclic voltammograms. All values were reported vs ferrocene, with the oxidation of ferrocene measured and corrected to zero for all experiments.

Fluorescence lifetime studies. The fluorescence lifetime measurements were carried out using a Picoquant Fluotime 200 Time Correlated Single Photon Counting setup employing an LDH 470 picosecond diode laser (Picoquant) with excitation wavelength at 466 nm as the excitation source. The laser was controlled by a PDL 800 B picosecond laser driver from Picoquant. The excitation rate was 10 MHz and the detection frequency was less than 100 kHz. Photons were collected at the magic angle.

Synthesis. **8-Hydroxymethyl-2,6-diethyl-1,3,5,7-tetramethyl pyrromethene fluoroborate** was prepared as described in the literature.[40]

3-Cyano-2,4-dimethyl pyrrole, 17: was prepared as described in the literature with minor modifications.[33,42] A mixture of 3-aminocrotonitrile (1.46 g, 17.8 mmol, 2 eq.) and glycine N'-methoxy-N'-methylamide HBr salt (1.77 g, 8.89 mmol, 1 eq.) in dry ethanol was stirred under argon at 50^0C. After 16h the reaction mixture was concentrated *in vacuo*. The solid residue was washed with DCM and the organic fractions were concentrated. The solid residue was used for the next step without further purification. The overall yield of 3-cyano-2,4-dimethyl pyrrole was 54%: ^{1}H NMR (500 MHz, $CDCl_3$) δ 8.38 (br, 1H), 6.38 (s, 1H), 2.37 (s, 3H), 2.13 (s, 3H); ^{13}C NMR (125 MHz, $CDCl_3$) δ 136.9, 121.8, 117.1, 114.7, 92.6, 12.3, 10.6.

8-Acetoxymethyl-1,3,5,7-tetramethyl pyrromethene fluoroborate, 1: 2, 4-dimethyl pyrrole (0.2 g, 2.1 mmol, 2 eq) was dissolved in dry CH_2Cl_2. Acetoxyacetyl chloride (0.14 ml, 1.3 mmol, 1.2 eq) was added to the solution and the reaction was left stirring at 40 ^{0}C under argon. After 2 h it was cooled to room temperature and diisopropylethylamine (0.73 ml, 4.2 mmol, 4 eq) was added followed after 15 min by drop-wise addition of BF_3•OEt_2 (0.53 ml, 4.2 mmol, 4 eq). During the addition of BF_3•OEt_2 the color changed from pale yellow to dark red. The reaction was stopped after 15 min, the solvent was evaporated under reduced pressure and the crude reaction mixture was loaded onto a silica gel flash column and eluted with 50% ethyl acetate/hexane to give **1** as orange-green crystals (0.25 g, 75% yield): ^{1}H NMR (500 MHz, $CDCl_3$) δ 6.08 (s, 2H), 5.29 (s, 2H), 2.53 (s, 6H), 2.35 (s, 6H), 2.13 (s, 3H); ^{13}C NMR (125 MHz, $CDCl_3$) δ 170.5, 156.6, 141.5, 133.3, 132.6, 122.3, 57.8, 20.6, 15.6, 14.7; HRMS (ESI) for $C_{16}H_{19}N_2O_2BF_2$ (M^{+Na}) calcd 343.1400, found 343.1396; FTIR: 965, 1074, 1190, 1510, 1551, 1742 cm^{-1}.

8-Acetoxymethyl-2-chloro-1,3,5,7-tetramethyl pyrromethene fluoroborate, 2: 8-Acetoxymethyl-1,3,5,7-tetramethyl pyrromethene fluoroborate, **1** (0.2 g, 0.62 mmol, 1 eq.) was dissolved in 3 ml dry THF under argon and cooled to -78^0C. N-chlorosuccinimide (0.17 g, 1.3 mmol. 2 eq.) dissolved in 2 ml dry THF was added drop-wise to the solution. The reaction mixture was stirred for 15 min at -78^0C after which it was warmed up to room

temperature and stirred for additional 12 h. The solution was diluted with CH_2Cl_2 and washed with brine. The organic layer was dried with $MgSO_4$ and the solvent was next evaporated under reduced pressure. The solid residue was loaded onto a silica gel flash column and eluted with dichloromethane to give **2** as red-green crystals (0.17 g, 76 % yield): ^{1}H NMR (500 MHz, $CDCl_3$) δ 6.13 (s, 1H), 5.28 (s, 2H), 2.54 (s, 6H), 2.37 (s, 3H), 2.33 (s, 3H), 2.13 (s, 3H); ^{13}C NMR (125 MHz, $CDCl_3$) δ 170.4, 159.2, 151.1, 143.3, 134.5, 133.7, 133.5, 130.1, 123.2, 123.1, 122.4, 57.8, 20.5, 15.8, 14.8, 12.7, 12.4; HRMS (ESI) for $C_{16}H_{18}N_2O_2BClF_2$ (M^{+Na}) calcd 377.10101, found 377.10206; FTIR: 643, 720, 965, 1160,1183, 1552, 1742 cm^{-1}.

8-Acetoxymethyl-2,6-dichloro-1,3,5,7-tetramethyl pyrromethene fluoroborate, 3: 8-Acetoxymethyl-1,3,5,7-tetramethyl pyrromethene fluoroborate, **1** (0.2 g, 0.62 mmol, 1 eq.) was dissolved in 3 ml of dry THF under argon and cooled to -78^{0}C. N-chlorosuccinimide (0.33 g, 2.5 mmol. 4 eq.) dissolved in 2 ml dry THF was added drop-wise to the solution. The reaction mixture was stirred for 15 min at -78^{0}C after which it was warmed up to room temperature and stirred for additional 36 h. The solution was diluted with CH_2Cl_2 and washed with brine. The organic layer was dried with $MgSO_4$ and the solvent was evaporated under reduced pressure. The solid residue was loaded onto a silica gel flash column and eluted with dichloromethane to give **3** as purple-green crystals (0.22 g, 92 % yield). ^{1}H NMR (500 MHz, $CDCl_3$) δ 5.29 (s, 2H), 2.57 (s, 6H), 2.36 (s, 6H), 2.14 (s, 3H); ^{13}C NMR (125 MHz, $CDCl_3$) δ 170.3, 153.7, 136.2, 134.1, 130.9, 123.6, 57.7, 20.6, 12.9, 12.6; HRMS (ESI) for $C_{16}H_{17}N_2O_2BCl_2F_2$ (M^-) calcd 387.06554, found 387.06563; FTIR: 600, 720, 992, 1178, 1555, 1742 cm^{-1}.

8-Acetoxymethyl-2-cyano-1,3,5,7-tetramethyl pyrromethene fluoroborate, 4: 3-cyano-2,4-dimethyl-pyrrole, **17** (0.2 g, 1.7 mmol, 1 eq) was dissolved in acetoxyacetyl chloride (0.91ml, 8.5 mmol, 5 eq). The reaction was left stirring at 45 ^{0}C under argon for 4 h until it turned dark green. The solution was evaporated to dryness under reduced pressure and dried under vacuum for 1h. A green solid (**18**) was obtained which was redissolved in 2 ml of dry

dichlomethane to yield a *ca*. 1 M solution of **18** to which 2,4-dimethylpyrrole (0.21 ml, 2.1 mmol, 1.2 eq) was added. The solution was refluxed at 40^0C under argon for 1 h. The reaction mixture was next cooled to room temperature and 8 ml of dry dichloromethane were added (0.1 M solution). After the addition of diisopropylethylamine (1.2 ml, 6.8 mmol, 4 eq) the solution turned pale yellow. The reaction was left stirring for 15 min. BF_3•OEt_2 (1.5 ml, 13.6 mmol, 8 eq) was next added drop-wise. The color changed from pale yellow to dark red after a few min. After 30 min the reaction was stopped. The solvent was evaporated under reduced pressure and the residue was loaded onto a silica gel flash column and eluted with dichloromethane to give **4** as an orange powder (0.13g, 46% yield): ^{1}H NMR (500 MHz, $CDCl_3$) δ 6.28 (s, 1H), 5.32 (s, 2H), 2.63 (s, 3H), 2.60 (s, 3H), 2.48 (s, 3H), 2.45 (s, 3H), 2.14 (s, 3H); ^{13}C NMR (125 MHz, $CDCl_3$) δ 170.2, 164.7, 154.7, 146.6, 140.4, 136.2, 134.9, 129.8, 125.7, 114.8, 57.3, 20.5, 16.3, 15.4, 14.0, 13.4; HRMS (ESI) for $C_{17}H_{18}N_3O_2BF_2$ ($M^{+\ Na}$) calcd 368.1352, found 368.1347; FTIR: 1033, 1109, 1224, 1579, 1738, 2215 cm^{-1}.

8-Acetoxymethyl-2,6-dicyano-1,3,5,7-tetramethyl pyrromethene fluoroborate, 5: 3-cyano-2, 4-dimethyl-pyrrole, **17** (0.8 g, 6.7 mmol, 2 eq) was dissolved in dry CH_2Cl_2 to yield a 3 M solution. Acetoxyacetyl chloride (0.43 ml, 4 mmol, 1.2 eq) was added to the solution and the reaction was left stirring at 40 ^{0}C under argon for 24 h until it turned dark green. The reaction mixture was allowed to cool down to room temperature and the solution was diluted to 0.3 M with dry CH_2Cl_2. Diisopropylethylamine (2.3 ml, 13.4 mmol, 4 eq) was added after which the reaction mixture turned pale yellow. The reaction was left stirring at room temperature under argon for 15 min. BF_3•OEt_2 (1.7 ml, 13.4 mmol, 4 eq) was added drop-wise. The color changed from pale yellow to dark red after a few min. The reaction was stopped after 15 min. The solvent was evaporated under reduced pressure and the crude reaction mixture was loaded onto a silica gel flash column and eluted with 50% ethyl acetate/hexane followed by a second silica gel flash column with CH_2Cl_2 to give **5** as a red powder (0.76 g, 31 % yield): ^{1}H NMR (500 MHz, $CDCl_3$) δ 5.36 (s, 2H), 2.71 (s, 6H), 2.61 (s, 6H), 2.16 (s, 3H); ^{13}C NMR (125 MHz, $CDCl_3$) δ 170.1, 160.9, 148.1, 139.4, 132.9, 113.5, 57.1,

20.7, 15.4, 14.3; HRMS (ESI) for $C_{18}H_{17}N_4O_2BF_2$ (M^-) calcd 369.1329, found 369.1329; FTIR: 1004, 1189, 1551, 1736, 2222 cm^{-1}.

General procedures for the hydrolysis of acetoxy Bodipy derivatives

Procedure 1

Meso-acetoxymethyl Bodipy dyes **1**, **3** or **5** (1 eq) were dissolved in dry THF under argon to yield a 0.05 M solution. $LiOH.H_2O$ (5 eq) was dissolved in a volume of water equal to the volume of THF employed in dissolving the Bodipy dye. The aqueous LiOH solution and the Bodipy solution in THF were combined. The reaction mixture was left stirring for 4 h at room temperature under argon and then extracted with ethyl acetate (3 x 100 ml). The combined organic layers were washed with saturated aqueous NH_4Cl solution (3 x 100 ml) and brine (1 x 100 ml) and dried over $MgSO_4$, filtered and evaporated under reduced pressure to afford the corresponding alcohol as an amorphous solid. The crude product was loaded onto a silica gel flash column and eluted with 50 % ethyl acetate/ hexane.

Procedure 2

Meso-acetoxymethyl Bodipy dyes **2** or **4** (1 eq) were dissolved in acetone to yield 0.02 M solution. 4M HCl in water were added to the solution for final HCl concentration of 1.3 M. The reaction mixture was stirred at 40^0C under argon until the starting material was consumed. The solution was diluted with ethyl acetate, washed with brine three times, dried over $MgSO_4$ and the solvent was evaporated under reduced pressure. The crude product was purified by flash column chromatography with 50 % ethyl acetate/ hexane.

8-Hydroxymethyl-1,3,5,7-tetramethyl pyrromethene fluoroborate, 6: 8-Acetoxymethyl-1,3,5,7-tetramethyl pyrromethene fluoroborate, **1** (0.2 g; 0.62 mmol) was stirred for 4 h in the presence of LiOH (0.13 g; 3.1 mmol) according to procedure 1 described above, to give **6** as an orange powder (0.12 g; 70%). ^{1}H NMR (500 MHz, d_6-DMSO) δ 6.21 (s, 2H), 5.52 (t, 1H), 4.70 (d, J=5.1 Hz, 2H), 2.47 (s, 6H), 2.39 (s, 6H); ^{13}C NMR (125 MHz, d_6-DMSO) δ 154.9, 142.5, 141.4, 132.2, 122.0, 54.6, 15.6, 14.7; HRMS (ESI) for $C_{14}H_{17}N_2OBF_2$ ($M^{+\ Na}$) calcd 301.1294, found 301.1292; FTIR: 958, 1156, 1203, 1510, 1558, 3549 cm^{-1}.

8-Hydroxymethyl-2-chloro-1,3,5,7-tetramethyl pyrromethene fluoroborate, 7: 8-Acetoxymethyl-2-chloro-1,3,5,7-tetramethyl pyrromethene fluoroborate, **2** (0.15 g, 0.42 mmol, 1 eq.) was stirred for 16 h in the presence of HCl according to procedure 2 described above, to give **7** as a red powder with quantitative yield (0.13 g). ^{1}H NMR (500 MHz, d_6-DMSO) δ 6.35 (s, 1H), 5.62-5.64 (t, 1H), 4.70-4.71 (d, J=5.1 Hz, 2H), 2.50 (s, 3H), 2.45 (s, 3H), 2.44 (s, 3H), 2.41 (s, 3H); ^{13}C NMR (125 MHz, d_6-DMSO) δ 158.9, 147.7, 145.5, 141.9, 134.8, 133.4, 129.5, 123.6, 120.4, 54.6, 15.9, 14.9, 12.6, 12.4; HRMS (ESI) for $C_{14}H_{16}N_2OBClF_2$ (M^-) calcd 311.09395, found 311.09379; FTIR: 648, 720, 978, 1308, 1552, 3544 cm^{-1}.

8-Hydroxymethyl-2,6-dichloro-1,3,5,7-tetramethyl pyrromethene fluoroborate, 8: 8-Acetoxymethyl-2,6-dichloro-1,3,5,7-tetramethyl pyrromethene fluoroborate, **3** (0.22 g; 0.57 mmol) was stirred for 4 h in the presence of LiOH (0.12 g; 2.9 mmol) according to procedure 1 described above to give **8** as red-green crystals (0.17 g; 84%). ^{1}H NMR (500 MHz, $CDCl_3$) δ 4.92-4.91 (d, J=5.1 Hz, 2H), 2.55 (s, 6H), 2.50 (s, 6H); ^{13}C NMR (125 MHz, $CDCl_3$) δ 153.3, 138.6, 136.1, 130.5, 123.3, 55.9, 22.9, 12.9, 12.6; HRMS (ESI) for $C_{14}H_{15}N_2OBCl_2F_2$ (M^-) calcd 345.05498, found 345.05507; FTIR: 606, 718, 996, 1052, 1552, 3544 cm^{-1}.

8-Hydroxymethyl-2-cyano-1,3,5,7-tetramethyl pyrromethene fluoroborate, 9: 8-Acetoxymethyl-2-cyano-1,3,5,7-tetramethyl pyrromethene fluoroborate, **4** (0.08 g, 0.23 mmol, 1 eq.) was stirred for 4 h in the presence of HCl according to procedure 2 described above to give **9** as an orange powder with quantitative yield. ^{1}H NMR (500 MHz, $CDCl_3$) δ 6.27 (s, 1H), 4.93 (s, 2H), 2.63 (s, 3H), 2.62 (s, 3H), 2.59 (s, 3H), 2.56 (s, 3H); ^{13}C NMR (125 MHz, $CDCl_3$) δ 164.0, 154.5, 146.5, 140.4, 139.3, 135.6, 129.5, 125.4, 114.9, 55.7, 16.2, 15.3, 13.9, 13.4; HRMS (ESI) for $C_{15}H_{16}N_3OBF_2$ (M^-) calcd 302.12817, found 302.12786; FTIR: 976, 1063, 1190, 1558, 2223, 3537 cm^{-1}.

8-Hydroxymethyl-2,6-dicyano-1,3,5,7-tetramethyl pyrromethene fluoroborate, 10: 8-Acetoxymethyl-2,6-dicyano-1,3,5,7-tetramethyl pyrromethene fluoroborate, **5** (0.2 g; 0.54mmol) was stirred for 4 h in the

presence of LiOH (0.11 g; 2.7 mmol) according to procedure 1 described above to give **10** as a red powder (0.15 g; 83%). ^{1}H NMR (400 MHz, d_6-acetone) δ 2.85 (s, 2H), 2.78 (s, 6H), 2.66 (s, 6H); ^{13}C NMR (75 MHz, d_6-acetone) δ 158.9, 148.5, 146.7, 132.5, 113.1, 54.8, 14.1, 13.0; HRMS (ESI) for $C_{16}H_{15}N_4OBF_2$ (M^-) calcd 327.1223, found 327.1227; FTIR: 1000, 1197, 1551, 2223, 3549 cm^{-1}.

General procedure for the synthesis of aldehyde Bodipy derivatives (Dess-Martin oxidation)

Dess-Martin periodinane (1.5 eq) was dissolved in dry dichloromethane. To the suspension was slowly added a solution of *meso*-acetoxymethyl Bodipy dyes PMOH, **6**, **7**, **8**, **9**, or **10** (1 eq) in dry dichloromethane at 0ºC under argon. After 10 min the ice bath was removed and the reaction mixture was left stirring at room temperature for extended periods of time as detailed below. The reaction mixture was extracted with saturated aqueous $Na_2S_2O_3$ followed by saturated aqueous $NaHCO_3$ and brine. The combined organic solutions were dried over $MgSO_4$. The solvent was evaporated and the residue was purified using flash column chromatography with dichloromethane as the eluent.

8-Formyl-2,6-diethyl-1,3,5,7-tetramethyl pyrromethene fluoroborate, 11: Reaction of 8-hydroxymethyl-2,6-diethyl-1,3,5,7-tetramethyl pyrromethene fluoroborate, **PMOH** (0.1 g, 0.3 mmol) and Dess-Martin periodinane (0.19 g; 0.45 mmol) took place for 15 min according to the procedure described above to give **11** as a purple powder (0.073 g; 74%). ^{1}H NMR (500 MHz, $CDCl_3$) δ 10.61 (s, 1H), 2.51 (s, 6H), 2.39-2.34 (q, J=7.6 Hz, J=7.5 Hz, 4H), 2.04 (s, 6H), 1.05-1.02 (t, J=7.7 Hz, J=7.5 Hz, 6H); ^{13}C NMR (125 MHz, $CDCl_3$) δ 194.1, 156.7, 136.4, 134.8, 133.6, 17.1, 14.6, 12.9, 12.8; HRMS (ESI) for $C_{18}H_{23}N_2OBF_2$ (M^-) calcd 333.19443, found 333.19453; FTIR: 979, 1183, 1319, 1551, 1711 cm^{-1}.

8-Formyl-1,3,5,7-tetramethyl pyrromethene fluoroborate, 12: Reaction of 8-hydroxymethyl-1,3,5,7-tetramethyl pyrromethene fluoroborate, **6** (0.1 g, 0.35 mmol) and Dess-Martin periodinane (0.23 g; 0.53 mmol) took place for 30 min according to the procedure described above to give **12** as a brown-green powder (0.083 g; 86%). ^{1}H NMR (500 MHz, $CDCl_3$) δ 10.57 (s, 1H), 6.08 (s, 2H), 2.54 (s, 6H), 2.13 (s, 6H); ^{13}C NMR (125 MHz, $CDCl_3$) δ 193.0, 158.5, 141.5, 135.9,

128.8, 121.8, 30.9, 15.4, 14.8; HRMS (ESI) for $C_{14}H_{15}N_2OBF_2$ (M^-) calcd 275.11727, found 275.11677; FTIR: 965, 1061, 1190, 1306, 1510, 1558, 1715 cm^{-1}.

8-Formyl-2-chloro-1,3,5,7-tetramethyl pyrromethene fluoroborate, 13: Reaction of 8-hydroxymethyl-2-chloro-1,3,5,7-tetramethyl pyrromethene fluoroborate, **7** (0.1 g, 0.32 mmol) and Dess-Martin periodinane (0.2 g; 0.48 mmol) took place for 15 min according to the procedure described above to give **13** as a purple-green powder (0.08 g; 80%). ^1H NMR (500 MHz, $CDCl_3$) δ 10.54 (s, 1H), 6.11, (s, 1H), 2.54, (s, 6H), 2.12 (s, 3H), 2.09 (s, 3H); ^{13}C NMR (125 MHz, $CDCl_3$) δ 192.6, 160.9, 152.8, 143.2, 136.1, 134.7, 129.6, 126.0, 122.6, 122.3, 15.5, 15.0, 12.7, 12.5; HRMS (ESI) for $C_{14}H_{14}N_2OBClF_2$ (M^-) calcd 309.07830, found 309.07788; FTIR: 642, 818, 1550, 1710 cm^{-1}.

8-Formyl-2,6-dichloro-1,3,5,7-tetramethyl pyrromethene fluoroborate, 14: Reaction of 8-hydroxymethyl-2, 6-dichloro-1,3,5,7-tetramethyl pyrromethene fluoroborate, **8** (0.1 g, 0.29 mmol) and Dess-Martin periodinane (0.18 g; 0.43 mmol) took place for 30 min according to the procedure described above to give **14** as a purple-green powder (0.08 g; 80%). ^1H NMR (500 MHz, $CDCl_3$) δ 10.55 (s, 1H), 2.57 (s, 6H), 2.12 (s, 6H); ^{13}C NMR (125 MHz, $CDCl_3$) δ 192.1, 155.5, 136.3, 136.2, 126.9, 123.4, 12.9, 12.8; HRMS (ESI) for $C_{14}H_{13}N_2OBCl_2F_2$ (M^-) calcd 343.03933, found 343.03892; FTIR: 600, 676, 990, 1182, 1554, 1716 cm^{-1}.

8-Formyl-2-cyano-1,3,5,7-tetramethyl pyrromethene fluoroborate, 15: Reaction of 8-hydroxymethyl-2-cyano-1,3,5,7-tetramethyl pyrromethene fluoroborate, **9** (0.1 g, 0.33 mmol) and Dess-Martin periodinane (0.21 g; 0.5 mmol) took place for 1h according to the procedure described above to give **15** as a brown-green powder (0.09 g; 91%). ^1H NMR (500 MHz, $CDCl_3$) δ 10.56 (s, 1H), 6.28 (s, 1H), 2.63 (s, 3H), 2.61 (s, 3H), 2.25 (s, 3H), 2.17 (s, 3H); ^{13}C NMR (125 MHz, $CDCl_3$) δ 191.6, 166.6, 156.3, 146.4, 140.7, 136.9, 132.4, 125.9, 125.2, 114.3, 103.5, 15.8, 15.6, 14.0, 13.5; HRMS (ESI) for $C_{15}H_{14}N_3OBF_2$ (M^-) calcd 300.11143, found 300.11236; FTIR: 976, 1059, 1316, 1549, 2220, 1714 cm^{-1}.

8-Formyl-2,6-dicyano-1,3,5,7-tetramethyl pyrromethene fluoroborate, 16: Reaction of 8-hydroxymethyl-2,6-dicyano-1,3,5,7-tetramethyl pyrromethene fluoroborate, **10** (0.1 g, 0.3 mmol) and Dess-Martin periodinane (0.19 g; 0.45 mmol) took place for 1.5 h according to the procedure described above to give **16** as a purple powder (0.095 g; 97%). ^{1}H NMR (500 MHz, $CDCl_3$) δ 10.59 (s, 1H), 2.73 (s, 6H), 2.36 (s, 6H); ^{13}C NMR (125 MHz, $CDCl_3$) δ 190.2, 162.4, 147.8, 140.2, 128.8, 112.8, 107.3, 14.9, 14.2; HRMS (ESI) for $C_{16}H_{13}N_4OBF_2$ (M^-) calcd 325.10777, found 325.10689; FTIR: 995, 1197, 1313, 1545, 1718, 2228 cm^{-1}.

8-(N-butyl)-methylimine-2,6-diethyl-1,3,5,7-tetramethyl pyrromethene fluoroborate (20) Butylamine (0.02 g, 0.27 mmol, 1.5 eq) and Dabco (0.12 g, 1.08 mmol, 6 eq) were dissolved in 1 ml dry toluene under argon. The solution was heated to 90^0C. Titanium chloride (0.27 ml of 1M in dichloromethane, 1.5 eq) was added dropwise to the heated reaction mixture, followed by the addition of 1 ml toluene solution of 8-Formyl-2,6-diethyl-1,3,5,7-tetramethyl pyrromethene fluoroborate **11** (0.06 g, 0.18 mmol, 1 eq). After 3 h of reflux the reaction mixture was cooled to room temperature. The formed precipitate was filtered and washed with dichloromethane. The solvent was evaporated under reduced pressure and the residue was purified using flash column chromatography with hexane/ethyl acetate = 10/1. A purple powder was obtained (0.058 g, 83%); ^{1}H NMR (500 MHz, $CDCl_3$) δ 8.50 (s, 1H), 3.66-3.70 (dt, 2H), 2.49 (s, 6H), 2.33-2.37 (q, 4H), 2.01 (s, 6H), 1.72-1.77 (quintet, 2H), 1.44-1.51 (sextet, 2H), 1.01-1.04 (t, 6H), 0.96-0.99 (t, 3H); ^{13}C NMR (125 MHz, $CDCl_3$) δ 157.1, 154.8, 136.9, 134.8, 132.8, 129.9, 62.1, 31.9, 30.8, 17.1, 14.7, 13.9, 13.8, 12.6; HRMS (ESI) for $C_{22}H_{32}BF_2N_3$ (M^+) calcd 388.27301 found 388.27342; FTIR: 1651, 1538, 1321, 1190, 1043, 961 cm^{-1}

8-(N-butyl)-methylimine-2-chloro-1,3,5,7-tetramethyl pyrromethene fluoroborate (21) 8-Formyl-2-chloro-1,3,5,7-tetramethyl pyrromethene fluoroborate **13** (0.015g, 0.05 mmol, 1 eq) was dissolved in 1 ml of dry dichloromethane. Butylamine (0.006 g, 0.075 mmol, 1.5 eq) was added to the solution. The reaction was left stirring under argon at room temperature for 10 h after which the solvent was evaporated under reduced pressure. The product was

purified by column chromatography from CH_2Cl_2 to yield a purple powder (0.015 g, 85 %). ^{1}H NMR (500 MHz, $CDCl_3$) δ 8.49 (s, 1H), 6.09 (s, 1H), 3.72-3.69 (dt, 2H, J=6.1 Hz, J=1.5 Hz), 2.54 (s, 6H), 2.11 (s, 3H), 2.09 (s, 3H), 1.78-1.72 (quintet, 2H), 1.50-1.46 (sextet, 2H), 0.99-0.97 (t, 3H, J=7.3 Hz); ^{13}C NMR (125 MHz, $CDCl_3$) δ 159.2, 155.8, 151.1, 143.5, 136.5, 134.9, 131.4, 127.9, 122.1, 62.2, 31.9, 20.8, 16.7, 14.9, 13.9, 13.8, 12.4; MS (ESI) for $C_{18}H_{23}BClF_2N_3$ (M^-) calcd 364.16416 found 364.30; FTIR: 1655, 1550, 1313, 1190, 987 cm^{-1}

8-(N-butyl)-methylamine-2,6-diethyl-1,3,5,7-tetramethyl pyrromethene fluoroborate (22) 8-(N-butyl)-methylimine-2,6-diethyl-1,3,5,7-tetramethyl pyrromethene fluoroborate **20** (0.05 g, 0.13 mmol, 1 eq) was dissolved in dry methanol. $NaCNBH_3$ (0.012 g, 0.2 mmol, 1.5 eq) was added to the solution and the reaction mixture was left stirring at room temperature under argon. After 2 h the reaction mixture was condensed under reduced pressure and purified by column chromatography from CH_2Cl_2. The product was isolated as red powder (0.048 g, 95%) ^{1}H NMR (500 MHz, $CDCl_3$) δ 3.70 (s, 2H), 2.72-2.74 (t, 2H), 2.49 (s, 6H), 2.37-2.42 (m, 10H), 1.49-1.54 (quintet, 2H), 1.35-1.41 (sextet, 2H), 1.03-1.07 (t, 6H), 0.91-0.94 (t, 3H); ^{13}C NMR (125 MHz, $CDCl_3$) δ 153.4, 136.3, 132.8, 131.8, 50.1, 45.5, 32.2, 20.5, 17.2, 14.7, 13.9, 12.5; HRMS (ESI) for $C_{22}H_{34}BF_2N_3$ (M^+) calcd 390.28866 found 390.28879; FTIR: 1546, 1345, 1190, 972 cm^{-1}

8-(N-butyl)-methylamine-2-chloro-1,3,5,7-tetramethyl pyrromethene fluoroborate (23) 8-(N-butyl)-methylimine-2-chloro-1,3,5,7-tetramethyl pyrromethene fluoroborate **21** (0.01 g, 0.027 mmol, 1 eq) was dissolved in 1 ml of dry methanol. $NaCNBH_3$ (0.005 g, 0. 81 mmol, 3 eq) was added to the solution and the reaction mixture was left stirring at room temperature under argon. After 2 h the reaction mixture was condensed under reduced pressure and purified by column chromatography from CH_2Cl_2. The product was isolated as red powder (0.08 g, 81%) ^{1}H NMR (500 MHz, $CDCl_3$) δ 6.11 (s, 1H), 3.92 (s, 2H), 2.72-2.75 (t, 2H, J=7.1 Hz, J=6.8 Hz), 2.53 (s, 6H), 2.48 (s, 3H), 2.46 (s, 3H), 1.54-1.50 (m, 2H), 1.40-1.36 (sextet, 2H), 0.94-0.91 (t, 3H, J=7.4 Hz); ^{13}C NMR (125 MHz, $CDCl_3$) δ 157.5, 149.7, 142.9, 140.7, 134.3, 133.0, 122.6, 50.2, 45.3, 32.3, 20.5,

15.7, 14.7, 13.9, 12.5, 12.2; MS (ESI) for $C_{18}H_{25}BClF_2N_3$ (M^-) cald 367.17981 found 366.22; FTIR: 1550, 1475, 1358, 1990, 980 cm^{-1}

4.5. References

1. Alfred, T. & Franz-Heinrich, K. Difluorboryl-Komplexe von Di- und Tripyrrylmethenen. *Justus Liebigs Annalen der Chemie* 718, 208-223, **1968**.
2. Haugland, R.P. *Handbook of Fluorescent Probes and Research Products*, (Molecular Probes, Inc., Eugene, OR, 2005).
3. Johnson, I.D., Kang, H.C. & Haugland, R.P. Fluorescent membrane probes incorporating dipyrrometheneboron difluoride fluorophores. *Analytical Biochemistry* 198, 228-237, **1991**.
4. Loudet, A. & Burgess, K. BODIPY Dyes and Their Derivatives: Syntheses and Spectroscopic Properties. *Chemical Reviews* 107, 4891-4932, **2007**.
5. Wood, T.E. & Thompson, A. Advances in the Chemistry of Dipyrrins and Their Complexes. *Chemical Reviews* 107, 1831-1861, **2007**.
6. Gilles, U., Raymond, Z. & Anthony, H. The Chemistry of Fluorescent Bodipy Dyes: Versatility Unsurpassed13. *Angewandte Chemie International Edition* 47, 1184-1201, **2008**.
7. Ziessel, R., Ulrich, G. & Harriman, A. The chemistry of Bodipy: a new El Dorado for fluorescence tools. *New Journal of Chemistry* 31, 496-501, **2007**.
8. Arbeloa, F.L.p., Bañuelos, J., Martínez, V., Arbeloa, T. & Arbeloa, I.L.p. Structural, photophysical and lasing properties of pyrromethene dyes. *International Reviews in Physical Chemistry* 24, 339 - 374, **2005**.
9. Qin, W., Rohand, T., Dehaen, W., Clifford, J.N., Driesen, K., Beljonne, D., Van Averbeke, B., Van der Auweraer, M. & Boens, N.l. Boron Dipyrromethene Analogs with Phenyl, Styryl, and Ethynylphenyl Substituents: Synthesis, Photophysics, Electrochemistry, and Quantum-Chemical Calculations. *Journal of Physical Chemistry A* 111, 8588-8597, **2007**.
10. Qin, W., Baruah, M., Van der Auweraer, M., De Schryver, F.C. & Boens, N.l. Photophysical Properties of Borondipyrromethene Analogues in Solution. *Journal of Physical Chemistry A* 109, 7371-7384, **2005**.
11. Korlach, J., Schwille, P., Webb, W.W. & Feigenson, G.W. Characterization of lipid bilayer phases by confocal microscopy and fluorescence correlation spectroscopy. *Proceedings of the National Academy of Sciences, USA* 96, 8461-8466, **1999**.
12. Drummen, G.P.C., van Liebergen, L.C.M., Op den Kamp, J.A.F. & Post, J.A. C11-BODIPY581/591, an oxidation-sensitive fluorescent lipid peroxidation probe: (micro)spectroscopic characterization and validation of methodology. *Free Radical Biology and Medicine* 33, 473-490, **2002**.
13. Pap, E.H.W., Drummen, G.P.C., Winter, V.J., Kooij, T.W.A., Rijken, P., Wirtz, K.W.A., Op den Kamp, J.A.F., Hage, W.J. & Post, J.A. Ratio-fluorescence microscopy of lipid oxidation in living cells using C11-BODIPY581/591. *FEBS Letters* 453, 278-282, **1999**.
14. Lemcke, S., Hönnscheidt, C., Waschatko, G., Bopp, A., Lütjohann, D., Bertram, N. & Gehrig-Burger, K. DHEA-Bodipy-A functional fluorescent DHEA analog for live cell imaging. *Molecular and Cellular Endocrinology* 314, 31-40.
15. Singh, K.K., Parwaresch, R. & Krupp, G. Rapid kinetic characterization of hammerhead ribozymes by real-time monitoring of fluorescence resonance energy transfer (FRET). *RNA* 5, 1348-1356, **1999**.
16. Danell, A.S. & Parks, J.H. FRET measurements of trapped oligonucleotide duplexes. *International Journal of Mass Spectrometry* 229, 35-45, **2003**.
17. Zeng, L., Miller, E.W., Pralle, A., Isacoff, E.Y. & Chang, C.J. A Selective Turn-On Fluorescent Sensor for Imaging Copper in Living Cells. *Journal of the American Chemical Society* 128, 10-11, **2005**.
18. Yuan, M., Li, Y., Li, J., Li, C., Liu, X., Lv, J., Xu, J., Liu, H., Wang, S. & Zhu, D. A Colorimetric and Fluorometric Dual-Modal Assay for Mercury Ion by a Molecule. *Organic Letters* 9, 2313-2316, **2007**.
19. Wang, J. & Qian, X. A Series of Polyamide Receptor Based PET Fluorescent Sensor Molecules: Positively Cooperative Hg2+ Ion Binding with High Sensitivity. *Organic Letters* 8, 3721-3724, **2006**.

20. Baruah, M., Qin, W., Vallée, R.A.L., Beljonne, D., Rohand, T., Dehaen, W. & Boens, N. A Highly Potassium-Selective Ratiometric Fluorescent Indicator Based on BODIPY Azacrown Ether Excitable with Visible Light. *Organic Letters* 7, 4377-4380, **2005**.
21. Bozdemir, O.A., Sozmen, F., Buyukcakir, O., Guliyev, R., Cakmak, Y. & Akkaya, E.U. Reaction-Based Sensing of Fluoride Ions Using Built-In Triggers for Intramolecular Charge Transfer and Photoinduced Electron Transfer. *Organic Letters* 12, 1400-1403, **2010**.
22. Peng, X., Du, J., Fan, J., Wang, J., Wu, Y., Zhao, J., Sun, S. & Xu, T. A Selective Fluorescent Sensor for Imaging Cd2+ in Living Cells. *Journal of the American Chemical Society* 129, 1500-1501, **2007**.
23. Krumova, K., Oleynik, P., Karam, P. & Cosa, G. Phenol-Based Lipophilic Fluorescent Antioxidant Indicators: A Rational Approach. *Journal of Organic Chemistry* 74, 3641-3651, **2009**.
24. Oleynik, P., Ishihara, Y. & Cosa, G. Design and Synthesis of a BODIPY-α±-Tocopherol Adduct for Use as an Off/On Fluorescent Antioxidant Indicator. *Journal of the American Chemical Society* 129, 1842-1843, **2007**.
25. Khatchadourian, A., Krumova, K., Boridy, S., Ngo, A.T., Maysinger, D. & Cosa, G. Molecular Imaging of Lipid Peroxyl Radicals in Living Cells with a BODIPYâˆ’Î±-Tocopherol Adduct. *Biochemistry* 48, 5658-5668, **2009**.
26. Gabe, Y., Ueno, T., Urano, Y., Kojima, H. & Nagano, T. Tunable design strategy for fluorescence probes based on 4-substituted BODIPY chromophore: improvement of highly sensitive fluorescence probe for nitric oxide. *Analytical and Bioanalytical Chemistry* 386, 621-626, **2006**.
27. Yasuyuki, Y., Yumiko, T., Akinori, M., Masahiko, I. & Shin, A. BODIPY-Based Fluorescent Redox Potential Sensors that Utilize Reversible Redox Properties of Flavin. *ChemBioChem* 9, 853-856, **2008**.
28. Sun, Z.-N., Wang, H.-L., Liu, F.-Q., Chen, Y., Tam, P.K.H. & Yang, D. BODIPY-Based Fluorescent Probe for Peroxynitrite Detection and Imaging in Living Cells. *Organic Letters* 11, 1887-1890, **2009**.
29. Andrew, C.B., Graeme, C., Kristopher, J.E., Ross, W.H. & William, C. Redox-Controlled Fluorescence Modulation in a BODIPY-Quinone Dyad. *European Journal of Organic Chemistry* 2008, 2705-2713, **2008**.
30. Sun, Z.-N., Liu, F.-Q., Chen, Y., Tam, P.K.H. & Yang, D. A Highly Specific BODIPY-Based Fluorescent Probe for the Detection of Hypochlorous Acid. *Organic Letters* 10, 2171-2174, **2008**.
31. Gabe, Y., Urano, Y., Kikuchi, K., Kojima, H. & Nagano, T. Highly Sensitive Fluorescence Probes for Nitric Oxide Based on Boron Dipyrromethene Chromophore-Rational Design of Potentially Useful Bioimaging Fluorescence Probe. *Journal of the American Chemical Society* 126, 3357-3367, **2004**.
32. de Silva, A.P., Gunaratne, H.Q.N., Gunnlaugsson, T., Huxley, A.J.M., McCoy, C.P., Rademacher, J.T. & Rice, T.E. Signaling Recognition Events with Fluorescent Sensors and Switches. *Chemical Reviews* 97, 1515-1566, **1997**.
33. Ueno, T., Urano, Y., Kojima, H. & Nagano, T. Mechanism-Based Molecular Design of Highly Selective Fluorescence Probes for Nitrative Stress. *Journal of the American Chemical Society* 128, 10640-10641, **2006**.
34. Ueno, T., Urano, Y., Setsukinai, K., Takakusa, H., Kojima, H., Kikuchi, K., Ohkubo, K., Fukuzumi, S. & Nagano, T. Rational principles for modulating fluorescence properties of fluorescein. *Journal of the American Chemical Society* 126, 14079-14085, **2004**.
35. Turro, N.J., Ramamurthy, V. & Scaiano, J.C. *Modern Molecular Photochemistry of Organic Molecules*, 1084 (University Science Books, Sausalito, CA, 2010).
36. Kim, H., Burghart, A., Welch, M.B., Reibenspies, J. & Burgess, K. Synthesis and spectroscopic properties of a new 4-bora-3a,4a-diaza-s-indacene (BODIPY (R)) dye. *Chemical Communications*, 1889-1890, **1999**.
37. Thoresen, L.H., Kim, H., Welch, M.B., Burghart, A. & Burgess, K. Synthesis of 3,5-Diaryl-4,4-difluoro-4-bora-3a,4a-diaza-s-indacene (BODIPY®) Dyes. *Synlett* 1998, 1276-1278, **1998**.

38. Prieto, J.B., Arbeloa, F.L., Martínez, V.M., López, T.A., Amat-Guerri, F., Liras, M. & Arbeloa, I.L. Photophysical properties of a new 8-phenyl analogue of the laser dye PM567 in different solvents: internal conversion mechanisms. *Chemical Physics Letters* 385, 29-35, **2004**.
39. Matthias, K., Thomas, G., Stefan, H., Jörg, D. & Josef, B. Electrogenerated Chemiluminescence and Proton-Dependent Switching of Fluorescence: Functionalized Difluoroboradiaza-s-indacenes. *Angewandte Chemie, International Edition in English* 36, 1333-1335, **1997**.
40. Amat-Guerri, F., Liras, M., Carrascoso, M.L. & Sastre, R. Methacrylate-tethered analogs of the laser dye PM567-synthesis, copolymerization with methyl methacrylate and photostability of the copolymers. *Photochemistry and Photobiology* 77, 577-584, **2003**.
41. Li, L., Nguyen, B. & Burgess, K. Functionalization of the 4,4-difluoro-4-bora-3a,4a-diaza-s-indacene (BODIPY) core. *Bioorganic & Medicinal Chemistry Letters* 18, 3112-3116, **2008**.
42. Alberola, A., González Ortega, A., Luisa Sádaba, M. & Sañudo, C. Versatility of Weinreb amides in the Knorr pyrrole synthesis. *Tetrahedron* 55, 6555-6566, **1999**.
43. degradation.
44. Prieto, J.B., Arbeloa, T., Liras, M., Martínez, V.M. & Arbeloa, F.L. Concerning the color change of pyrromethene 650 dye in electron-donor solvents. *Journal of Photochemistry and Photobiology A: Chemistry* 184, 298-305, **2006**.
45. Cieslik-Boczula, K., Burgess, K., Li, L.L., Nguyen, B., Pandey, L., De Borggraeve, W.M., Van der Auweraer, M. & Boens, N. Photophysics and stability of cyano-substituted boradiazaindacene dyes. *Photochemical & Photobiological Sciences* 8, 1006-1015, **2009**.
46. Arbeloa, F.L., Prieto, J.B., Martínez, V.M., López, T.A. & Arbeloa, I.L. Intramolecular Charge Transfer in Pyrromethene Laser Dyes: Photophysical Behaviour of PM650. *ChemPhysChem* 5, 1762-1771, **2004**.
47. Meyer, S.D. & Schreiber, S.L. Acceleration of the Dess-Martin Oxidation by Water. *Journal of Organic Chemistry* 59, 7549-7552, **1994**.
48. Lai, R.Y., Fabrizio, E.F., Lu, L., Jenekhe, S.A. & Bard, A.J. Synthesis, Cyclic Voltammetric Studies, and Electrogenerated Chemiluminescence of a New DonorAcceptor Molecule: 3,7-[Bis[4-phenyl-2-quinolyl]]-10-methylphenothiazine. *Journal of the American Chemical Society* 123, 9112-9118, **2001**.
49. Lai, R.Y. & Bard, A.J. Electrogenerated Chemiluminescence 71. Photophysical, Electrochemical, and Electrogenerated Chemiluminescent Properties of Selected Dipyrromethene-BF2 Dyes. *Journal of Physical Chemistry B* 107, 5036-5042, **2003**.
50. Gaussian.
51. Koch, W. & Holthausen, M.C. *A Chemist's Guide to Density Functional Theory*, 1-300 (Wiley-VCH, Weinheim, Germany, 2000).

How Lipid Unsaturation, Peroxyl Radical Partitioning and Chromanol Lipophilic Tail Affect the Antioxidant Activity of α-Tocopherol: Direct Visualization via High Throughput Fluorescence Studies Conducted with Fluorogenic α-Tocopherol Analogues

Katerina Krumova, Sayuri Friedland, and Gonzalo Cosa, *J. Am. Chem. Soc*., **2012**, 134 (24), 10102–10113

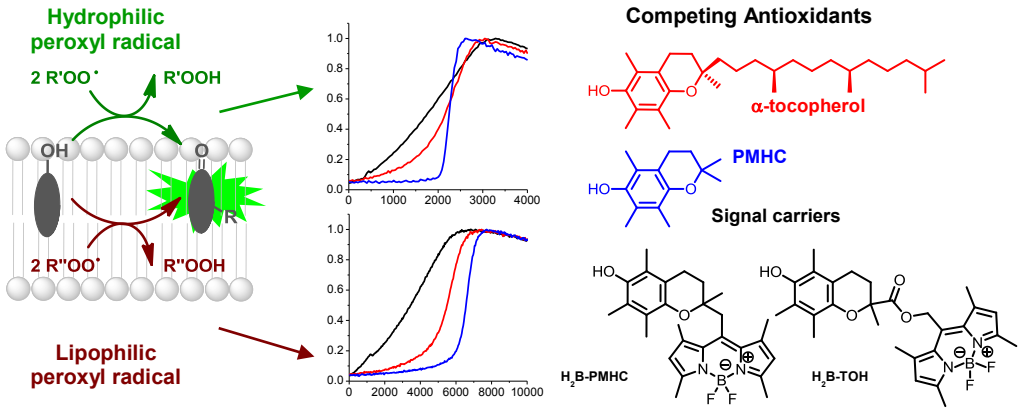

Preface

In previous chapters we established the mechanism through which BTOH operates and the requirements that need to be met in order to improve its sensitivity and reactivity. The sensitivity arises from the photoinduced electron transfer (PeT) that operates in BTOH. We anticipated that by favoring the PeT upon using fluorophores with higher reduction potential, we would make the "off" state less emissive. This will lead to higher on/off ratios and improved sensitivity. In this chapter we report the preparation of 2 highly sensitive fluorogenic α-tocopherol analogues by utilizing one of the newly synthesized Bodipy fluorophores described in chapter 4 bearing H-substitution on positions C-2 and C-6 as a reporter segment. The 2 probes undergo >100 fold fluorescence intensity enhancement upon reaction with peroxyl radicals in solution and >30 fold emission enhancement in heterogeneous media (liposome suspensions). The probes consist of a chromanol moiety coupled to the *meso* position of the Bodipy fluorophore. The coupling is accomplished through two different functional groups which enables tuning the reactivity of the probes towards H-atom abstraction by peroxyl radicals. In this chapter we investigate the effect on the radical scavenging reactivity of the fluorogenic probes bearing a methylene (in H_2B-PMHC) vs. ester linker (in H_2B-TOH). We next discuss the application of the two new probes for the development of a high-throughput fluorescence assay for monitoring kinetics of peroxyl radical reactions in liposomes. The evolution of the fluorescence intensity over time provides a rapid facile method to conduct competitive kinetic studies in the presence of α-tocopherol and analogues. Studies are conducted in 6 different liposome solutions prepared from poly- and mono-unsaturated, and saturated (fluid vs. gel phase) lipids, in the presence of either hydrophilic or lipophilic peroxyl radicals. A quantitative treatment is formulated for the temporal evolution of the intensity in terms of relative rate constants of H-atom abstraction (k_{inh}) from the various tocopherol analogues. Combined, the new probes, the fluorescence assay, and the data analysis provide a new method to obtain in a rapid parallel format relative antioxidant activities in phospholipid membranes. Altogether, a novel, facile method of study, new

insights, and a quantitative understanding on the critical role of lipid diversity in modulating antioxidant activity in the lipid milieu is reported.

5.1. Introduction

A member of the vitamin E family of compounds, α-tocopherol (TOH) has long been recognized as the most active naturally occurring lipid soluble antioxidant (Scheme 5.1 and Figure 5.1).[1] Interest on the antioxidant and anti-inflammatory properties of TOH has led to multiple studies proposing among others the benefit of TOH in mitigating cardiovascular disease,[2] slowing Alzheimer's disease progression,[3] and most recently in promoting plasma membrane repair.[4] TOH has also attracted attention due to its nonantioxidant functions, in particular its emerging role as a cellular signaling molecule, including modulation of the activity of protein kinase C[5] and phosphatidylinositol 3-kinase, as well as regulation of a number of genes.[6]

The paradigm of TOH antioxidant activity in autoxidation reactions has been laid out in a number of studies conducted over the past 30 years in homogeneous solution and in the presence of initiators. See Scheme 5.1, reactions 1 to 6, where LH represents a bis-allylic methylene moiety in a polyunsaturated fatty acid (PUFA), and Ri is the rate of initiation of lipid peroxidation.

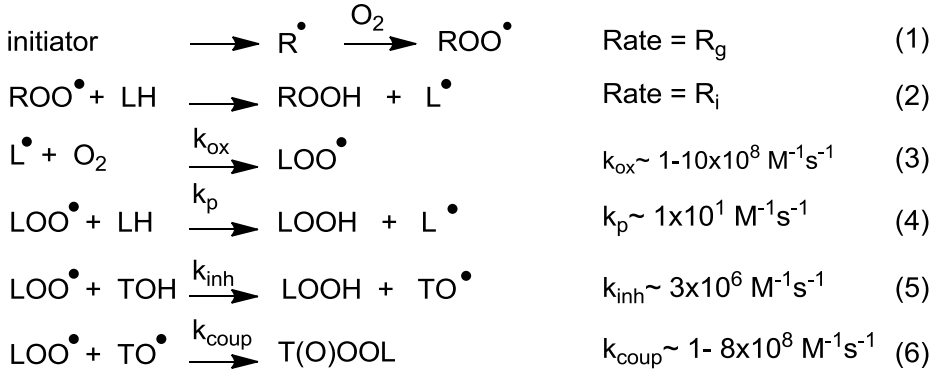

Scheme 5.1. Lipid oxidation in the presence of a free radical initiator (ROO●) and TOH, here LH represents a bis-allylic methylene moiety. The listed rate constants were obtained in homogeneous solutions. Equations 3,[7] 4,[8] 5,[1] 6.[9]

In a first elementary step TOH reacts with a peroxyl radical ($ROO^{\bullet}$ or $LOO^{\bullet}$) via H-atom transfer to yield a tocopheroxyl radical ($TO^{\bullet}$, Equation 5) and a hydroperoxide ROOH/LOOH. Analysis of the rate law for the overall process shows that the antioxidant activity of TOH is given by the rate constant for this

second order reaction (k_{inh}, the rate constants of H-atom abstraction). In the next elementary step, the $TO^{\bullet}$ initially formed rapidly scavenges a second $ROO^{\bullet}$ / $LOO^{\bullet}$ to yield addition products (e.g. tocopherones, Equation 6).[1,10-12] In the presence of initiators and in homogeneous solution TOH thus scavenges 2 peroxyl radicals, and the rate of generation R_g of peroxyl radicals may be equaled to the rate of initiation R_i of lipid peroxidation and is calculated by measuring the rate of consumption of TOH (see Equation 7).[1]

$$-\frac{d[TOH]}{dt} = k_{inh}^{TOH} \times [LOO^{\bullet}] \times [TOH] = \frac{R_g}{2} \qquad (7)$$

Whereas the antioxidant activity of TOH, its analogues,[13] and other natural and synthetic lipophilic phenolic compounds including catechols,[14] dihydroquinones,[15-17] naphthyridinols,[18] etc. are well established in homogeneous solution in organic solvents, their quantification in model lipid membranes is significantly more difficult to perform. Structural and stereoelectronic effects account for TOH rapid H-atom transfer to peroxyl free radicals in homogeneous solution.[1] When TOH is embedded in lipid membranes, in addition to its inherent chemical reactivity both its localization/accessibility and mobility in the heterogeneous media play a role in modulating its relative rate of free radical scavenging.[8,10,19-31] In line with the above, a ~1000-fold reduction in k_{inh} has been reported for TOH in phospholipid membranes vs in organic solution,[20] mostly attributed to TOH physical inaccessibility by attacking radicals and only minimally due to hydrogen bonding to water (hydrogen atom transfer cannot take place between a phenol antioxidant (AOH) when hydrogen bonded to the solvent, for steric reasons[32-34]). In fact, estimates of the drop in k_{inh} for TOH based solely on the interaction with water place the value at 8×10^5 $M^{-1}s^{-1}$, only 4-fold lower than the 3×10^6 $M^{-1}s^{-1}$ value reported in styrene.[19]

The strong effect imparted on k_{inh} by the physical-chemical heterogeneity of the phospholipid membrane-water interface is highlighted by the different antioxidant activities measured for 2,2,5,7,8-pentamethyl-6-hydroxy-chroman (PMHC, a TOH analogue lacking the phytyl tail) and TOH (see Figure 5.1 for their chemical structures), a topic which was recently reviewed.[8] Both molecules

have the same inherent chemical reactivity towards peroxyl radicals arising from the conserved chromanol moiety, yet within phospholipid membranes and due to its higher mobility, PMHC is a more potent antioxidant than TOH.[8] While significant body of research has been dedicated to the role of the media on antioxidant activities, how the rich diversity in the lipid membrane composition affects the mobility and consequently the relative antioxidant activity of TOH, however, is still poorly understood.[35-39]

In order to provide a quantitative understanding on the role that the lipid environment plays on the relative antioxidant activities of TOH and TOH analogues, we have developed a fluorescence based method to study the relative antioxidant activities of TOH and TOH analogues in a rapid parallel format. The method relies on 3 key elements: 1) The preparation of 2 new highly sensitive fluorogenic TOH analogues that follow conceptually the design of the first generation probe B-TOH that we recently reported,[40,41] yet they have a much higher sensitivity. The new probes reported here undergo > 30 fold fluorescence intensity enhancements upon reaction with peroxyl radicals. Their reactivity towards peroxyl radicals was further tuned to provide suitable references for competitive kinetic studies using the probes as signal carriers. 2) A simple high throughput fluorescence assay for a microplate reader that relies on the high sensitivity of the 2 new probes and that reports real time $ROO^{\bullet}$ reaction dynamics with TOH and its analogues in compartmented systems. 3) A quantitative treatment of the temporal evolution of the fluorescence intensity wherefrom the kinetic information is obtained for the various conditions analyzed.

Using this new method we show here how the membrane fluidity (gel vs. liquid crystalline phase), the extent of lipid unsaturation, the type of peroxyl radical used (lipophilic vs. hydrophilic), and the lipophilic tail in the free radical scavenger all affect the relative antioxidant dynamics of TOH and TOH analogues. Quantitative results validate the robustness of the new method described. Most importantly, they provide a wealth of information and new insights on the critical role of lipid diversity in modulating antioxidant activity in the lipid milieu.

5.2. Results and Discussion

5.2.1. Preparation of the New Probes

The 2 new fluorogenic antioxidants synthesized for our studies are shown in Figure 5.1. The 2 segment receptor-reporter probes consist of a chromanol moiety coupled to the *meso* position of a Bodipy fluorophore, either via an ester linker (meso-methanoyl Bodipy-6-hydroxy-2,5,7,8-tetramethylchromane-2-carboxylic acid or H_2B-TOH) or via a methylene linker (Bodipy-2,2,5,7,8-pentamethyl-6-hydroxy-chroman adduct or H_2B-PMHC).

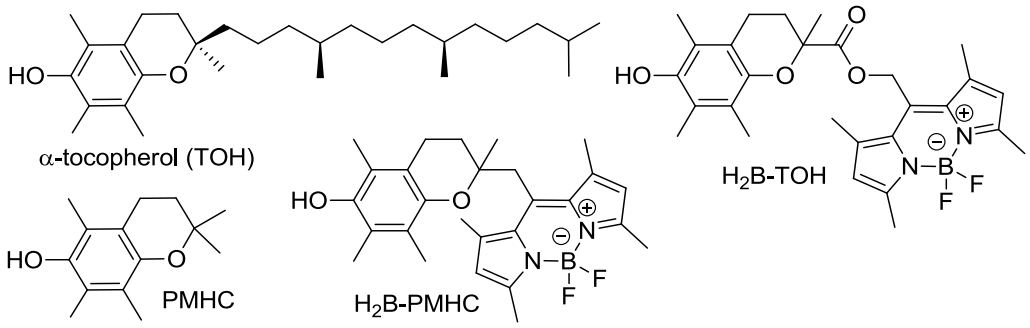

Figure 5.1. Structures of TOH, PMHC, and the new probes H2B-TOH and H2B-PMHC.

The new fluorogenic antioxidants follow the conceptual design of the first generation probe B-TOH.[40,41] They rely on an intramolecular off-on switch based on photoinduced electron transfer[42] from the chromanol to the Bodipy moiety. The chromanol moiety quenches the emission of the fluorophore until it is oxidized following reaction with peroxyl radicals.[40,41,43] A Bodipy dye with improved redox potential recently prepared by us[44] was utilized as the reporter segment both in H_2B-TOH and in H_2B-PMHC. Favorable photoinduced electron transfer from the chromanol to the Bodipy group ensures an excellent contrast between the dark (reduced) and emissive (oxidized) state, a condition required for the high throughput fluorescence method described here.

H_2B-TOH was prepared following the coupling of 6-hydroxy-2,5,7,8-tetramethylchromane-2-carboxylic acid, commercially known as Trolox, to the Bodipy dye 8-hydroxymethyl-1,3,5,7-tetramethyl pyrromethene fluoroborate via a new route involving Mitsunobu reaction. This methodology gave the product with much better yields than the coupling we originally reported in preparing B-

TOH, and involving EDC.[41] The new compound was prepared with a 67% yield. H_2B-TOH undergoes a ca. 30-fold intensity enhancement upon scavenging peroxyl radicals when embedded in lipid membranes, a marked improvement over the 4-fold enhancement[43] originally reported for B-TOH under similar conditions.

The rationale behind the preparation of H_2B-PMHC was to tune the rate constants of H-atom abstraction (k_{inh}) or antioxidant activity of the probe by utilizing a methylene rather than an ester linker to couple the Bodipy dye to the chromanol moiety. It has been found experimentally that TOH has a larger k_{inh} value than Trolox with k_{inh} = 3.2 x 10^6 $M^{-1}s^{-1}$ and k_{inh} = 1.1 x 10^6 $M^{-1}s^{-1}$, respectively, in styrene.[13] The lower value recorded for Trolox is due to the electron withdrawing effect of the carboxylic moiety which strengthens the phenol O-H bond.[13] We reasoned that by replacing the carbonyl linker by a methylene linker in our probes, we would achieve a similar difference in reactivity between H_2B-TOH and H_2B-PMHC (see Scheme 5.2).

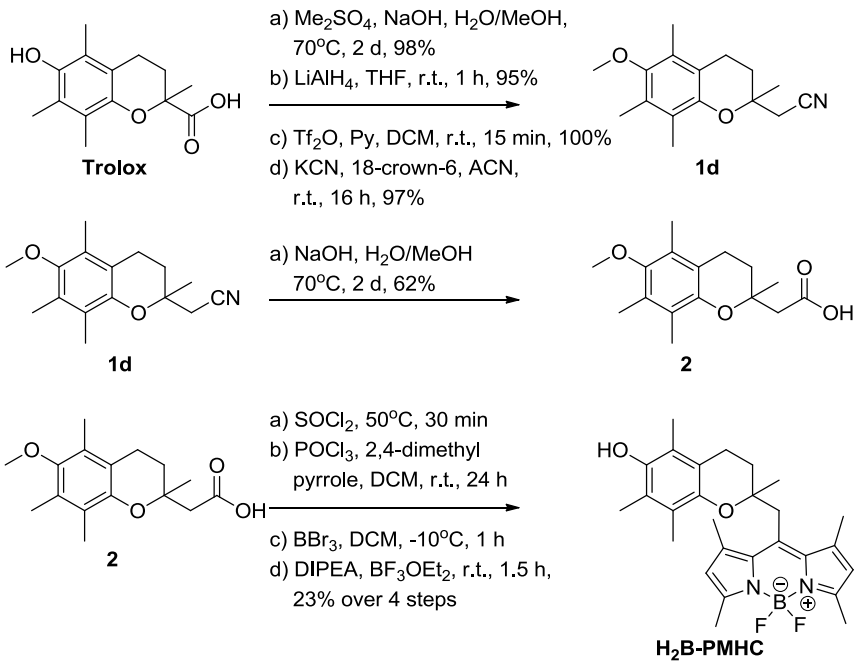

Scheme 5.2. Preparation of H_2B-PMHC.

Key in designing H_2B-PMHC was also to minimize the distance between the receptor and reporter segments to ensure that efficient photoinduced electron transfer takes place from the chromanol to the Bodipy segment ensuring a dark

"off state" and better overall sensitivity for the off-on probe. We thus initially considered preparing the probe by building the Bodipy dye directly onto the acid chloride derivative of Trolox. We were however unsuccessful in our attempts, presumably due to the steric crowding around the quaternary carbon in the chromanol ring. We thus extended the aliphatic chain in Trolox by first reducing the acid group to an alcohol, followed by the insertion of a good leaving group (triflate), substitution by nitrile (**1d** in Scheme 5.2), and hydrolysis to obtain the desired acid 2-(6-methoxy-2,5,7,8-tetramethylchroman-2-yl)-acetic acid (**2** in Scheme 5.2). The acid chloride was next prepared and it was reacted with 2 equivalents of 2,4-dimethyl pyrrole in the presence of phosphorus oxychloride. The organic compound was subsequently deprotected with BBr_3 and following addition of DIPEA and $BF_3.OEt_2$ we obtained H_2B-PMHC in 23% yield from **2**.

5.2.2. Fluorescence Assay

The 2 new probes were used as signal carriers in competitive kinetic studies in the presence of TOH and PMHC. These studies yielded relative antioxidant activity values in model lipid membranes for either TOH or PMHC vs. either H_2B-TOH or H_2B-PMHC. In our assay, we used a microplate reader to monitor over time the emission intensity enhancement of membrane embedded H_2B-TOH or H_2B-PMHC upon scavenging peroxyl radicals when alone or in the presence of competing antioxidants.

We conducted our experiments with liposomes prepared from 6 different glycerophospholipids chosen based both on the degree of unsaturation in their fatty acid chains and on their transition temperature (Tm). We prepared aqueous dispersions of liposomes of L-*α*-phosphocholine (eggPC, a natural mixture containing saturated, unsaturated and polyunsaturated fatty acids, mostly 16:0 and 18:1-*cis*-9), 1,2-dilinoleoyl-*sn*-glycero-3-phosphocholine (DLPC, 18:2-*cis*-9, *cis*-12 polyunsaturated fatty acids, Tm = -53 ^{o}C), 1,2-dioleoyl-*sn*-glycero-3-phosphocholine (DOPC, 18:1-*cis*-9 unsaturated fatty acids, Tm = -20 ^{o}C), 1-palmitoyl-2-oleoyl-*sn*-glycero-3-phosphocholine (POPC, 16:0 saturated and 18:1-*cis*-9 unsaturated fatty acid, Tm = -2 ^{o}C), 1,2-dimyristoyl-*sn*-glycero-3-

phosphocholine (DMPC, 14:0 saturated fatty acids, Tm = 23 ^{o}C), and 1,2-dipalmitoyl-*sn*-glycero-3-phosphocholine (DPPC, 16:0 saturated fatty acids, Tm = 41 ^{o}C). The liposome dispersions were prepared following standard protocols involving the hydration and subsequent extrusion of lipid films through 100 nm polycarbonate films.[45] The pH 6.7, 10 mM phosphate buffer saline solutions were 150 mM in NaCl and $1x10^{-3}$ M in lipid (ca. $1x10^{-8}$ M in liposomes).[45]

Liposome dispersions were supplemented with acetonitrile solutions containing increasing concentrations of H_2B-TOH (or H_2-B-PMHC) ranging from $8.5x10^{-7}$ M to $6.1x10^{-6}$ M. Alternatively, in competing kinetic studies, a constant concentration of H_2B-TOH (or H_2-B-PMHC) of $1x10^{-7}$ M was used with either PMHC or TOH at concentrations ranging from $7.5x10^{-7}$ M to $6x10^{-6}$ M. The lipid:antioxidant ([LH]:[AOH]) mole ratio in our experiments extended from $1x10^{4}$ to $1.7x10^{2}$, within the range of values encountered in the membranes of many cells,[35,36,46] and below the critical value for [LH]:[AOH] = $1x10^{5}$ above which lipid peroxidation via a chain reaction will be observed for polyunsaturated fatty acids (PUFA).[23] Under our experimental conditions in the presence of an antioxidant the kinetic chain length for PUFA lipid autoxidation ν is negligible, $\nu_{AOH}<<1$ (see Equation 8 and Scheme 5.1 for k_p and k_{inh} values).

$$\upsilon_{TOH} = \frac{k_p}{2k_{inh}} \times \frac{[LH]}{[TOH]} \qquad (8)$$

The liposome solutions were injected into the wells of a microplate reader tray and after equilibrating at 37 °C, azo free-radical initiator solutions were injected into the wells. We utilized as a source of peroxyl radicals either 2,2'-azobis(2-amidinopropane) monohydrochloride (ABAP) a charged hydrophilic initiator with a half-life of 579.4 $x10^{3}$ s at 37^{o}C,[22,47] or 2,2'-Azobis(4-methoxy-2,4-dimethyl valeronitrile) (MeO-AMVN) a lipophilic initiator with a half-life of 12.8 $x10^{3}$ s at 37 ^{o}C (Scheme 5.3).[30] Peroxyl radicals generated from ABAP are foreseen to react with the antioxidants at the water/membrane interface[10] approaching from the water[31] whereas those from MeO-AMVN are expected to react approaching from the membrane hydrophobic core.[30] Values for R_g may be estimated from the thermolysis rate constant of the azo initiator "k_i" and the

escape fraction of free radicals from geminate recombination "e", see Equation 9 and Scheme 5.3.[22,28,30,47,48]

$$R_g = 2ek_i[Azo-initiator] \quad (9)$$

Under the concentrations used ($9x10^{-3}$ M for ABAP, $2x10^{-4}$ M for MeO-AMVN), at 37°C and under air saturated conditions, peroxyl radicals are generated at a constant rate R_g of $1x10^{-8}$ Ms^{-1} in water[22,23,47] and toluene[30], respectively. Geminate recombination (Eq. 10) has been shown to reduce by 11-fold the generation rate of lipophilic peroxyl radicals from MeO-AMVN in lipid membranes, so the estimated value for R_g is ~$0.91x10^{-9}$ for MeO-AMVN in liposome solutions.[30]

Altogether, 4 antioxidant compounds were studied at 6 different concentrations in model membranes prepared from 6 different lipids in the presence of 2 types of peroxyl radicals, in triplicates.

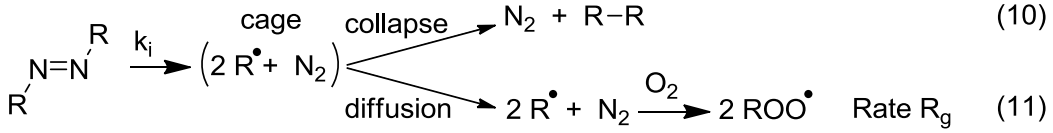

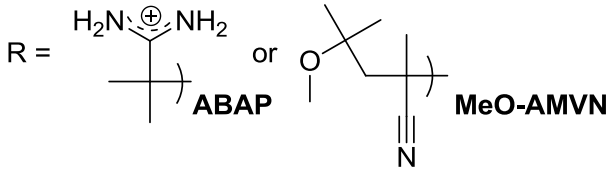

Scheme 5.3. Thermolysis of azo initiators.[22,30,47]

5.2.2.1. Results Obtained with H_2B-PMHC, EggPC and ABAP

Figure 5.2A displays representative intensity-time trajectories recorded in solutions containing ABAP, EggPC liposomes and increasing concentrations of membrane embedded H_2B-PMHC. We recorded fluorescence intensity enhancements of ca. 100-fold, where the maximum emission intensity achieved was proportional to the initial concentration of the fluorogenic antioxidant used.

A linear increase in fluorescence intensity with time is observed following reaction of membrane-embedded H_2B-PMHC with hydrophilic peroxyl radicals. The linear increase in fluorescence intensity and concomitant linear drop in [H_2B-PMHC] with time is consistent with the mechanism shown in Scheme 5.1 which

predicts a rate law which is zero order for the consumption of a TOH antioxidant or analogue such as H_2B-PMHC.[23] See also Equations 7 and 12, where "α" is the proportionality constant between fluorescence intensity and [H_2B-PMHC] and is related to the fluorescence detection efficiency of our setup and to the emission quantum yield of oxidized H_2B-PMHC.

$$\alpha \times \frac{d[Intensity]}{dt} = -\frac{d[H_2B-PMHC]}{dt} = \frac{R_g}{2} \qquad (12)$$

Figures 5.2B and 5.2C display results obtained with increasing concentrations of membrane embedded TOH or PMHC and a small, constant amount of H_2B-PMHC as a signal carrier, unless otherwise identical conditions to those used in acquiring the data of Figure 5.2A. In both sets of data the maximum emission intensity achieved is the same in each run, and proportional to the amount of H_2B-PMHC used as signal carrier (note however that different microplate settings were used in acquiring data for Figure 5.2A and data for Figures 5.2B and C) .

A linear increase in fluorescence intensity with time is observed for experiments conducted with TOH, with a slope which is inversely proportional to the initial [TOH] (Figure 5.2B). These results indicate that the peroxyl radicals generated upon thermolysis of ABAP do not discriminate between both antioxidants and react with the same rate constant with fluorogenic H_2B-PMHC and with TOH, i.e., $k_{inh}^{TOH}/k_{inh}^{H2B\text{-}TOH} \sim 1$ (see also below). The decreasing slope with increasing [TOH] simply indicates that of the total antioxidant load (AOH, where $[AOH]_0 = [H_2B\text{-}PMHC]_0 + [TOH]_0$) reacting at any given time, a decreasing fraction is fluorogenic. An induction period in the intensity profile is observed for experiments with PMHC when ABAP is used (Figure 5.2C). These results highlight the higher reactivity (antioxidant activity) of membrane-embedded PMHC over H_2B-PMHC towards hydrophilic peroxyl radicals.

We conclude based on the observations listed above that the reactivity order towards scavenging hydrophilic peroxyl radicals at the water/membrane interface in EggPC liposomes is thus PMHC > TOH = H_2B-PMHC.

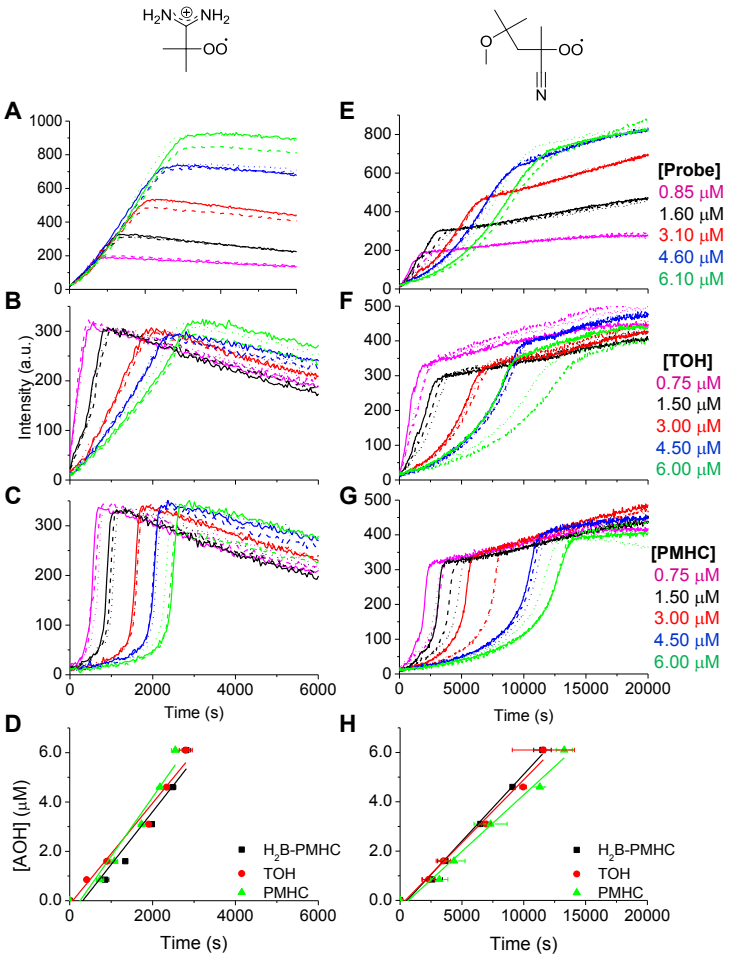

Figure 5.2. Fluorescence intensity-time profiles recorded in triplicates in 1 mM EggPC and 9 mM ABAP solutions with increasing concentrations (see figure captions for the values) of A) H_2B-PMHC B) TOH + 0.1 μM H_2B-PMHC and C) PMHC + 0.1 μM H_2B-PMHC. D) Increasing antioxidant concentration vs. time required for its consumption (τ). Panels E to H show similar data acquired in 1 mM EggPC with 200 μM MeO-AMVN.

5.2.2.2. Results Obtained with H_2B-PMHC, EggPC and MeO-AMVN

Qualitatively, the results obtained in experiments involving the generation of lipophilic peroxyl radicals within EggPC liposomes followed the same trend as those described above using ABAP. Thus a linear increase in fluorescence intensity with time was recorded for H_2B-PMHC, the lipophilic peroxyl radicals reacted with the same rate with TOH and H_2B-PMHC as reflected by a linear increase in intensity, and PMHC outcompeted H_2B-PMHC giving rise to induction periods (see Figures 5.2E to 5.2G). The major difference we encountered when comparing to experiments conducted with ABAP lies in the loss of linearity in the intensity plots occurring at lower LH:H_2BTOH molecular

ratios (experiments conducted with $4.5x10^{-6}$ M and $6x10^{-6}$ M total antioxidant load), and which we assign to a larger time required for establishing steady state conditions given the small Ri value with MeO-AMVN, which is 10-fold lower than with ABAP under our experimental conditions due to free radical recombination within the membrane (Equation 10).[30] Depletion of MeO-AMVN, that has a half-life of 12,800 s, may also contribute to the loss of linearity. Another important difference is that the shape of the induction period observed with PMHC is significantly less pronounced for lipophilic peroxyl radicals than for hydrophilic peroxyl radicals (Figures 5.2C vs. 5.2G).

5.2.2.3. Results Obtained with H_2B-PMHC and All Other Lipids

The outcome of analogous experiments as those described above and conducted on liposomes prepared with DLPC, DOPC, POPC, DMPC, or DPPC are displayed in the appendix for chapter 5, Figures A5.2-A5.6. The results obtained in these lipids with either hydrophilic or lipophilic peroxyl radicals follow the same trend as that described above for EggPC liposomes.

In summary, from these qualitative observations we conclude that the antioxidant activity towards either lipophilic or hydrophilic peroxyl radicals follows the trend PMHC > TOH = H_2B-PMHC. The 3 molecules differ solely in the structure of their lipophilic tail yet they have the same inherent chemical reactivity given by their identical chromanol moiety. Our results highlight that both TOH and H_2B-PMHC exhibit a restricted (yet similar) mobility and accessibility within the bilayer when compared to PMHC, a result of their large lipophilic tails. Differences in the antioxidant activities of these 3 compounds thus arise from membrane induced changes in accessibility and mobility. In fact, all 3 molecules exhibit similar antioxidant activity in homogeneous solution, where competing kinetic studies show small yet identical induction periods with either PMHC or TOH, see Figure 5.3.

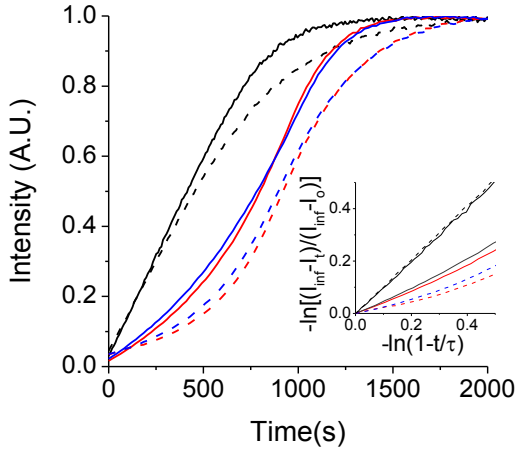

Figure 5.3. Fluorescence intensity-time profiles recorded in acetonitrile with 2,2'-Azobis(2-methylbutyronitrile) and: **solid black line)** H_2B-PMHC 9.5 μM; **solid red line)** TOH 9.0 μM + H_2B- PMHC 0.5 μM and **solid blue line)** PMHC 9.0 μM + H_2B- PMHC 0.5 μM. Results in dashed lines correspond to: **dash black line)** H_2B-TOH 9.5 μM; **dash red line)** TOH 9.0 μM + H_2B-TOH 0.5 μM and **dash blue line)** PMHC 9.0 μM + H_2B-TOH 0.5 μM. The inset shows the data plotted according to equation 20, wherefrom we obtain values for $k_{inh}^{PMHC}/k_{inh}^{\alpha\text{-tocopherol}} \sim 1$, $k_{inh}^{H2B\text{-}PMHC}/k_{inh}^{PMHC} = 0.49$, $k_{inh}^{H2B\text{-}TOH}/k_{inh}^{PMHC} = 0.27$, and $k_{inh}^{H2B\text{-}PMHC}/k_{inh}^{H2B\text{-}TOH} = 1.8$.

A quantitative treatment of the fluorescence intensity-time profiles is presented in the following section wherefrom the relative antioxidant activities of PMHC, TOH, H_2B-PMHC, and H_2B-TOH are estimated for the various conditions.

5.2.2.4. Results obtained with H_2B-TOH and All Other Lipids

Results from a series of experiments where we monitored the fluorogenic antioxidant H_2B-TOH in EggPC liposomes using either ABAP or MeO-AMVN azo initiators are displayed in Figures 5.4A to 5.4C and 5.4E to 5.4G, respectively. Figures A5.8 to A5.12 in the appendix for chapter 5 display the results gathered with DLPC, DOPC, POPC, DMPC or DPPC. With H_2B-TOH in the presence of peroxyl radicals we recorded fluorescence intensity enhancements of ca. 30-fold with time, where the maximum emission intensity achieved was proportional to the initial concentration of H_2B-TOH employed.

A linear increase in intensity with time is observed following reaction of membrane-embedded H_2B-TOH with peroxyl radicals generated upon thermolysis of either ABAP or MeO-AMVN (Figures 5.4A and 5.4E, respectively). Notably,

and as we described for experiments with H_2B-PMHC above, deviations from linearity occur at small LH:H_2B-TOH molecular ratios when lipophilic peroxyl radicals are produced.

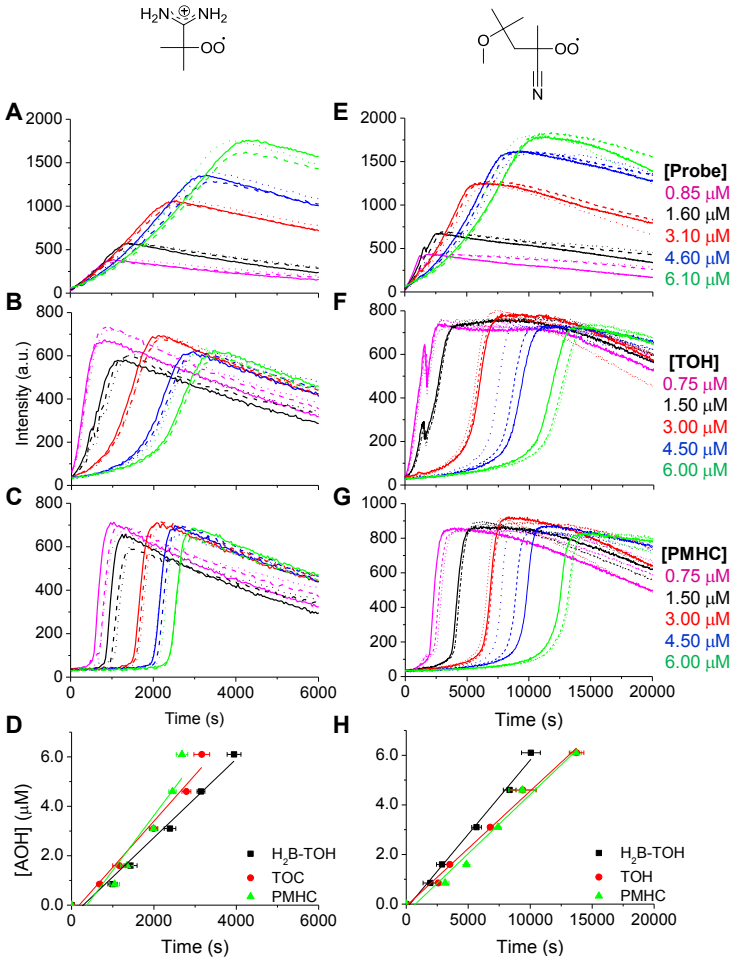

Figure 5.4. Fluorescence intensity-time profiles recorded in triplicates in 1 mM EggPC and 9 mM ABAP solutions with increasing concentrations (see figure captions for the values) of A) H_2B-TOH B) TOH + 0.1 μM H_2B-TOH and C) PMHC + 0.1 μM H_2B-TOH. D) Increasing antioxidant concentration vs. time required for its consumption (τ). Panels E to H show similar data acquired in 1 mM EggPC with 200 μM MeO-AMVN.

In all lipid suspensions examined an induction period in the intensity profile is observed in experiments conducted with TOH and H_2B-TOH as a signal carrier and either ABAP or MeO-AMVN as a source of peroxyl radicals. The induction periods are significantly more pronounced in competitive kinetic studies with PMHC. These results highlight the higher reactivity of membrane-embedded TOH over H_2B-TOH towards both hydrophilic and lipophilic peroxyl radicals. They also show qualitatively that PMHC is more reactive than TOH. The

reactivity order towards scavenging peroxyl radicals is thus PMHC > TOH > H_2B-TOH in all lipids examined with either lipophilic or hydrophilic peroxyl radicals.

The lower reactivity towards peroxyl radicals recorded for H_2B-TOH over TOH may be ascribed to its lower inherent chemical reactivity (see also Figure 5.3 for homogeneous solution studies which show that $k_{inh}^{H2B\text{-}TOH}/k_{inh}^{TOH} \sim 0.25$).[49] The inherent lower reactivity of H_2B-TOH arises from the electron-withdrawing effect of the carbonyl moiety in the ester linker functionality, which strengthens the phenol O-H bond.[13] Although the effect of a vicinal carbonyl on the antioxidant activity of a chromanol in homogeneous solution was established ca. 25 years ago, to our knowledge such an effect was not explored within lipid membranes. Here we show that the lipid membrane does not exert a leveling effect on antioxidant activities and our results with H_2B-TOH and TOH illustrate that even slight inherent chemical reactivity differences are translated to the heterogeneous water-lipid interface.

The higher reactivity of PMHC over TOH for peroxyl radicals within lipid membranes has been described as arising from the higher accessibility and mobility of the former over the latter in this media. We show qualitatively that whereas the induction periods recorded with hydrophilic peroxyl radicals are more pronounced with PMHC than with TOH, for lipophilic peroxyl radicals the induction curves are similar for both antioxidants. A more in depth discussion is presented following the quantitative analysis below.

5.2.3. Quantitative Analysis

5.2.3.1. Rates of Antioxidant Consumption

The intensity-time trajectories recorded not only provide qualitative (*vide supra*) and quantitative (*vide infra*) information on the relative antioxidant activity of the 4 antioxidant studied, but they also enable us to calculate the rates of antioxidant consumption and the stoichiometric coefficient for peroxyl radical scavenging by TOH and TOH analogues, under the range of conditions explored.

Alternatively, they may provide for an efficient way to determine rates of initiation of free radicals in a simple rapid manner (see Equation 7 and 12).

The rates of antioxidant consumption may be calculated from the slope of the linear correlation between the concentration of total antioxidant load ([AOH], where $[AOH]_0 = [\text{fluorogenic antioxidant}]_0 + [\text{non-fluorogenic antioxidant}]_0$) and τ, the time required for its consumption. Figures 5.2D and 5.2H illustrate the linear dependence of the initial antioxidant concentration [AOH] with τ for experiments conducted in EggPC with H_2B-PMHC and either ABAP or MeO-AMVN, respectively. Figures 5.4D and 5.3H illustrate similar data obtained in EggPC with H_2B-TOH. Results with all other lipids are illustrated in Figures A5.1 to A5.12 in the appendix for chapter 5. Values of τ were experimentally determined for each initial [AOH] from the intensity-time trajectories such as those shown in figures 5.2A-C, 5.2E-G, 5.4A-C or 5.4E-G. The value of τ corresponded to the time at the intercept of the straight lines tangential to the linear increase in intensity and the subsequent linear change in intensity arising from Bodipy degradation.[40,41]

The rates of antioxidant consumption we measured were roughly the same for all 4 antioxidants tested in all 6 lipids for a given type of azo initiator (either ABAP or MeO-AMVN) consistent with all 4 antioxidants having a stoichiometric coefficient of 2 for peroxyl radical scavenging. The rates measured in the 6 different lipids are illustrated in the accompanying bar plots (Figures 5.5A and 5.5B, respectively for experiments with H_2B-PMHC, and Figures 5.5C and 5.5D, respectively for experiments with H_2B-TOH); see also accompanying plots and Table 5.1.

The rate values we measured with ABAP, in the range of 1.5×10^{-9} Ms^{-1} to 2.5×10^{-9} Ms^{-1}, are 2- to 3-fold lower than the theoretical estimate of 5×10^{-9} Ms^{-1} ($R_g/2$, see also Equation 9 and accompanying discussion). Presumably a wastage reaction accounting for ca. 60% of the produced $ROO^{\bullet}$ (and involving their bimolecular self-reaction) is taking place in the aqueous phase. Careful analysis of the bar plots show that with increasing unsaturation in the lipid utilized the rate of hydrophilic peroxyl radical consumption increases. Antioxidants embedded in

saturated lipids do not efficiently scavenge hydrophilic peroxyl radicals, presumably a result of their lower accessibility.

The rate values obtained with MeO-AMVN ($0.5x10^{-9}$ Ms^{-1} to $0.7x10^{-9}$ Ms^{-1}) are ca. 10-fold lower than those expected in homogeneous solution with toluene as a solvent ($5x10^{-9}$ Ms^{-1}).[30] The discrepancy may be accounted for by geminate recombination within membranes (Equation 10 in Scheme 5.3) which has been shown to reduce by 11-fold the generation rate R_g of lipophilic peroxyl radicals from MeO-AMVN.[30] Lipophilic peroxyl radicals are scavenged with the same efficiency by all 4 antioxidants studied regardless of the nature of their aliphatic tail or the lipid membrane they are embedded into.

In closing we also note that experiments in DMPC and DPPC are devoid of significant error, particularly when ABAP is used, possibly the result of a poor partitioning of the probe within saturated lipids. The low quality of the data prevents an accurate determination of the rate of consumption of AOH.

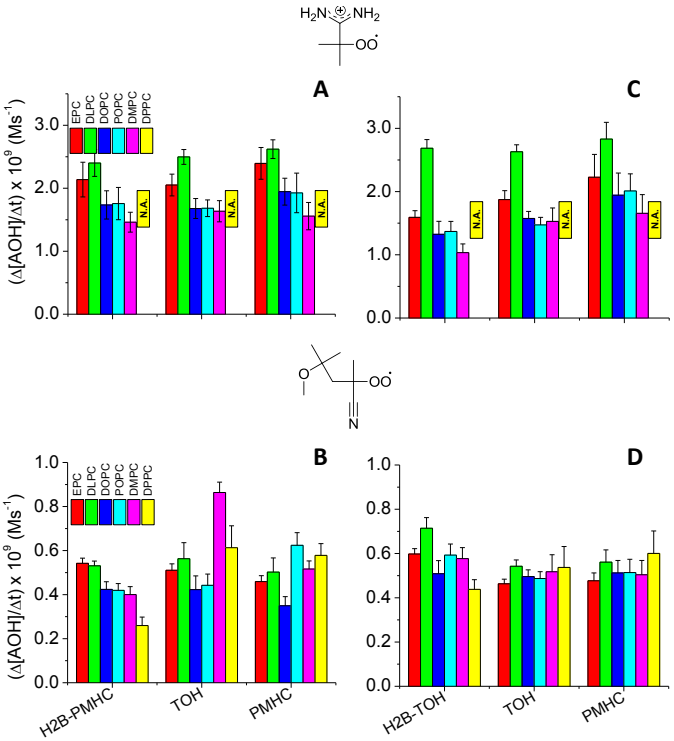

Figure 5.5. Rate of consumption of antioxidants determined in the presence of peroxyl radicals in six different lipids. Panels A and B show the rates determined upon generation of peroxyl radicals from 9 mM ABAP and 200 μM MeO-AMVN, respectively, data acquired with the probe H_2B-PMHC. Panels C and D show similar data acquired with the probe H_2B-TOH.

H_2B-TOH	***ABAP***					
	EggPC	**DLPC**	**DOPC**	**POPC**	**DMPC**	**DPPC**
H_2B-TOH	1.59 ± 0.11	2.69 ± 0.14	1.32 ± 0.21	1.37 ± 0.16	1.03 ± 0.14	N.A.
H_2B-TOH+TOH	1.87 ± 0.14	2.63 ± 0.11	1.57 ± 0.11	1.47 ± 0.12	1.53 ± 0.21	N.A.
H_2B-TOH+PMHC	2.23 ± 0.36	2.83 ± 0.26	1.94 ± 0.35	2.01 ± 0.27	1.66 ± 0.29	N.A.
	MeO-AMVN					
	EggPC	**DLPC**	**DOPC**	**POPC**	**DMPC**	**DPPC**
H_2B-TOH	0.59 ± 0.02	0.71 ± 0.05	0.51 ± 0.06	0.59 ± 0.05	0.58 ± 0.05	0.44 ± 0.04
H_2B-TOH+TOH	0.46 ± 0.02	0.54 ± 0.03	0.49 ± 0.03	0.48 ± 0.08	0.52 ± 0.08	0.54 ± 0.09
H_2B-TOH+PMHC	0.47 ± 0.03	0.56 ± 0.05	0.51 ± 0.06	0.51 ± 0.06	0.50 ± 0.06	0.60 ± 0.1

H_2B-PMHC	***ABAP***					
	EggPC	**DLPC**	**DOPC**	**POPC**	**DMPC**	**DPPC**
H_2B-PMHC	2.1 ± 0.3	2.4 ± 0.2	1.7 ± 0.2	1.8 ± 0.3	1.5 ± 0.2	N.A.
H_2B-PMHC+TOH	2.1 ± 0.2	2.5 ± 0.1	1.7 ± 0.2	1.7 ± 0.1	1.6 ± 0.2	N.A.
H_2B-PMHC+PMHC	2.4 ± 0.3	2.6 ± 0.1	1.9 ± 0.2	1.9 ± 0.3	1.6 ± 0.2	N.A.
	MeO-AMVN					
	EggPC	**DLPC**	**DOPC**	**POPC**	**DMPC**	**DPPC**
H_2B-PMHC	0.54 ±0.02	0.53 ± 0.02	0.42 ± 0.03	0.42 ± 0.03	0.40 ± 0.04	0.49 ± 0.1
H_2B-PMHC+TOH	0.51 ± 0.03	0.56 ± 0.07	0.42 ± 0.06	0.44 ± 0.05	0.86 ± 0.05	0.61 ± 0.1
H_2B-PMHC+PMHC	0.46 ± 0.03	0.50 ± 0.06	0.35 ± 0.04	0.62 ± 0.06	0.51 ± 0.04	0.58 ± 0.05

Table 5.1. Rate of consumption of antioxidants. Units of nMs^{-1}. Calculated from the linear fit of [AOH] vs τ plots for ABAP $9x10^{-3}$ M (Figures A5.1 to A5.6), and MeO-AMVN 200 μM (Figures A5.7 to A5.12).

5.2.3.2. Relative Antioxidant Activity

The fluorescence intensity-time profiles may be further analyzed in order to determine the relative rate constants of H-atom abstraction for the various TOH analogues competing with the fluorogenic antioxidants.

The analysis of the rate law for the mechanism shown in Scheme 5.1 involving lipid autoxidation in the presence of a free radical initiator $ROO^{\bullet}$ and TOH, and including a new antioxidant e.g. H_2B-TOH, shows that the rate of consumption of TOH may be described by Equation 13. This equation is obtained upon substituting in Equation 7 with the expression for $[LOO^{\bullet}]$ under steady state conditions in the presence of 2 different antioxidants, e.g. H_2B-TOH and TOH.

$$-\frac{d[TOH]}{dt} = k_{inh}^{TOH}\left[\frac{R_i}{2\left(k_{inh}^{TOH}[TOH] + k_{inh}^{H_2B\text{-}TOH}[H_2B\text{-}TOH]\right)}\right][TOH] \qquad (13)$$

A similar expression to the one above may be utilized to calculate the rate of consumption of H_2B-TOH (or H_2B-PMHC) in the presence of TOH, see Equation 14:

$$-\frac{d[H_2B\text{-}TOH]}{dt} = k_{inh}^{H_2B\text{-}TOH}\left[\frac{R_i}{2\left(k_{inh}^{TOH}[TOH]+k_{inh}^{H_2B\text{-}TOH}[H_2B\text{-}TOH]\right)}\right][H_2B\text{-}TOH] \quad (14)$$

Based on the relative values of k_{inh} three different regimes may be obtained for the rate of consumption of H_2B-TOH:

i) When k_{inh}^{TOH} [TOH] << $k_{inh}^{H2B\text{-}TOH}$ [H_2B-TOH], the fluorogenic antioxidant consumption takes place unaffected by the presence of TOH.

$$-\frac{d[H_2B\text{-}TOH]}{dt} = \frac{R_i}{2} \quad (15)$$

ii) When k_{inh}^{TOH} [TOH] = $k_{inh}^{H2B\text{-}TOH}$ [H_2B-TOH], the rate of consumption of the fluorogenic antioxidant is slowed down by the factor β, the ratio of fluorogenic antioxidant to total antioxidant.

$$-\frac{d[H_2B\text{-}TOH]}{dt} = \left[\frac{R_i}{2([TOH]+[H_2B\text{-}TOH])}\right][H_2B\text{-}TOH] = \frac{R_i}{2}\frac{[H_2B\text{-}TOH]}{[AOH]} = \frac{R_i\beta}{2} \quad (16)$$

iii) When k_{inh}^{TOH} [TOH] >> $k_{inh}^{H2B\text{-}TOH}$ [H_2B-TOH] the differential equation obtained (17) may be solved by approximating $[TOH]_t$ to the value obtained from the integral of Equation 7, where τ is the time required for consuming the total [TOH], see Equation 18 (a similar methodology is utilized in the analysis of the temporal evolution of oxygen uptake in the presence of antioxidants[10,13,20,47,50]).

$$-\frac{d[H_2B\text{-}TOH]}{dt} = k_{inh}^{H_2B\text{-}TOH}\left[\frac{R_i}{2k_{inh}^{TOH}[TOH]}\right][H_2B\text{-}TOH] \quad (17)$$

$$-\frac{d[H_2B\text{-}TOH]}{dt} = k_{inh}^{H_2B\text{-}TOH}\left[\frac{1}{k_{inh}^{TOH}(\tau-t)}\right][H_2B\text{-}TOH] \quad (18)$$

Following integration, Equation 19 is obtained which may be further rearranged upon replacing the ratio $[H_2B\text{-}TOH]_t/[H_2B\text{-}TOH]_o$ in terms of the fluorescence intensities recorded in our experiment, obtaining expression 20,

where I_o, I_t and I_∞ are the initial intensity, the intensity at time "t" and the intensity at the maximum).[51]

$$-\ln\left(\frac{[H_2B\text{-}TOH]_t}{[H_2B\text{-}TOH]_o}\right) = -\frac{k_{inh}^{H_2B\text{-}TOH}}{k_{inh}^{TOH}}\ln\left(1-\frac{t}{\tau}\right) \quad (19)$$

$$-\ln\left(\frac{I_\infty - I_t}{I_\infty - I_o}\right) = -\frac{k_{inh}^{H_2B-TOH}}{k_{inh}^{TOH}}\ln\left(1-\frac{t}{\tau}\right) \quad (20)$$

The above expression provides a simple way to determine the relative antioxidant activities for H_2B-TOH and TOH ($k_{inh}^{H_2B\text{-}TOH}/k_{inh}^{TOH}$) from the analysis of the initial slope of a plot of $-\ln((I_\infty - I_t)/(I_\infty - I_o))$ vs. $-\ln(1 - t/\tau)$. Such protocol is directly extendable to studies with PMHC or any other antioxidant. In an analogous manner studies may be conducted with the more reactive fluorogenic antioxidant H_2B-PMHC. Equation 20 provides a more general way to evaluate the data than an analysis based on the initial slopes of intensity-time profiles.

Figure 5.6 shows fluorescence intensity-time traces acquired with 4.5 x 10^{-6} M of either TOH or PMHC and 0.1 x 10^{-6} M of either H_2B-TOH or H_2B-PMHC, in all 6 lipids and with ABAP. Also shown are results acquired with MeO-AMVN as the source of peroxyl radicals, with 1.5 or 3 x 10^{-6} M of either TOH or PMHC and 0.1 x 10^{-6} M of either H_2B-TOH or H_2B-PMHC. The insets show the intensity analysis according to Equation 20 for trajectories with probe alone and with probe and either TOH or PMHC. Note that whereas the expected slope is 1 for trajectories acquired with the probe alone and analyzed according to Equation 20, small deviations are observed when the actual fluorescence intensity enhancement is not linear with time.

Table 5.2 and Table 5.3 list the relative antioxidant activities recorded in our studies in the presence of hydrophilic and lipophilic peroxyl radicals, respectively.

Lipid	$\frac{k_{inh}^{H2B-PMHC}}{k_{inh}^{TOH}}$	$\frac{k_{inh}^{H2B-PMHC}}{k_{inh}^{PMHC}}$	$\frac{k_{inh}^{H2B-TOH}}{k_{inh}^{TOH}}$	$\frac{k_{inh}^{H2B-TOH}}{k_{inh}^{PMHC}}$
EggPC	0.94±0.02	0.10±0.01	0.39±0.02	≤0.01
DLPC	0.80±0.04	0.11±0.02	0.20±0.02	≤0.01
DOPC	0.96±0.03	0.11±0.01	0.31±0.02	≤0.01
POPC	1.10±0.01	0.13±0.02	0.37±0.02	≤0.01
DMPC	1.25±0.05	0.18±0.01	0.43±0.01	≤0.01
DPPC	1.17±0.1	0.10±0.02	0.56±0.01	≤0.01

Table 5.2. Relative antioxidant activities in the presence of hydrophilic peroxyl radicals (ABAP). The errors reported are those recovered from analyzing individual fluorescence intensity−time traces. Deviations from the average for three independent experiments are typically within 10%.

Lipid	$\frac{k_{inh}^{H2B-PMHC}}{k_{inh}^{TOH}}$	$\frac{k_{inh}^{H2B-PMHC}}{k_{inh}^{PMHC}}$	$\frac{k_{inh}^{H2B-TOH}}{k_{inh}^{TOH}}$	$\frac{k_{inh}^{H2B-TOH}}{k_{inh}^{PMHC}}$
EggPC	0.57±0.03	0.18±0.02	0.17±0.01	0.06±0.01
DLPC	0.41±0.02	0.18±0.02	0.09±0.01	0.05±0.01
DOPC	0.52±0.02	0.13±0.03	0.12±0.01	0.05±0.01
POPC	0.75±0.02	0.14±0.02	0.19±0.01	0.05±0.01
DMPC	0.96±0.03	0.20±0.01	0.21±0.01	0.06±0.01
DPPC	0.96±0.02	0.30±0.02	0.21±0.02	0.01±0.01

Table 5.3. Relative antioxidant activities in the presence of lipophilic peroxyl radicals (MeO-AMVN). The errors reported are those recovered from analyzing individual fluorescence intensity−time traces. Deviations from the average for three independent experiments are typically within 10%.

A number of key new quantitative results are obtained upon inspection of the data tabulated, these are listed below.

I) The relative antioxidant activities of chromanols in homogeneous solution, arising from their inherent chemical reactivity, readily translate to the microheterogeneous environment at the water lipid interface, thus a similar value for $k_{inh}^{H2B-PMHC}/k_{inh}^{H2B-TOH}$ (in the range of 2 to 3) is recorded in both homogeneous solution and in liposome suspensions with hydrophilic or lipophilic peroxyl radicals. Although the effect of a vicinal carbonyl on the antioxidant activity of a chromanol in homogeneous solution was established ca. 25 years ago, to our knowledge such an effect was not explored within lipid membranes. Interestingly, the lipid membrane does not exert a leveling effect on antioxidant activities and our results with H_2B-TOH and H_2B-PMHC illustrate that even slight inherent chemical reactivity differences are translated to the heterogeneous water-lipid interface.

II) The relative antioxidant activity between tocopherol analogues with the same inherent chemical reactivity but bearing short (PMHC) and long (α-tocopherol) aliphatic tails $k_{inh}^{PMHC}/k_{inh}^{TOH}$ ranges from ca. 7 to ca. 9.4 (with the exception of DPPC for which it is ca. 14) in the presence of hydrophilic peroxyl radicals, and on average, a value of 8 is found. Our results place in quantitative terms a long known qualitative observation.[8]

III) Lipophilic peroxyl radicals showed reduced discrimination between antioxidants bearing long and short aliphatic tails with $k_{inh}^{PMHC}/k_{inh}^{TOH}$ in the range of 3 to 5 when calculated from competing experiments performed with H_2B-PMHC and in the range of 2 to 4 when calculated from competing experiments conducted with H_2B-TOH for most lipid membranes. On average, the value lies between 3 and 4, based on either set of experiments. Notably, $k_{inh}^{PMHC}/k_{inh}^{TOH}$ is lower for DLPC, and exceptionally large for DPPC when acquired with H_2B-TOH.

Points II and III constitute to our knowledge the first quantitative results on the relative antioxidant activity of TOH analogues bearing short vs. long aliphatic tails. The higher reactivity of PMHC over TOH towards hydrophilic peroxyl radicals has been ascribed to the higher accessibility to peroxyl free radicals and higher mobility of the former over the latter in this media.[8] Our results show that accessibility to the antioxidant by the hydrophilic peroxyl radical (a constraint imposed on hydrophilic but not lipophilic peroxyl radicals), plays a significant role, yet the relative mobility of the peroxyl radical and the antioxidant (a factor common to both types of peroxyl radicals) is the dominant factor accounting for the difference between PMHC and TOH antioxidant activities in lipid membranes. We do however note that lipids are enriched with MeO-AMVN (a 2/10 MeO-AMVN/lipid mole ratio was used to ensure peroxyl radicals were generated at a sufficiently large rate) so the differences we observe between experiments conducted with hydrophilic vs lipophilic peroxyl radicals may also arise from differences in the lipid membrane fluidity due to the inclusion of MeO-AMVN within the membranes.

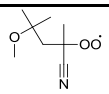

	H_2B-PMHC	H_2B-TOH	H_2B-PMHC	H_2B-TOH
EggPC				
DLPC				
DOPC				
POPC				
DMPC				
DPPC				

Figure 5.6. Fluorescence intensity−time traces acquired with ABAP and 4.5×10^{-6} M of either TOH or PMHC and 0.1×10^{-6} M of either H_2B-TOH or H_2B-PMHC in 1 mM lipids. Also shown are results acquired with MeO-AMVN as the source of peroxyl radicals, with 1.5×10^{-6} M of either TOH or PMHC and 0.1×10^{-6}M H_2B-PMHC, and with 0.1×10^{-6}M H_2B-TOH and 3.0×10^{-6} M of either TOH or PMHC. The inset shows the analysis according to eq 20. **Black**, trajectories acquired with the probe alone; **red**, competitive kinetic experiments with the probe and TOH; and **blue**, competitive kinetic experiments with the probe and PMHC (in all cases the total load of antioxidant is the same).

Inspection of the traces in Figure 5.6 provides additional information, thus as described before: IV) Antioxidants embedded in saturated lipids do not efficiently scavenge hydrophilic peroxyl radicals, presumably a result of their lower accessibility, this translates in turn to larger times for antioxidant consumption. It may thus be observed in going down the left two columns in Figure 5.6 that increasing times are required to consume the antioxidants as saturation in the lipids increases.

The above results add to a previous observation (vide supra), namely: V) Lipophilic peroxyl radicals are scavenged with roughly the same efficiency by all 4 antioxidants studied regardless of the nature of their aliphatic tail or the lipid membrane they are embedded into.

A note of caution should be introduced to help rationalize the distribution of intensity-time traces around an average value for identical experimental conditions. Given the high activation energies for the thermolysis of AIBN (ca. 130 kJ/mol) or MeO-AMVN (ca. 115 kJ/mol) these reactions are extremely sensitive to temperature. A change of 1 ^{o}C degree at 37 ^{o}C introduces changes of 15% and 13%, respectively, in the thermolysis rate constant k_i (see equation 9) of these azo initiators. A gradient of up to 1 ^{o}C across the wellplate was encountered in our experiments and this affected the end point value (maximum intensity point) for triplicates. The relative antioxidant activity analysis based on equation 20 however should not be affected significantly provided the τ value used is that recorded for each trajectory in e.g. Figure 5.6.

5.3. Conclusions

In conclusion, the two new fluorogenic TOH analogues reported here and characterized by a different inherent chemical reactivity and large sensitivity have

enabled to develop a high throughput fluorescent method to study real-time the dynamics of antioxidant consumption in model lipid membranes. Our results illustrate that mobility and to a lesser extent physical accessibility account for the larger relative antioxidant activity of tocopherol analogues bearing short (PMHC) over long (α-tocopherol) aliphatic tails, but that otherwise have the same inherent chemical reactivity. The results also illustrate that the microheterogeneous nature of the water lipid interface does not exert a leveling effect on the antioxidant activities of TOH analogues that have different inherent chemicals reactivity towards H-atom abstraction.

The method we have developed is readily extendable to lipid mixtures including cholesterol, natural lipid mixtures and should prove a powerful tool for oxidative lipidomics and we argue a range of analytical studies with the purpose of determining the extent of lipid degradation in e.g. foods and oils. The new probes may be further utilized towards rapidly evaluating the rate of initiation of free radical reactions in complex systems with available fluorescence spectrometers. We also recognize the potential of the new probes towards imaging reactive oxygen species in live cells studies.

5.4. Experimental Section

Materials

(±) 6-hydroxy-2,5,7,8-tetramethylchromane-2-carboxylic acid (Trolox), α-tocopherol (TOH), 2,2,5,7,8-pentamethyl-6-chromanol (PMHC), diisopropyl azodicarboxylate, triphenylphosphine, and 2,2´-azobis-(2-methylpropionamidine) dihydrochloride (ABAP) were purchased from Sigma-Aldrich (Oakville, Ontario, Canada). 2,2'-Azobis(4-methoxy-2.4-dimethyl valeronitrile) (MeO-AMVN) was supplied by Wako Pure Chemical Industries, Ltd. L-α-phosphocholine (EggPC), 1,2-dilinoleoyl-*sn*-glycero-3-phosphocholine (DLPC), 1,2-dioleoyl-*sn*-glycero-3-phosphocholine (DOPC), 1-palmitoyl-2-oleoyl-*sn*-glycero-3-phosphocholine (POPC), 1,2-dimyristoyl-**sn**-glycero-3-phosphocholine (DMPC), and 1,2-dipalmitoyl-**sn**-glycero-3-phosphocholine (DPPC) were obtained from Avanti

Polar Lipids, (Alabaster, Al). All chemicals were used without further purification. Water was purified by a Millipore MilliQ system.

Methods

Absorption and emission spectra were recorded on a Cary 5000 UV-VIS-NIR and Cary Eclipse fluorescence spectrophotometers, respectively, using 1 cm x 1 cm quartz cuvettes. H_2B-TOH concentrations for wellplate assays were determined by measuring the absorption at λ_{max} 517 nm in acetonitrile and using a molar absorption coefficient of 65,000 $M^{-1}cm^{-1}$. H_2B-PMHC concentrations for wellplate assays were determined by measuring the absorption at λ_{max} 506 nm in acetonitrile and using a molar absorption coefficient of 57,400 $M^{-1}cm^{-1}$. A Biotek Synergy 2 Multi-Mode microplate reader was used to record the intensity time trajectories of the fluorogenic antioxidant H_2B-TOH and H_2B-PMHC. For experiments conducted with H_2B-TOH the fluorescence emission was recorded at 535 nm upon excitation at 490 nm. For experiments conducted with H_2B-PMHC the fluorescence emission was recorded at 520 nm upon excitation at 485 nm. The emission was monitored for 14 h at 40 s time intervals. ^{1}H-NMR and ^{13}C-NMR spectra were recorded on a Varian VNMRS 500 instrument at 500MHz and 125 MHz respectively. ESI mass spectra were measured on a Thermo Scientific Exactive Orbitrap.

Liposome preparation

Aqueous solutions 20 mM in lipids were prepared as follows. 137 mg of Egg PC, 141 mg of DLPC, 141 mg of DOPC, 137 mg of POPC, 122 mg of DMPC and 132 mg of DPPC were weighed in six dry vials and dissolved with minimal amount of chloroform. The solvent was evaporated with a stream of argon while rotating the sample vial to create a thin film on the vial wall. The films were left under vacuum to remove excess solvent. After 1 hour the aliquots of Egg PC, DLPC, DOPC, POPC, DMPC and DPPC were hydrated with 9 ml of a pH 6.7, 10 mM phosphate buffer saline solution 150 mM in NaCl, yielding 20 mM lipid suspensions. The lipid suspensions were subjected to 3 freeze-thaw-sonication-vortex cycles, where each cycle involved storing the vials with the solutions in dry ice for 4 minutes, thawing at 37 ^{o}C for 4 minutes, followed by 4

minute sonication. After the third cycle the lipid suspensions were extruded 15 times using an Avanti mini extruder with one 100 nm polycarbonate membrane. Liposomes roughly 100 nm in diameter and each containing *ca.* 100,000 Egg PC, DLPC, DOPC, POPC, DMPC, DPPC lipids were thus obtained.[1]

Microplate Assays

Increasing concentration of H_2B-TOH. H_2B-TOH was embedded in the lipid membranes as follows. A stock 130.7 μM H_2B-TOH solution in acetonitrile was prepared. H_2B-TOH concentration was determined by measuring the absorption at λ_{max} 517 nm in acetonitrile and using its molar extinction coefficient of 65,000 $M^{-1}cm^{-1}$. Five 64.3 μL aliquots of 20 mM EggPC, DLPC, DOPC, POPC, DMPC and DPPC (30 aliquots in total) were placed in microcentrifuge tubes and were further diluted with 100 μl of the phosphate buffer saline solution utilized in lipid hydration, to yield 7.8 mM lipid suspensions. To the five aliquots of a given lipid, increasing amounts of H_2B-TOH stock solution were added (8.4, 15.7, 30.5, 45.3, 60 μl respectively). The solutions were subsequently diluted with the phosphate buffer saline solution, to yield 1.2 ml of solutions 1.07 mM in lipids and 0.91, 1.71, 3.32, 4.93 or 6.54 μM in H_2B-TOH. From each of the lipid suspensions three aliquots of 280 μl were loaded into 3 different wells of a microplate reader tray. The solutions were left equilibrating at 37 ^oC for 15 min after which 20 μl of free-radical initiator were added to each of the wells. The initiator solutions utilized were either 0.135 M in ABAP in a pH 6.7 phosphate buffer saline solution, or 3.0 mM in 2MeO-AMVN in acetonitrile. The final solutions were 1 mM in lipids, 10 nM in liposomes, 0.85, 1.6, 3.1, 4.6 or 6.1 μM in H_2B-TOH, and 9 mM in ABAP or 200 μM in MeO-AMVN.

Increasing concentrations of PMHC or TOH with 0.1 μM H_2B-TOH. PMHC or TOH and H_2B-TOH were embedded in the lipid membranes as follows. Two antioxidant stock solutions were prepared containing: A) 12.9 μM H_2B-TOH in acetonitrile, B) 128.6 μM TOH or PMHC in acetonitrile. Lipid aliquots were prepared next as described above. To the five aliquots of a given lipid 10 μl of stock solution A (H_2B-TOH) and increasing amounts (7.5, 15, 30, 45 and 60 μl respectively) of stock solution B (TOH or PMHC) were added. The solutions

were subsequently diluted with the phosphate buffer saline solution, to yield 1.2 ml of solutions of 1.07 mM in lipids, 0.107 μM in H_2B-TOH and 0.8, 1.61, 3.21, 4.82 or 6.43 μM in TOH or PMHC. The lipid suspensions were handled as described in the previous section for H_2B-TOH only, including the addition of azo-initiators. The final solutions were 1 mM in lipids, 10 nM in liposomes, 0.1 μM in H_2B-TOH, 0.75, 1.5, 3.0, 4.5 or 6.0 μM in TOH or PMHC, and 9 mM in ABAP or 200 μM in MeO-AMVN.

Experiments with H_2B-PMHC. H_2B-PMHC was embedded in the lipid membranes as described above for experiments conducted with H_2B-TOH or H_2B-TOH and TOH or PMHC. H_2B-PMHC concentration was determined by measuring the absorption at λ_{max} 506 nm in acetonitrile and using its molar extinction coefficient of 57,400 $M^{-1}cm^{-1}$. The procedure we followed was analogous to that described for H_2B-TOH.

Synthesis

8-Hydroxymethyl-1,3,5,7-tetramethyl pyrromethene fluoroborate was prepared as described in the literature.[3]

8-((±)6-Hydroxy-2,5,7,8-tetramethylchromane-2-carbonyloxy)-methyl-1,3,5,7-tetramethyl pyrromethene fluoroborate, (H_2B-TOH). Trolox (0.1 g, 0.4 mmol, 1.5 eq), 8-Hydroxymethyl-1,3,5,7-tetramethyl pyrromethene fluoroborate (0.074 g, 0.27 mmol, 1 eq) and triphenylphosphine (0.105 g, 0.4 mmol, 1.5 eq) were dissolved in 5 ml dry THF under argon. The reaction mixture was left stirring for 5 min at 0^0C and diisopropyl azodicarboxylate (0.081 g, 0.4 mmol, 1.5 eq) was added dropwise. After 10 min the ice bath was removed and the solution was left to warm up to room temperature. The reaction was left stirring at room temperature for 2 h. The solvent was evaporated under reduced pressure and the residue was directly loaded onto a silica gel flash column and eluted with 1/1 hexane/dichloromethane 1% methanol. The product was isolated as an orange powder (0.91 g, 67% yield): ^{1}H NMR (500 MHz, $CDCl_3$) δ ppm 6.00 (s, 2H), 5.33 (d, J = 5.0 Hz, 1H), 5.11 (d, J = 4.7 Hz, 1H), 4.29 (s, 1H), 2.54-2.61 (m, 1H), 2.52, (s, 6H), 2.43-2.48 (m, 2H), 2.14 (s, 6H), 2.01 (s, 3H), 1.95 (s, 3H), 1.93 (s, 3H), 1.90-1.92 (m, 1H), 1.63 (s, 3H); ^{13}C (125 MHz, $CDCl_3$) δ ppm

173.9, 156.4, 145.9, 145.4, 141.4, 132.7, 132.3, 122.9, 122.1, 121.8, 118.9, 116.7, 57.7, 30.9, 25.6, 21.0, 15.3, 14.7, 12.1, 11.5, 11.0; HRMS (ESI^+) for $C_{28}H_{33}N_2O_4BF_2Na$ ($M^{+.Na}$) calcd 533.2394, found 533.2393; FTIR: 3523, 1733, 1550, 1508, 1158, 975, 712 cm^{-1}.

6-Methoxy-2,5,7,8-tetramethylchroman-2-carboxylate, 1a. **1a** was prepared as described in the literature.[52] 6-Hydroxy-2,5,7,8-tetramethylchroman-2-carboxylic acid (Trolox, 1g, 4 mmol) was dissolved in 10 ml methanol and dimethylsulfate (4.5 ml, 48 mmol) was added. Sodium hydroxide (2 g, 48 mmol) was dissolved in 10 ml water and added dropwise to the solution. The reaction mixture was left stirring under argon at 70°C for 2 days. The mixture was allowed to cool to room temperature and was poured in water, followed by extraction of the aqueous phase twice with dichloromethane and once with ethyl acetate. The organic extracts were washed with saturated aqueous NH_4Cl solution, brine and were dried over $MgSO_4$. After evaporation of the solvent under reduced pressure the oily residue was loaded onto a silica gel flash column and eluted with 10 % ethyl acetate/ hexanes. Compound **1a** was obtained as oil (1.1 g, 98 % yield). ^1H NMR ($CDCl_3$,500MHz): δ = 3.70 (s, 3 H), 3.65 (s, 3 H), 2.64 - 2.64 (m, 1 H), 2.59 - 2.70 (m, 1 H), 2.40 - 2.57 (m, 2 H), 2.23 (s, 3 H), 2.20 (s, 3 H), 2.14 (s, 3 H), 1.82 - 1.94 (m, 1 H), 1.64 ppm (s, 3 H); ^{13}C NMR ($CDCl_3$, 126MHz): δ = 174.2, 150.1, 147.7, 128.0, 125.6, 122.8, 117.1, 77.1, 60.3, 52.3, 30.5, 25.4, 20.9, 12.6, 11.8, 11.6 ppm; MS (ESI^-) for $C_{16}H_{21}O_4$ (M^-) calcd 277.15, found 277.13; FTIR: 1751, 1753, 1453, 1250, 1102, 1080 cm^{-1}.

(6-Methoxy-2,5,7,8-tetramethylchroman-2-yl)-methanol, 1b. **1b** was prepared as described in the literature.[53] Lithium aluminum hydride (0.55 g, 14.4 mmol) was suspended in 15 ml dry THF under argon at -78°C. To the stirring suspension a solution of methyl 6-methoxy-2,5,7,8-tetramethylchroman-2-carboxylate **1a** (1 g, 3.6 mmol) in 10 ml dry THF was added dropwise. The reaction mixture was allowed to slowly warm up to room temperature and was left stirring for 1 h. It was quenched by dropwise addition of water followed by extraction with ethyl acetate. The organic fraction was washed with saturated aqueous NH_4Cl solution, brine, dried over $MgSO_4$ and the solvent was evaporated

under reduced pressure. No further purification was required. Compound **1b** was obtained as white solid (0.85 g, 95 % yield). ^{1}H NMR ($CDCl_3$, 500MHz): δ = 3.55 - 3.72 (m, 5 H), 2.56 - 2.73 (m, 2 H), 2.21 (s, 3 H), 2.17 (s, 3 H), 2.07 - 2.13 (s, 3 H), 1.95 - 2.06 (m, 2 H), 1.75 (ddd, *J*=13.5, 6.2, 4.8 Hz, 1 H), 1.25 ppm (s, 3 H); ^{13}C NMR ($CDCl_3$, 126MHz): δ = 149.8, 147.1, 127.7, 126.2, 122.2, 117.2, 75.0, 69.4, 60.4, 27.5, 20.5, 20.1, 12.6, 11.9, 11.7 ppm. MS (ESI^+) for $C_{15}H_{23}O_3$ (M^+) calcd 251.16, found 251.09; FTIR: 3260, 1451, 1245, 1043 cm^{-1}.

(6-Methoxy-2,5,7,8-tetramethylchroman-2-yl)-methyl trifluoro-methanesulfonate, 1c. **1c** was prepared as described in the literature.[53] (6-Methoxy-2,5,7,8-tetramethylchroman-2-yl)methanol **1b** (0.85 g, 3.4 mmol) was dissolved in 15 ml dry dichloromethane under argon, cooled to 0°C and pyridine (0.55 ml, 6.8 mmol) was added. Triflic anhydride (0.86 ml, 5.1 mmol) was added dropwise and the reaction mixture was left stirring for 15 min at room temperature. The solution was then filtered through silica gel to remove the excess Tf_2O and triflic acid. The silica gel was further washed with 50 % dichloromethane/hexanes. The filtrate was evaporated to dryness under reduced pressure to give compound **1c** as white solid in quantitative yield (1.3 g). ^{1}H NMR ($CDCl_3$, 500MHz): δ = 4.48 (q, *J*=1.0 Hz, 2 H), 3.65 (s, 3 H), 2.68 (t, *J*=6.7 Hz, 2 H), 2.19 - 2.28 (m, 3 H), 2.17 (s, 3 H), 2.10 (s, 3 H), 1.95 - 2.05 (m, 1 H), 1.81 - 1.92 (m, 1 H), 1.38 ppm (s, 3 H); ^{13}C NMR ($CDCl_3$, 126MHz): δ = 150.3, 146.3, 128.6, 125.9, 123.4, 122.5, 120.7, 119.9, 117.4, 116.6, 114.8, 79.6, 73.2, 72.9, 60.4, 60.4, 27.7, 21.0, 19.7, 12.5, 11.7 ppm. MS (ESI^+) for $C_{16}H_{21}F_3O_5S$ (M^+) calcd 383.11, found 382.94; FTIR: 1459, 1401, 1385, 1203, 1137 cm^{-1}.

2-(6-Methoxy-2,5,7,8-tetramethylchroman-2-yl)-acetonitrile, 1d. (6-Methoxy-2,5,7,8-tetramethylchroman-2-yl)-methyl trifluoromethane-sulfonate, **1c** (1.3 g, 3.4 mmol), 18-crown-6-ether (1.8 g, 6.8 mmol) and potassium cyanide (0.44 g, 6.8 mmol) were dissolved in 24 ml dry acetonitrile at room temperature under argon. The reaction mixture was left stirring for 16 h and diluted with ethyl acetate. The organic solution was washed twice with brine, dried over $MgSO_4$ and the solvent was evaporated under reduced pressure. No further purification was required. Compound **1d** was obtained as oil (0.86 g, 97 % yield). ^{1}H NMR

($CDCl_3$, 400MHz): δ = 3.64 (s, 3 H), 2.55 - 2.74 (m, 4 H), 2.19 (s, 3 H), 2.15 (s, 3 H), 2.11 (s, 3 H), 1.87 - 2.07 (m, 2 H), 1.49 ppm (s, 3 H); ^{13}C NMR ($CDCl_3$, 101MHz): δ = 150.3, 146.4, 128.6, 126.0, 123.5, 117.1, 116.5, 72.5, 60.4, 30.8, 28.5, 24.6, 20.3, 12.6, 11.8, 11.7 ppm. HRMS (ESI^+) for $C_{16}H_{22}O_2N$ (M^+) calcd 260.1645, found 260.1641; FTIR: 2246, 1454, 1252, 1162, 1087 cm^{-1}

2-(6-Methoxy-2,5,7,8-tetramethylchroman-2-yl)-acetic acid, 2. 2-(6-Methoxy-2,5,7,8-tetramethylchroman-2-yl)-acetonitrile, **1d** (0.86 g, 3.3 mmol) was dissolved in 5 ml of methanol. Potassium hydroxide (5.6 g, 100 mmol) was dissolved in 8 ml of water and added to the solution to yield final concentration of compound **1d** 0.25 M and of potassium hydroxide 7.7 M. The reaction mixture was stirring at 70°C under argon for 24 h or until all the starting material was consumed. The solution was acidified with 6 M HCl and extracted with ethyl acetate. The organic extract was washed with brine, dried over $MgSO_4$ and the solvent was evaporated under reduced pressure. The oily residue was loaded onto a short silica gel flash column and eluted with 50 % ethyl acetate/ hexanes. Compound **2** was obtained as white oily solid (0.57 g, 62 % yield). ^1H NMR ($CDCl_3$, 400MHz): δ = 9.57 - 11.38 (bs, 1 H), 3.66 (s, 3 H), 2.69 (d, *J*=4.7 Hz, 2 H), 2.65 (t, *J*=6.8 Hz, 2 H), 2.21 (s, 4 H), 2.17 (s, 3 H), 2.03 - 2.14 (m, 5 H), 1.94 (dt, *J*=13.8, 7.0 Hz, 1 H), 1.48 ppm (s, 3 H); ^{13}C NMR ($CDCl_3$, 101MHz): δ = 176.4, 149.9, 146.8, 128.2, 125.9, 123.2, 117.2, 73.4, 60.4, 44.0, 31.0, 24.7, 20.5, 12.6, 11.8, 11.7 ppm. HRMS (ESI^-) for $C_{16}H_{21}O_4$ (M^-) calcd 277.1445, found 277.1441; FTIR: 3500, 1701, 1447, 1252, 1084 cm^{-1}

8-((6-hydroxy-2,5,7,8-tetramethylchroman-2-yl)-methyl)-1,3,5,7-tetramethyl Pyrromethene Fluoroborate, 3 (H_2B-PMHC). 2-(6-Methoxy-2,5,7,8-tetramethylchroman-2-yl)-acetic acid, **2** (0.17 g, 0.6 mmol) was dissolved in 0.7 ml thionyl chloride and refluxed at 50°C under argon for 1 h. The reaction mixture was diluted with 20 ml dry toluene and the solvent was evaporated to dryness under reduced pressure. The coevaporation with toluene was repeated two more times and the oily residue was dried under high vacuum for 2 h to ensure that all the thionyl chloride was removed. Without further purification the oily residue was dissolved in 5 ml dry dichloromethane. Phosphorus oxychloride

(0.55 ml, 6 mmol) was added dropwise. The reaction mixture was stirred for 5 min at room temperature followed by dropwise addition of 2,4-dimethyl pyrrole (0.13 ml, 1.3 mmol). The reaction mixture was left stirring at room temperature under argon for 24 h. It was diluted with dichloromethane, washed with brine, dried over $MgSO_4$ and the solvent was evaporated under reduced pressure. The oily residue was redissolved in 5 ml dry dichloromethane and the solution was cooled to -10°C. BBr_3 (0.55 ml, 6 mmol) was added dropwise, the reaction mixture was stirred for 1 h at -10°C. It was quenched with water and extracted with dichloromethane. The organic extract was washed with brine, dried over $MgSO_4$ and the solvent was evaporated under reduced pressure. The oily residue was redissolved in 1 ml dry dichloromethane and 12 ml dry toluene. Diisopropylethylamine (0.4 ml) was added followed after 15 min by very slow dropwise addition of $BF_3.OEt_2$ (0.6 ml) at 0°C. After stirring for 1.5 h at room temperature the solvent was evaporated under reduced pressure and the residue was loaded onto a silica gel flash column and eluted with 30 % ethyl acetate/ hexanes. Compound **3** was obtained as red-orange solid (0.07 g, 23 % yield over 4 steps). ^{1}H NMR ($CDCl_3$, 500MHz): δ = 6.04 (s, 2 H), 4.20 (s, 1 H), 3.42 - 3.56 (m, 2 H), 2.57 - 2.74 (m, 2 H), 2.53 (s, 3 H), 2.52 (s, 3 H), 2.50 (s, 3 H), 2.43 (s, 3 H), 2.09 (s, 3 H), 2.08 (s, 3 H), 1.90 - 1.98 (m, 2 H), 1.77 (s, 3 H), 1.18 ^{13}C NMR ($CDCl_3$, 126MHz): δ = 153.9, 153.1, 145.0, 144.7, 142.7, 141.2, 140.2, 134.6, 133.7, 123.3, 122.1, 122.0, 121.3, 118.3, 116.8, 75.6, 38.8, 33.4, 20.8, 17.6, 17.6, 14.5, 12.1, 11.5, 11.2 ppm. HRMS (ESI^+) for $C_{27}H_{34}N_2O_2BF_2$ (M^+) calcd 467.2676, found 467.2683; FTIR: 3547, 1543, 1194, 1152 cm^{-1}

5.5. References

1. Burton, G.W. & Ingold, K.U. Vitamin E: application of the principles of physical organic chemistry to the exploration of its structure and function. *Accounts of Chemical Research* 19, 194-201, **1986**.
2. Singh, U., Devaraj, S. & Jialal, I. VITAMIN E, OXIDATIVE STRESS, AND INFLAMMATION. *Annual Review of Nutrition* 25, 151-174, **2005**.
3. Sano, M., Ernesto, C., Thomas, R.G., Klauber, M.R., Schafer, K., Grundman, M., Woodbury, P., Growdon, J., Cotman, C.W., Pfeiffer, E., Schneider, L.S. & Thal, L.J. A Controlled Trial of Selegiline, Alpha-Tocopherol, or Both as Treatment for Alzheimer's Disease. *New England Journal of Medicine* 336, 1216-1222, **1997**.
4. Howard, A.C., McNeil, A.K. & McNeil, P.L. Promotion of plasma membrane repair by vitamin E. *Nat Commun* 2, 597, **2011**.
5. Boscoboinik, D., Szewczyk, A., Hensey, C. & Azzi, A. Inhibition of cell proliferation by alpha-tocopherol. Role of protein kinase C. *Journal of Biological Chemistry* 266, 6188-6194, **1991**.
6. Azzi, A., Gysin, R., Kempna, P., Munteanu, A., Negis, Y., Villacorta, L., Visarius, T. & Zingg, J.-M. Vitamin E Mediates Cell Signaling and Regulation of Gene Expression. *Annals of the New York Academy of Sciences* 1031, 86-95, **2004**.
7. Hasegawa, K. & Patterson, L.K. PULSE RADIOLYSIS STUDIES IN MODEL LIPID SYSTEMS: FORMATION AND BEHAVIOR OF PEROXY RADICALS IN FATTY ACIDS. *Photochemistry and Photobiology* 28, 817-823, **1978**.
8. Niki, E. & Noguchi, N. Dynamics of Antioxidant Action of Vitamin E. *Accounts of Chemical Research* 37, 45-51, **2004**.
9. Jonsson, M., Lind, J., Reitberger, T., Eriksen, T.E. & Merenyi, G. Free radical combination reactions involving phenoxyl radicals. *Journal of Physical Chemistry* 97, 8229-8233, **1993**.
10. Barclay, L.R.C. Model biomembranes: quantitative studies of peroxidation, antioxidant action, partitioning, and oxidative stress. *Canadian Journal of Chemistry* 71, 1-16, **1993**.
11. Liebler, D.C., Baker, P.F. & Kaysen, K.L. Oxidation of vitamin E: evidence for competing autoxidation and peroxyl radical trapping reactions of the tocopheroxyl radical. *Journal of the American Chemical Society* 112, 6995-7000, **1990**.
12. Liebler, D.C., Burr, J.A., Matsumoto, S. & Matsuo, M. Reactions of the vitamin E model compound 2,2,5,7,8-pentamethylchroman-6-ol with peroxyl radicals. *Chemical Research in Toxicology* 6, 351-355, **1993**.
13. Burton, G.W., Doba, T., Gabe, E., Hughes, L., Lee, F.L., Prasad, L. & Ingold, K.U. Autoxidation of biological molecules. 4. Maximizing the antioxidant activity of phenols. *Journal of the American Chemical Society* 107, 7053-7065, **1985**.
14. Barclay, L.R.C., Edwards, C.E. & Vinqvist, M.R. Media Effects on Antioxidant Activities of Phenols and Catechols. *Journal of the American Chemical Society* 121, 6226-6231, **1999**.
15. Barclay, L.R.C., Vinqvist, M.R., Mukai, K., Itoh, S. & Morimoto, H. Chain-breaking phenolic antioxidants: steric and electronic effects in polyalkylchromanols, tocopherol analogs, hydroquinones, and superior antioxidants of the polyalkylbenzochromanol and naphthofuran class. *The Journal of Organic Chemistry* 58, 7416-7420, **1993**.
16. Roginsky, V., Barsukova, T., Loshadkin, D. & Pliss, E. Substituted p-hydroquinones as inhibitors of lipid peroxidation. *Chemistry and Physics of Lipids* 125, 49-58, **2003**.
17. Loshadkin, D., Roginsky, V. & Pliss, E. Substituted p-hydroquinones as a chain-breaking antioxidant during the oxidation of styrene. *International Journal of Chemical Kinetics* 34, 162-171, **2002**.
18. Nam, T.-g., Rector, C.L., Kim, H.-y., Sonnen, A.F.P., Meyer, R., Nau, W.M., Atkinson, J., Rintoul, J., Pratt, D.A. & Porter, N.A. Tetrahydro-1,8-naphthyridinol Analogues of α-Tocopherol as Antioxidants in Lipid Membranes and Low-Density Lipoproteins. *Journal of the American Chemical Society* 129, 10211-10219, **2007**.

19. Valgimigli, L., Ingold, K.U. & Lusztyk, J. Antioxidant Activities of Vitamin E Analogues in Water and a Kamlet-Taft beta Value for Water. *Journal of the American Chemical Society* 118, 3545-3549, **1996**.
20. Barclay, L.R.C., Baskin, K.A., Dakin, K.A., Lock, S.J. & Vinqvist, M.R. The antioxidant activities of phenolic antioxidants in free radical peroxidation of phospholipid membranes. *Canadian Journal of Chemistry* 68, 2258-69, **1990**.
21. Bowry, V.W. & Ingold, K.U. The Unexpected Role of Vitamin E (a-Tocopherol) in the Peroxidation of Human Low-Density Lipoprotein. *Accounts of Chemical Research* 32, 27-34, **1999**.
22. Bedard, L., Young, M.J., Hall, D., Paul, T. & Ingold, K.U. Quantitative Studies on the Peroxidation of Human Low-Density Lipoprotein Initiated by Superoxide and by Charged and Neutral Alkylperoxyl Radicals. *Journal of the American Chemical Society* 123, 12439-12448, **2001**.
23. Alessi, M., Paul, T., Scaiano, J.C. & Ingold, K.U. The Contrasting Kinetics of Peroxidation of Vitamin E-Containing Phospholipid Unilamellar Vesicles and Human Low-Density Lipoprotein. *J. Am. Chem. Soc.* 124, 6957-6965, **2002**.
24. Gramlich, G., Zhang, J. & Nau, W.M. Diffusion of a-Tocopherol in Membrane Models: Probing the Kinetics of Vitamin E Antioxidant Action by Fluorescence in Real Time. *Journal of the American Chemical Society* 126, 5482-5492, **2004**.
25. Barclay, L.R.C. & Vinqvist, M.R. Membrane peroxidation: Inhibiting effects of water-soluble antioxidants on phospholipids of different charge types. *Free Radical Biology and Medicine* 16, 779-788, **1994**.
26. Nam, T.-g., Rector, C.L., Kim, H.-y., Sonnen, A.F.P., Meyer, R., Nau, W.M., Atkinson, J., Rintoul, J., Pratt, D.A. & Porter, N.A. Tetrahydro-1,8-naphthyridinol Analogues of Î±-Tocopherol as Antioxidants in Lipid Membranes and Low-Density Lipoproteins. *Journal of the American Chemical Society* 129, 10211-10219, **2007**.
27. Sonnen, A.F.P., Bakirci, H., Netscher, T. & Nau, W.M. Effect of Temperature, Cholesterol Content, and Antioxidant Structure on the Mobility of Vitamin E Constituents in Biomembrane Models Studied by Laterally Diffusion-Controlled Fluorescence Quenching. *Journal of the American Chemical Society* 127, 15575-15584, **2005**.
28. Culbertson, S.M. & Porter, N.A. Unsymmetrical Azo Initiators Increase Efficiency of Radical Generation in Aqueous Dispersions, Liposomal Membranes, and Lipoproteins. *Journal of the American Chemical Society* 122, 4032-4038, **2000**.
29. Culbertson, S.M., Vinqvist, M.R., Barclay, L.R.C. & Porter, N.A. Minimizing Tocopherol-Mediated Radical Phase Transfer in Low-Density Lipoprotein Oxidation with an Amphiphilic Unsymmetrical Azo Initiator. *Journal of the American Chemical Society* 123, 8951-8960, **2001**.
30. Noguchi, N., Yamashita, H., Gotoh, N., Yamamoto, Y., Numano, R. & Niki, E. 2,2′-Azobis (4-Methoxy-2,4-Dimethylvaleronitrile), a New Lipid-Soluble Azo Initiator: Application to Oxidations of Lipids and Low-Density Lipoprotein in Solution and in Aqueous Dispersions. *Free Radical Biology and Medicine* 24, 259-268, **1998**.
31. Takahashi, M., Tsuchiya, J. & Niki, E. Scavenging of radicals by vitamin E in the membranes as studied by spin labeling. *Journal of the American Chemical Society* 111, 6350-6353, **1989**.
32. Avila, D.V., Ingold, K.U., Lusztyk, J., Green, W.H. & Procopio, D.R. Dramatic Solvent Effects on the Absolute Rate Constants for Abstraction of the Hydroxylic Hydrogen Atom from tert-Butyl Hydroperoxide and Phenol by the Cumyloxyl Radical. The Role of Hydrogen Bonding. *Journal of the American Chemical Society* 117, 2929-2930, **1995**.
33. Litwinienko, G. & Ingold, K.U. Solvent Effects on the Rates and Mechanisms of Reaction of Phenols with Free Radicals. *Accounts of Chemical Research* 40, 222-230, **2007**.
34. Snelgrove, D.W., Lusztyk, J., Banks, J.T., Mulder, P. & Ingold, K.U. Kinetic Solvent Effects on Hydrogen-Atom Abstractions: Reliable, Quantitative Predictions via a Single Empirical Equation1. *Journal of the American Chemical Society* 123, 469-477, **2000**.

35. Wang, X. & Quinn, P.J. Vitamin E and its function in membranes. *Progress in Lipid Research* 38, 309-336, **1999**.
36. Wang, X. & Quinn, P.J. The location and function of vitamin E in membranes (Review). *Molecular Membrane Biology* 17, 143 - 156, **2000**.
37. Quinn, P.J. Molecular associations of vitamin E. in *Vitamin E: Vitamins and Hormones Advances in Research and Applications*, Vol. 76 67-+ (Elsevier, Amsterdam, 2007).
38. Atkinson, J., Harroun, T., Wassall, S.R., Stillwell, W. & Katsaras, J. The location and behavior of alpha-tocopherol in membranes. *Molecular Nutrition & Food Research* 54, 641-651, **2010**.
39. Qin, S.-S., Yu, Z.-W. & Yu, Y.-X. Structural and Kinetic Properties of alfa-Tocopherol in Phospholipid Bilayers, a Molecular Dynamics Simulation Study. *Journal of Physical Chemistry B* 113, 16537-16546, **2009**.
40. Krumova, K., Oleynik, P., Karam, P. & Cosa, G. Phenol-Based Lipophilic Fluorescent Antioxidant Indicators: A Rational Approach. *Journal of Organic Chemistry* 74, 3641-3651, **2009**.
41. Oleynik, P., Ishihara, Y. & Cosa, G. Design and Synthesis of a BODIPY-alfa-Tocopherol Adduct for Use as an Off/On Fluorescent Antioxidant Indicator. *Journal of the American Chemical Society* 129, 1842-1843, **2007**.
42. de Silva, A.P., Gunaratne, H.Q.N., Gunnlaugsson, T., Huxley, A.J.M., McCoy, C.P., Rademacher, J.T. & Rice, T.E. Signaling Recognition Events with Fluorescent Sensors and Switches. *Chemical Reviews* 97, 1515-1566, **1997**.
43. Khatchadourian, A., Krumova, K., Boridy, S., Ngo, A.T., Maysinger, D. & Cosa, G. Molecular Imaging of Lipid Peroxyl Radicals in Living Cells with a BODIPY-Tocopherol Adduct. *Biochemistry* 48, 5658-5668, **2009**.
44. Krumova, K. & Cosa, G. Bodipy Dyes with Tunable Redox Potentials and Functional Groups for Further Tethering: Preparation, Electrochemical, and Spectroscopic Characterization. *Journal of the American Chemical Society* 132, 17560–17569, **2010**.
45. Torchilin, V.P. & Weissig, V. (eds.). *Liposomes*, (Oxford University Press Inc., NY, 2003).
46. Buttriss, J.L. & Diplock, A.T. The ga-tocopherol and phospholipid fatty acid content of rat liver subcellular membranes in vitamin E and selenium deficiency. *Biochimica et Biophysica Acta (BBA) - Lipids and Lipid Metabolism* 963, 61-69, **1988**.
47. Barclay, L.R.C., Locke, S.J., MacNeil, J.M., VanKessel, J., Burton, G.W. & Ingold, K.U. Autoxidation of micelles and model membranes. Quantitative kinetic measurements can be made by using either water-soluble or lipid-soluble initiators with water-soluble or lipid-soluble chain-breaking antioxidants. *Journal of the American Chemical Society* 106, 2479-2481, **1984**.
48. Maillard, B., Ingold, K.U. & Scaiano, J.C. Rate constants for the reactions of free radicals with oxygen in solution. *Journal of the American Chemical Society* 105, 5095-5099, **1983**.
49. We recently showed via oxygen uptake studies in styrene solution at 30^{o}C (ref. 44) that TOH antioxidant activity towards peroxyl radicals is ca. 1.6 fold larger than that of B-TOH, i.e., $k_{inh}^{TOH}/ k_{inh}^{B\text{-}TOH} = 1.6$. B-TOH bears ethyl groups in the BODIPY equatorial positions instead of H atoms as is the case for H_2B-TOH. The results acquired with B-TOH are extendable to H_2B-TOH since such structural modification only affects the photophysical properties of the probes yet it has no effect on their antioxidant activity.
50. Barclay, L.R.C. & Ingold, K.U. Autoxidation of biological molecules. 2. Autoxidation of a model membrane. Comparison of the autoxidation of egg lecithin phosphatidylcholine in water and in chlorobenzene. *Journal of the American Chemical Society* 103, 6478-6485, **1981**.
51. Equaiton 20 requires for the experimental quantity observed to reach a plateau as the reaction is complete. Due to slow degradation of the probe once it is turned on as a result of further reaction between the peroxyl radical and presumably the pyrrole units in the bodipy, in our experiments the intensity does not reach a plateau, but rather decreases slowly. We thus use the intensity at the maximum as that corresponding to I_{∞}.

52. Koufaki, M., Theodorou, E., Galaris, D., Nousis, L., Katsanou, E.S. & Alexis, M.N. Chroman/Catechol Hybrids: Synthesis and Evaluation of Their Activity against Oxidative Stress Induced Cellular Damage. *Journal of Medicinal Chemistry* 49, 300-306, **2005**.
53. Huang, J.-W., Shiau, C.-W., Yang, J., Wang, D.-S., Chiu, H.-C., Chen, C.-Y. & Chen, C.-S. Development of Small-Molecule Cyclin D1-Ablative Agents. *Journal of Medicinal Chemistry* 49, 4684-4689, **2006**.

Imaging Peroxyl Radicals within the Mitochondrial Lipid Membrane of Live Cells

Katerina Krumova, Lana Greene, Gonzalo Cosa, *manuscript in preparation*

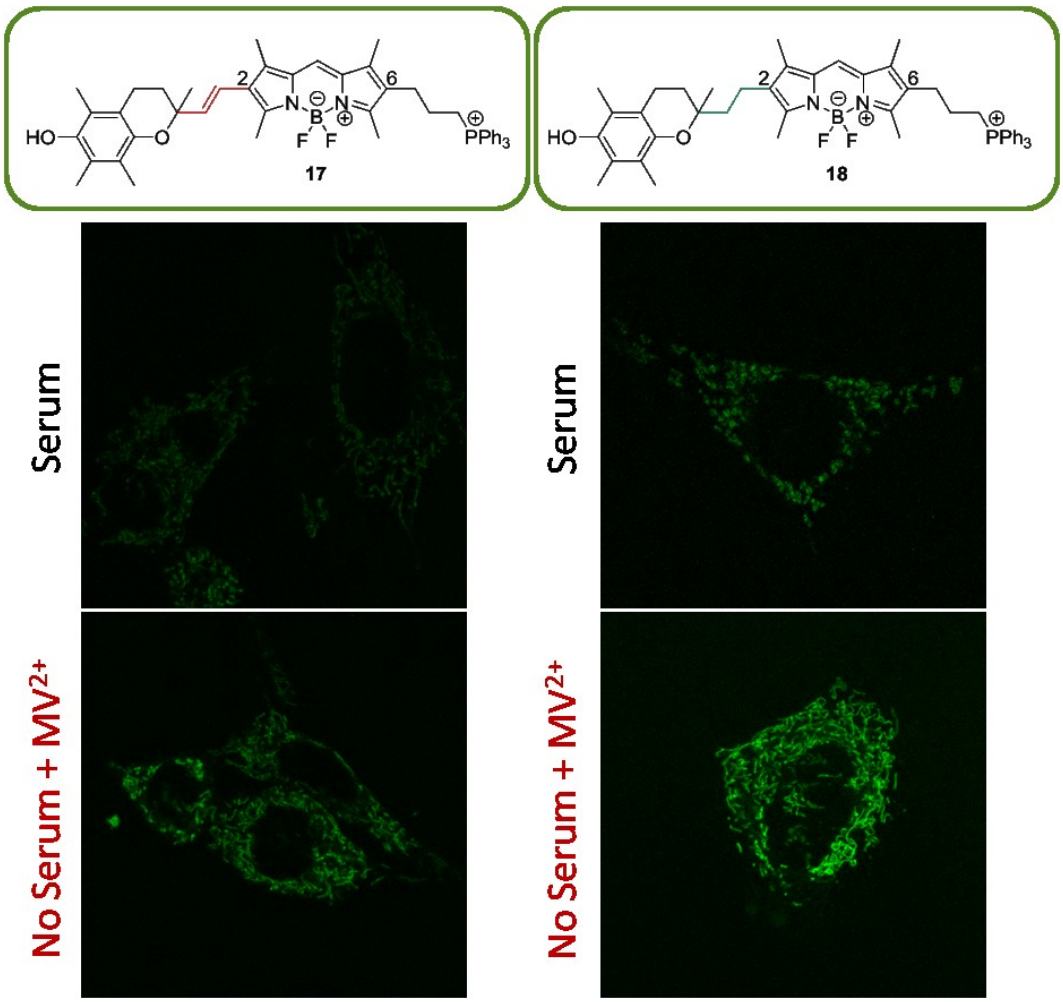

Preface

In previous chapters we discussed the preparation of the first (B-TOH) and second (H_2B-TOH and H_2B-PMHC) generation of lipophilic fluorogenic probes for the specific imaging of ROS in the lipid membrane of live cells. Studies performed in homogeneous solution, on suspensions of model lipid membranes (liposomes), and in live cells demonstrate the potential of the fluorogenic antioxidants as chemical tools that can elucidate the biological consequences of the chemistry of ROS.

To better understand the importance of the subcellular localization and trafficking of ROS we need however to develop fluorogenic sensors capable of targeting specific organelles. In the following chapter we describe the design and synthesis of the third generation of ROS-sensitive fluorogenic indicators (Mito-B-v-TOH and Mito-B-e-TOH) equipped with functional groups that lead to their preferential accumulation in mitochondria. The specificity and sensitivity of the newly developed probes towards peroxyl radicals were tested in liposomes utilizing the high throughput fluorescence assay described in chapter 5. Additionally, we explore the ability of Mito-B-v-TOH and Mito-B-e-TOH to visualize oxidative stress changes in the mitochondria of live fibroblast cells triggered upon treatment of the cell culture with methyl viologen. Control studies with healthy cells and co-localization studies with mitochondrial markers further establish the potential of our new probes for studying the chemistry of ROS in complex biological systems.

6.1. Introduction

Mitochondria play an essential role in the normal cell functioning and survival. They are referred to as the "powerhouse of the cell" as they are a major production site of cellular energy.[1] Energy is generated during the oxidative phosphorylation process that relies on the electron transport chains (respiratory chains) in the inner mitochondrial membrane. During this process, electrons are transferred from electron donors (typically sugars) to oxygen via a series of relay systems, resulting in reduction of oxygen to water and release of energy that is stored in the form of adenosine triphosphate (ATP).[2]

Mitochondria are involved not only in the energy production of the cell but also in variety of signalling processes, metabolism of biomolecules, and calcium homeostasis modulation.[3] They play a crucial role in apoptotic cell death by releasing proapoptotic factors from the intermembrane space, thus committing the cell to die.[4]

Given its critical role it is not surprising that mitochondrial malfunction leads to variety of biological and pathological events disrupting the normal functioning of the cell. There is a complex relationship between mitochondrial damage and remarkable range of health issues, aging, and various diseases.[3,5,6]

In nearly all cases the mitochondrial dysfunction is caused by reactive oxygen species (ROS) produced as side products along the electron transport chain.[7-9] Here the highly reductive environment of the mitochondrial electron transport chains is responsible for the generation of ROS. The redox systems involved in oxidative phosphorylation, such as NADPH, flavoproteins, Fe-S clusters, and ubisemiquinone have sufficient reduction potential to participate in monovalent reduction of molecular oxygen.[8]

Targeting mitochondria with ROS scavengers (antioxidants) or compounds that interfere with the unique biochemistry in mitochondria is emerging as a novel approach in drug discovery towards treatment of degenerative diseases.[10-12] Advances in this area are dependent on the understanding of the relationship between the redox state within mitochondria and cellular processes. Such an understanding requires in turn appropriate tools to interrogate and study the

chemistry and biology of ROS in mitochondria. Fluorescence imaging with ROS-sensitive fluorogenic probes which specifically target mitochondria is a powerful non-invasive approach to tackle the study of ROS production and consumption within this organelle.

In order to successfully develop mitochondria-targeting fluorogenic probes however a number of requirements have to be met. For a molecule to target an organelle it must first cross the cellular membrane, which possesses a complex structure that prohibits free access to intracellular compartments. Additionally all organelles are separated from the cytosol by lipid membranes that might differ in lipid composition but have no distinguishing features that can afford directing molecules in a specific manner. One way to selectively target mitochondria is to take advantage of their electrochemical potential. The mitochondrion is comprised of four different compartments: the outer mitochondrial membrane (OMM), the inner mitochondrial membrane (IMM), the intermembrane space (IMS), and the matrix (Figure 6.1). A unique feature of the IMM is its strong negative potential of -180 mV maintained across the membrane.

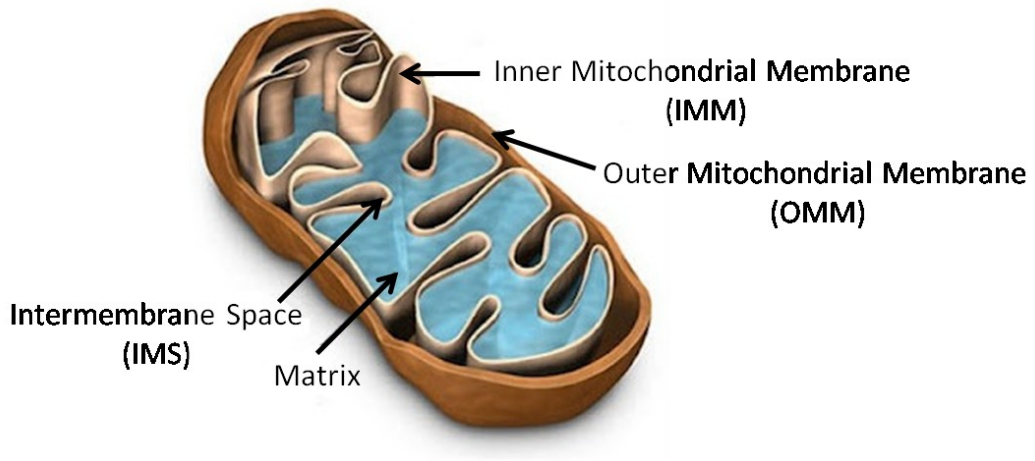

Figure 6.1. Structure of mitochondria.[13]

A few strategies have emerged as viable approaches to target mitochondria. These involve the use of cationic proteins and peptides,[14-17] as well as lipophilic cationic compounds.[3,18,19] Delocalized lipophilic cations such as triphenylphosphonium cation (TPP) are particularly good first at passing through

the phospholipid membrane without requiring any specific uptake mechanism and next at accumulating in mitochondria. The use of phosphonium groups have been pioneered by Murphy[3,20-24] and subsequently utilized by others[11,25-29] to selectively direct attached cargo or fluorescent probes to mitochondria.

The activation energy required to transport a lipophilic cation through the lipid membrane depends on both the Born energy, which raises the activation energy, and the hydrophobic energy, which lowers it.[3]

The Born energy (W_B) is the energy required to transfer a monovalent, spherical ion of charge Z and radius r from an aqueous phase of dielectric constant ε_1 into the center of a bilayer of dielectric constant ε_2. It is expressed by equation (1) below:[30]

$$W_B = \frac{Z^2}{8\pi\varepsilon_0 r} \times \left(\frac{1}{\varepsilon_1 - \varepsilon_2} \right) \tag{1}$$

When the transfer is from water (ε_2=80) to bulk lipid membrane (ε_1=2) the Born energy is given by:

$$W_B \approx \frac{81 \times Z^2}{r} kcal/mol \tag{2}$$

The Born energy term poses the most significant energy barrier to ion transport. We may appreciate both from equation (1) and (2) that the larger the radius of the ion the smaller the energy required for moving the ion into the membrane.

The hydrophobic energy is the energy required to move an uncharged molecule with the same radius r through the membrane. It is an attractive force and the greater the hydrophobic surface area of the cation the larger the magnitude of the hydrophobic energy. The hydrophobic energy term generally lowers the overall activation energy for the transport. For TPP the large hydrophobic radius of 4.2 Å lowers the Born energy and increases the hydrophobic energy, thus enabling it to readily pass through the membrane.[3]

Lipophilic cations are taken up from the positively charged outer leaflet of the IMM into the negatively charged inner leaflet until a sufficiently large concentration gradient is built up to equalize the electrochemical potential of the

molecules on both sides. When the compound uptake is equilibrated with the membrane potential, the ratio of the cation concentration inside and outside of the membrane will be given by the Nernst equation:

$$\Delta\psi = -\frac{RT}{F}\ln\left(\frac{[cation_{in}]}{[cation_{out}]}\right) \qquad (3)$$

This relationship predicts that for the plasma membrane, characterized with a potential ranging from -30 to -60 mV with respect to extracellular space, TPP will accumulate in a 5 to 10-fold excess into the cytoplasm. Further for the mitochondrial inner membrane with a typical potential of -140 to -180 mV, TPP will accumulate in a several hundred-fold excess within the mitochondria.[3,17]

Building on our previous work on 2 segment receptor-reporter fluorogenic antioxidants [31-33] here we describe the design, synthesis, and characterization of lipophilic fluorogenic probes (Mito-B-v-TOH and Mito-B-e-TOH) which are ROS-sensitive and specifically target the mitochondrial lipid membrane.

The new probes consist of 3 segments: a receptor, a reporter, and a mitochondria targeting element (e.g. a lipophilic cation such as TPP; Figure 6.2). A chromanol ring with the chemical structure of the potent free radical scavenger α-tocopherol constitutes the receptor segment. The reporter segment consists of a Bodipy fluorophore whose excited state deactivation is sensitive to redox chemical changes in the receptor moiety. The lipophilicity of the Bodipy dye also ensures partitioning in the lipid membrane. For the mitochondria-targeting segment we selected a triphenylphosphonium cation appended via a lipophilic tail to the Bodipy dye. The two probes reported differ in the use of a vinyl or an ethyl functionality to couple the receptor and the reporter segments.

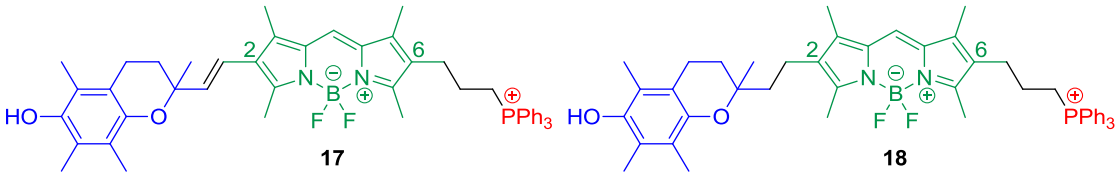

Figure 6.2. Structures of mitochondria-targeting fluorogenic antioxidants **17** (Mito-B-v-TOH) and **18** (Mito-B-e-TOH). The three segments are colored for visualization.

The two newly prepared probes are shown to be sensitive to the presence of ROS species (mostly lipid peroxyl radicals) generated in the mitochondrial membrane of live fibroblast cells upon treatment with methyl viologen as a source of stress. Control studies with healthy cells and co-localization studies with mitochondrial markers unequivocally establish the suitability of the new compounds towards imaging ROS production in the mitochondrial membrane of live cells with high sensitivity. The live cell studies together with the photophysical properties of the new probes and their chemical reactivity towards peroxyl radicals reported here altogether anticipate that Mito-B-e-TOH and Mito-B-v-TOH may become versatile tools in the study of mitochondrial physiology and mitochondrial dysfunction in the presence of reactive oxygen species (ROS).

6.2. Results and Discussion

6.2.1. Design of Mitochondria-Targeting Fluorogenic Antioxidants

The choice of the 3 segments and linkers utilized in building the probes Mito-B-v-TOH (**17**) and Mito-B-e-TOH (**18**) ensured that the new compounds would have: i) A high specificity towards lipid peroxyl radicals, the dominant species in lipid membranes encountered following ROS stress; ii) An absorption and emission in the visible range, to minimize excitation of cellular components; iii) An affinity for the hydrophobic environment within the lipid bilayer; iv) A photoinduced electron transfer (PeT) molecular switch which is controlled by reaction with ROS. Here the receptor readily quenches the emission of the reporter and upon oxidation of the receptor by reaction with ROS PeT is turned off and emission in the reporter segment is restored; v) A largely delocalized positively charged segment for preferential accumulation of the probe in the mitochondrial membrane, which in addition does not interfere with PeT; vi) Short linkers between receptor and reporter segments to favor PeT.

On the basis of the above concepts we selected as the receptor-reporter-targeting trio the α-tocopherol chromanol moiety, a Bodipy fluorophore, and the TPP cation, respectively. From our previous work, we have established that the redox potentials of Bodipy dyes are easily tuneable to afford exergonic PeT from

the chromanol moiety.[31,34] Additionally, synthetic modifications to the fluorophore allow for a facile introduction of the mitochondria-targeting phosphonium tag. We employed vinyl or ethyl linkers as means to minimize the distance between the receptor and reporter segments, favoring PeT. The design of the fluorogenic probes further relied on the coupling of the receptor and the reporter at the equatorial positions of the Bodipy core (C2 adn C6). We expected this construct to be minimally disruptive of the lipid packing in the membrane as the molecule may align with the lipids within the bilayer, rather than exist as a propeller as is the case with our previously reported fluorogenic antioxidants B-TOH, H_2B-TOH, and H_2B-PMHC.

6.2.2. Synthesis of Mitochondria-Targeting Fluorogenic Antioxidants

An important consideration in the synthetic route chosen is the stage at which installation of the phosphonium targeting group takes place. We planned to introduce the TPP tag in the final step of the synthesis in order to circumvent potential complications arising from possible incompatibility with the reagents and functionalities used. We rationalized that synthetically it would be more feasible to first couple the chromanol and the pyrrole bearing aldehyde functionality on the α-position through a vinyl linker (segment A in Scheme 6.1) via Heck coupling and next use the resulting compound to build an asymmetric Bodipy dye bearing a chromanol moiety. This approach would additionally allow for the conversion of the vinyl linker into an ethyl linker.

Traditionally asymmetric Bodipy dyes are prepared by condensation of a pyrrole with a free α-position and a pyrrole carrying an α-aldehyde.[35] We envisioned that the pyrrole with a free α-position could additionally have a propyl chloride group (segment B in Scheme 6.1). Thus, the introduction of a good leaving group allows for installation of the TPP through a nucleophilic substitution reaction once the Bodipy framework is built (See Scheme 6.1).

The synthetic approach outlined in Schemes 6.2, 6.3, and 6.4 meets all the criteria discussed above.

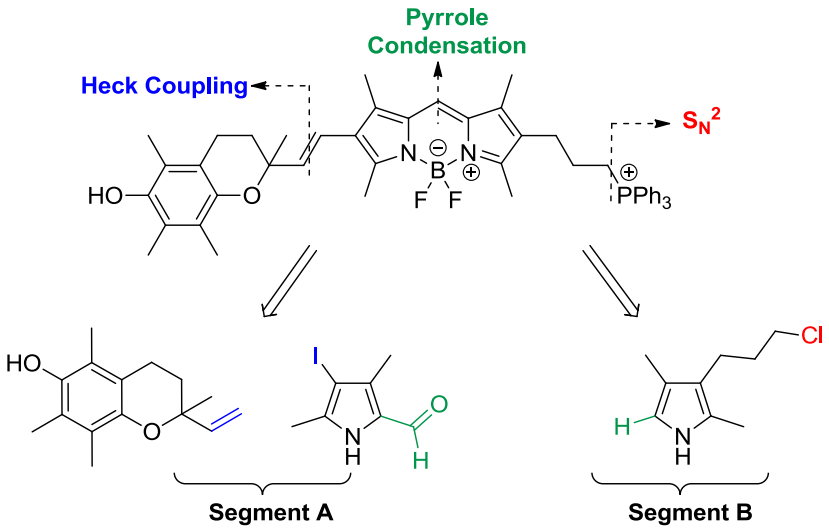

Scheme 6.1. Retrosynthetic analysis of mitochondria-targeting fluorogenic probes.

In order to accomplish the Heck coupling we installed an alkene group on the chromanol ring and an iodide on the α-formyl-pyrrole. To prepare the chromanol alkene we utilized the Wittig reaction. The chromanol aldehyde, **1**, necessary for the Wittig reaction was in turn prepared by Dess-Martin oxidation of the corresponding alcohol, the synthesis of which was previously reported by us.[33]

The aldehyde undergoes Wittig reaction with iodo-(methyl)-triphenylphosphorane to afford the terminal chromanol alkene, **2** (Scheme 6.2). The synthesis of the iodo-formyl pyrrole, **3**, necessary for the Heck coupling, was previously reported by Burgess *et al*.[36] We initially attempted a direct coupling of **2** and **3**, using palladium acetate $Pd(OAc)_2$ as a catalyst under basic conditions (triethylamine, TEA). Formation of the coupling product was not observed however, possibly due to deactivation of the catalyst by the NH-group in the pyrrole. We established that the nitrogen on the pyrrole should be protected in order for the reaction to take place. Traditional protecting groups used for pyrroles such as tert-butyloxycarbonyl (Boc) and benzoyl (Bz) groups were not amenable to our synthetic conditions as they got easily deprotected under the high temperatures (100°C) required for of the Heck reaction. After investigating several possibilities we selected the methoxymethyl (MOM) moiety as the most

suitable protecting group to use. Protecting **3** with methoxymethyl bromide yielded the desired pyrrole, **4** (Scheme 6.2).

We subsequently proceeded with the Heck coupling of compounds **2** and **4**. The standard Heck coupling conditions involving TEA and $Pd(OAc)_2$ in dimethylformamide (DMF) at 100°C led exclusively to deiodination of pyrrole **4**. Examining the mechanism of the reaction we concluded that the loss of iodine was possibly due to the base used. We modified the conditions employing potassium acetate, tetrabutylammonium bromide, and 5% $Pd(OAc)_2$ (Scheme 6.2).[37] The reaction was heated to 100 °C for 24 h. It was stopped before full conversion was observed, due to partial decomposition of the product. The coupling yielded the desired chromanol-pyrrole adduct **5** with 44 % yield. Deiodination was still observed but only with a 15 % yield. A total of 23% of the starting chromanol alkene was recovered after the reaction.

In order to subject compound **5** to a condensation with the pyrrole bearing a free α-position to form the Bodipy fluorophore, a removal of both protecting groups (MOM on the pyrrole and methoxy on the chromanol) was necessary. MOM deprotection proved to be challenging as most of the product decomposed under the acidic conditions used (HCl or trifluoroacetic acid). Only 10 % yield was achieved. We thus developed an alternative two-step deprotection approach (Scheme 6.2). In the first step addition of BBr_3 at -10 °C removed both the methoxy group on the phenol as well as the methoxy part of the MOM protection to yield **6** (Segment A in Scheme 6.1). Compound **6** is a hemi-aminal, which was hydrolysed to formaldehyde and fully deprotected pyrrole **7** following treatment with 1 M NaOH.[38] Maintaining the right temperature throughout the reaction of the formation of **6** was crucial. An increase in the temperature led to decomposition of the intermediate **6**.

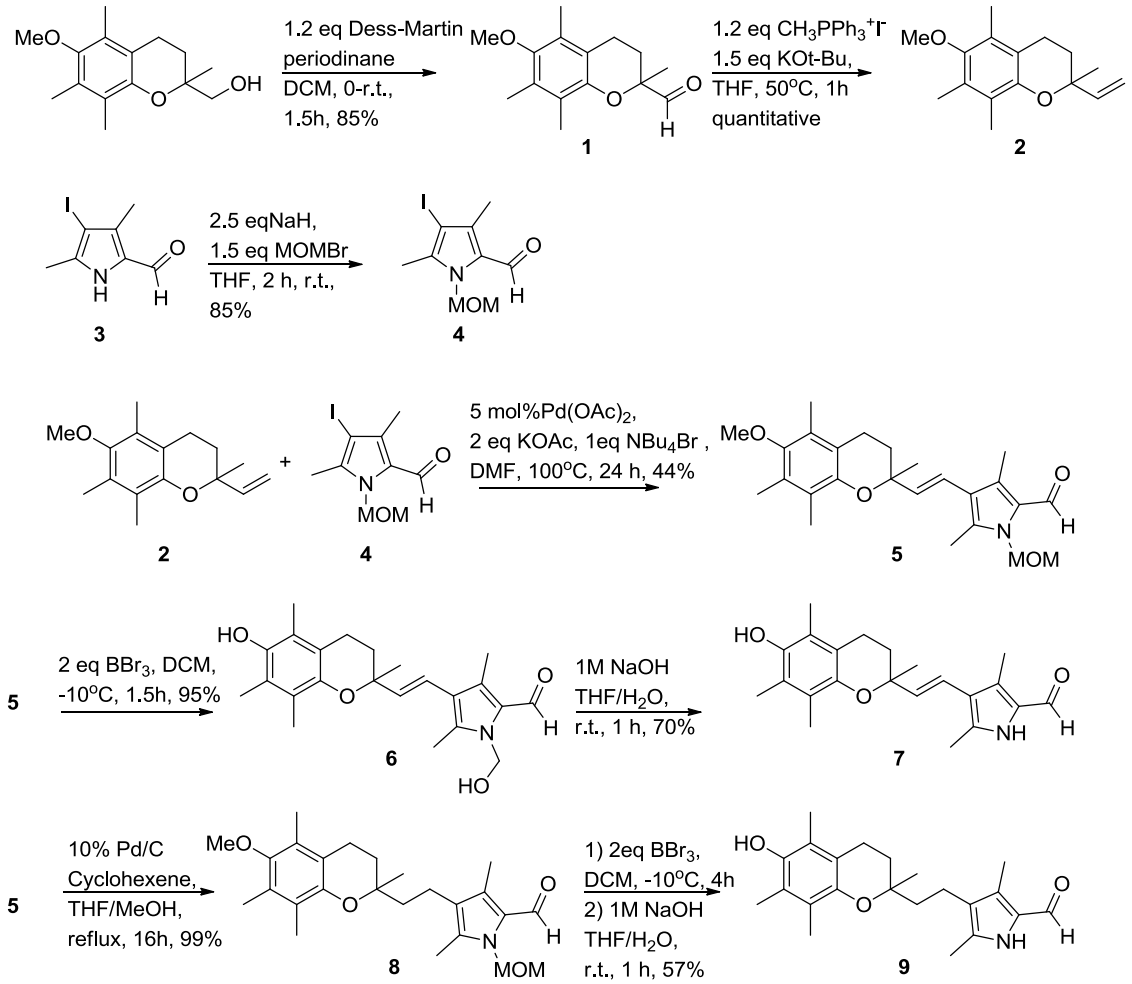

Scheme 6.2. Synthesis of Segment A.

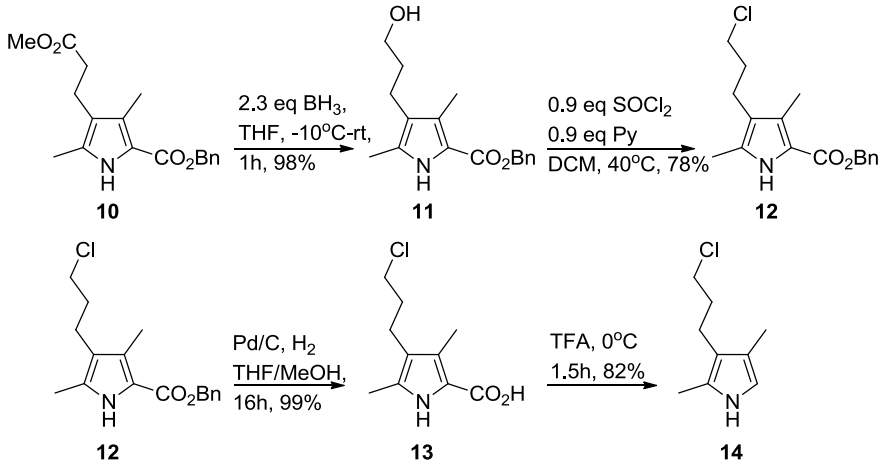

Scheme 6.3. Synthesis of Segment B.

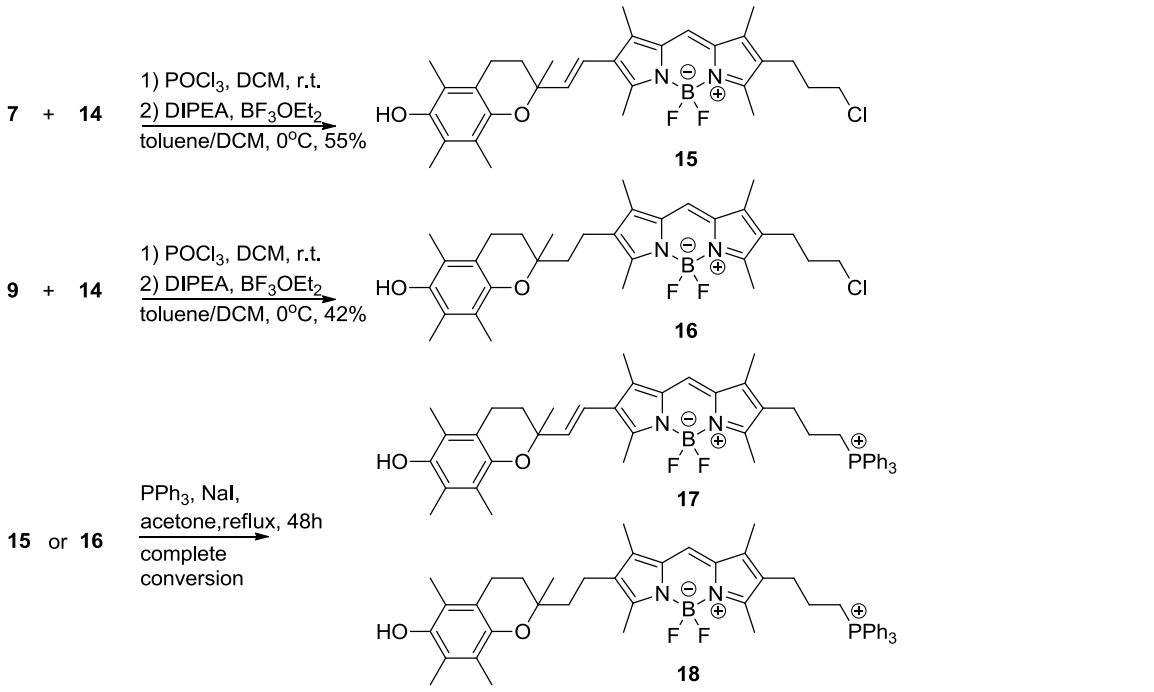

Scheme 6.4. Synthesis of mitochondria-targeting fluorogenic probes Mito-B-V-TOH (**17**) and Mito-B-e-TOH (**18**) and their precursors.

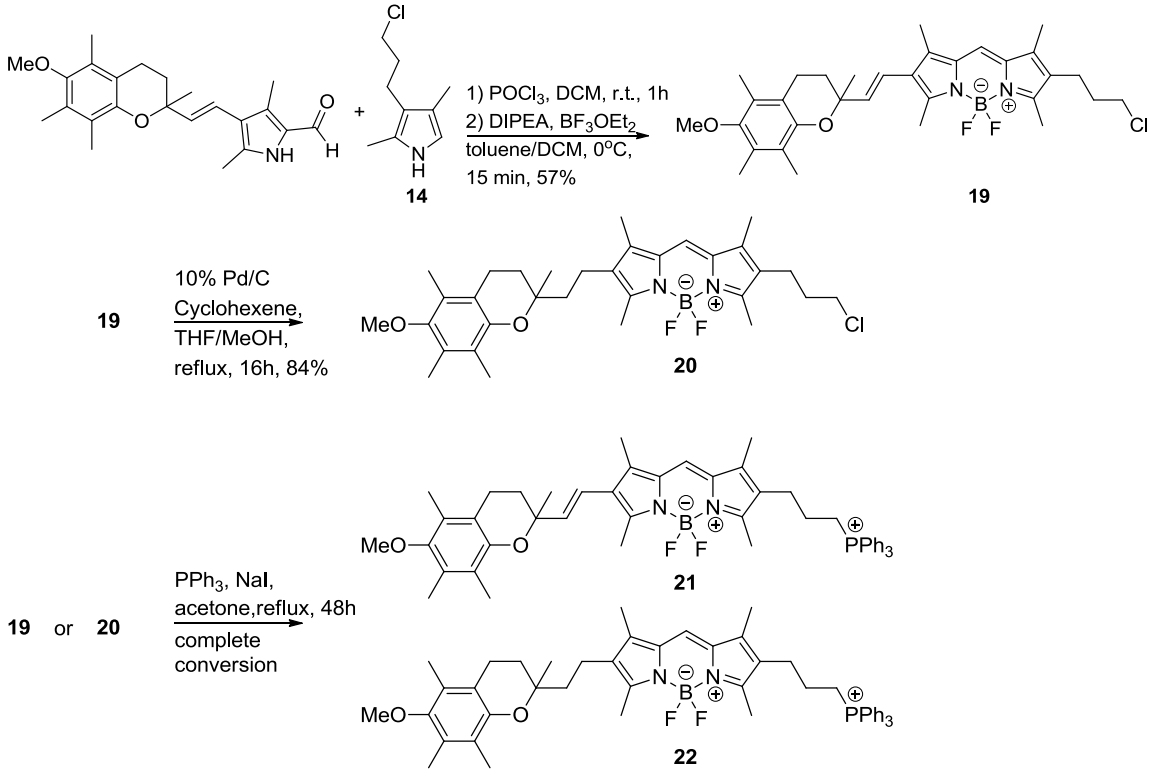

Scheme 6.5. Synthesis of fluorescent mitochondria-targeting control compounds **21** and **22** and their precursors.

Compound **5** was additionally used as a starting material for the synthesis of the chromanol-pyrrole adduct **9**, with an ethyl linkage (Scheme 6.2). Standard hydrogenation conditions (10% Pd/C and H_2 gas) were initially used to reduce the vinyl group. However, additionally to the reduction of the double bond, reduction of the α-aldehyde was observed. The use of milder reduction conditions was required. The conversion of cyclohexene to benzene was employed as a source of H_2 and in the presence of Pd/C as a catalyst the reduction afforded compound **8** with quantitative yields. Full deprotection of **8** under the conditions described above yielded compound **9**.

We next proceeded with the preparation of the pyrrole with free α-position (segment B in Scheme 6.1). We started with a reduction of the methyl ester to an alcohol (**11**) in the commercially available pyrrole **10** (Scheme 6.3) using BH_3.[39,40] Further, the alcohol in the propyl chain was converted into a good leaving group, namely a chloride, utilizing thionyl chloride and pyridine, yielding pyrrole **12**. Deprotection of the benzyl ester **12** using Pd/C and H_2 gas, followed by decarboxylation of pyrrole **13** with trifluoroacetic acid, yielded pyrrole **14** with a free α-position.

Having prepared all the necessary segments to assemble the precursor Bodipy for the mitochondria-targeting fluorogenic antioxidants, we proceeded with their condensation. Pyrrole **14** was subjected to a condensation reaction with either pyrrole **7** or **9** in the presence of phosphorus oxychloride (Scheme 6.4). Complexation of the so formed dipyrromethenes with BF_3.OEt and diisopropylethylamine yielded the chormanol-Bodipy adducts **15** and **16**.

The final step in the synthesis of the 2 new fluorogenic antioxidants **17** and **18** was the nucleophilic substitution of the chloride in the lipophilic tail of the Bodipy dye with triphenylphosphene to install the positively charged phosphonium tag (Scheme 6.4). The substitution was facilitated by the use of sodium iodide.

Control compounds **21** and **22** were prepared, bearing the methoxy protecting group on the chromanol ring. To prepare **21** and **22** compound **5** was partially deprotected, here only the pyrrole protecting MOM-group was removed.

The resulting compound was subjected to a condensation reaction with pyrrole **14** (Scheme 6.5), yielding compound **19** which bears a vinyl linker. The corresponding analogue with an ethyl linker, compound **20**, was obtained upon reduction of **19** in the presence of cyclohexene and Pd/C. The TPP segment was installed following the method described above, yielding the control fluorescent mitochondria-targeting compounds **21** and **22**.

6.2.3. Spectroscopic Properties of Fluorogenic Antioxidants

Listed in Table 6.1 are the absorption and emission maxima, emission quantum yields, and absorption extinction coefficients of compounds **15** to **22** determined in acetonitrile. Figure 6.3 displays the absorption and emission spectra for these compounds measured in acetonitrile.

The absorption and emission bands of the fluorogenic antioxidants **15** and **17**, and the control compounds **19** and **21** (all bearing a vinyl linker) are centered around 535 and 580 nm, respectively. For compounds **16** and **18**, and control compounds **20** and **22** (bearing an ethyl linker) the corresponding bands are observed at 525 and 535 nm. A shift to lower energies is observed for the probes bearing a vinyl linker relative to the corresponding compounds with an ethyl linker. This is due to the extended conjugation in the former Bodipy fluorophores. Additionally the fluorophores bearing a vinyl linker have a much larger Stokes shift, and a lesser defined absorption and emission vibronic pattern possibly the result of the extended conjugation into the non-rigid vinyl linker (Figure 6.3).

Control studies with compounds **19** to **22**, bearing a methoxy protected phenol, provided further insight on the role of PeT and on the effect of the vinyl vs the saturated linking moiety in the emission quantum yield of our probes. Our previous work has established that a methoxy protected chromanol may not undergo PeT with the Bodipy fluorophore bearing H-groups at positions C2 and C6.

	Abs λ_{max} (nm)	Em λ_{max} (nm)	Φ_f	$\varepsilon \times 10^3$ ($M^{-1}cm^{-1}$)
15	536	582	0.04	34
16	525	535	0.07	61
17	537	572	0.02	34
18	525	535	0.06	61
19	536	585	0.30	34
20	525	535	1.00	61
21	536	582	0.23	34
22	525	535	0.77	61

Table 6.1. Photophysical properties of dyes **15** to **22** in acetonitrile at room temperature. Quantum yields were measured using PM605 in acetonitrile as a standard (Φ_{st} = 0.72).

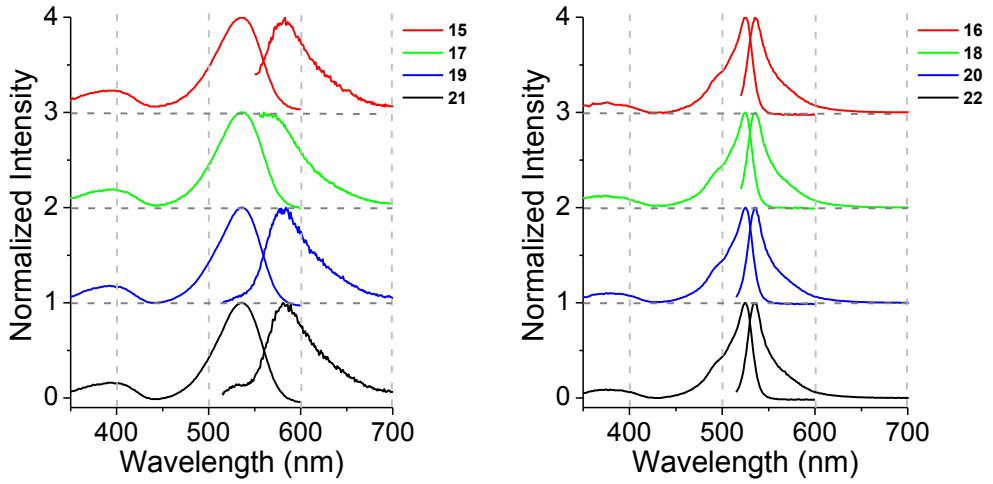

Figure 6.3. Normalized absorption and emission spectra obtained in acetonitrile for compounds **15** - **22**. Plots are offset with respect to each other in the ordinate axis to facilitate comparison.

The 10-fold lower quantum yields in compounds **15** to **18** when compared to their respective counterparts compounds **19** to **22**, respectively, are consistent with emission quenching via intramolecular PeT, occurring from the chromanol moiety to the Bodipy fluorophore. We may thus anticipate that at best ten-fold enhancement is expected for the new fluorogenic probes upon reaction with ROS.

The presence of a vinyl group in **15** and **17** can lead to an additional decrease in the emission quantum yields when compared to the emission of **16** and **18**, respectively. Arguably this is a result of energy dissipation in the excited state via non-radiative pathways such as *cis-trans*-isomerization of the double

bond upon excitation. Consistent with energy dissipation in the double bond, our results indicate that the quantum yields of **19** and **21** were 2 to 3-fold smaller than those of compounds **20** and **22** where an ethyl and not a vinyl moiety serves as a linking segment. Thus, higher emission intensity is expected from Bodipy compounds where the vinyl moiety is reduced.

Compounds **19** to **22** not only provide for controls in ensemble spectroscopic studies but also in microscopy studies on live cells, where they provide a measure of the maximum emission intensity enhancements to be expected upon staining cells with fluorogenic markers following treatment with ROS generators (see below).

6.2.4. Radical Scavenging Activity of Fluorogenic Antioxidants

In order to investigate their reactivity the new probes fluorogenic antioxidants **15 - 19** were subjected to reaction with peroxyl radicals, generated via thermolysis of azo-initiators in homogeneous (acetonitrile solution) and micro-heterogeneous media (liposome suspension). The kinetic studies conducted follow the experimental procedures and analysis described in chapters 2 and 5. Three different azo-initiators, two lipophilic and one hydrophilic, were used (Figure 6.4) to examine the effect of the site of radical generation on the reactivity and sensitivity of the probes.

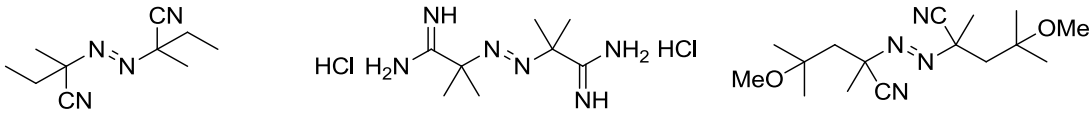

2,2'-Azobis(2-methylbutyronitrile) **(AMBN)**

2,2'-Azobis(2-methylpropionamidine) dihydrochloride **(ABAP)**

2,2'-Azobis(4-methoxy-2,4-dimethyl valeronitrile) **(MeO-AMVN)**

Figure 6.4. Structures of azo-initiators used in reactivity studies of **15-19** in acetonitrile solutions (AMBN) and liposomal suspensions (ABAP and MeO-AMVN). AMBN and MeO-AMVN are lipophilic radical initiators, whereas ABAP is hydrophilic radical initiator.

Competitive kinetic studies in the presence of two types of antioxidants (α-tocopherol and PMHC, Figure 6.5) allowed us to further investigate the relative inherent reactivity of the new fluorogenic probes in homogeneous solution. Using competitive kinetic studies we additionally examined the relative localization and

mobility for the new mitochondria-targeting fluorogenic antioxidants vs α-tocopherol and PMHC in lipid membranes. Here, we applied the high-throughput fluorescence assay described in Chapter 5.

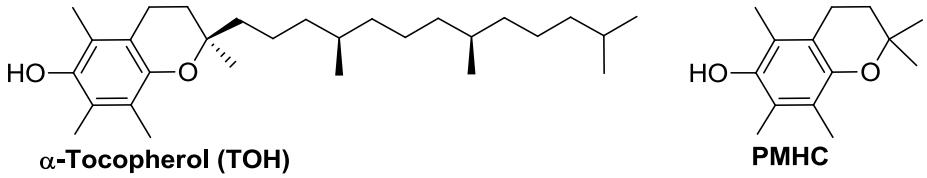

Figure 6.5. Structures of TOH and PMHC.

6.2.4.1. Kinetic Studies in Homogeneous Solutions

Emission intensities of 9.5 μM solutions of **15-19** in acetonitrile were recorded for 4000 s with peroxyl radicals formed following thermolysis of 84.5 mM AMBN at 37 °C. Additionally, competitive kinetic studies were performed in the presence of 9 μM α-tocopherol (TOH) or PMHC and 0.5 μM compounds **15-19** (Figure 6.6).

Upon scavenging of peroxyl radicals by the chromanol receptor segment in compounds **15-18** a linear increase in fluorescence intensity is observed over time in acetonitrile solutions (Figure 6.6). The linear increase in intensity is consistent with the rate law which is expected to be zero order in antioxidant concentration. The rate law for antioxidant consumption follows Equation 4

$$\frac{-d[AOH]}{dt} = \frac{R_i}{2} \qquad (4)$$

where R_i is the rate of generation of peroxyl radicals via thermolysis of the azo-initiator AMBN. The on/off ratio in compounds **15** to **18** was in the range of 10 to 20 fold. The emission enhancements are comparable to those reported for BTOH under similar conditions.[31,32] B-TOH and the new probes all have electron donating groups (EDG) in the C2 and C6 positions of the Bodipy fluorophore. As discussed in previous chapters, EDG in these positions decrease the reduction potential of the reporter, making the PeT less exergonic.[31,34] This in turn leads to brighter "off" state and a concomitant lower sensitivity to ROS for the fluorogenic probes.

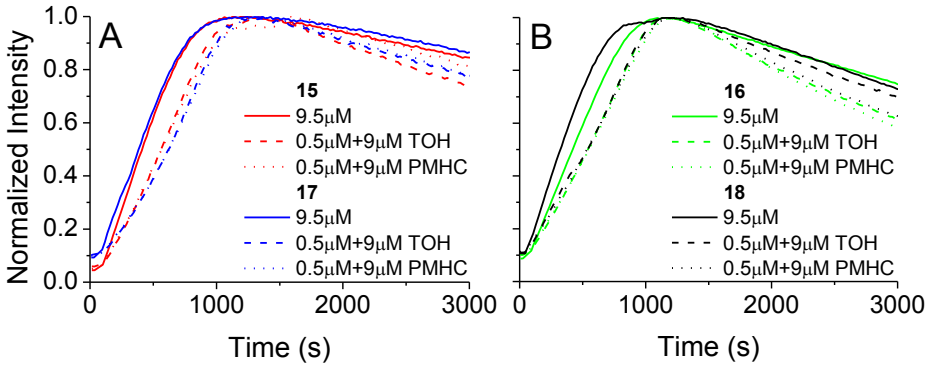

Figure 6.6. Fluorescence intensity-time profiles recorded in acetonitrile with 2,2'-Azobis(2-methylbutyronitrile) (AMBN) at 37 °C. All fluorogenic probes were excited at 510 nm and emission intensity was followed at 570 nm. Solid lines: 9.5 μM fluorogenic probes **15**-**18**. Dashed lines: 9.0 μM TOH + 0.5 μM fluorogenic probes **15**-**18**. Dotted lines: 9.0 μM PMHC + 0.5 μM fluorogenic probes **15**-**1**8. Plot A and B represent kinetic studies with fluorogenic antioxidants bearing a vinyl or an ethyl linker, respectively.

No emission enhancement was observed in compound **19**, which has a protected phenol and cannot undergo H-abstraction by peroxyl radicals. Instead, a linear drop in emission intensity with time was recorded. This result is consistent with the onset of radical-mediated Bodipy degradation.

Figure 6.6 additionally displays the results of competitive kinetic studies performed in the presence of 9 μM α-tocopherol (TOH) or 9 μM PMHC and 0.5 μM of compounds **15** (similar studies were conducted with compounds **16** to **19**). The emission intensities showed a linear increase with time for both antioxidants (TOH and PMHC) and all indicators. No induction period was observed with either antioxidant. These results indicate that the peroxyl radicals do not discriminate between the antioxidants and react with the same rate constant with the fluorogenic indicators and with α-tocopherol and PMHC. The inherent chemical reactivity of the chromanol ring in the fluorogenic probes is thus on par with the reactivity of α-tocopherol and PMHC and is not diminished by the coupling to the Bodipy segment.

6.2.4.2. Kinetic Studies in Heterogeneous Liposomal Suspensions

In order to evaluate the peroxyl radical scavenging activity of the fluorogenic antioxidants when embedded in lipid membranes we applied the high-

throughput fluorescence method described in Chapter 5. We utilized in our studies hydrophilic (ABAP) and lipophilic (MeO-AMVN) azo-initiators to generate peroxyl radicals at 37 °C.

The left panel in Figure 6.7 displays intensity-time trajectories obtained for solutions containing ABAP. We recorded fluorescence intensity enhancements of ca. 6-fold. A linear increase in fluorescence intensity with time was observed regardless whereas the total antioxidant load consisted of the fluorogenic probe (**15-18**) alone or the fluorogenic probe (**15-18**) and α-tocopherol present at a mole ratio of 1:45 probe: α-tocopherol. In stark contrast a clear induction period in the emission enhancement was observed when experiments were conducted with a 1:45 mol ratio mixture of probe: PMHC under the same conditions. We can ascribe the differences in antioxidant activity of these 3 classes of compounds (probe, α-tocopherol and PMHC) to membrane induced changes in accessibility and mobility. The fluorogenic probes and α-tocopherol arguably are positioned deeper in the lipid membrane and are less mobile relative to PMHC due to the highly lipophilic nature of the Bodipy fluorophores and the phytyl tail, respectively. We may conclude that the bulky triphenylphosphonium tag does not significantly modify the reactivity or positioning in the membrane for the probe in comparison to α-tocopherol.

Qualitatively similar results were obtained in experiments involving the generation of lipophilic peroxyl radicals (MeO-AMVN) within EggPC liposomes (Figure 6.7 right panel). α-Tocopherol and either of the fluorogenic probes **15-18** reacted with the same rate as reflected by the linear increase in intensity in competitive kinetic studies. PMHC however outcompetes all of the probes **15-18** as can be inferred from the sigmoidal intensity growth with time in competitive kinetic studies.

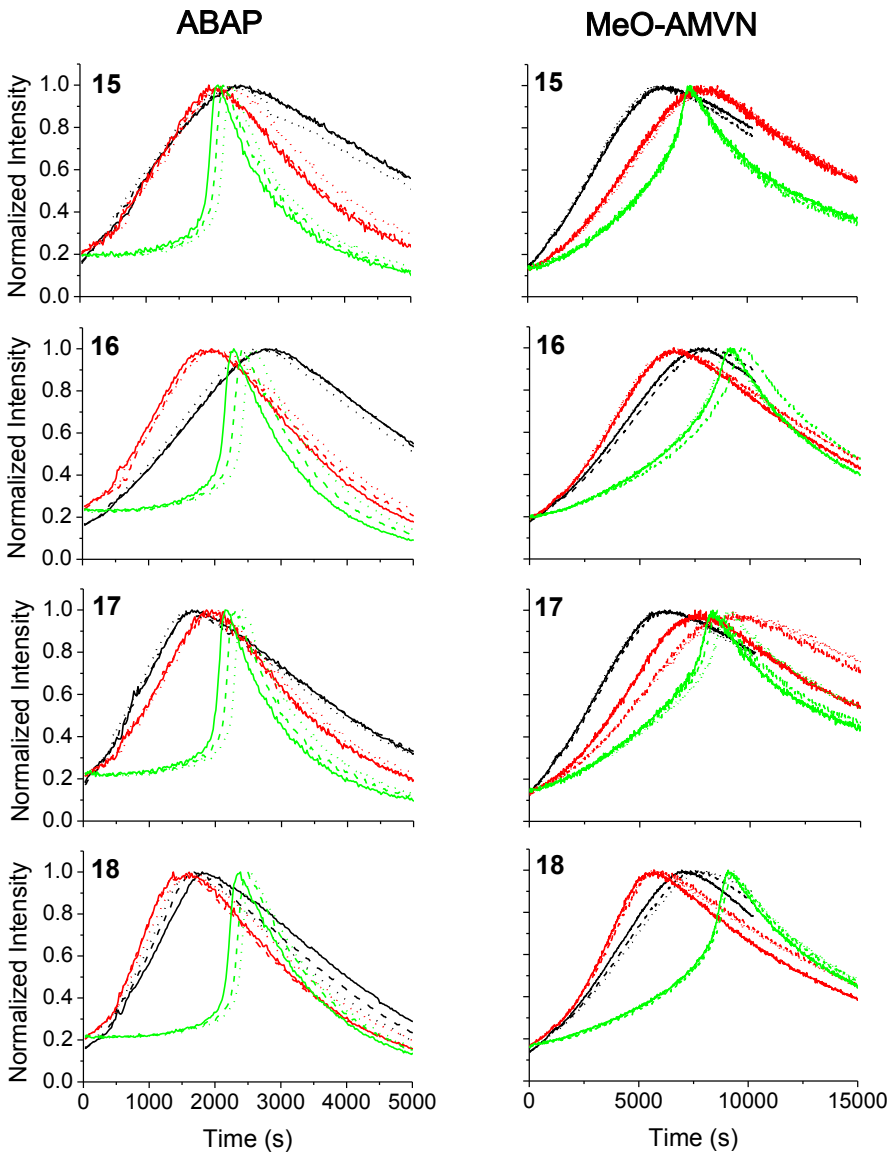

Figure 6.7. Fluorescence intensity-time profiles recorded in triplicates in 1 mM EggPC and 9 mM ABAP solutions (left panel) with: **Black)** 4.6 μM fluorogenic antioxidants **15-18** **Red)** 4.5 μM TOH + 0.1 μM probes **15-18** and **Green)** 4.5 μM PMHC + 0.1 μMprobes **15-18**. Right panel shows similar data acquired in 1 mM EggPC with 200 μM MeO-AMVN.

6.3. Imaging ROS in the Mitochondria of Living Cells

Fluorogenic antioxidants Mito-B-v-TOH and Mito-B-e-TOH were next tested for their ability to target mitochondria and report on the production of ROS in living biological system. Control compounds **19**, **20**, **21**, **22**, assisted in identifying specific (**21**, **22**) vs non-specific (**19**, **20**) targeting, as well as in estimating the expected fluorescent enhancements. Co-localization studies were

also performed with the commercially available red emissive mitochondria targeting dye MitoTracker Deep Red.

We first performed a series of studies involving fluorogenic probes Mito-B-v-TOH (**17)** and Mito-B-e-TOH (**18**) and their non-targeting fluorescent analogues **19** and **20** in order to check whereas the probe localizes in mitochondria. As a model cell line we used NIH 3T3 mouse embryo fibroblast cells cultured in growth media. Fibroblast cells were stained with a 1 μM solution of the fluorogenic probes Mito-B-v-TOH or Mito-B-e-TOH at 37 °C for 5 min. The staining solutions also contained 200 nM MitoTracker Deep Red (a commercially available mitochondrial indicator). The cells exhibit measurable levels of fluorescence (in the region of 500 nm to 620 nm) in discrete subcellular locations as determined by confocal microscopy upon selective excitation of Mito-B-v-TOH or Mito-B-e-TOH at 488 nm (Figure 6.8 A1 and Figure 6.9 A1, respectively). Selective excitation of MitoTracker Deep Red at 633 nm and emission collection in the region extending from 650 to 740 nm gave rise to similar images as those obtained with compounds **17** and **18** (Figure 6.8 A2 and Figure 6.9 A2, respectively). Co-localization experiments of probes Mito-B-v-TOH or Mito-B-e-TOH with MitoTracker Deep Red established that the observed fluorescence from the probes is localized in the mitochondria of the live cells used (Figure 6.8 A3 and Figure 6.9 A3, respectively). The fluorescent analogues **21** and **22** also showed co-localization with MitoTracker Deep Red under the same imaging conditions (Figure 6.8.B and Figure 6.9.B, respectively)

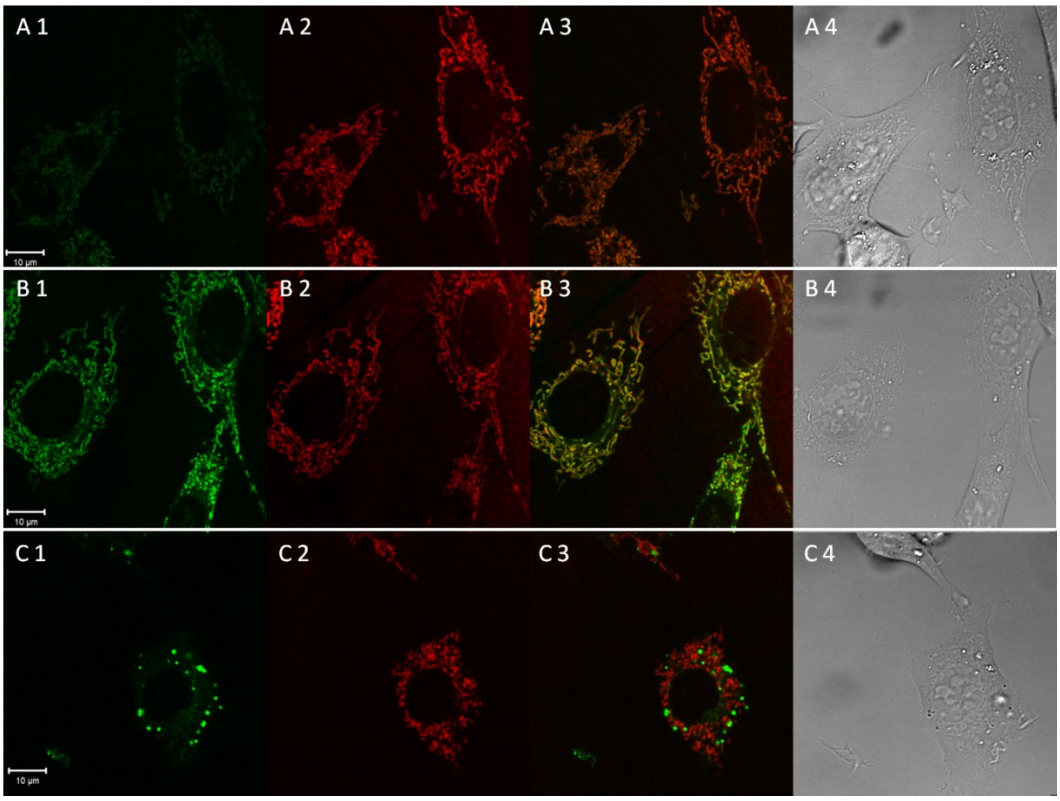

Figure 6.8. Confocal fluorescence images of live NIH 3T3 mouse embryo fibroblast cells. Cells were incubated with 1 μM probes **19**, **17**, **21** (all bearing vinyl linker) together with 200 nM MitoTracker Deep Red at 37 °C for 5 min. Images display emission intensities collected in optical windows between 500 and 620 nm (for probes **19, 17, 21**) upon excitation at 488 nm (5 % laser power) and between 650 and 740 nm (for MitoTracker Deep Red) upon excitation at 633 nm (8% laser power): **Panel A1)** probe **17** (Mito-B-v-TOH), **A2)** MitoTracker Deep Red, **A3)** overlay of 1 and 2, **A4)** bright field image; **Panel B1)** probe **21**, **B2)** MitoTracker Deep Red, **B3)** overlay of 1 and 2, **B4)** bright field image; **Panel C1)** probe **19**, **C2)** MitoTracker Deep Red, **C3)** overlay of 1 and 2, **C4)** bright field image. Scale bar is 10 μm.

We conducted control experiments under the same conditions described above using probes **19** and **20** that lack the phosphonium tag (Figure 6.8.C and Figure 6.9.C, respectively). No co-localization was observed after co-staining with MitoTracker Deep Red. The above experiments confirm that the TPP cationic segment is successful in targeting the fluorogenic compounds Mito-B-v-TOH or Mito-B-e-TOH to mitochondria.

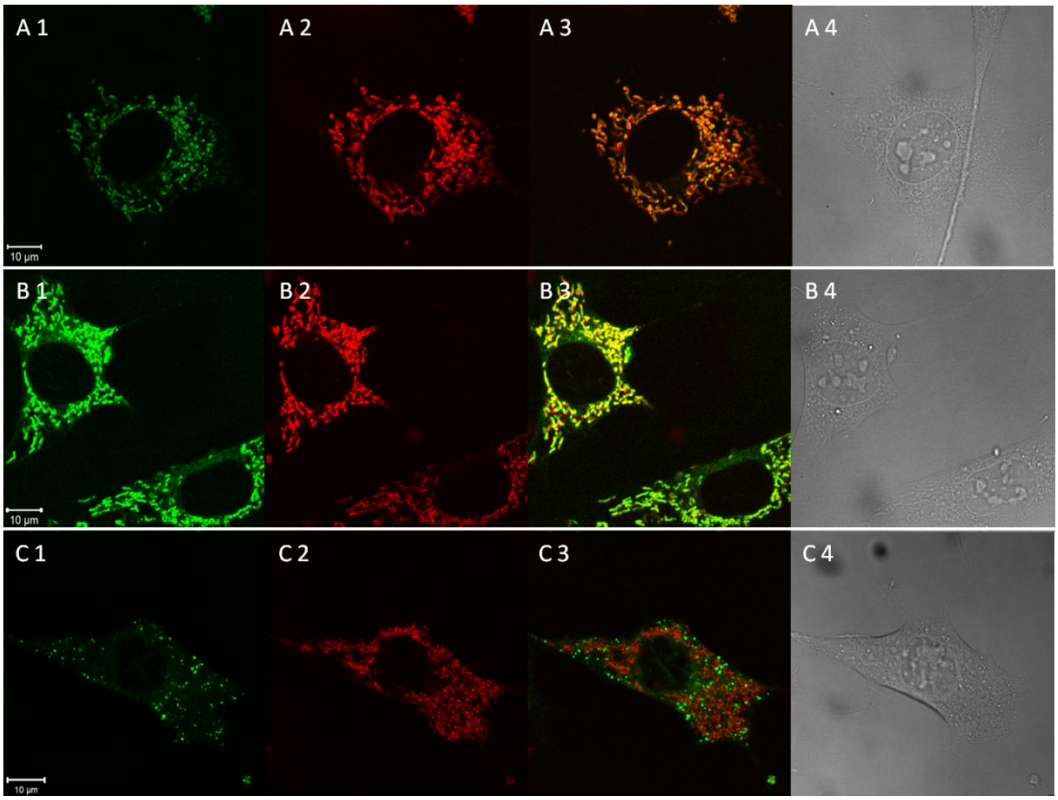

Figure 6.9. Confocal fluorescence images of live NIH 3T3 mouse embryo fibroblast cells. Cells were incubated with 1 μM probes **18**, **22**, **20** (all bearing ethyl linker) together with 200 nM MitoTracker Deep Red at 37 °C for 5 min. Images display emission intensities collected in optical windows between 500 and 620 nm (for probes **18**, **22**, **20**) upon excitation at 488 nm (5 % laser power) and between 650 and 740 nm (for MitoTracker Deep Red) upon excitation at 633 nm (8% laser power): **Panel A1)** probe **18** (Mito-B-e-TOH), **A2)** MitoTracker Deep Red, **A3)** overlay of 1 and 2, **A4)** bright field image; **Panel B1)** probe **22**, **B2)** MitoTracker Deep Red, **B3)** overlay of 1 and 2, **B4)** bright field image; **Panel C1)** probe **20**, **C2)** MitoTracker Deep Red, **C3)** overlay of 1 and 2, **C4)** bright field image. Scale bar is 10 μm.

The images described above where collected with a 100x magnification objective to enable better resolution of the intracellular features. Imaging with lower magnification indicated that the results are extendable to all the cells in the imaging chamber. Further confirmation of the validity of the results is provided by confocal microscopy images acquired after sequential scanning along the z-axis of the cells. This allows for a 3 dimensional visualization of the cells and their organelle position, as well as the visualization of the distribution of fluorogenic probes and MitoTracker Deep Red. Our bright field transmission measurements additionally indicate that the cells are viable throughout the experiment (Figure 6.8 and 6.9). Taken together, these data establish that fluorogenic antioxidants **17** and **18** and their fluorescent analogues **21** and **22**

accumulate preferentially in cell mitochondrial membrane due to the lipophilic cationic segment (phosphonium tag) introduced in their structure.

Having established that the fluorogenic probes Mito-B-v-TOH and Mito-B-e-TOH can respond to peroxyl radical in homogeneous and heterogeneous media and can preferentially accumulate in mitochondria, we next tested for their ability of to detect ROS in live cells (Figure 6.10). Methyl viologen was used as a source of ROS in our experiments.[41]

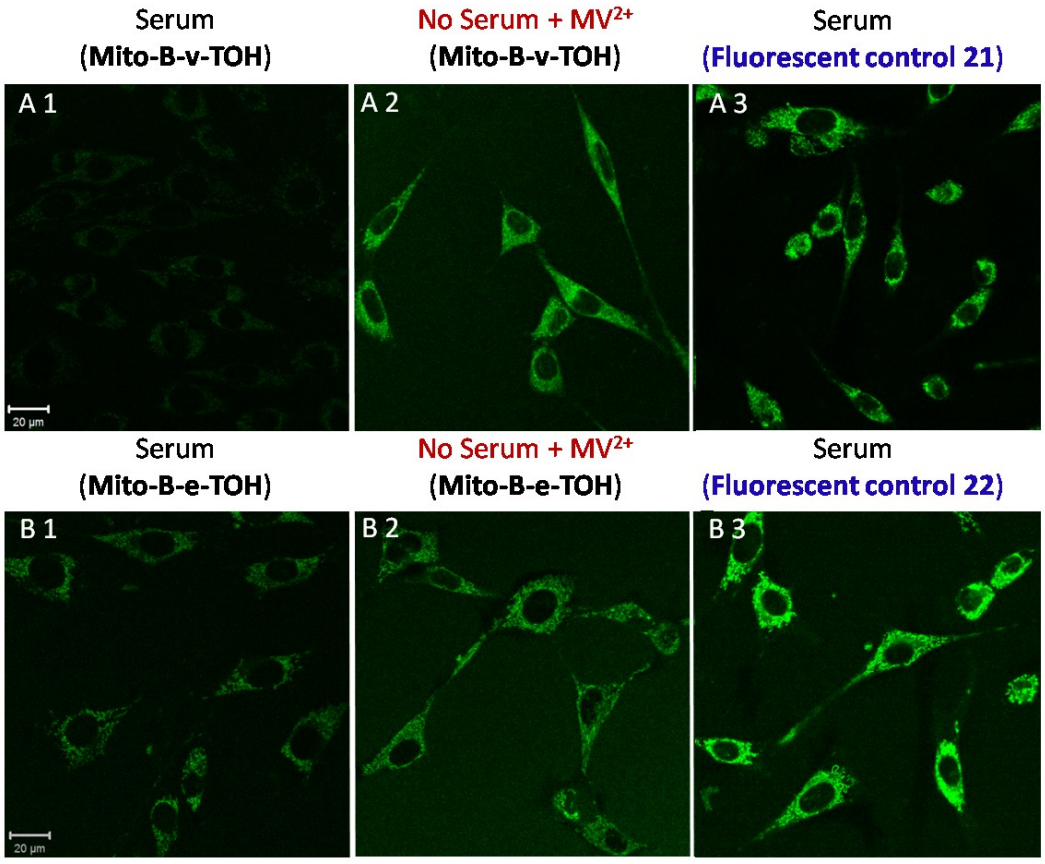

Figure 6.10. Detection of ROS with mitochondria-targeting fluorogenic probes **17 (panel A)** and **18 (panel B)** in live NIH 3T3 mouse embryo fibroblast cells. Cells were incubated with 1 µM probes **17** or **18** at 37 °C for 5 min. Confocal fluorescence images display emission intensities recorded 20 min after incubation with the probes and collected in optical windows between 500 and 620 nm upon excitation at 488 nm (5 % laser power): **1)** Fibroblast cells in the presence of 10 % FBS; **2)** Fibroblast cells deprived of growth factors (FBS) and additionally stressed with 1mM MV^{2+} (methyl viologen) for 4 h; **3)** Fibroblast cells in the presence of 10 % FBS incubated with 1 µM mitochondria-targeting fluorescent probes **21** (panel A) or **22** (panel B).

Fibroblast cells were cultured in media deprived of growth factors and supplemented with 1 mM MV^{2+} (methyl viologen) for 4 h. The cells were incubated with 1 µM probes **17** or **18** for 5 min at 37 °C and imaged by confocal

microscopy. Control cells were cultured in media with growth factors and no MV^{2+} under otherwise identical conditions, stained with 1 μM probes **17** or **18**, and imaged under the same conditions. The emission intensity was followed for 20 min. Marked emission enhancements were observed in the stressed cells stained with probes Mito-B-v-TOH or Mito-B-e-TOH (Figure 6.10 A2 and B2, respectively) relative to healthy cells in growth media (Figure 6.10 A1 and B1). The emission enhancements we recorded were of ca. 8-fold for Mito-B-v-TOH and 2-fold for Mito-B-e-TOH. This confirms that the mitochondria-targeting fluorogenic antioxidants can report the increased production of ROS in the mitochondria of treated cells relative to that of healthy cells.

Control studies conducted with emissive analogues **21** and **22** and healthy cells with growth factor and no MeV^{+2} further enabled us to evaluate the maximum sensitivity that could be achieved with the probes (Figure 6.10 A3 and B3, respectively). The recorded intensities were ca. 7-fold and 4-fold higher for compounds **21** and **22**, respectively, than those observed with their fluorogenic analogues Mito-B-v-TOH or Mito-B-e-TOH, respectively, in healthy cells under the same conditions (where both Mito-B-v-TOH and Mito-B-e-TOH remain in the off-state due to lack of ROS source). These results show that Mito-B-v-TOH and Mito-B-e-TOH reached the maximum emission enhancements expected to be observed in cells under oxidative stress.

6.4. Conclusions

In this study we have described the synthesis, chemical properties (including reactivity, partitioning, sensitivity, and organelle targeting capabilities), as well as biological applications of the two new mitochondria-targeting fluorogenic probes Mito-B-v-TOH and Mito-B-e-TOH (and of a series of related compounds prepared as controls).

The strategy for the synthesis of the mitochondria-targeting fluorogenic probes involves building the Bodipy fluorophore (reporter segment) onto the chromanol ring that serves as a receptor moiety. We exploit the Heck reaction as a means to achieve the coupling of the two segments. Additionally, synthetic

modifications to the fluorophore allow for a facile introduction of the mitochondria-targeting phosphonium tag. The synthetic approach utilized in preparing the new probes provides a useful convergent methodology for the development of a scaffold of fluorogenic antioxidants and more generally functionalized Bodipy dyes.

Given the synthetic constraints, the first fluorogenic antioxidants targeting mitochondria are not optimized towards PeT. We are currently improving the sensitivity of the two probes by introducing electron-withdrawing groups in the Bodipy core to afford a more exergonic PeT from the receptor to the reporter moiety.

Reactivity studies performed in homogeneous solution and in aqueous dispersions of model lipid membranes (liposomes), demonstrate the specificity and sensitivity of the new fluorogenic antioxidants Mito-B-v-TOH and Mito-B-e-TOH towards peroxyl radicals. Fluorescence co-localization studies in live mouse embryo fibroblast cells with MitoTracker Deep Red confirmed that the two probes preferentially accumulate in mitochondria. Fluorescence confocal microscopy experiments with the same cell line further establish that Mito-B-v-TOH and Mito-B-e-TOH are chemically and spatially specific probes that readily report on the presence of ROS within the lipid membrane of the mitochondria of cells undergoing oxidative stress. We are currently pursuing to optimize the sensitivity of the two probes by introducing electron-withdrawing groups in the Bodipy core to afford a more exergonic PeT from the receptor to the reporter moiety.

The findings reported here demonstrate that mitochondria-targeted fluorogenic antioxidants such as Mito-B-v-TOH and Mito-B-e-TOH may be successfully used to investigate the role of oxidative stress in pathologies involving mitochondrial dysfunction.

6.5. Experimental Section

Materials. 2,2'-Azobis(4-methoxy-2.4-dimethyl valeronitrile) (MeO-AMVN) and 2,2'-Azobis(2-methylbutyronitrile) (AMBN) were supplied by Wako Pure Chemical Industries, Ltd. L-α-phosphocholine (EggPC) was obtained from

Avanti Polar Lipids, (Alabaster, Al). All other chemicals were purchased from Sigma-Aldrich (Oakville, Ontario, Canada) and were used without further purification. Water was purified by a Millipore MilliQ system

Instrumentation. Absorption and emission spectra were recorded on a Cary 5000 UV-VIS-NIR and Cary Eclipse Fluorescence Spectrophotomeres, using 1 cm x 1 cm quartz quvettes. 1H NMR and 13C NMR spectra were recorded on a Varian VNMRS 500 instrument at 500MHz and 126 MHz respectively. ESI mass spectra were measured on a Thermo Scientific Exactive Orbitrap.

Fluorescence Quantum Yields were measured following the procedure described in chapter 4.

Steady state fluorescence studies. A Cary Eclipse Spectrophotometer with temperature controller was utilized to measure the emission intensity profiles of A) 9.5 μM compounds **15** to **18** and B) 9.0 μM α-tocopherol or PMHC solutions with 0.5 μM compounds **15** to **18** in 3 ml actonitrile. Fluorescence was recorded at 570 nm upon exciting at 510 nm using 2.5 nm excitation and 2.5 (for case A) or 5 nm (for case B) emission slits. 2.875 mL of acetonitrile solutions containing compounds **15** to **18** with or without α-tocopherol or PMHC were incubated for 10 min at 37°C before 125 μL of AMBN 2.028 M in acetonitrile were added to each cuvette for final AMBN concentration of 84.5 mM. The emission intensity was followed at 2.5 s intervals for 4000 s.

Liposome Preparation and Microplate Assays were conducted following the procedure from chapter 5.

Cell Preparation and Staining. NIH 3T3 mouse embryo fibroblast cells were cultured in Dulbecco's Modified Eagle Medium (DMEM) containing high glucose with L-gilutamine, phenol red, and sodium pyruvate (Gibco®), supplemented with 10% fetal bovine serum (FBS) and 1% penicillin-streptomycin. Cells were maintained at 37˚C (5% CO_2) in a humidified atmosphere. Cells were trypsinized and split 1/40 once a week. For fluorescence microscopy, cells were passed, split 1/5, plated on 35 mm glass imaging dish (World Precision Instruments, Inc.) coated with fibronectin (1μg/ml), and cultured in DMEM containing growth factors 1 day prior to imaging. For all experiments

solutions of dyes were prepared as follows. 60 μM MitoTracker Deep Red (Molecular Probes®) or 300 μM of **17**, **18**, **19**, **20**, **21**, and **22** stock solutions in DMSO were prepared. 10 μl of each stock solution were added to 3 ml of Dulbecco's Modified Eagle Medium (DMEM) containing high glucose with L-gilutamine, without phenol red, sodium pyruvate (Gibco®), or HEPES. Cells were incubated with the DMEM solutions with final concentrations of 200 nM MitoTracker Deep Red and 1 μM of either **17**, **18**, **19**, **20**, **21**, or **22** for 5 min at 37˚C (5% CO_2) in a humidified atmosphere. The DMEM solutions were removed and exchanged with DMEM containing high glucose, L-gilutamine, and 10% fetal bovine serum (FBS), without phenol red, or sodium pyruvate.

Cells stressed with methyl viologen. NIH 3T3 mouse embryo fibroblast cells were prepared as described above. The DMEM growth media was removed 4 h prior to imaging and substituted with 1.5 ml of DMEM containing 1mM MV^{2+} (methyl viologen) and glucose with L-gilutamine, without phenol red, sodium pyruvate (Gibco®), or HEPES. After 4 hours the MV^{2+} solution was removed, cells were washed with Dulbecco's Phosphate-Buffered Saline (DPBS), stained as described above, and the media was exchanged to DMEM containing high glucose with L-gilutamine, without phenol red, sodium pyruvate (Gibco®), or HEPES.

Fluorescence imaging experiments. Confocal fluorescence imaging studies were performed using Zeiss LSM 710 laser scanning microscope and C-Apochromat 40x/1.20 W Korr M27 water-immersion objective lens or Plan-Apochromat 100x/1.40 oil-immersion objective lens. Excitation of cells loaded with both dyes **17**, **18**, **19**, **20**, **21**, or **22** and MitoTracker Deep Red at 488 nm and 633 nm was carried out with Ar and HeNe lasers, respectively, using MBS 488/543/633 dichrioc beam splitter. Emission was collected using META detector between 500-620 nm and 650-740 nm, respectively, using sequential scans.

Calculations for cell fluorescence. All quantifications were performed using ImageJ software following a protocol previously published.[42,43] For

corrected total cell fluorescence (CTCF) calculations the following formula was used:

$$CTCF = IntDensity - (CellArea \times BkgFluorescence) \quad (5)$$

where *IntDensity* is the integrated intensity of the pixels for one cell, *CellArea* is the number of pixels in the same cell, and *BkgFluorescence* is the average signal per pixel for a region with no cells.

Synthesis. **6-methoxy-2,5,7,8-tetramethylchroman-2-carbaldehyde, 1.** (6-Methoxy-2,5,7,8-tetramethylchroman-2-yl)-methanol (0.82 g, 3.3 mmol, 1 eq) and $NaHCO_3$ (0.55 g, 6.6 mmol, 2 eq) were dissolved in 20 ml dry dichloromethane under argon and cooled to 0^0C. Dess-Martin periodinane (1.66 g, 4 mmol, 1.2 eq) was slowly added and the reaction mixture was stirred at room temperature for 2 h. It was diluted with dichloromethane and washed twice with saturated aqueous $NaHCO_3$, brine, dried over $MgSO_4$ and the solvent was evaporated under reduced pressure. The white solid residue was loaded onto a silica gel flash column and eluted with 20 % ethyl acetate/ hexanes. Compound **1** was obtained as white solid (0.7 g, 2.8 mmol, 84.5 % yield). ^{1}H NMR ($CDCl_3$, 300MHz): δ = 9.65 (s, 1 H), 3.65 (s, 3 H), 2.47 - 2.68 (m, 2 H), 2.25 - 2.35 (m, 1 H), 2.24 (s, 3 H), 2.22 (s, 3 H), 2.14 (s, 3 H), 1.76 - 1.92 (m, 1 H), 1.42 ppm (s, 3 H); ^{13}C NMR ($CDCl_3$, 75MHz): δ = 204.3, 150.4, 147.3, 128.4, 126.1, 123.1, 117.7, 80.4, 60.3, 27.7, 21.5, 20.3, 12.6, 11.9, 11.7 ppm; MS (ESI^-) for $C_{15}H_{19}O_3$ (M^-) calcd 247.13, found 247.11; FTIR: 2935, 1730, 1452, 1249, 1085, 986 cm^{-1}.

6-methoxy-2,5,7,8-tetramethyl-2-vinylchroman, 2. Potassium tert-butoxide (0.47 g, 4.2 mmol, 1.5 eq) was dissolved in 10 ml dry THF. The solution was cooled to 0^0C and 6-methoxy-2,5,7,8-tetramethylchroman-2-carbaldehyde, **1**, (0.7 g, 2.8 mmol, 1 eq), dissolved in 10 ml dry THF, was added dropwise. Methyltriphenylphosphonium iodide (1.36 g, 3.36 mmol. 1.2 eq) was slowly added and the reaction was heated to 60 ^{0}C. After 1 h it was cooled to room temperature and filtered to remove the excess methyltriphenylphosphonium iodide. The solvent was removed under reduced pressure and the oily residue was loaded onto a silica gel flash column and eluted with 20 % ethyl acetate/ hexanes. Compound **2** was obtained as white transparent oil in quantitative yield (0.65 g,

2.8 mmol). ^{1}H NMR ($CDCl_3$, 400MHz): δ = 5.88 (dd, *J*=17.2, 10.9 Hz, 1 H), 5.15 (dd, *J*=17.4, 1.4 Hz, 1 H), 5.05 (dd, *J*=10.7, 1.4 Hz, 1 H), 3.65 (s, 3 H), 2.41 - 2.69 (m, 2 H), 2.22 (s, 3 H), 2.18 (s, 3 H), 2.15 (s, 3 H), 1.95 (dt, *J*=13.4, 5.8 Hz, 1 H), 1.83 (ddd, *J*=13.4, 9.5, 6.1 Hz, 1 H), 1.42 ppm (s, 3 H); ^{13}C NMR ($CDCl_3$, 75MHz): δ = 149.6, 147.7, 141.9, 127.8, 125.7, 122.5, 117.7, 113.3, 75.5, 60.4, 31.8, 27.0, 20.8, 12.6, 11.8, 11.7 ppm; HRMS (ESI^+) for $C_{16}H_{23}O_2$ (M^+) calcd 247.16926, found 247.16881; FTIR: 2926, 1452, 1400, 1249, 1082, 915 cm^{-1}.

2-Carbaldehyde-3,5-dimethyl pyrrole and **2-Carbaldehyde-3,5-dimethyl-4-iodo pyrrole, 3**, were prepared according to procedures previously reported by Burgess *et al*.[36]

2-Carbaldehyde-3,5-dimethyl-4-iodo-1-(methoxymethyl) pyrrole, 4. Sodium hydride (0.18 g,7.7 mmol, 2.6 eq) was suspended in 10 ml dry THF at -78^{0}C under argon. 2-Carbaldehyde-3,5-dimethyl-4-iodo pyrrole, **3**, (0.75 g, 3 mmol, 1eq) was dissolved in 10 ml dry THF and added dropwise to the suspension followed by an addition of methoxymethyl bromide (0.36 ml, 4.5 mmol, 1.5 eq). The reaction was stirred for 2 h at room temperature under argon and quenched by dropwise addition of water at 0^{0}C. The mixture was diluted with ethyl acetate and the organic layer was washed with brine, dried over $MgSO_4$ and the solvent was evaporated under reduced pressure. The oily residue was loaded onto a silica gel flash column and eluted with 20 % ethyl acetate/ hexanes. Compound **4** was obtained as white transparent oil (0.75 g, 2.6 mmol, 85 % yield). ^{1}H NMR ($CDCl_3$, 500MHz): δ = 9.61 (s, 1 H), 5.69 (s, 2 H), 3.23 (s, 3 H), 2.30 (s, 3 H), 2.22 ppm (s, 3 H); ^{13}C NMR ($CDCl_3$, 126MHz): δ = 177.3, 141.4, 138.1, 128.6, 75.1, 74.6, 55.7, 13.1, 13.0 ppm; HRMS (ESI^+) for $C_9H_{13}O_2NI$ (M^+) calcd 293.99855, found 293.99843; FTIR: 2819, 1645, 1482, 1375, 1082, 912, 682 cm^{-1}.

(E)-4-(2-(6-methoxy-2,5,7,8-tetramethylchroman-2-yl)vinyl)-1-(methoxymethyl)-3,5-dimethyl-2-carbaldehyde pyrrole, 5. 6-methoxy-2,5,7,8-tetramethyl-2-vinylchroman, **2**, (0.34 g, 1.5 mmol, 1 eq), 2-carbaldehyde-3,5-dimethyl-4-iodo-1-(methoxymethyl) pyrrole, **4**, (0.55 g, 1.9 mmol, 1.3 eq), potassium acetate (0.37 g, 3.8 mmol, 2.6 eq) and tetrabutylammonium bromide

(0.6 g, 1.9 mmol, 1.3 eq) were dissolved in dry, degassed dimethylformamide under argon. $Pd(OAc)_2$ (20 mg, 88 nmol, 0.06 eq) was added and the solution was heated to 110^0C. The reaction mixture was left stirring for 24 h after which it was cooled to room temperature and diluted with ethyl acetate. The organic layer was washed with saturated aqueous NH_4Cl solution, brine, dried over Na_2SO_4 and the solvent was evaporated under reduced pressure. The dark brown oil was loaded onto a silica gel flash column and eluted with 30 % ethyl acetate/ hexanes. Compound **5** was obtained as pale yellow oil (0.26 g, 0.64 mmol, 44 % yield). ^{1}H NMR ($CDCl_3$, 500MHz): δ = 9.66 (s, 1 H), 6.28 (d, *J*=16.1 Hz, 1 H), 5.76 (d, *J*=16.1 Hz, 1 H), 5.71 (s, 2 H), 3.62 (s, 3 H), 3.27 (s, 3 H), 2.59 - 2.68 (m, 1 H), 2.47 - 2.58 (m, 1 H), 2.24 (s, 3 H), 2.21 (s, 9 H), 2.12 (s, 3 H), 1.97 - 2.05 (m, 1 H), 1.86 - 1.95 (m, 1 H), 1.50 ppm (s, 3 H); ^{13}C NMR ($CDCl_3$, 126 MHz): δ = 177.3, 149.6, 147.7, 138.4, 134.9, 133.9, 127.8, 127.4, 125.7, 122.4, 120.6, 119.4, 117.8, 75.5, 74.4, 60.4, 55.6, 32.4, 27.8, 21.1, 12.6, 11.8, 11.7, 10.3, 9.8 ppm; HRMS (ESI^+) for $C_{25}H_{34}O_4N$ (M^+) calcd 412.24824, found 412.24726; FTIR: 2926, 1642, 1149, 1367, 1252, 1082, 730 cm^{-1}.

(E)-4-(2-(6-hydroxy-2,5,7,8-tetramethylchroman-2-yl)vinyl)-1-(hydroxymethyl)-3,5-dimethyl-2-carbaldehyde pyrrole, 6. (E)-4-(2-(6-methoxy-2,5,7,8-tetramethylchroman-2-yl)vinyl)-1-(methoxymethyl)-3,5-dimethyl-2-carbaldehyde pyrrole, **5**, (0.2 g, 0.5 mmol, 1eq) was dissolved in 6 ml of dry dichloromethane, cooled to -10^0C and placed under argon. 1 M BBr_3 in dichloromethane (1 ml, 2 eq) was added dropwise and the reaction mixture was stirred for 1.5 h at -10^0C. 10 ml of water were added to quench the reaction. It was diluted with dichloromethane and the organic layer was washed with water, dried over Na_2SO_4 and the solvent was evaporated under reduced pressure. No further purification was required. Compound **6** was obtained as pale yellow solid (0.18 g, 0.47 mmol, 95 % yield). ^{1}H NMR ($CDCl_3$, 400MHz): δ = 9.48 (s, 1 H), 6.27 (d, *J*=16.4 Hz, 1 H), 5.74 (d, *J*=16.0 Hz, 1 H), 5.36 (s, 3 H), 4.36 (s, 1 H), 2.60 - 2.73 (m, 1 H), 2.55 (dd, *J*=9.6, 6.4 Hz, 1 H), 2.25 (s, 3 H), 2.21 (s, 6 H), 2.17 (s, 3 H), 2.08 (s, 3 H), 1.95 - 2.04 (m, 1 H), 1.83 - 1.95 (m, 1 H), 1.48 ppm (s, 3 H); ^{13}C NMR ($CDCl_3$, 75MHz): δ = 177.2, 145.5, 144.8, 137.9, 135.4, 134.9,

128.2, 122.0, 121.1, 120.4, 119.2, 118.5, 117.4, 75.3, 68.4, 32.5, 27.7, 21.2, 12.2, 11.9, 11.3, 10.4, 10.0 ppm; HRMS (ESI^+) for $C_{23}H_{30}O_4N$ (M^+) calcd 384.21693, found 384.21721; FTIR: 3396, 2915, 1604, 1330, 1056, 967 cm^{-1}.

(E)-4-(2-(6-hydroxy-2,5,7,8-tetramethylchroman-2-yl)vinyl)-3,5-dimethyl-2-carbaldehyde pyrrole, 7. (E)-4-(2-(6-hydroxy-2,5,7,8-tetramethylchroman-2-yl)vinyl)-1-(hydroxymethyl)-3,5-dimethyl-2-carbaldehyde pyrrole, **6**, (0.18 g, 0.47 mmol) was dissolved in 8 ml THF. 10 ml of 1 M aqueous NaOH were added to the solution and the reaction mixture was left stirring for 1 h at room temperature under argon. The reaction mixture was diluted with dichloromethane and the organic layer was washed with water and brine, dried over Na_2SO_4 and the solvent was evaporated under reduced pressure. The oily residue was loaded onto a silica gel flash column and eluted with 50 % ethyl acetate/ hexanes. Compound **7** was obtained as pale yellow oil (0.110 g, 0.33 mmol, 70 % yield). ^1H NMR ($CDCl_3$, 400MHz): δ = 9.80 (br. s, 1 H), 9.43 (s, 1 H), 6.31 (d, *J*=16.4 Hz, 1 H), 5.74 (d, *J*=16.1 Hz, 1 H), 4.63 (br. s, 1 H), 2.47 - 2.73 (m, 2 H), 2.26 (s, 3 H), 2.23 (s, 3 H), 2.22 (s, 3 H), 2.18 (s, 3 H), 2.17 (s, 2 H), 2.09 (s, 3 H), 1.84 - 2.04 (m, 3 H), 1.47 ppm (s, 3 H); ^{13}C NMR ($CDCl_3$, 75MHz): δ = 176.2, 145.5, 144.8, 136.3, 133.3, 131.6, 128.0, 122.1, 121.1, 120.2, 119.5, 118.6, 117.5, 75.3, 32.6, 30.9, 27.7, 21.2, 12.7, 12.3, 11.9, 11.3, 9.8 ppm; HRMS (ESI^+) for $C_{22}H_{28}O_3N$ (M^+) calcd 354.20637, found 354.20595; FTIR: 3241, 2922, 1615, 1437, 1252, 1082, 904, 727 cm^{-1}.

4-(2-(6-methoxy-2,5,7,8-tetramethylchroman-2-yl)ethyl)-1-(methoxy-methyl)-3,5-dimethyl-1H-pyrrole-2-carbaldehyde, 8. (E)-4-(2-(6-methoxy-2,5,7,8-tetramethylchroman-2-yl)vinyl)-1-(methoxymethyl)-3,5-dimethyl-2-carbaldehyde pyrrole, **5**, (0.11 g, 0.27 mmol) and palladinised carbon Pd/C (11 mg, 10% w/w) were dissolved in 2ml THF, 8 ml methanol, and 2 ml cyclohexene. The reaction mixture was placed under argon and heated to 70 °C for 16 h. The solution was cooled to room temperature and filtered through Celite to remove Pd/C. The solvent was evaporated under reduced pressure. No further purification was required. Compound **8** was obtained as colourless oil (0.11 g, 0.27 mmol, 99 % yield). ^1H NMR ($CDCl_3$, 400MHz): δ = 9.62 (s, 1 H), 5.63 -

5.74 (m, 2 H), 3.63 (s, 3 H), 3.29 (s, 3 H), 2.58 - 2.67 (m, 2 H), 2.47 - 2.58 (m, 2 H), 2.21 (s, 3 H), 2.19 (s, 3 H), 2.17 (s, 3 H), 2.15 (s, 7 H), 1.78 - 1.94 (m, 3 H), 1.54 - 1.73 (m, 2 H), 1.34 ppm (s, 3 H); ^{13}C NMR ($CDCl_3$, 75MHz): δ = 176.8, 149.6, 147.5, 137.9, 134.6, 129.5, 127.9, 127.2, 125.9, 123.2, 122.9, 117.5, 115.4, 74.4, 74.2, 60.4, 55.5, 40.2, 31.4, 23.6, 20.6, 17.7, 12.6, 11.8, 11.7, 9.4, 8.6 ppm; FTIR: 2926, 1645, 1452, 1252, 1089 cm^{-1}.

4-(2-(6-hydroxy-2,5,7,8-tetramethylchroman-2-yl)ethyl)-3,5-dimethyl-1H-pyrrole-2-carbaldehyde, 9. 4-(2-(6-methoxy-2,5,7,8-tetramethyl-chroman-2-yl)ethyl)-1-(methoxy-methyl)-3,5-dimethyl-1H-pyrrole-2-carb-aldehyde, **8,** (0.11 g, 0.27 mmol, 1 eq) was dissolved in 4 ml of dry dichloromethane, cooled to -10^{0}C and placed under argon. 1 M BBr_3 in dichloromethane (0.54 ml, 2 eq) was added dropwise and the reaction mixture was stirred for 4 h at -10^{0}C. 6 ml of water were added to quench the reaction. It was diluted with dichloromethane and the organic layer was washed with water, dried over Na_2SO_4 and the solvent was evaporated under reduced pressure. The oily residue was directly used in the next step without further purification. The oily residue was dissolved in 5 ml THF. 8 ml of 1 M aqueous NaOH were added to the solution and the reaction mixture was left stirring for 1 h at room temperature under argon. The reaction mixture was diluted with dichloromethane and the organic layer was washed with water and brine, dried over Na_2SO_4 and the solvent was evaporated under reduced pressure. The oily residue was loaded onto a silica gel flash column and eluted with 50 % ethyl acetate/ hexanes. Compound **9** was obtained as pale yellow oil (0.054 g, 0.15 mmol, 57 % yield). ^{1}H NMR ($CDCl_3$, 500MHz): δ = 9.47 (s, 1 H), 9.07 (br. s., 2 H), 2.72 (dt, *J*=11.3, 5.5 Hz, 2 H), 2.58 - 2.67 (m, 3 H), 2.29 (s, 3 H), 2.28 (s, 3 H), 2.10 - 2.24 (m, 3 H), 2.09 (s, 3 H), 2.02 (br. s., 3 H), 2.01 (br. s., 3 H), 1.87 - 1.99 (m, 5 H), 1.86 (s, 4 H), 1.63 ppm (s, 3 H); ^{13}C NMR ($CDCl_3$, 126MHz): δ = 187.5, 187.1, 175.8, 143.0, 141.0, 140.7, 140.4, 134.8, 129.5, 127.9, 121.8, 121.1, 114.5, 77.3, 77.0, 76.8, 71.8, 45.8, 43.6, 31.1, 23.5, 20.2, 12.4, 12.3, 12.2, 11.7 ppm; FTIR: 3237, 2922, 1619, 1441, 1371, 712 cm^{-1}.

Compounds **11** to **14** were prepared according to previously reported procedures[39,40] with modification described below.

Benzyl 4-(3-hydroxypropyl)-3,5-dimethyl-1H-pyrrole-2-carboxylate, **11**. Benzyl 4-(3-methoxy-3-oxopropyl)-3,5-dimethyl-1H-pyrrole-2-carboxylate, **10**, (1 g, 3.2 mmol, 1 eq) was dissolve in 15 ml dry THF and the solution was cooled to -10^0C. 1 M BH_3 in THF (7.4 ml, 2.3 eq) was added dropwise, the reaction mixture was warmed to room temperature and left stirring for 1 h under argon. The reaction was quenched by addition of 10 ml methanol. The solvent was evaporated under reduced pressure. The white solid was loaded onto a silica gel flash column and eluted with 60 % ethyl acetate/ hexanes. Compound **11** was obtained as white solid (0.9 g, 3.1 mmol, 98 % yield). ^{1}H NMR ($CDCl_3$, 500MHz): δ = 9.41 (br. s., 1 H), 7.28 - 7.49 (m, 5 H), 5.32 (s, 2 H), 3.63 (t, *J*=6.5 Hz, 2 H), 2.46 (t, *J*=7.5 Hz, 2 H), 2.41 (s, 1 H), 2.32 (s, 3 H), 2.18 (s, 3 H), 1.67 - 1.75 ppm (m, 2 H); ^{13}C NMR ($CDCl_3$, 126MHz): δ = 161.8, 136.7, 130.7, 128.5, 128.0, 128.0, 127.7, 121.5, 116.4, 65.5, 62.2, 33.5, 20.2, 11.4, 10.9 ppm; FTIR: 3389, 3300, 2941, 1659, 1500, 1437, 1260, 693, 616 cm^{-1}.

Benzyl 4-(3-chloropropyl)-3,5-dimethyl-1H-pyrrole-2-carboxylate, 12. Benzyl 4-(3-hydroxypropyl)-3,5-dimethyl-1H-pyrrole-2-carboxylate, **11**, (0.9 g, 3.1 mmol, 1 eq) was dissolved in 15 ml dry dichloromethane. Pyridine (0.22 ml, 2.8 mmol, 0.9 eq) was added to the solution, followed by a quick addition of thionyl chloride (0.2 ml, 2.8 mmol, 0.9 eq). The reaction mixture was heated to 40^0C and stirred for 3 h under argon. It was diluted with dichloromethane and washed with saturated aqueous $NaHCO_3$, saturated aqueous NH_4Cl and brine, dried over $MgSO_4$ and the solvent was evaporated under reduced pressure. The white solid residue was loaded onto a silica gel flash column and eluted with 20 % ethyl acetate/ hexanes. Compound **12** was obtained as white solid (0.74 g, 2.4 mmol, 78 % yield). ^{1}H NMR ($CDCl_3$, 400MHz): δ = 8.83 (br. s., 1 H), 7.28 - 7.48 (m, 5 H), 5.30 (s, 2 H), 3.50 (t, *J*=6.4 Hz, 2 H), 2.54 (t, *J*=7.2 Hz, 2 H), 2.29 (s, 3 H), 2.21 (s, 3 H), 1.90 ppm (quin, *J*=6.8 Hz, 2 H); ^{13}C NMR ($CDCl_3$, 75MHz): δ = 162.0, 136.7, 131.2, 128.6, 128.0, 127.9, 127.6, 120.3, 116.7, 65.5, 44.5, 33.4, 21.0, 11.4, 11.0 ppm; FTIR: 3315, 2915, 1659, 1500, 1452, 1271, 1089, 693 cm^{-1}.

4-(3-chloropropyl)-3,5-dimethyl-1H-pyrrole-2-carboxylic acid, 13. Benzyl 4-(3-chloropropyl)-3,5-dimethyl-1H-pyrrole-2-carboxylate, **12**, (0.7 g, 2.3

mmol, 1 eq) was dissolved in 3 ml THF and 15 ml methanol and palladised charcoal (Pd/C, 0.07 g, 10 w%) was added. The hydrogenation was carried in the dark, under atmospheric pressure with a balloon with H_2 gas. The reaction was left stirring at room temperature for 16 h. The solution was filtered through a bed of Celite and evaporated to dryness under reduced pressure to give compound **13** as a brown-red solid (0.49 g, 2.27 mmol, 99 %). ^{1}H NMR ($CDCl_3$, 400MHz): δ = 13.21 (br. s, 1 H), 4.68 (br. s., 2 H), 3.54 (t, *J*=5.7 Hz, 2 H), 2.48 - 2.68 (m, 5 H), 2.25 (s, 3 H), 1.76 - 1.97 ppm (m, 2 H); ^{13}C NMR ($CDCl_3$, 75MHz): δ = 166.8, 132.5, 129.8, 121.0, 116.1, 44.5, 33.3, 21.0, 11.5, 10.8 ppm; FTIR: 3311, 3228, 2926, 1611, 1463, 1249, 1093, 715, 694 cm^{-1}.

4-(3-chloropropyl)-3,5-dimethyl pyrrole, 14. 4-(3-chloropropyl)-3,5-dimethyl-1H-pyrrole-2-carboxylic acid, **13**, (0.1 g, 0.46 mmol, 1 eq) was dissolved in 2 ml trifluoroacetic acid. The reaction mixture was left stirring for 1.5 h at 0^{0}C after which the TFA was evaporated with a stream of argon. The oily residue was dissolved in ethyl acetate and washed three times with saturated aqueous $NaHCO_3$, brine, dried over Na_2SO_4 and the solvent was evaporated under reduced pressure. No further purification was required. Compound **14** was obtained as pink oil (0.65 g, 0.38 mmol, 82 % yield) ^{1}H NMR ($CDCl_3$, 300MHz): δ = 7.55 (br. s., 1 H), 6.42 (s, 1 H), 3.57 (t, *J*=6.6 Hz, 2 H), 2.57 (t, *J*=7.3 Hz, 2 H), 2.21 (s, 3 H), 2.06 (s, 3 H), 1.96 ppm (quin, *J*=6.9 Hz, 2 H); ^{13}C NMR ($CDCl_3$, 75MHz): δ = 124.3, 118.0, 116.9, 113.1, 44.9, 33.7, 21.3, 11.4, 10.5 ppm; HRMS (ESI$^+$) for $C_9H_{15}NCl$ (M^+) calcd 172.08875, found 172.08853; FTIR: 3363, 2911, 1682, 1585, 1434, 1289, 1093, 737, 641, 586 cm^{-1}.

(E)-6-(2-(6-hydroxy-2,5,7,8-tetramethylchroman-2-yl)vinyl)-2-(3-chloropropyl)-1,3,5,7-tetramethyl Pyrromethene Fluoroborate, 15. 4-(3-Chloropropyl)-3,5-dimethyl pyrrole, **14**, (0.053 g, 0.31 mmol, 1.1 eq) and (E)-4-(2-(6-hydroxy-2,5,7,8-tetramethylchroman-2-yl)vinyl)-3,5-dimethyl-2-carbaldehyde pyrrole, **7**, (0.1 g, 0.28 mmol, 1eq) were dissolved in 6 ml dry dichloromethane. Phosphorus oxychloride (0.13 ml, 1.4 mmol, 5 eq) was added dropwise and the reaction mixture was stirred for 2 h at room temperature under argon. It was diluted with dichloromethane and washed with water and brine,

dried over Na_2SO_4 and the solvent was evaporated under reduced pressure. The residue was redissolved in 5 ml dry dichloromethane and 25 ml dry toluene. The solution was cooled to -10^0C and diisopropylethylamine (0.5 ml, 2.8 mmol, 10 eq) was added dropwise. After stirring for 10 min $BF_3.OEt_2$ (0.6 ml, 4.8 mmol, 17 eq) was added dropwise. The reaction mixture was left stirring at room temperature for half an hour. It was diluted with ethyl acetate and washed with water and brine, dried over Na_2SO_4 and the solvent was evaporated under reduced pressure. The residue was loaded onto a silica gel flash column and eluted with 30 % ethyl acetate/ hexanes. Compound **15** was obtained as red-purple solid (85 mg, 0.15 mmol, 55 % yield). ^{1}H NMR ($CDCl_3$, 400MHz): δ = 6.99 (s, 1 H), 6.30 (d, *J*=16.4 Hz, 1 H), 5.85 (d, *J*=16.0 Hz, 1 H), 4.23 (br. s., 1 H), 3.53 (t, *J*=6.3 Hz, 2 H), 2.58 - 2.73 (m, *J*=4.7 Hz, 2 H), 2.51 - 2.58 (m, 3 H), 2.50 (s, 3 H), 2.46 (s, 3 H), 2.23 (s, 3 H), 2.16 - 2.21 (m, *J*=3.1 Hz, 9 H), 2.09 (s, 3 H), 1.95 - 2.06 (m, 2 H), 1.84 - 1.95 (m, 4 H), 1.49 ppm (s, 3 H); ^{13}C NMR ($CDCl_3$, 75MHz): δ = 155.8, 155.1, 145.5, 144.8, 138.0, 135.9, 135.1, 132.9, 132.5, 128.7, 126.4, 122.1, 121.0, 119.2, 118.5, 117.4, 75.3, 44.3, 32.6, 27.7, 21.2, 21.0, 13.4, 12.8, 12.2, 11.9, 11.3, 10.7, 9.6 ppm; HRMS (ESI^+) for $C_{31}H_{39}O_2N_2BClF_2$ (M^+) calcd 555.27557, found 555.27664; FTIR: 3555, 2919, 1596, 1445, 1222, 682, 656 cm^{-1}.

6-(2-(6-hydroxy-2,5,7,8-tetramethylchroman-2-yl)ethyl)-2-(3-chloropropyl)-1,3,5,7-tetramethyl Pyrromethene Fluoroborate, 16. Compound **16** was prepared following the procedure for the synthesis of compound **15**. 4-(3-Chloropropyl)-3,5-dimethyl pyrrole, **14**, (0.028 g, 0.17 mmol, 1.1 eq), (E)-4-(2-(6-hydroxy-2,5,7,8-tetramethylchroman-2-yl)vinyl)-3,5-dimethyl-2-carbaldehyde pyrrole, **9**, (0.054 g, 0.15 mmol, 1eq), and phosphorus oxychloride (0.07 ml, 0.75 mmol, 5 eq) were dissolved in 3 ml dry dichloromethane. Compound **16** was obtained as orange solid (35 mg, 0.063mmol, 42% yield). ^{1}H NMR ($cdcl_3$, 500MHz): d = 6.94 (s, 1 H), 4.26 (br. s., 1 H), 3.53 (t, *J*=6.2 Hz, 2 H), 2.64 (t, *J*=6.6 Hz, 2 H), 2.50 - 2.58 (m, 4 H), 2.49 (s, 3 H), 2.41 (s, 3 H), 2.14 - 2.19 (m, *J*=4.4 Hz, 9 H), 2.11 (s, 3 H), 2.09 (s, 3 H), 1.77 - 1.95 (m, 5 H), 1.52 - 1.74 (m, 2 H), 1.32 ppm (s, 3 H); ^{13}C NMR ($cdcl_3$, 126MHz): δ = 155.7, 154.2, 145.2, 144.8, 137.4, 137.2, 132.7, 132.2, 130.3,

127.9, 122.5, 121.2, 118.7, 118.6, 117.2, 77.3, 77.0, 76.8, 73.9, 44.3, 39.4, 32.7, 31.7, 25.6, 23.5, 21.0, 21.0, 20.7, 17.9, 14.2, 12.6, 12.4, 12.2, 11.8, 11.3, 9.6, 9.3 ppm; MS (ESI^+) for $C_{31}H_{41}O_2N_2BClF_2Na$ (M^{+Na}) calcd 579.27, found 579.26; FTIR: 3549, 2922, 1601, 1471, 1219, 1063, 689, 649 cm^{-1}.

(E)-6-(2-(6-hydroxy-2,5,7,8-tetramethylchroman-2-yl)vinyl)-2-(3-(triphenylphosphonio)-propyl)-1,3,5,7-tetramethyl Pyrromethene Fluoroborate, 17. (E)-6-(2-(6-hydroxy-2,5,7,8-tetramethylchroman-2-yl)vinyl)-2-(3-chloropropyl)-1,3,5,7-tetramethyl Pyrromethene Fluoroborate, **15**, (50 mg, 0.09 mmol, 1 eq), triphenylphosphine (0.12 g, 0.45 mmol, 5 eq) and sodium iodide (13 mg, 0.09 mmol, 1 eq) were dissolved in 6 ml acetone. The reaction mixture was refluxed for 24 h or till all the starting dye was consumed, after which the solvent was evaporated to dryness under reduced pressure. The residue was redissolved in dichloromethane, washed with water, dried over Na_2SO_4 and the solvent was evaporated under reduced pressure. The solid was redissolved in 5 ml dichloromethane and precipitated from 150 ml diethyl ether. The purple solid was filtered and no further purification was required. Compound **16** was obtained as purple solid (63 mg, 0.08 mmol, 90 % yield). ^1H NMR ($CDCl_3$, 400MHz): δ = 7.55 - 7.85 (m, 22 H), 6.98 (s, 1 H), 6.27 (d, *J*=16.0 Hz, 1 H), 5.83 (d, *J*=16.4 Hz, 1 H), 4.32 (s, 1 H), 3.73 - 3.89 (m, 2 H), 2.83 (t, *J*=7.2 Hz, 2 H), 2.45 - 2.73 (m, 3 H), 2.42 (s, 3 H), 2.29 (s, 3 H), 2.19 (d, *J*=2.7 Hz, 6 H), 2.12 - 2.17 (m, 10 H), 2.06 (s, 3 H), 1.93 - 2.02 (m, 2 H), 1.83 - 1.93 (m, 2 H), 1.66 - 1.83 (m, 3 H), 1.46 ppm (s, 3 H); ^{13}C NMR ($CDCl_3$, 75MHz): δ = 155.5, 155.0, 145.4, 144.9, 138.9, 136.4, 135.4, 135.1, 135.1, 133.7, 133.5, 133.2, 132.7, 130.6, 130.5, 127.9, 126.6, 122.0, 121.1, 119.6, 119.0, 118.6, 118.5, 117.4, 75.3, 32.5, 31.0, 29.3, 27.7, 24.4, 24.1, 22.8, 22.2, 21.5, 21.2, 14.2, 13.4, 13.0, 12.3, 11.9, 11.4, 10.8, 10.5 ppm; MS (ESI^+) for $C_{49}H_{53}O_2N_2BF_2P^+$ (M^+) calcd 781.39, found 781.50; FTIR: 3390, 2960, 1634, 1593, 1434, 737, 719, 690 cm^{-1}.

6-(2-(6-hydroxy-2,5,7,8-tetramethylchroman-2-yl)ethyl)-2-(3-(triphenylphosphonio)-propyl)-1,3,5,7-tetramethyl Pyrromethene Fluoroborate, 18. Compound **18** was prepared following the procedure for the synthesis of compound **17**. 6-(2-(6-hydroxy-2,5,7,8-tetramethylchroman-2-

yl)ethyl)-2-(3-chloropropyl)-1,3,5,7-tetramethyl Pyrromethene Fluoroborate, **16**, (30 mg, 0.054 mmol, 1 eq), triphenylphosphine (70 mg, 0.27 mmol, 5 eq) and sodium iodide (8 mg, 0.05 mmol, 1 eq) were dissolved in 3 ml acetone. Compound **18** was obtained as an orange solid (40 mg, 0.051 mmol, 95% yield). ^{1}H NMR ($CDCl_3$, 500MHz): δ = 7.58 - 7.82 (m, 15 H), 6.93 (s, 1 H), 4.31 (s, 1 H), 3.66 - 3.84 (m, 2 H), 2.81 (t, *J*=7.1 Hz, 2 H), 2.56 - 2.66 (m, 2 H), 2.48 (t, *J*=8.6 Hz, 2 H), 2.37 (s, 3 H), 2.28 (s, 3 H), 2.10 - 2.21 (m, 9 H), 2.08 (s, 3 H), 2.06 (s, 3 H), 1.70 - 1.89 (m, 4 H), 1.50 - 1.70 (m, 2 H), 1.29 ppm (s, 3 H); ^{13}C NMR ($CDCl_3$, 126 MHz): δ = 156.2, 153.3, 145.2, 144.8, 138.0, 138.0, 135.1, 135.1, 133.6, 133.6, 133.0, 132.0, 130.6, 130.5, 127.0, 122.4, 121.2, 119.2, 118.7, 118.3, 117.6, 117.1, 73.8, 53.5, 39.3, 31.6, 31.0, 29.3, 24.3, 24.1, 23.5, 22.8, 22.8, 22.0, 21.6, 20.7, 17.9, 12.8, 12.5, 12.3, 11.8, 11.4, 10.5, 9.3 ppm; MS (ESI^+) for $C_{49}H_{55}O_2N_2BF_2P^+$ (M^+) calcd 783.41, found 783.43; FTIR: 3374, 2919, 1601, 1434, 1223, 1193, 968, 723, 686, 653 cm^{-1}.

(E)-6-(2-(6-methoxy-2,5,7,8-tetramethylchroman-2-yl)vinyl)-2-(3-chloropropyl)-1,3,5,7-tetramethyl Pyrromethene Fluoroborate, 19. Compound **19** was prepared following the procedure for the synthesis of compound **15**. (E)-4-(2-(6-methoxy-2,5,7,8-tetramethylchroman-2-yl)vinyl-3,5-dimethyl-2-carbaldehyde pyrrole (0.12 g, 0.32 mmol, 1 eq), 4-(3-chloropropyl)-3,5-dimethyl pyrrole **14** (0.06 g, 0.35 mmol, 1.1 eq) and phosphorus oxychloride (0.15 ml, 1.6 mmol, 5 eq) were dissolved in 3 ml dry dichloromethane. Compound **19** was obtained as purple solid (0.1 g, 0.18 mmol, 57% yield). ^{1}H NMR ($CDCl_3$, 500MHz): δ = 7.00 (s, 1 H), 6.30 (d, *J*=16.4 Hz, 1 H), 5.86 (d, *J*=16.1 Hz, 1 H), 3.63 (s, 3 H), 3.54 (t, *J*=6.2 Hz, 2 H), 2.60 - 2.70 (m, 1 H), 2.52 - 2.59 (m, 2 H), 2.51 (s, 3 H), 2.46 (s, 3 H), 2.22 (s, 6 H), 2.20 (s, 3 H), 2.18 (s, 3 H), 2.13 (s, 3 H), 1.97 - 2.10 (m, 2 H), 1.92 (p, *J*=13.9, 6.7 Hz, 2 H), 1.51 (s, 3 H) ppm; ^{13}C NMR ($CDCl_3$, 126MHz): δ = 155.8, 155.0, 149.7, 147.6, 138.0, 135.9, 135.1, 132.9, 132.4, 128.7, 127.7, 126.4, 125.7, 122.4, 119.2, 119.1, 117.7, 75.5, 60.3, 44.2, 32.5, 32.4, 30.9, 27.6, 21.0, 21.0, 13.3, 12.7, 12.5, 11.8, 11.6, 10.6, 9.6 ppm; FTIR: 2926, 1604, 1459, 1230, 1060, 686, 660 cm^{-1}.

6-(2-(6-methoxy-2,5,7,8-tetramethylchroman-2-yl)ethyl)-2-(3-chloropropyl)-1,3,5,7-tetramethyl Pyrromethene Fluoroborate, 20. Compound **20** was prepared following the procedure for the synthesis of compound **8**. (E)-6-(2-(6-methoxy-2,5,7,8-tetramethylchroman-2-yl)vinyl)-2-(3-chloropropyl)-1,3,5,7-tetramethyl Pyrromethene Fluoroborate **19** (30 mg, 0.053 mmol, 1 eq) and palladinised carbon Pd/C (3 mg, 10% w/w) were dissolved in 1 ml THF, 2 ml methanol, and 1 ml cyclohexene. The reaction mixture was placed under argon and heated to 70 °C for 16 h. Compound **20** was obtained as orange solid (26 mg, 0.045 mmol, 84% yield). ^{1}H NMR ($CDCl_3$, 500MHz): δ = 6.94 (s, 1 H), 3.59 - 3.67 (m, 3 H), 3.53 (t, *J*=6.2 Hz, 2 H), 2.62 (t, *J*=6.8 Hz, 2 H), 2.49 - 2.58 (m, 4 H), 2.48 (s, 3 H), 2.40 (s, 3 H), 2.19 (s, 3 H), 2.18 (s, 3 H), 2.14 (s, 6 H), 2.08 (s, 3 H), 1.79 - 1.94 (m, 4 H), 1.57 - 1.73 (m, 3 H), 1.33 (s, 3 H) ppm; ^{13}C NMR ($CDCl_3$, 126MHz): δ = 155.6, 154.3, 149.7, 147.5, 137.3, 137.2, 132.7, 132.2, 130.3, 127.9, 125.9, 122.9, 118.8, 117.5, 74.1, 60.4, 44.3, 39.5, 32.7, 31.5, 23.6, 21.0, 20.6, 17.9, 12.6, 12.5, 12.4, 11.8, 11.7, 9.6, 9.2 ppm

(E)-6-(2-(6-methoxy-2,5,7,8-tetramethylchroman-2-yl)vinyl)-2-(3-(triphenylphosphonio)-propyl)-1,3,5,7-tetramethyl Pyrromethene Fluoroborate, 21. Compound **21** was prepared following the procedure for the synthesis of compound **17**. (E)-6-(2-(6-methoxy-2,5,7,8-tetramethylchroman-2-yl)vinyl)-2-(3-chloropropyl)-1,3,5,7-tetramethyl Pyrromethene Fluoroborate, **19**, (35 mg, 0.06 mmol, 1 eq), triphenylphosphine (0.08 g, 0.3 mmol, 5 eq) and sodium iodide (37 mg, 0.24 mmol, 4 eq) were dissolved in 3 ml acetone. The reaction mixture was refluxed for 48 h or till all the starting dye was consumed. Compound **21** was obtained as purple solid (47 mg, 0.059 mmol, 97 % yield). ^{1}H NMR ($CDCl_3$, 500MHz): δ = 7.71 - 7.84 (m, 7 H), 7.59 - 7.71 (m, 5 H), 6.99 (s, 1 H), 6.26 (d, *J*=16.1 Hz, 1 H), 5.83 (d, *J*=16.1 Hz, 1 H), 3.75 - 3.89 (m, 2 H), 3.60 (s, 3 H), 2.82 – 2.85 (t, *J*=7.2 Hz, 2 H), 2.55 - 2.67 (m, 1 H), 2.43 - 2.56 (m, 1 H), 2.42 (s, 3 H), 2.29 (s, 3 H), 2.21 (s, 3 H), 2.19 (s, 6 H), 2.16 (s, 3 H), 2.10 (s, 3 H), 1.95 - 2.02 (m, 1 H), 1.88 (ddd, *J*=13.3, 9.7, 5.9 Hz, 1 H), 1.72 - 1.82 (m, 2 H), 1.47 (s, 3 H) ppm; ^{13}C NMR ($CDCl_3$, 126MHz): δ = 155.5, 155.1, 149.7, 147.7, 139.0, 136.4, 135.3, 135.1, 135.1, 133.7, 133.6, 132.7, 132.7, 130.6, 130.5, 128.0,

127.8, 126.6, 125.7, 122.4, 119.6, 119.1, 118.3, 117.7, 117.7, 75.5, 60.4, 32.4, 27.7, 24.3, 24.2, 22.8, 22.8, 22.1, 21.7, 21.1, 13.3, 12.9, 12.5, 11.8, 11.7, 10.7, 10.5, 1.9 ppm; FTIR: 2926, 1593, 1434, 1227, 967, 723, 690 cm^{-1}.

(E)-6-(2-(6-methoxy-2,5,7,8-tetramethylchroman-2-yl)ethyl)-2-(3-(triphenylphosphonio)-propyl)-1,3,5,7-tetramethyl Pyrromethene Fluoroborate, 22. Compound **22** was prepared following the procedure for the synthesis of compound **17**. (E)-6-(2-(6-methoxy-2,5,7,8-tetramethylchroman-2-yl)ethyl)-2-(3-chloropropyl)-1,3,5,7-tetramethyl Pyrromethene Fluoroborate, **20**, (20 mg, 0.035 mmol, 1 eq), triphenylphosphine (46 mg, 0.18 mmol, 5 eq) and sodium iodide (21 mg, 0.14 mmol, 4 eq) were dissolved in 3 ml acetone. The reaction mixture was refluxed for 48 h or till all the starting dye was consumed. Compound **22** was obtained as orange solid (26 mg, 0.033 mmol, 94 % yield). ^{1}H NMR ($CDCl_3$, 500MHz): δ = 7.63 - 7.83 (m, 15 H), 6.95 (s, 1 H), 3.80 (m., 2 H), 3.62 (s, 3 H), 2.83 (t, *J*=6.8 Hz, 2 H), 2.60 (t, *J*=6.7 Hz, 2 H), 2.50 (t, *J*=8.6 Hz, 2 H), 2.39 (s, 3 H), 2.28 (s, 3 H), 2.23 (s, 3 H), 2.18 (s, 3 H), 2.13 (s, 6 H), 2.07 (s, 3 H), 1.73 - 1.92 (m, 4 H), 1.63 - 1.72 (m, 3 H), 1.32 (s, 3 H) ppm; ^{13}C NMR ($CDCl_3$,126MHz): δ = 156.2, 153.4, 149.7, 147.4, 138.2, 137.9, 135.1, 135.1, 133.7, 133.6, 133.4, 133.3, 132.9, 132.0, 130.6, 130.5, 127.9, 127.1, 125.9, 122.8, 119.2, 118.4, 117.7, 117.4, 74.1, 60.4, 39.5, 31.4, 24.2, 24.1, 23.6, 22.8, 22.8, 21.9, 21.5, 20.6, 17.9, 12.8, 12.5, 12.4, 11.8, 11.7, 10.5, 9.3 ppm; FTIR: 2923, 1597, 1434, 1227, 1189, 971, 727, 689, 652 cm^{-1}

6.6. References

1. McBride, H.M., Neuspiel, M. & Wasiak, S. Mitochondria: More Than Just a Powerhouse. *Current Biology* 16, R551-R560, **2006**.
2. Scheffler, I.E. Mitochondrial Electron Transport and Oxidative Phosphorylation. in *Mitochondria* 141-245 (John Wiley & Sons, Inc., 2002).
3. Murphy, M.P. & Smith, R.A.J. Targeting Antioxidants to Mitochondria by Conjugation to Lipophilic Cations. *Annual Review of Pharmacology and Toxicology* 47, 629-656, **2007**.
4. Green, D.R. & Kroemer, G. The Pathophysiology of Mitochondrial Cell Death. *Science* 305, 626-629, **2004**.
5. Dickinson, B.C. & Chang, C.J. Chemistry and biology of reactive oxygen species in signaling or stress responses. *Nat Chem Biol* 7, 504-511, **2011**.
6. Green & John C. Reed, D.R. Mitochondria and Apoptosis. *Science* 281, 1309-1312, **1998**.
7. Finkel, T. & Holbrook, N.J. Oxidants, oxidative stress and the biology of ageing. *Nature* 408, 239-247, **2000**.
8. Turrens, J.F. Mitochondrial formation of reactive oxygen species. *The Journal of Physiology* 552, 335-344, **2003**.
9. Murphy, M.P. How mitochondria produce reactive oxygen species. *Biochem J* 417, 1-13, **2009**.
10. Szewczyk, A. & Wojtczak, L. Mitochondria as a Pharmacological Target. *Pharmacological Reviews* 54, 101-127, **2002**.
11. Mukhopadhyay, A. & Weiner, H. Delivery of drugs and macromolecules to mitochondria. *Advanced Drug Delivery Reviews* 59, 729-738, **2007**.
12. Szeto, H. Mitochondria-targeted peptide antioxidants: Novel neuroprotective agents. *The AAPS Journal* 8, E521-E531, **2006**.
13. http://micro.magnet.fsu.edu/cells/mitochondria/mitochondria.html.
14. Horton, K.L., Stewart, K.M., Fonseca, S.B., Guo, Q. & Kelley, S.O. Mitochondria-Penetrating Peptides. *Chemistry & Biology* 15, 375-382, **2008**.
15. Stewart, K.M., Horton, K.L. & Kelley, S.O. Cell-penetrating peptides as delivery vehicles for biology and medicine. *Organic & Biomolecular Chemistry* 6, 2242-2255, **2008**.
16. Yousif, L.F., Stewart, K.M., Horton, K.L. & Kelley, S.O. Mitochondria-Penetrating Peptides: Sequence Effects and Model Cargo Transport. *ChemBioChem* 10, 2081-2088, **2009**.
17. Yousif, L.F., Stewart, K.M. & Kelley, S.O. Targeting Mitochondria with Organelle-Specific Compounds: Strategies and Applications. *ChemBioChem* 10, 1939-1950, **2009**.
18. Hoye, A.T.D., Jennifer E.; Wipf, Peter; Fink, Mitchell P.; Kagan, Valerian E. Targeting Mitochondria. *Accounts of Chemical Research* 41, 87-97, **2008**.
19. Koide, Y., Urano, Y., Kenmoku, S., Kojima, H. & Nagano, T. Design and Synthesis of Fluorescent Probes for Selective Detection of Highly Reactive Oxygen Species in Mitochondria of Living Cells. *Journal of the American Chemical Society* 129, 10324-10325, **2007**.
20. James, A.M., Sharpley, M.S., Manas, A.-R.B., Frerman, F.E., Hirst, J., Smith, R.A.J. & Murphy, M.P. Interaction of the Mitochondria-targeted Antioxidant MitoQ with Phospholipid Bilayers and Ubiquinone Oxidoreductases. *Journal of Biological Chemistry* 282, 14708-14718, **2007**.
21. Murphy, M.P. Selective targeting of bioactive compounds to mitochondria. *Trends in Biotechnology* 15, 326-330, **1997**.
22. Murphy, M.P. Development of lipophilic cations as therapies for disorders due to mitochondrial dysfunction. *Expert Opinion on Biological Therapy* 1, 753-764, **2001**.
23. Porteous, C.M., Logan, A., Evans, C., Ledgerwood, E.C., Menon, D.K., Aigbirhio, F., Smith, R.A.J. & Murphy, M.P. Rapid uptake of lipophilic triphenylphosphonium cations by mitochondria in vivo following intravenous injection: Implications for mitochondria-specific therapies and probes. *Biochimica et Biophysica Acta (BBA) - General Subjects* 1800, 1009-1017, **2010**.
24. Ross, M.F., Prime, T.A., Abakumova, I., James, A.M., Porteous, C.M., Smith, R.A.J. & Murphy, M.P. Rapid and extensive uptake and activation of hydrophobic triphenylphosphonium cations within cells. *Biochem J* 411, 633-645, **2008**.
25. Abu-Gosh, S.E., Kolvazon, N., Tirosh, B., Ringel, I. & Yavin, E. Multiple Triphenylphosphonium Cations Shuttle a Hydrophilic Peptide into Mitochondria. *Molecular Pharmaceutics* 6, 1138-1144, **2009**.

26. Biasutto, L., Mattarei, A., Marotta, E., Bradaschia, A., Sassi, N., Garbisa, S., Zoratti, M. & Paradisi, C. Development of mitochondria-targeted derivatives of resveratrol. *Bioorganic & Medicinal Chemistry Letters* 18, 5594-5597, **2008**.
27. Dickinson, B.C. & Chang, C.J. A Targetable Fluorescent Probe for Imaging Hydrogen Peroxide in the Mitochondria of Living Cells. *Journal of the American Chemical Society* 130, 9638-9639, **2008**.
28. Dickinson, B.C., Srikun, D. & Chang, C.J. Mitochondrial-targeted fluorescent probes for reactive oxygen species. *Current Opinion in Chemical Biology* 14, 50-56, **2010**.
29. Dodani, S.C., Leary, S.C., Cobine, P.A., Winge, D.R. & Chang, C.J. A Targetable Fluorescent Sensor Reveals That Copper-Deficient SCO1 and SCO2 Patient Cells Prioritize Mitochondrial Copper Homeostasis. *Journal of the American Chemical Society* 133, 8606-8616, **2011**.
30. Honig, B.H., Hubbell, W.L. & Flewelling, R.F. Electrostatic Interactions in Membranes and Proteins. *Annual Review of Biophysics and Biophysical Chemistry* 15, 163-193, **1986**.
31. Krumova, K., Oleynik, P., Karam, P. & Cosa, G. Phenol-Based Lipophilic Fluorescent Antioxidant Indicators: A Rational Approach. *The Journal of Organic Chemistry* 74, 3641-3651, **2009**.
32. Oleynik, P., Ishihara, Y. & Cosa, G. Design and Synthesis of a BODIPY-a-Tocopherol Adduct for Use as an Off/On Fluorescent Antioxidant Indicator. *Journal of the American Chemical Society* 129, 1842-1843, **2007**.
33. Chatgilialoglu, C. & Ferreri, C. Trans Lipids: The Free Radical Path. *Accounts of Chemical Research* 38, 441-448, **2005**.
34. Krumova, K. & Cosa, G. Bodipy Dyes with Tunable Redox Potentials and Functional Groups for Further Tethering: Preparation, Electrochemical, and Spectroscopic Characterization. *Journal of the American Chemical Society* 132, 17560-17569, **2010**.
35. Loudet, A. & Burgess, K. BODIPY Dyes and Their Derivatives: Syntheses and Spectroscopic Properties. *Chemical Reviews* 107, 4891-4932, **2007**.
36. Wan, C.-W., Burghart, A., Chen, J., Bergström, F., Johansson, L.B.Å., Wolford, M.F., Kim, T.G., Topp, M.R., Hochstrasser, R.M. & Burgess, K. Anthracene–BODIPY Cassettes: Syntheses and Energy Transfer. *Chemistry – A European Journal* 9, 4430-4441, **2003**.
37. Tietze, L.F., Kettschau, G., Heuschert, U. & Nordmann, G. Highly Efficient Synthesis of Linear Pyrrole Oligomers by Twofold Heck Reactions. *Chemistry – A European Journal* 7, 368-373, **2001**.
38. Macor, J.E., Forman, J.T., Post, R.J. & Ryan, K. Synthesis and reactivity of pyrrolo[3,2-e]indole: Removal of a N-BOM group from an unactivated indole. *Tetrahedron Letters* 38, 1673-1676, **1997**.
39. Holmes, R.T., Lu, J., Mwakwari, C. & Smith, K.M. Syntheses of protoporphyrin-IX derivatives bearing extended propionate side-chains. *CORD Conference Proceedings* 2010, 5-16, **2009**.
40. Tu, B., Wang, C. & Ma, J. ChemInform Abstract: Improved Synthesis of Symmetrical Dipyrromethenes. *ChemInform* 30, no-no, **1999**.
41. Khatchadourian, A., Krumova, K., Boridy, S., Ngo, A.T., Maysinger, D. & Cosa, G. Molecular Imaging of Lipid Peroxyl Radicals in Living Cells with a BODIPY−α-Tocopherol Adduct. *Biochemistry* 48, 5658-5668, **2009**.
42. Gavet, O. & Pines, J. Progressive Activation of CyclinB1-Cdk1 Coordinates Entry to Mitosis. *Developmental Cell* 18, 533-543, **2010**.
43. Burgess, A., Vigneron, S., Brioudes, E., Labbé, J.-C., Lorca, T. & Castro, A. Loss of human Greatwall results in G2 arrest and multiple mitotic defects due to deregulation of the cyclin B-Cdc2/PP2A balance. *Proceedings of the National Academy of Sciences* **2010**.

7.1 Concluding Remarks

This thesis describes our efforts in preparing a family of lipophilic fluorogenic probes for the specific imaging of ROS in the lipid membrane of live cells. In designing the new probes we sought to optimize their i) reactivity, ii) specificity, iii) partitioning, iv) sensitivity, as well as their v) organelle targeting characteristics.

The optimization of the 5 criteria described above resulted in a series of new probes that consist of a receptor and a reporter segment where a third organelle-targeting segment was additionally incorporated at a later stage. In order to fulfill the 5 requirements i) the receptor segment in the new probes was chosen to contain a chromanol unit similar or identical to that of α-tocopherol, the most potent naturally occurring lipophilic antioxidant. ii) The choice of this receptor ensured that the new probes will readily and specifically react with peroxyl radicals, the chain carriers in lipid membrane peroxidation. iii) The reporter segment selected consisted of a Bodipy fluorophore, a lipophilic dye that provides for preferential partitioning of the probes within the membrane and further ensures the reporting of redox changes in the receptor segment. iv) The sensitivity of the fluorogenic probes was controlled by an off-on intramolecular switch based on photoinduced electron transfer (PeT). Upon peroxyl radical scavenging, oxidation of the receptor segment deactivates an otherwise efficient intramolecular fluorescence deactivation mechanism based on PeT, leading to fluorescence enhancement. v) Finally suitable decoration enabled for specific mitochondria targeting within cells.

The studies described in this thesis ultimately provide a roadmap to navigate through the conception of a first generation probe and to underpin its mechanism of action. With the mechanistic information in hand we were next able to optimize the receptor, the reporter and their linking segment towards achieving a highly sensitive and reactive probe. The journey further involved the development of novel assays, the acquisition of key mechanistic information on lipid peroxidation in model lipid membranes, and the optimization of live cells studies with both non-targeting and targeting ROS sensitive fluorogenic probes.

Specifically, in chapter 2 we described the investigation of the molecular mechanism operating in the off-on switching in the first generation lipophilic fluorogenic probe, namely B-TOH. Through mechanistic studies including laser flash photolysis, electrochemistry, and DFT calculations we were able to establish that photoinduced electron transfer occurs from the receptor to the reporter segment, thus rendering the probe non–emissive. Upon peroxyl radical scavenging, oxidation of the receptor segment deactivates PeT leading to a 10-fold fluorescence enhancement observed in homogeneous solutions.

In Chapter 3 we demonstrated the scope and limitations for the potential application of B-TOH as a novel sensor suitable for peroxyl radical detection in cells both under physiological and pathological conditions. Reactivity studies performed in model lipid membranes underscored the antioxidant activity of B-TOH. B-TOH was also able to report on the oxidative status of cells under states of growth factor withdrawal and externally induced oxidative stress. However, when BTOH was embedded in lipid membranes we observed a marked decrease in sensitivity leading to only 5-fold emission enhancement upon scavenging peroxyl radicals, compared to the 10-fold enhancement recorded in homogeneous solution.

These results underlined the need for improvement of the sensitivity of the first generation fluorogenic sensors. The information gained in chapters 2 and 3 allowed us to determine the electrochemical and spectroscopic requirements that need to be met for the reporter (fluorophore) segment in order to modulate the sensitivity of B-TOH.

Aiming at fulfilling these requirements in Chapter 4 we discussed the preparation, electrochemical and spectroscopic characterization of 16 new Bodipy dyes with diverse redox properties and versatile tethering potential. Substitution at positions C2 and C6 with electron donating or withdrawing groups (Et, H, Cl or CN) enabled tuning the redox potentials within a *ca.* 0.7 eV without substantially changing the absorption and emission spectra, or the HOMO-LUMO bandgap. In the new series of Bodipy dyes we introduced hydroxymethyl or formyl groups at the *meso* position of the Bodipy core, which proved to be convenient

functionalities for covalent tethering to both electrophiles and nucleophiles. The non-emissive *meso*-formyl Bodipy dyes additionally provide unique opportunities as fluorogenic probes of nucleophilic attack by *e.g.* alcohols, thiols and amine groups and as fluorescent labeling agents where uncoupled fluorophores will not contribute to the fluorescence background.

The effect that the substituents in the Bodipy fluorophores have on the sensitivity of the fluorogenic antioxidants is clearly demonstrated in Chapter 5 by the second generation probes (H_2B-TOH and H_2B-PMHC) prepared by us. Emission enhancements of up to 100-fold were observed upon reaction of H_2B-TOH or H_2B-PMHC with peroxyl radicals. Further, in Chapter 5 we investigated the effect on the sensitivity of the probes and on their reactivity towards peroxyl radicals when a methylene (in H_2B-PMHC) vs. ester linker (in H_2B-TOH) was used to couple the receptor and reporter segments. The higher sensitivity of H_2B-PMHC is due to the shorter methylene linker that favors PeT. Additionally the ester linker utilized in H_2B-TOH reduces the radical scavenging reactivity of the phenol segment by strengthening the phenolic O-H BDE through its electron-withdrawing properties.

The potential of the improved probes H_2B-TOH and H_2B-PMHC is demonstrated in the high-throughput fluorescence assay for monitoring kinetics of peroxyl radical reactions in liposomes that we further developed. The evolution of the fluorescence intensity over time provides a rapid, facile method to conduct competitive kinetic studies in the presence of α-tocopherol and analogues. This novel method gives new insights and a quantitative understanding on the critical role of lipid diversity in modulating antioxidant activity in the lipid milieu. Our results illustrate that the relative antioxidant activities of chromanols in homogeneous solution, arising from their inherent chemical reactivity, readily translate to the microheterogeneous environment at the water lipid interface. We conclude that mobility and to a lesser extent physical accessibility account for the larger relative antioxidant activity of tocopherol analogues bearing short (PMHC) over long (α-tocopherol) aliphatic tails, but that otherwise have the same inherent chemical reactivity.

The synthetic methodologies developed and discussed in Chapters 4 and 5 enabled us to expand the scope of the fluorogenic probes to specific organelle targeting. In Chapter 6 we addressed the synthetic challenges encountered during the development of the third generation of fluorogenic sensors for detection of ROS in mitochondria. Specific accumulation in mitochondria was observed in live cells. The radical scavenging activity of the new probes was demonstrated in both liposome suspensions and live cells under oxidative stress conditions. Targeting mitochondria with ROS scavengers (antioxidants) will further advance our understanding of the complex relationship between the redox state within mitochondria and vital cellular processes.

We anticipate that the novel scaffold of fluorogenic antioxidants described in this thesis should prove useful for creating new multifunctional probes that extend our ability to study ROS biology.

7.2. New Directions

The study of ROS production in biological systems and the correlation of ROS chemistry with its biology ultimately requires better imaging capabilities which will in turn demand not only the development of novel probes, but also novel imaging strategies to be applied. Thus, both synthetic and instrumental efforts are required to advance the field forward.

From the viewpoint of the synthesis of novel probes, we anticipate that by using the criteria and methodologies we had developed it will be possible to expand the family of fluorogenic antioxidants to enable for both emission color tuning and reactivity tuning.

We have initiated the development of fluorogenic probes with increasing reactivity towards ROS and with distinct emission spectra, for identification. Ultimately a reactivity/color palette for reactive oxygen species will be generated that will enable exploring the reactivity of the free radicals being formed at any given time in cells/tissues and correlating this to cellular responses over time. The highly sensitive and ROS specific lipophilic fluorescent probes will allow us

to study and assess the effect of synthetic potent antioxidants in bulk cell studies and in single cells studies.

A similar rational design strategy may also be applicable to other biomolecules of interest for the development of various bifunctional fluorogenic probes. Recently, we have initiated the development of a fluorogenic Coenzyme Q_{10} (ubiquinone) analogue as a probe to monitor the oxidative status in mitochondrial electron transport chains in live cells. The ubiquinone moiety is redox active serving as a mobile electron carrier in the mitochondrial inner membrane. Furthermore, the reduced form of CoQ_{10} (ubiqinol) has an important protective function as a chain breaking antioxidant, terminating lipid peroxidation in phospholipid bilayers. The fluorogenic probe will be suitable for studying many central nervous system degenerative diseases and age-related disorders associated with oxidative stress, such as Parkinson's and Alzheimer's diseases.

Further developments will involve tethering fluorophores to neurotransmitters such as adrenaline, dopamine, and other related catecholamines. Under oxidative stress conditions the catecholamines undergo oxidation to quinones, which disrupts the signalling capabilities of catecholamines to receptors in the nervous system. By preparing catecholamine-fluorophore probes, we will permit real-time imaging of neurotransmitter oxidation in neurone cell cultures.

We expect the proposed probes to be a useful tool for a range of biological and pathological investigations that will greatly extends our ability to study the biology of ROS.

Regarding the instrumental design, we believe that novel high resolution strategies in fluorescence microscopy such as STORM,[1] PALM,[2,3] STED,[4,5] SOFI,[6] etc, may become critical in studying ROS production within mitochondria. These methodologies have instrumental constraints but also place pressure on the performance of the dyes. The synergy of instrument and probe development will surely enable a great progress in the future towards the study of ROS production in biological systems and the correlation of ROS chemistry with its biology.

7.3. References

1. Rust, M.J., Bates, M. & Zhuang, X. Sub-diffraction-limit imaging by stochastic optical reconstruction microscopy (STORM). *Nat Meth* 3, 793-796, **2006**.
2. Betzig, E., Patterson, G.H., Sougrat, R., Lindwasser, O.W., Olenych, S., Bonifacino, J.S., Davidson, M.W., Lippincott-Schwartz, J. & Hess, H.F. Imaging Intracellular Fluorescent Proteins at Nanometer Resolution. *Science* 313, 1642-1645, **2006**.
3. Hess, S.T., Girirajan, T.P.K. & Mason, M.D. Ultra-High Resolution Imaging by Fluorescence Photoactivation Localization Microscopy. *Biophysical journal* 91, 4258-4272, **2006**.
4. Klar, T.A., Jakobs, S., Dyba, M., Egner, A. & Hell, S.W. Fluorescence microscopy with diffraction resolution barrier broken by stimulated emission. *Proceedings of the National Academy of Sciences* 97, 8206-8210, **2000**.
5. Hell, S.W. & Wichmann, J. Breaking the diffraction resolution limit by stimulated emission: stimulated-emission-depletion fluorescence microscopy. *Opt. Lett.* 19, 780-782, **1994**.
6. Dedecker, P., Mo, G.C.H., Dertinger, T. & Zhang, J. Widely accessible method for superresolution fluorescence imaging of living systems. *Proceedings of the National Academy of Sciences* 109, 10909-10914, **2012**.

8. Appendices

8.1. Appendix Chapter 2

3,5-di-tert-butyl-4-hydroxybenzyloxymethyl-2,6-diethyl -1,3,5,7-tetramethyl pyrromethene fluoroborate (**B-BHB**)

INDEX	FREQUENCY	PPM	HEIGHT
1	3157.242	7.891	20.7
2	2904.885	7.260	24.7
3	2294.534	5.735	10.0
4	2205.329	5.512	15.7
5	2120.818	5.300	5.0
6	1011.231	2.527	34.9
7	959.585	2.398	10.9
8	952.152	2.380	11.8
9	944.718	2.361	5.1
10	918.895	2.297	40.7
11	628.578	1.572	9.0
12	588.680	1.471	10.9
13	574.594	1.436	162.0
14	422.007	1.055	11.3
15	414.182	1.035	25.0
16	406.748	1.017	13.0

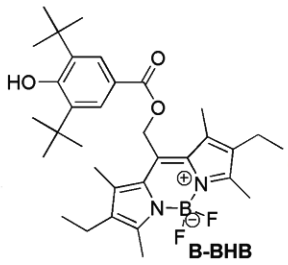

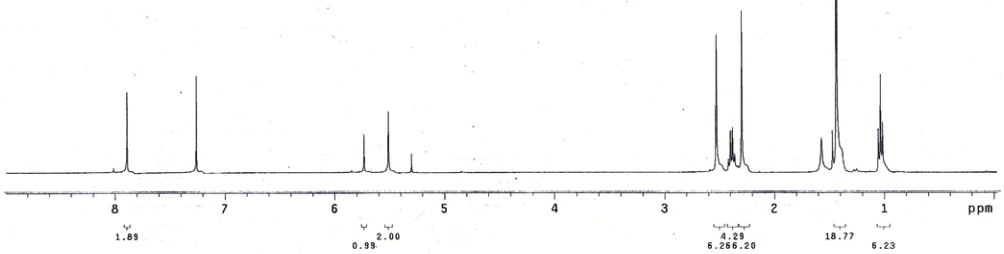

STANDARD CARBON PARAMETERS

Pulse Sequence: s2pul
Solvent: CDCl3
Ambient temperature
User: l-14-87
UNITY-500 "dante"

Relax. delay 1.500 sec
Pulse 45.0 degrees
Acq. time 1.300 sec
Width 30807.5 Hz
2508 repetitions
OBSERVE C13, 125.6895203 MHz
DECOUPLE H1, 499.9008858 MHz
Power 41 dB
continuously on
WALTZ-16 modulated
DATA PROCESSING
Line broadening 1.0 Hz
FT size 131072
Total time 7 hr, 48 min, 33 sec

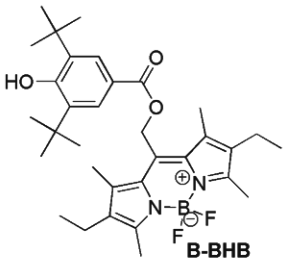

8.2. Appendix Chapter 4

3-cyano-2,4-dimethyl pyrrole (**17**)

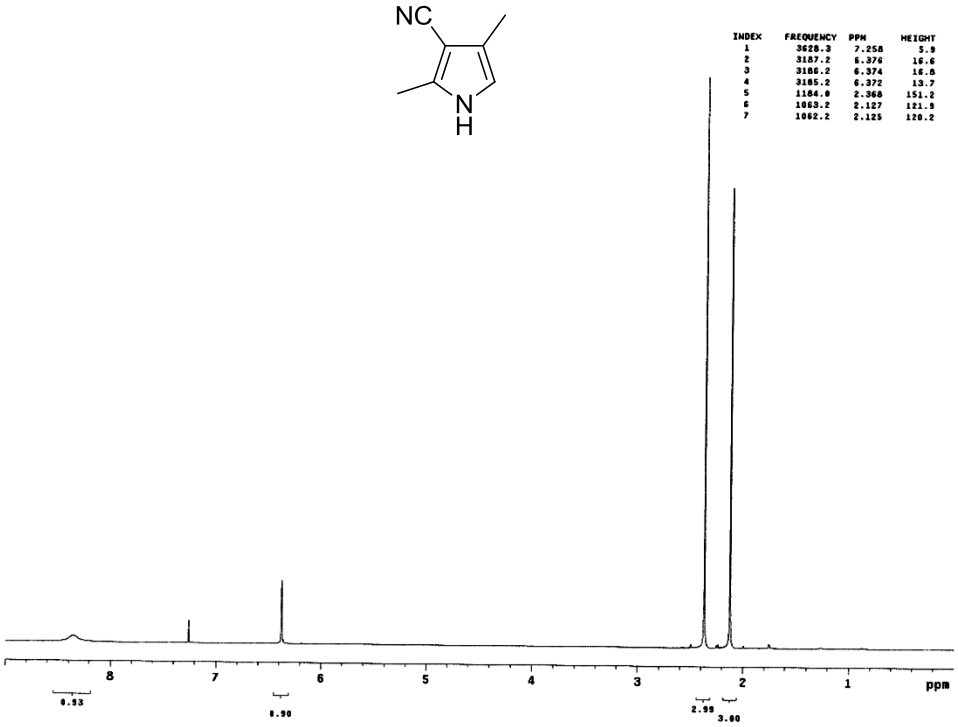

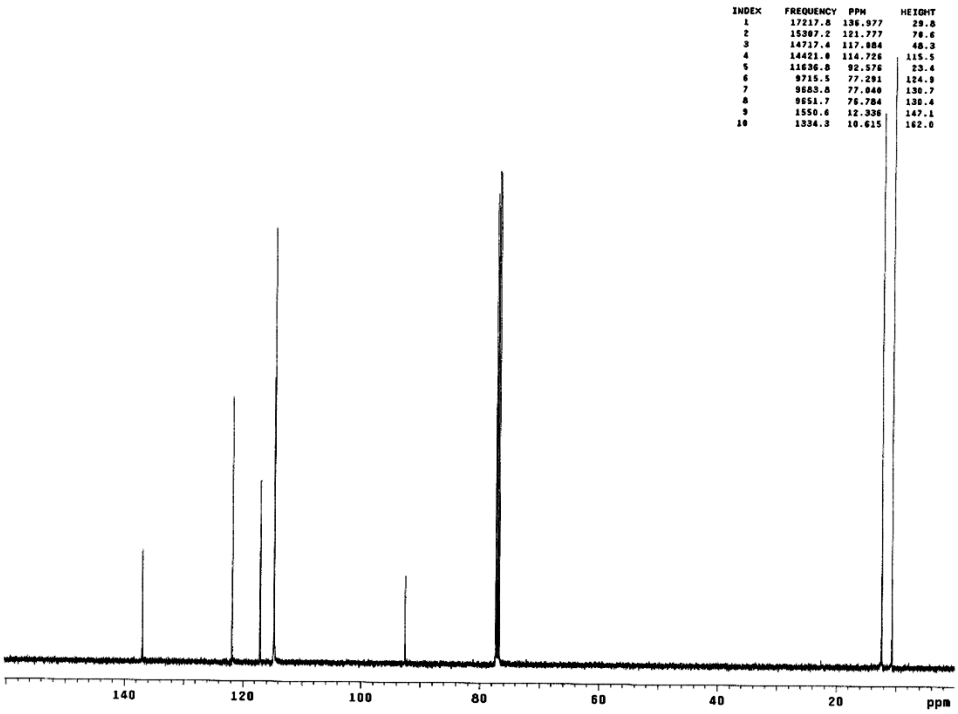

8-Acetoxymethyl-1,3,5,7-tetramethyl pyrromethene fluoroborate (**1**)

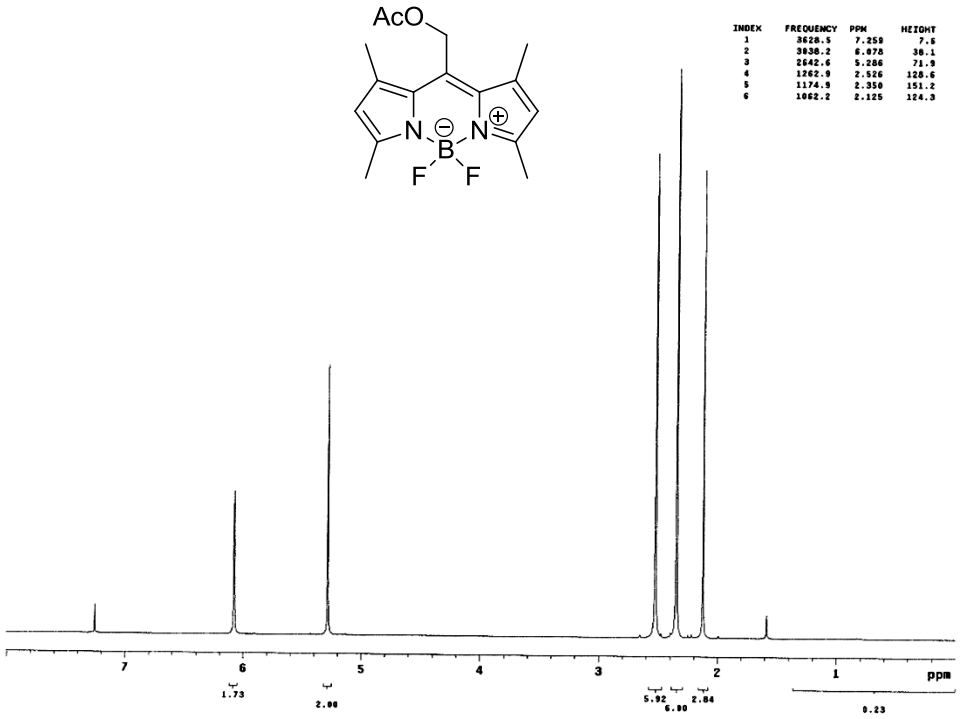

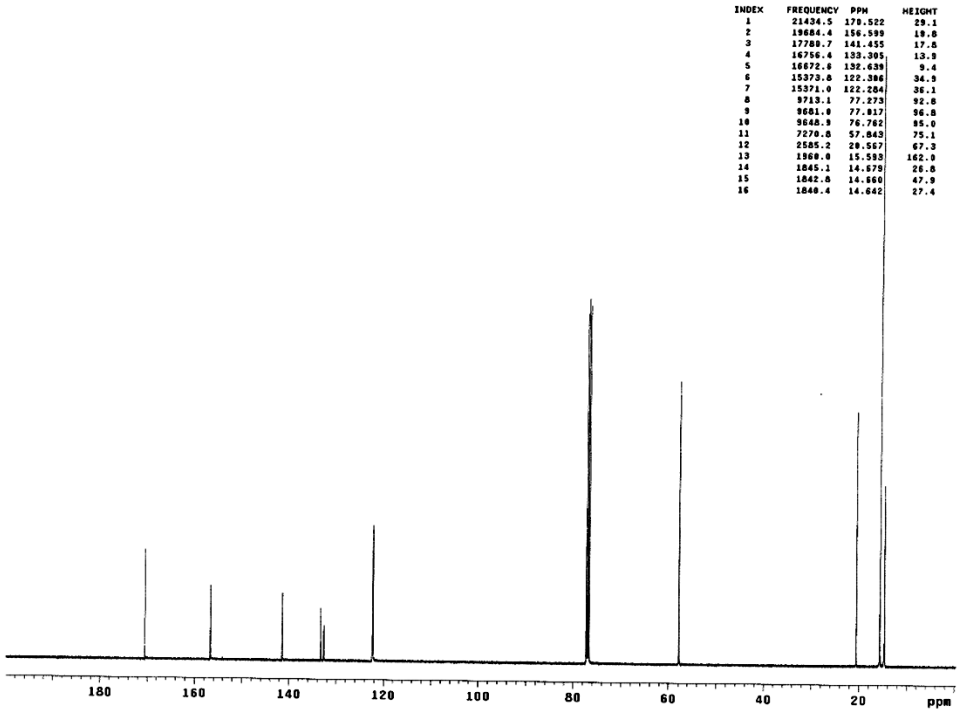

8-Acetoxymethyl-2-chloro-1,3,5,7-tetramethyl pyrromethene fluoroborate (**2**)

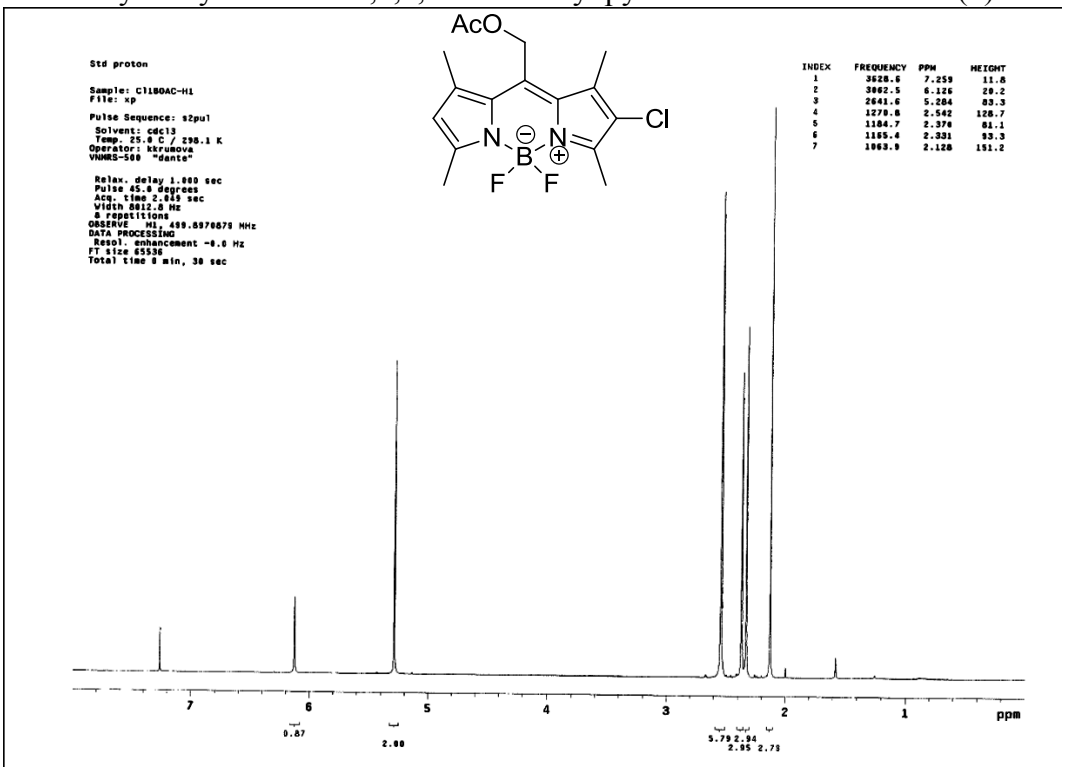

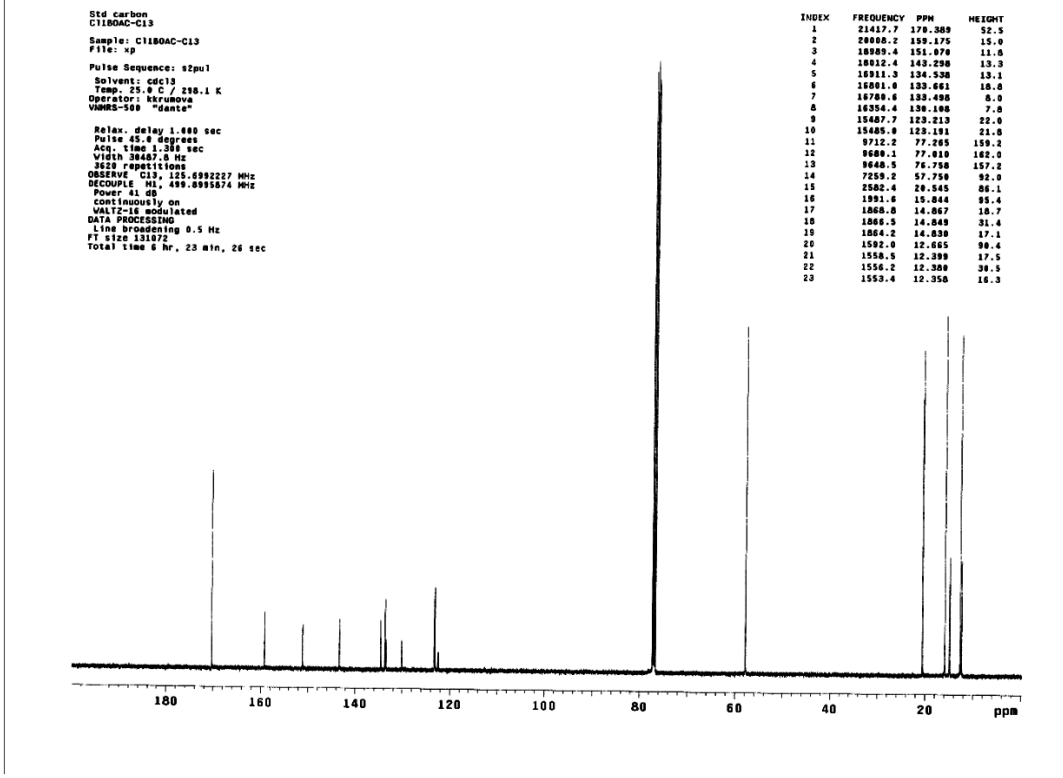

8-Acetoxymethyl-2,6-dichloro-1,3,5,7-tetramethyl pyrromethene fluoroborate (**3**)

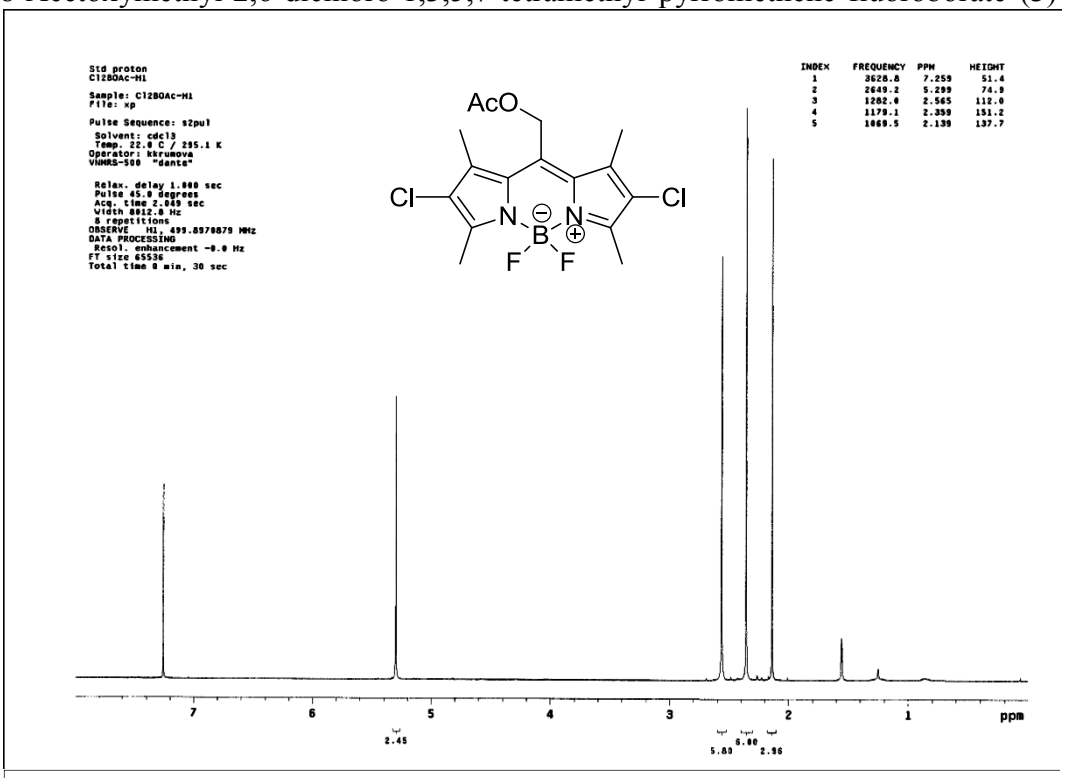

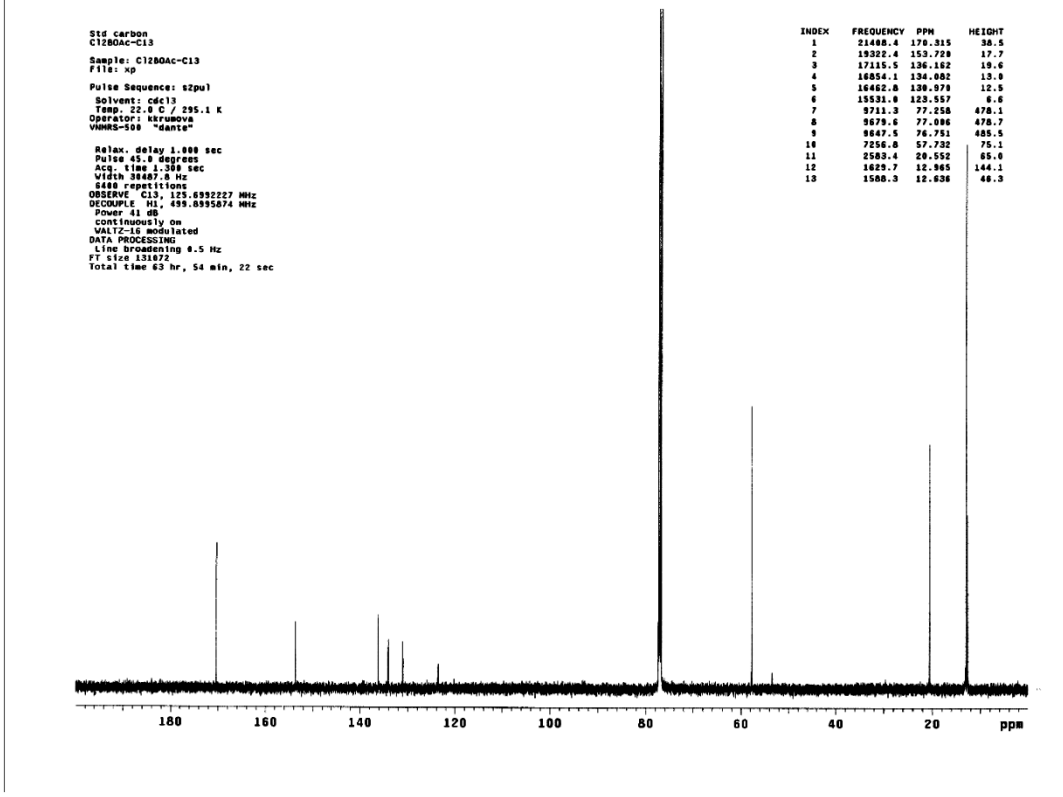

8-Acetoxymethyl-2-cyano-1,3,5,7-tetramethyl pyrromethene fluoroborate (**4**)

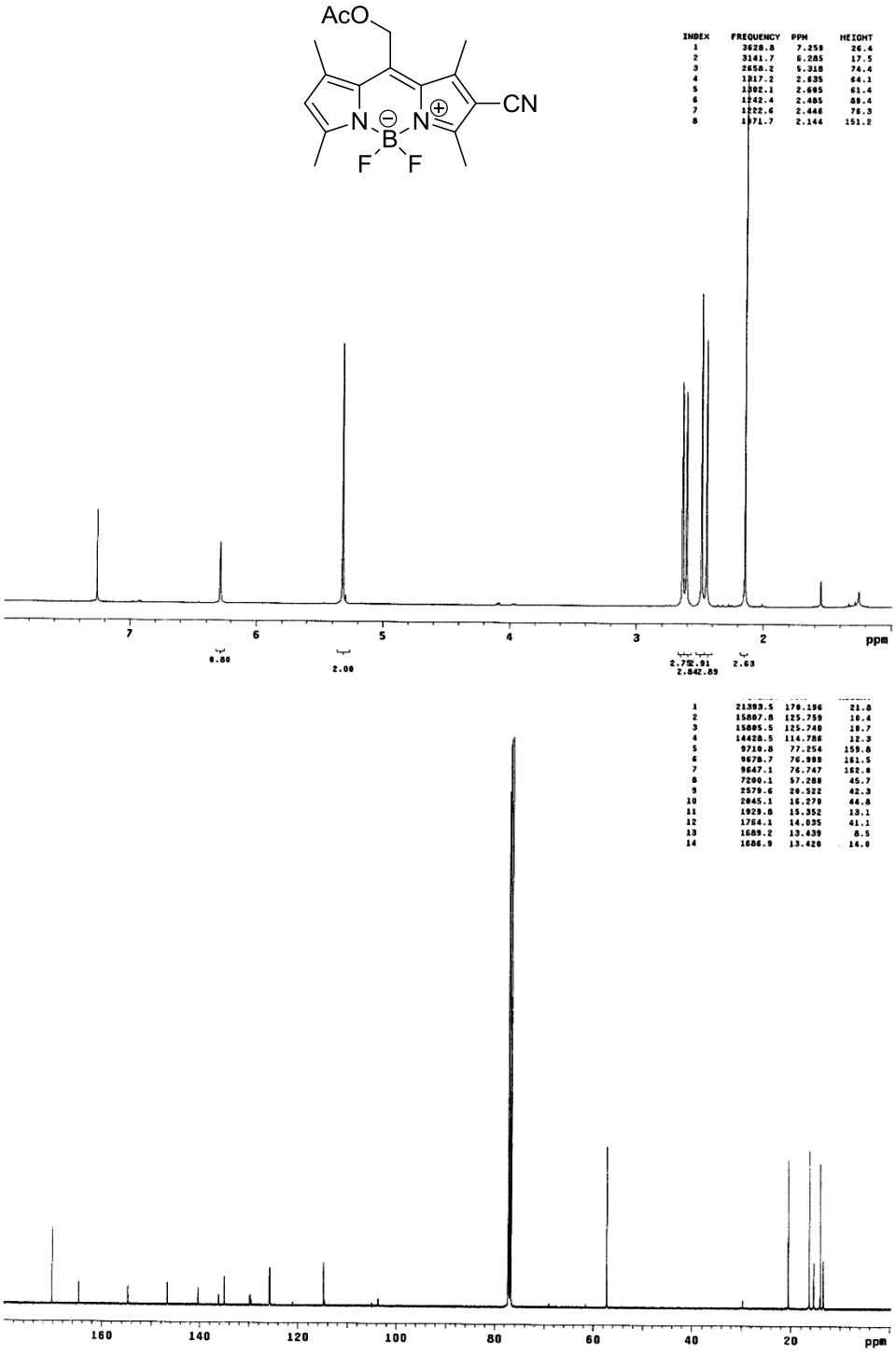

8-Acetoxymethyl-2,6-dicyano-1,3,5,7-tetramethyl pyrromethene fluoroborate (**5**)

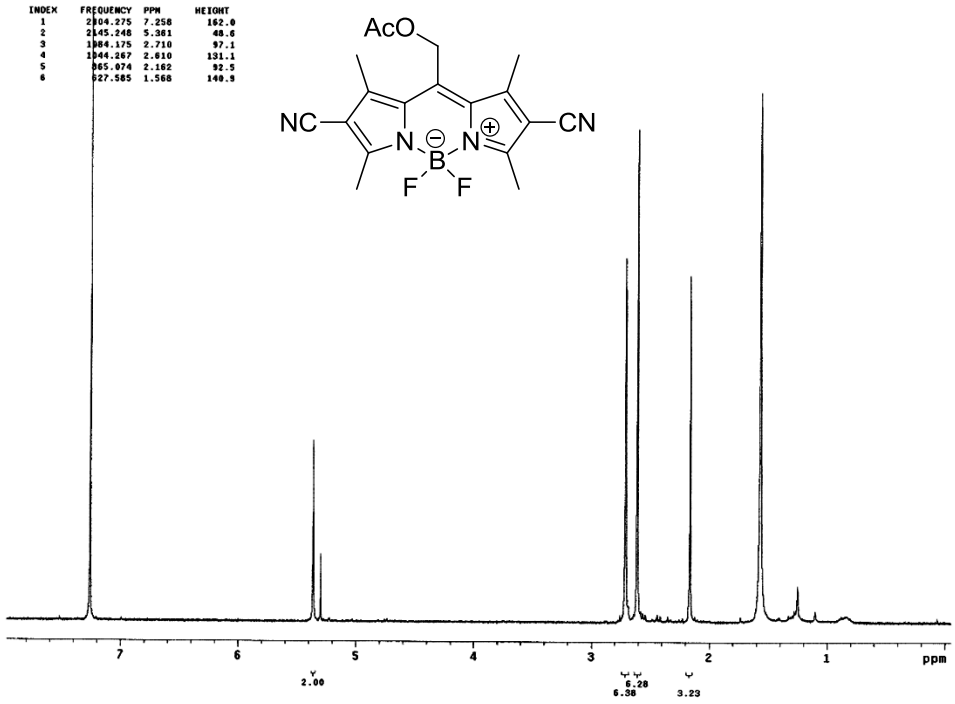

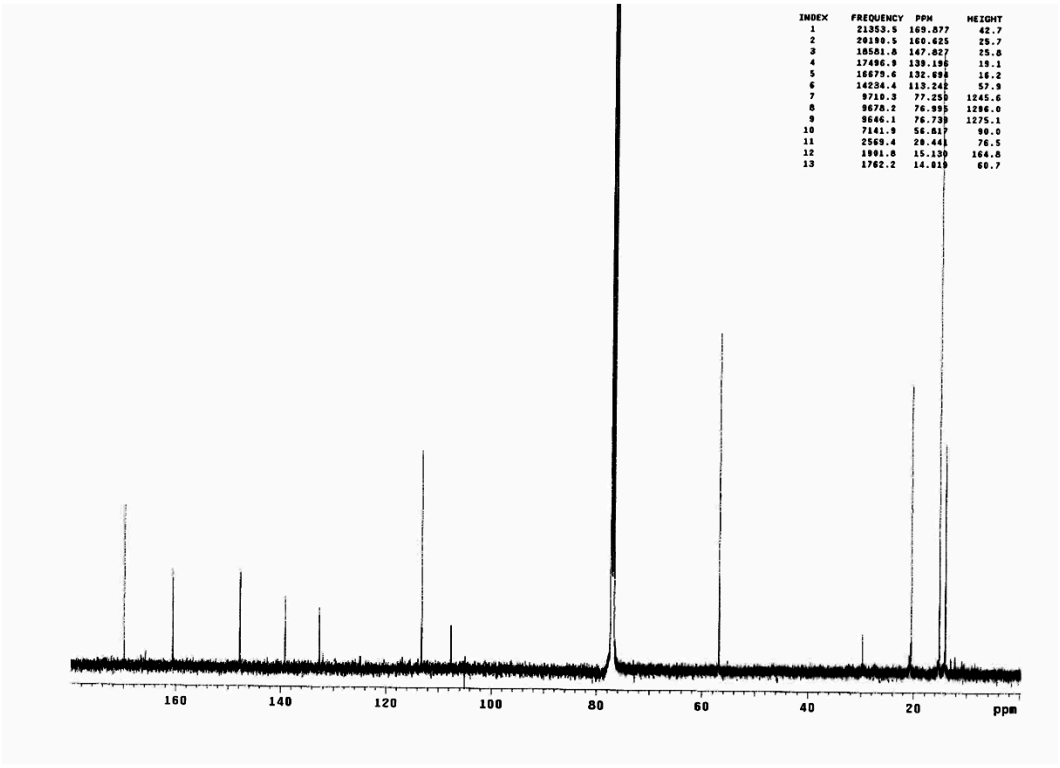

8-Hydroxymethyl-1,3,5,7-tetramethyl pyrromethene fluoroborate (**6**)

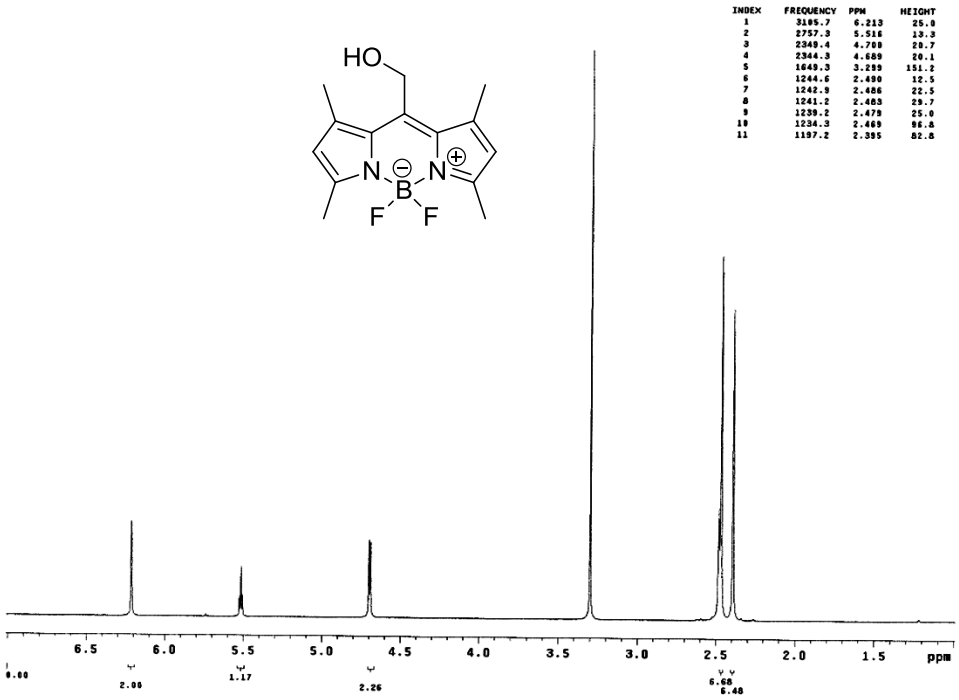

INDEX	FREQUENCY	PPM	HEIGHT
1	3105.7	6.213	25.0
2	2757.3	5.516	13.3
3	2349.4	4.700	28.7
4	2344.3	4.689	20.1
5	1649.3	3.299	151.2
6	1244.6	2.490	12.5
7	1242.9	2.486	22.5
8	1241.2	2.483	29.7
9	1239.2	2.479	25.0
10	1234.3	2.469	96.8
11	1197.2	2.395	82.8

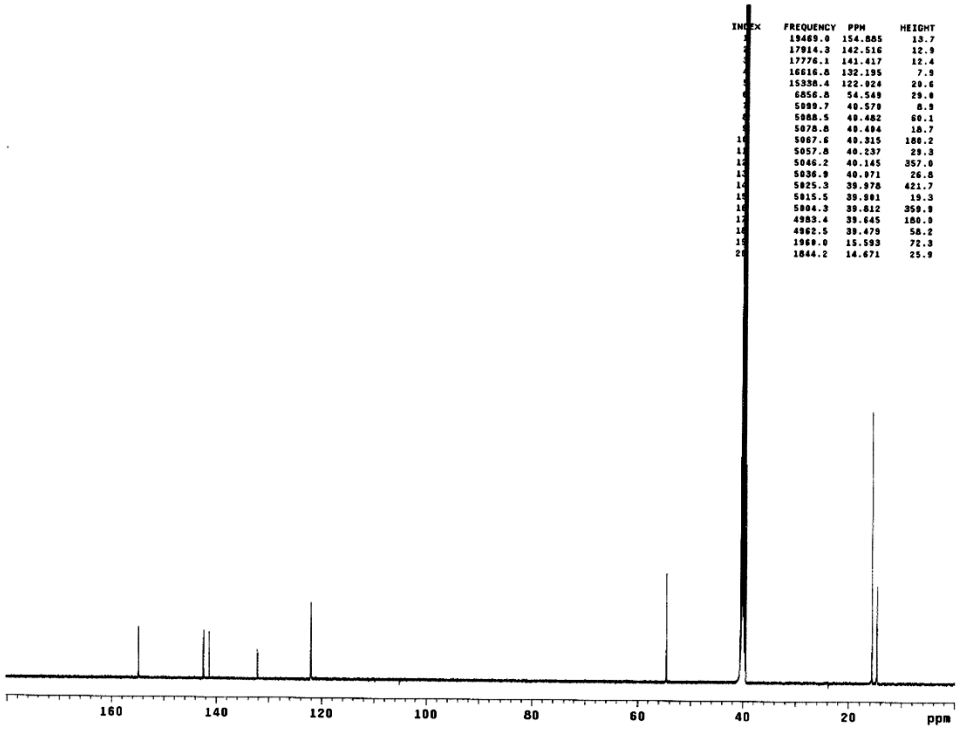

INDEX	FREQUENCY	PPM	HEIGHT
1	19469.0	154.885	13.7
2	17914.3	142.516	12.9
3	17776.1	141.417	12.4
4	16616.8	132.195	7.9
5	15338.4	122.024	20.6
6	6856.8	54.549	29.8
7	5089.7	40.579	8.9
8	5088.5	40.482	60.1
9	5078.8	40.404	18.7
10	5067.6	40.315	180.2
11	5057.8	40.237	29.3
12	5046.2	40.145	357.8
13	5036.9	40.071	26.8
14	5025.3	39.978	421.7
15	5015.5	39.901	19.3
16	5004.3	39.812	359.9
17	4983.4	39.645	180.8
18	4962.5	39.479	58.2
19	1968.0	15.593	72.3
20	1844.2	14.671	25.9

8-Hydroxymethyl-2-chloro-1,3,5,7-tetramethyl pyrromethene fluoroborate (**7**)

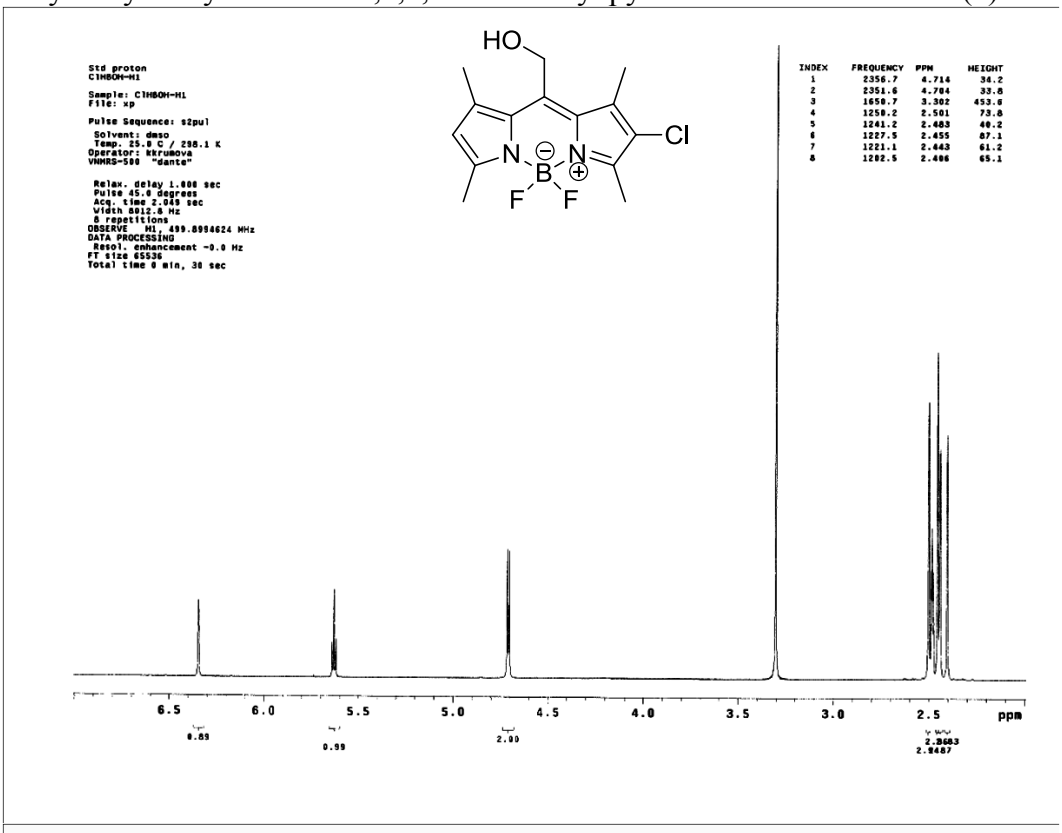

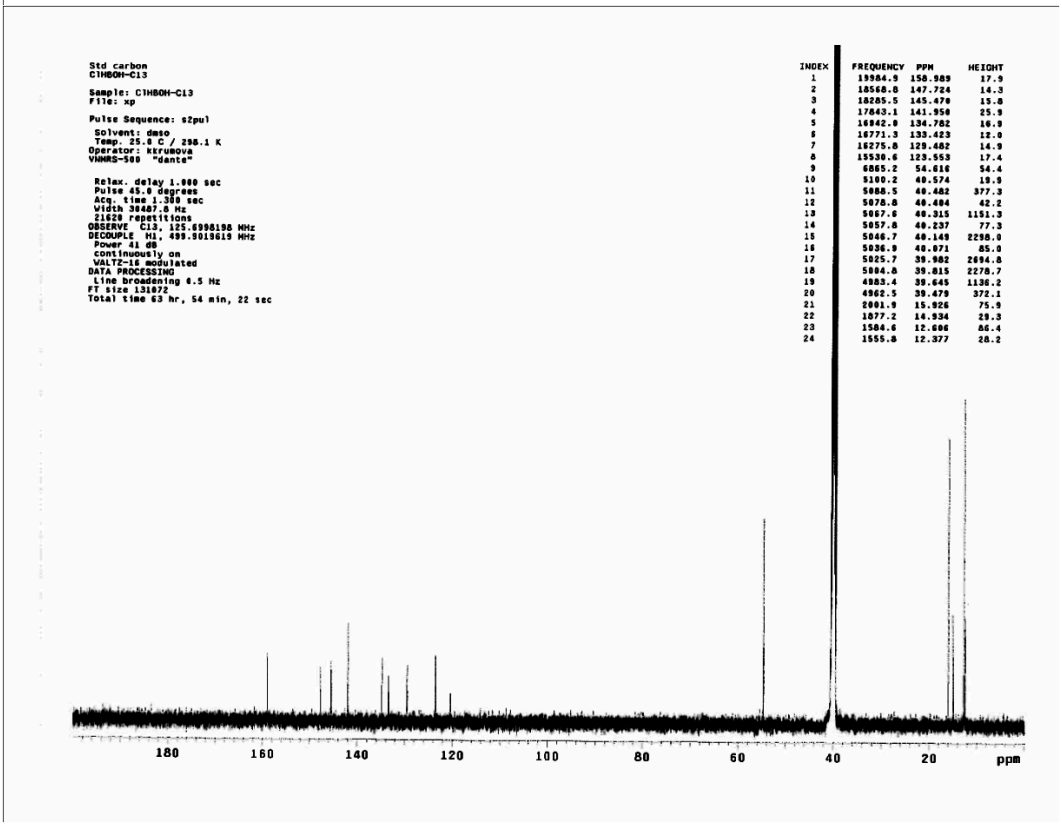

8-Hydroxymethyl-2,6-dichloro-1,3,5,7-tetramethyl pyrromethene fluoroborate (**8**)

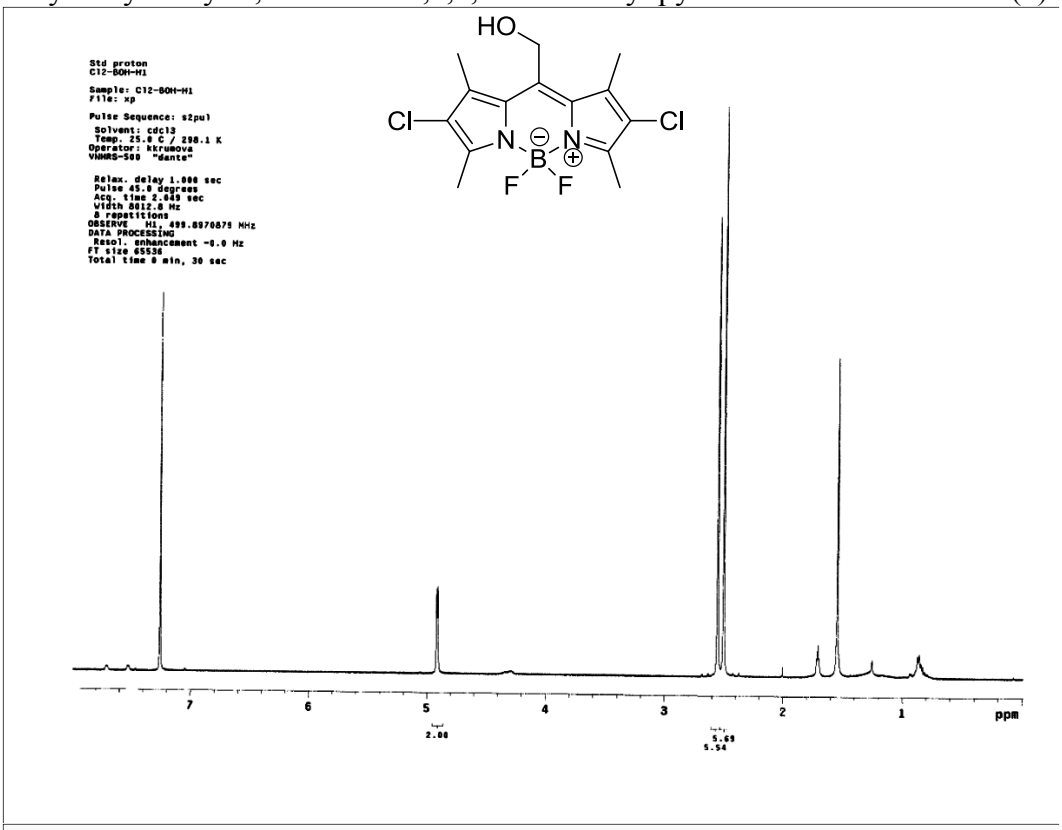

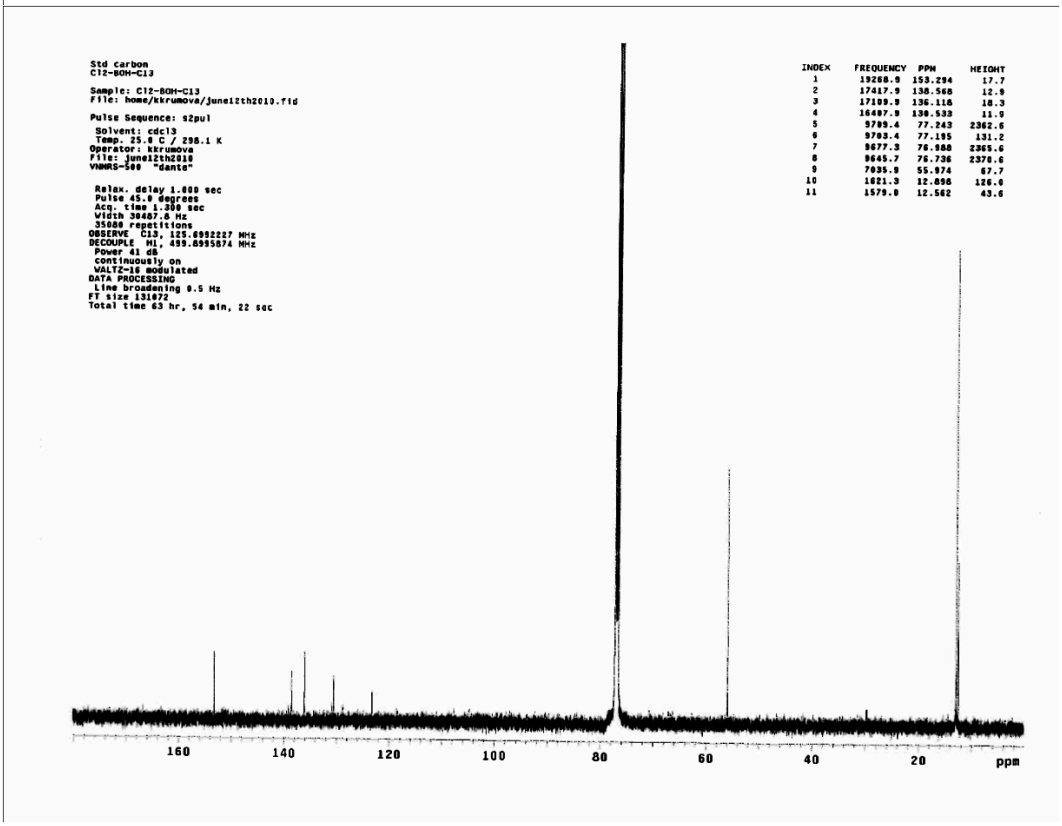

8-Hydroxymethyl-2-cyano-1,3,5,7-tetramethyl pyrromethene fluoroborate (**9**)

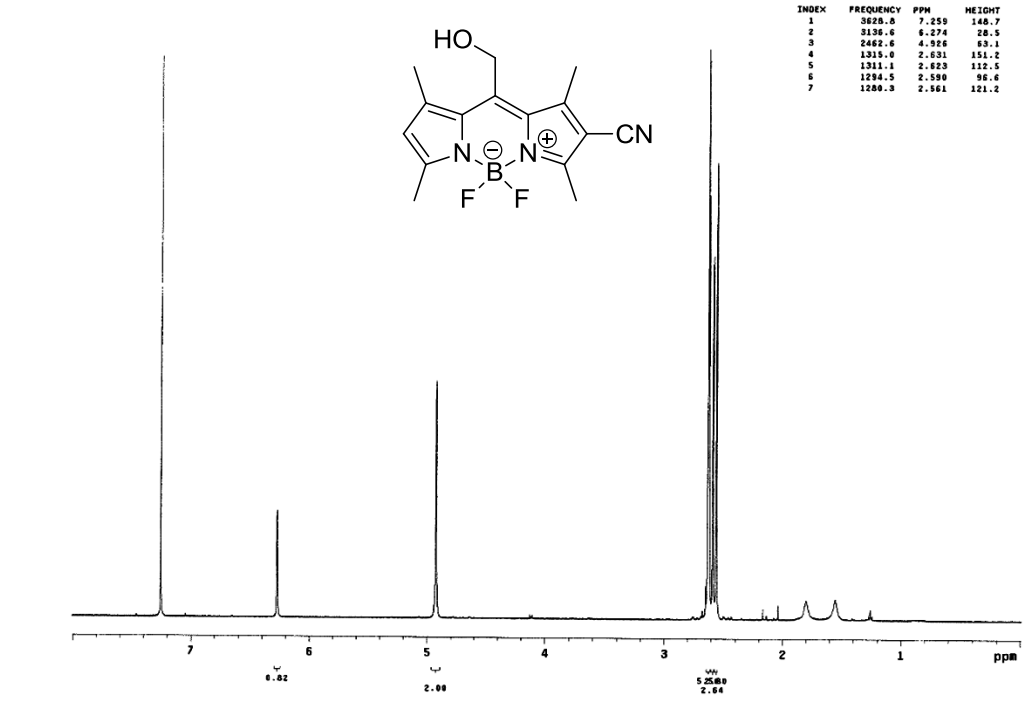

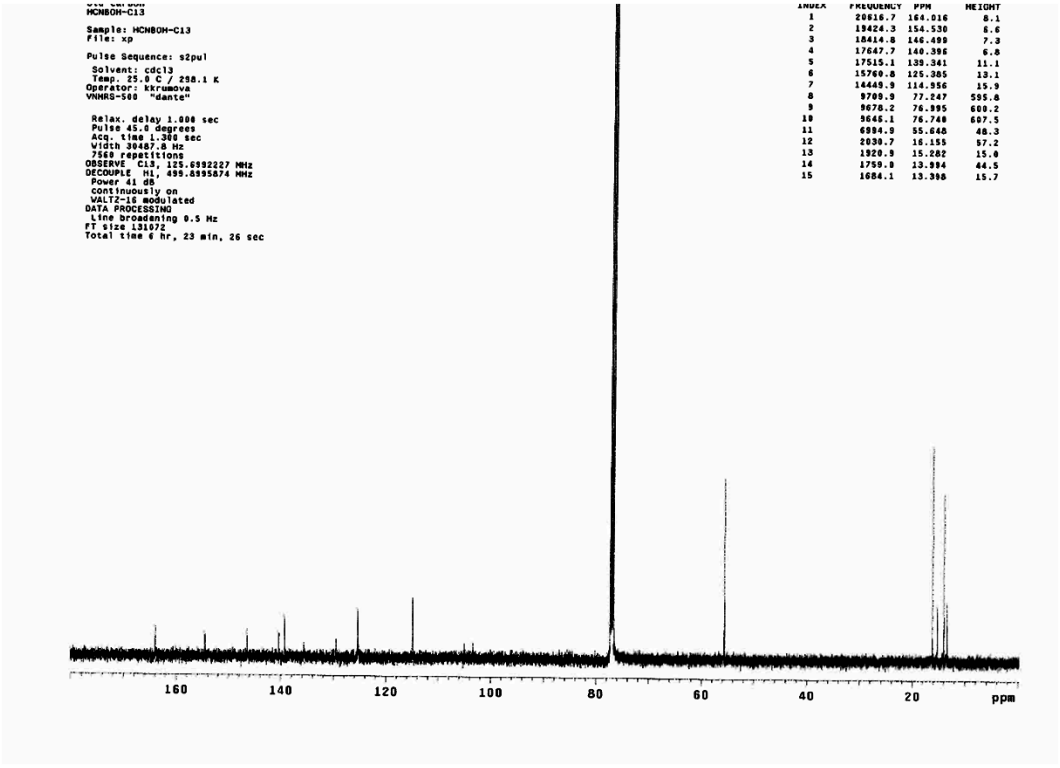

8-Hydroxymethyl-2,6-dicyano-1,3,5,7-tetramethyl pyrromethene fluoroborate (**10**)

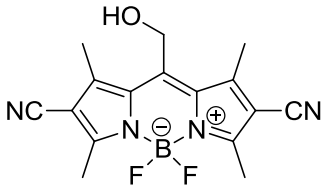

INDEX	FREQUENCY	PPM	HEIGHT
1	2537.7	5.076	26.8
2	1410.4	2.821	151.2
3	1391.1	2.783	97.7
4	1331.2	2.663	66.5
5	1029.9	2.060	12.1
6	1027.7	2.056	22.1
7	1025.5	2.051	30.3
8	1023.6	2.048	21.5

INDEX	FREQUENCY	PPM	HEIGHT
1	25817.2	205.388	89.4
2	25797.7	205.232	5722.3
3	25777.2	205.070	72.8
4	19981.2	158.960	17.8
5	18667.9	148.512	20.9
6	18446.9	146.754	14.4
7	14218.7	113.116	52.6
8	6868.4	54.680	93.5
9	6874.9	54.693	12.7
10	3705.9	29.482	29.7
11	3693.4	29.382	534.8
12	3686.4	29.327	65.8
13	3673.8	29.227	1655.3
14	3666.9	29.172	110.5
15	3654.8	29.075	3347.5
16	3647.8	29.020	114.4
17	3635.2	28.920	4347.5
18	3628.2	28.864	93.9
19	3615.7	28.764	3597.5
20	3598.6	28.613	1966.5
21	3577.1	28.457	678.3
22	1771.1	14.090	186.9
23	1637.6	13.028	33.1
24	1635.3	13.010	54.9
25	1632.5	12.987	30.9

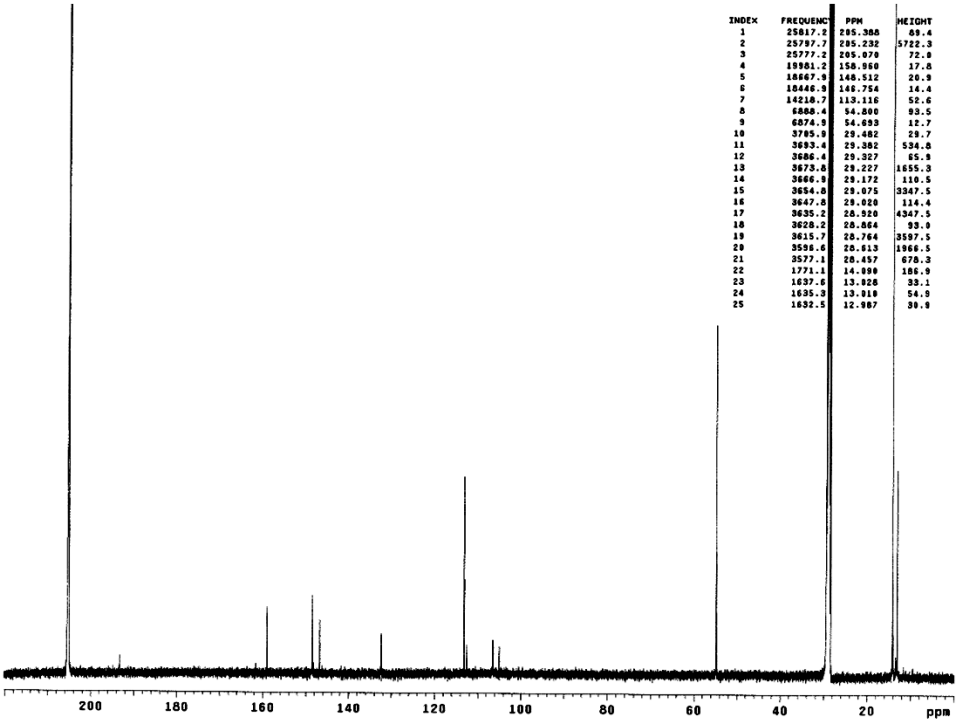

8-Formyl-2,6-diethyl-1,3,5,7-tetramethyl pyrromethene fluoroborate (**11**)

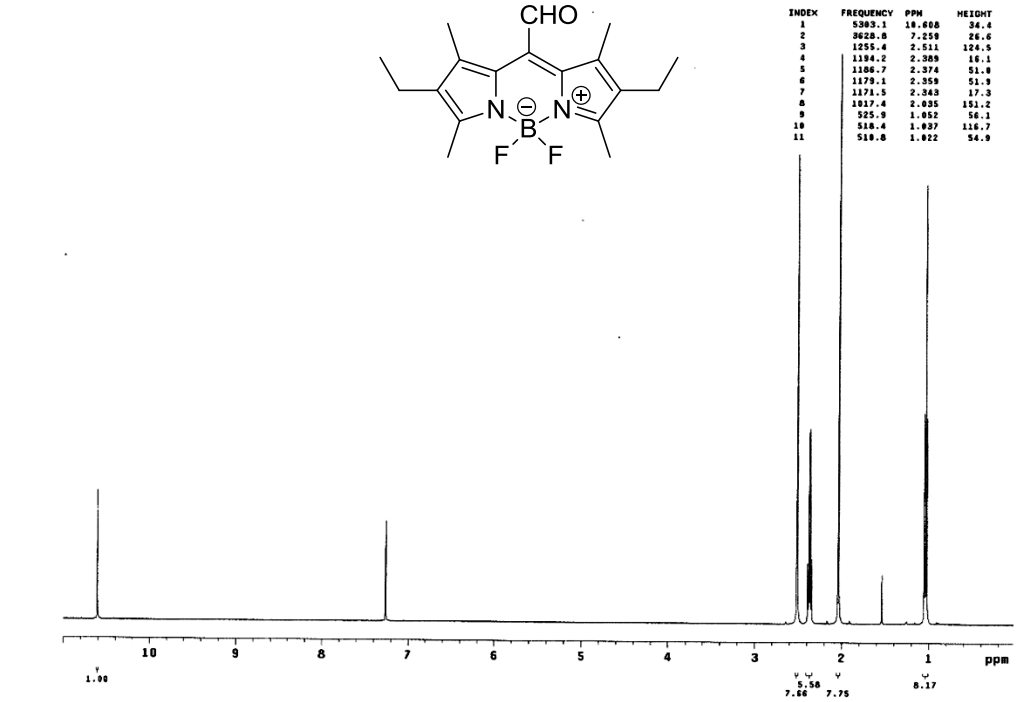

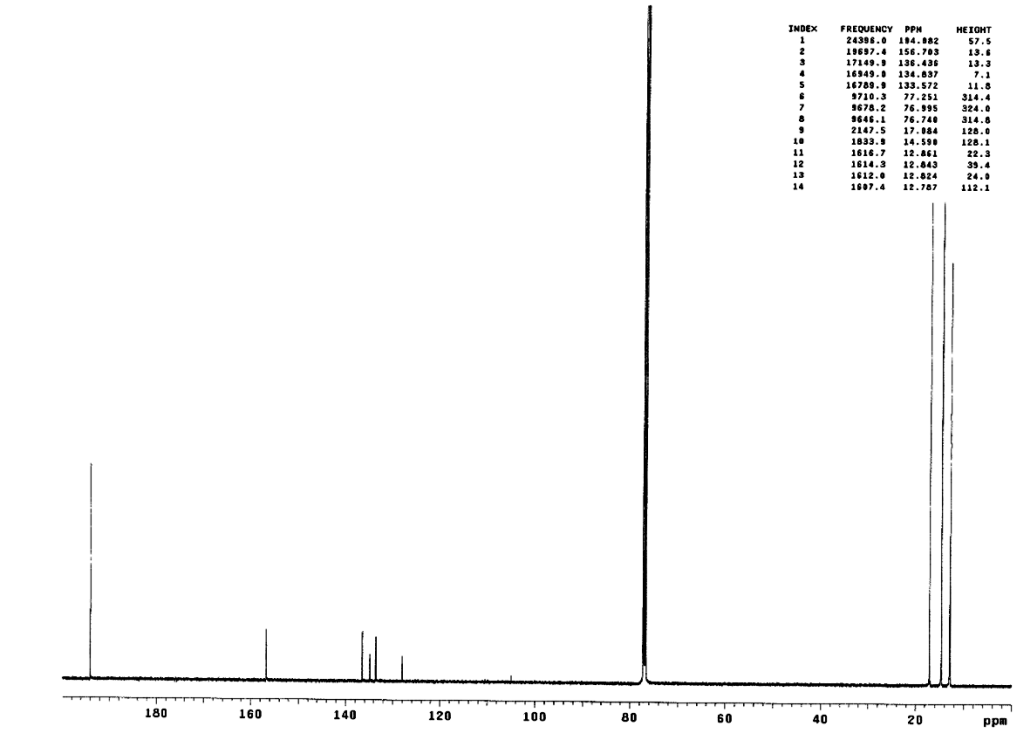

8-Formyl-1,3,5,7-tetramethyl pyrromethene fluoroborate (**12**)

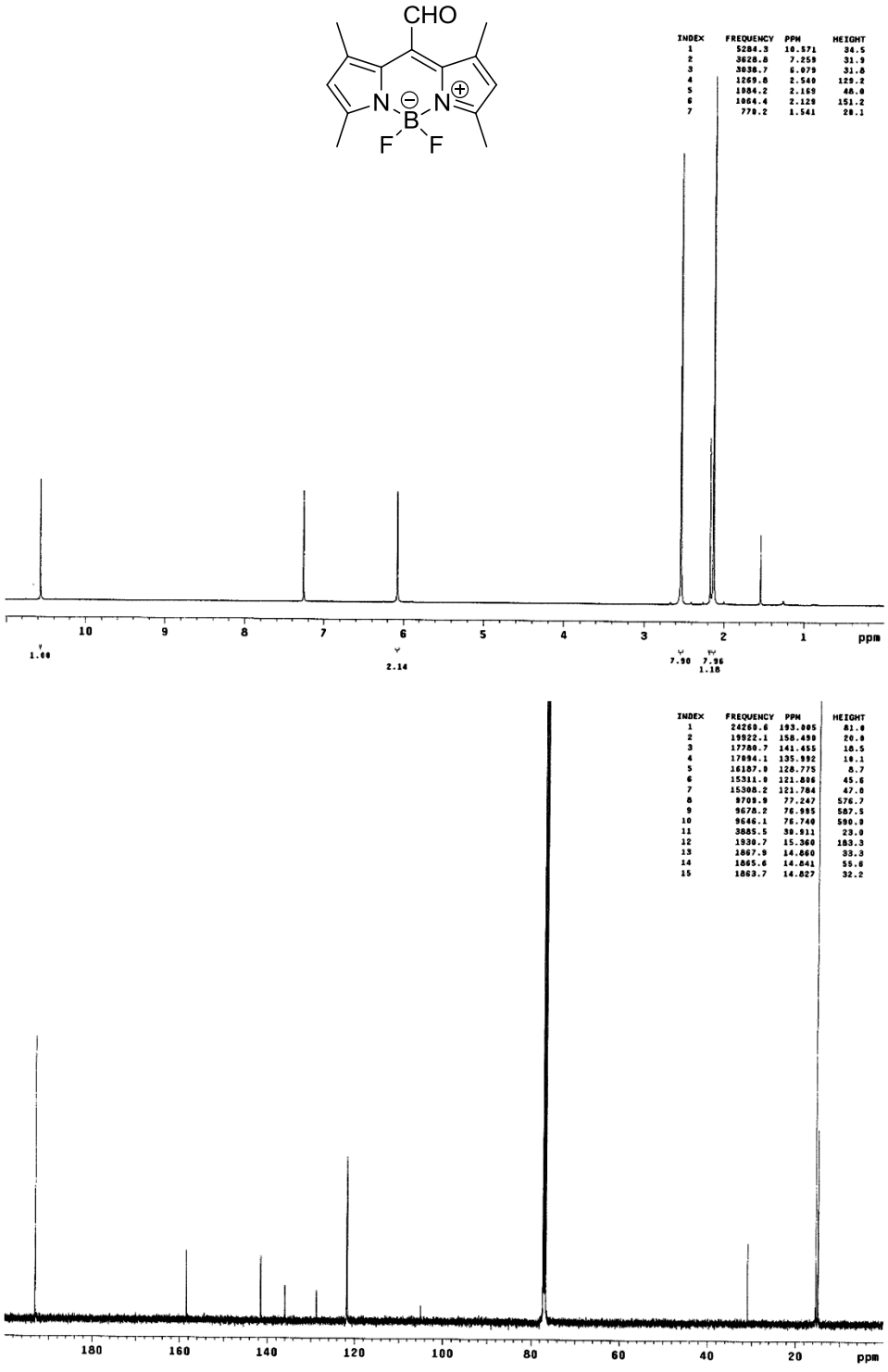

8-Formyl-2-chloro-1,3,5,7-tetramethyl pyrromethene fluoroborate (**13**)

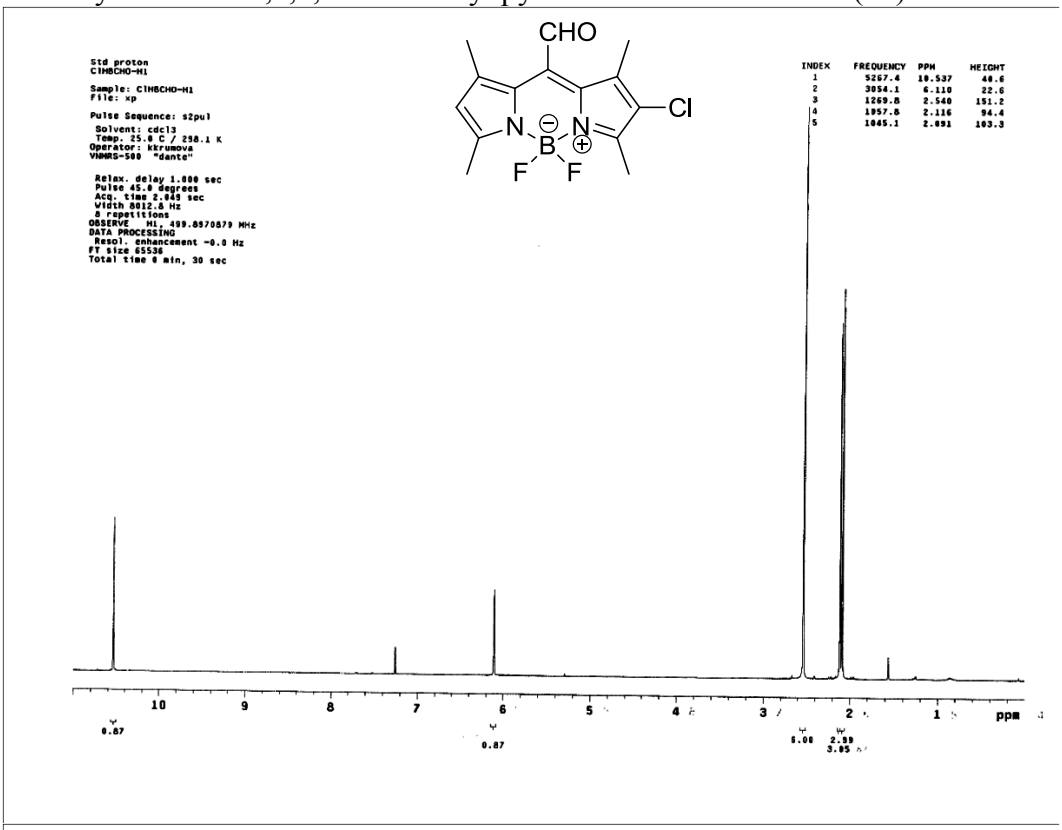

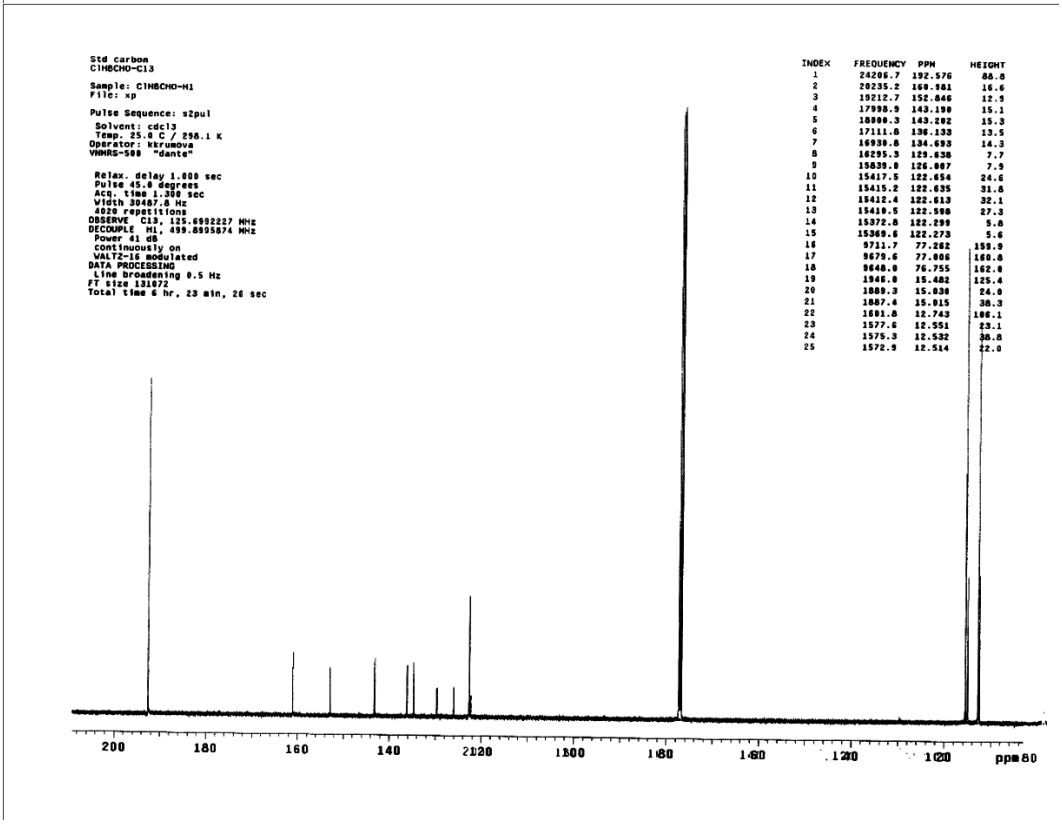

8-Formyl-2,6-dichloro-1,3,5,7-tetramethyl pyrromethene fluoroborate (**14**)

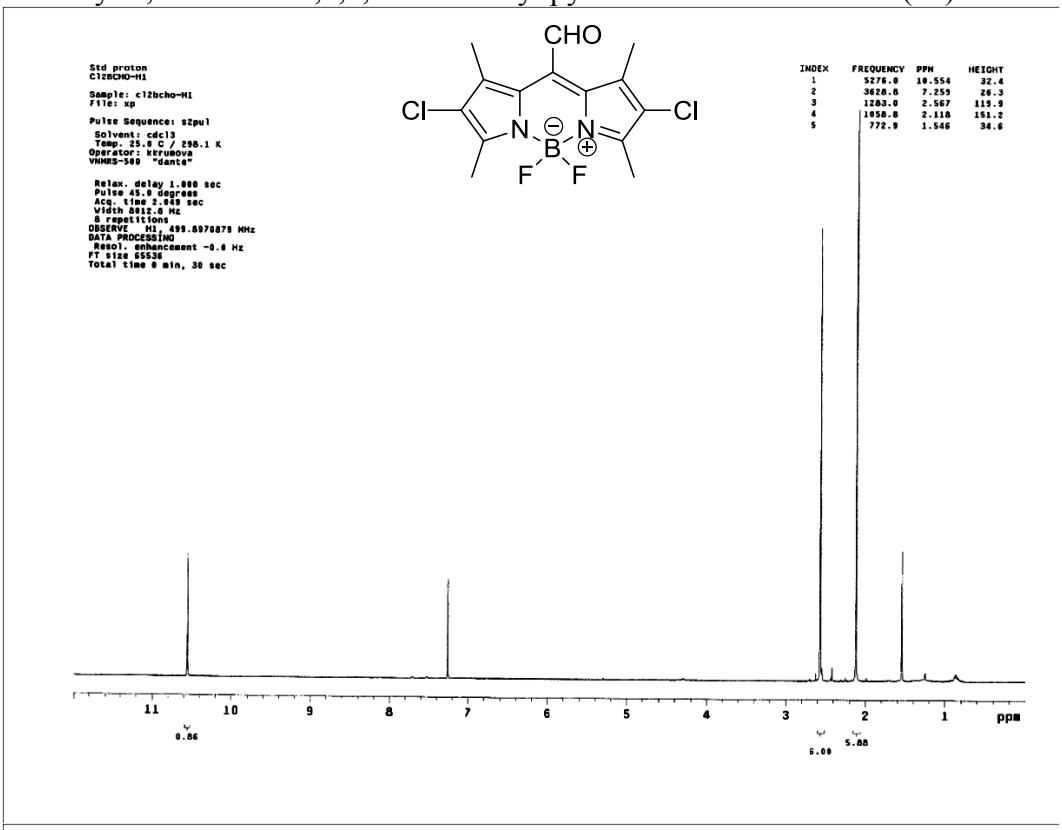

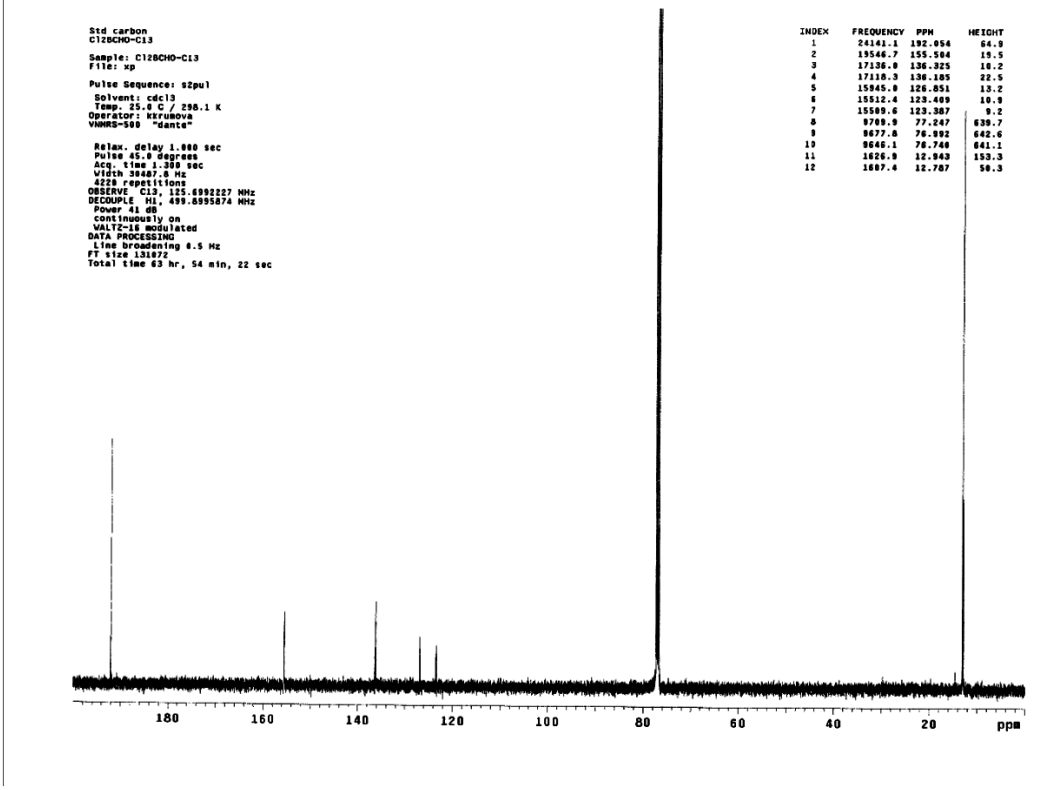

8-Formyl-2-cyano-1,3,5,7-tetramethyl pyrromethene fluoroborate (**15**)

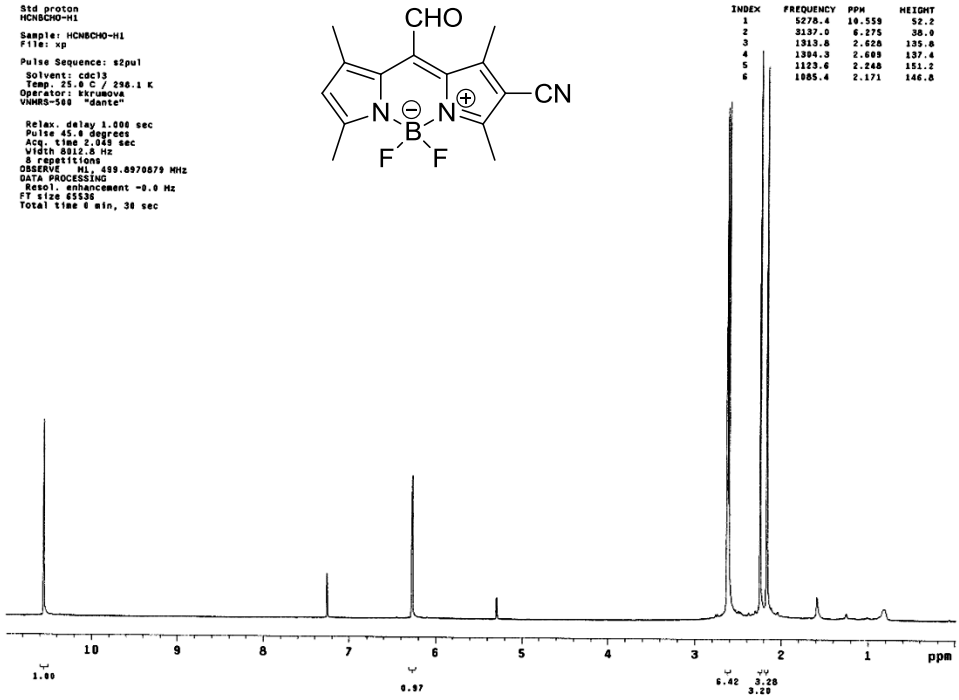

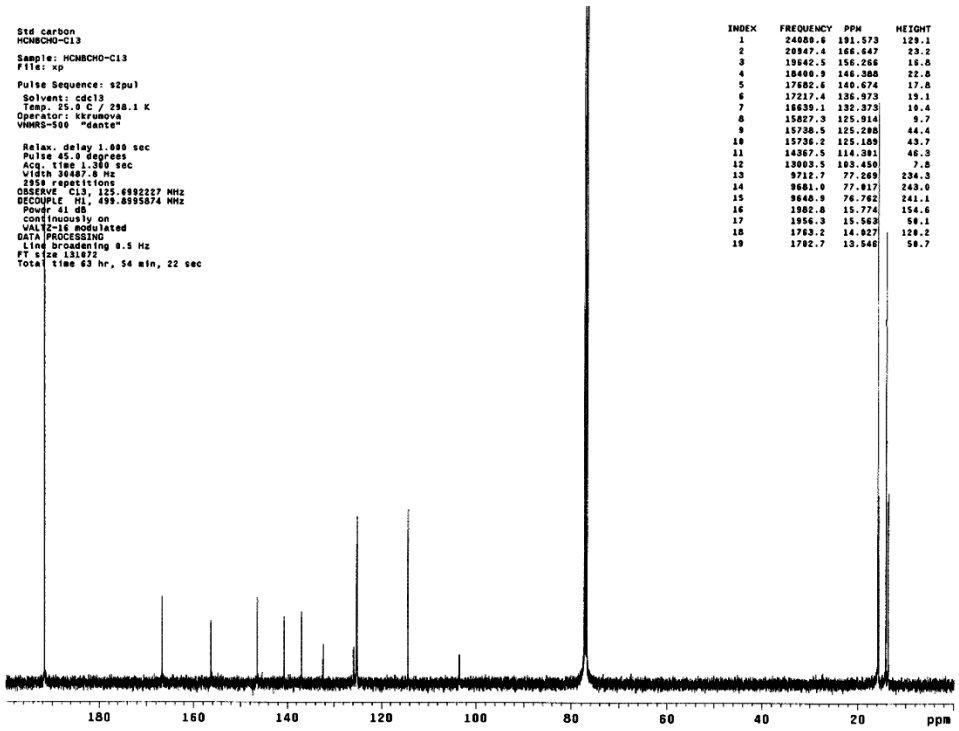

8-Formyl-2,6-dicyano-1,3,5,7-tetramethyl pyrromethene fluoroborate (**16**)

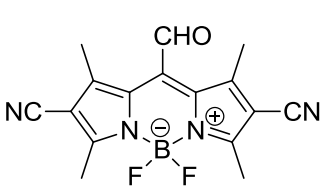

INDEX	FREQUENCY	PPM	HEIGHT
1	5297.7	10.598	14.1
2	3634.2	7.270	17.1
3	1366.6	2.734	69.6
4	1179.1	2.359	75.6

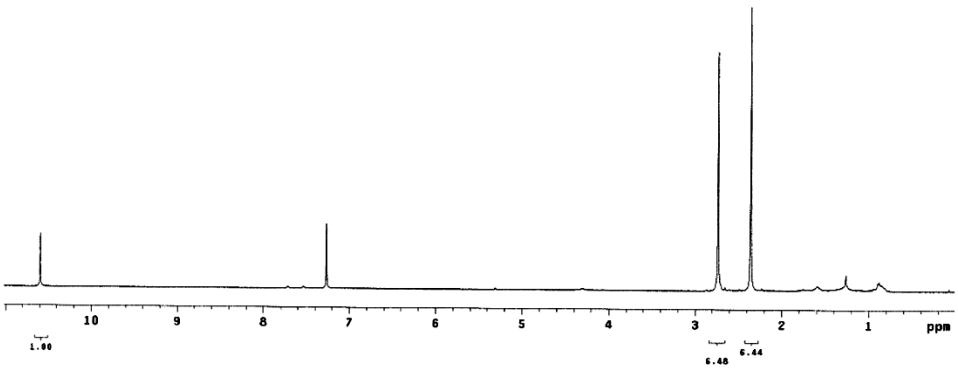

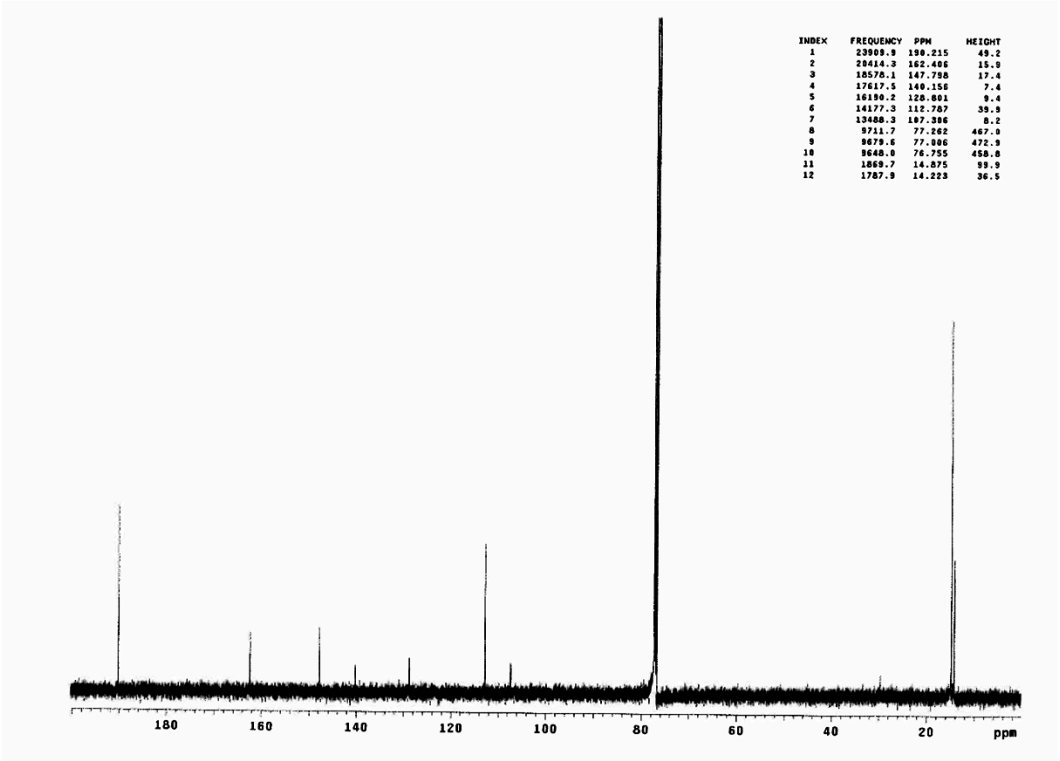

INDEX	FREQUENCY	PPM	HEIGHT
1	23909.9	190.215	49.2
2	20414.3	162.406	15.0
3	18570.1	147.758	17.4
4	17617.5	140.156	7.4
5	16190.2	128.801	9.4
6	14177.3	112.787	39.9
7	13488.3	107.306	8.2
8	9711.7	77.262	467.9
9	9679.6	77.006	472.9
10	9648.0	76.755	458.8
11	1869.7	14.875	99.9
12	1787.9	14.223	36.5

8-(N-butyl)-methylimine-2,6-diethyl-1,3,5,7-tetramethyl pyrromethene fluoroborate (**20**)

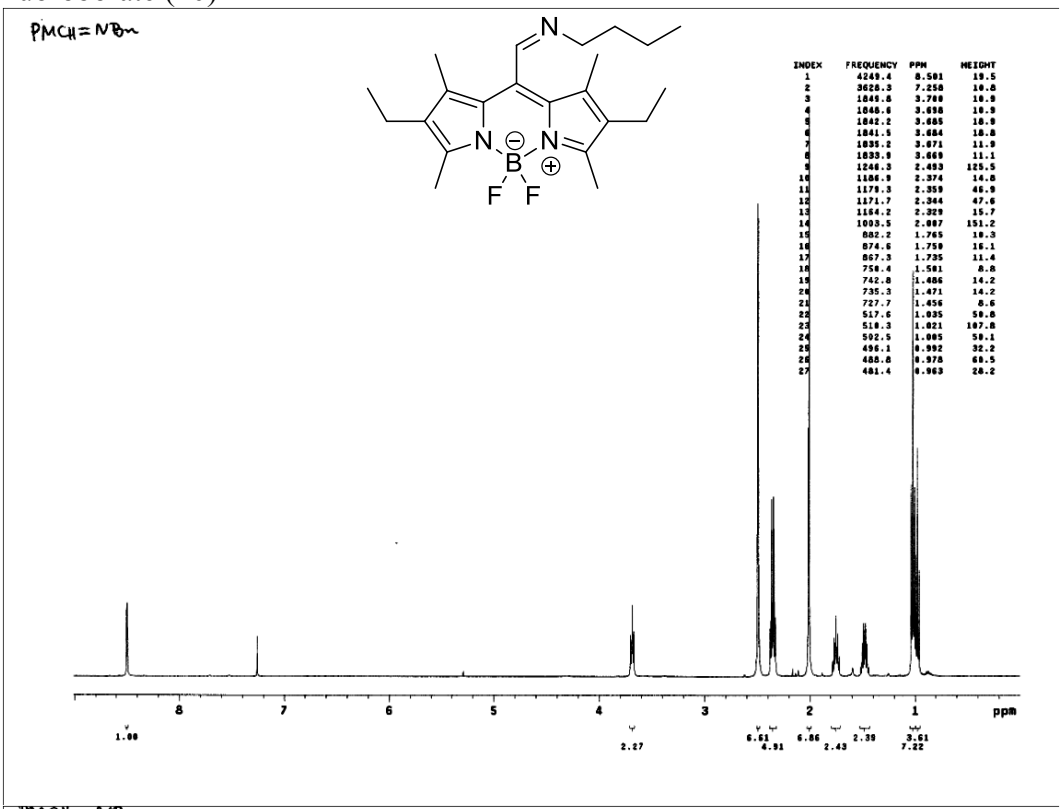

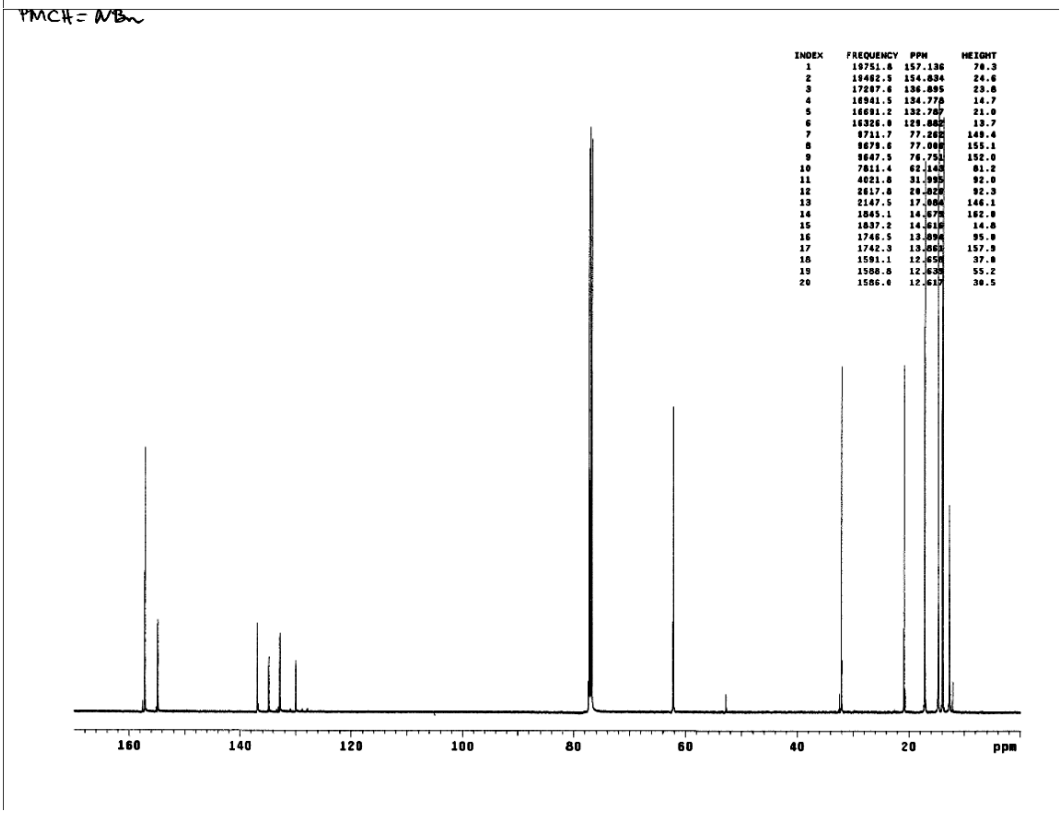

8-(N-butyl)-methylimine-2-chloro-1,3,5,7-tetramethyl pyrromethene fluoroborate (**21**)

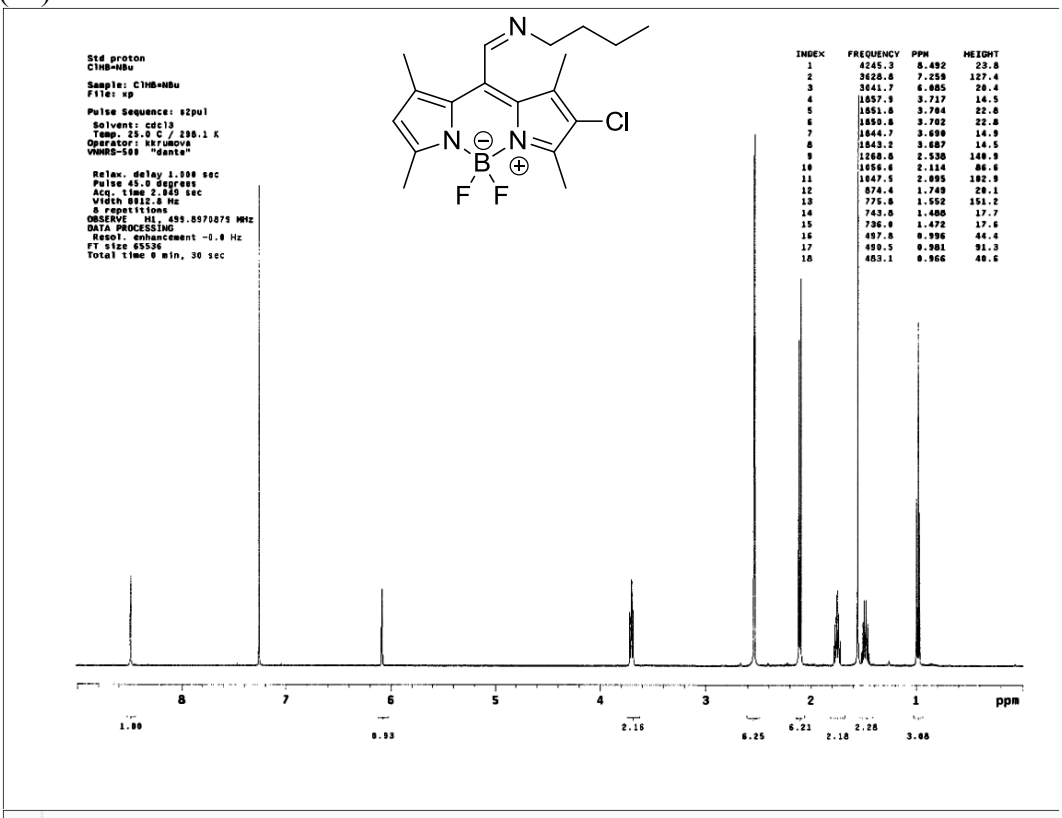

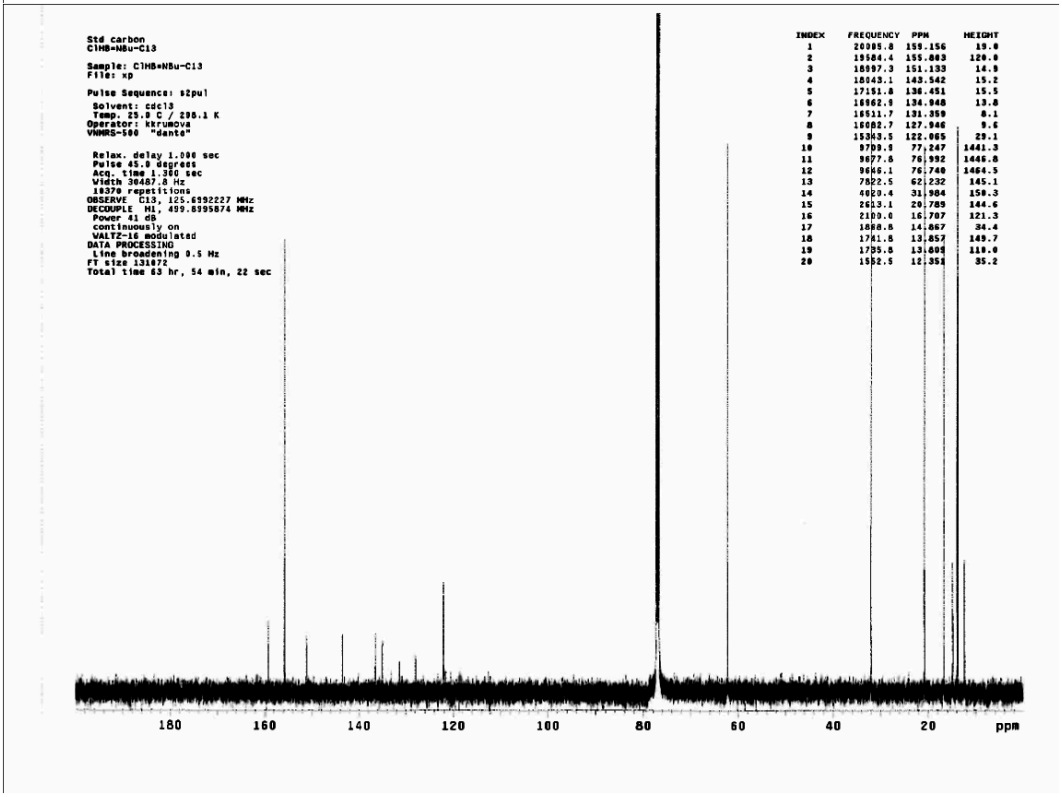

8-(N-butyl)-methylamine-2,6-diethyl-1,3,5,7-tetramethyl pyrromethene fluoroborate (**22**)

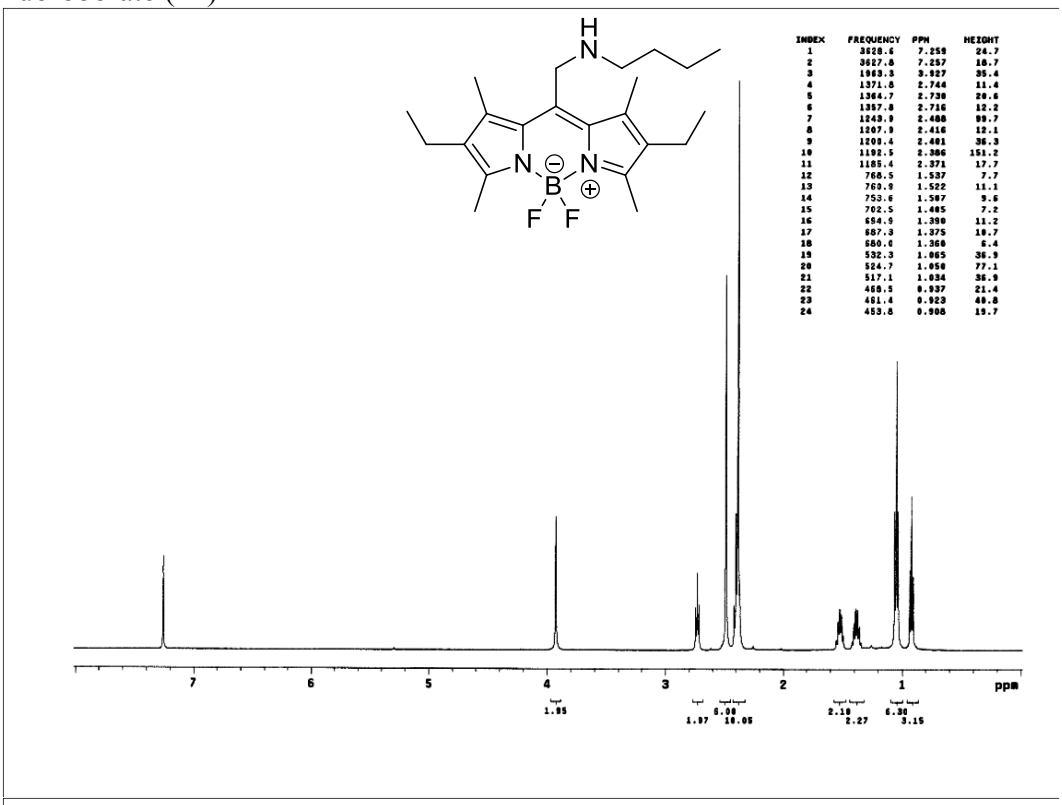

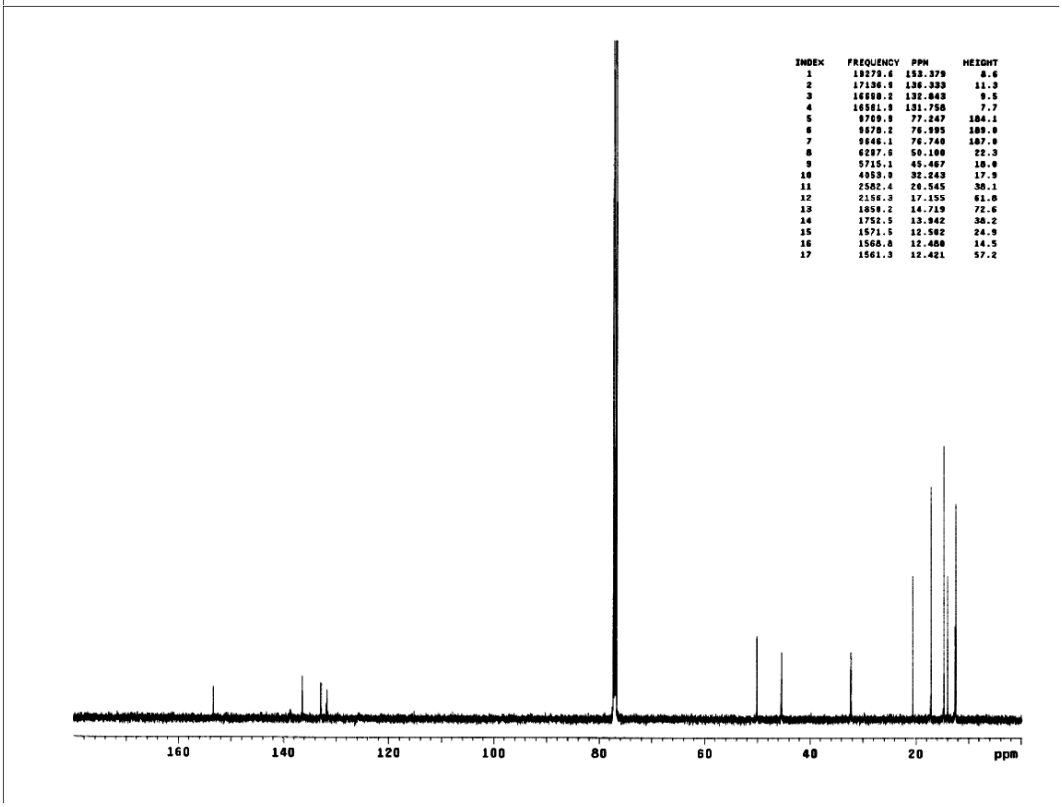

8-(N-butyl)-methylamine-2-chloro-1,3,5,7-tetramethyl pyrromethene fluoroborate (**23**)

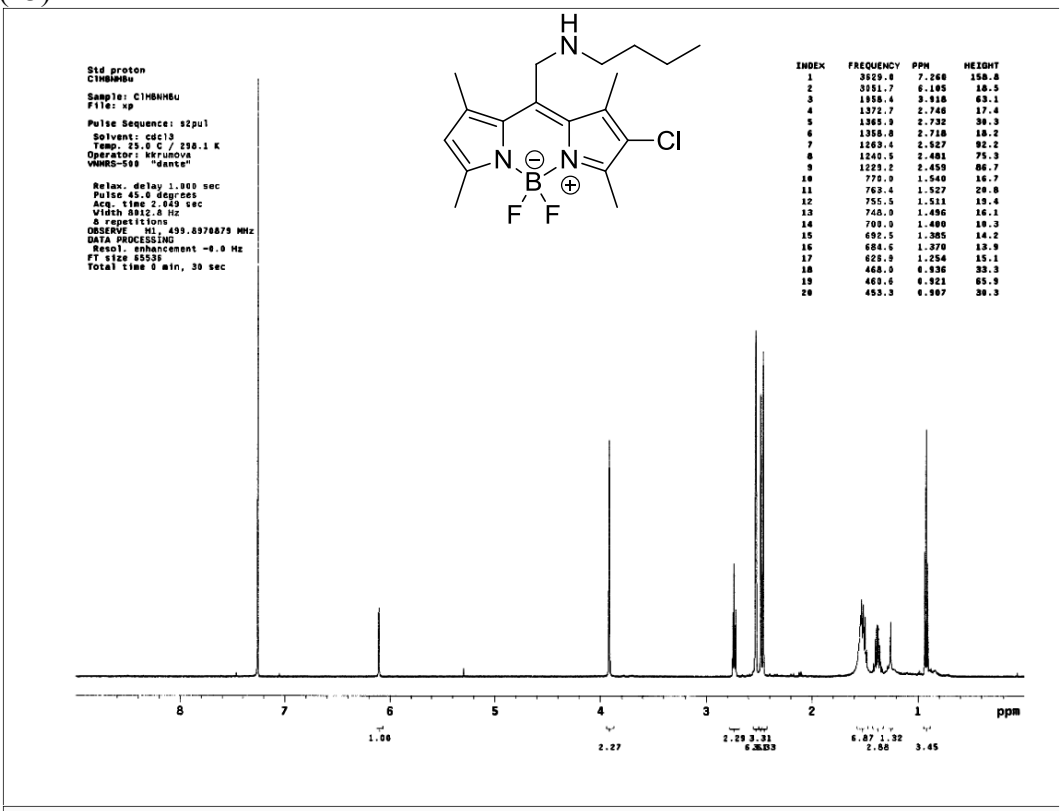

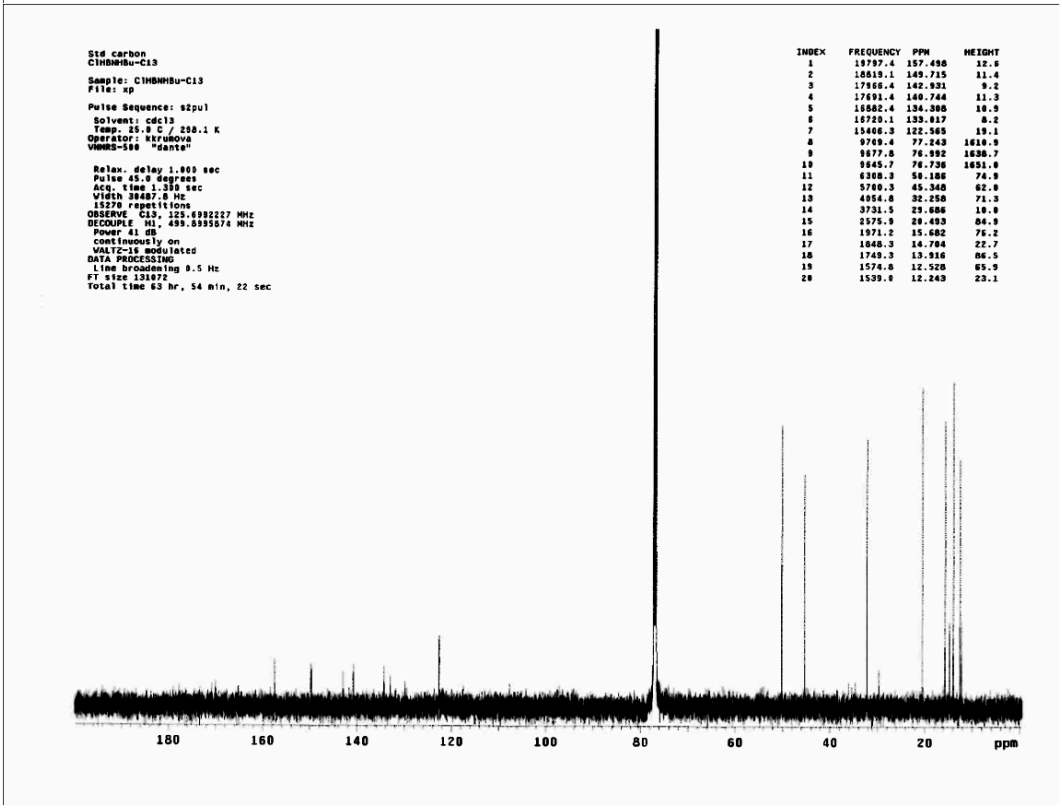

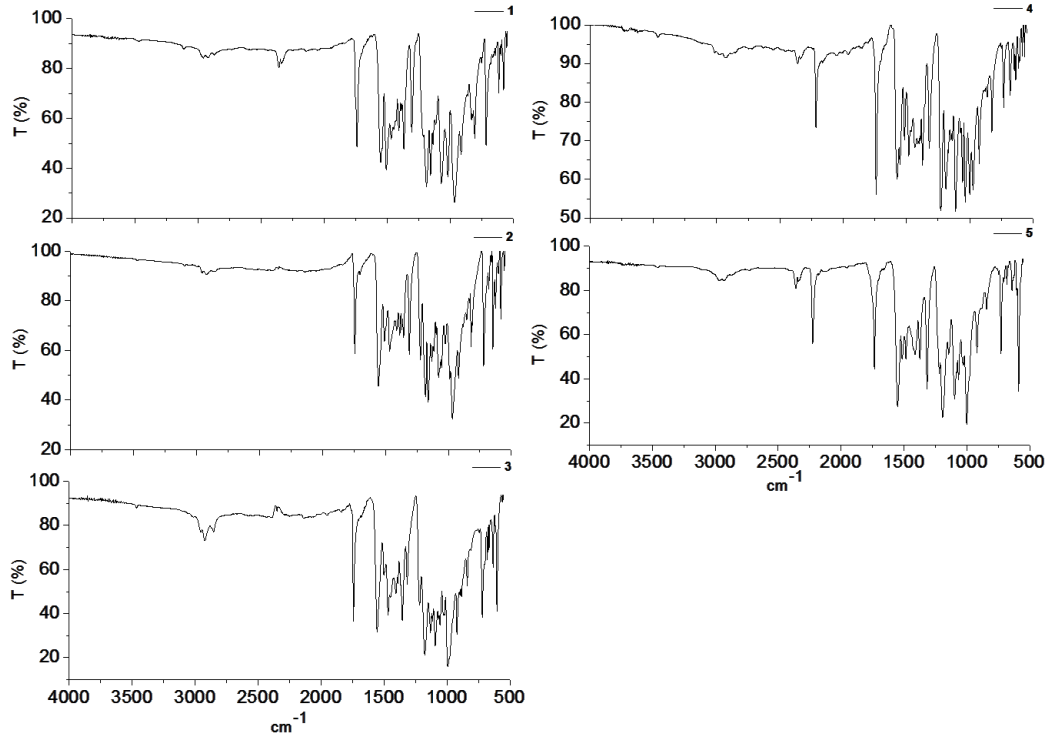
1
2
3
4
5
T (%)
cm-1
4000 3500 3000 2500 2000 1500 1000 500

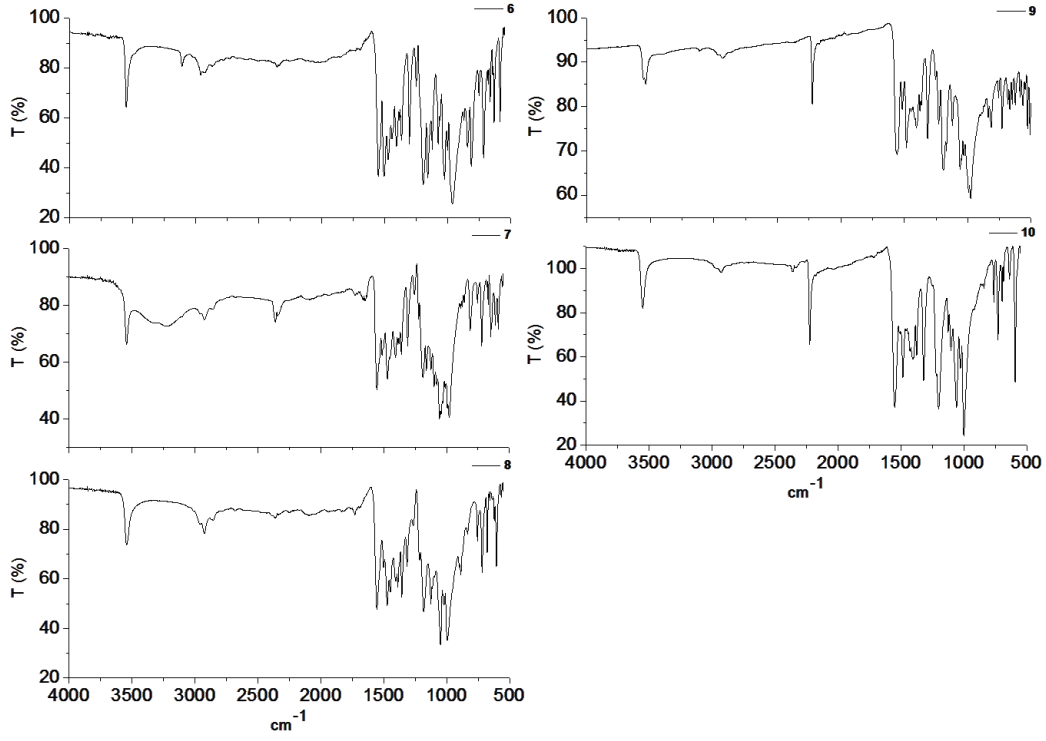
6
7
8
9
10
T (%)
cm-1
4000 3500 3000 2500 2000 1500 1000 500

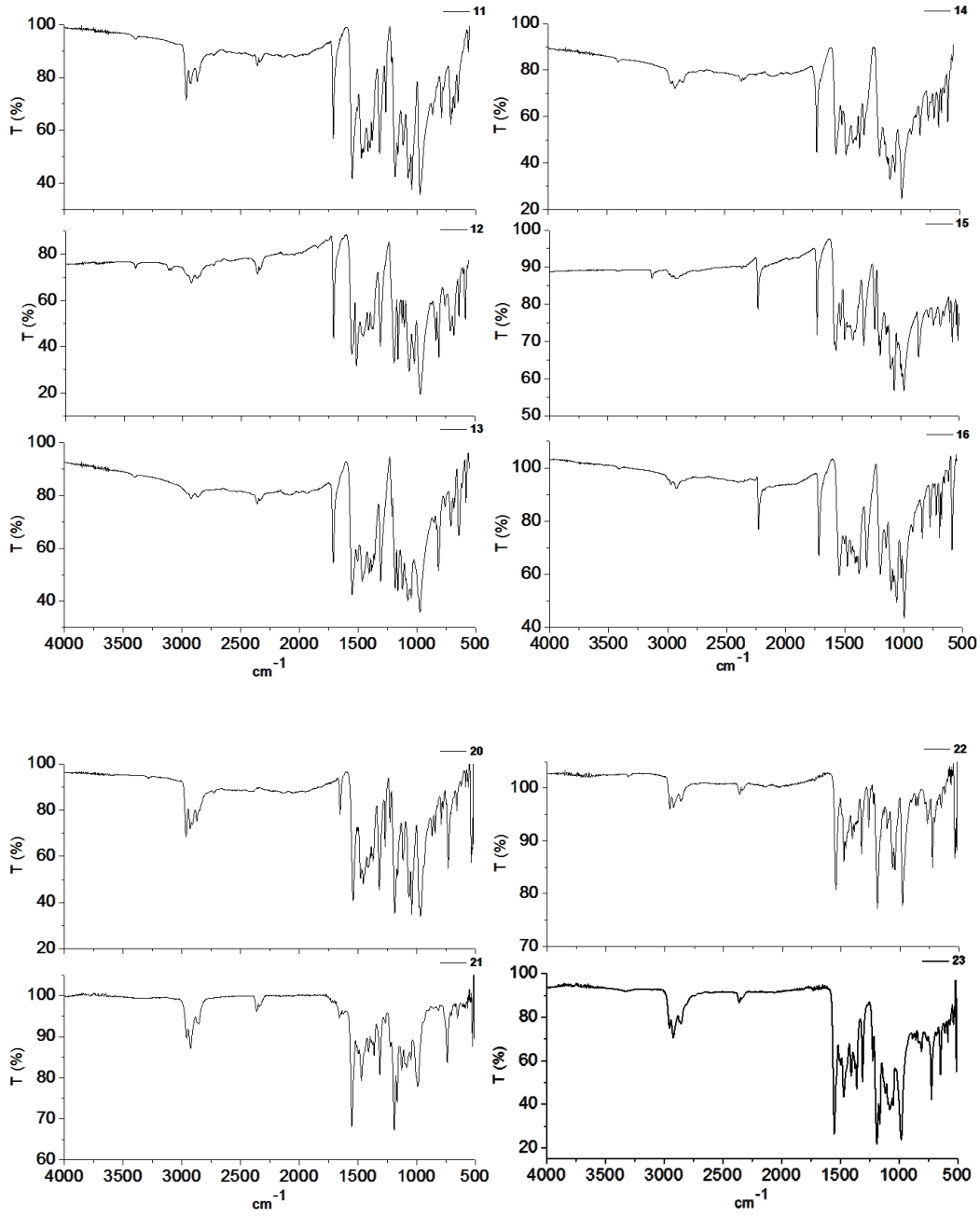
11
12
13
14
15
16
20
21
22
23
T (%)
cm-1
4000 3500 3000 2500 2000 1500 1000 500

8.3. Appendix Chapter 5

Table A5.1. Lipids used in this study.

Lipid	Structure	Transition Temperature
L-α-phosphocholine (EggPC)	natural mixture containing saturated, unsaturated and polyunsaturated fatty acids, mostly 16:0 and 18:1-cis-9	
1,2-dilinoleoyl-*sn*-glycero-3-phosphocholine (DLPC)	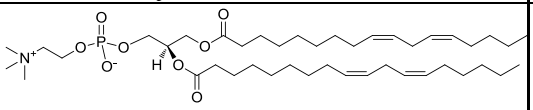 18:2-cis-9, cis-12 polyunsaturated fatty acids	-53°C
1,2-dioleoyl-*sn*-glycero-3-phosphocholine (DOPC)	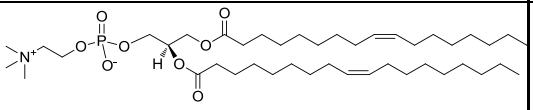 18:1-cis-9 unsaturated fatty acids	-20°C
1-palmitoyl-2-oleoyl-*sn*-glycero-3-phosphocholine (POPC)	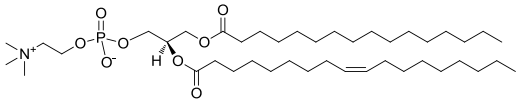 16:0 saturated and 18:1-cis-9 unsaturated fatty acid	2°C
1,2-dimyristoyl-*sn*-glycero-3-phosphocholine (DMPC)	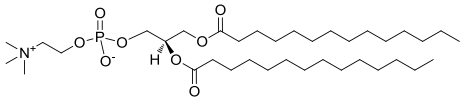 14:0 saturated fatty acids	23°C
1,2-dipalmitoyl-*sn*-glycero-3-phosphocholine (DPPC)	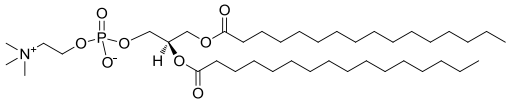 16:0 saturated fatty acids	41°C

EggPC and H_2B-PMHC

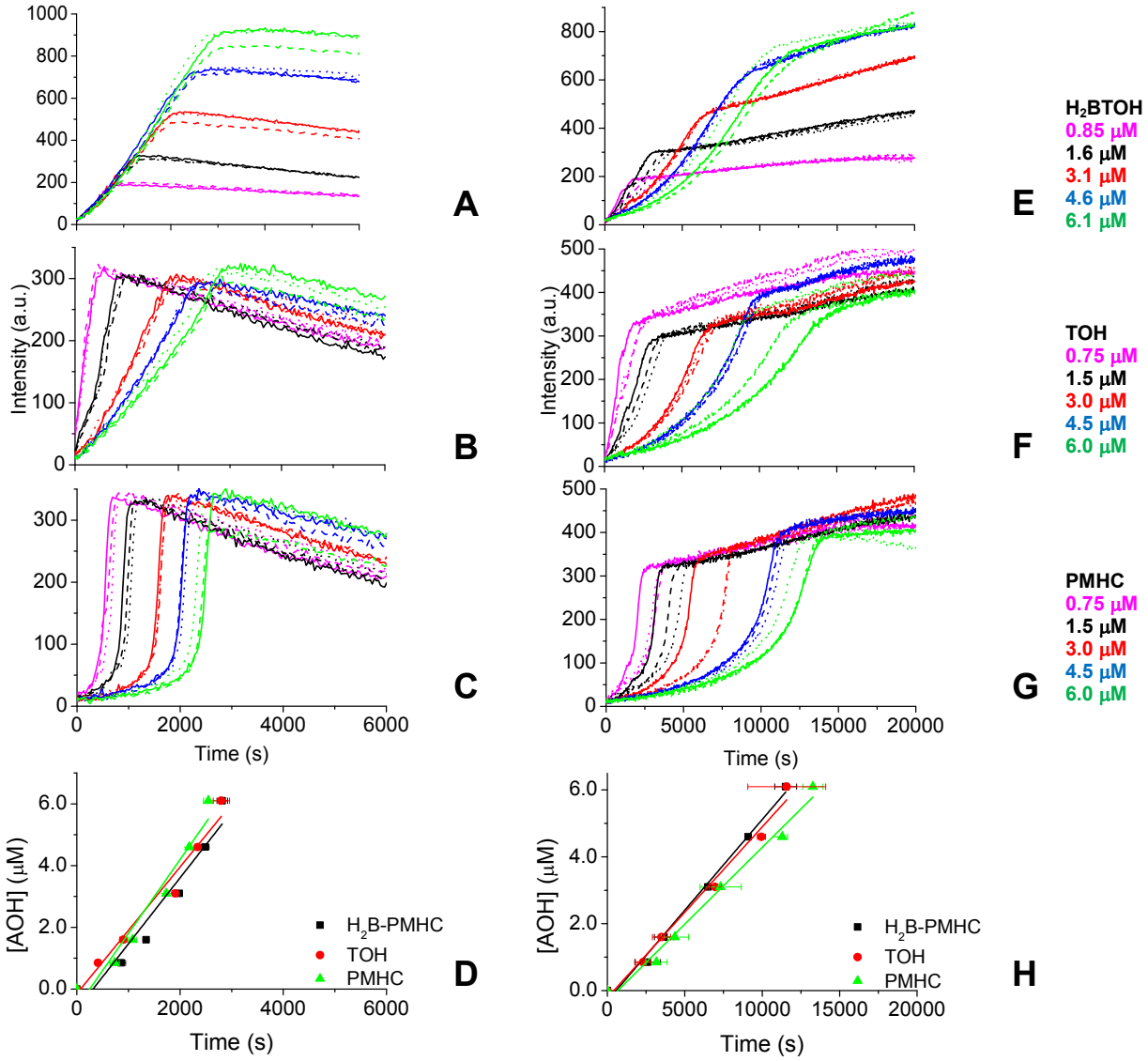

Figure A5.1. Fluorescence intensity-time profiles recorded in triplicates in 1 mM EggPC and $9x10^{-3}$ M ABAP solutions with increasing concentrations (see figure captions for the values) of A) H_2B-PMHC B) TOH + 0.1 μM H_2B-PMHC and C) PMHC + 0.1 μM H_2B-PMHC. D) Increasing antioxidant concentration vs. time required for its consumption (τ). Panels E to H show similar data acquired with $2x10^{-4}$ M MeO-AMVN.

DLPC and H_2B-PMHC

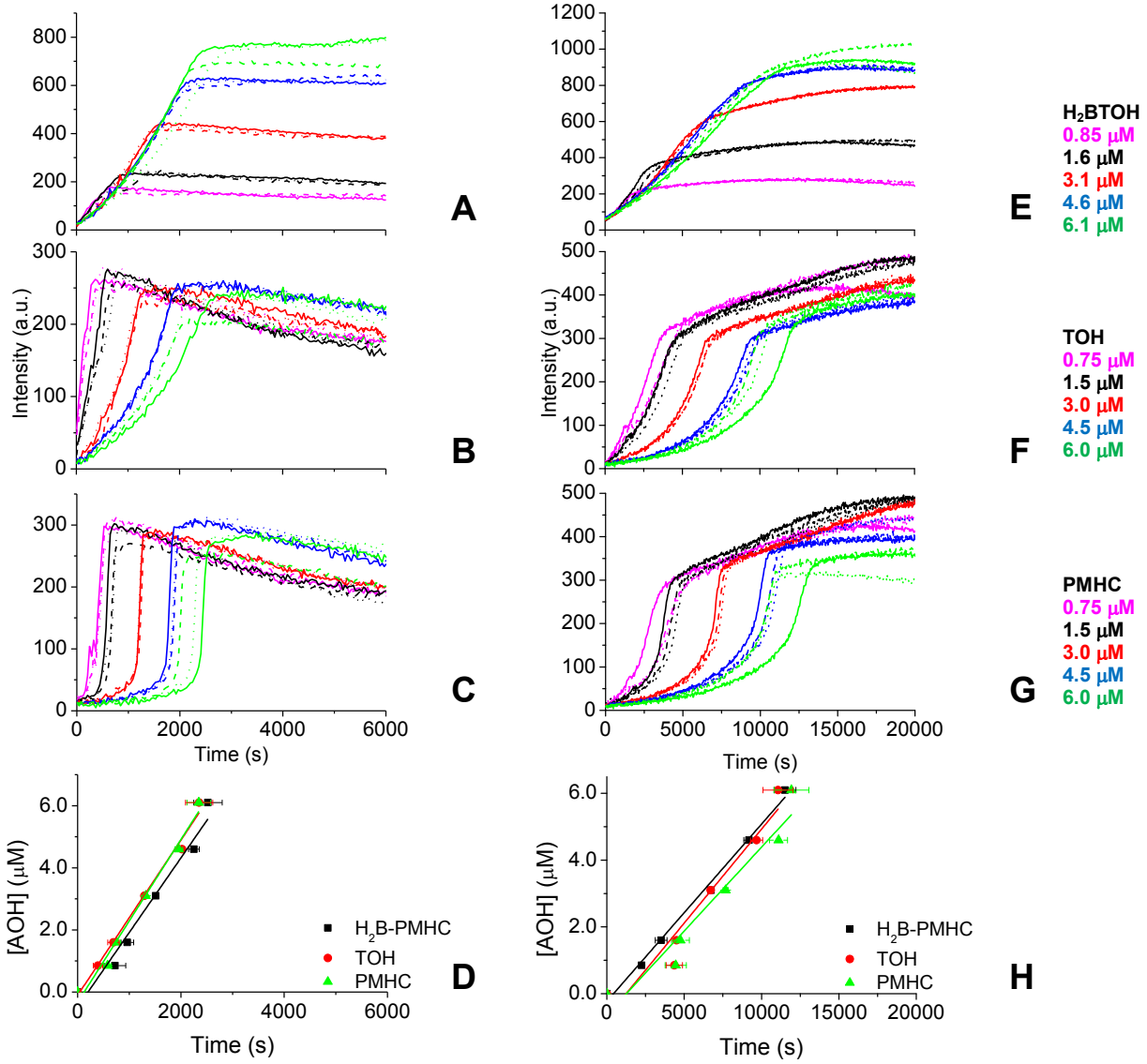

Figure A5.2. Fluorescence intensity-time profiles recorded in triplicates in 1 mM DLPC and $9x10^{-3}$ M ABAP solutions with increasing concentrations (see figure captions for the values) of A) H_2B-PMHC B) TOH + 0.1 μM H_2B-PMHC and C) PMHC + 0.1 μM H_2B-PMHC. D) Increasing antioxidant concentration vs. time required for its consumption (τ). Panels E to H show similar data acquired with $2x10^{-4}$ M MeO-AMVN.

DOPC and H_2B-PMHC

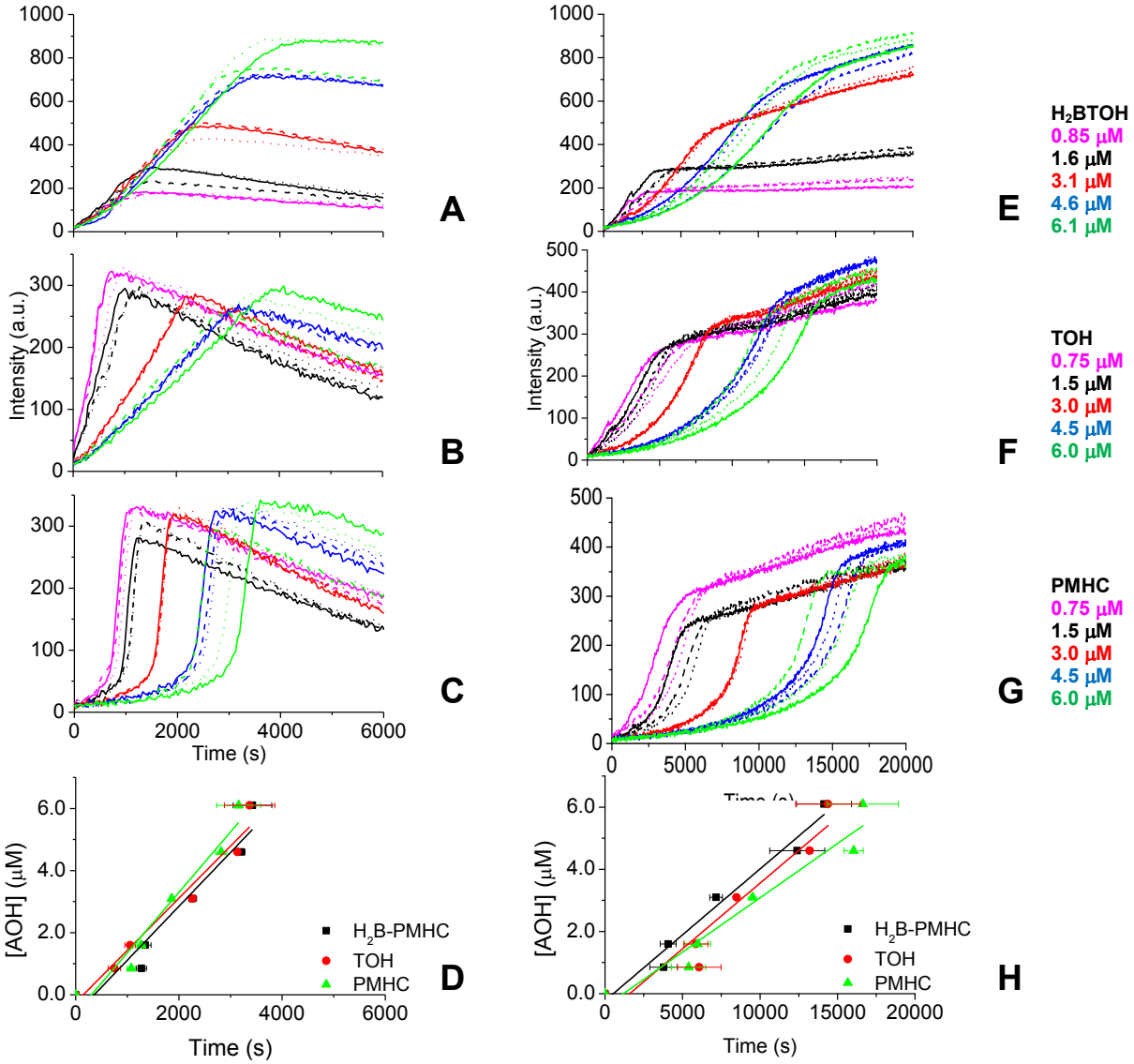

Figure A5.3. Fluorescence intensity-time profiles recorded in triplicates in 1 mM DOPC and $9x10^{-3}$ M ABAP solutions with increasing concentrations (see figure captions for the values) of A) H_2B-PMHC B) TOH + 0.1 μM H_2B-PMHC and C) PMHC + 0.1 μM H_2B-PMHC. D) Increasing antioxidant concentration vs. time required for its consumption (τ). Panels E to H show similar data acquired with $2x10^{-4}$ M MeO-AMVN.

POPC and H_2B-PMHC

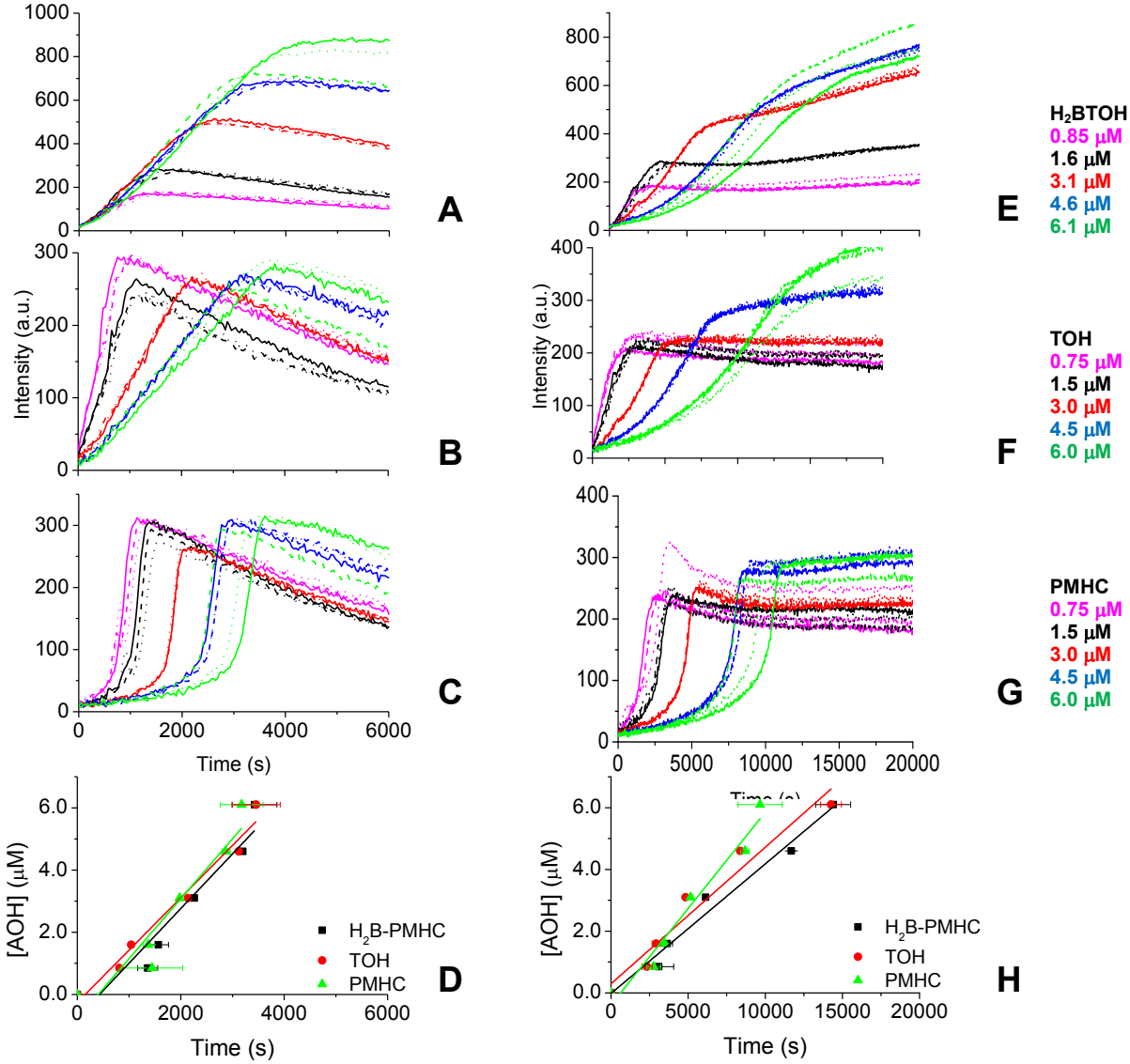

Figure A5.4. Fluorescence intensity-time profiles recorded in triplicates in 1 mM POPC and $9x10^{-3}$ M ABAP solutions with increasing concentrations (see figure captions for the values) of A) H_2B-PMHC B) TOH + 0.1 μM H_2B-PMHC and C) PMHC + 0.1 μM H_2B-PMHC. D) Increasing antioxidant concentration vs. time required for its consumption (τ). Panels E to H show similar data acquired with $2x10^{-4}$ M MeO-AMVN.

DMPC and H_2B-PMHC

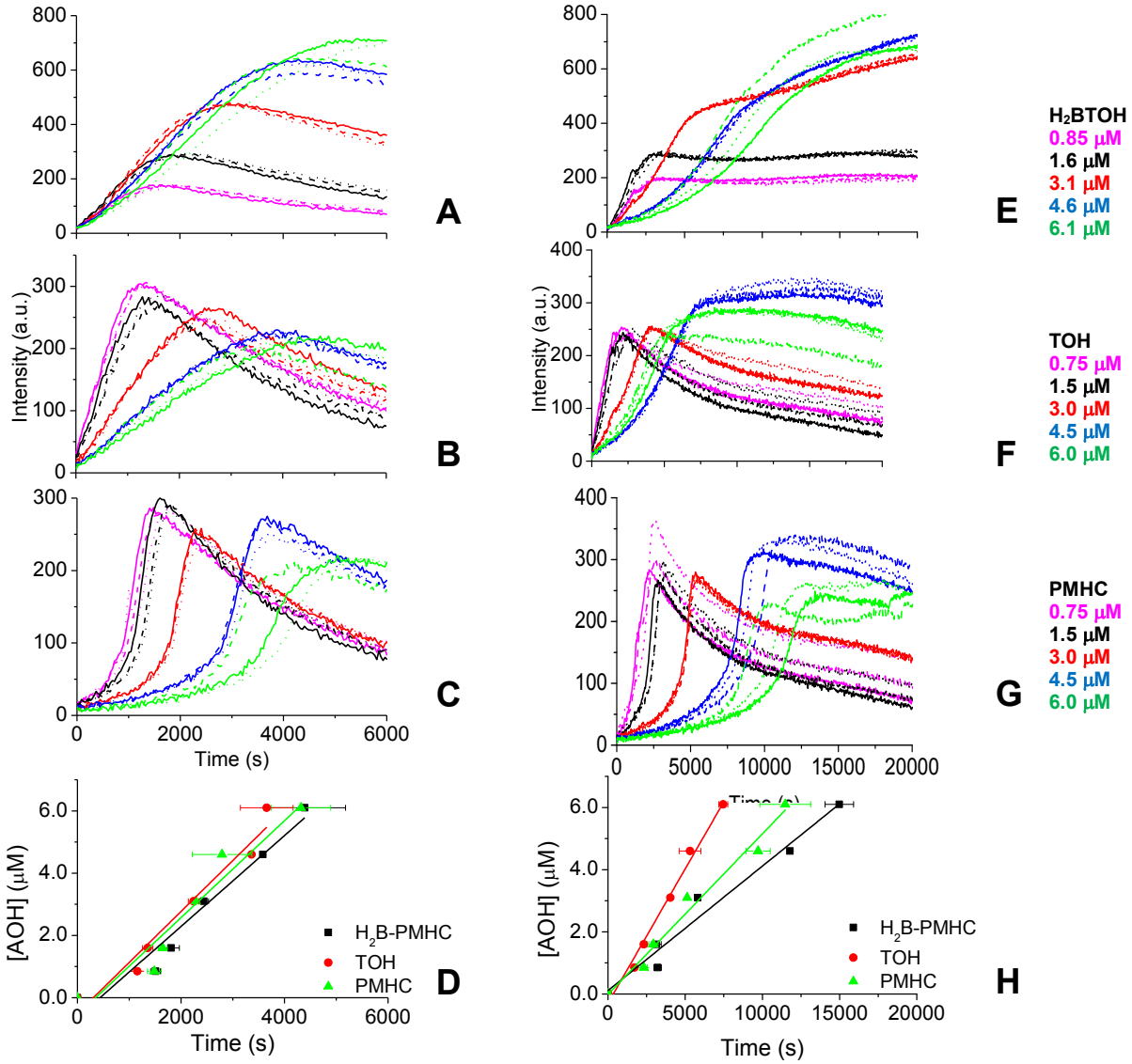

Figure A5.5. Fluorescence intensity-time profiles recorded in triplicates in 1 mM DMPC and $9x10^{-3}$ M ABAP solutions with increasing concentrations (see figure captions for the values) of A) H_2B-PMHC B) TOH + 0.1 μM H_2B-PMHC and C) PMHC + 0.1 μM H_2B-PMHC. D) Increasing antioxidant concentration vs. time required for its consumption (τ). Panels E to H show similar data acquired with $2x10^{-4}$ M MeO-AMVN.

DPPC and H_2B-PMHC

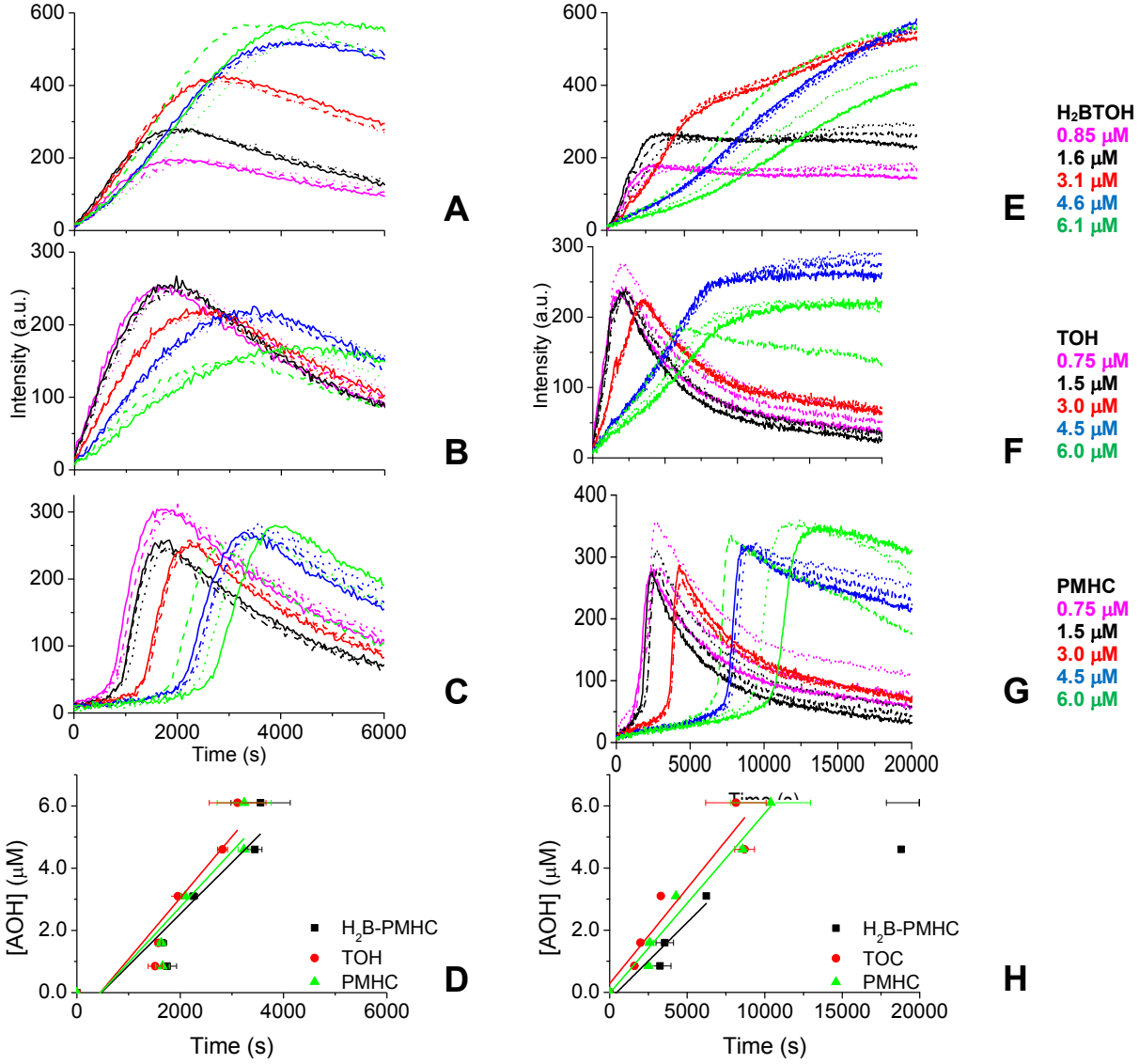

Figure A5.6. Fluorescence intensity-time profiles recorded in triplicates in 1 mM DPPC and $9x10^{-3}$ M ABAP solutions with increasing concentrations (see figure captions for the values) of A) H_2B-PMHC B) TOH + 0.1 μM H_2B-PMHC and C) PMHC + 0.1 μM H_2B-PMHC. D) Increasing antioxidant concentration vs. time required for its consumption (τ). Panels E to H show similar data acquired with $2x10^{-4}$ M MeO-AMVN.

EggPC and H_2B-TOH

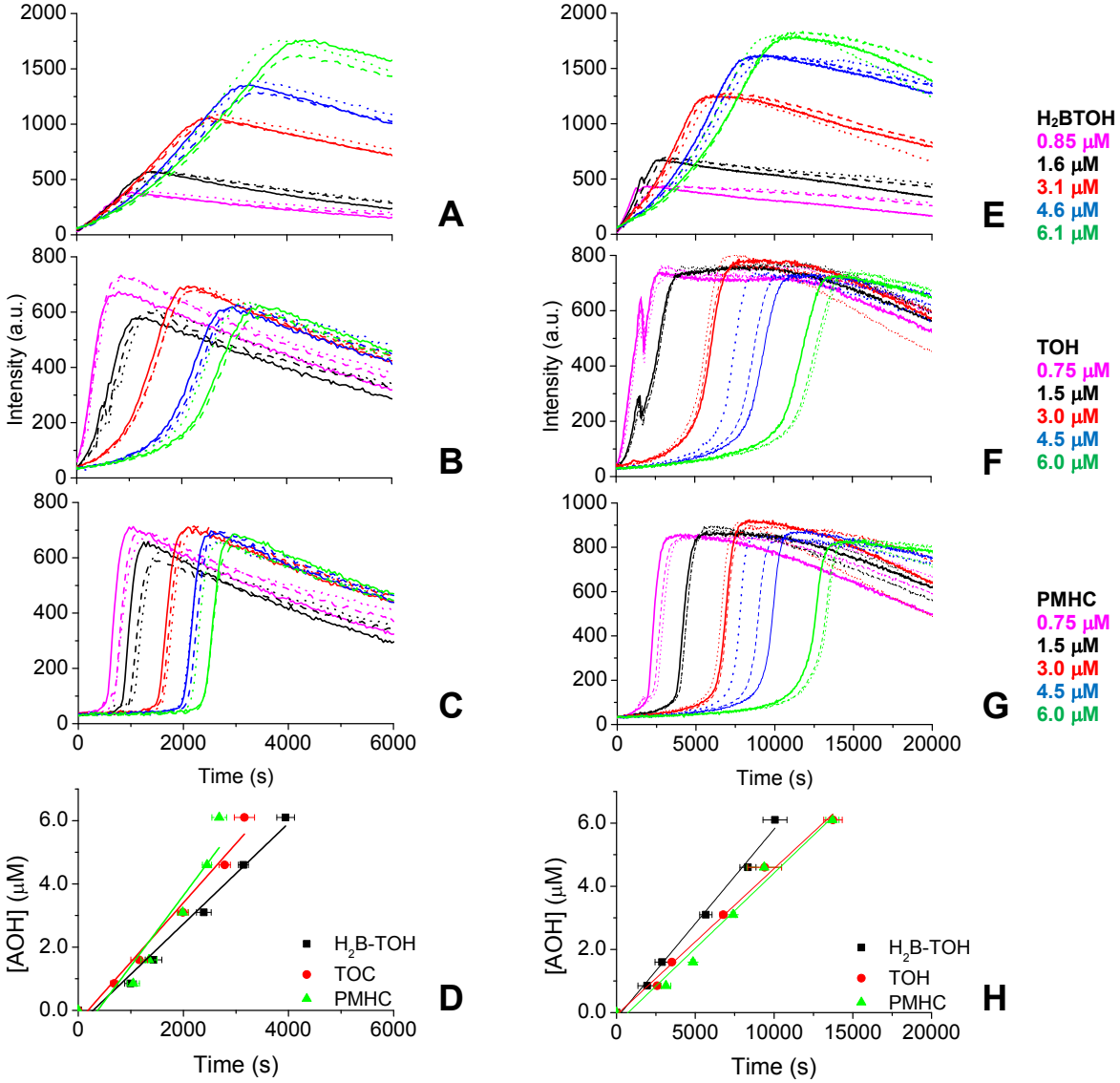

Figure A5.7. Fluorescence intensity-time profiles recorded in triplicates in 1 mM EggPC and $9x10^{-3}$ M ABAP solutions with increasing concentrations (see figure captions for the values) of A) H_2B-TOH B) TOH + 0.1 μM H_2B-TOH and C) PMHC + 0.1 μM H_2B-TOH. D) Increasing antioxidant concentration vs. time required for its consumption (τ). Panels E to H show similar data acquired with $2x10^{-4}$ M MeO-AMVN.

DLPC and H_2B-TOH

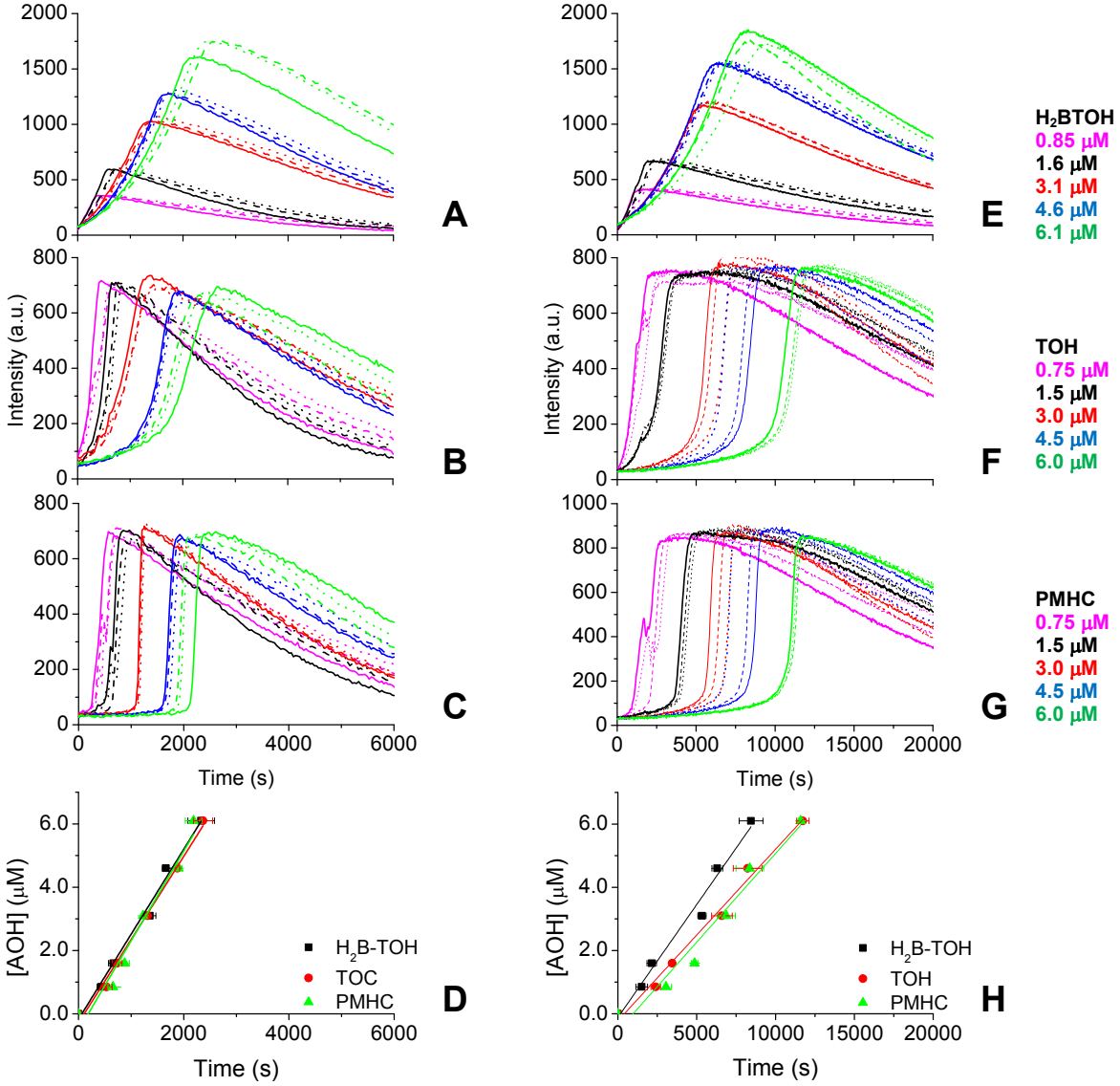

Figure A5.8. Fluorescence intensity-time profiles recorded in triplicates in 1 mM DLPC and $9x10^{-3}$ M ABAP solutions with increasing concentrations (see figure captions for the values) of A) H_2B-TOH B) TOH + 0.1 μM H_2B-TOH and C) PMHC + 0.1 μM H_2B-TOH. D) Increasing antioxidant concentration vs. time required for its consumption (τ). Panels E to H show similar data acquired with $2x10^{-4}$ M MeO-AMVN.

DOPC and H_2B-TOH

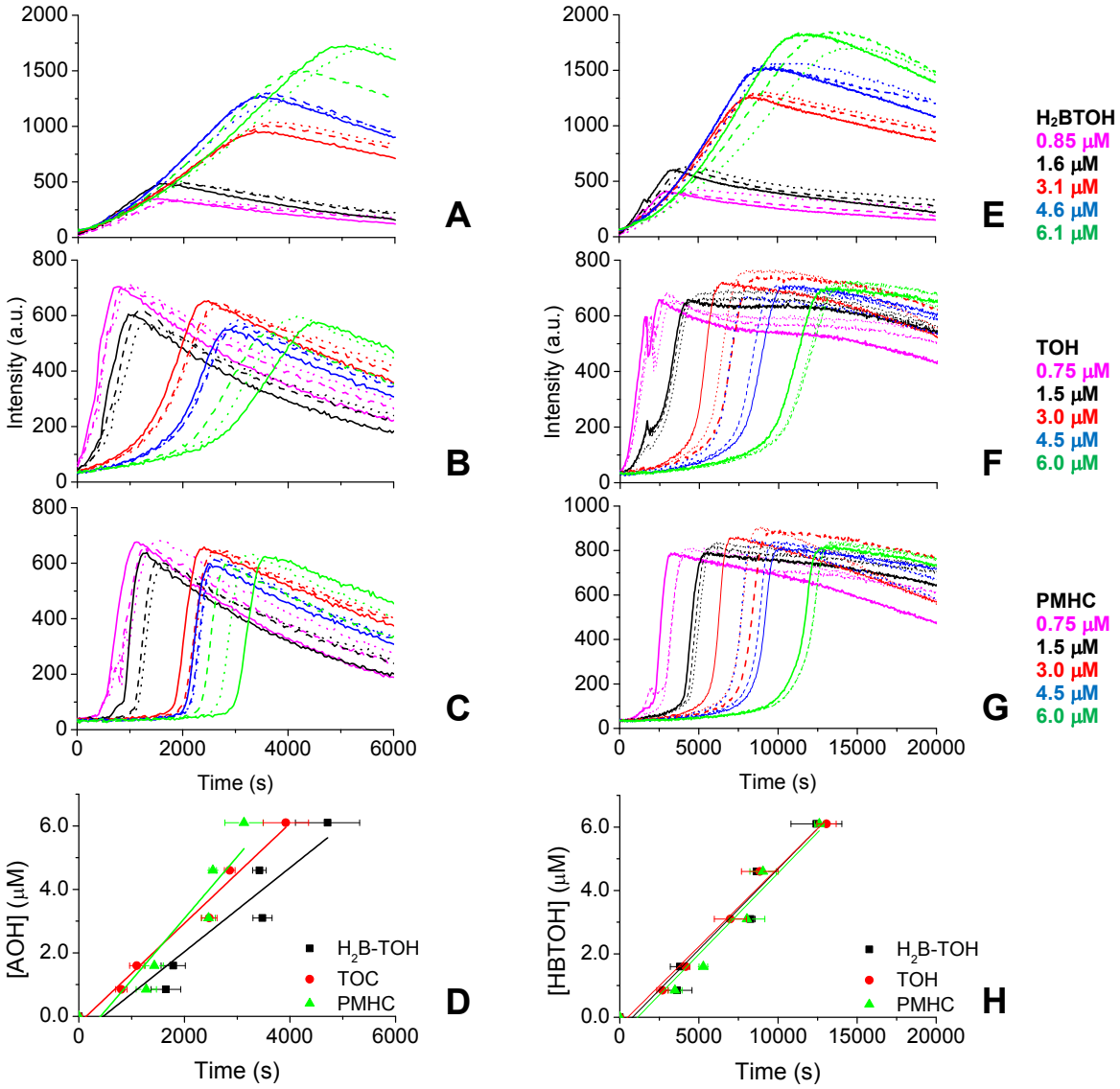

Figure A5.9. Fluorescence intensity-time profiles recorded in triplicates in 1 mM DOPC and $9x10^{-3}$ M ABAP solutions with increasing concentrations (see figure captions for the values) of A) H_2B-TOH B) TOH + 0.1 μM H_2B-TOH and C) PMHC + 0.1 μM H_2B-TOH. D) Increasing antioxidant concentration vs. time required for its consumption (τ). Panels E to H show similar data acquired with $2x10^{-4}$ M MeO-AMVN.

POPC and H_2B-TOH

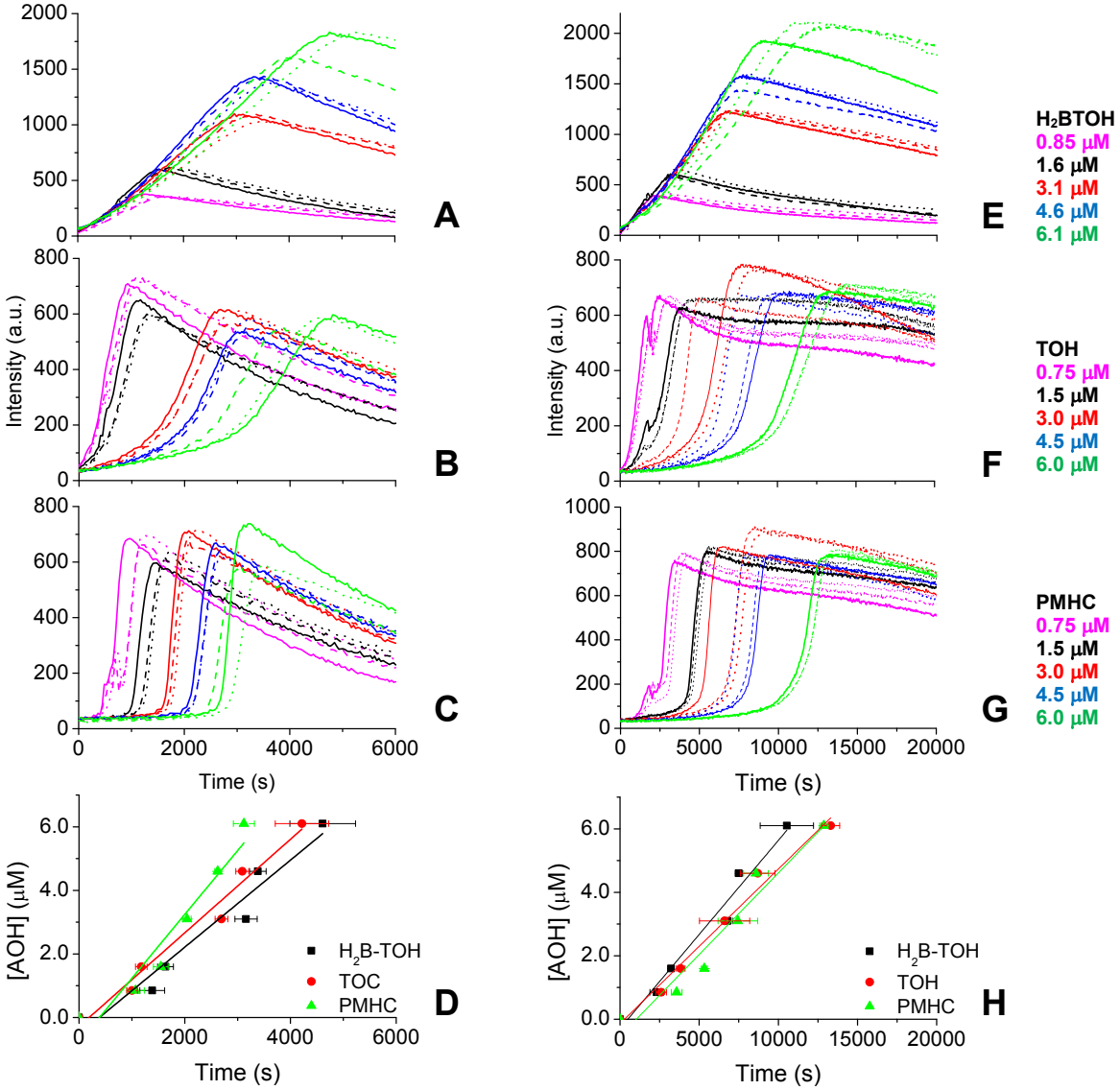

Figure A5.10. Fluorescence intensity-time profiles recorded in triplicates in 1 mM POPC and $9x10^{-3}$ M ABAP solutions with increasing concentrations (see figure captions for the values) of A) H_2B-TOH B) TOH + 0.1 μM H_2B-TOH and C) PMHC + 0.1 μM H_2B-TOH. D) Increasing antioxidant concentration vs. time required for its consumption (τ). Panels E to H show similar data acquired with $2x10^{-4}$ M MeO-AMVN.

DMPC and H_2B-TOH

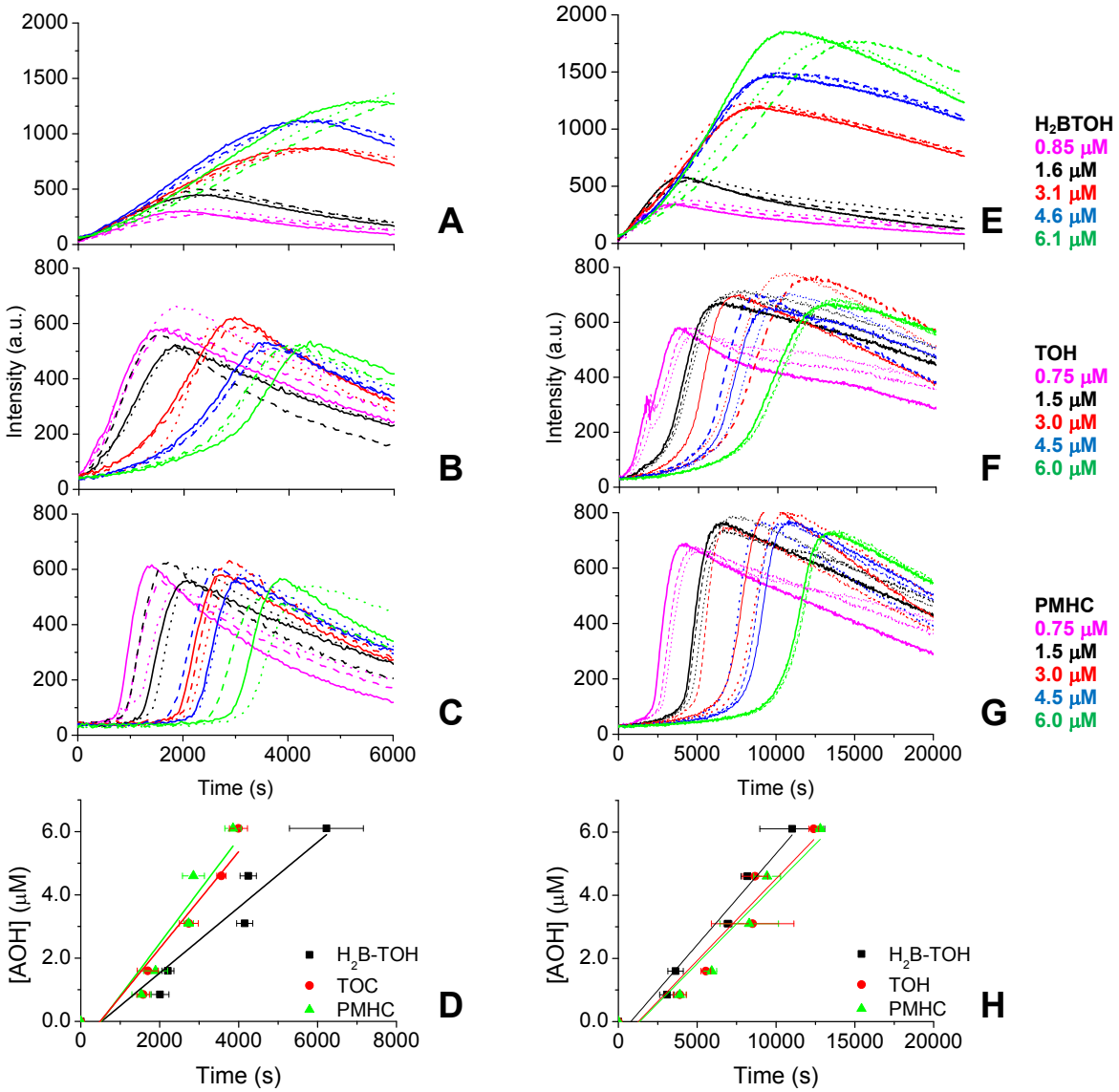

Figure A5.11. Fluorescence intensity-time profiles recorded in triplicates in 1 mM DMPC and $9x10^{-3}$ M ABAP solutions with increasing concentrations (see figure captions for the values) of A) H_2B-TOH B) TOH + 0.1 μM H_2B-TOH and C) PMHC + 0.1 μM H_2B-TOH. D) Increasing antioxidant concentration vs. time required for its consumption (τ). Panels E to H show similar data acquired with $2x10^{-4}$ M MeO-AMVN.

DPPC and H_2B-TOH

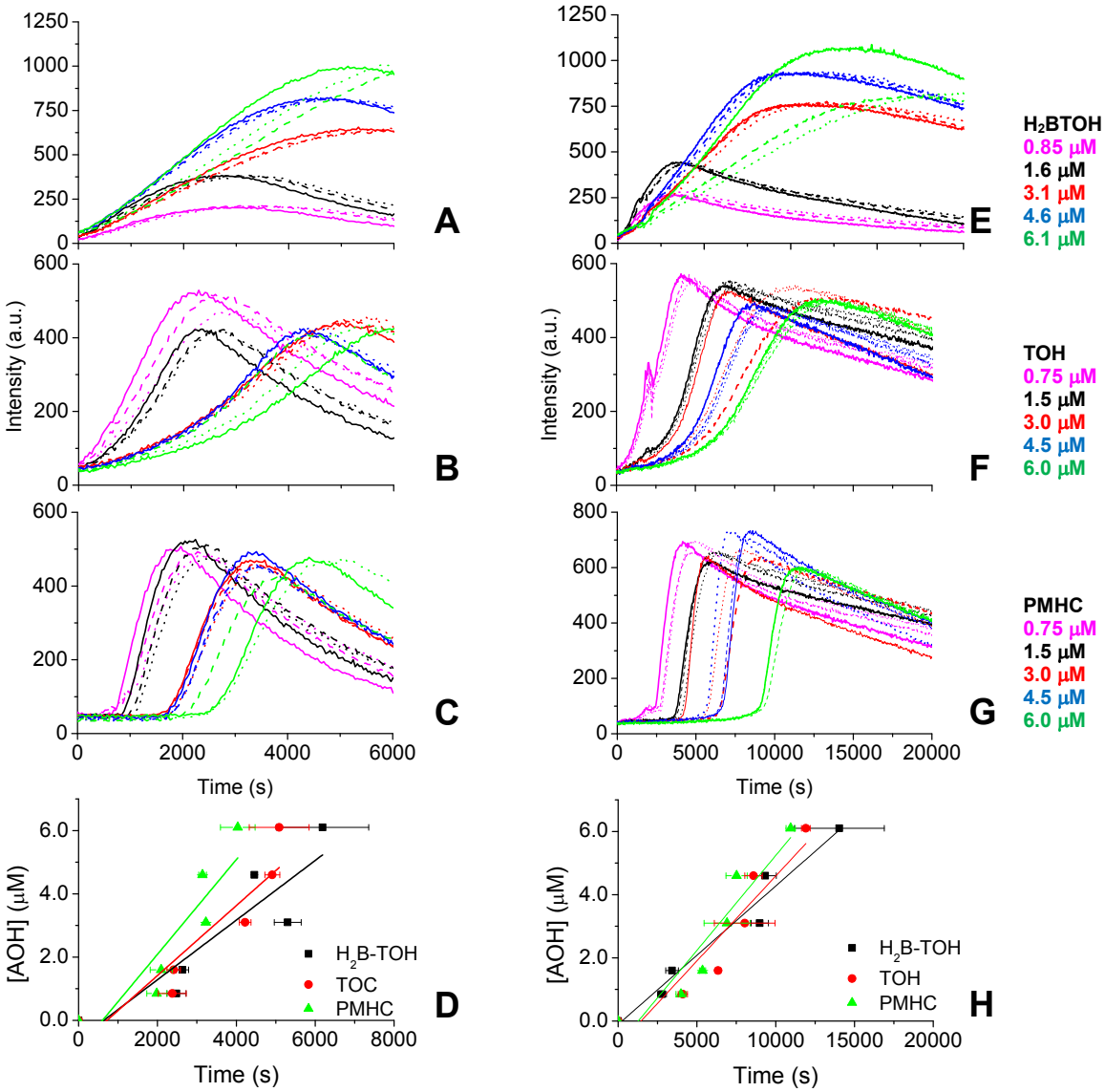

Figure A5.12. Fluorescence intensity-time profiles recorded in triplicates in 1 mM DPPC and $9x10^{-3}$ M ABAP solutions with increasing concentrations (see figure captions for the values) of A) H_2B-TOH B) TOH + 0.1 μM H_2B-TOH and C) PMHC + 0.1 μM H_2B-TOH. D) Increasing antioxidant concentration vs. time required for its consumption (τ). Panels E to H show similar data acquired with $2x10^{-4}$ M MeO-AMVN.

HBTOH-H1

No.	(ppm)	(Hz)	Height
1	1.55	773.9	0.3915
2	1.63	816.2	0.9821
3	1.93	965.7	0.6904
4	1.95	973.5	0.6653
5	2.01	1002.6	0.6831
6	2.14	1067.6	0.2796
7	2.45	1225.4	0.0937
8	2.47	1234.4	0.1708
9	2.52	1261.8	1.0000
10	4.29	2143.8	0.0854

No.	(ppm)	(Hz)	Height
11	4.29	2145.8	0.1465
12	4.30	2148.0	0.0796
13	5.08	2540.7	0.1538
14	5.11	2553.0	0.1850
15	5.30	2649.3	0.1882
16	5.33	2664.2	0.1873
17	5.35	2676.2	0.1541
18	6.01	3003.2	0.2829
19	7.26	3628.7	0.9256

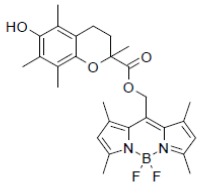

H2BTOH-C13

No.	(ppm)	(Hz)	Height
1	11.03	832.4	0.2172
2	11.54	870.5	0.2266
3	12.05	909.2	0.2462
4	14.67	1107.2	0.1978
5	15.29	1153.6	0.4913
6	21.03	1586.5	0.2598
7	25.61	1932.6	0.3856
8	30.95	2335.1	0.2852
9	57.67	4351.4	0.2777
10	76.59	5778.9	1.9482
11	77.01	5811.0	2.0000
12	77.21	5825.9	0.0805
13	77.44	5843.1	1.9604

No.	(ppm)	(Hz)	Height
14	116.73	8808.1	0.2094
15	118.97	8977.3	0.1388
16	121.77	9188.5	0.1681
17	122.11	9213.9	0.1842
18	122.90	9273.6	0.1665
19	132.31	9983.5	0.0654
20	132.66	10010.1	0.1066
21	141.43	10671.8	0.1141
22	145.44	10974.3	0.1416
23	145.83	11004.1	0.1025
24	156.39	11800.8	0.1134
25	173.90	13121.6	0.1506

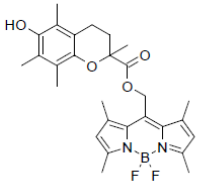

MeOTrolox-CO2Me-H1

No.	(ppm)	(Hz)	Height
1	1.64	820.6	0.7884
2	1.88	941.2	0.0429
3	1.89	945.3	0.0433
4	1.90	947.5	0.0452
5	1.91	952.4	0.0461
6	2.14	1067.8	0.5524
7	2.20	1101.4	0.5445
8	2.23	1113.6	0.5353
9	2.44	1220.2	0.0423

No.	(ppm)	(Hz)	Height
10	2.45	1223.4	0.0511
11	2.45	1226.6	0.0532
12	2.47	1236.6	0.0546
13	2.48	1239.0	0.0809
14	2.51	1256.4	0.0428
15	3.65	1822.5	0.9310
16	3.70	1850.4	1.0000
17	5.27	2632.9	0.1011

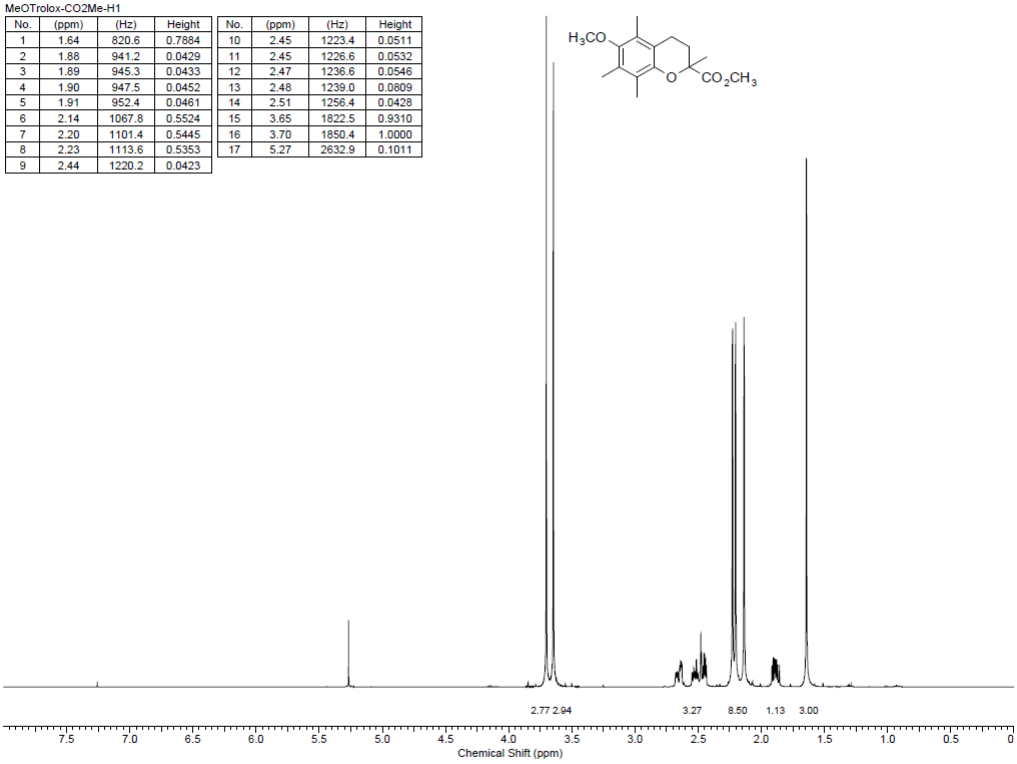

MeOTrolox-CO2Me-C13

No.	(ppm)	(Hz)	Height
1	11.63	1462.3	0.7083
2	11.81	1484.6	0.5572
3	12.55	1578.1	0.5430
4	20.86	2623.0	0.7000
5	25.44	3197.5	0.8401
6	30.48	3832.1	0.8568
7	52.28	6571.7	0.2490
8	52.31	6575.4	0.2736
9	60.23	7571.9	0.2462
10	60.26	7575.2	0.2837
11	76.95	9673.3	0.2836

No.	(ppm)	(Hz)	Height
12	77.13	9695.6	1.0000
13	77.20	9704.9	0.3083
14	77.45	9737.0	0.2853
15	117.12	14723.7	0.7493
16	122.84	15442.4	0.5890
17	125.63	15793.7	0.6579
18	128.02	16093.3	0.6005
19	147.66	18562.6	0.5147
20	150.14	18874.8	0.5635
21	174.24	21903.8	0.5777

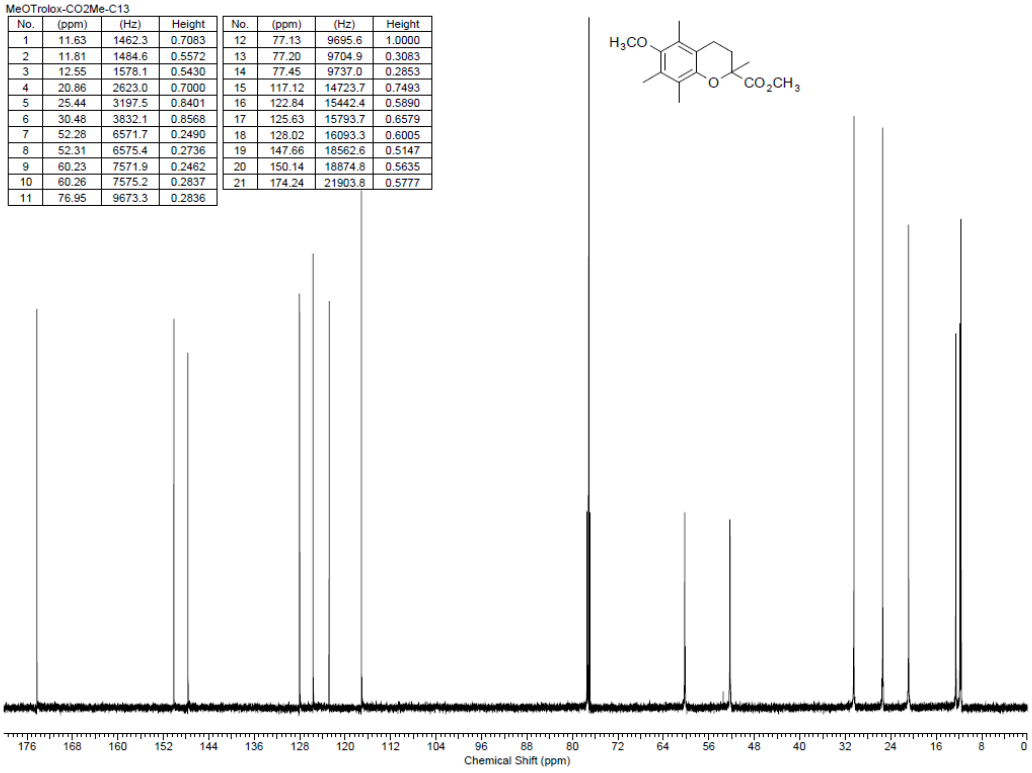

MeOTrCH2OH-H1

No.	(ppm)	(Hz)	Height
1	1.25	622.6	0.7228
2	1.76	879.6	0.0717
3	2.00	1000.9	0.0663
4	2.03	1014.3	0.1572
5	2.11	1053.4	0.6250
6	2.17	1084.3	0.6416
7	2.21	1103.1	0.6243

No.	(ppm)	(Hz)	Height
8	2.65	1326.1	0.1089
9	2.67	1333.2	0.1081
10	2.68	1337.6	0.0629
11	3.59	1796.4	0.0938
12	3.62	1807.6	0.1861
13	3.65	1825.0	1.0000
14	3.68	1837.9	0.1035

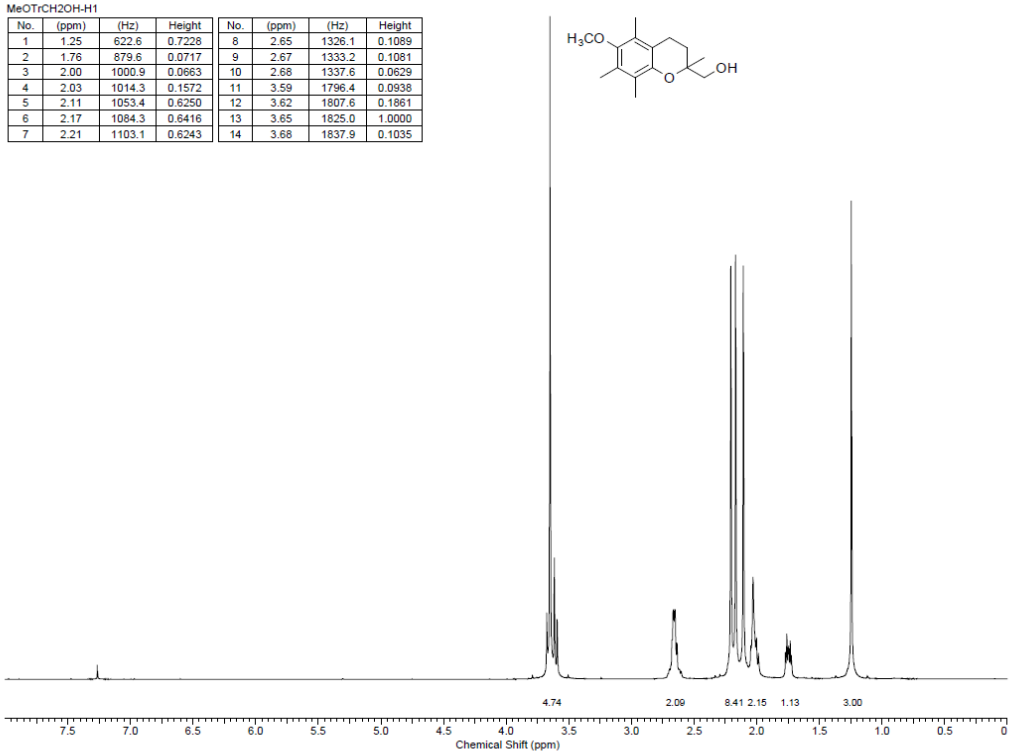

MeOTrCH2OH-C13

No.	(ppm)	(Hz)	Height
1	11.71	1472.0	0.6183
2	11.85	1489.3	0.6562
3	12.55	1578.1	0.6057
4	20.14	2531.8	0.7359
5	20.55	2583.0	0.9977
6	27.65	3476.2	1.0000
7	60.40	7592.9	0.2190
8	60.41	7594.7	0.2917
9	69.35	8718.2	0.5441
10	75.34	9470.9	0.5520

No.	(ppm)	(Hz)	Height
11	76.80	9655.2	0.6814
12	77.06	9687.3	0.7151
13	77.31	9719.4	0.6789
14	117.55	14777.6	0.3828
15	122.87	15446.6	0.2981
16	125.97	15836.5	0.3520
17	128.03	16095.1	0.3519
18	147.14	18497.0	0.2893
19	149.85	18837.6	0.2841

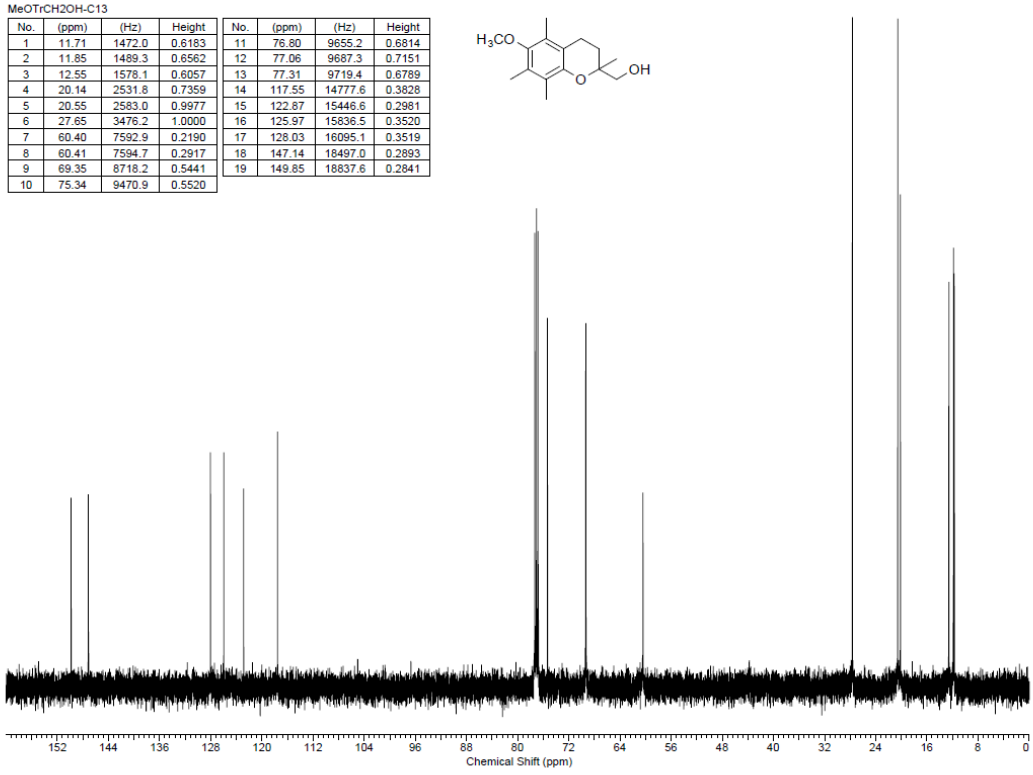

MeOTrCH2OTf-H1

No.	(ppm)	(Hz)	Height	No.	(ppm)	(Hz)	Height
1	1.38	688.4	0.8330	10	2.21	1105.0	0.7621
2	1.85	926.3	0.0760	11	2.66	1331.7	0.1352
3	1.87	932.4	0.0769	12	2.68	1338.3	0.2095
4	1.88	939.7	0.1044	13	2.69	1345.2	0.1208
5	1.99	994.0	0.0958	14	3.65	1826.2	1.0000
6	2.00	1000.6	0.0706	15	4.44	2218.4	0.1012
7	2.02	1007.7	0.0721	16	4.46	2228.7	0.1866
8	2.10	1052.0	0.7425	17	4.50	2248.0	0.1903
9	2.17	1085.2	0.7636	18	4.52	2258.1	0.0998

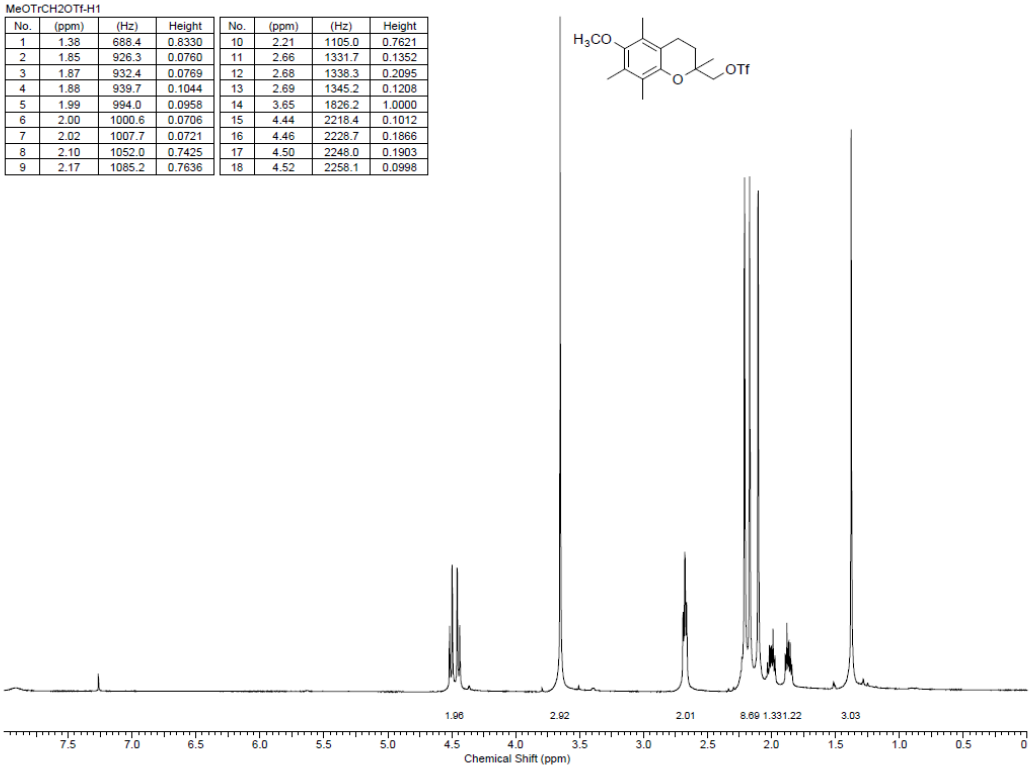

MeOTrCH2OTf-C13

No.	(ppm)	(Hz)	Height	No.	(ppm)	(Hz)	Height
1	11.67	1466.5	0.8689	12	79.64	10012.0	0.6201
2	12.53	1575.8	0.4433	13	114.83	14435.7	0.0400
3	19.68	2474.6	0.5543	14	116.56	14652.5	0.4615
4	21.01	2640.7	0.6672	15	117.37	14755.3	0.1213
5	27.71	3484.1	1.0000	16	119.92	15074.9	0.1291
6	60.35	7587.3	0.2594	17	122.46	15394.5	0.0446
7	60.38	7591.0	0.2636	18	123.37	15509.4	0.3799
8	72.87	9161.1	0.5468	19	125.90	15827.6	0.4041
9	76.77	9651.4	0.5245	20	128.56	16161.2	0.3724
10	77.03	9683.1	0.5251	21	146.35	18397.9	0.3076
11	77.28	9715.2	0.5118	22	150.27	18891.1	0.3240

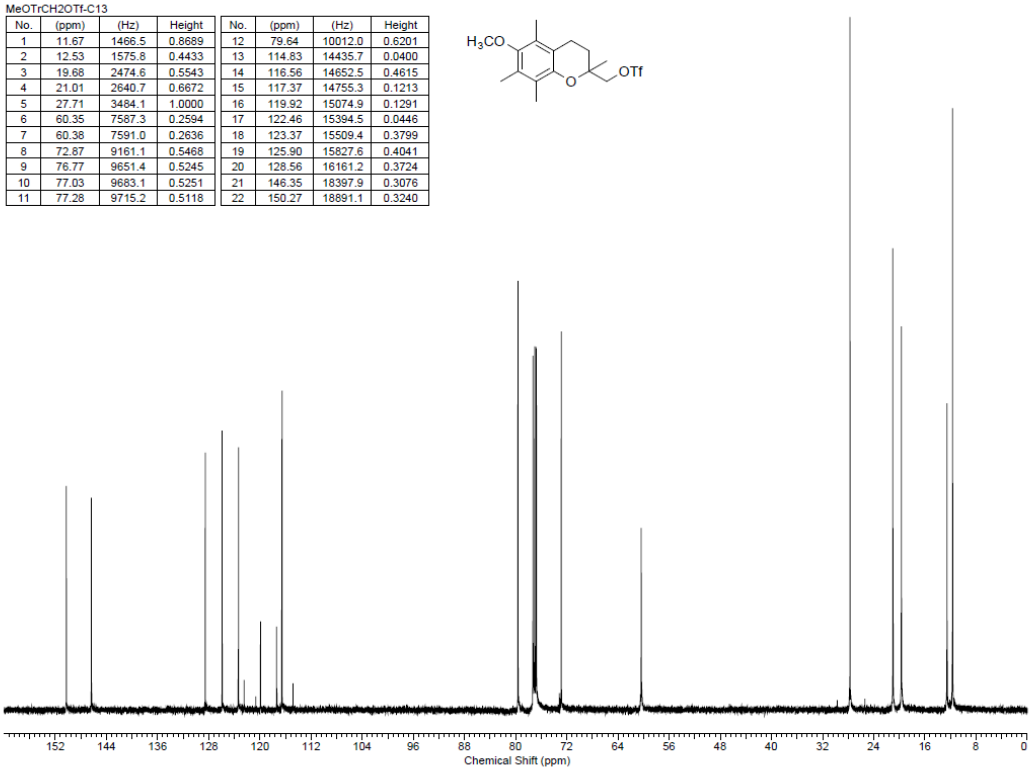

MeOTrCH2CN

No.	(ppm)	(Hz)	Height
1	1.49	596.3	0.7387
2	1.91	765.9	0.0445
3	1.93	772.9	0.0648
4	1.95	779.6	0.0989
5	1.97	786.6	0.0509
6	2.00	800.3	0.0826
7	2.02	806.9	0.0643
8	2.11	842.5	0.5786

No.	(ppm)	(Hz)	Height
9	2.15	861.6	0.6086
10	2.19	878.1	0.5862
11	2.59	1037.1	0.0449
12	2.63	1053.5	0.3083
13	2.64	1057.8	0.2728
14	2.66	1062.5	0.0881
15	3.64	1455.6	1.0000

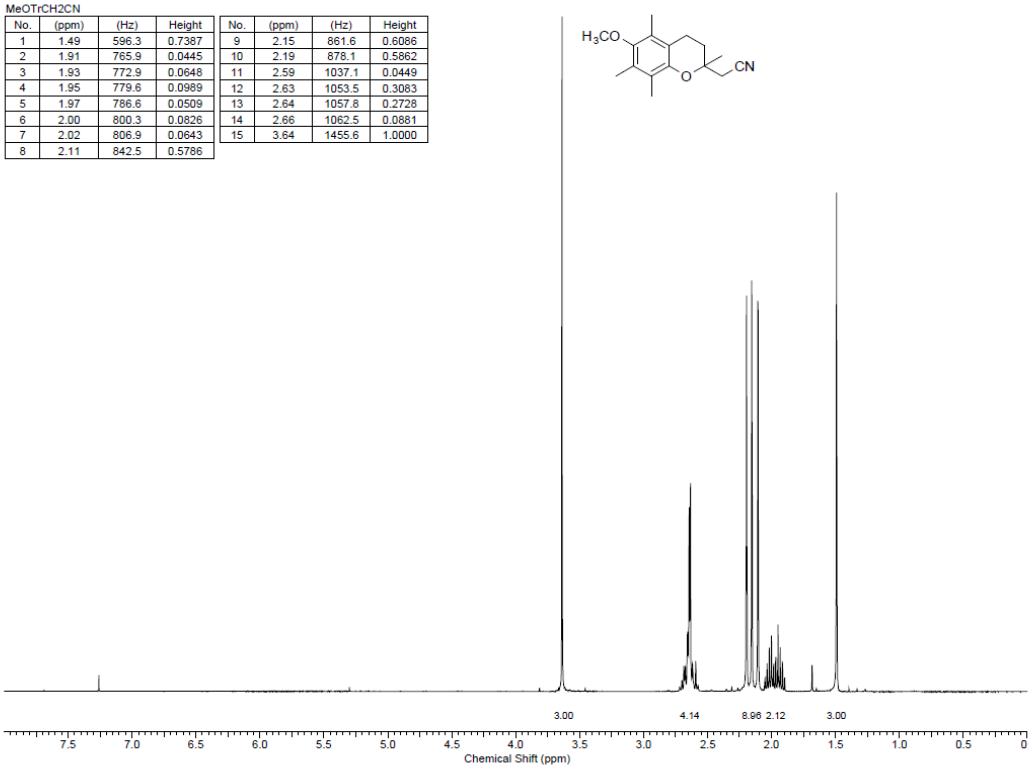

MeOTrolox-CH2CN-C13

No.	(ppm)	(Hz)	Height
1	11.70	882.7	0.7679
2	11.76	887.1	0.7775
3	12.57	948.5	0.8363
4	20.26	1528.5	0.9249
5	24.51	1849.1	1.0000
6	28.51	2151.5	0.9860
7	30.77	2321.8	0.9274
8	60.37	4555.4	0.9076
9	69.27	5226.6	0.2164
10	72.50	5470.4	0.6828

No.	(ppm)	(Hz)	Height
11	76.78	5793.9	0.2823
12	77.20	5825.4	0.2889
13	77.63	5857.4	0.2670
14	116.59	8797.6	0.3789
15	117.13	8838.5	0.4161
16	123.42	9312.9	0.3019
17	125.98	9506.4	0.3577
18	128.50	9696.6	0.3788
19	146.40	11046.7	0.2500
20	150.30	11340.8	0.2905

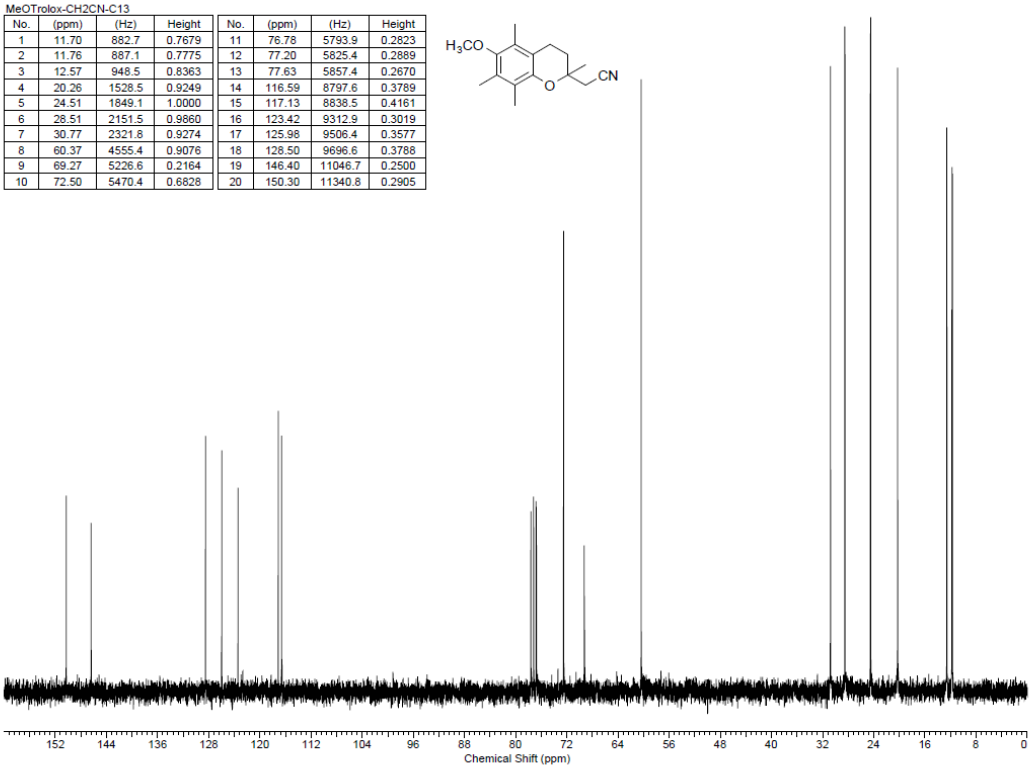

MeO-Trolox-CH2COOH

No.	(ppm)	(Hz)	Height
1	1.48	593.6	0.7534
2	1.94	776.1	0.0669
3	1.96	782.7	0.0794
4	2.07	829.6	0.0978
5	2.08	830.4	0.0974
6	2.09	836.2	0.1059
7	2.10	841.3	0.6908
8	2.17	868.7	0.7033

No.	(ppm)	(Hz)	Height
9	2.21	884.3	0.7050
10	2.64	1055.1	0.1029
11	2.65	1061.7	0.1980
12	2.67	1068.8	0.1007
13	2.69	1074.6	0.2610
14	2.70	1079.3	0.2469
15	3.66	1465.0	1.0000
16	5.30	2121.5	0.2574

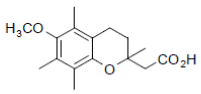

MeOTrCH2COOH-C13

No.	(ppm)	(Hz)	Height
1	11.69	1176.6	0.6372
2	11.75	1182.5	0.8165
3	12.57	1265.1	0.6739
4	20.48	2060.5	0.6024
5	24.67	2482.1	0.8959
6	31.05	3124.2	0.6462
7	43.96	4423.1	0.7030
8	60.39	6076.5	1.0000
9	73.45	7390.2	0.8773
10	76.76	7724.1	0.3832

No.	(ppm)	(Hz)	Height
11	77.08	7755.8	0.4422
12	77.39	7787.5	0.3924
13	117.16	11788.8	0.6400
14	123.21	12397.0	0.4174
15	125.92	12670.4	0.5526
16	128.16	12895.3	0.3560
17	146.81	14772.1	0.3813
18	149.91	15083.9	0.3247
19	176.42	17751.0	0.3932

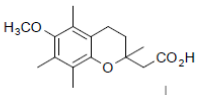

HOTRCH2HB-H1

No.	(ppm)	(Hz)	Height
1	1.18	590.5	1.0000
2	1.56	782.0	0.0906
3	1.77	882.5	0.8574
4	1.92	960.3	0.0790
5	1.93	963.5	0.1003
6	1.93	966.6	0.1474
7	1.94	971.0	0.1649
8	1.95	975.7	0.1669
9	2.08	1041.7	0.9252
10	2.09	1046.1	0.9289

No.	(ppm)	(Hz)	Height
11	2.43	1213.1	0.8124
12	2.50	1251.8	0.8647
13	2.52	1257.6	0.6542
14	2.53	1266.9	0.6182
15	2.68	1339.1	0.1002
16	3.49	1746.5	0.2569
17	3.51	1753.3	0.2421
18	4.20	2099.3	0.2698
19	6.04	3020.3	0.4093
20	7.26	3628.4	0.2398

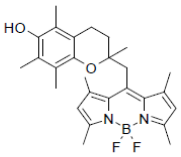

HOTRCH2HB-C13

No.	(ppm)	(Hz)	Height
1	11.22	1410.2	0.1336
2	11.53	1449.7	0.1533
3	12.13	1524.6	0.1189
4	14.53	1827.0	0.0608
5	17.57	2208.9	0.1072
6	17.59	2210.8	0.1348
7	20.80	2614.6	0.2261
8	33.45	4204.7	0.2261
9	38.77	4874.2	0.1114
10	75.57	9500.2	0.2140
11	76.75	9648.2	0.9888
12	77.00	9680.3	1.0000
13	77.26	9711.9	0.9491
14	116.81	14685.1	0.1299

No.	(ppm)	(Hz)	Height
15	118.30	14872.1	0.1338
16	121.27	15245.2	0.1273
17	121.99	15335.9	0.0498
18	122.06	15344.7	0.0474
19	123.34	15505.7	0.1155
20	133.67	16804.1	0.0298
21	134.61	16922.3	0.0309
22	140.18	17622.9	0.0461
23	141.20	17750.8	0.0835
24	142.66	17934.6	0.0498
25	144.72	18193.7	0.1129
26	145.00	18228.1	0.1275
27	153.05	19240.4	0.0511
28	153.93	19351.2	0.0528

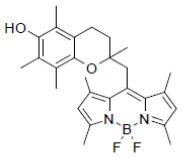

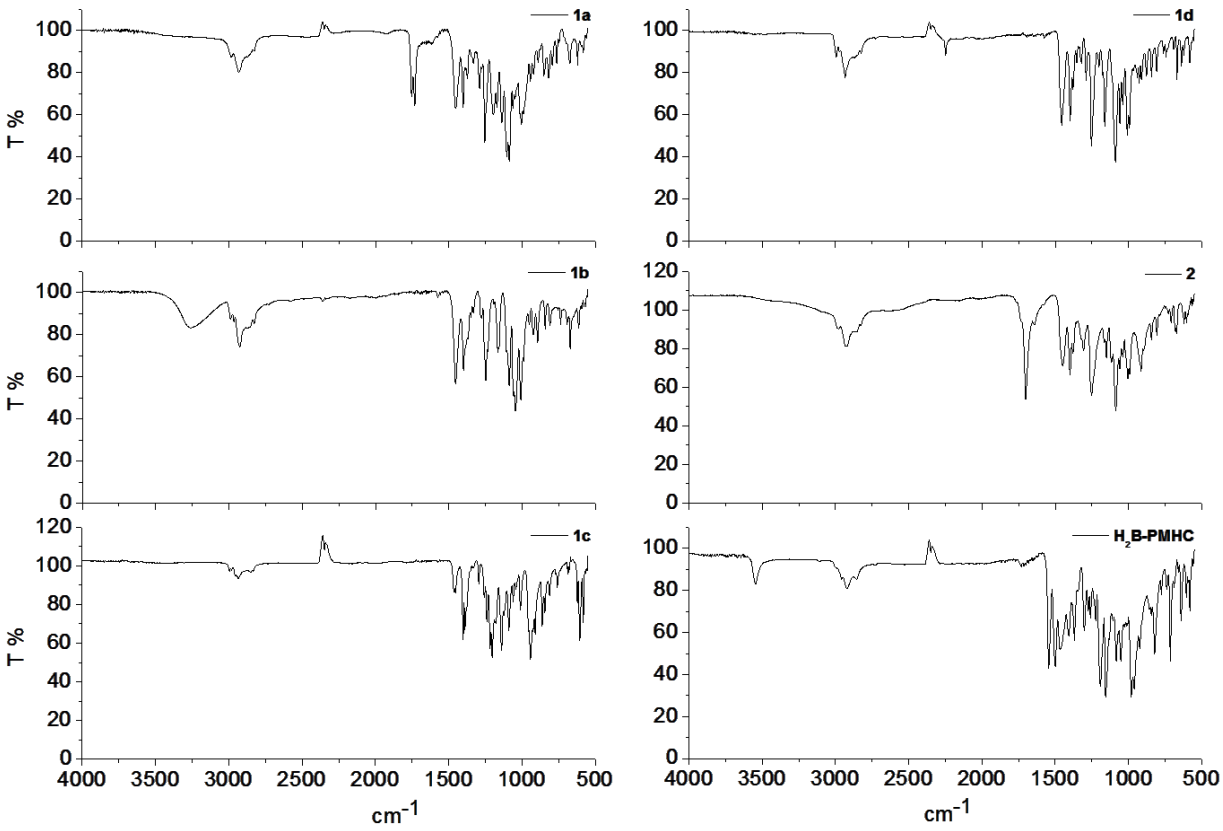
1a
1d
1b
2
1c
H2B-PMHC
T %
cm-1
4000 3500 3000 2500 2000 1500 1000 500

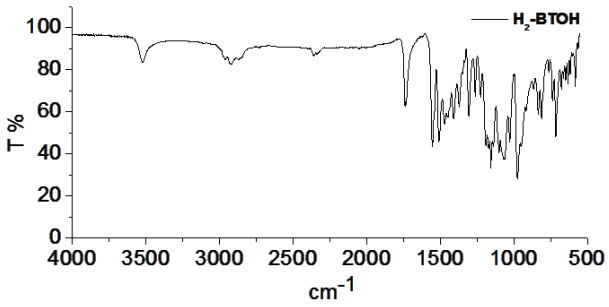
H2-BTOH
T %
cm-1
4000 3500 3000 2500 2000 1500 1000 500

8.4. Appendix Chapter 6

6-methoxy-2,5,7,8-tetramethylchroman-2-carbaldehyde, **1**

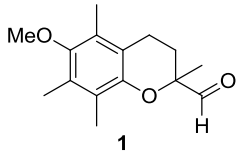

1

MeOTrolox-CHO

No.	(ppm)	(Hz)	Height	No.	(ppm)	(Hz)
1	9.65	2895.3	0.2038	15	2.24	671.1
2	9.65	2894.1	0.1829	16	2.22	665.6
3	3.65	1095.4	1.0000	17	2.14	640.9
4	2.62	784.8	0.0348	18	1.88	564.5
5	2.59	778.4	0.0783	19	1.86	557.4
6	2.57	772.5	0.0696	20	1.85	556.3
7	2.54	762.6	0.0389	21	1.85	555.4
8	2.33	698.7	0.0350	22	1.85	554.2
9	2.31	693.7	0.0390	23	1.84	550.7
10	2.31	692.2	0.0405	24	1.83	549.5
11	2.29	687.2	0.0341	25	1.83	548.3
12	2.28	684.9	0.0427	26	1.81	541.9
13	2.27	679.9	0.0599	27	1.42	427.3
14	2.26	678.7	0.0617	28	0.13	39.9

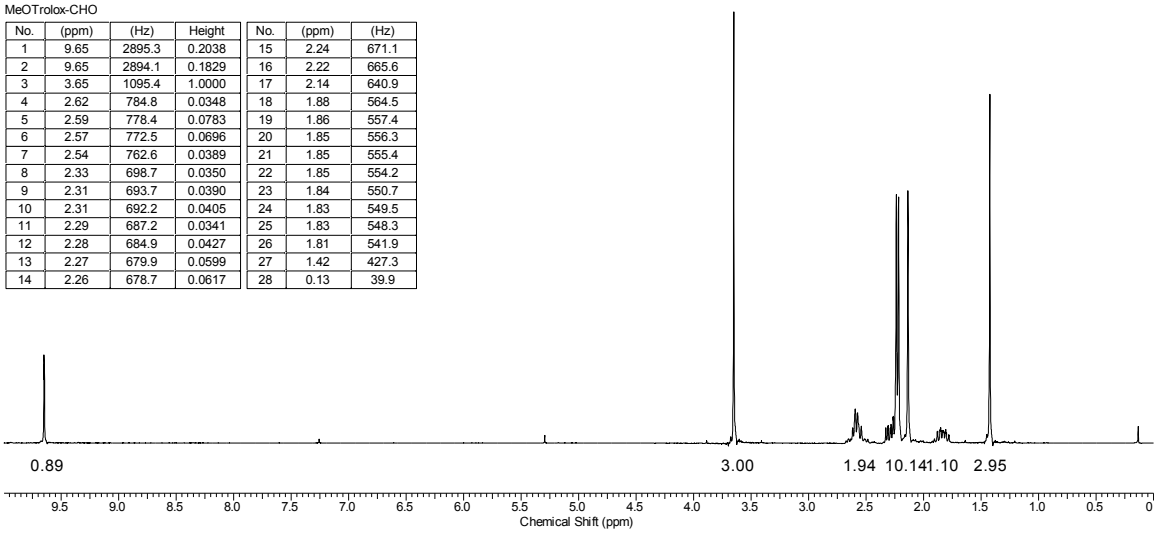

MeOTrolox-CHO-C13

No.	(ppm)	(Hz)	Height	No.	(ppm)	(Hz)
1	204.30	15416.0	0.6888	10	77.16	5822.1
2	150.42	11350.2	0.1803	11	76.73	5790.0
3	147.33	11116.9	0.1973	12	60.34	4553.2
4	128.37	9686.1	0.2980	13	27.74	2092.9
5	126.12	9516.9	0.2803	14	21.55	1625.8
6	123.09	9288.0	0.2089	15	20.27	1529.6
7	117.70	8881.6	0.3762	16	12.58	949.0
8	80.41	6067.5	0.4847	17	11.89	897.1
9	77.58	5854.1	0.2171	18	11.66	879.9

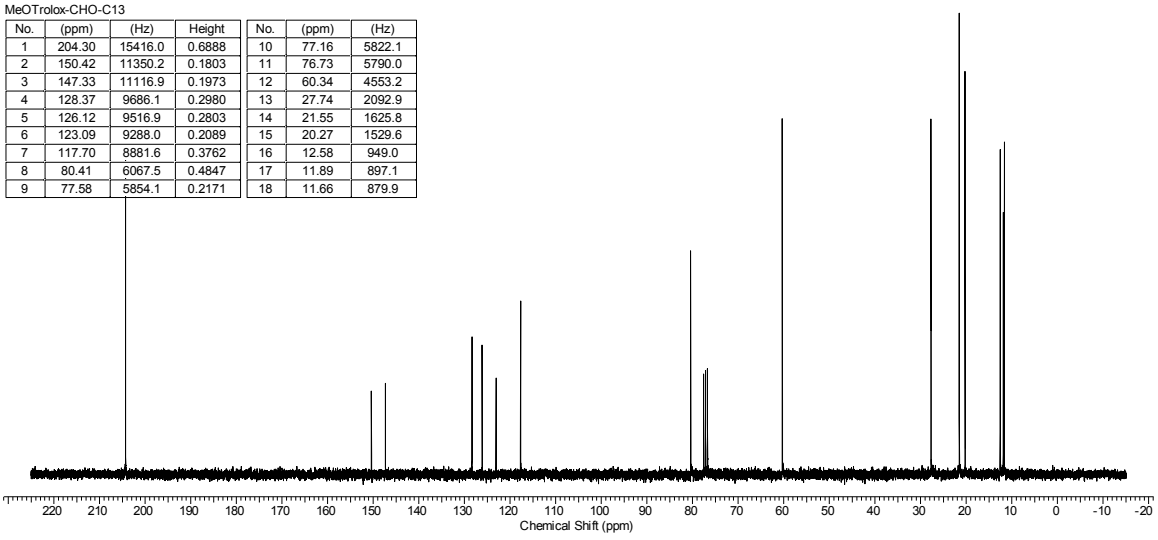

6-methoxy-2,5,7,8-tetramethyl-2-vinylchroman, **2**

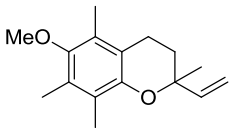

2

MeOTr-CH=CH2-fr1

No.	(ppm)	(Hz)	Height
1	5.92	2367.3	0.0842
2	5.89	2356.4	0.0864
3	5.87	2350.1	0.0955
4	5.85	2339.2	0.0968
5	5.17	2068.7	0.1252
6	5.17	2067.6	0.1225
7	5.13	2051.6	0.1103
8	5.12	2050.0	0.1075
9	5.06	2025.0	0.1258
10	5.06	2023.4	0.1143
11	5.03	2014.0	0.1186
12	5.03	2012.9	0.1119
13	3.65	1459.9	1.0000
14	2.63	1053.5	0.0344
15	2.62	1047.7	0.0227
16	2.61	1042.6	0.0450
17	2.59	1036.7	0.0811
18	2.58	1031.2	0.0467
19	2.55	1021.5	0.0380
20	2.54	1014.8	0.0473

No.	(ppm)	(Hz)	Height
21	2.53	1012.1	0.0473
22	2.51	1005.4	0.0528
23	2.22	888.6	0.7342
24	2.18	870.6	0.7320
25	2.15	858.9	0.7398
26	1.98	793.3	0.0325
27	1.97	787.4	0.0475
28	1.95	781.5	0.0425
29	1.95	779.6	0.0588
30	1.93	774.1	0.0808
31	1.92	768.2	0.0466
32	1.86	746.0	0.0502
33	1.85	740.1	0.0558
34	1.84	736.6	0.0576
35	1.83	732.7	0.0446
36	1.83	730.3	0.0538
37	1.82	726.4	0.0348
38	1.81	723.3	0.0342
39	1.79	717.1	0.0274
40	1.42	567.4	0.8608

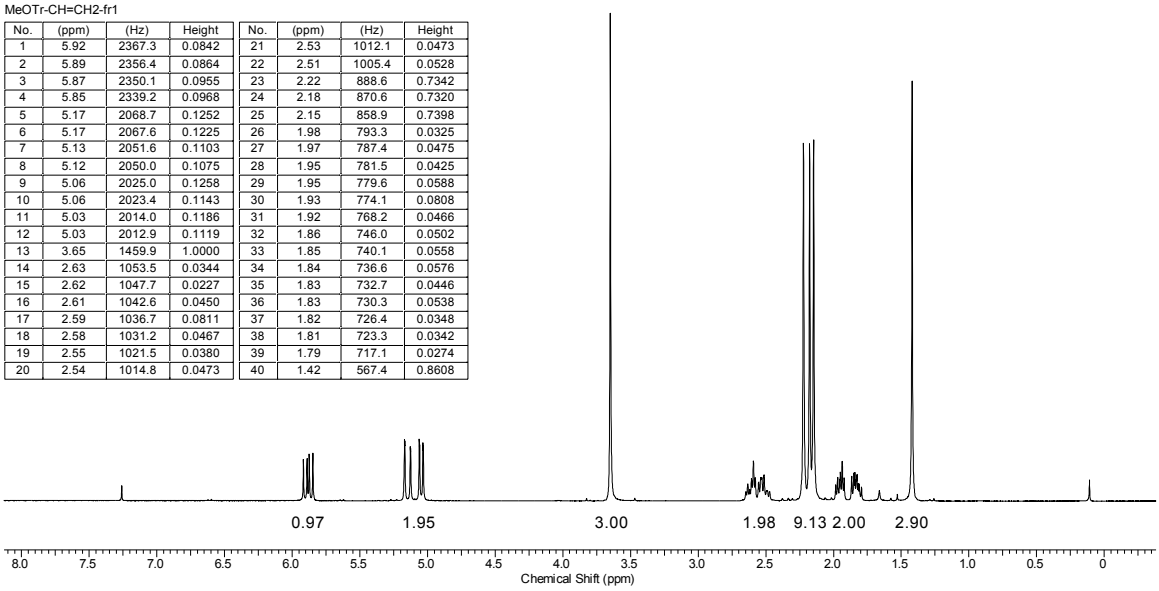

MeOTrolox-CH=CH2-C13

No.	(ppm)	(Hz)	Height
1	149.56	11285.5	0.1629
2	147.75	11148.4	0.2377
3	141.87	10705.0	0.7326
4	127.75	9639.6	0.2671
5	125.65	9481.5	0.2248
6	122.50	9243.8	0.2398
7	117.65	8877.8	0.2842
8	113.27	8547.2	0.7950
9	77.47	5845.8	0.5305
10	77.05	5813.8	0.5296
11	76.63	5782.2	0.5373
12	75.47	5694.9	0.4054
13	60.39	4557.1	0.6799
14	31.80	2399.2	1.0000
15	27.04	2040.4	0.9025
16	20.85	1573.2	0.9045

No.	(ppm)	(Hz)	Height
17	12.58	949.6	0.6778
18	11.82	892.1	0.6141
19	11.71	883.3	0.7015

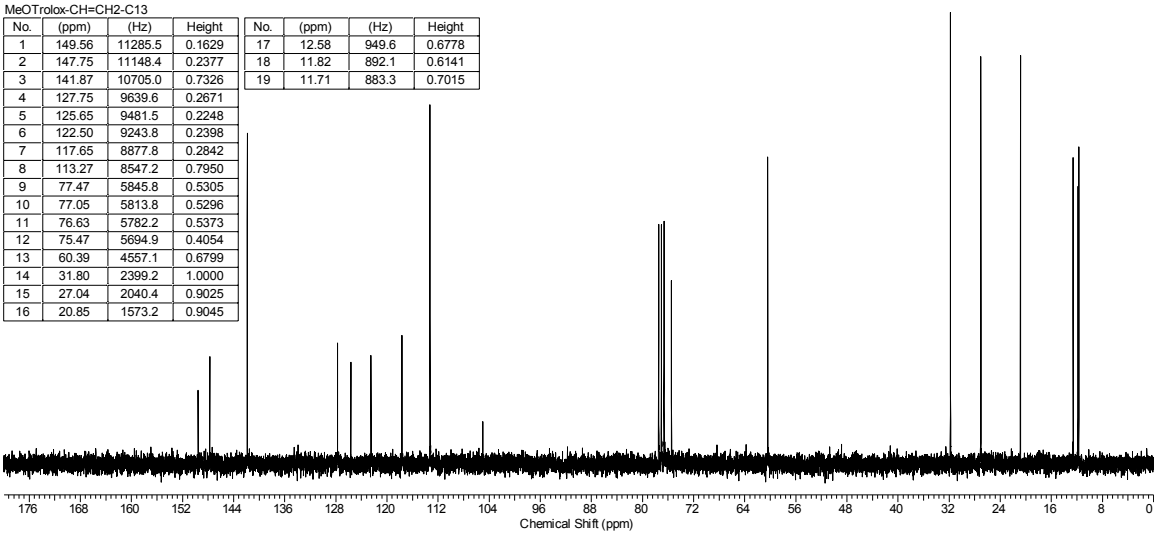

2-Carbaldehyde-3,5-dimethyl-4-iodo pyrrole, **3**

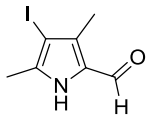

3

I-CHO-dimethyl-pyrrole-H1

No.	(ppm)	(Hz)	Height
1	10.67	5336.3	0.0200
2	9.48	4737.2	0.3046
3	2.35	1174.5	0.9181
4	2.27	1135.9	1.0000

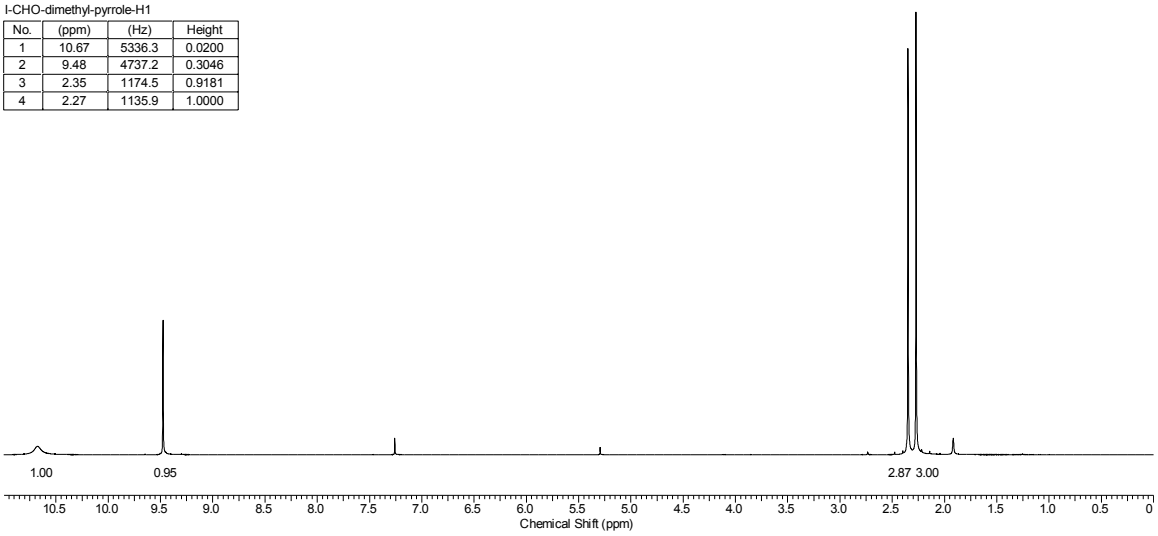

CHO-I-pyrrole-C13

No.	(ppm)	(Hz)	Height
1	176.19	22149.9	0.6743
2	140.20	17624.3	0.1061
3	136.89	17208.8	0.0889
4	129.07	16226.3	0.2307
5	72.65	9133.2	0.1150
6	14.31	1799.6	0.7365
7	12.68	1593.9	0.4716

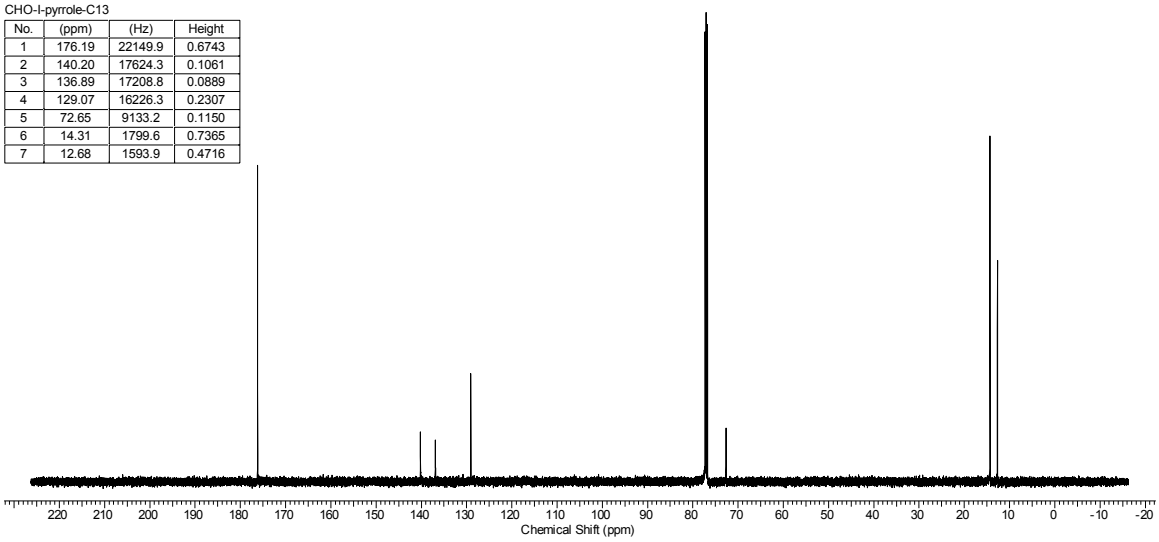

2-Carbaldehyde-3,5-dimethyl-4-iodo-1-(methoxymethyl) pyrrole, **4**

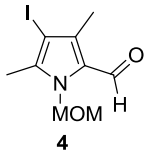

4

MOM-I-CHO-dimethylpyrrole

No.	(ppm)	(Hz)	Height
1	9.61	4803.5	0.2914
2	5.69	2845.4	0.6243
3	3.23	1612.2	1.0000
4	2.30	1150.3	0.8388
5	2.22	1111.7	0.8049

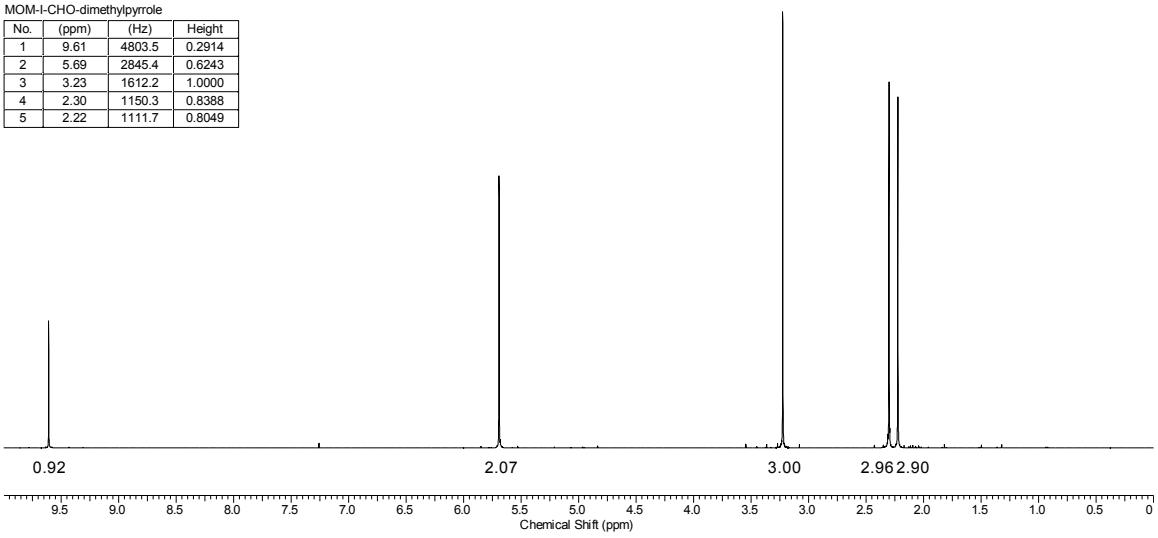

MOM-CHO-I-pyrrole-C13

No.	(ppm)	(Hz)	Height
1	177.27	17837.2	0.9483
2	141.43	14231.0	0.1212
3	138.14	13899.3	0.1420
4	128.55	12935.1	0.1673
5	75.06	7552.3	0.7463
6	74.58	7504.4	0.1861
7	55.67	5601.8	1.0000
8	13.09	1316.7	0.5234
9	13.04	1312.3	0.6162

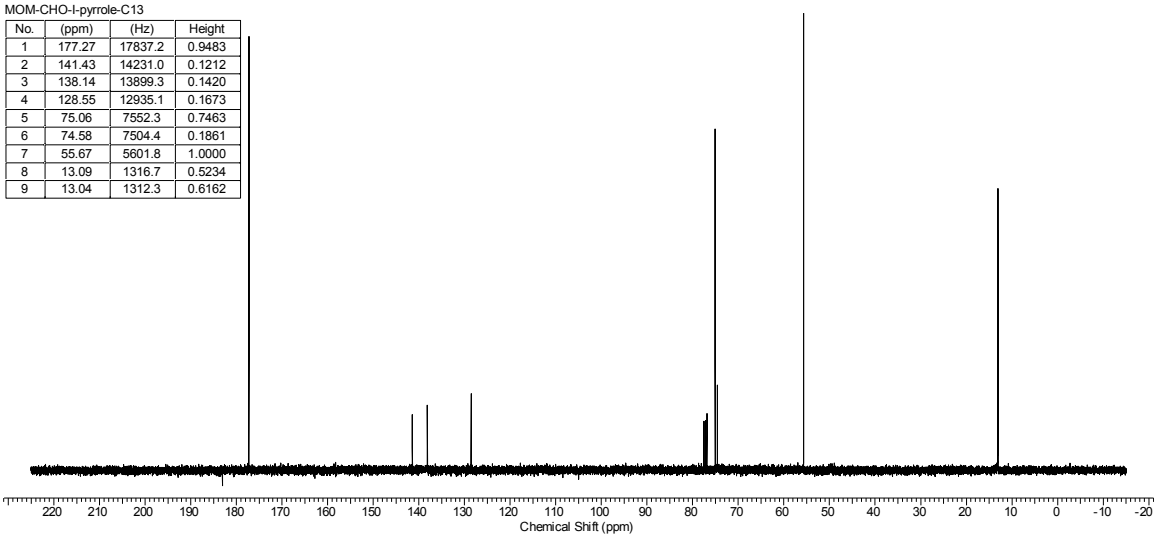

(E)-4-(2-(6-methoxy-2,5,7,8-tetramethylchroman-2-yl)vinyl)-1-(methoxymethyl)-3,5-dimethyl-2-carbaldehyde pyrrole, **5**

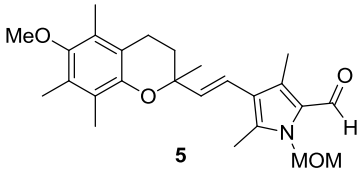

5

MeOTrCH=CH-pyrrole-MOM

No.	(ppm)	(Hz)	Height
1	9.66	4829.9	0.1373
2	6.30	3147.9	0.0914
3	6.26	3131.8	0.1035
4	5.78	2887.3	0.1136
5	5.74	2870.9	0.1003
6	5.71	2855.5	0.3267
7	3.62	1809.3	0.6545
8	3.27	1636.7	0.6978
9	2.65	1326.6	0.0194
10	2.63	1315.6	0.0195
11	2.62	1310.0	0.0342
12	2.61	1304.6	0.0191
13	2.54	1271.3	0.0191
14	2.54	1268.2	0.0193
15	2.52	1261.6	0.0252

No.	(ppm)	(Hz)	Height
16	2.24	1119.0	0.5842
17	2.21	1103.1	1.0000
18	2.12	1058.6	0.4402
19	2.02	1010.4	0.0226
20	2.01	1003.1	0.0285
21	2.00	997.9	0.0349
22	1.99	997.0	0.0347
23	1.98	991.8	0.0225
24	1.93	965.7	0.0242
25	1.92	959.5	0.0277
26	1.91	955.9	0.0276
27	1.90	952.2	0.0201
28	1.90	949.8	0.0263
29	1.50	748.3	0.5243

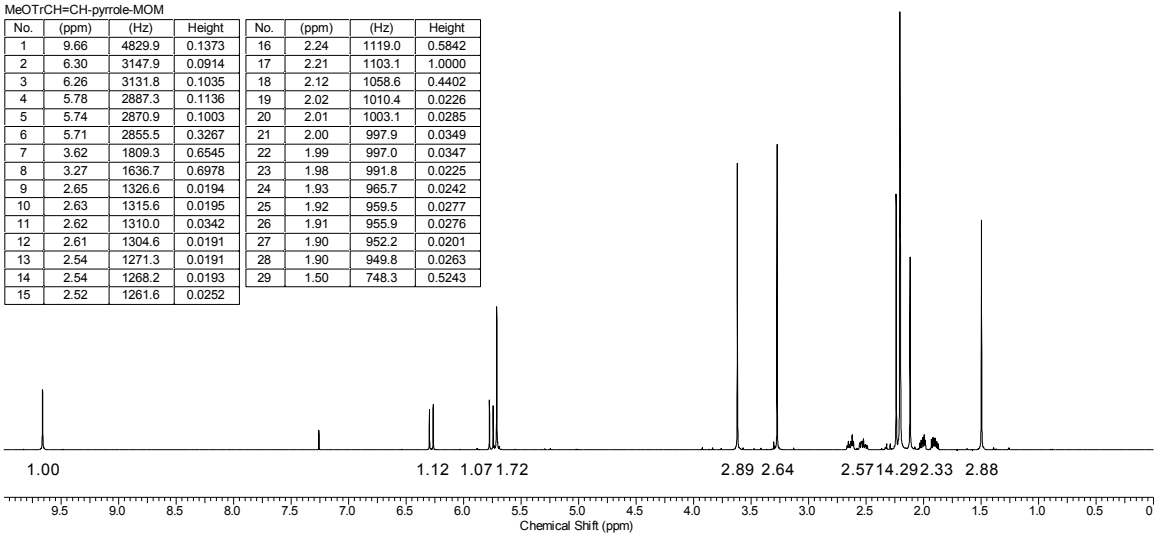

MeOTrCH=CH-pyrrole-MOM-C13

No.	(ppm)	(Hz)	Height
1	177.29	22287.1	0.5628
2	149.64	18812.0	0.3117
3	147.74	18572.8	0.3012
4	138.44	17403.3	0.1533
5	134.90	16958.6	0.6635
6	133.91	16833.9	0.1445
7	127.76	16061.6	0.3867
8	127.44	16020.2	0.1787
9	125.74	15807.1	0.3806
10	122.41	15388.9	0.3890
11	120.59	15159.1	0.3809
12	119.42	15012.1	0.5510
13	117.76	14804.1	0.3536
14	77.30	9717.5	0.9545
15	77.04	9685.4	1.0000
16	76.79	9653.3	0.9888
17	75.54	9496.1	0.5953
18	74.36	9348.6	0.5903
19	60.39	7591.5	0.6155
20	55.55	6983.4	0.8654

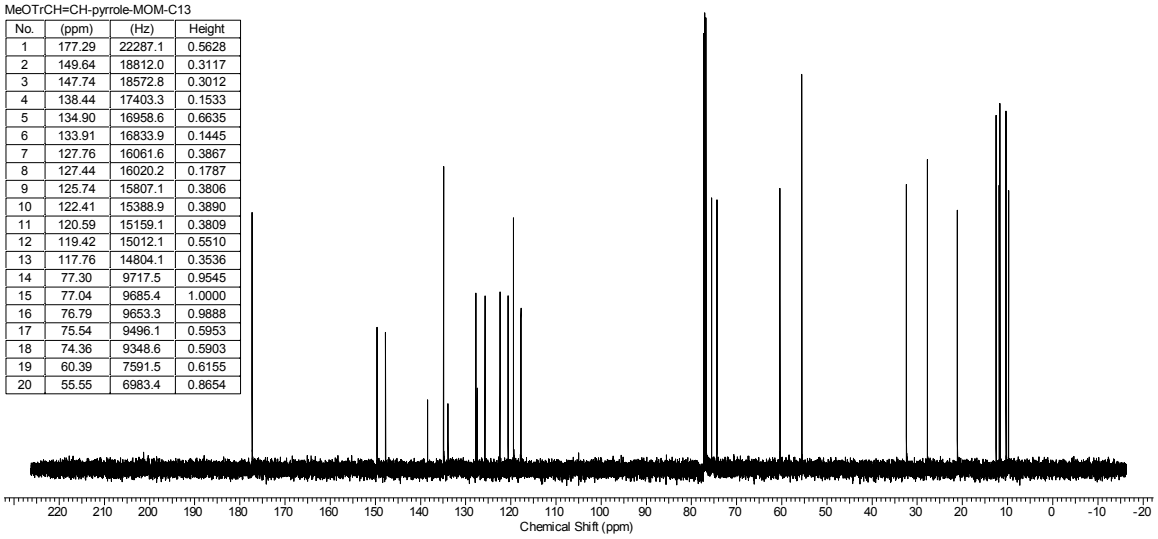

(E)-4-(2-(6-hydroxy-2,5,7,8-tetramethylchroman-2-yl)vinyl)-1-(hydroxymethyl)-3,5-dimethyl-2-carbaldehyde pyrrole, **6**

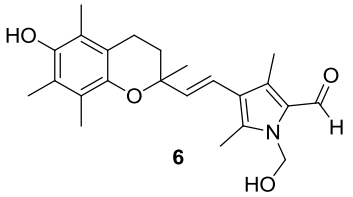

6

HOTr-CH=CH-CHO-pyrrole-CH2OH

No.	(ppm)	(Hz)	Height	No.	(ppm)	(Hz)
1	9.48	3792.1	0.2346	18	2.21	885.9
2	6.29	2515.4	0.0979	19	2.17	870.2
3	6.25	2499.0	0.1214	20	2.08	832.3
4	5.76	2306.3	0.1245	21	2.03	814.0
5	5.72	2290.3	0.1144	22	2.02	808.9
6	5.36	2146.5	0.6530	23	2.02	807.7
7	4.36	1743.6	0.1150	24	2.01	802.6
8	2.68	1073.1	0.0192	25	2.00	800.7
9	2.65	1062.1	0.0209	26	1.99	795.6
10	2.64	1056.6	0.0365	27	1.99	794.4
11	2.63	1051.2	0.0208	28	1.97	789.4
12	2.57	1029.3	0.0168	29	1.93	773.3
13	2.56	1023.0	0.0211	30	1.92	767.1
14	2.55	1019.9	0.0216	31	1.91	763.6
15	2.53	1013.3	0.0268	32	1.90	760.0
16	2.25	900.7	0.7328	33	1.89	757.3
17	2.23	894.1	0.0210	34	1.88	753.8

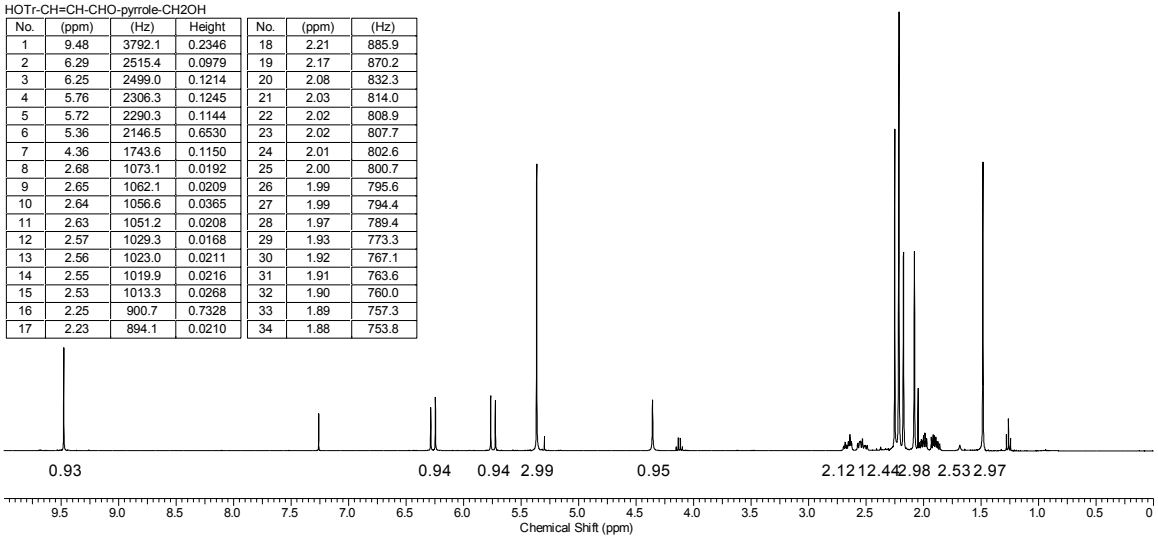

HOTrCH=CH-CHO-pyrrole-CH2OH-C13

No.	(ppm)	(Hz)	Height
1	177.19	13370.4	0.5448
2	145.47	10977.0	0.2452
3	144.82	10927.8	0.2451
4	137.88	10403.7	0.1700
5	135.39	10215.7	0.5012
6	134.90	10179.2	0.2204
7	128.15	9670.0	0.1477
8	122.04	9208.9	0.1941
9	121.08	9136.5	0.2345
10	120.38	9083.4	0.2386
11	119.23	8996.6	0.4755
12	118.53	8944.1	0.2842
13	117.43	8860.6	0.2878
14	75.28	5680.5	0.3494
15	68.39	5160.8	0.5271
16	32.51	2453.4	0.4726
17	27.66	2087.4	0.5212
18	21.22	1600.9	0.4085
19	12.25	924.2	0.4208
20	11.87	895.4	0.3651
21	11.30	852.8	0.3710
22	10.38	783.2	0.4599
23	10.01	755.5	0.4245

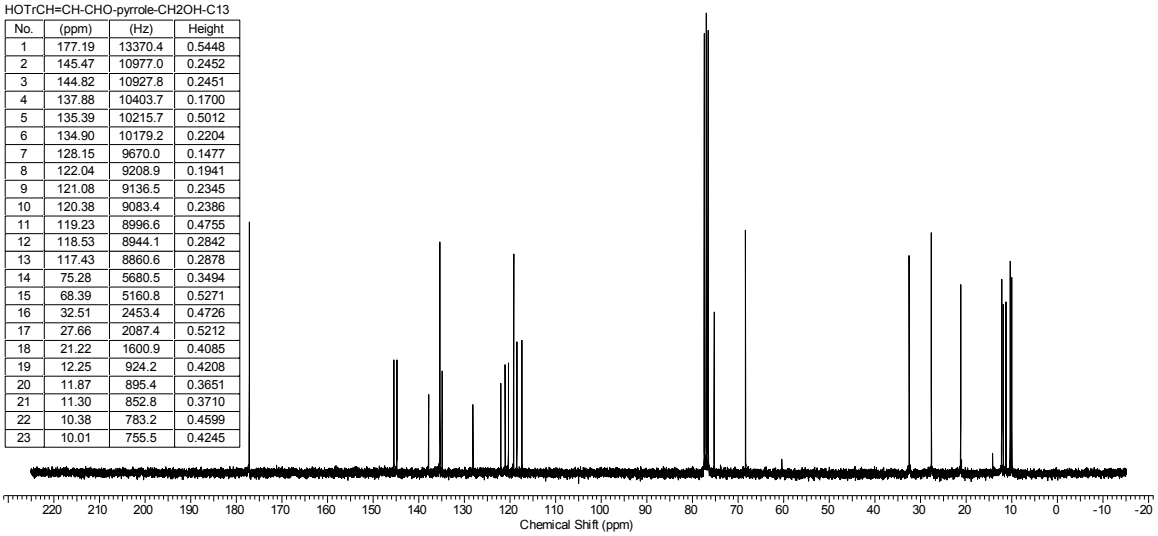

(E)-4-(2-(6-hydroxy-2,5,7,8-tetramethylchroman-2-yl)vinyl)-3,5-dimethyl-2-carbaldehyde pyrrole, **7**

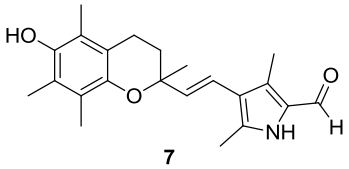

7

HOTr-CH=CH-pyrrole-CHO-H1

No.	(ppm)	(Hz)	Height	No.	(ppm)	(Hz)
1	9.79	3917.5	0.0148	18	2.22	886.7
2	9.45	3781.5	0.2218	19	2.18	872.6
3	6.33	2532.2	0.0651	20	2.17	868.3
4	6.29	2515.8	0.0756	21	2.15	860.1
5	5.79	2316.9	0.0619	22	2.14	858.1
6	5.75	2300.5	0.0555	23	2.14	856.6
7	4.63	1852.3	0.0187	24	2.08	833.9
8	2.67	1069.9	0.0104	25	2.06	822.6
9	2.65	1058.6	0.0127	26	2.03	812.0
10	2.63	1053.5	0.0263	27	2.01	806.2
11	2.62	1047.7	0.0141	28	2.01	802.6
12	2.58	1033.2	0.0103	29	2.00	798.3
13	2.57	1026.6	0.0150	30	1.98	792.5
14	2.56	1024.2	0.0154	31	1.97	787.0
15	2.54	1017.6	0.0171	32	1.92	770.2
16	2.26	903.5	0.6616	33	1.91	764.0
17	2.23	892.9	0.5794	34	1.90	760.4

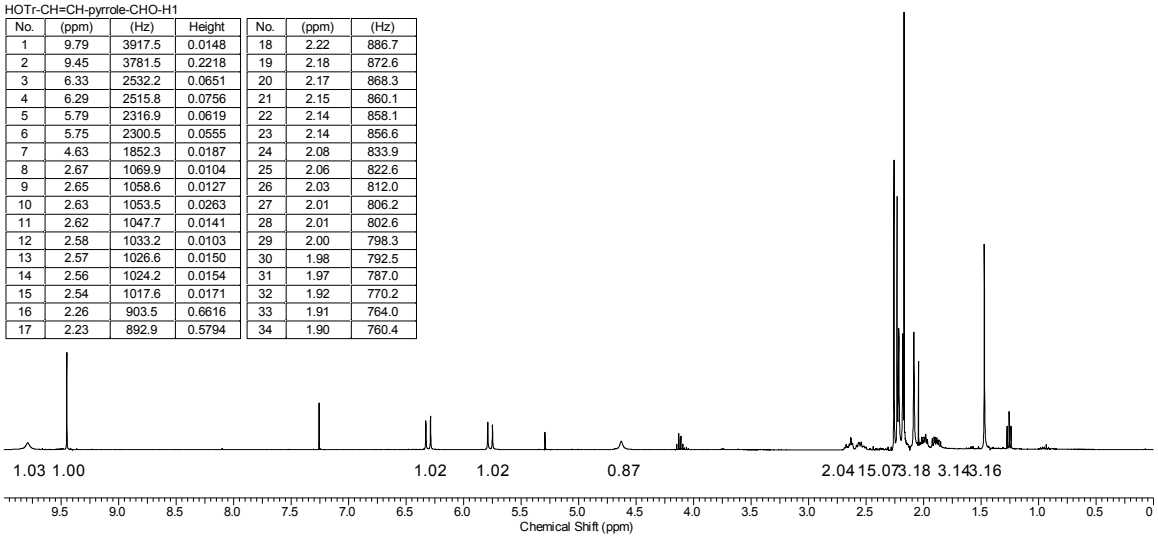

HOTrCH=CH-CHO-pyrrole-C13

No.	(ppm)	(Hz)	Height	No.	(ppm)	(Hz)	Height
1	176.17	13293.6	0.2938	13	117.47	8864.0	0.1817
2	145.53	10980.9	0.1748	14	75.28	5680.5	0.2880
3	144.77	10924.0	0.1877	15	32.59	2458.9	0.3196
4	136.29	10284.3	0.1681	16	30.95	2335.1	0.1320
5	133.27	10056.5	0.3347	17	27.68	2088.5	0.3726
6	131.60	9930.4	0.0799	18	21.22	1600.9	0.3048
7	127.98	9657.3	0.2122	19	12.68	956.8	0.3783
8	122.07	9211.2	0.1759	20	12.28	926.9	0.2710
9	121.12	9139.3	0.1738	21	11.87	895.4	0.2841
10	120.15	9066.3	0.1660	22	11.35	856.2	0.2672
11	119.46	9014.3	0.4329	23	9.79	739.0	0.3282
12	118.58	8948.0	0.1888				

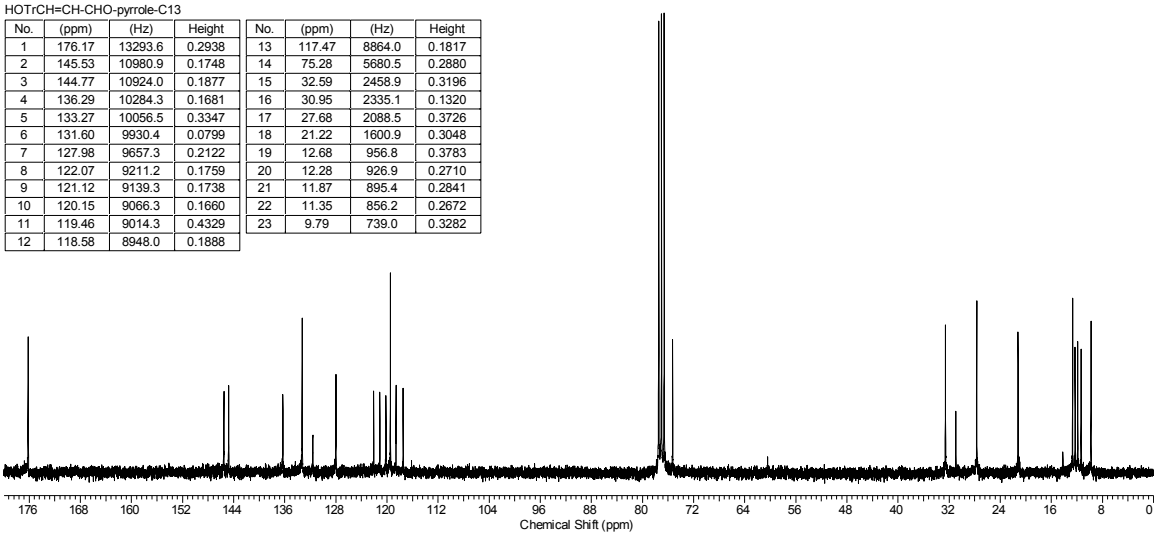

4-(2-(6-methoxy-2,5,7,8-tetramethylchroman-2-yl)ethyl)-1-(methoxy-methyl)-3,5-dimethyl-1H-pyrrole-2-carbaldehyde, **8**

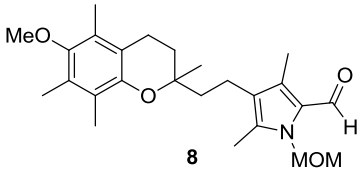

8

MeOTr-CH2CH2-pyrrole-CHO-MOM-c-Hexene-Pd

No.	(ppm)	(Hz)	Height	No.	(ppm)	(Hz)	Height
1	9.62	3850.3	0.2053	14	2.19	877.7	0.6511
2	5.71	2285.6	0.0521	15	2.17	869.9	0.6012
3	5.70	2282.1	0.1510	16	2.15	861.3	1.0000
4	5.69	2277.4	0.1493	17	2.11	844.8	0.0500
5	3.64	1456.0	0.6740	18	1.89	757.3	0.0435
6	3.29	1318.1	0.7155	19	1.88	750.3	0.0777
7	2.64	1057.8	0.0566	20	1.85	741.3	0.1112
8	2.63	1051.2	0.1242	21	1.84	734.6	0.0454
9	2.61	1044.1	0.0794	22	1.66	664.7	0.0431
10	2.56	1022.6	0.0723	23	1.64	656.1	0.0534
11	2.53	1013.7	0.1037	24	1.62	647.9	0.0440
12	2.51	1005.4	0.0811	25	1.34	536.5	0.5473
13	2.21	882.7	0.5189				

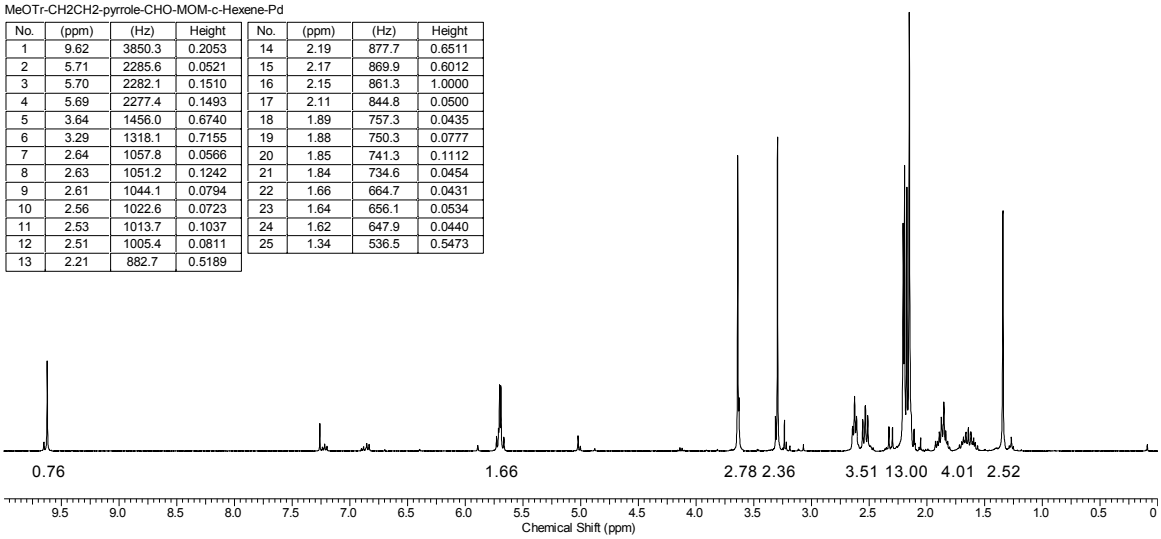

MeOTrCH2CH2-pyrrole-CHO-MOM-c-HexenePd-C13

No.	(ppm)	(Hz)	Height	No.	(ppm)	(Hz)	Height	No.	(ppm)	(Hz)	Height
1	176.77	13338.3	0.8610	10	123.17	9294.1	0.5938	19	31.40	2369.4	0.9657
2	149.59	11287.7	0.3456	11	122.86	9270.9	0.4049	20	23.62	1782.2	0.9845
3	147.53	11132.4	0.3471	12	117.48	8864.5	0.5497	21	20.61	1555.0	0.7933
4	137.93	10408.1	0.2226	13	115.36	8704.7	0.1785	22	17.74	1338.3	0.7125
5	134.59	10155.5	0.1912	14	74.38	5612.5	0.7015	23	12.56	947.4	0.6335
6	129.49	9771.2	0.1626	15	74.18	5597.0	0.9889	24	11.82	891.5	0.6929
7	127.90	9650.7	0.4241	16	60.42	4558.7	0.3634	25	11.70	882.7	0.7011
8	127.23	9600.4	0.3319	17	55.51	4188.9	0.4730	26	9.42	710.8	0.6097
9	125.90	9500.3	0.4425	18	40.24	3036.1	0.9333	27	8.60	648.8	0.4394

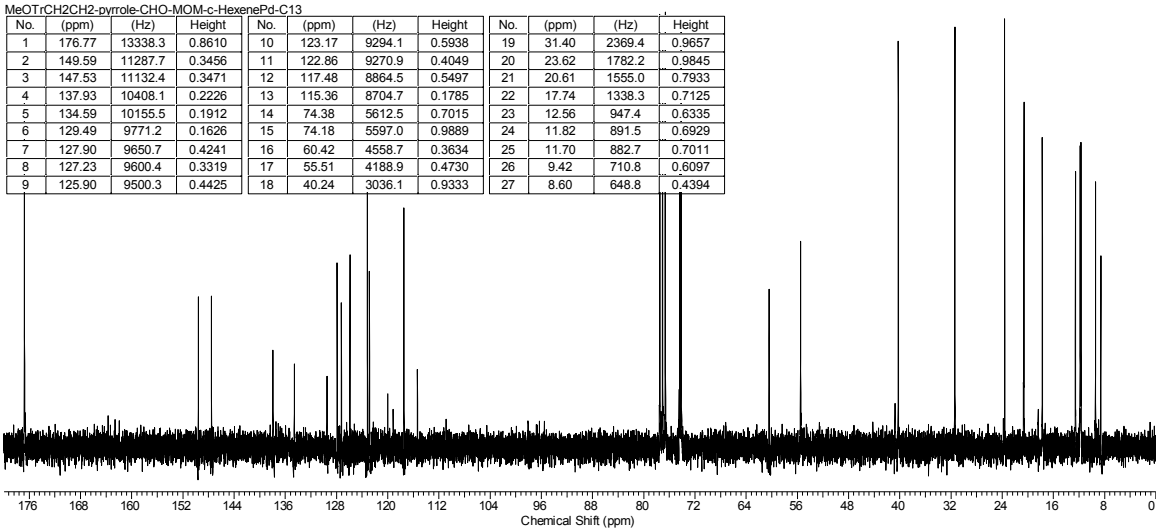

4-(2-(6-hydroxy-2,5,7,8-tetramethylchroman-2-yl)ethyl)-3,5-dimethyl-1H-pyrrole-2-carbaldehyde, **9**

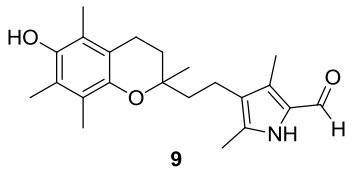

9

HOTrCH2CH2-P-CHO-H1

No.	(ppm)	(Hz)	Height
1	9.47	4735.0	0.3060
2	9.07	4535.9	0.0483
3	7.26	3628.7	0.9569
4	2.73	1365.0	0.1241
5	2.72	1359.1	0.1275
6	2.71	1353.5	0.1313
7	2.64	1322.0	0.1435
8	2.63	1312.9	0.2008
9	2.61	1304.8	0.1665
10	2.29	1146.6	0.9838
11	2.28	1137.8	1.0000
12	2.13	1066.2	0.1494
13	2.09	1043.2	0.9979
14	2.02	1008.9	0.7735

No.	(ppm)	(Hz)
15	2.01	1005.3
16	1.96	978.9
17	1.94	969.8
18	1.93	966.9
19	1.92	960.8
20	1.91	956.4
21	1.90	950.5
22	1.89	943.4
23	1.87	937.3
24	1.86	929.5
25	1.63	813.3

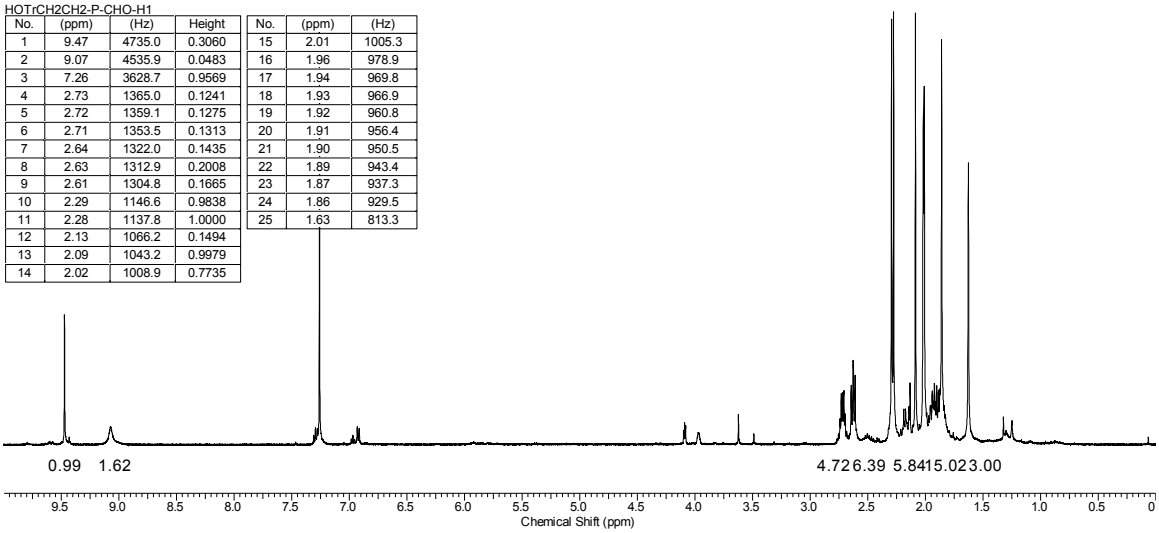

HOTrCH2CH2-P-CHO-C13

No.	(ppm)	(Hz)	Height
1	187.52	23573.9	0.0452
2	187.10	23520.4	0.0477
3	175.83	22103.8	0.0324
4	143.02	17979.7	0.0592
5	140.95	17719.2	0.0513
6	140.74	17693.1	0.0496
7	140.38	17647.5	0.0444
8	134.85	16952.0	0.0179
9	129.52	16282.1	0.0349
10	127.95	16084.9	0.0400
11	121.79	15310.8	0.0204
12	121.11	15225.6	0.0216
13	114.51	14395.7	0.0367

No.	(ppm)	(Hz)	Height
14	77.26	9712.4	0.9793
15	77.00	9680.3	1.0000
16	76.75	9648.6	0.9681
17	71.82	9029.0	0.0903
18	45.76	5752.0	0.1083
19	43.58	5478.0	0.1048
20	31.06	3904.2	0.1073
21	23.54	2958.9	0.1100
22	20.18	2537.4	0.0987
23	12.43	1562.3	0.1182
24	12.30	1546.5	0.1156
25	12.15	1527.9	0.1107
26	11.65	1464.6	0.0911

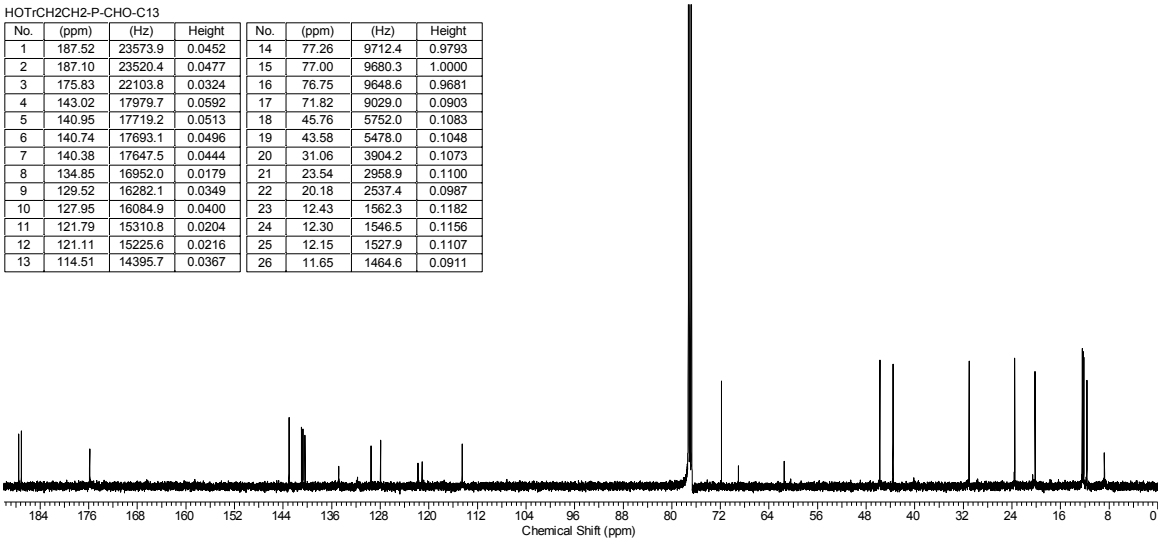

Benzyl 4-(3-chloropropyl)-3,5-dimethyl-1H-pyrrole-2-carboxylate, **12**

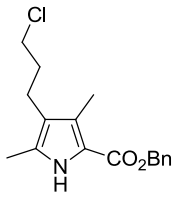

12

ClCH2CH2CH2-Me2pyrrole-COOBn-fr1

No.	(ppm)	(Hz)	Height	No.	(ppm)	(Hz)	Height
1	8.83	3532.6	0.0361	14	3.52	1408.7	0.1729
2	7.43	2973.0	0.1189	15	3.50	1402.1	0.3454
3	7.41	2966.4	0.2305	16	3.49	1395.8	0.1841
4	7.40	2959.7	0.1060	17	2.56	1023.0	0.1489
5	7.39	2958.1	0.1187	18	2.54	1016.0	0.2652
6	7.39	2956.2	0.0626	19	2.52	1008.6	0.1632
7	7.38	2951.5	0.2243	20	2.29	917.5	1.0000
8	7.36	2944.1	0.1201	21	2.21	883.9	0.9676
9	7.35	2940.2	0.0791	22	1.93	773.7	0.0500
10	7.34	2938.6	0.0990	23	1.92	767.1	0.1423
11	7.33	2934.3	0.0461	24	1.90	760.0	0.1798
12	7.33	2931.6	0.0848	25	1.88	753.0	0.1259
13	5.30	2121.9	0.5926	26	1.87	746.4	0.0375

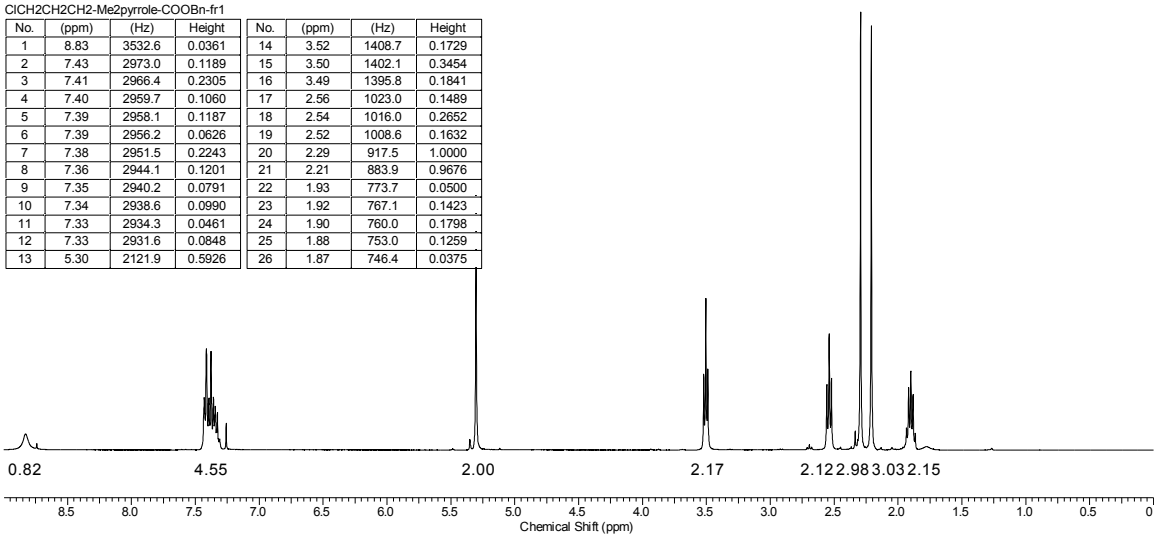

ClCH2CH2CH2-Me2-pyrrole-COOBn-C13

No.	(ppm)	(Hz)	Height
1	161.97	12222.1	0.0760
2	136.74	10318.0	0.2148
3	131.25	9903.3	0.1581
4	128.58	9702.1	1.0000
5	128.04	9661.7	0.4363
6	127.93	9653.5	0.8739
7	127.55	9624.7	0.1013
8	120.34	9080.7	0.2915
9	116.70	8805.9	0.1928
10	65.54	4945.8	0.4015
11	44.52	3359.6	0.3878
12	33.44	2523.1	0.3915
13	21.03	1587.1	0.2992
14	11.43	862.2	0.3664
15	11.02	831.3	0.3296

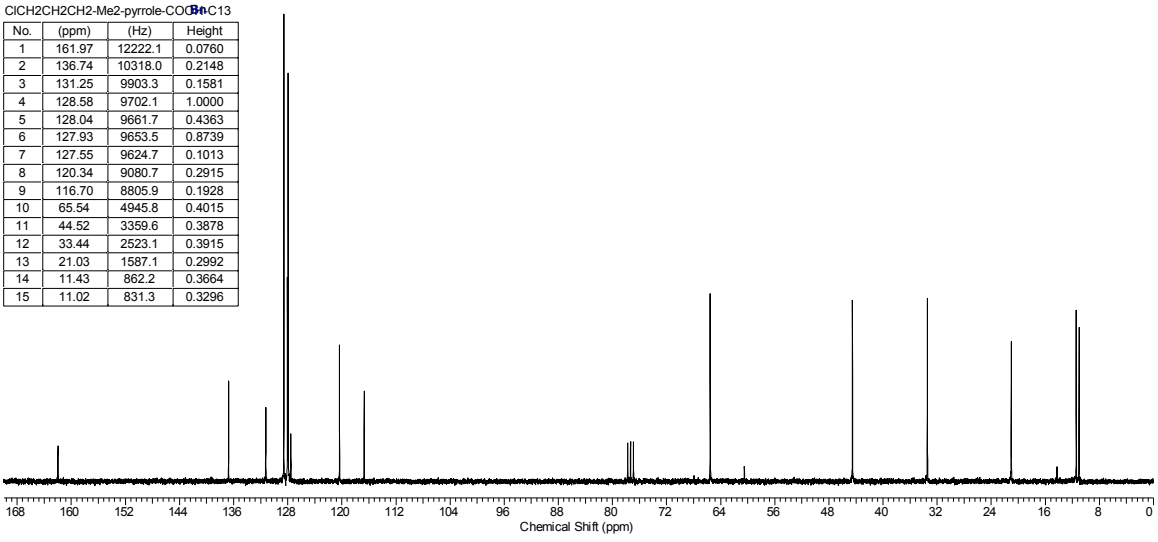

4-(3-chloropropyl)-3,5-dimethyl-1H-pyrrole-2-carboxylic acid, **13**

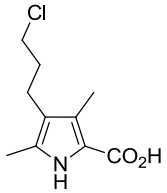

13

ClCH2CH2CH2-Me2-pyrrole-COOH

No.	(ppm)	(Hz)	Height	No.	(ppm)	(Hz)	Height
1	13.16	5265.7	0.0112	9	2.27	909.7	1.0000
2	4.68	1873.4	0.1531	10	2.23	894.1	0.0634
3	3.55	1421.6	0.2102	11	2.20	880.4	0.0523
4	3.54	1416.2	0.3281	12	1.94	776.8	0.0621
5	3.52	1410.3	0.2020	13	1.93	771.0	0.1510
6	2.63	1054.3	0.1743	14	1.91	762.8	0.1847
7	2.62	1046.5	0.2893	15	1.89	756.5	0.1489
8	2.59	1035.1	0.6371	16	1.87	749.9	0.0709

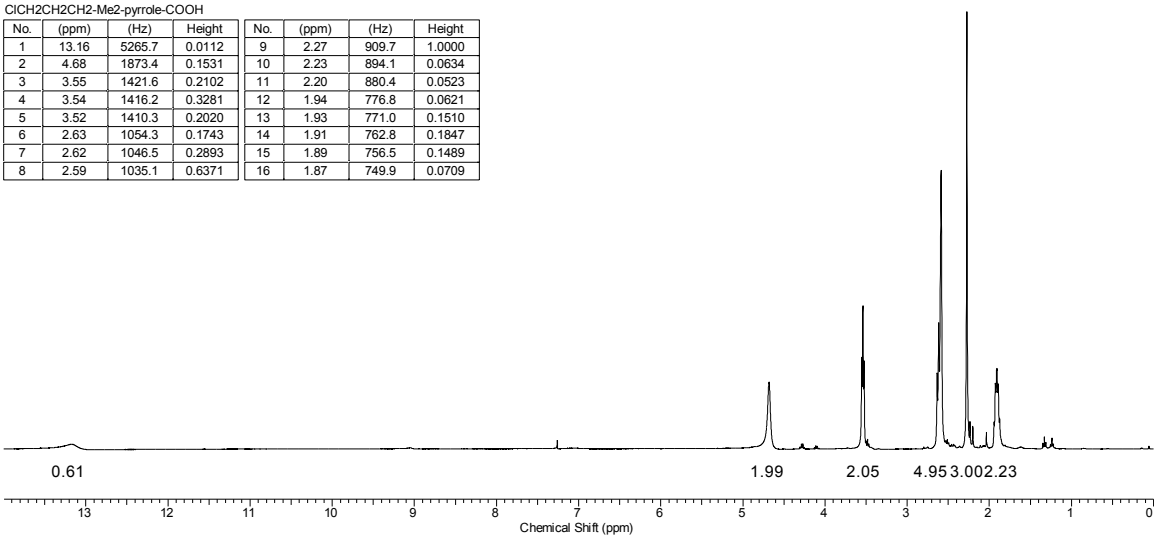

ClCH2CH2CH2-pyrrole-COOH-C13

No.	(ppm)	(Hz)	Height
1	166.81	12587.0	0.2805
2	132.46	9995.1	0.6036
3	129.83	9796.6	0.5486
4	121.01	9131.0	0.7663
5	116.07	8758.4	0.3861
6	77.59	5854.7	0.2520
7	77.16	5822.6	0.2663
8	76.74	5790.5	0.2572
9	44.49	3356.8	1.0000
10	33.27	2510.4	0.9190
11	20.97	1582.6	0.5578
12	11.52	869.4	0.6697
13	10.80	815.2	0.7473

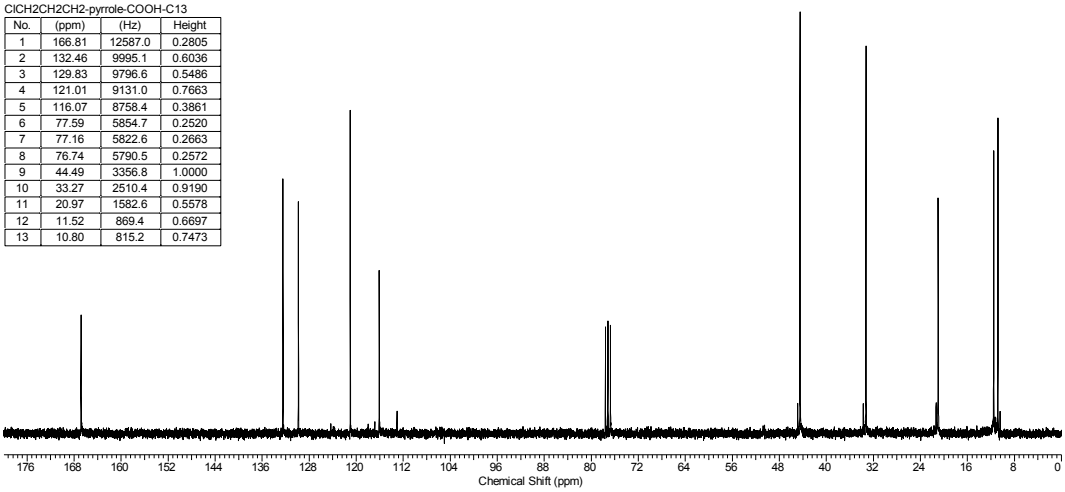

4-(3-chloropropyl)-3,5-dimethyl pyrrole, **14**

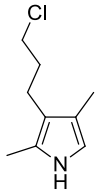

14

ClCH2CH2CH2-pyrrole-H1

No.	(ppm)	(Hz)	Height
1	7.55	2266.7	0.0262
2	6.42	1926.8	0.1116
3	3.59	1077.0	0.1877
4	3.57	1070.2	0.3832
5	3.55	1063.8	0.2085
6	2.60	779.8	0.1612
7	2.58	772.8	0.2873
8	2.55	765.2	0.1884
9	2.21	664.4	1.0000
10	2.06	619.6	0.8696
11	2.01	603.4	0.0597
12	1.99	596.7	0.1693
13	1.96	589.4	0.2070
14	1.94	582.6	0.1574
15	1.92	575.9	0.0489

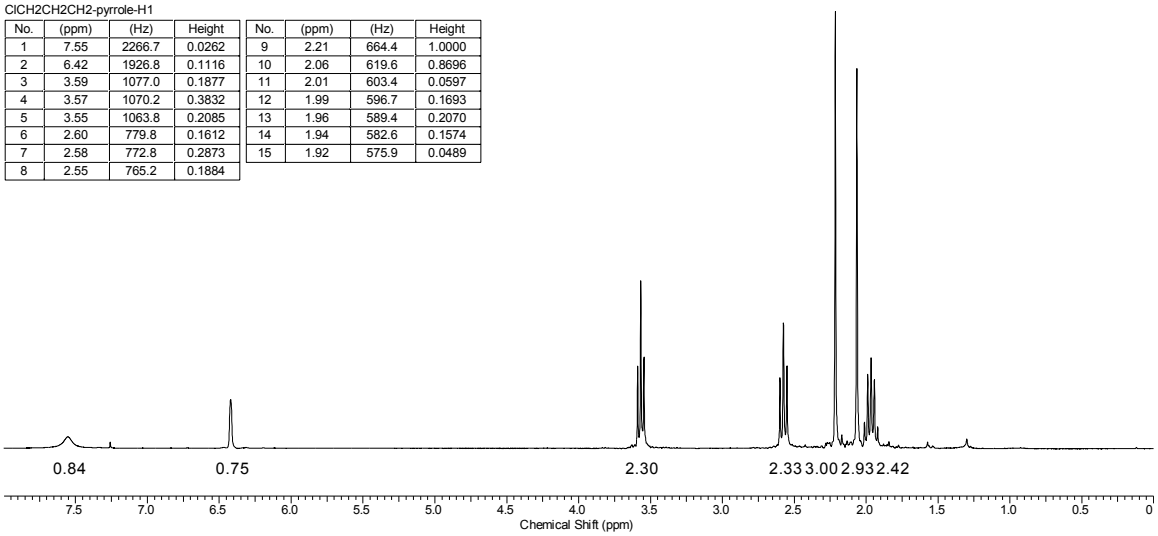

ClCH2CH2CH2-pyrrole-C13

No.	(ppm)	(Hz)	Height
1	124.32	9380.9	0.1556
2	118.01	8904.9	0.2306
3	116.89	8820.3	0.2424
4	113.06	8531.1	0.7167
5	44.85	3384.4	0.7894
6	33.69	2542.4	0.8985
7	21.32	1608.6	1.0000
8	11.35	856.7	0.4827
9	10.45	788.7	0.4784

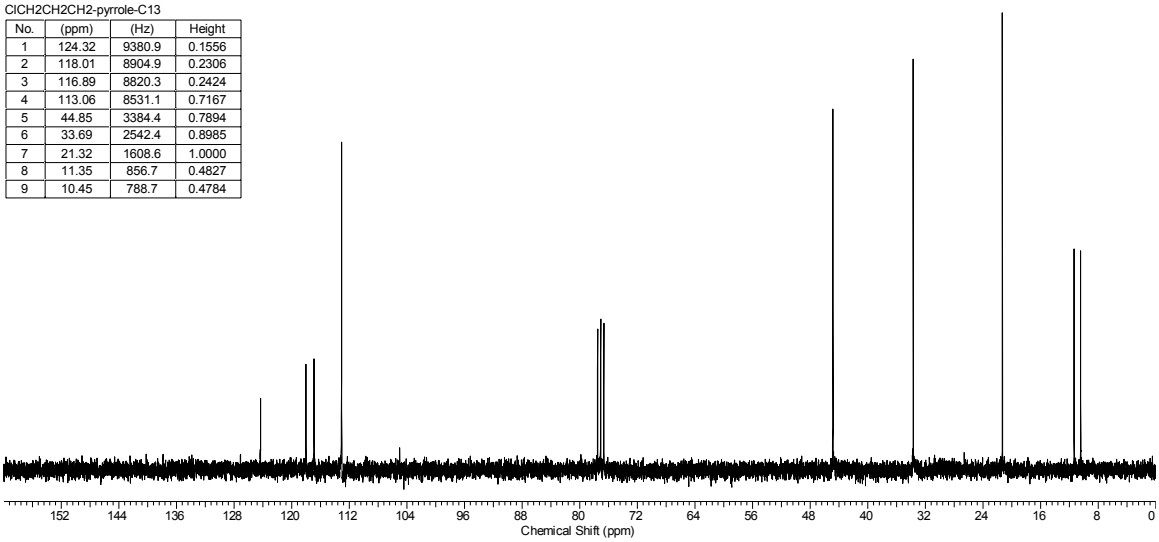

(E)-6-(2-(6-hydroxy-2,5,7,8-tetramethylchroman-2-yl)vinyl)-2-(3-chloropropyl)-1,3,5,7-tetramethyl Pyrromethene Fluoroborate, **15**

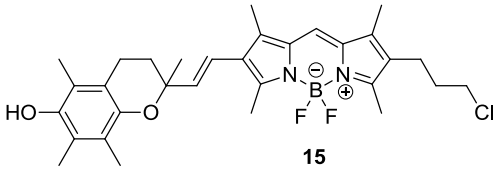

15

HOTrCH=CH-B-CH2CH2CH2Cl-H1-good

No.	(ppm)	(Hz)	Height	No.	(ppm)	(Hz)	Height
1	6.99	2795.2	0.2328	18	2.19	876.1	0.6818
2	6.32	2530.6	0.0805	19	2.18	873.0	1.0000
3	6.28	2514.2	0.0954	20	2.09	834.7	0.4003
4	5.87	2348.9	0.0845	21	2.05	819.8	0.1044
5	5.83	2332.9	0.0721	22	2.03	812.0	0.0458
6	4.23	1693.6	0.0151	23	2.01	804.6	0.0534
7	3.55	1419.7	0.1310	24	2.00	798.7	0.0546
8	3.53	1413.4	0.2525	25	1.98	793.3	0.0344
9	3.52	1407.2	0.1339	26	1.94	776.1	0.0572
10	2.65	1059.0	0.0407	27	1.92	769.8	0.1181
11	2.63	1054.3	0.0422	28	1.91	763.6	0.1291
12	2.57	1026.9	0.1261	29	1.90	762.0	0.1363
13	2.55	1019.5	0.1777	30	1.89	755.4	0.1058
14	2.53	1012.1	0.1303	31	1.88	752.2	0.0421
15	2.50	999.2	0.4718	32	1.87	749.1	0.0442
16	2.46	984.7	0.4698	33	1.49	594.4	0.5381
17	2.23	891.7	0.3910				

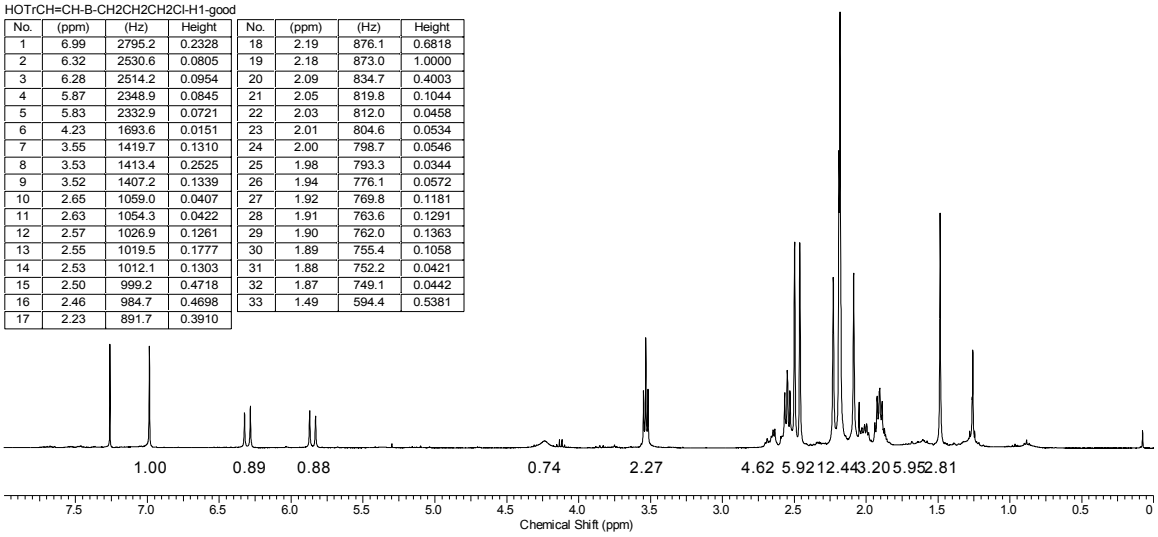

ClCH2CH2CH2-B-CH=CH-TrOH-C13-good

No.	(ppm)	(Hz)	Height	No.	(ppm)	(Hz)	Height
1	155.78	11754.9	0.0479	16	117.43	8860.6	0.0862
2	155.12	11704.6	0.0481	17	75.35	5685.5	0.1285
3	145.47	10976.5	0.0776	18	44.30	3342.4	0.2244
4	144.81	10927.3	0.0798	19	32.57	2457.8	0.2889
5	138.02	10414.8	0.0598	20	27.69	2089.6	0.1490
6	135.91	10255.0	0.0504	21	21.22	1600.9	0.1332
7	135.12	10195.8	0.1369	22	21.00	1584.8	0.2071
8	132.88	10026.6	0.0436	23	13.38	1009.3	0.0770
9	132.45	9994.6	0.0451	24	12.75	962.3	0.0757
10	128.68	9709.8	0.0510	25	12.23	923.1	0.1124
11	126.40	9537.9	0.0416	26	11.88	896.5	0.1156
12	122.09	9212.3	0.0783	27	11.30	852.8	0.1125
13	121.05	9133.8	0.0754	28	10.75	810.8	0.1833
14	119.20	8994.4	0.2526	29	9.64	727.3	0.1808
15	118.48	8940.2	0.0785				

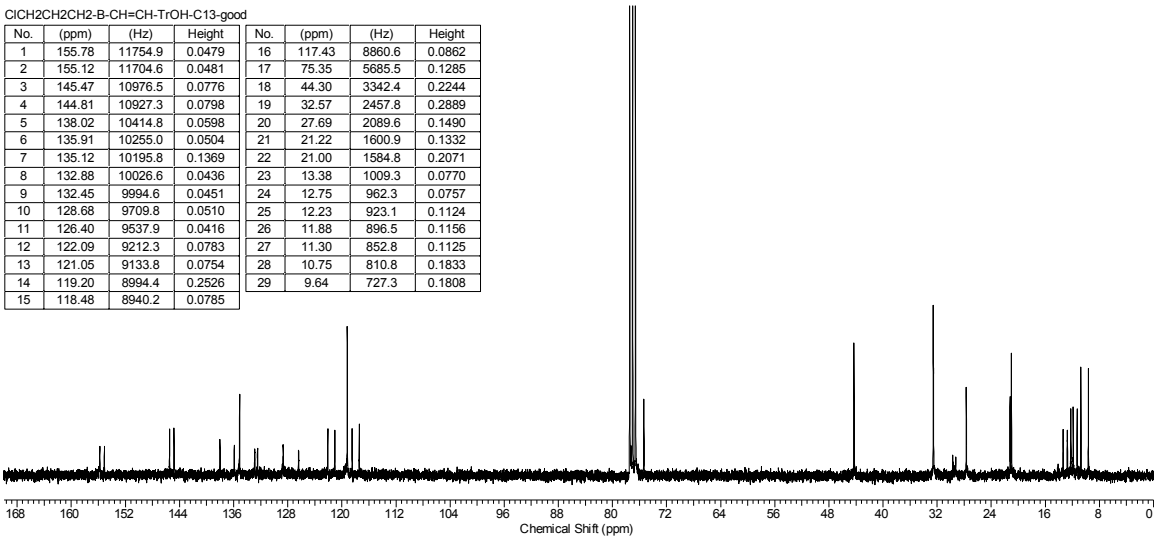

6-(2-(6-hydroxy-2,5,7,8-tetramethylchroman-2-yl)ethyl)-2-(3-chloropropyl)-1,3,5,7-tetramethyl Pyrromethene Fluoroborate, **16**

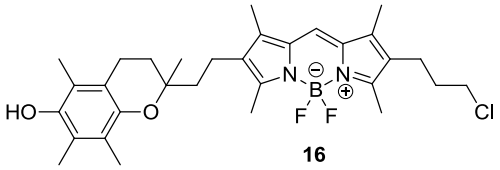

16

HOTrCH2CH2-B-Pr-Cl-fr2-H1

No.	(ppm)	(Hz)	Height
1	7.26	3628.7	0.1951
2	6.94	3467.8	0.3437
3	4.26	2130.9	0.0673
4	3.54	1770.9	0.1781
5	3.53	1764.6	0.3492
6	3.52	1758.5	0.1745
7	2.64	1320.0	0.1380
8	2.56	1278.2	0.1484
9	2.54	1271.1	0.2340
10	2.53	1265.5	0.1611
11	2.53	1263.5	0.1901
12	2.51	1256.7	0.1770
13	2.50	1248.1	0.1582
14	2.49	1243.5	0.6897
15	2.41	1202.9	0.6600
16	2.17	1087.2	0.9774
17	2.17	1082.8	1.0000
18	2.11	1053.9	0.5268
19	2.09	1044.2	0.8313
20	2.05	1023.6	0.4745
21	1.91	953.4	0.1554
22	1.69	846.3	0.0404
23	1.60	800.6	0.0426
24	1.32	662.2	0.7444
25	1.26	631.1	0.2489

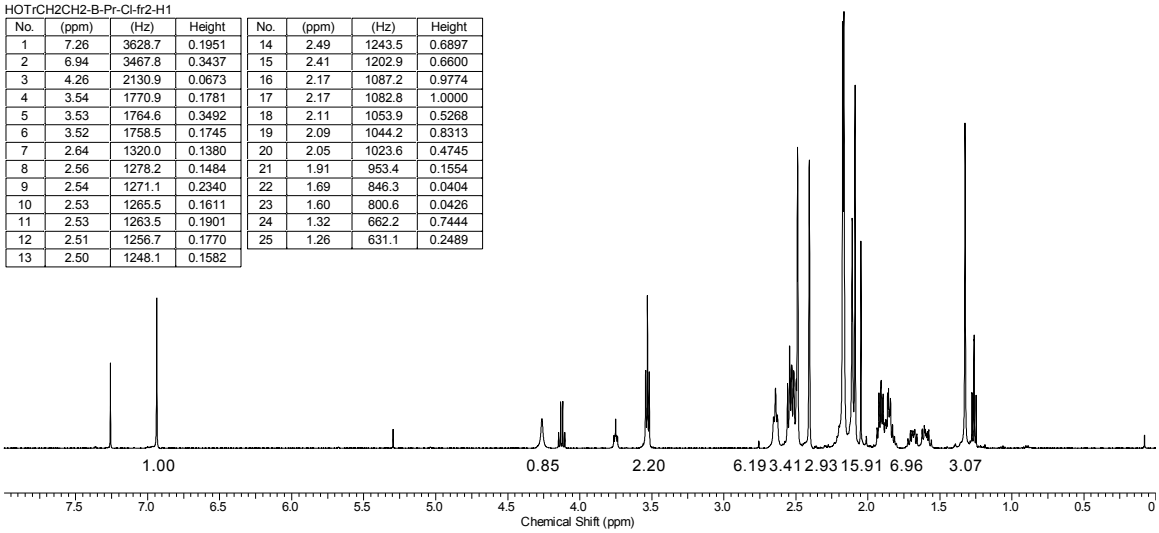

HOTrCH2CH2-B-Pr-Cl-fr2-C13

No.	(ppm)	(Hz)	Height
1	155.68	19571.2	0.1078
2	154.18	19382.8	0.1052
3	145.24	18257.9	0.2410
4	144.79	18202.1	0.2252
5	137.36	17268.4	0.1101
6	137.17	17243.7	0.1105
7	132.71	16683.6	0.0938
8	132.18	16616.2	0.0951
9	130.32	16383.1	0.1091
10	127.89	16077.0	0.1033
11	122.52	15402.4	0.2236
12	121.18	15233.5	0.1997
13	118.75	14927.9	0.3715
14	118.64	14913.9	0.2148
15	117.18	14731.6	0.2545
16	73.86	9285.3	0.4597
17	44.32	5572.0	0.5168
18	39.42	4955.1	0.4134
19	32.68	4108.9	0.6493
20	31.68	3982.8	0.4138
21	25.60	3218.5	0.0986
22	23.50	2953.7	0.5082
23	21.05	2645.8	0.1934
24	21.03	2643.5	0.5254
25	20.71	2603.9	0.3789
26	17.93	2254.1	0.4424
27	14.20	1784.7	0.1525
28	12.61	1585.6	0.2199
29	12.43	1562.8	
30	12.19	1533.0	
31	11.83	1487.4	
32	11.28	1417.6	
33	9.58	1204.1	
34	9.26	1163.6	

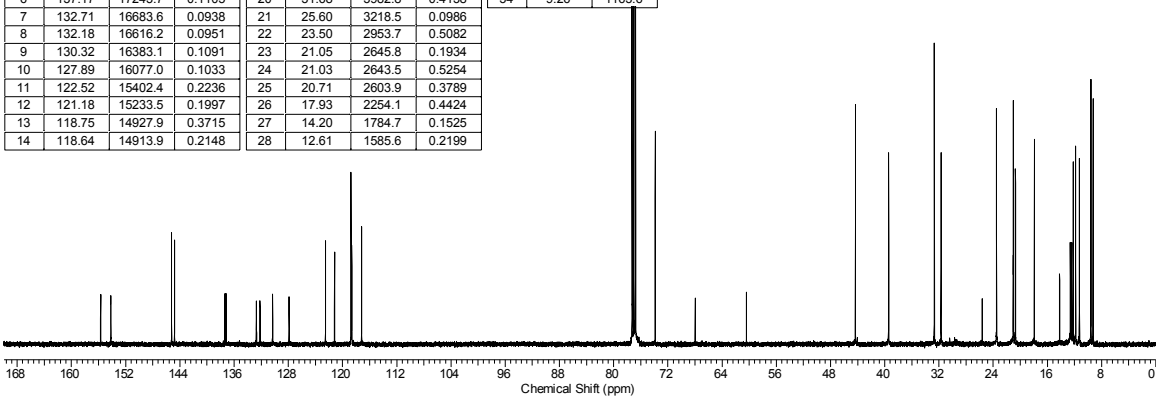

(E)-6-(2-(6-hydroxy-2,5,7,8-tetramethylchroman-2-yl)vinyl)-2-(3-(triphenylphosphonio)-propyl)-1,3,5,7-tetramethyl Pyrromethene Fluoroborate, **17**

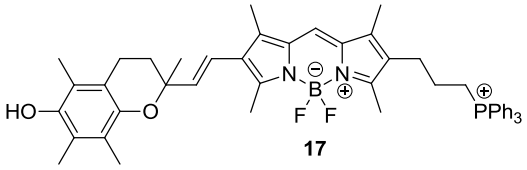

17

Mito-TrOH-exsPPh3

No.	(ppm)	(Hz)	Height	No.	(ppm)	(Hz)	Height
1	7.77	3109.0	0.1596	18	4.32	1729.6	0.0694
2	7.76	3105.5	0.1504	19	3.82	1526.7	0.0314
3	7.76	3103.5	0.1888	20	3.81	1523.6	0.0328
4	7.75	3101.6	0.2268	21	3.78	1511.1	0.0398
5	7.74	3096.5	0.1968	22	2.84	1138.3	0.0359
6	7.72	3089.1	0.2026	23	2.83	1131.3	0.0694
7	7.68	3073.8	0.1596	24	2.81	1123.9	0.0376
8	7.67	3069.9	0.1822	25	2.62	1048.4	0.0671
9	7.66	3066.0	0.1678	26	2.42	968.3	0.2514
10	7.65	3062.5	0.1764	27	2.29	916.7	0.2403
11	7.64	3058.2	0.0936	28	2.20	878.8	0.3562
12	7.64	3055.1	0.0746	29	2.19	876.1	0.3193
13	6.98	2791.7	0.1231	30	2.17	868.3	0.0378
14	6.29	2516.2	0.0581	31	2.15	860.9	1.0000
15	6.25	2500.2	0.0706	32	2.06	822.6	0.3137
16	5.85	2341.1	0.0752	33	2.00	801.5	0.0252
17	5.81	2324.7	0.0613	34	1.99	794.4	0.0307

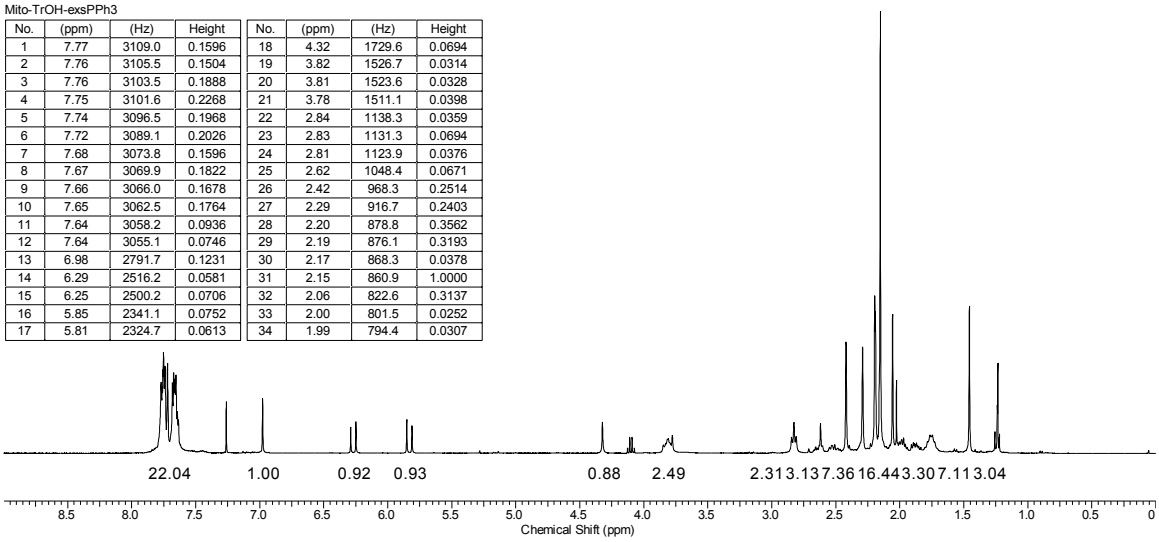

Mito-TrOH-C13

No.	(ppm)	(Hz)	Height	No.	(ppm)	(Hz)	Height
1	155.52	11735.0	0.0539	20	119.64	9027.6	0.1042
2	154.98	11694.7	0.0583	21	119.04	8982.3	0.1443
3	145.40	10971.5	0.0703	22	118.58	8948.0	0.1085
4	144.85	10930.0	0.0886	23	118.51	8942.5	0.1636
5	138.87	10478.9	0.0624	24	117.38	8856.8	0.2265
6	136.40	10292.6	0.0657	25	75.33	5683.8	0.1550
7	135.36	10213.5	0.1643	26	32.50	2452.3	0.0990
8	135.14	10196.9	0.2996	27	30.96	2336.2	0.0841
9	135.11	10194.7	0.3104	28	29.25	2207.4	0.0740
10	133.68	10086.9	0.6473	29	27.68	2088.5	0.1535
11	133.55	10077.0	0.6340	30	24.38	1839.7	0.0505
12	133.22	10052.6	0.0340	31	24.14	1821.5	0.0445
13	132.67	10010.6	0.1205	32	22.82	1722.0	0.0680
14	130.62	9856.4	0.6649	33	22.20	1675.5	0.0442
15	130.46	9844.2	0.6355	34	21.55	1625.8	0.0396
16	127.93	9652.9	0.0772	35	21.20	1599.8	0.1028
17	126.59	9551.7	0.0578	36	14.19	1070.7	0.0355
18	122.00	9205.6	0.0832	37	13.38	1009.3	0.0769
19	121.13	9140.4	0.0901	38	12.96	977.8	0.0796

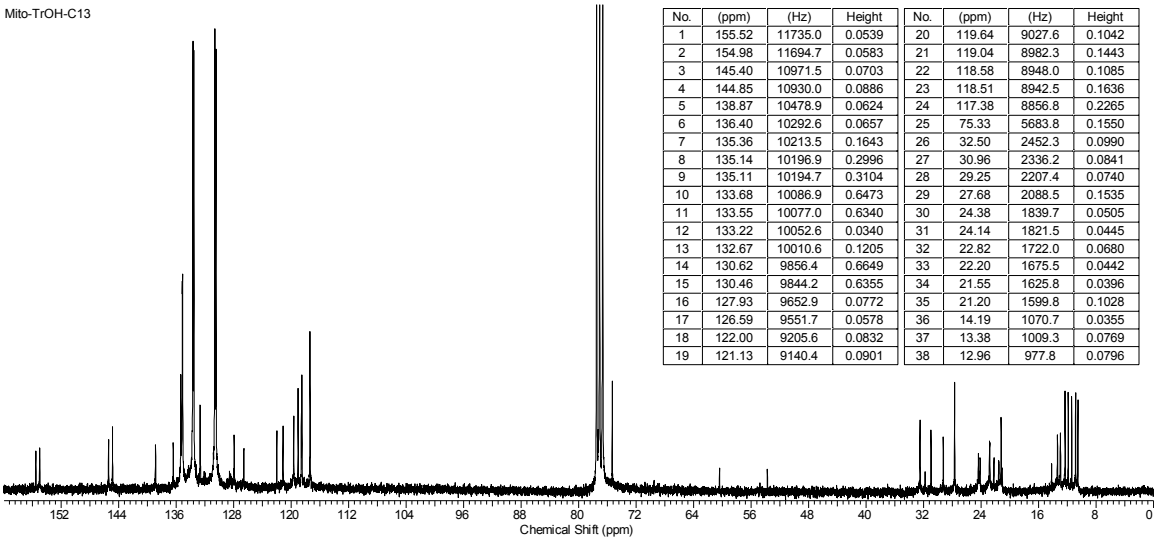

6-(2-(6-hydroxy-2,5,7,8-tetramethylchroman-2-yl)ethyl)-2-(3-(triphenylphosphonio)-propyl)-1,3,5,7-tetramethyl Pyrromethene Fluoroborate, **18**

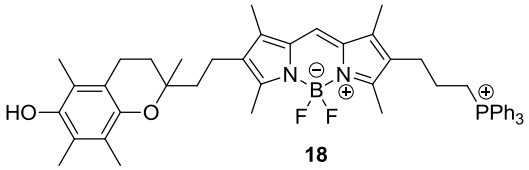

18

HOTrCH2CH2-B-Pr-PPh3-H1

No.	(ppm)	(Hz)	Height	No.	(ppm)	(Hz)	Height	No.	(ppm)	(Hz)	Height
1	7.78	3888.6	0.1651	9	2.28	1141.5	0.8352	17	1.81	905.5	0.1580
2	7.65	3821.9	0.2122	10	2.17	1086.7	0.9759	18	1.80	898.4	0.1210
3	6.93	3464.6	0.4228	11	2.16	1079.6	0.1833	19	1.29	646.5	0.9219
4	4.31	2156.1	0.2619	12	2.15	1075.2	0.9213				
5	2.81	1404.9	0.2496	13	2.14	1067.4	0.9287				
6	2.61	1302.6	0.1753	14	2.13	1064.5	0.8962				
7	2.48	1240.0	0.1890	15	2.08	1039.8	0.7893				
8	2.37	1186.2	0.8188	16	2.06	1030.7	1.0000				

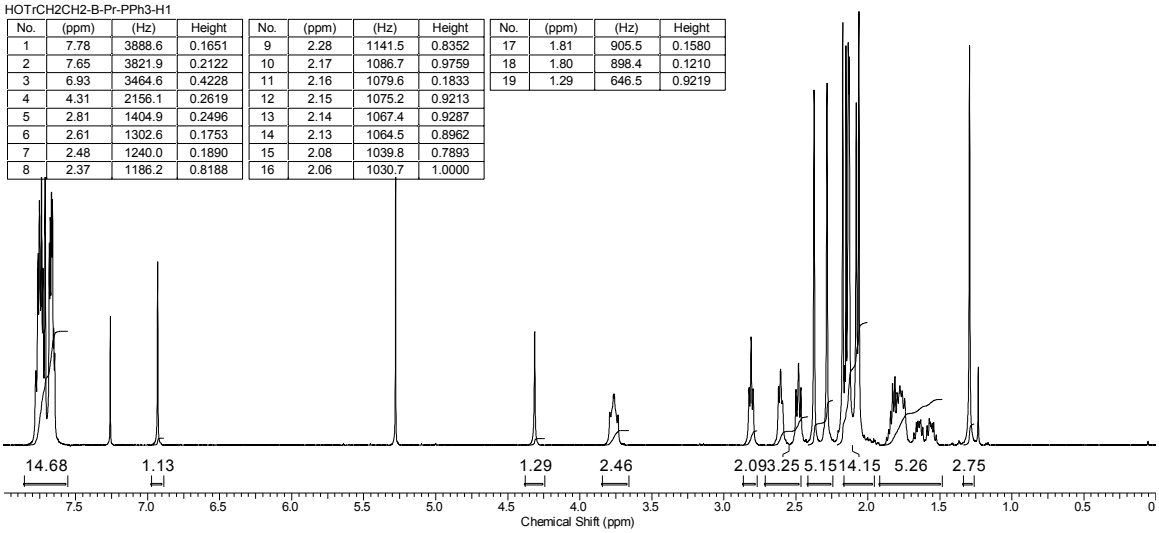

HOTrCH2CH2-B-Pr-PPh3-C13

No.	(ppm)	(Hz)	Height	No.	(ppm)	(Hz)	Height	No.	(ppm)	(Hz)	Height	No.	(ppm)	(Hz)	Height
1	156.24	19641.9	0.0595	12	131.97	16590.1	0.0625	23	73.82	9280.2	0.1769	34	21.96	2760.2	0.0548
2	153.34	19277.2	0.0583	13	130.60	16418.4	0.7889	24	53.50	6725.2	0.0551	35	21.55	2709.5	0.0590
3	145.16	18248.1	0.0901	14	130.50	16405.9	0.7406	25	39.35	4946.3	0.1250	36	20.69	2601.1	0.1237
4	144.82	18205.8	0.1017	15	127.03	15969.0	0.0652	26	31.63	3976.8	0.1330	37	17.91	2251.7	0.1251
5	138.00	17347.9	0.0771	16	122.43	15391.2	0.1001	27	30.96	3892.1	0.0651	38	12.83	1613.0	0.1037
6	137.97	17344.7	0.0756	17	121.24	15241.0	0.0965	28	29.25	3677.6	0.0382	39	12.47	1567.4	0.1020
7	135.14	16988.3	0.2577	18	119.19	14984.2	0.1280	29	24.26	3049.6	0.0682	40	12.29	1544.6	0.1783
8	135.11	16985.5	0.2610	19	118.71	14923.2	0.0996	30	24.12	3032.4	0.0659	41	11.83	1487.4	0.1970
9	133.64	16799.9	0.7515	20	118.29	14871.1	0.1844	31	23.48	2952.4	0.2221	42	11.38	1430.6	0.1900
10	133.56	16789.7	0.7024	21	117.61	14785.1	0.1744	32	22.83	2869.5	0.0757	43	10.46	1314.3	0.2396
11	132.95	16713.9	0.0668	22	117.14	14725.5	0.1049	33	22.80	2865.8	0.0733	44	9.34	1174.8	0.2319

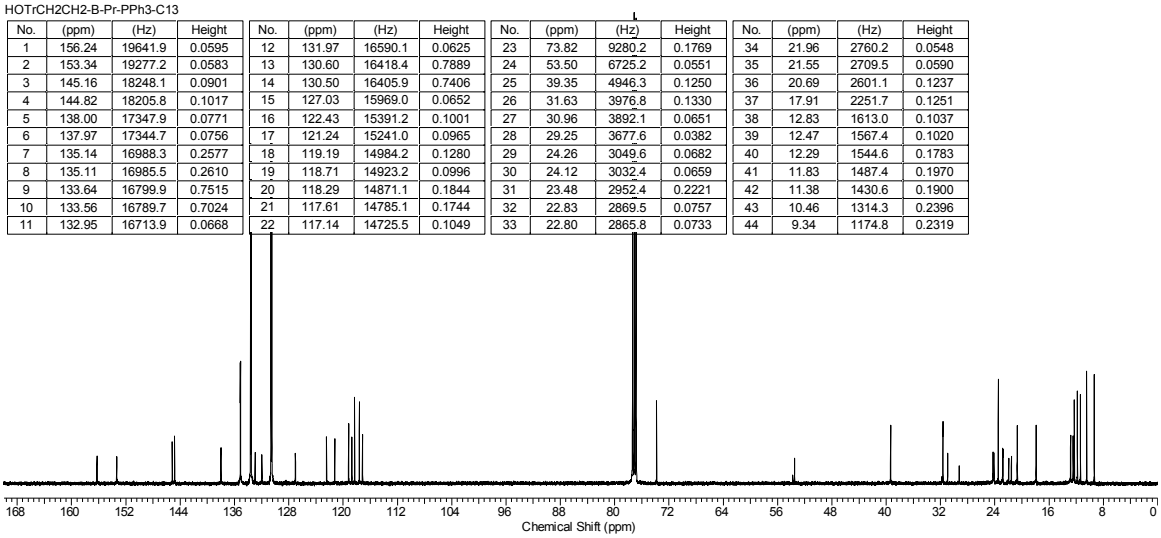

(E)-6-(2-(6-methoxy-2,5,7,8-tetramethylchroman-2-yl)vinyl)-2-(3-chloropropyl)-1,3,5,7-tetramethyl Pyrromethene Fluoroborate, **19**

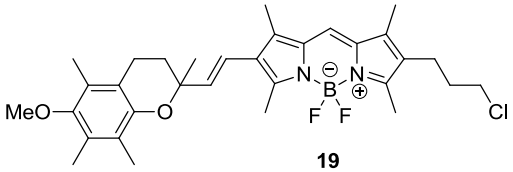

19

MeOTrC=C-B-Pr-Cl-H1-new

No.	(ppm)	(Hz)	Height
1	7.00	3499.0	0.2034
2	6.32	3159.9	0.1043
3	6.29	3143.5	0.1197
4	5.87	2936.4	0.1256
5	5.84	2920.2	0.1110
6	3.63	1816.1	0.7042
7	3.55	1777.0	0.1187
8	3.54	1770.6	0.2141
9	2.51	1254.7	0.4874
10	2.46	1230.2	0.4804
11	2.22	1111.1	1.0000
12	2.20	1099.4	0.5867
13	2.18	1091.8	0.7280
14	2.18	1090.8	0.7299
15	2.13	1066.4	0.5799
16	1.51	753.6	0.5937

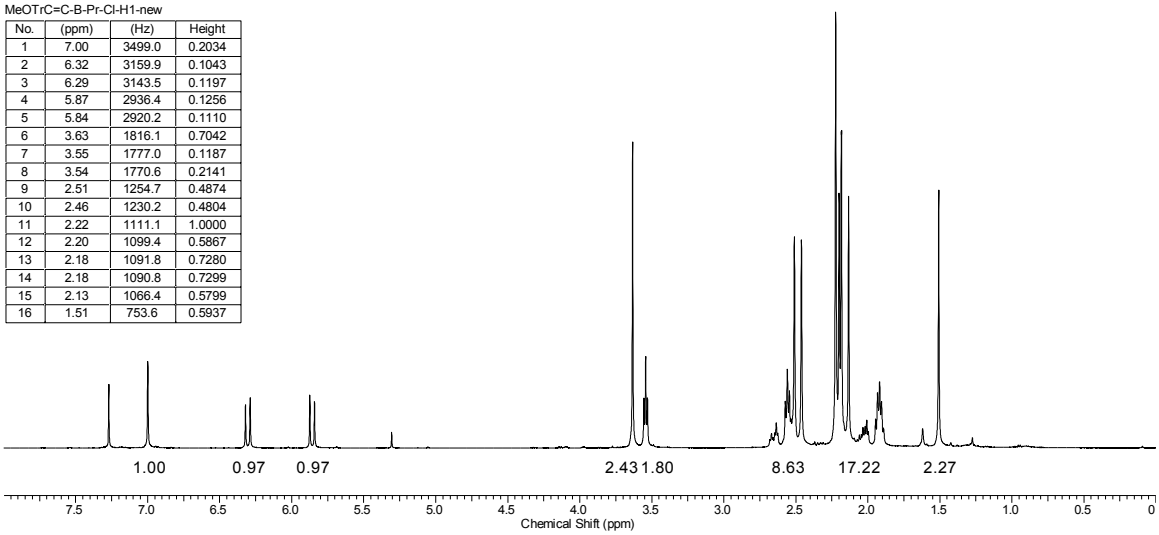

No.	(ppm)	(Hz)	Height
1	155.80	19585.6	0.1068
2	154.98	19482.3	0.1019
3	149.67	18814.8	0.2030
4	147.65	18561.2	0.2282
5	137.99	17347.0	0.1095
6	135.85	17078.1	0.1163
7	135.09	16982.7	0.5111
8	132.86	16702.2	0.0942
9	132.40	16644.1	0.0980

No.	(ppm)	(Hz)	Height
10	128.67	16175.1	0.1086
11	127.74	16058.8	0.2386
12	126.39	15889.0	0.0857
13	125.70	15801.6	0.2430
14	122.37	15383.3	0.2227
15	119.18	14982.8	0.4977
16	119.15	14978.1	0.3678
17	117.68	14793.9	0.2611
18	75.52	9493.3	0.4115

No.	(ppm)	(Hz)	Height
19	60.32	7583.1	0.4731
20	44.22	5559.4	0.5144
21	32.53	4089.8	0.5887
22	32.38	4070.7	0.4475
23	30.86	3879.5	0.1210
24	27.64	3474.3	0.5541
25	21.05	2646.2	0.4556
26	20.97	2636.5	0.4991
27	13.25	1666.0	0.2381

No.	(ppm)	(Hz)	Height
28	12.69	1595.3	0.2599
29	12.51	1572.5	0.5110
30	11.80	1483.7	0.5145
31	11.63	1461.8	0.5419
32	10.60	1332.5	0.5069
33	9.57	1203.1	0.4775

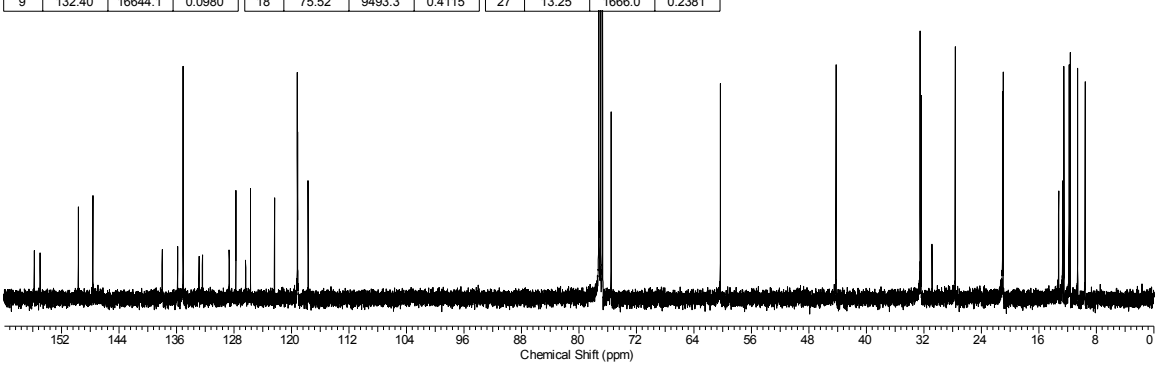

6-(2-(6-methoxy-2,5,7,8-tetramethylchroman-2-yl)ethyl)-2-(3-chloropropyl)-1,3,5,7-tetramethyl Pyrromethene Fluoroborate, **20**

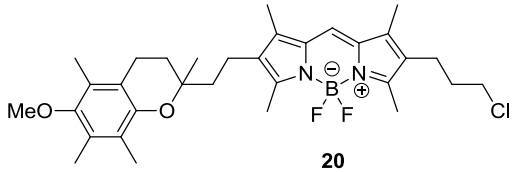

20

No.	(ppm)	(Hz)	Height
1	6.94	3466.8	0.2065
2	3.63	1813.0	1.0000
3	3.53	1764.3	0.2142
4	2.62	1308.7	0.1062
5	2.54	1271.3	0.1296
6	2.53	1264.0	0.1478
7	2.49	1247.1	0.1022
8	2.40	1199.7	0.3704
9	2.19	1096.2	0.5210
10	2.18	1087.9	0.4773
11	2.14	1069.8	0.8496
12	2.08	1039.5	0.4660
13	1.94	967.4	0.0262

No.	(ppm)	(Hz)	Height
14	1.91	954.7	0.0822
15	1.86	930.4	0.0242
16	1.86	928.5	0.0385
17	1.85	925.6	0.0354
18	1.84	922.1	0.0710
19	1.82	908.4	0.0225
20	1.70	852.2	0.0194
21	1.70	850.0	0.0158
22	1.69	845.3	0.0264
23	1.69	842.4	0.0182
24	1.66	828.5	0.0222
25	1.61	804.8	0.0413
26	1.60	798.6	0.0253

No.	(ppm)	(Hz)
27	1.59	795.0
28	1.58	788.9
29	1.33	665.1

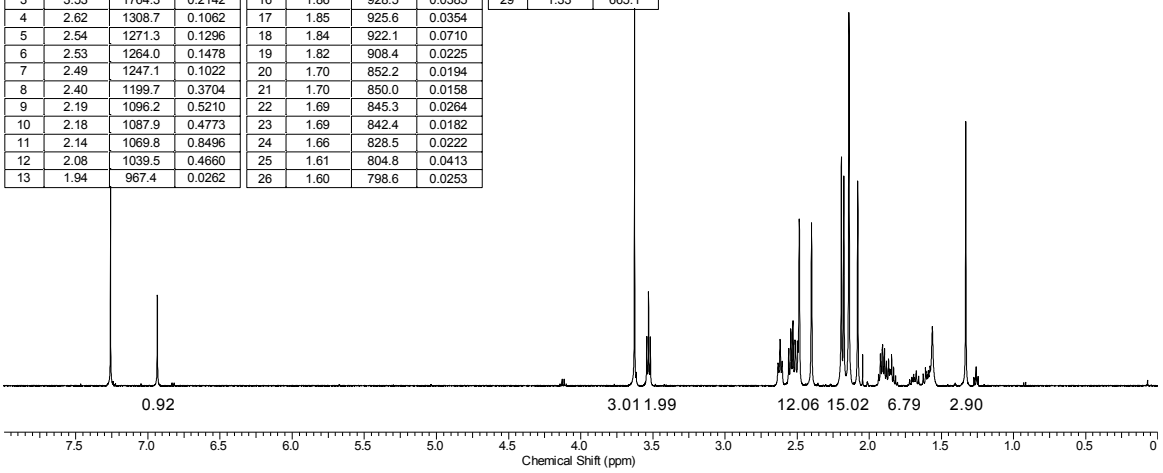

No.	(ppm)	(Hz)	Height
1	155.62	19562.8	0.0171
2	154.25	19391.6	0.0187
3	149.65	18812.9	0.0413
4	147.47	18539.4	0.0483
5	137.34	17265.6	0.0164
6	137.20	17247.9	0.0181
7	132.69	16680.8	0.0163
8	132.19	16617.6	0.0164
9	130.27	16376.1	0.0177
10	127.91	16080.2	0.0681
11	125.91	15828.1	0.0556
12	122.88	15447.1	0.0535
13	118.76	14929.3	0.0615
14	117.47	14766.9	0.0635
15	74.11	9316.5	0.0859
16	60.43	7597.1	0.0872

No.	(ppm)	(Hz)	Height
17	44.32	5571.5	0.0900
18	39.48	4963.0	0.0844
19	32.67	4107.5	0.1059
20	31.48	3957.7	0.0809
21	23.64	2971.4	0.1111
22	21.02	2643.0	0.0922
23	20.59	2588.6	0.0761
24	17.91	2251.3	0.0714
25	12.62	1587.0	0.0396
26	12.54	1576.3	0.1089
27	12.40	1559.0	0.0355
28	11.81	1484.6	0.0988
29	11.68	1468.3	0.1081
30	9.59	1205.9	0.0987
31	9.23	1160.3	0.0946

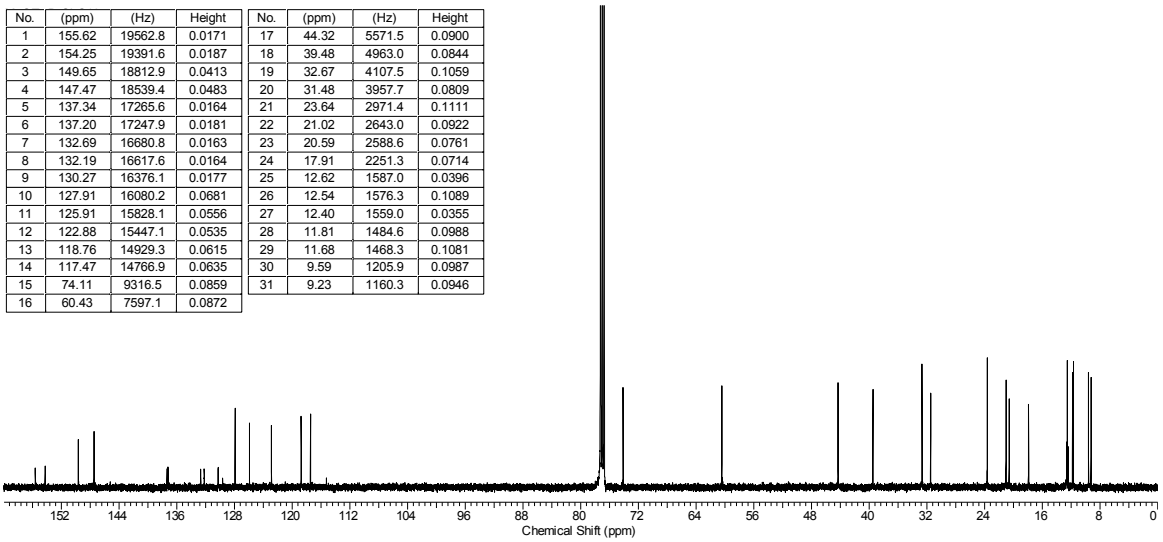

(E)-6-(2-(6-methoxy-2,5,7,8-tetramethylchroman-2-yl)vinyl)-2-(3-(triphenylphosphonio)-propyl)-1,3,5,7-tetramethyl Pyrromethene Fluoroborate, **21**

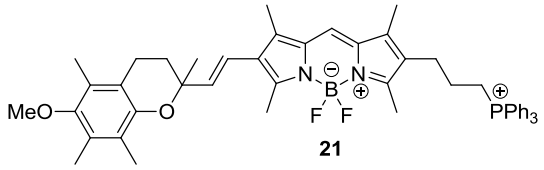

21

No.	(ppm)	(Hz)	Height
1	7.78	3890.4	0.0726
2	7.78	3888.4	0.0846
3	7.78	3887.2	0.0793
4	7.77	3885.5	0.1910
5	7.77	3884.2	0.2267
6	7.77	3883.0	0.3221
7	7.76	3881.1	0.1928
8	7.76	3879.1	0.1455
9	7.75	3876.4	0.3709
10	7.75	3872.3	0.2468
11	7.73	3866.6	0.0826
12	7.73	3864.7	0.2971
13	7.73	3863.2	0.2149
14	7.69	3841.9	0.2151
15	7.68	3838.8	0.2353

No.	(ppm)	(Hz)	Height
16	7.67	3834.4	0.2265
17	7.66	3830.9	0.2476
18	7.65	3826.5	0.1108
19	7.65	3823.1	0.0988
20	6.99	3492.7	0.2257
21	6.28	3138.6	0.1192
22	6.25	3122.5	0.1384
23	5.85	2922.5	0.1530
24	5.81	2906.3	0.1267
25	3.82	1909.8	0.0483
26	3.60	1798.6	0.8526
27	2.84	1417.6	0.1152
28	2.60	1300.9	0.0391
29	2.49	1245.9	0.0304
30	2.42	1207.3	0.4038

No.	(ppm)	(Hz)	Height
31	2.29	1146.9	0.3988
32	2.21	1105.0	0.4880
33	2.19	1092.8	0.9362
34	2.16	1077.9	0.4893
35	2.10	1047.3	0.5598
36	1.99	996.7	1.0000
37	1.88	941.0	0.0301
38	1.77	887.2	0.0496
39	1.47	735.8	0.6431

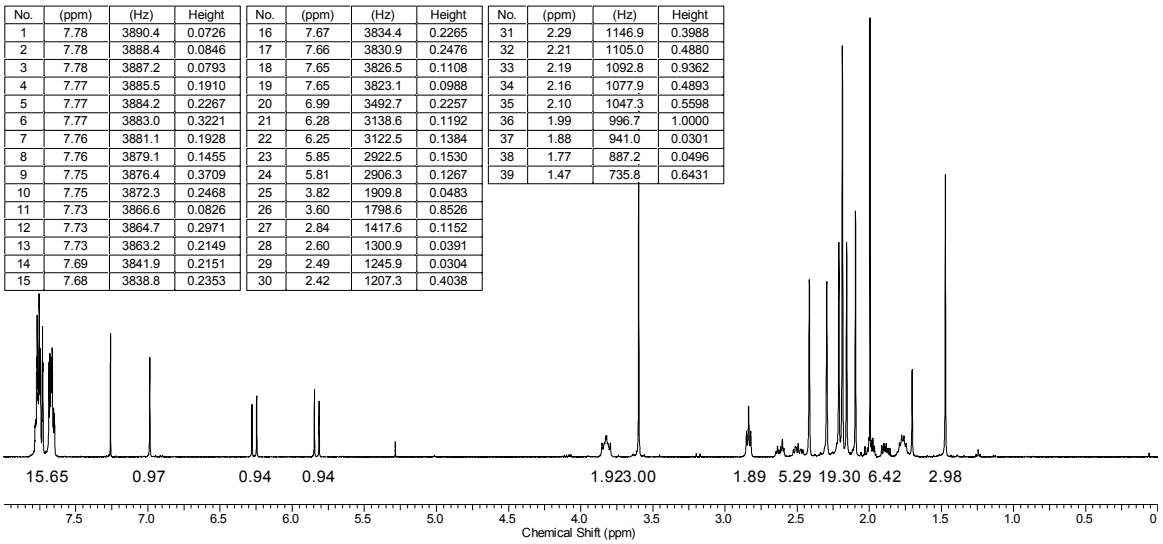

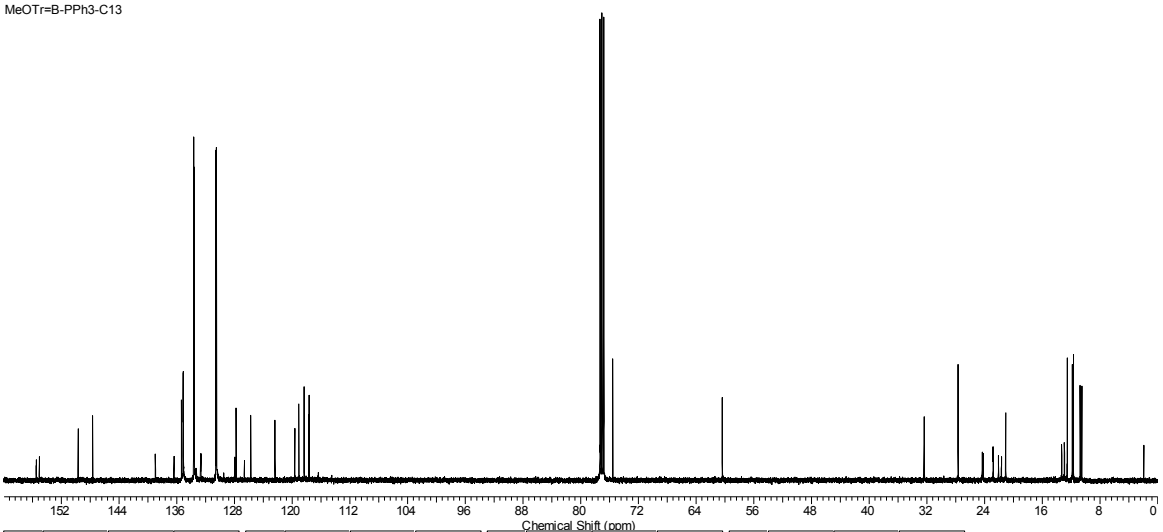

No.	(ppm)	(Hz)	Height
1	155.48	19545.6	0.0448
2	155.05	19492.1	0.0511
3	149.68	18816.2	0.1116
4	147.66	18562.1	0.1394
5	138.97	17469.8	0.0574
6	136.38	17145.1	0.0523
7	135.35	17014.8	0.1727
8	135.12	16986.0	0.2316
9	135.10	16983.2	0.2341
10	133.66	16802.7	0.7342
11	133.58	16792.5	0.6705

No.	(ppm)	(Hz)	Height
12	132.71	16682.7	0.0572
13	132.65	16676.2	0.0581
14	130.58	16416.1	0.7067
15	130.48	16403.6	0.7126
16	127.95	16085.3	0.0505
17	127.77	16062.6	0.1556
18	126.63	15919.3	0.0429
19	125.74	15807.1	0.1404
20	122.39	15385.7	0.1292
21	119.65	15041.4	0.1122
22	119.08	14969.3	0.1650

No.	(ppm)	(Hz)	Height
23	118.34	14876.3	0.2008
24	117.71	14798.1	0.1412
25	117.65	14790.2	0.1831
26	75.55	9497.4	0.2608
27	60.37	7588.7	0.1778
28	32.38	4070.7	0.1372
29	27.67	3478.0	0.2483
30	24.33	3058.0	0.0616
31	24.18	3040.3	0.0585
32	22.83	2870.5	0.0732
33	22.80	2866.3	0.0715

No.	(ppm)	(Hz)	Height
34	22.08	2775.1	0.0538
35	21.67	2724.4	0.0518
36	21.08	2649.5	0.1457
37	13.31	1673.0	0.0779
38	12.93	1626.0	0.0816
39	12.55	1577.2	0.2622
40	11.84	1488.3	0.2489
41	11.67	1466.9	0.2695
42	10.75	1351.1	0.2041
43	10.53	1323.6	0.2029
44	1.93	242.9	0.0764

(E)-6-(2-(6-methoxy-2,5,7,8-tetramethylchroman-2-yl)ethyl)-2-(3-(triphenylphosphonio)-propyl)-1,3,5,7-tetramethyl Pyrromethene Fluoroborate, **22**

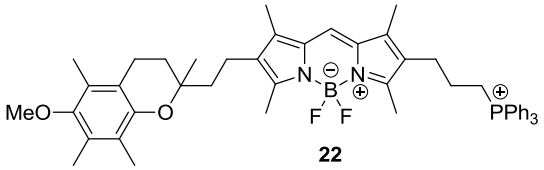

22

No.	(ppm)	(Hz)	Height
1	7.77	3886.2	0.1790
2	7.77	3884.0	0.2065
3	7.76	3879.8	0.1620
4	7.76	3879.6	0.1633
5	7.75	3876.2	0.2487
6	7.74	3871.3	0.1602
7	7.70	3848.3	0.1719
8	7.69	3844.9	0.2026
9	7.68	3840.7	0.2330
10	7.67	3833.1	0.1059
11	7.66	3829.7	0.0821
12	6.95	3472.4	0.1674
13	3.80	1901.3	0.0398
14	3.62	1808.6	0.5696
15	3.62	1807.6	0.5361
16	2.83	1414.6	0.0868

No.	(ppm)	(Hz)	Height
17	2.60	1302.1	0.0895
18	2.59	1295.3	0.0472
19	2.52	1258.6	0.0554
20	2.50	1250.1	0.0828
21	2.48	1241.5	0.0560
22	2.39	1194.5	0.3542
23	2.13	1063.5	1.0000
24	1.85	926.0	0.0545
25	1.85	922.9	0.0376
26	1.82	909.2	0.0498
27	1.81	902.3	0.0458
28	1.79	896.5	0.0449
29	1.67	835.8	0.0405
30	1.65	827.0	0.2043
31	1.60	798.2	0.0316
32	1.32	658.8	0.4717

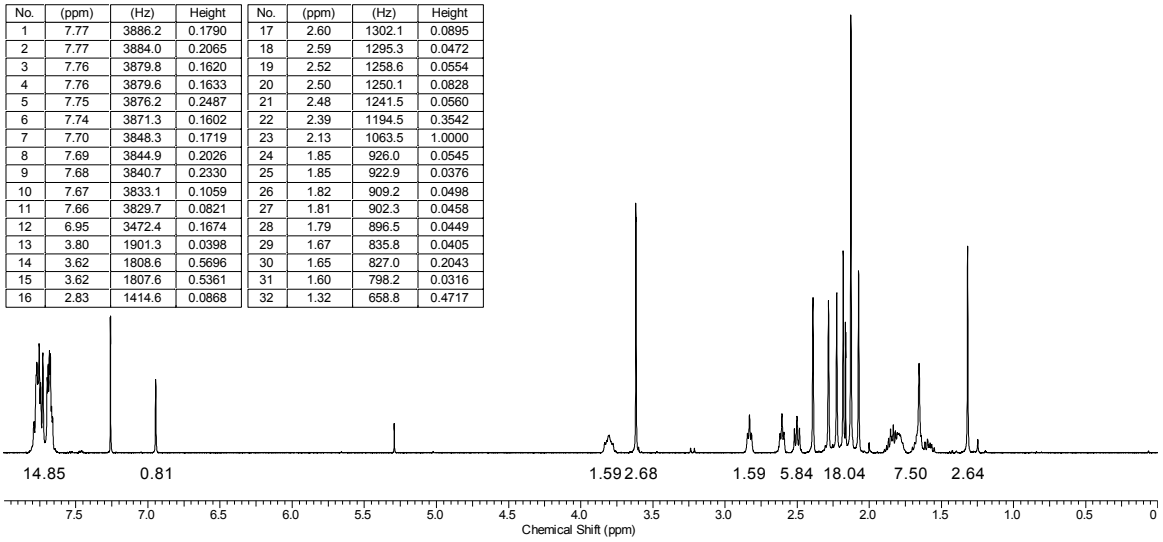

No.	(ppm)	(Hz)	Height
1	156.19	19634.9	0.0337
2	153.37	19280.4	0.0299
3	149.66	18813.8	0.0813
4	147.44	18535.2	0.0787
5	138.25	17379.6	0.0309
6	137.90	17335.8	0.0321
7	135.09	16982.7	0.1458
8	135.07	16979.5	0.1548
9	133.67	16804.1	0.3912
10	133.59	16793.9	0.4303
11	133.37	16766.0	0.0313

No.	(ppm)	(Hz)	Height
12	133.28	16755.3	0.0324
13	132.93	16711.1	0.0282
14	132.01	16595.7	0.0361
15	130.59	16416.6	0.4038
16	130.49	16404.0	0.4166
17	127.91	16079.8	0.0839
18	127.05	15971.8	0.0366
19	125.91	15828.1	0.0821
20	122.84	15442.9	0.0730
21	119.21	14986.5	0.0794
22	118.40	14884.6	0.1203

No.	(ppm)	(Hz)	Height
23	117.72	14798.6	0.1154
24	117.44	14764.1	0.0939
25	74.09	9313.7	0.1640
26	60.42	7596.1	0.1184
27	39.46	4961.1	0.0891
28	31.45	3953.5	0.0955
29	24.21	3044.0	0.0440
30	24.07	3026.3	0.0343
31	23.61	2968.6	0.1554
32	22.83	2870.5	0.0450
33	22.80	2866.3	0.0478

No.	(ppm)	(Hz)	Height
34	21.92	2755.1	0.0337
35	21.51	2703.9	0.0377
36	20.58	2586.7	0.0822
37	17.90	2250.3	0.0775
38	12.78	1606.0	0.0560
39	12.53	1575.3	0.1581
40	12.43	1562.8	0.0538
41	11.80	1483.7	0.1433
42	11.67	1467.4	0.1681
43	10.51	1321.8	0.1201
44	9.29	1167.3	0.1300

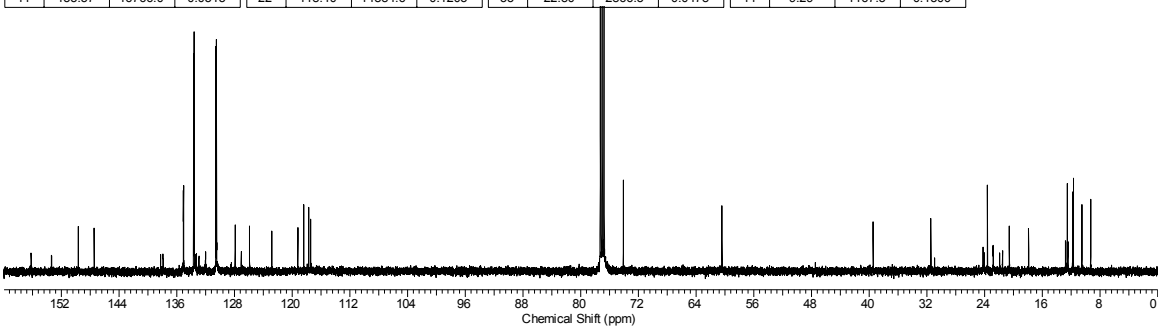

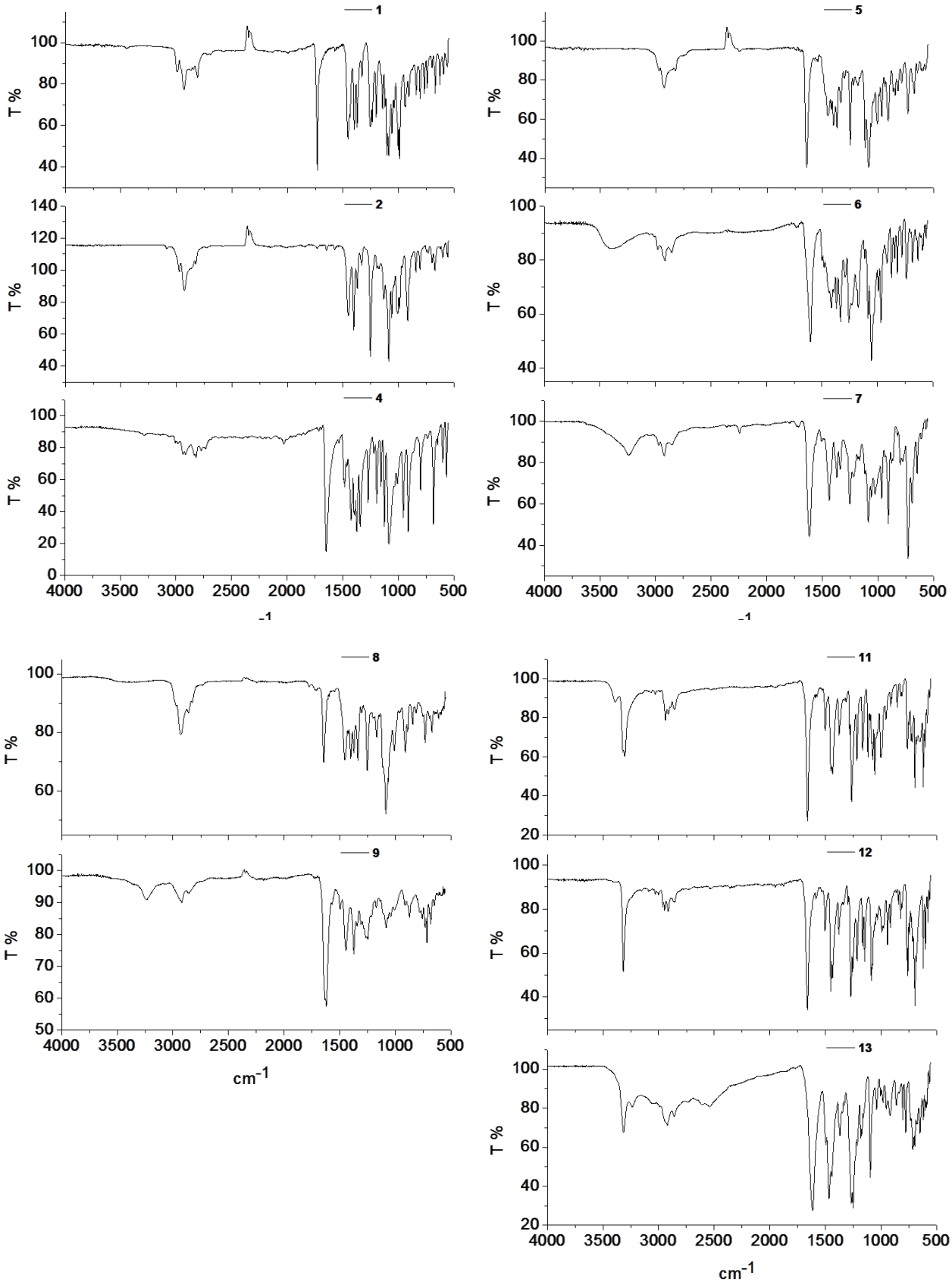
1
2
4
5
6
7
8
9
11
12
13
T %
cm-1

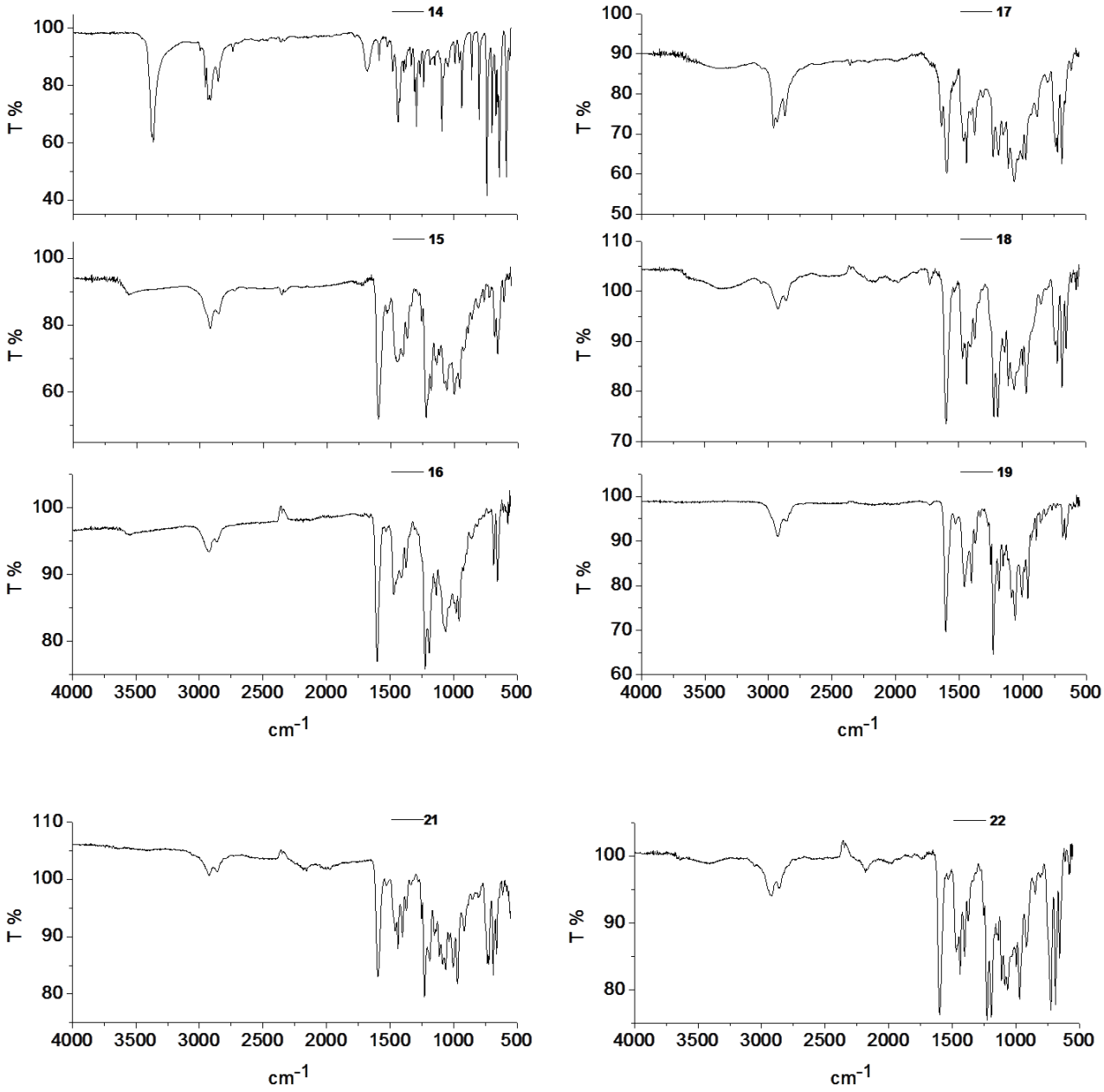
14
15
16
17
18
19
21
22
T %
cm-1
4000 3500 3000 2500 2000 1500 1000 500